

**Научном већу Института за физику у Београду**

Београд, 17. 4. 2018. године

**Предмет: Молба за покретање поступка за избор у звање виши научни сарадник**

Молим Научно веће Института за физику у Београду да, у складу с Правилником о поступку и начину вредновања и квантитативном исказивању научно-истраживачких резултата истраживача, покрене поступак за мој избор у звање виши научни сарадник.

У прилогу достављам:

1. Мишљење руководиоца пројекта са предлогом чланова комисије за избор у звање
2. Образложење за превремено покретање избора у звање
3. Стручну биографију
4. Преглед научне активности
5. Елементе за квалитативну оцену научног доприноса
6. Елементе за квантитативну оцену научног доприноса
7. Списак објављених радова и њихове копије
8. Податке о цитираности радова
9. Фотокопију решења о избору у претходно звање
10. Доказе о испуњености наведених квалитативних услова

С поштовањем,

---

др Игор Франовић

научни сарадник,

Институт за физику у Београду

## **Научном већу Института за физику у Београду**

Београд, 17. април 2018. године

**Предмет: Мишљење руководиоца пројекта о избору др Игора Франовића у звање виши научни сарадник**

Др Игор Франовић је запослен у Лабораторији за примену рачунара у науци, у оквиру Националног центра изузетних вредности за изучавање комплексних система Института за физику у Београду и ангажован је на пројекту основних истраживања Министарства просвете, науке и технолошког развоја Републике Србије ОН171017, под називом "Моделирање и нумеричке симулације сложених вишечестичних физичких система". На поменутом пројекту ради на темама из статистичке физике и нелинеарне динамике. С обзиром да далеко превазилази све предвиђене услове у складу са Правилником о поступку, начину вредновања и квантитативном исказивању научноистраживачких резултата истраживача МПНТР, сагласан сам са покретањем поступка за избор др Игора Франовића у звање виши научни сарадник по убрзаном поступку.

За састав комисије за избор др Игора Франовића у звање виши научни сарадник предлагем:

- (1) др Антун Балаж, научни саветник, Институт за физику у Београду
- (2) др Александар Белић, научни саветник, Институт за физику у Београду
- (3) проф. др Милан Кнежевић, редовни професор Физичког факултета Универзитета у Београду

Руководилац пројекта ОН171017

др Антун Балаж  
научни саветник

## Научном већу Института за физику у Београду

**Предмет: Образложење за убрзано покретање поступка за избор др Игора Франовића у звање виши научни сарадник**

Др Игор Франовић је запослен у Лабораторији за примену рачунара у науци, у оквиру Националног центра изузетних вредности за изучавање комплексних система Института за физику у Београду и ангажован је на пројекту основних истраживања Министарства просвете, науке и технолошког развоја Републике Србије ОН171017, под називом "Моделирање и нумеричке симулације сложених вишечестичних физичких система". На поменутом пројекту ради на темама из статистичке физике и нелинеарне динамике.

Др Франовић је изабран у звање научни сарадник 17. децембра 2014. године, односно пре 3 године и 4 месеца. Од тада је остварио изузетне научне резултате, што се може видети по томе да је објавио чак 15 радова у часописима са ISI листе. Од тога је 11 радова објављено у часописима категорије M21a (међународни часописи изузетних вредности), док је 4 објављено у часописима категорије M21 (врхунски међународни часописи). Такође, др Франовић је у том периоду одржао више предавања на међународним скуповима, од којих су два била предавања по позиву. Према бази *ISI Web of Science*, радови др Франовића укупно су цитирани 134 пута, док је број цитата без аутоцитата 82. Према бази *Scopus*, укупан број цитата је 146, док је број цитата без аутоцитата 91. Према подацима с обе базе, Хиршов индекс радова др Франовића је 8.

Укупан импакт фактор радова др Игора Франовића износи 78.126, а у периоду након одлуке Научног већа Института за физику о предлогу за стицање претходног научног звања радова укупан импакт фактор је 38.881. Часописи у којима објављује др Франовић су цењени по свом угледу и водећи у његовим областима рада. Међу поменутиим часописима посебно се истичу *Physical Review Letters*, *Scientific Reports*, *Nonlinear Dynamics*, *Physical Review E*, *Chaos* и *Europhysics Letters*. Истичемо да је др Франовић прошле године именован за Associate Editor-а у међународном часопису из области нелинеарне динамике *Chaos, Solitons & Fractals* који издаје Elsevier. Рецензент је за часописе *Scientific Reports*, *Chaos*, *Europhysics Letters*, *Physics Letters A*, *European Physical Journal B*, *Neural Networks*, *Nonlinear Processes in Geophysics*.

Др Франовић руководи билатералним пројектом сарадње Републике Србије и Савезне Републике Немачке под називом *Emergent Dynamics in Systems of Coupled Excitable Units*. Такође, у оквиру националног пројекта ОН171017, *Моделирање и нумеричке симулације сложених вишечестичних система*, руководилац је потпројекта *Самоорганизација у спрегнутим ексцитабилним системима*. Др Франовић има широку научну сарадњу с колегама из иностранства, укључујући групу професора Владимира Некоркина с Института примењене физике Руске

академије наука у Нижњем Новгороду, групу Матијаса Волфрума с Вајерштраас института у Берлину, као и проф. Магјажа Перца с Универзитета у Марибору и проф. Јиргена Куртса с Универзитета Хумболт у Берлину.

Др Франовић је тренутно руководиоца рада на докторској дисертацији Иве Бачић у Центру изузетних вредности за изучавање комплексних система Института за физику у Београду. Завршетак рада на тој тези очекује се током 2019. године.

На Институту за физику у Београду, др Франовић је увео нове методе у проучавање емергентних феномена у системима под утицајем шума и кашњења у интеракцијама. Знања и искуства које је стекао у теоријском моделовању, аналитичким методама и техникама анализе динамике комплексних система успешно преноси млађим сарадницима у Лабораторији за примену рачунара у науци у оквиру Центра изузетних вредности за изучавање комплексних система.

С обзиром да далеко превазилази све предвиђене квантитативне и квалитативне услове, као и да је у тренутно научно звање научни сарадник изабран пре више од три године, у складу са Законом о научноистраживачкој делатности и Правилником о поступку, начину вредновања и квантитативном исказивању научноистраживачких резултата истраживача МПНТР предлажемо да се за колегу др Игорa Франовића покрене убрзани поступак за избор у звање виши научни сарадник.

У Београду, 17. априла 2018. године

Предложени чланови комисије:

др Антун Балаж  
научни саветник  
Институт за физику у Београду

др Александар Белић  
научни саветник  
Институт за физику у Београду

проф. др Милан Кнежевић  
редовни професор Физичког факултета  
Универзитета у Београду

### 3. БИОГРАФСКИ ПОДАЦИ О КАНДИДАТУ

Др Игор Франовић је рођен 25.2.1979. године у Београду. Завршио је Пету београдску гимназију 1997. године, након чега је уписао основне студије на Физичком факултету у Београду, смер теоријска и експериментална физика. Дипломирао је 2002. године с просечном оценом 9.43, одбранивши дипломски рад на тему *Анализа Јан-Телер (Jahn-Teller)-овог ефекта на примеру прелазног метал-комплекса  $[Cr(NH_3)_6]^{3+}$*  под руководством проф. др Драгољуба Белића. Магистарске студије на Физичком факултету у Београду, смер теоријска физика кондензованог стања, завршио је с просечном оценом 10,00, а магистарску тезу под насловом *Перколациони фазни прелази на просторно-временским фракталним структурама у ex-vivo и in-vitro неуронским културама* одбранио је 2011. године. Ментор на изради магистарске тезе је био доц. др Владимира Миљковића, а у тези је показано како се уводећи претпоставку о функционалним ансамблима транзијентно синхронизованих неурона могу објаснити механизам настанка и фракталне карактеристике патерна пропагације активности на мезоскопским неуронским мрежама. Докторат под насловом *Collective dynamics and self-organisation of stochastic neuronal systems influenced by synaptic time delay* одбранио је 2013. године на Физичком факултету у Београду. Радом на тези је руководио проф. др Никола Бурић, а у оквиру тезе су анализирани аналогije у процесу самоорганизације колективне активности између система спрегнутих аутономних осцилатора и система куплованих екситабилних јединица, при чему је применом методе средњег поља развијен ефективни модел макроскопске динамике популације екситабилних јединица изложених шуму и кашњењу у интеракцијама.

Од 2004.-2006. године, Игор Франовић је на матичном факултету, као стипендиста Министарства науке и заштите животне средине, учествовао на пројекту *Фазни прелази и нелинеарне појаве у биолошким и неорганским материјалима*, којим је руководио проф. др Сава Милошевић. Од јануара 2008. године до јануара 2011. године био је запослен као истраживач-приправник на Физичком факултету у Београду у оквиру пројекта *Фазни прелази и карактеризација неорганских и органских система*, којим је руководио проф. др Мићо Митровић. Од јануара 2011. године био је запослен на Физичком факултету у Београду као истраживач-приправник, а затим и као истраживач-сарадник (од фебруара 2012. до марта 2014. године) у оквиру пројекта бр. 171015 Министарства просвете и науке Републике Србије под називом *Фазни прелази и карактеризација неорганских и органских система*, којим руководи проф. др Сунчица Елезовић-Хацић. Од марта 2014. године ради у Лабораторији за примену рачунара у науци у оквиру Центра изузетних вредности за изучавање комплексних система Института за физику у Београду, где је ангажован на националном пројекту ОН171017, *Моделирање и нумеричке симулације сложених вишечестичних система*, као руководиоца потпројекта *Самоорганизација у спрегнутим екситабилним системима*. Такође, др Франовић руководи истраживањем на теми *Емергентна динамика на комплексним мрежама: стохастички ефекти, кашњење у интеракцијама*,

*адаптивност* у оквиру Центра изузетних вредности за изучавање комплексних система.

Истраживачки рад др Франовића обухвата области теорије нелинеарне динамике, стохастичких процеса и теорије комплексних мрежа, а као водеће теме истраживања се издвајају (а) самоорганизација у системима спрегнутих ексцитабилних јединица, (б) развој методе средњег поља за анализу стабилности и бифуркација система стохастичких диференцијалних једначина с кашњењем, као и (в) коефекти топологије, шума и кашњења у интеракцијама на динамику структурних и функционалних неуронских мрежа. Његов досадашњи рад укључује 29 радова у међународним часописима, као и 2 поглавља у књизи. Од 29 радова, 19 је објављено у часописима изузетних вредности категорије M21a, као што су *Physical Review Letters*, *Scientific Reports*, *Chaos*, *Communications in Nonlinear Science and Numerical Simulation* и *Physical Review E*. Др Франовић је добитник награде за најбољег младог истраживача Физичког факултета у Београду за 2013. годину. Има развијену међународну научну сарадњу с истраживачким групама из Русије, Немачке и Словеније. Ментор је на докторским студијама Иве Бачић, за чију тезу се очекује да буде завршена 2019. године. Руководилац је билатералног пројекта сарадње између Републике Србије и Савезне Републике Немачке *Emergent Dynamics in Systems of Coupled Excitable Units*. Такође, др Франовић је Associate Editor у врхунском међународном часопису *Chaos, Solitons & Fractals*.

#### 4. ПРЕГЛЕД НАУЧНЕ АКТИВНОСТИ

Др Игор Франовић се бави теоријском анализом само-организације и генеричких форми емергентног понашања у комплексним системима, чија је локална динамика представљена моделима спрегнутих осцилатора или ексцитабилних јединица. У свом раду користи концепте и методе из неколико различитих области физике, укључујући теорију нелинеарне динамике, статистичку физику и теорију комплексних мрежа, док се као главна мотивација и потенцијалне области примене добијених резултата истичу дескрипција, предвиђање и контрола колективног понашања неуронских мрежа и других биолошких система.

У ширем контексту, проучавање емергентних феномена заснованих на синхронизацији великог броја елемената, као главном принципу само-организације који даје квалитативно нове форме понашања које није могуће предвидети или извести из особина локалне динамике, представља парадигму за карактеризацију макроскопске динамике бројних реалних система, од физике, хемије и биологије, преко инжењерства и технологије до социологије и економије. При том, класа ексцитабилних система, чије је карактеристично понашање одређено тиме што им се параметри налазе у близини бифуркације која преводи систем из стационарног стања у осцилаторни режим, је у фокусу савремених истраживања како због теоријског значаја, тако и због могућности практичне примене, пре свега у биофизици. Комплексности колективног понашања система спрегнутих ексцитабилних јединица доприносе особине локалне динамике, која типично подразумева вишеструке временске скале, значајан утицај шума и кашњења у интеракцијама, као и организација по схеми модуларних комплексних мрежа, како на структурном, тако и на функционалном нивоу. Проучавање емергентне динамике на оваквим системима већ је довело до настанка значајних нових теоријских концепата, као што су методе анализе различитих форми пропегативних и локализованих патерна активности, технике анализе стабилности и бифуркација система стохастичких диференцијалних једначина са и без кашњења, као и установљење појма адаптивних мрежа.

У досадашњем раду, др Франовић се бавио развојем квантитативних метода анализе генеричких форми емергентног понашања у системима спрегнутих ексцитабилних или осцилаторних јединица, као и развојем нових аналитичких метода за анализу стабилности и бифуркација макроскопске динамике стохастичких система с кашњењем у интеракцијама. Рад др Франовића се може поделити у следеће подтеме:

- само-организација у системима спрегнутих ексцитабилних јединица под утицајем шума и кашњења у интеракцијама
- проблем активације у системима спрегнутих ексцитабилних јединица с вишеструким изворима шума
- развој методе средњег поља за анализу стабилности и бифуркација система стохастичких диференцијалних једначина са и без кашњења
- мултистабилност и споре стохастичке флукуације средње активности на комплексним неуронским мрежама

- динамика мотива неурона са шумом и кашњењем у интеракцијама
- патерни пропагације синхронизоване активности у мезоскопским неуронским мрежама
- примена теорије нелинеарне динамике у интердисциплинарним истраживањима
- неуређене конфигурације кинетичког Изинговог модела на комплексним мрежама

#### 4.1 Само-организација у системима спрегнутих ексциtabilних јединица под утицајем шума и кашњења у интеракцијама

Циљ истраживања у оквиру ове теме, коју је др Франовић покренуо као докторанд, састоји се у испитивању и продубљивању аналогije између колективног понашања интерагујућих фазних осцилатора и популација састављених од ексциtabilних елемената, који су типични за неуронске и друге биолошке системе. Главни допринос др Франовића у овој области састоји се у томе што је експлицитно показано да системи ексциtabilних јединица, представљених парадигматским Fitzhugh-Nagumo моделом, могу да испоље комплексне феномене самоорганизације, засноване на синхронизацији локалних активности. У том контексту, уочен је феномен спонтане кластер-синхронизације на хомогеној популацији, који настаје једино услед садејства ексциtabilности јединица, шума и кашњења у интеракцијама. Утврђено је да се механизам кластерована заснива на конкуренцији две карактеристичне временске скале, где једна одговара осцилаторној моди изазваној шумом, а друга моди вођеној кашњењем. Поред асимптотски стабилних дво- и тро-кластер партиција, уочена су и тро-кластер стања динамичког карактера. Утврђено је да стабилност дво-кластер стања важи и у термодинамичком лимесу. Детаљном анализом, др Франовић је показао да је кластероване резонантни феномен у односу на кашњење у интеракцијама, који опстаје и у случају комплексних топологија повезаности неурона (scale-free мреже), као и при неуниформним вредностима локалних параметара. Утврђено је да глобална бифуркација ефективног модела добијеног применом методе средњег поља (mean-field method) указује на области параметара система у којима се може очекивати појава кластерована. Наведени резултати приказани су у следећим радовима:

- *Spontaneous Formation of Synchronization Clusters in Homogenous Neuronal Ensembles Induced by Noise and Interaction Delays*  
**I. Franović, K. Todorović, N. Vasović, and N. Burić**  
Phys. Rev. Lett. **108**, 094101 (2012)
- *Cluster Synchronization of Spiking Induced by Noise and Interaction Delays in Homogenous Neuronal Ensembles*  
**I. Franović, K. Todorović, N. Vasović, and N. Burić**  
Chaos **22**, 033147 (2012)



## 4.2 Проблем активације у системима спрегнутих ексцитабилних јединица с вишеструким изворима шума

У оквиру ове теме, др Франовић се бавио анализом threshold понашања и статистичких карактеристика процеса активације у системима једне и две ексцитабилне јединице, као и популације ексцитабилних јединица под утицајем интринзичног и екстерног шума. По први пут су размотрени ефекти интермедијерних интензитета шума који леже изван области применљивости теорије великих флукуација. Као најважнији резултат, др Франовић је показао да постоје универзалне статистичке особине процеса активације за сва три посматрана система, а да је универзалност квалитативно одређена стохастичком бифуркацијом која одговара прелазу из стохастички стабилне фиксне тачке у стохастички стабилан гранични циклус. Постојање стохастичке бифуркације доказано је применом ефективних модела стохастичке динамике система, заснованих на методи кумуланата допуњеној гаусијанском closure хипотезом.

Поред тога, важан резултат представља увођење релевантних граничних услова за проблеме активације у ексцитабилним системима: у случају једне јединице, одређени су гранични услови који омогућавају директну генерализацију на системе од две јединице, док су у случају популације размотрене три различите формулације догађаја активације, које карактеришу различите аспекте threshold понашања и улогу кохеренције активности појединачних јединица у процесу активације. Описани резултати представљени су у следећим радовима:

- *Activation Process in Excitable Systems with Multiple Noise Sources: One and Two Interacting Units*  
**I. Franović**, K. Todorović, M. Perc, N. Vasović, and N. Burić  
Phys. Rev. E **92**, 062911 (2015)
- *Activation Process in Excitable Systems with Multiple Noise Sources: Large Number of Units*  
**I. Franović**, M. Perc, K. Todorović, S. Kostić, and N. Burić  
Phys. Rev. E **92**, 062912 (2015)

## 4.3 Развој методе средњег поља за анализу стабилности и бифуркација система стохастичких диференцијалних једначина са и без кашњења

У оквиру ове теме, фокус истраживања је на развоју и примени методе средњег поља при анализи стохастичке стабилности и стохастичких бифуркација макроскопске динамике неуронских популација. Најважнији резултати др Франовића у овој области се односе на (а) прецизну формулацију релевантних апроксимација на којима се заснива примена методе средњег поља у макроскопским системима стохастичких ексцитабилних јединица с кашњењем у интеракцијама; (б) развој ефективних модела колективне динамике у случају популација ексцитабилних јединица; (в) извођење редукованог модела глобалне динамике популације стохастичких неуронских мапа.

Приликом примени mean-field методе, од изузетног је значаја питање да ли су апроксимације иза mean-field модела универзалног карактера, или је потребно да се прилагођавају конкретној класи система која се проучава. У истраживању др Франовића експлицитно је показано да апроксимације немају универзалну форму, већ морају да буду прилагођене конкретној класи система којој припада посматрани модел. У случају спрегнутих ексциtabilних система, дефинисане су две релевантне апроксимације, назване *гаусијанска апроксимација* и *апроксимација о квази-независности*. При том, испоставља се да формулација прве апроксимације мора да узме у обзир релаксациони карактер осцилација типичан за ексциtabilне јединице, док је нарушење друге апроксимације могуће предвидети на самоусаглашен начин анализом динамике коју приказује модел добијен применом методе средњег поља.

Поред тога, др Франовић је демонстрирао да ефективни модели засновани на методи средњег поља могу да на квалитативно исправан начин опишу стабилност егзактног система, сценарије за појаву и супресију колективне моде, као и мултистабилне режиме егзактног система, примењујући их на примерима интерагујућих популација ексциtabilних јединица, као и популацијама стохастичких неуронских мапа. Поред квалитативног поклапања, у смислу генеричких форми бифуркација и одговарајућих области параметара појединих емергентних режима, утврђено је да ефективни модели са задовољавајућом тачношћу предвиђају: (а) статистичке карактеристике релевантних временских серија егзактног система, (б) одговор популације на спољашње стимулације мале амплитуде, задат кривама фазног одговора, као и одговор на пертурбације коначне амплитуде. Наведени резултати представљени су у следећим радовима:

- *Persistence and Failure of Mean-field Approximations Adapted to a Class of Systems of Delay-coupled Excitable Units*  
**I. Franović**, K. Todorović, N. Vasović, and N. Burić:  
Phys. Rev. E **89**, 022926 (2014)
- *Mean-field Dynamics of a Population of Stochastic Map Neurons*  
**I. Franović**, O. V. Maslennikov, I. Bačić, and V. I. Nekorkin  
Phys. Rev. E **96**, 012226 (2017)
- *Mean-field Approximation of Two Coupled Populations of Excitable Units*  
**I. Franović**, K. Todorović, N. Vasović, and N. Burić  
Phys. Rev. E **87**, 012922 (2013)
- *Stability, Bifurcations, and Dynamics of Global Variables of a System of Bursting Neurons*  
**I. Franović**, K. Todorović, N. Vasović, and N. Burić  
Chaos **21**, 033109 (2011)

#### 4.4 Мултистабилност и споре стохастичке флукуације средње активности на модуларним неуронским мрежама

У оквиру ове области, др Франовић се бави анализом проблема макроскопске варијабилности, која представља емергентну форму колективног понашања на неуронским мрежама. Наиме, познато је да се активност неурона може описати као двоструки стохастички процес, који се с једне стране манифестује као микроскопска варијабилност у временским серијама појединачних неурона, и с друге стране, као макроскопска варијабилност, која се опажа на дугим временским скалама, и укључује споре стохастичке флукуације средње фреквенције емитовања импулса. Споре флукуације настају услед спонтаног алтернирања између епизода повишене активности неурона и епизода релативног мировања. Таква алтернирајућа (switching) динамика између различитих колективних стања је од посебног значаја за пирамидалне неуроне у неокортексу, и сматра се да представља динамичку парадигму за реализацију различитих форми учења и меморије. Циљ истраживања је да се утврде услови који омогућавају појаву switching динамике, при чему је акценат стављен на садејство различитих типова шума, кашњења у интеракцијама и хетерогености топологије интеракција мреже. Између осталог, разматран је и случај кластерованих мрежа неурона, које су нарочито заступљене у кортексу.

Главни резултат досадашњег истраживања представља развој ефикасног модел колективне активности кластероване мреже rate неурона, који омогућава да се процене различити доприноси ефикасном макроскопском шуму, као и да се одреде области параметара где је могуће очекивати switching динамику. Од посебног значаја за могуће апликације је чињеница да се механизми switching динамике у случајним и модуларним неуронским мрежама квалитативно разликују, при чему је показано да кластеровање доприноси мултистабилности мреже, чинећи switching феномен робуснијим. Наведени резултати објављени су у следећим радовима:

- *Clustering Promotes Switching Dynamics in Networks of Noisy Neurons*  
**I. Franović** and V. Klinshov  
Chaos **28**, 023111 (2018)
- *Slow Rate Fluctuations in a Network of Noisy Neurons with Coupling Delay*  
**I. Franović** and V. Klinshov  
EPL **116**, 48002 (2016)
- *Mean-field Dynamics of a Random Neural Network with Noise*  
V. Klinshov and **I. Franović**  
Phys. Rev. E **92**, 062813 (2015)

#### 4.5 Динамика мотива неурона са шумом и кашњењем у интеракцијама

Акцент истраживања у овој области је на анализи динамичких режима и феномена стохастичке фазне синхронизације на типичним бинарним или тернарним мотивима неурона. Од посебног значаја су управо триплетни, који чине основне јединице грађе комплексних неуронских мрежа. Циљ истраживања се састоји у систематском одређивању односа између структурних мотива, задатих анатомском повезаношћу неуронске мреже, и функционалних мотива, који одражавају актуелну динамику јединица или њихово стање синхронизованости. Др Франовић се бавио моделима који укључују две парадигматске форме локалне динамике неурона: *bursting* динамику задату Рулковљевим мапама и ексцитабилну динамику представљену Fitzhugh-Nagumo моделом.

У случају *bursting* неурона, главни резултат представља одређивање механизма настанка *burst* синхронизације и патерна активности карактеристичних за поједине мотиве применом теорије сингуларне пертурбације (анализа у фазној равни). Важан допринос представља и дефинисање два типа функционалних мотива, при чему су идентификовани управо они функционални мотиви који највише доприносе успостављању *burst* синхронизације између јединица.

У случају ексцитабилне локалне динамике, анализиране су стохастичка стабилност, као и стања синхронизације различитих осцилаторних мода у систему од две спрегнуте јединице у присуству два независна извора шума (интринзични шум у јонским каналима и спољашњи синаптички шум), као и два типа кашњења у интеракцијама. Посматрани систем је значајан у светлу испитивања односа особине ексцитабилности и вишеструких карактеристичних временских скала. Питање коефекта шума и кашњења у модификовању ексцитабилног понашања у дуговременском лимесу третирано је применом методе статистичке линеаризације, при чему је показано да карактер шума (интринзични или екстерни) примарно утиче на прилагођавање фреквенција између јединица, као и на резултат конкуренције између осцилаторних мода вођених шумом или кашњењем.

Описани резултати представљени су у следећим радовима:

- *Stability, Coherent Spiking and Synchronization in Noisy Excitable Systems with Coupling and Internal Delays*  
**I. Franović, K. Todorović, N. Vasović, and N. Burić:**  
Commun. Nonlinear Sci. Numer. Simulat. **19**, 3202 (2014)
- *The Effects of Synaptic Time Delay on Motifs of Chemically Coupled Rulkov Model Neurons*  
**I. Franović and V. Lj. Miljković:**  
Commun. Nonlinear Sci. Numer. Simulat. **16**, 623 (2011)

- *Functional Motifs: a Novel Perspective on Burst Synchronization and Regularization of Neurons Coupled Via Delayed Inhibitory Synapses*  
I. Franović and V. Lj. Miljković  
Chaos Soliton. Fract. **44**, 122 (2011)
- *Phase Plane Approach to Cooperative Rhythms in Neuron Motifs with Delayed Inhibitory Synapses*  
I. Franović and V. Lj. Miljković:  
EPL **92**, 68007 (2011)
- *Possibilities of Introducing Different Functional Circuits on Top of a Structural Neuron Triplet: Where Do the Gains Lie?*  
I. Franović and V. Lj. Miljković:  
Chaos Soliton. Fract. **45**, 527 (2012)
- *Power Law Behavior Related to Mutual Synchronization of Chemically Coupled Map Neurons*  
I. Franović and V. Lj. Miljković:  
Eur. Phys. J. B **76**, 613 (2010)

#### **4.6 Патерни пропагације синхронизоване активности у мезоскопским неуронским мрежама**

Истраживањем у оквиру ове теме др Франовић се бавио током магистарских студија на Физичком факултету у Београду. Основна идеја се састојала у томе да се процес пропагације патерна транзијентне синхронизоване активности у мезоскопским неуронским система представи моделом перколације на разуђеним мрежама насталим одстрањивањем веза с дводимензионалне решетке с интеракцијама најближих суседа, или с интеракцијама најближих и наредних најближих суседа. Транзијентна синхронизација, као основни мод локалне динамике чворова мреже, моделована је увођењем претпоставке о функционалним ансамблима неурона, чија се примарна активност састоји у емитовању пакета приближно синхронизованих акционих потенцијала (импулса).

Показано је да настанак просторно-временских патерна активности, тзв. *synfire* ланаца, представља критичну појаву, која зависи од вероватноће повезаности између неуронских популација на чворовима мреже. Применом методе скалирања на коначним системима, одређена је зависност критичне вероватноће од параметара локалне динамике и јачине интеракција, а анализирано је и како на фракталне особине перколационог кластера утиче топологије интеракција. Као најважнији резултат, утврђено је како класе универзалности посматраних фазних прелаза зависе од карактеристика динамике неуронских популација на чворовима мреже, при чему се

добијени резултати поклапају с подацима из релевантних експерименталних истраживања.

Наведени резултати приказани су у радовима:

- *Percolation Transition at Growing Spatiotemporal Fractal Patterns in Models of Mesoscopic Neural Networks*  
I. Franović and V. Lj. Miljković:  
Phys. Rev. E **79**, 061923 (2009).
- *Fractal Properties of Percolation Clusters in Euclidian Neural Networks*  
I. Franović and V. Lj. Miljković:  
Chaos Soliton. Fract. **39**, 1418 (2009).

#### **4.7 Примена теорије нелинеарне динамике у интердисциплинарним истраживањима**

У оквиру ове теме, др Франовић се бави применом теорије нелинеарне динамике на моделовање комплексног понашања сеизмичких раседа, геолошких структура одговорних за настанак земљотреса. Конкретно, третиране су три групе проблема, укључујући (а) анализу осетљивости парадигматских модела раседа на спољашње пертурбације, (б) настанак колективне моде у сложеним раседима под утицајем шума и кашњења у интеракцијама и (в) механизам настанка апериодичних временских серија на једноставним (монокомпонентним) раседима.

Током анализе групе проблема (а), користећи методу кривих фазног одговора (*phase response curves*) првог и другог реда, експлицитно је демонстриран низ нетривијалних ефеката, укључујући: нарушење принципа суперпозиције при деловању сукцесивних пертурбација услед јаке нелинеарности модела, сложену зависност промене фазе сеизмичког циклуса од параметара и комплексности раседа, као и постојање дуговременског ефекта пертурбација, како у случају монокомпонентних, тако и у случају сложених раседа.

Поводом круга питања (б), детаљно су испитани коефекти сеизмичког шума и кашњења у интеракцијама на појаву колективне моде у два класа модела комплексних раседа. За оба сценарија, развијен је *mean-field* модел који на квалитативно исправан начин описује колективну динамику раседа, чиме је показано да се метод средњег поља може успешно примењивати и у случају система чији елементи имају дисконтинуалну и *stiff* динамику. Бифуркационом анализом ефективних модела утврђено је постојање области параметера који подржавају бистабилну динамику, којој у егзактним системима одговарају комплексне апериодичне осцилације чија статистика квалитативно задовољава релевантне сеизмичке законе скалирања, као што је Гутенберг-Рихтеров (Gutenberg-Richter) закон.

У оквиру целине (в), показано да сасвим једноставан модел монокомпонентног раседа, представљеног канонским Burridge-Кнорoff моделом, може да генерише комплексне форме понашања захваљујући меморијском ефекту, уведеном у типични модел трења између масивног блока и контактне површине раседа. На основу спроведене бифуркационе анализе, показано је да се прелазак у хаос одвија према Ruelle-Takens-Newhouse сценарију.

Наведени резултати представљени су у следећим радовима:

- *Phase Response Curves for Models of Earthquake Fault Dynamics*  
**I. Franović**, S. Kostić, M. Perc, V. Klinshov, V. I. Nekorkin, and J. Kurths  
Chaos **26**, 063105 (2016)
- *Triggered Dynamics in a Model of Different Fault Creep Regimes*  
S. Kostić, **I. Franović**, M. Perc, N. Vasović, and K. Todorović  
Sci. Rep. **4**, 5401 (2014),
- *Dynamics of Fault Motion in a Stochastic Spring-slider Model with Varying Neighboring Interactions and Time-delayed Coupling*  
S. Kostić, N. Vasović, **I. Franović**, K. Todorović, V. Klinshov, and V. I. Nekorkin  
Nonlinear Dyn. **87**, 2563 (2017)
- *Friction Memory Effect in Complex Dynamics of Earthquake Model*  
S. Kostić, **I. Franović**, K. Todorović, and N. Vasović:  
Nonlinear Dyn. **73**, 1933 (2013)
- *Earthquake Nucleation in a Stochastic Fault Model of Globally Coupled Units with Interaction Delays*  
N. Vasović, S. Kostić, **I. Franović**, and K. Todorović:  
Commun. Nonlinear Sci. Numer. Simulat. **38**, 117 (2016)
- *Nonlinear Dynamics Behind the Seismic Cycle: One-dimensional Phenomenological Modeling*  
S. Kostić, N. Vasović, K. Todorović, and **I. Franović**  
Chaos Soliton. Fract. **106**, 310 (2018)
- *Complex Dynamics of Spring-Block Earthquake Model Under Periodic Parameter Perturbations*  
S. Kostić, N. Vasović, **I. Franović**, and K. Todorović  
J. Comput. Nonlin. Dyn. **9**, 031019 (2014)
- *Dynamics of Landslide Model with Time Delay and Periodic Parameter Perturbations*  
S. Kostić, N. Vasović, **I. Franović**, D. Jevremović, D. Mitrović, and K. Todorović:  
Commun. Nonlinear Sci. Numer. Simulat. **19**, 3346 (2014)

- *Dynamics of Simple Earthquake Model with Time Delay and Variation of Friction Strength*  
S. Kostić, N. Vasović, **I. Franović**, and K. Todorović  
Nonlinear Proc. Geoph. **20**, 857 (2013)

#### **4.8 Неуређене конфигурације кинетичког Ising-овог модела на комплексним мрежама**

У оквиру ове теме, др Франовић се бави проблемом процеса уређивања и структуром неуређених конфигурација кинетичког Ising-овог (Glauber-овог) модела на нултој температури, задатог на комплексним мрежама. Разматрани су различити примери комплексних мрежа укључујући случај Watts-Strogatz-ових мрежа добијених преповезивањем регуларне дводимензионалне решетке, као и парадигматских хетерогених двослојних мрежа (two-layer networks) с мултиплекс или случајном структуром веза између слојева. Као главни резултат, показано је да у small-world режиму систем не постиже уређеност у термодинамичком лимесу, већ завршава у метастабилним активним конфигурацијама састављеним из два домена, који одговарају кластерованом стању на почетној решетки. За интермедијерне вероватноће преповезивања, додатно се појављују неуређене конфигурације с малим, изолованим капљицама спинова супротне оријентације. У случају двослојних мрежа, показано је да карактер коначног стања квалитативно зависи од структуре интеракција између слојева. Описани резултати представљени су у раду:

- *Disordered Configurations of the Glauber Model in Two-dimensional Networks*  
Ваћић, **I. Franović**, and M. Perc:  
EPL **120**, 68001 (2017), ИФ 2.095 за 2014. годину



## 5. ЕЛЕМЕНТИ ЗА КВАЛИТАТИВНУ ОЦЕНУ НАУЧНОГ ДОПРИНОСА КАНДИДАТА

### 5.1 Квалитет научних резултата

#### 5.1.1 Научни ниво и значај резултата, утицај научних радова

Др Игор Франовић је у свом досадашњем раду дао кључни допринос у истраживању на укупно 29 радова објављених у међународним часописима с ISI листе, као и 2 поглавља у књизи, од којих је једно објављено у истакнутој монографији међународног значаја. Од 29 радова, 19 је објављено у часописима М21а категорије (међународни часописи изузетних вредности), 7 у часописима категорије М21 (врхунски међународни часописи), док је 3 објављено у часописима категорије М22.

У периоду након доношења одлуке Научног већа Института за физику о предлогу за стицање претходног научног звања, др Франовић је објавио 15 радова у часописима с ISI листе. Од тога је 11 радова објављено у часописима категорије М21а (међународни часописи изузетних вредности), док је 4 објављено у часописима категорије М21 (врхунски међународни часописи). Такође, др Франовић је у том периоду одржао више предавања на међународним скуповима, од којих су два била предавања по позиву.

Као пет најзначајнијих радова др Франовића могуће је издвојити:

1. *Clustering Promotes Switching Dynamics in Networks of Noisy Neurons*  
**I. Franović** and V. Klinshov  
Chaos **28**, 023111 (2018), М21а, цитиран 0 пута;
2. *Mean-field dynamics of a population of stochastic map neurons*  
I. Franović, O.V. Maslennikov, I. Ваčić, and V. I. Nekorkin,  
Phys. Rev. E **96**, 012226 (2017), М21, цитиран 0 пута;
3. *Activation Process in Excitable Systems with Multiple Noise Sources: One and Two Interacting Units*  
**I. Franović**, K. Todorović, M. Perc, N. Vasović, and N. Burić  
Phys. Rev. E **92**, 062911 (2015), М21а, цитиран 13 пута;
4. *Activation Process in Excitable Systems with Multiple Noise Sources: Large Number of Units*  
**I. Franović**, M. Perc, K. Todorović, S. Kostić, and N. Burić  
Phys. Rev. E **92**, 062912 (2015), М21а, цитиран 14 пута;
5. *Spontaneous Formation of Synchronization Clusters in Homogenous Neuronal Ensembles Induced by Noise and Interaction Delays*  
**I. Franović**, K. Todorović, N. Vasović, and N. Burić  
Phys. Rev. Lett. **108**, 094101 (2012), М21а, цитиран 17 пута;

У првом раду, детаљно је испитан емергентни феномен макроскопске варијабилности на модуларним неуронским мрежама. Макроскопска варијабилност се опажа на временским скалама много дужим од карактеристичног времена локалне динамике неурона, а манифестује се кроз појаву спорих стохастичких флукуација средње фреквенције емитовања импулса мреже. Споре флукуације последица су кохерентних спонтаних прелазака неурона између тзв. *up*-стања повећане активности неурона и тзв. *down*-стања релативног мировања неурона. Оваква колективна алтернирајућа (*switching*) динамика представља динамичку парадигму за одређене процесе учења и меморије. У раду су утврђени услови за појаву *switching* динамике, с акцентом на садејство различитих типова шума и хетерогености у топологији мреже. Применом методе средњег поља, по први пут је развијен ефективни модел колективне динамике за модуларну (кластеровану) неуронску мрежу, при чему је њена колективна динамика приказана преко спрегнутих стохастичких *mean-field* система другог реда који одражавају активности појединачних кластера. Бифуркационом анализом ефективних модела у термодинамичком лимесу утврђене су разлике у генеричким механизмима *switching* динамике код некластерованих и кластерованих мрежа. У првом случају, механизам је аналоган стохастичкој честици у *double-well* потенцијалу. У другом случају, показано је да кластеровање непосредно подстиче мултистабилност колективне динамике, што значајно утиче на повећање робусности *switching* феномена.

У другом раду, по први пут је добијен ефективни модел колективне динамике ансамбла куплованих стохастичких неуронских мапа. Значај неуронских мапа лежи у томе што на нумерички ефикасан начин могу да репродукују све релевантне форме динамике неурона, пружајући основу за разумевање колективног понашања типичних функционалних модула у неуронским системима, као што су кортикалне колоне и микроколоне. У теоријском смислу, развој ефективног модела ансамбла куплованих стохастичких дискретних система је нарочито важан, пошто је примена стандардних техника заснованих на Фокер-Планковом формализму немогућа. У конкретном случају, ефективни модел макроскопске динамике је добијен применом методе средњег поља, засноване на теорији кумуланата допуњеној гаусијанском *closure* хипотезом. Модел је искоришћен за анализу емергентних режима, као и одговора популације на спољашњу стимулацију. Утврђено је да ефективни модел на квалитативно исправан начин може да опише стабилност и бифуркације егзактног система, као и све генеричке форме макроскопског понашања, укључујући макроскопску ексцитабилност, *subthreshold* осцилације, периодични или хаотични *spiking* режим, као и хаотичну *bursting* динамику. Од посебног значаја је чињеница да је по први пут експлицитно уведен појам макроскопске ексцитабилности, према којем је под одређеним условима популацију ексцитабилних јединица могуће третирати као макроскопски ексцитабилни елемент, који на одговарајућу стимулацију може да одговори емисијом једног импулса или серије повезаних импулса. Користећи ефективни модел, утврђене су области параметара у којима се појављују различите форме макроскопске ексцитабилности.

Поред квалитативног поклапања између домена параметара који одговарају појединим режима егзактног система и ефективног модела, експлицитно је показано да

ефективни модел може са задовољавајућом тачношћу да предвиди квантитативне карактеристике временских серија егзактног система, као што су средњи *interspike* или *interburst* интервали. Такође је утврђено да ефективни модел с изузетно високом тачношћу може да репродукује криве фазног одговора егзактног система, које описују типичан одговор популације на малу пертурбацију. Испоставило се да осим одговора на малу пертурбацију, ефективни модел може да предвиди и одговор популације на стимулацију коначне амплитуде и трајања чак и при интермедијерним интензитетима шума.

Трећи и четврти рад третирају комплементарне теме (објављени су као *sequel* у Phys. Rev. E), и односе се на проблем *threshold* динамике и процеса активације у системима од једне или две купловане ексцитабилне јединице, као и популације ексцитабилних јединица под утицајем спољашњег и унутрашњег шума. Добијени резултати важе у области интермедијерних интензитета шума, где није могуће применити класичну теорију великих флукуација. За сва три посматрана система, показано је да се нумерички добијене највероватније трајекторије активације поклапају са трајекторијама генерисаним ефективним системом хамилтонијанских једначина. У случају једне ексцитабилне јединице, важан резултат представља увођење релевантних граничних услова за проблем активације, који омогућавају директну генерализацију на системе од две ексцитабилне јединице. У случају популације, применом одговарајућег *mean-field* модела је први пут експлицитно показана особина макроскопске ексцитабилности. Поред тога, уведене су три различите формулације догађаја активације за глобалне варијабле ансамбла јединица, при чему свака од формулација карактерише различите аспекте *threshold* понашања и улоге кохеренције активности појединачних јединица у догађају активације. За системе од једне и две јединице, као и популацију ексцитабилних елемената, демонстрирано је да постоје универзалне статистичке особине процеса активације, описане средњим временом до првог импулса и одговарајућим коефицијентом варијације. У том контексту, најважнији резултат поменутог рада представља чињеница да универзалност потиче од стохастичке бифуркације која одговара прелазу из стохастички стабилне фиксне тачке у стохастички стабилан гранични циклус.

У петом раду је показано да системи спрегнутих ексцитабилних јединица, представљени парадигматским Фицхју-Нагумо (Fitzhugh-Nagumo) моделом, могу да испоље емергентни феномен спонтане кластер-синхронизације. До овакве форме само-организовања, засноване на синхронизацији локалних активности, долази услед садејства ексцитабилне динамике типа II, одређене двома карактеристичним временским скалама, шума и кашњења у интеракцијама. Експлицитно је показано да се ефекат кластерована заснива на конкуренцији две осцилаторне моде, од којих једна одговара осцилацијама индукованим шумом, док друга мода настаје као последица кашњења у интеракцијама. На локалном нивоу, механизам кластерована је објашњен успостављањем аналогије између стохастичке динамике ексцитабилних јединица и честица у *double-well* потенцијалу. Уочено је да постоје два типа кластерована, укључујући асимптотски стабилне дво- и тро-кластер конфигурације, као и динамичке

тро-кластер конфигурације. Демонстрирано је да кластеровање има карактер резонантног феномена у односу на кашњење у интеракцијама, одржавајући се у случају хетерогености топологије мреже, као и хетерогености локалних параметара система. Утвршено је да глобална бифуркација ефективног модела добијеног на основу методе средњег поља (*mean-field method*) може да предвиди појаву кластеровања у појединим областима параметара система.

### 5.1.2 Позитивна цитираност научних радова кандидата

Према бази *ISI Web of Science*, радови др Франовића укупно су цитирани 134 пута, док је број цитата без аутоцитата 82. Према бази *Scopus*, укупан број цитата је 146, док је број цитата без аутоцитата 91. Према подацима с обе базе, Хиршов индекс радова др Франовића је 8.

Прилог: подаци о цитираности радова из интернет базе *ISI Web of Science*

### 5.1.3 Параметри квалитета часописа

Као битан елемент за процену квалитета научних радова служи и импакт-фактор часописа у којима су радови објављени. Др Франовић је објављивао радове у часописима категорија M21a, M21 и M22, при чему су подвучени импакт-фактори часописа у којима су публиковани радови након одлуке Научног већа Института за физику о предлогу за стицање претходног научног звања:

- 1 рад у *Physical Review Letters* (ИФ 7.943)
- 1 рад у *Scientific Reports* (ИФ 5.578)
- 2 рада у часопису *Nonlinear Dynamics* (ИФ 3.464 за један рад и ИФ 3.009 за други рад)
- 4 рада у часопису *Communications in Nonlinear Science and Numerical Simulations* (ИФ 2.866 за три рада и ИФ 2.806 за један рад)
- 7 радова у часопису *Physical Review E* (ИФ 2.366 за један рад, ИФ 2.326 за 5 радова и ИФ 2.508 за један рад)
- 4 рада у часопису *Chaos* (ИФ 2.283 за два рада, 2.188 за један рад и 2.081 за један рад)
- 3 рада у часопису *Europhysics Letters* (ИФ 2.893 за један рад и ИФ 2.095 за два рада)
- 4 рада у часопису *Chaos, solitons & fractals* (ИФ 3.315 за два рада, ИФ 1.611 за један рад и ИФ 1.268 за један рад)
- 1 рад у часопису *Nonlinear Processes in Geophysics* (ИФ 1.692)
- 1 рад у часопису *European Physical Journal B* (ИФ 1.575)
- 1 рад у часопису *Journal of Computational Nonlinear Dynamics* (ИФ 1.530)

Укупан импакт-фактор радова др Франовића износи 78.126, а фактор утицаја радова у периоду након одлуке Научног већа Института за физику о предлогу за стицање претходног научног звања радова је 38.881. Часописи у којима објављује др Франовић су цењени по свом угледу и водећи у његовим областима рада. Међу поменути

часописима посебно се истичу *Physical Review Letters*, *Scientific Reports*, *Nonlinear Dynamics*, *Physical Review E*, *Chaos* и *Europhysics Letters*.

Додатни библиометријски показатељи према Упутству о начину писања извештаја о изборима у звања које је усвојио Матични научни одбор за физику приказани су у следећој табели:

	<b>ИФ</b>	<b>М</b>	<b>СНИП</b>
<b>Укупно</b>	38.881	134.99	15.822
<b>Усредњено по чланку</b>	2.592	8.999	1.055
<b>Усредњено по аутору</b>	10.342	41.167	4.099

#### **5.1.4 Степен самосталности и степен учешћа у реализацији радова у научним центрима у земљи и иностранству**

Од 29 објављених радова, др Франовић је први аутор на 19 радова, други наведени аутор на 4 рада, трећи аутор на 5 радова, и последњи аутор на једној публикацији. На радовима који су објављени у периоду након одлуке Научног већа Института за физику о предлогу за стицање претходног научног звања, др Франовић је први аутор на 7 публикација, други наведени аутор на 3 рада, трећи наведени аутор на 4 рада и последњи аутор на једној публикацији.

При изради поменутих публикација, др Франовић је учествовао у осмишљавању и формулацији проблема, конструкцији релевантних нумеричких симулација и прикупљању података, развоју теоријских метода за анализу добијених резултата, као и писању радова.

Током магистарских студија на Физичком факултету у Београду, др Франовић се првенствено бавио развојем теоријских и квантитативних метода за анализу односа структурних и функционалних неуронских мотива, као и применом теорије сингуларне пертурбације на анализу феномена стохастичке фазне синхронизације у системима *bursting* неурона. Током докторских студија, у сарадњи с проф. др Николом Бурићем с Института за физику у Београду, др Франовић је започео истраживање у области емергентне динамике на системима ексцитабилних јединица под утицајем шума и кашњења у интеракцијама. У том контексту, започет је развој нове методе за анализу стабилности и (стохастичких) бифуркација система стохастичких диференцијалних једначина, као и система стохастичких диференцијалних једначина с кашњењем. Након завршеног доктората, др Франовић је почео да се бави проблемом активације и *threshold* динамике у системима спрегнутих ексцитабилних јединица, указујући на значај адекватне формулације граничних услова, као и универзалност статистичких карактеристика процеса активације у системима ексцитабилних јединица под утицајем интринзичног и екстерног шума коначног (интермедијерног интензитета). Показано је да универзалне карактеристике потичу од стохастичке бифуркације која преводи систем из стохастички стабилне фиксне тачке у осцилаторни режим. Поред ове теме, у сарадњи с колегама из Русије, др Франовић је покренуо истраживање усмерено ка

анализи емергентног феномена макроскопске варијабилности на модулларним неуронским мрежама, при чему је по први пут развијен ефективни модел колективне динамике модулларне мреже, којим је могуће анализирати мултистабилност мреже и switching динамiku између одговарајућих колективних стања.

Др Франовић руководи билатералним пројектом сарадње Републике Србије и Савезне Републике Немачке под називом *Emergent Dynamics in Systems of Coupled Excitable Units*. Такође, у оквиру националног пројекта ОН171017, *Моделирање и нумеричке симулације сложених вишечестичних система*, руководилац је потпројекта *Самоорганизација у спрегнутим ексцитабилним системима*.

Др Франовић има широку научну сарадњу с колегама из иностранства, укључујући групу професора Владимира Некоркина с Института примењене физике Руске академије наука у Нижњем Новгороду, групу Матијаса Волфрума с Вајерштрас института у Берлину, као и проф. Матјажа Перца с Универзитета у Марибору и проф. Јиргена Куртса с Универзитета Хумболт у Берлину.

### **5.1.5 Награде**

Др Франовић је добитник награде за најбољег младог истраживача Физичког факултета у Београду за 2013. годину.

Прилог: диплома о награди

### **5.2 Ангажованост у формирању научних кадрова**

Др Франовић је тренутно руководиоца рада на докторској дисертацији Иве Бачић у Центру изузетних вредности за изучавање комплексних система Института за физику у Београду. Завршетак рада на тој тези очекује се током 2019. године.

Поред тога, др Франовић је током школске 2015/2016. године водио пројекат студентске праксе *Комплексност и динамика самоорганизације у популацијама стохастичких ексцитабилних јединица*, на коме је учествовало пет студената завршних година Физичког факултета у Београду.

Прилог: потврда о менторству руководиоца пројекта, извештај о раду истраживача-докторанта

### **5.3 Нормирање броја коауторских радова, патената и техничких решења**

Сви радови др Франовића објављени након одлуке Научног већа Института за физику о предлогу за стицање претходног научног звања укључују резултате комплексних нумеричких симулација. Од тога, тринаест радова има пет или мање коаутора, тако да улазе пуном тежином на број коаутора. Три рада има имају више од пет коаутора, при чему радови објављени у часописима *Nonlinear Dynamics* (2017), *Chaos* (2016) и *Communications in Nonlinear Science and Numerical Simulations* (2014) имају по шест коаутора, тако да носе по 8.33 нормираних поена. Укупан број поена др Франовића према М20 публикацијама у релевантном периоду пре нормирања износи

152, а након нормирања 146.99. Број поена одузет нормирањем чини мање од 10% од укупног броја поена на основу M20 публикација.

#### **5.4 Руковођење пројектима, потпројектима и пројектним задацима**

Др Франовић руководи билатералним пројектом сарадње Републике Србије и Савезне Републике Немачке под називом „*Emergent Dynamics in Systems of Coupled Excitable Units*“.

У оквиру националног пројекта ОН171017, *Моделирање и нумеричке симулације сложених вишечестичних система*, др Франовић је руководилац потпројекта *Самоорганизација у спрегнутим екситабилним системима*. Поред тога, др Франовић руководи истраживањем на теми *Емергентна динамика на комплексним мрежама: стохастички ефекти, кашњење у интеракцијама, адаптивност* у Центру изузетних вредности за изучавање комплексних система.

У периоду 2015.-2016. године, др Франовић је учествовао на пројекту билатералне сарадње између Републике Србије и Републике Португала *Noise and measurement errors in multi-parti quantum security protocols*.

Прилог: web страна Министарства просвете, науке и технолошког развоја о прихваћеним пројектима билатералне сарадње с Немачком за пројектни циклус 2017.-2018. године, потврда руководиоца пројекта о руковођењу потпројектом, потврда руководиоца Центра изузетних вредности о руковођењу истраживачком темом

#### **5.5 Активност у научним и научно-стручним друштвима**

Др Франовић је Associate Editor у међународном часопису из области нелинеарне динамике *Chaos, Solitons & Fractals* који издаје Elsevier.

Рецензент је за часописе *Scientific Reports, Chaos, Europhysics Letters, Physics Letters A, European Physical Journal B, Neural Networks, Nonlinear Processes in Geophysics*.

Поред тога, члан је Одсека за квантну и математичку физику Друштва физичара Србије.

Био је организатор и копредседавајући радионице *Nikola Burić Memorial Workshop*, одржане децембра 2016. године.

Прилог: web страна о уредништву часописа, писма уредништва рецензенту, web страница конференције

#### **5.6 Утицајност научних резултата**

Утицај научних радова др Франовића детаљно је приказан у одељку 5.1 овог документа. Комплетан списак радова и цитата дат је у прилогу.

## 5.7 Конкретан допринос кандидата у реализацији радова у земљи и иностранству

Др Франовић је значајно допринео сваком раду у чијој припреми је учествовао. Од 16 радова објављених у периоду након одлуке Научног већа Института за физику о предлогу за стицање претходног научног звања, сви радови су урађени у сарадњи с колегама из земље и иностранства. Др Франовић је у овим радовима имао кључни допринос: на 8 радова је први аутор, а на 3 рада је наведен као други аутор. Током израде ових публикација, он је осмислио тему истраживања, и радио је на развоју одговарајућих нумеричких симулација, прикупљању и анализи релевантних података, развоју теоријских модела, метода и техника анализа проблема, писању радова, а такође је био у комуникацији с уредником часописа при слању рада за објављивање.

На Институту за физику у Београду, др Франовић је увео нове методе у проучавање емергентних феномена у системима под утицајем шума и кашњења у интеракцијама. Знања и искуства које је стекао у теоријском моделовању, аналитичким методама и техникама анализе динамике комплексних система успешно преноси млађим сарадницима у Лабораторији за примену рачунара у науци у оквиру Центра изузетних вредности за изучавање комплексних система.

## 5.8 Уводна предавања на конференцијама и друга предавања

Након претходног избора у звање, др Франовић је одржао следећа предавања по позиву:

- **Igor Franović, Kristina Todorović, Nebojša Vasović and N. Burić**  
*Mean Field Dynamics of Networks of Delay-coupled Noisy Excitable Units*  
International Conference of Numerical Analysis and Applied Mathematics (ICNAAM 2015), Minisymposium “Dynamical Networks with Complex Links“  
22–28 September 2015, Rhodes, Greece, M31;  
AIP Conf. Proc. 1738, 210004 (2016), DOI: 10.1063/1.4951987, American Institute of Physics
- **I. Franović and V.V. Klinshov**  
*Mean-field analysis of stability and slow rate fluctuations in a network of noisy neurons with coupling delay*  
Topical problems of Nonlinear Wave Physics (NWP-2017), 22–28 July, 2017  
Moscow, St Petersburg, Russia, M32

Поред тога, одржао је и следећа предавања на међународним конференцијама:

- **Igor Franović, Kristina Todorović, Nebojša Vasović and Nikola Burić**  
*Mean-field treatment of collective motion in systems of delay-coupled stochastic excitable units*  
XXXIV Dynamics Days Europe, 8-12 September 2014, Bayreuth, Germany, M34



- **Igor Franović**, Kristina Todorović, Nebojša Vasović and Nikola Burić  
*Mean-field Dynamics of Systems of Delay-coupled Noisy Excitable Units*,  
The 19th Symposium on Condensed Matter Physics – SFKM 2015,  
7-11 September 2015, Belgrade, Serbia, M34
- **Igor Franović**, Matjaž Perc and Kristina Todorović  
*Activation process in systems of excitable units with multiple noise sources*  
XXXVI Dynamics Days Europe,  
6 June -10 June 2016, Corfu, Greece, M34
- **I. Franović**  
*Switching dynamics in networks of stochastic rate-based neurons*  
Analysis and Modeling of Complex Oscillatory Systems (AMCOS),  
19–23 March, 2018  
Barcelona, Spain, M34

У оквиру међународне сарадње, др Франовић је одржао следећа предавања на иностраним универзитетима и институтима:

- **Igor Franović**  
*Mean-field Treatment of Collective Dynamics in Systems of Delay-coupled Excitable Units*  
Универзитет Хумболт, Факултет математике и природних наука, Одељење за статистичку физику, нелинеарну динамику и стохастичке процесе,  
12. фебруар 2015, Берлин, Немачка
- **Igor Franović**  
*Statistical Physics of Neural Systems with Noise and Delay*  
Институт за примењену физику Руске академије наука у Нижњем Новгороду,  
13. август 2015, Нижњи Новгород, Русија
- **Igor Franović**  
*Mean-field Analysis of Activation Process in Assemblies of Coupled Noisy Excitable Units*  
Seminar in Nonlinear Dynamics, Weierstrass Institute for Applied Analysis and Stochastics,  
11. мај 2016, Берлин, Немачка
- **Igor Franović**  
*Analysis of Activation Process in Coupled Noisy Excitable Systems*  
Универзитет Хумболт, Факултет математике и природних наука, Одељење за статистичку физику, нелинеарну динамику и стохастичке процесе,  
13.5.2016, Берлин, Немачка

- **Igor Franović**

*Mean-field Approach for Analysis of Collective Dynamics and Activation Processes in Coupled Noisy Excitable Systems*

Институт за примењену физику Руске академије наука у Нижњем Новгороду,  
9.6.2016, Нижњи Новгород, Русија

- **I. Franović**

*Bistability, rate oscillations and slow rate fluctuations in networks of noisy neurons with coupling delay*

Oberseminar Nonlinear Dynamics, Weierstrass Institute for Applied Analysis and Stochastics, 27th June 2017

## 6. ЕЛЕМЕНТИ ЗА КВАНТИТАТИВНУ ОЦЕНУ НАУЧНОГ ДОПРИНОСА КАНДИДАТА

Остварени резултати у периоду након одлуке Научног већа Института за физику о предлогу за стицање претходног научног звања дати су у табели. Према бази ISI Web of Science, радови др Франовића укупно су цитирани 134 пута, док је број цитата без ауоцитата 82. Према бази Scopus, укупан број цитата је 146, док је број цитата без ауоцитата 91. Према подацима обе базе, Хиршов индекс радова др Франовића је 8.

Категорија	М бодова	Број	Укупно М	Нормирани број
Категорија	по раду	радова	бодова	М бодова
M13	7	1	1	7
M21a	10	10	100	94.99
M21	8	5	40	40
M31	3.5	1	3.5	3.5
M32	1.5	1	1.5	1.5
M33	1	5	5	5
M34	0.5	6	6	3

Поређење оствареног броја М-бодова с минималним квантитативним условима за избор у звање виши научни сарадник:

Минималан број М бодова		Услов - 150% минималног броја бодова*	Остварено (нормирано)
Укупно	50	75	<b>154.99</b>
M10+M20+M31+M32+M33 +M41+M42	40	60	<b>152.49</b>
M11+M12+M21+M22+M23	30	45	<b>134.99</b>

\* Минималан број М бодова због убрзаног покретања поступка за избор звање виши научни сарадник

## 7. СПИСАК РАДОВА ДР ИГОРА ФРАНОВИЋА

### 7.1 Поглавље у истакнутој монографији међународног значаја (M13)

#### Радови објављени након претходног избора у звање

1. Srđan Kostić, Nebojša Vasović, Kristina Todorović, and **Igor Franović**  
*Nonlinear Dynamics Behind The Seismogenic Fault Motion – A Review On Dynamics Of Single-Array Spring-Block Models*  
in Wayne Coleman (ed.), “Earthquakes: Monitoring Technology, Disaster Management and Impact Assessment“, p. 1-60, Nova Science Publishers (2017)

### 7.2 Радови у међународним часописима изузетних вредности (M21a)

#### Радови објављени након претходног избора у звање

1. **I. Franović** and V. Klinshov:  
*Clustering Promotes Switching Dynamics in Networks of Noisy Neurons*  
Chaos **28**, 023111 (2018), ИФ 2.283 за 2016. годину
2. S. Kostić, N. Vasović, **I. Franović**, K. Todorović, V. Klinshov, and V. I. Nekorkin:  
*Dynamics of Fault Motion in a Stochastic Spring-slider Model with Varying Neighboring Interactions and Time-delayed Coupling*  
Nonlinear Dyn. **87**, 2563 (2017), ИФ 3.464 за 2016. годину
3. **I. Franović**, S. Kostić, M. Perc, V. Klinshov, V. I. Nekorkin, and J. Kurths:  
*Phase Response Curves for Models of Earthquake Fault Dynamics*  
Chaos **26**, 063105 (2016), ИФ 2.283 за 2016. Годину
4. N. Vasović, S. Kostić, **I. Franović**, and K. Todorović:  
*Earthquake Nucleation in a Stochastic Fault Model of Globally Coupled Units with Interaction Delays*  
Commun. Nonlinear Sci. Numer. Simulat. **38**, 117 (2016), ИФ 2.866 за 2014. годину
5. **I. Franović**, K. Todorović, M. Perc, N. Vasović, and N. Burić:  
*Activation Process in Excitable Systems with Multiple Noise Sources: One and Two Interacting Units*  
Phys. Rev. E **92**, 062911 (2015), ИФ 2.326 за 2013. годину
6. **I. Franović**, M. Perc, K. Todorović, S. Kostić, and N. Burić:  
*Activation Process in Excitable Systems with Multiple Noise Sources: Large Number of Units*  
Phys. Rev. E **92**, 062912 (2015), ИФ 2.326 за 2013. годину

7. V. Klinshov and **I. Franović**:  
*Mean-field Dynamics of a Random Neural Network with Noise*  
Phys. Rev. E **92**, 062813 (2015), ИФ 2.326 за 2013. Годину

**Радови публиковани после одлуке Научног већа о предлогу за стицање претходног научног звања**

1. **I. Franović**, K. Todorović, N. Vasović, and N. Burić:  
*Stability, Coherent Spiking and Synchronization in Noisy Excitable Systems with Coupling and Internal Delays*  
Commun. Nonlinear Sci. Numer. Simulat. **19**, 3202 (2014), ИФ 2.866 за 2014. годину
2. S. Kostić, **I. Franović**, M. Perc, N. Vasović, and K. Todorović:  
*Triggered Dynamics in a Model of Different Fault Creep Regimes*  
Sci. Rep. **4**, 5401 (2014), ИФ 5.578 за 2014. Годину
3. S. Kostić, N. Vasović, **I. Franović**, D. Jevremović, D. Mitrović, and K. Todorović:  
*Dynamics of Landslide Model with Time Delay and Periodic Parameter Perturbations*  
Commun. Nonlinear Sci. Numer. Simulat. **19**, 3346 (2014), ИФ 2.866 за 2014. годину

**Радови објављени пре претходног избора у звање**

1. **I. Franović**, K. Todorović, N. Vasović, and N. Burić:  
*Persistence and Failure of Mean-field Approximations Adapted to a Class of Systems of Delay-coupled Excitable Units*  
Phys. Rev. E **89**, 022926 (2014), ИФ 2.326 за 2013. годину
2. S. Kostić, **I. Franović**, K. Todorović, and N. Vasović:  
*Friction Memory Effect in Complex Dynamics of Earthquake Model*  
Nonlinear Dyn. **73**, 1933 (2013), ИФ 3.009 за 2012. годину
3. **I. Franović**, K. Todorović, N. Vasović, and N. Burić:  
*Mean-field Approximation of Two Coupled Populations of Excitable Units*  
Phys. Rev. E **87**, 012922 (2013), ИФ 2.326 за 2013. годину
4. **I. Franović**, K. Todorović, N. Vasović, and N. Burić:  
*Cluster Synchronization of Spiking Induced by Noise and Interaction Delays in Homogenous Neuronal Ensembles*  
Chaos **22**, 033147 (2012), ИФ 2.188 за 2012. годину
5. **I. Franović**, K. Todorović, N. Vasović, and N. Burić:

*Spontaneous Formation of Synchronization Clusters in Homogenous Neuronal Ensembles Induced by Noise and Interaction Delays*  
Phys. Rev. Lett. **108**, 094101 (2012), ИФ 7.943 за 2012. Годину

6. **I. Franović** and V. Lj. Miljković:  
*The Effects of Synaptic Time Delay on Motifs of Chemically Coupled Rulkov Model Neurons*  
Commun. Nonlinear Sci. Numer. Simulat. **16**, 623 (2011), ИФ 2.806 за 2011. годину
7. **I. Franović**, K. Todorović, N. Vasović, and N. Burić:  
*Stability, Bifurcations, and Dynamics of Global Variables of a System of Bursting Neurons*  
Chaos **21**, 033109 (2011), ИФ 2.081 за 2010. годину
8. **I. Franović** and V. Lj. Miljković:  
*Functional Motifs: a Novel Perspective on Burst Synchronization and Regularization of Neurons Coupled Via Delayed Inhibitory Synapses*  
Chaos Soliton. Fract. **44**, 122 (2011), ИФ 3.315 за 2009. годину
9. **I. Franović** and V. Lj. Miljković:  
*Phase Plane Approach to Cooperative Rhythms in Neuron Motifs with Delayed Inhibitory Synapses*  
EPL **92**, 68007 (2011), ИФ 2.893 за 2009. годину
10. **I. Franović** and V. Lj. Miljković:  
*Percolation Transition at Growing Spatiotemporal Fractal Patterns in Models of Mesoscopic Neural Networks*  
Phys. Rev. E **79**, 061923 (2009), ИФ 2.508 за 2008. годину
11. **I. Franović** and V. Lj. Miljković:  
*Fractal Properties of Percolation Clusters in Euclidian Neural Networks*  
Chaos Soliton. Fract. **39**, 1418 (2009), ИФ 3.315 за 2009. годину

### **7.3 Радови у врхунским међународним часописима (M21)**

#### **Радови објављени после претходног избора у звање**

1. I. Bačić, **I. Franović**, and M. Perc:  
*Disordered Configurations of the Glauber Model in Two-dimensional Networks*  
EPL **120**, 68001 (2017), ИФ 2.095 за 2014. годину
2. S. Kostić, N. Vasović, K. Todorović, and **I. Franović**:  
*Nonlinear Dynamics Behind the Seismic Cycle: One-dimensional Phenomenological*

### *Modeling*

Chaos Soliton. Fract. **106**, 310 (2018), ИФ 1.611 за 2015. годину

3. **I. Franović**, O. V. Maslennikov, I. Bačić, and V. I. Nekorkin:  
*Mean-field Dynamics of a Population of Stochastic Map Neurons*  
Phys. Rev. E **96**, 012226 (2017), ИФ 2.366 за 2016. годину
4. **I. Franović** and V. Klinshov:  
*Slow Rate Fluctuations in a Network of Noisy Neurons with Coupling Delay*  
EPL **116**, 48002 (2016), ИФ 2.095 за 2014. Годину

### **Радови публиковани после одлуке Научног већа о предлогу за стицање претходног научног звања**

1. S. Kostić, N. Vasović, **I. Franović**, and K. Todorović:  
*Complex Dynamics of Spring-Block Earthquake Model Under Periodic Parameter Perturbations*  
J. Comput. Nonlin. Dyn. **9**, 031019 (2014), ИФ 1.530 за 2013. годину

### **7.4 Радови у истакнутим међународним часописима (M22)**

#### **Радови објављени пре претходног избора у звање**

1. S. Kostić, N. Vasović, **I. Franović**, and K. Todorović:  
*Dynamics of Simple Earthquake Model with Time Delay and Variation of Friction Strength*  
Nonlinear Proc. Geoph. **20**, 857 (2013), ИФ 1.692 за 2013. годину
2. **I. Franović** and V. Lj. Miljković:  
*Possibilities of Introducing Different Functional Circuits on Top of a Structural Neuron Triplet: Where Do the Gains Lie?*  
Chaos Soliton. Fract. **45**, 527 (2012), ИФ 1.268 за 2010. годину
3. **I. Franović** and V. Lj. Miljković:  
*Power Law Behavior Related to Mutual Synchronization of Chemically Coupled Map Neurons*  
Eur. Phys. J. B **76**, 613 (2010), ИФ 1.575 за 2010. годину

### **7.5 Предавања по позиву с међународних скупова штампана у целини (M31)**

#### **Радови објављени после претходног избора у звање**

1. **Igor Franović**, Kristina Todorović, Nebojša Vasović and N. Burić

*Mean Field Dynamics of Networks of Delay-coupled Noisy Excitable Units*  
International Conference of Numerical Analysis and Applied Mathematics (ICNAAM  
2015), Minisymposium “Dynamical Networks with Complex Links“  
22–28 September 2015, Rhodes, Greece,  
AIP Conf. Proc. 1738, 210004 (2016), DOI: 10.1063/1.4951987, American Institute of  
Physics

## 7.6 Предавања по позиву с међународних скупова штампана у изводу (M32)

### Радови објављени после претходног избора у звање

1. **I. Franović** and V.V. Klinshov  
*Mean-field analysis of stability and slow rate fluctuations in a network of  
noisy neurons with coupling delay*  
Topical problems of Nonlinear Wave Physics (NWP-2017), 22–28 July, 2017  
Moscow, St Petersburg, Russia

## 7.7 Саопштења с међународних скупова штампана у целини (M33)

### Радови објављени после претходног избора у звање

1. K. Todorović, **I. Franović**, N. Vasović and S. Kostić  
*Mean-field approximation of two coupled populations of excitable units modeled by  
Fitzhugh-Nagumo elements*  
4th South-East European Conference on Computational Mechanics, isbn: 978-86-  
921243-0-3, Kragujevac, 3.-4. jul 2017
2. K. Todorović, **I. Franović**, N. Vasović and S. Kostić,  
*Spontaneous formation of synchronization clusters in neuronal populations induced  
by noise and interaction delays*  
6th Internacional Congress of Serbian Society of Mechanics, Tara, Serbia, isbn: 978-  
86-909973-6-7, 19.-21. jun 2017
3. Srđan Kostić, Nebojša Vasović, Dragutin Jevremović, Duško Sunarić, **Igor Franović**  
and Kristina Todorović  
*Complex Dynamics of Landslides with Time Delay Under External Seismic Triggering  
Effect*  
IAEG XII Congress "Engineering Geology for Society and Territory", Torino 2014,  
Engineering Geology for Society and Territory, vol. 2: Landslide processes, Springer  
(2015), p. 1353-1356, DOI: 10.1007/978-3-319-09057-3\_328

### Радови објављени после одлуке Научног већа о предлогу за стицање претходног научног звања



1. S. Kostić, N. Vasović, **I. Franović** and K. Todorović,  
*Assessment of blast induced ground vibrations by artificial neural network*  
Proceedings of 12th Symposium on Neural Network Applications in Electrical Engineering (NEUREL) 55-60, 2014

#### **Радови објављени пре претходног избора у звање**

1. **I. Franović** and V. Miljković  
*Percolation approach to formation of synfire chains in two dimensional neural networks*  
Proceedings of 8th Symposium on Neural Network Applications in Electrical Engineering (NEUREL) 69-72, 2006

### **7.8 Саопштења с међународних скупова штампана у изводу (M34)**

#### **Радови објављени после претходног избора у звање**

1. O.V. Maslennikov, **I. Franović** and V.I. Nekorkin  
*Mean-field model for a network of globally coupled stochastic map-based neurons*  
Topical problems of Nonlinear Wave Physics (NWP-2017),  
22–28 July 2017, Moscow, St Petersburg, Russia
2. V. Klinshov and **I. Franović**  
*Bistability, Rate Oscillations and Slow Rate Fluctuations in a Neural Network with Noise and Coupling Delays*  
XXXVII Dynamics Days Europe, June 5–9, 2017, Szeged, Hungary
3. **Igor Franović**, Matjaž Perc and Kristina Todorović  
*Activation process in systems of excitable units with multiple noise sources*  
XXXVI Dynamics Days Europe, 6 June -10 June 2016, Corfu, Greece
4. **Igor Franović**, Kristina Todorović, Nebojša Vasović and Nikola Burić  
*Mean-field Dynamics of Systems of Delay-coupled Noisy Excitable Units*  
The 19th Symposium on Condensed Matter Physics – SFKM 2015,  
7-11 September 2015, Belgrade, Serbia
5. **Igor Franović**, Kristina Todorović, Nebojsa Vasović and Nikola Burić  
*Mean-field treatment of collective motion in systems of delay-coupled stochastic excitable units*  
XXXIV Dynamics Days Europe, 8-12 September 2014, Bayreuth, Germany



## ПОТВРДА О РУКОВОЂЕЊУ ПОТПРОЈЕКТОМ

Овим потврђујем да научни сарадник **др Игор Франовић** за кога се покреће избор у звање виши научни сарадник, у оквиру Лабораторије за примену рачунара у науци Националног центра изузетних вредности за изучавање комплексних система Института за физику у Београду, односно у оквиру пројекта ОН171017 „Моделирање и нумеричке симулације сложених вишечестичних система“ руководи потпројектом: „Самоорганизација у спрегнутим екситабилним системима“. На поменутом потпројекту су ангажовани следећи истраживачи: др Игор Франовић, др Нели-Кристина Тодоровић-Васовић, др Небојша Васовић, Ива Бачић.

Београд, 17. април 2018. године

др Антун Балаж  
научни саветник  
Руководилац пројекта ОН171017  
Руководилац Центра за изучавање комплексних  
система Института за физику у Београду



Република Србија  
МИНИСТАРСТВО ПРОСВЕТЕ,  
НАУКЕ И ТЕХНОЛОШКОГ  
РАЗВОЈА

Број: 451-03-01413/2016-09/6

Датум: 09.01.2017.

Београд, Немањина 22-26

Институт за физику  
- Игор Франовић -

Прегревица 118  
11 080 Београд

Поштовани господине Франовићу,

Обавештавамо Вас да је у оквиру Програма билатералне научне и технолошке сарадње између Републике Србије и Немачке службе за академску размену (ДААД), а на основу спроведених процедура оцене пројеката у обе државе, усвојена листа за финансирање пројеката у двогодишњем периоду са почетком реализације од 1. јануара 2017. године.

Са задовољством Вас обавештавамо да је Ваш пројекат „Емергентна динамика у системима спрегнутих екситабилних јединица” одобрен за финансирање.

Желимо да напоменемо да реализација пројекта треба да допринесе даљем унапређењу сарадње, омогући учешће младих истраживача и помогне генерисању новог пројектног предлога којим би се конкурисало у другим програмима међународне сарадње (нпр. Хоризонт 2020).

Обе стране финансираће пројекат према условима наведеним у Конкурсу, тако да страна која шаље покрива трошкове превоза истраживача између две институције, а страна која прима истраживаче, покрива трошкове њиховог боравка и локалног превоза који су неопходни за реализацију сарадње на одобреном пројекту.

Захтеви за рефундацију трошкова путовања српских истраживача, односно трошкова боравка немачких истраживача, достављају се на обрасцу који можете преузети на интернет адреси Министарства, у огранку међународна научна сарадња, уз одговарајућу пратећу документацију.

Руководиоци одобрених пројеката за финансирање, дужни су да доставе годишњи и завршни извештај о реализацији пројекта, у року од 15 дана након завршетка пројектне године, односно након завршетка пројекта, у форми која се такође, налази на интернет адреси Министарства. Саставни део извештаја су и прилози који садрже резултате билатералног пројекта: реализоване посете, учешће младих истраживача, радна верзија или копија објављеног рада у међународном часопису, назив пројекта и назив потенцијалног програма или јавног позива на који се конкурише у смислу наставка сарадње, агенда и листа учесника заједничких радионица.

Информација о свим одобреним пројектима објављена је на интернет страници Министарства просвете, науке и технолошког развоја.

Истовремено бих желео да Вам честитам на одобреном пројекту и пожелим успешну реализацију пројектних активности.

С поштовањем,



Проф. др Владимир Подовић, државни секретар

Проф. др Виктор Недовић, в. д. Помоћник министра

Милица Голубовић Тасевска, саветник

Министарство просвете, науке и технолошког развоја Републике Србије и  
Немачка служба за академску размену – ДААД

*Ministry of Education Science and Technological Development of the Republic of Serbia  
and Deutcher Akademischer Austauschdienst – DAAD*

**Пројектни циклус / Project years 2017-2018**

	<i>Srpski rukovodilac projekta i srpska institucija</i>  <i>Serbian applicant and Serbian institution</i>	<i>Nemački rukovodilac projekta i nemačka institucija</i>  <i>German applicant and German institution</i>	<i>Naziv projekta</i>  <i>Project title</i>
1.	Prof. dr Zoran V. POPOVIĆ  Institut za fiziku,  Univerzitet u Beogradu	PD Dr. Rudolf HACKL  Walter-Meissner- Institute, München	Fluktuacije naelektrisanja i spina u FeSe supstituisanim sumporom  <i>Spin-and Charge Instabilities in Sulfur- substituted FeSe</i>
2.	Dr Goran ISIĆ  Institut za fiziku,  Univerzitet u Beogradu	Prof. Dr. Thomas PERTSCH  University of Jena	Rezonantne nanostrukture za kontrolu spontane emisije (RESONANCE)  <i>Resonant Nanostructures for Controlling Spontaneous Emission (RWESONANCE)</i>
3.	Dr Antun BALAŽ  Institut za fiziku,  Univerzitet u Beogradu	PD. Dr. Axel PELSTER  TU Kaiserslautern	Boze Ajnštajn kondenzacija svetlosti (BEC-L)  <i>Bose-Einstein Condensation of Light (BEC—L)</i>

4.	Prof. dr Pavle ANĐUS Biološki fakultet, Univerzitet u Beogradu	Dr. Alexander KRANZ Fraunhofer Institute, Leipzig	Primena naprednih tehnika oslikavanja u ispitivanju promena krvomoždane barijere u ALSu  <i>Advanced imaging of blood-brain barrier alterations in ALS</i>
5.	Dr Aleksandra ĐUKIĆ VUJOVIĆ Tehnološko-metalurški fakultet, Univerzitet u Beogradu	Prof. Dr. Christian GUSBETH Karlsruhe Institute of Technology	Integrirana ekstrakcija pulsniim električnim poljem i mlečno-kiselinska fermentacija za proizvodnju ekstrakata mikroalgi obogaćenih probioticima  (PEF4AlgBiotics) <i>Integrated pulsed electric field extraction and lactic acid bacteria fermentation for the production of micro algal extracts fortified with probiotics</i> (PEF4AlgBiotics)
6.	Dr Igor FRANOVIĆ Institu za fiziku, Univerzitet u Beogradu	Dr. Matthias WOLFRUM Weierstrass Institute for Applied Analysis and Stochastics, Berlin(WIAS)	Emergentna dinamika u sistemima spregnutih ekscitabilnih jedinica  <i>Emergent Dynamics in Systems of Coupled Excitable Units</i>
7.	Dr Vladimir PANIĆ Institut za hemiju, tehnologiju i metalurgiju, Univerzitet u Beogradu	Prof. Dr.-Ing. Bernd FRIEDRICH RWTH, Aachen	Novi pristupi sintezi za dobijanje uredjenih struktura multikomponentnih metalnih oksida kao uniformnih prevlaka aktiviranih titanskih anoda  <i>Novel designs of synthesis of multicomponent metal oxides</i>

8.	Prof. dr Žarko ČOJBAŠIĆ Mašinski fakultet, Univerzitet u Nišu	Prof. Dr. Manfred ZEHN  TU Berlin	Pametni mehanotronički sistemi i strukture  <i>Smart Mechatronic Systems and Structures</i>
9.	Prof. dr Zora DAJIĆ STEVANOVIĆ  Poljoprivredni fakultet,  Univerzitet u Beogradu	Dr. Hartwig SCHULZ  Julius Kühn Institute, Berlin	Primena infracrvene i Ramanove spektroskopije u cilju identifikacije i lokalizacije različitih bioaktivnih supstanci u lekovitom i aromatičnom bilju  <i>Application of infrared (IR) and Raman spectroscopy for identification and localization of various bioactive substances in various medical and aromatic plants</i>
10.	Prof. dr Snežana SAVIĆ  Farmaceutski fakultet,  Univerzitet u Beogradu	Prof. Dr. Dominique Jasmin LUNTER  Eberhard-Karls Univeristät, Tübingen	Biosurfaktanti i biopolisaharidi/polimeri koji stvaraju film kao kozmetičke sirovine i prospektivni farmaceutski ekscipijensi: formulacija koloidnih i film- formirajućih sistema za isporuku aktivnih supstanci  <i>Biosurfactants and biopolysaccharides/fim- forming polymers as cosmetic raw materials and prospective pharmaceutical excipients: formulation of colloidal and film-forming delivery systems</i>



## ПОТВРДА О МЕНТОРСТВУ

Овим потврђујем да је научни сарадник **др Игор Франовић**, за кога се покреће избор у звање виши научни сарадник, у оквиру Лабораторије за примену рачунара у науци Националног центра изузетних вредности за изучавање комплексних система Института за физику у Београду, односно у оквиру пројекта ОН171017 „Моделирање и нумеричке симулације сложених вишечестичних система“, ментор за докторску тезу Иве Бачић. Она је студент треће године докторских студија на Физичком факултету Универзитета у Београду.

Београд, 17. април 2018. године

др Антун Балаж  
научни саветник  
Руководилац пројекта ОН171017  
Руководилац Центра за изучавање комплексних  
система Института за физику у Београду



Република Србија  
МИНИСТАРСТВО ПРОСВЕТЕ,  
НАУКЕ И ТЕХНОЛОШКОГ РАЗВОЈА  
БЕОГРАД  
Немањина 22-26

**ИЗВЕШТАЈ РУКОВОДИОЦА**  
**О РАДУ - ИСТРАЖИВАЧА ДОКТОРАНТА**  
укљученог на пројекат Министарства

**I. ОПШТИ ПОДАЦИ**

1. Име и презиме докторанта **Ива Бачић**
2. Институт - факултет (НИО запослења) **Институт за физику у Београду**
3. Ментор
  - име и презиме **др Игор Франовић**
  - звање **научни сарадник**
  - (НИО запослења ментора) **Институт за физику у Београду**
4. Ментор овог докторанта је од **октобра 2015. године**
5. Пројекат на коме је докторант ангажован
  - назив пројекта **Моделирање и нумеричке симулације сложених вишечестичних система**
  - евиденциони број пројекта **171017**

**II. АНГАЖОВАЊЕ ДОКТОРАНТА – ИСТРАЖИВАЧА ДОКТОРАНТА**

6. Врста ангажовања докторанта у оквиру научноистраживачког рада (написати конкретно шта је радио и да ли има публиковане радове/где и повезаност послова са докторатом)

Током 2017. године Ива је положила све престале испите на докторским студијама с оценом 10, а показала је и значајан напредак у усвајању релевантних аналитичких и нумеричких метода. Ива је учествовала у припреми публикације објављене у часопису *Physical Review E*, и тај рад ће бити саставни део њене докторске тезе. Поред тога, један од семинарских радова је проширен и припрема се за слање у часопис. Такође, Ива је партиципирала на билатералном пројекту са Савезном Републиком Немачком, у оквиру којег је имала прилику да сарађује с еминентним

**колегама из Берлина. Остварени су значајни резултати, за које очекујемо да ће бити приказани у две публикације које ће бити укључене у Ивин докторат.**

7. Да ли је докторант био ангажован на другим пословима у тој НИО:

а) не

б) да ( навести на којим):

8. Степен реализације плана и програма рада на пројекту (образложење)

**Предвиђени план и програм рада на пројекту су испуњени у потпуности. Поред овладавања релевантним аналитичким и нумеричким методама, које су обрађене у оквиру положених испита, Ива је учествовала у припреми рада који ће бити саставни део њене тезе. Такође, дала је и значајан допринос у међународној сарадњи у оквиру билатералног пројекта са Савезном Републиком Немачком.**

9. Планови и предлози за даље ангажовање докторанта:

а) наставити/продужити ангажовање...

б) не наставити/прекинути (образложите у вези са оценом датом у оквиру тачке 10) овог извештаја):

в) остало

10. Изнесите своје предлоге за побољшање услова и резултата рада докторанта чији сте ментор:

**У прилогу овог извештаја достављам документацију која чини његов ОБАВЕЗНИ саставни део:**

**1) Потврде са факултета о реализованим обавезама на докторским студијама (заокружити прилог а-в који се доставља)**

**а) о последњем овереном и уписаном семестру,**

**б) о положеним испитима и укупном просечном оценом на докторским студијама, или**

**в) потврду факултета о пријављеној/ одобреној теми доктората и реализацији.**

**2) оверену копију радне књижице (од 1-7 стране);**

**3) копија М-А обрасца (Потврда о поднетој пријави, промени, одјави на обавезно социјално осигурање).**

Датум ....16.1.2018. год.

Докторант

Ментор

---

Декан/Директор

---

Руководилац пројекта

МП

---

Република Србија  
**МИНИСТАРСТВО ПРОСВЕТЕ,  
НАУКЕ И ТЕХНОЛОШКОГ РАЗВОЈА**  
Комисија за стицање научних звања

Број:660-01-00042/240

17.12.2014. године

Београд

На основу члана 22. става 2. члана 70. став 5. Закона о научноистраживачкој делатности ("Службени гласник Републике Србије", број 110/05 и 50/06 – исправка и 18/10), члана 2. става 1. и 2. тачке 1 – 4.(прилози) и члана 38. Правилника о поступку и начину вредновања и квантитативном исказивању научноистраживачких резултата истраживача ("Службени гласник Републике Србије", број 38/08) и захтева који је поднео

**Физички факултет у Београду**

Комисија за стицање научних звања на седници одржаној 17.12.2014. године, донела је

**ОДЛУКУ  
О СТИЦАЊУ НАУЧНОГ ЗВАЊА**

**Др Игор Франовић**

стиче научно звање

**Научни сарадник**

у области природно-математичких наука - физика

**О Б Р А З Л О Ж Е Њ Е**

**Физички факултет у Београду**

утврдио је предлог број 19/4 од 23.04.2014. године на седници наставно-научног већа Факултета и поднео захтев Комисији за стицање научних звања број 19/6 од 05.05.2014. године за доношење одлуке о испуњености услова за стицање научног звања **Научни сарадник**.

Комисија за стицање научних звања је по претходно прибављеном позитивном мишљењу Матичног научног одбора за физику на седници одржаној 17.12.2014. године разматрала захтев и утврдила да именовани испуњава услове из члана 70. став 5. Закона о научноистраживачкој делатности ("Службени гласник Републике Србије", број 110/05 и 50/06 – исправка и 18/10), члана 2. става 1. и 2. тачке 1 – 4.(прилози) и члана 38. Правилника о поступку и начину вредновања и квантитативном исказивању научноистраживачких резултата истраживача ("Службени гласник Републике Србије", број 38/08) за стицање научног звања **Научни сарадник**, па је одлучила као у изреци ове одлуке.

Доношењем ове одлуке именовани стиче сва права која му на основу ње по закону припадају.

Одлуку доставити подносиоцу захтева, именованом и архиви Министарства просвете, науке и технолошког развоја у Београду.

**ПРЕДСЕДНИК КОМИСИЈЕ**

Др Станислава Стошић-Грујичић,

научни саветник

*С. Стошић-Грујичић*



**ДРЖАВНИ СЕКРЕТАР**

Др Александар Белић

*Александар Белић*



Vladimir &lt;rodos.net.2015@gmail.com&gt;

2/18/15 ☆



to me ▾

Dear Igor,

It is my great pleasure to invite you to take part in the Symposium "Dynamical Networks with Complex Links" which will take place in Rhodes, Greece, in 23-29 September 2015. The purpose of the Symposium is to bring together specialists from various areas studying networks with various aspects of complexity such as nonlinear connections, dynamical connections, plasticity, coupling delays, complex topology, etc. A number of prominent scientists have already declared taking part in the Symposium, including

Eckehard Schoell, Technical University Berlin, Germany

Juergen Kurths, Potsdam Institute for Climate Impact Research, Germany

Vadim Anishenko, Saratov State University, Russia

Boris Bezruchko, Saratov State University, Russia

Alexander Dmitriev, Kotelnikov Institute of Radio Engineering, Russia

Serhiy Yachuk, Weiersrass Institute for Applied Analysis and Stochastics, Germany

Larger Laurent, University of Franche-Comte, France

Jordi Soriano-Fradera, University of Barcelona, Spain

We organize the Symposium in the framework of the International Conference of Numerical Analysis and Applied Mathematics 2015 ([ICNAAM 2015](#)). This conference will take place in Rhodes, the island known as the pearl of the Mediterranean, in a luxurious [Rodos Palace Hotel](#). The Proceedings of ICNAAM 2015 will be published in the world-renowned AIP (American Institute of Physics) Conference Proceedings.

I am sure the Symposium will significantly benefit from your impact and hope you will agree to take part in it. I also encourage you to distribute the information about the Symposium between your colleagues and/or students who you feel can be interested in participation.

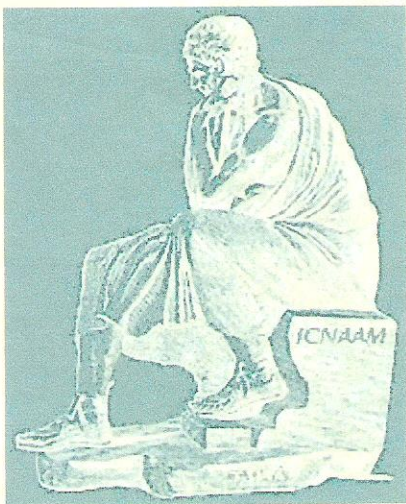
Yours sincerely,  
Vladimir Nekorkin

*International Conference of  
Numerical Analysis and Applied Mathematics 2015  
(ICNAAM 2015)  
Rodos Palace-Conference Center, Rhodes, Greece,  
23-29 September 2015*

*CERTIFICATION*

*We certify that Dr. Franovic Igor has participated in the International Conference of Numerical Analysis and Applied Mathematics 2015 (ICNAAM 2015) with presentation of a scientific paper entitled "Mean Field Dynamics of Networks of Delay-coupled Noisy Excitable Units".*

ICNAAM 2015



*On behalf of the  
Organizing Committee*



*Prof. T.E. Simos  
Academician of the EASA, EAS, EAASL  
President of the European Society of Computational Methods  
in Sciences, Engineering and Technology (ESCMSET)  
Chair ICNAAM 2015*



# AMCOS

Conference and Tutorial on  
Analysis and Modelling of Complex Oscillatory Systems

March 19-23, 2018

PRBB, Barcelona



Universitat  
Pompeu Fabra  
*Barcelona*



## Wednesday, 21 of March

cancelled	KL	<b>Damián H. Zanette</b> San Carlos de Bariloche, Argentina	Synchronization in micromechanical oscillators
9:40–10:10	CT	<b>Nicolas Fourcaud-Trocmé</b> Lyon, France	Evolution of slow and fast rhythm networks during learning of an olfactory discrimination task
10:10–10:45	IS	<b>Alex Roxin</b> Barcelona, Spain	Fluctuation-driven plasticity allows for flexible rewiring on neuronal assemblies
10:45–11:15	Coffee		
11:15–11:55	IS	<b>Florian Mormann</b> Bonn, Germany	Perception and memory at the level of single neurons in the human medial temporal lobe
11:55–12:45	IS	<b>Raffaella Burioni</b> Parma, Italy	Neuronal avalanches in cortex dynamics and the synchronization transition
12:45–14:00	Lunch		
14:00–14:30	CT	<b>Arindam Saha</b> Oldenburg, Germany	Emergence of Riddled Basins of Attraction in Delay-coupled FitzHugh-Nagumo Oscillators
14:30–15:05	IS	<b>Juan Restrepo</b> Colorado, USA	Uncovering low-dimensional macroscopic chaotic dynamics of large finite size complex systems
15:05–15:30	Coffee		
15:30–16:00	CT	<b>Igor Franovic</b> Belgrade, Serbia	Switching dynamics in networks of stochastic rate-based neurons
16:00–16:40	IS	<b>Tilo Schwalger</b> Lausanne, Switzerland	Finite-size effects in the mesoscopic dynamics of spiking neural networks
16:40–17:10	CT	<b>Helmut Schmidt</b> Barcelona, Spain	Network mechanisms underlying the role of oscillations in cognitive tasks
17:10–19:30	Poster session with Wine & Cheese		



# Clustering enhances switching dynamics in networks of stochastic rate-based neurons

I. Franović<sup>1</sup>

Scientific Computing Laboratory, Center for the Study of Complex Systems, Institute of Physics Belgrade, University of Belgrade,

Macroscopic variability is an emergent property of neural networks, typically manifested in slow rate oscillations, which consist in spontaneous switching between the episodes of elevated neuronal activity and the quiescent episodes. The switching dynamics between the collective states is especially relevant for activity of neocortical pyramidal neurons, and is believed to facilitate or mediate different types of learning and memory. We investigate the conditions that facilitate switching dynamics, focusing on the interplay between the different sources of noise and the heterogeneity in network topology. We consider clustered networks of rate-based neurons subjected to external and intrinsic noise, and derive a reduced model which describes the collective network dynamics in terms of a set of coupled second-order stochastic mean-field systems associated to each of the clusters. The model allows one to estimate the different contributions to effective macroscopic noise and qualitatively indicates the parameter domains where switching dynamics may occur. By analyzing the corresponding mean-field models in the thermodynamic limit, we demonstrate the differences in mechanisms behind the switching phenomenon in non-clustered and clustered networks. In case of a non-clustered random network, the mechanism resembles the motion of a noisy particle in a double-well potential. The mechanism changes due to clustering, which is shown to promote multistability. This makes the switching phenomenon gain robustness, occurring in the considerably broader parameter region than in the case of a non-clustered network.

## References

- [1] I. Franović and V. Klinshov, EPL 116, 48002 (2016).
- [2] I. Franović and V. Klinshov, submitted to Chaos (2017).
- [3] V. Klinshov and I. Franović, Phys. Rev. E 92, 062813 (2015).



University of Szeged  
**Faculty of Science  
and Informatics**

# XXXVII Dynamics Days Europe

June 5–9, 2017

Szeged, Hungary

Abstracts

**AIP** | **Chaos**  
An Interdisciplinary Journal of Nonlinear Science



**IOP** Publishing

19:00-19:20 Maxim V. Shamolin

**Variety of Integrable Cases in Dynamics of Nonconservative Variable Dissipation Systems**

19:20-19:40 Filippo Terragni

**Collocated POD and Simulation of Nonlinear Dynamics**

19:40-20:00 Gergely Röst

**Population Dynamics of Epidemic and Endemic States of Drug-resistance Emergence in Infectious Diseases with Delayed Treatment Initiation**

**CT17 NETWORKS (Room 215)**

*Discussion leader: István Z. Kiss*

17:40-18:00 GChiranjit Mitra

**Multi-node Basin Stability in Complex Dynamical Networks**

18:00-18:20 Vladimir Klinshov

**Bistability, Rate Oscillations and Slow Rate Fluctuations in a Neural Network with Noise and Coupling Delays**

18:20-18:40 František Muzika

**Symmetry Breaking in a Ring of Coupled Cells with Glycolytic Oscillatory Reaction**

18:40-19:00 Viktor Novičenko

**Control of Synchronization in Complex Oscillator Networks Via Time-delayed Feedback**

19:00-19:20 Márton Pósfai

**Fluctuations and Stability of Emergent Hierarchies in Social Systems**

19:20-19:40 Alberto Saa

**Network Asymmetries Favor Synchronization**

WEDNESDAY 7TH JUNE

8:45-10:50 PARALLEL SESSIONS

**MS1a CHEMO-HYDRODYNAMICS (Room 107)**

*Organizer: Marcello A. Budroni*

8:45- 9:10 Fabian Brau

**Flow Control of  $A + B \rightarrow C$  Fronts by Radial Injection**

9:10- 9:35 Uwe Tiele

**Sliding Drops – from Bifurcations for Single Drops to Ensemble Dynamics**

9:35-10:00 Karin Schwarzenberger

**Relaxation Oscillations of Solutal Marangoni Convection at Droplets and Chains of Droplet**

10:00-10:25 Reda Tiani

**Effects of Marangoni Flows on  $A + B \rightarrow C$  Reaction-diffusion Fronts**

10:25-10:50 Kay Huang

**Pattern Formation in Wet Granular Matter**

TUESDAY 18:00 – 18:20 (Room 215)

## **Bistability, Rate Oscillations and Slow Rate Fluctuations in a Neural Network with Noise and Coupling Delays**

*Vladimir Klinshov*<sup>1</sup>, and *Igor Franović*<sup>2</sup>

<sup>1</sup> Institute of Applied Physics of the Russian Academy of Sciences, Russia

<sup>2</sup> Scientific Computing Laboratory, Institute of Physics Belgrade, University of Belgrade, Belgrade, Serbia

A network of randomly coupled rate-based neurons influenced with different sources of noise and coupling delays is studied. A second-order stochastic mean-field model for the network dynamics is derived. This model is used to analyze the system dynamics and bifurcations in the thermodynamic limit, as well as to study the fluctuations due to the finite-size effect. Different types of noise, the internal and the external ones, were shown to have substantially different impact on the network dynamics. Although the both sources of noise give rise to stochastic fluctuations, only the external one affects the mean activity levels of the network.

In a wide interval of parameters the bistable dynamics of the network was observed with two different stable levels of activity coexisting. The origin of the bistability is related to the pitch-fork bifurcation. In the presence of coupling delays, the stationary levels may destabilize via Hopf bifurcations giving rise to stable oscillations of the mean rate. In the vicinity of the pitch-fork bifurcation, the noise-induced slow stochastic fluctuations of the mean rate were obtained. Their mechanism was shown to be associated to noise-induced transitions in a double-well potential. The developed mean-field model correctly predicts the parameter regions and the characteristics of the observed complex dynamical regimes.

### **References**

- [1] V. Klinshov and I. Franović, *Mean-field dynamics of a random neural network with noise*, Phys. Rev. E **92**, 062813 (2015).
- [2] I. Franović and V. Klinshov, *Slow rate fluctuations in a network of noisy neurons with coupling delay*, EPL **116**, 48002 (2016).

Vladimir Klinshov [redacted] > to me ↵

3/6/17

Dear Professor Franovic,

it is my pleasure to invite you to hold a talk at the parallel Nonlinear Dynamics and Complexity of the International Symposium Topical Problems of Nonlinear Wave Physics. The conference will be held on a boat traveling from Moscow to St. Petersburg from 22-28 July 2018.

Let me please remind you that the registration deadline expires on March 15. The form for registration and submission of the short summary is available at

<http://www.nwp.sci-nnov.ru/registration.html>

Best regards,  
Vladimir Klinshov,  
Scientific Secretary

=====

Dr Vladimir Klinshov, Ph.D.  
Institute of Applied Physics  
603950 Ulyanova str, 46  
Nizhny Novgorod, Russia

Tel: [redacted]  
email: [redacted]  
website: [redacted]

Russian Academy of Sciences  
Institute of Applied Physics



**International Symposium**  
**TOPICAL PROBLEMS**  
**OF NONLINEAR WAVE PHYSICS**

*22 – 28 July, 2017*

*Moscow – St. Petersburg, Russia*

**PROGRAM and ABSTRACTS**

Nizhny Novgorod, 2017

**NWP-1: Nonlinear Dynamics and Complexity**

**NWP-2: Lasers with High Peak and High Average Power**

**NWP-3: Nonlinear Phenomena in the Atmosphere and Ocean**

**WORKSHOP: Magnetic Fields in Laboratory High Energy Density Plasmas  
(LaB)**

**CREMLIN WORKSHOP: Key Technological Issues in Construction  
and Exploitation of 100 Pw Laser Lasers**

***Board of Chairs***

<b>Henrik Dijkstra,</b>	Utrecht University, The Netherlands
<b>Alexander Feigin,</b>	Institute of Applied Physics RAS, Russia
<b>Julien Fuchs,</b>	CNRS, Ecole Polytechnique, France
<b>Efim Khazanov,</b>	Institute of Applied Physics RAS, Russia
<b>Juergen Kurths,</b>	Potsdam Institute for Climate Impact Research, Germany
<b>Albert Luo,</b>	Southern Illinois University, USA
<b>Evgeny Mareev,</b>	Institute of Applied Physics RAS, Russia
<b>Catalin Miron,</b>	Extreme Light Infrastructure, Romania
<b>Vladimir Nekorkin,</b>	Institute of Applied Physics RAS, Russia
<b>Vladimir Rakov,</b>	University of Florida, USA
<b>Alexander Sergeev,</b>	Institute of Applied Physics RAS, Russia
<b>Ken-ichi Ueda,</b>	Institute for Laser Science, the University of Electro-Communications, Japan

## Organized by



**Institute of Applied Physics  
of the Russian Academy of Sciences**  
[www.iapras.ru](http://www.iapras.ru)



**GYCOM Ltd**  
[www.gycom.ru](http://www.gycom.ru)



**International Center for Advanced Studies  
in Nizhny Novgorod (INCAS)**  
[www.incas.iapras.ru](http://www.incas.iapras.ru)

## Supported by



[www.avesta.ru](http://www.avesta.ru)



[www.lasercomponents.ru](http://www.lasercomponents.ru)



[www.coherent.com](http://www.coherent.com)



[www.lasertrack.ru](http://www.lasertrack.ru)



[www.thalesgroup.com](http://www.thalesgroup.com)



[www.standa.it](http://www.standa.it)



[www.phcloud.ru](http://www.phcloud.ru)



[www.epj.org](http://www.epj.org)



7:30-8:30	Breakfast		
Session	NWP-1	NWP-2 & LaB	NWP-3
	Complex dynamics	Laser sources: extending limits	Climate dynamics – 2
	HALL B	HALL A	HALL C
8:30-10:30	8:30 <b>X. Leoncini</b> ( <i>France</i> ). Dynamics of systems with many degrees of freedom from long range-interactions to complex networks [Invited]	8:30 <b>I.E. Kozhevator</b> ( <i>Russia</i> ), <b>D.E. Silin</b> , <b>A.V. Pigasin</b> , <b>E.H. Kulikova</b> , and <b>S.B. Speransky</b> . Design and specifications of 630-mm phase shifting interferometer for the qualification of large aperture optics	8:30 <b>A.A. Tsonis</b> ( <i>USA</i> ) and <b>S. Kravtsov</b> . Insights into decadal climate variability from the synchronization of a network of major climate modes [Invited]
	9:00 <b>I. Franović</b> ( <i>Serbia</i> ) and <b>V.V. Klinshov</b> . Mean-field analysis of stability and slow rate fluctuations in a network of noisy neurons with coupling delay [Invited]	8:50 <b>A. Kudryashov</b> ( <i>Russia</i> ), <b>V. Samarkin</b> , <b>A. Aleksandrov</b> , <b>G. Borsoni</b> , <b>T. Jitsuno</b> , and <b>J. Sheldakova</b> . Large bimorph flexible mirror for Peta-Watt laser beam correction [Invited]	9:00 <b>N.A. Diansky</b> ( <i>Russia</i> ), <b>I.V. Solomonova</b> , <b>A.V. Gusev</b> , and <b>T.Yu. Vyrychalkina</b> . Effects of the North Atlantic thermohaline circulation on climate variability and Arctic climate change projections based on the combined scenario [Invited]
	9:30 <b>V.V. Klinshov</b> ( <i>Russia</i> ), <b>D.S. Shechapin</b> , <b>S. Yanchuk</b> , and <b>V.I. Nekorkin</b> . Multi-jittering regimes in networks with pulse delayed coupling	9:10 <b>E.A. Mironov</b> ( <i>Russia</i> ) and <b>O.V. Palashov</b> . Thermo-optical characteristics of uniaxial crystals	9:30 <b>A. Gritsun</b> ( <i>Russia</i> ) and <b>V. Lucarini</b> . Instability characteristics of blocking regimes in a simple quasi-geostrophic atmospheric model [Invited]
		9:25 <b>V.Yu. Venediktov</b> ( <i>Russia</i> ). Holographic wavefront sensors and high-power lasers	
		9:45 <b>V.N. Ginzburg</b> ( <i>Russia</i> ), <b>A.A. Kochetkov</b> , and <b>E.A. Khazanov</b> . Study of self-filtering and small-scale self-focusing suppression of high-intensity laser beams	
		10:00 <b>Yu. Zhao</b> ( <i>China</i> ), <b>J. Shao</b> , <b>Sh. Liu</b> , <b>M. Zhu</b> , <b>J. Chen</b> , and <b>Zh. Wu</b> . Thermal-dynamical analysis of femtosecond laser damage of optical coatings	
	10:15 <b>I. Shaikin</b> ( <i>Russia</i> ), <b>A. Kuzmin</b> , and <b>A. Shaykin</b> . Pump laser for multistage parametrical amplifier		
10:30-13:30	GORITSY <span style="float: right;">Bus tour</span>		
13:30-15:00	Lunch		

8:00-9:00	<b>Breakfast</b>		
	<b>HALL A</b>		
9:00-9:50	C.C. Kuranz (USA). Astrophysically relevant, magnetized high-energy-density physics experiments at the University of Michigan [Plenary talk 10]		
9:50-10:40	M. Hoshino (Japan). Wakefield acceleration in relativistic shocks: origin of ultra-high-energy cosmic rays [Plenary talk 11]		
10:40-11:00	<b>Coffee break</b>		
Session	<b>NWP-1</b>	<b>NWP-2 &amp; LaB</b>	<b>NWP-3</b>
	Neural networks – 2	LaB – 6	Atmosphere and ocean dynamics – 2
	<b>HALL B</b>	<b>HALL C</b>	<b>HALL C</b>
11:00-13:30	11:00 M. Masoliver and C. Masoller (Spain). Subthreshold signal encoding and transmission in coupled FitzHugh-Nagumo neurons [Invited]	11:00 L. Chen (UK). Magnetic field amplification and particle acceleration in laboratory astrophysics [Invited]	11:00 F. Qiao (China), Y. Yuan, C. Huang, D. Dai, J. Deng, and Z. Song. Wave turbulence interaction induced vertical mixing and its effects in ocean and climate models [Invited]
	11:30 U. Feudel (Germany), G. Ansmann, and K. Lehnertz. Self-induced switchings between multiple space-time patterns on complex networks of excitable units [Invited]	11:20 A.A. Andreev (Russia) and Z. Lech. Generation and detection of super-strong magnetic fields by ultra-intense laser pulses [Invited]	11:30 C. Guan (China) and D. Zhu. Numerical investigations of wave-induced mixing in upper ocean layer [Invited]
	S. Morfu, M. Bordet, M. Rossé, and J.M. Bilbault (France). Impact of perturbations on neuron response [Invited]	11:40 Ph. Korneev (Russia), E.d'Humieres, V.Tikhonchuk, and T. Pisarczyk. Laser-plasma magnetization for laboratory astrophysics [Invited]	12:00 I. Kamenkovich (USA), M. Rudko, and I. Rypina. Dynamics and transport characteristics of zonally elongated transients in the ocean [Invited]
	12:30 M. Courbage (France), L. Mangin, and F. Rozi. Respiratory neural network: activity, connectivity and synchronization [Invited]	12:00 I.F. Shaikhislamov (Russia), Yu.P. Zakharov, V.G. Posukh, A.V. Melekhov, and A.G. Ponomarenko. Collisionless super-Alfvénic interaction and generation of large amplitude pre-shock magnetosonic wave in laser plasma experiment [Invited]	12:30 J. Li (China), A.L. Kohout, H.H. Shen, and C. Guan. Effect of nonlinear wave-wave interaction on apparent wave attenuation in ice covered seas
	13:00 O.V. Maslennikov (Russia), I. Franović, and V.I. Nekorkin. Mean-field model for a network of globally coupled stochastic map-based neurons	12:20 S. Sakata (Japan), S. Lee, H. Sawada, Y. Iwasa, H. Morita, K. Matsuo, K.F.F. Law, T. Johzaki, H. Nagatomo, Y. Sentoku, A. Sunahara, A. Yao, Y. Arikawa, M. Hata, S. Kojima, Y. Abe, H. Kishimoto, K. Kanbayashi, A. Yogo, A. Morace, H. Sakagami, T. Ozaki, K. Yamanoi, T. Norimatsu, T. Shimizu, Y. Nakata, J. Kawanaka, S. Tokita, N. Miyanaga, M. Murakami, M. Nakai, H. Shiraga, H. Nishimura, K. Mima, H. Azechi, and S. Fujioka. First experimental demonstration of isochoric heating of a dense plasma core with assistance of external kilo-Tesla magnetic field [Invited]	13:00 S.V. Shagalov (Russia) and G.V. Rybushkina. Weakly supercritical dynamics of Rossby wave packets in barotropically unstable zonal JET flows
		12:40 Q. Moreno (France), M.E. Dieckmann, X. Ribeyre, S. Jequier, V.T Tikhonchuk, L. Gremillet, and E. d'Humières. PIC simulations for the study of collisionless shocks formation in laboratory astrophysics context [Invited]	
		13:00 V.M. Gubchenko (Russia). On kinetic approach to magnetic reconnection: from space to laser HED plasma [Invited]	

Nonlinear Dynamics and Complexity	Lasers with High Peak and High Average Power	Nonlinear Phenomena in the Atmosphere and Ocean
HALL B	HALL A	HALL C
Complex dynamics	Laser sources: extending limits	Climate dynamics – 2
<p><b>8:30</b>  <b>X. Leoncini</b> (<i>France</i>).  <b>Dynamics of systems with many degrees of freedom from long range-interactions to complex networks</b> [Invited]                      In this talk I will discuss the dynamics of systems with many degrees of freedom. We first will consider some results obtained in the case of long-range interacting systems with Hamiltonian dynamics. Starting from these we shall see how some of the properties can be transferred to the dynamics on networks, either on regular lattices or more complex networks.</p>	<p><b>8:30</b>  <b>I.E. Kozhevator</b> (<i>Russia</i>), D.E. Silin, A.V. Pigasin, E.H. Kulikova, and S.B. Speransky.  <b>Design and specifications of 630-mm phase shifting interferometer for the qualification of large aperture optics</b>                      A specialized phase shifting interferometer for qualification of large optics for extremely high-power laser systems has been designed and tested at IAP RAS. The interferometer will be used to assess homogeneity of blank material as well as in-process inspection information and final inspection qualification data. The 630 mm system is one of the largest Fizeau phase shifting interferometers ever manufactured in Russia. The interferometer has a high lateral resolution, but the most notable feature of this device is its high absolute precision. In this presentation we consider vibration and distortion control of interferometer optical elements and optical transfer function optimization. We also address the effects in the test cavity arising from measuring transmitted and reflected wavefronts of optics mounted at various angles, including the Brewster's angles.</p>	<p><b>8:30</b>  <b>A.A. Tsonis</b> (<i>USA</i>) and S. Kravtsov.  <b>Insights into decadal climate variability from the synchronization of a network of major climate modes</b> [Invited]                      We apply ideas from the theory of synchronized chaos to analyze a network of a few major climate indices and show evidence of major climate regime shifts that accompany, and perhaps even define, the observed and simulated decadal climate variability. We also detect differences in the dynamical structure of this variability between the models and observations, which can eventually help understand the current limitations of climate models and guide their further development.</p>
<p><b>9:00</b>  <b>I. Franović</b> (<i>Serbia</i>) and V.V. Klinshov.  <b>Mean-field analysis of stability and slow rate fluctuations in a network of noisy neurons with coupling delay</b> [Invited]                      We analyze the emergence of slow rate fluctuations and rate oscillations in random neuronal networks influenced by external and internal noise, as well as coupling delay. The second-order stochastic mean-field model is derived to examine (i) network's stability and bifurcations in the thermodynamic limit and (ii) fluctuations associated to finite-size effects. Regarding (i), external and internal noise are found to affect macroscopic dynamics in a fundamentally different fashion. Considering (ii), we demonstrate that slow rate fluctuations between two quasi-stationary states may be understood as noise-driven transitions in a double-well potential, whereas delay-noise interplay can yield fluctuations involving two oscillatory regimes.</p>	<p><b>8:50</b>  <b>A. Kudryashov</b> (<i>Russia</i>), V. Samarkin, A. Aleksandrov, G. Borsoni, T. Jitsuno, and J. Sheldakova.  <b>Large bimorph flexible mirror for Peta-Watt laser beam correction</b> [Invited]                      Two types of large bimorph deformable mirrors with the size of 410×468 mm and 320 mm were developed and tested. The results of the measurements of the response functions of all the actuators and of the surface shape of the deformable mirror are presented in this paper. The possibility of correction of the aberrations in high power lasers was demonstrated experimentally (to get Strehl number up to 0.7) and numerically.</p>	<p><b>9:00</b>  <b>N.A. Diansky</b> (<i>Russia</i>), I.V. Solomonova, A.V. Gusev, and T.Yu. Vyruchalkina.  <b>Effects of the North Atlantic thermohaline circulation on climate variability and Arctic climate change projections based on the combined scenario</b> [Invited]                      The combined scenario of climate change assessment is proposed based on the composition of “greenhouse” and “cyclic” effects. The forecast of atmospheric characteristics was made for 2010–2071 using the CORE datasets for 1948–2009. The prognostic run was made with the OGCM INMOM on reproducing thermohaline circulation and sea ice in the Atlantic and Arctic Oceans for 1948–2071. The interconnections were investigated amongst climate processes of the North Atlantic and Arctic.</p>
<p><b>9:30</b>  <b>V.V. Klinshov</b> (<i>Russia</i>), D.S. Shchapin, S. Yanchuk, and V.I. Nekorkin.  <b>Multi-jittering regimes in networks with pulse delayed coupling</b>                      We report a novel type of the dynamics in oscillatory networks with pulse delayed coupling. In such networks the regular low-periodic oscillations may destabilize giving birth to the higher-</p>	<p><b>9:10</b>  <b>E.A. Mironov</b> (<i>Russia</i>) and O.V. Palashov.  <b>Thermo-optical characteristics of uniaxial crystals</b>                      Thermally induced distortions of laser radiation caused by the photoelastic effect during high-power beam propagation through optical elements cut along the optical axis of uniaxial crystals have been investigated. The optical anisotropy parameter <math>\xi</math> and thermo-</p>	<p><b>9:30</b>  <b>A. Gritsun</b> (<i>Russia</i>) and V. Lucarini.  <b>Instability characteristics of blocking regimes in a simple quasi-geostrophic atmospheric model</b> [Invited]                      In this paper we study statistics and instability characteristics of blocking events in the three layer quasi-geostrophic model of atmosphere by Marshall and Molteni. It is shown that the model is</p>

<p><b>12:00</b> S. Morfu, M. Bordet, M. Rossé, and <b>J.M. Bilbault</b> (<i>France</i>). <b>Impact of perturbations on neuron response</b> [Invited] We propose an overview of the effects of deterministic and stochastic perturbations on the response of a neuron. Our study is based on numerical simulations and experiments with an elementary neural circuit. We use different excitations to highlight various phenomena such as Mode locking, Vibrational Resonance, Ghost Stochastic Resonance... We close the study with a lattice of coupled circuit.</p>	<p><b>11:40</b> <b>Ph. Korneev</b> (<i>Russia</i>), E. d’Humieres, V. Tikhonchuk, and T. Pisarczyk. <b>Laser-plasma magnetization for laboratory astrophysics</b> [Invited] Spontaneous plasma magnetization is a common process in laser-plasma interaction. The magnetic field amplitudes depend on laser intensity, and may reach kilotesla and even higher level in relativistic regime. One of the most interesting features of these fields is that they can be “frozen” inside the laser-generated plasmas, hot, low collisional, or even relativistic and collisionless. This property makes such plasmas very attractive for studies of astrophysical-related laboratory studies. Here, we present some possibilities to facilitate the generation of the magnetized collisionless plasmas with controllable magnetization.</p>	<p><b>12:00</b> <b>I. Kamenkovich</b> (<i>USA</i>), M. Rudko, and I. Rypina. <b>Dynamics and transport characteristics of zonally elongated transients in the ocean</b> [Invited] Oceanic flows with mesoscale eddies (length scale of 10–100 km) contain zonally-elongated large-scale transients (ZELTs) that can be detected in pressure anomalies as a spectral peak corresponding to long zonal and short meridional length scales, or as leading Empirical Orthogonal Functions. These patterns are generated and maintained by transient nonlinear forcing, associated with mesoscale eddies, and are, therefore, nonlinear phenomena. ZELTs play a key role in anisotropic material transport and in large-scale tracer distributions.</p>
<p><b>12:30</b> <b>M. Courbage</b> (<i>France</i>), L. Mangin, and F. Rozi. <b>Respiratory neural network: activity, connectivity and synchronization</b> [Invited] Chaos in the rhythmic activity is a major issue that has been discussed in many studies of neuro-science and physiology, and especially in the respiratory air flow. Here, we present the results of two studies concerning the activity and the connectivity of the respiratory neural network in healthy humans and patients with obstructive lung disease. Our results show an increase in the dynamic chaos of airway flow in patients, focusing on expiratory flow.</p>	<p><b>12:00</b> <b>I.F. Shaikhislamov</b> (<i>Russia</i>), Yu.P. Zakharov, V.G. Posukh, A.V. Melekhov, and A.G. Ponomarenko. <b>Collisionless super-Alfvénic interaction and generation of large amplitude pre-shock magnetosonic wave in laser plasma experiment</b> [Invited] We report the experiment on generation of strong super-Alfvénic magnetosonic perturbation by laser-produced plasma expanding in magnetized background under conditions when the magnetic cavity size reaches the ion gyroradius. Detailed measurements of plasma density and velocity, electric and magnetic fields are presented which demonstrate strong magnetic compression at the front and cavity dynamics, laser plasma deceleration and formation, with record efficiency of energy transfer 25%, of strong non-linear magnetosonic wave propagating through background plasma.</p>	<p><b>12:30</b> <b>J. Li</b> (<i>China</i>), A.L. Kohout, H.H. Shen, and C. Guan. <b>Effect of nonlinear wave-wave interaction on apparent wave attenuation in ice covered seas</b> Studies of wave propagation in ice covered seas have become increasingly more important due to the rapid reduction of sea ice in the Arctic Ocean. However, in some cases, it is still problematic to interpret the behaviors of measured apparent wave attenuation only with current wave-ice models. Inspired by previous speculation, the effect of nonlinear four-wave interactions on apparent wave damping during a field observation in marginal Antarctic is tested with discrete interaction approximation. The results show that the nonlinear wave-wave interaction does offset wave damping during stormy cases and for short waves in ice covered waters.</p>
<p><b>13:00</b> <b>O.V. Maslennikov</b> (<i>Russia</i>), I. Franović, and V.I. Nekorkin. <b>Mean-field model for a network of globally coupled stochastic map-based neurons</b> We analyze the emergent regimes and the stimulus-response relationship of a population of stochastic spiking neurons modeled by discrete-time systems by means of a mean-field (MF) model, derived within the framework of cumulant approach complemented by the Gaussian closure hypothesis. It is demonstrated that the MF model can qualitatively account for stability and bifurcations of the exact system, capturing all the generic forms of collective behavior, including macroscopic excitability, subthreshold oscillations, periodic or chaotic spiking, and chaotic bursting dynamics. Apart from qualitative analogies, we find a substantial quantitative agreement between the exact and the approximate system, as reflected in matching of the parameter domains admitting the different dynamical regimes, as well as the characteristic properties of the associated time series. The effective model is further shown to reproduce with sufficient accuracy the phase response curves of the exact system and the assembly’s response to external stimulation of finite amplitude and duration.</p>	<p><b>12:20</b> <b>S. Sakata</b> (<i>Japan</i>), S. Lee, H. Sawada, Y. Iwasa, H. Morita, K. Matsuo, K.F.F. Law, T. Johzaki, H. Nagatomo, Y. Sentoku, A. Sunahara, A. Yao, Y. Arikawa, M. Hata, S. Kojima, Y. Abe, H. Kishimoto, K. Kanbayashi, A. Yogo, A. Morace, H. Sakagami, T. Ozaki, K. Yamanoi, T. Norimatsu, T. Shimizu, Y. Nakata, J. Kawanaka, S. Tokita, N. Miyanaga, M. Murakami, M. Nakai, H. Shiraga, H. Nishimura, K. Mima, H. Azechi, and S. Fujioka. <b>First experimental demonstration of isochoric heating of a dense plasma core with assistance of external kilo-Tesla magnetic field</b> [Invited] We have demonstrated efficient heating of a compressed plasma by relativistic electron beams produced by LFEX laser with the assistance of external magnetic field. Emission from Cu tracer atoms contained in the compressed plasma was measured to infer the plasma temperature and the energy coupling efficiency from heating laser to core plasma. Li-like and He-like emission lines, which appeared only with assistance of the external magnetic field, suggest that the electron temperature was ~1.7 keV and density ~ 6 g/cc.</p>	<p><b>13:00</b> <b>S.V. Shagalov</b> (<i>Russia</i>) and G.V. Rybushkina. <b>Weakly supercritical dynamics of Rossby wave packets in barotropically unstable zonal JET flows</b> This study explores the supercritical dynamics of Rossby wave packets comprised of unstable barotropic and baroclinic normal modes feeding on the common critical layers (CL) of a stratified barotropically unstable zonal jet flow. Nonlinear generation mechanisms of slowly modulated wave-trains and CL potential vorticity patterns are examined for the regimes of weakly nonlinear and strongly nonlinear dissipative CL.</p>

**SEECCM 2017** 4th South-East European Conference on Computational Mechanics  
ECCOMAS Special Interest Conference  
3-5 July 2017 Kragujevac, Serbia



# ***SEECCM 2017***

**4<sup>th</sup> South-East European Conference  
on Computational Mechanics**

**03-04 July, Kragujevac, Serbia**

# Organizers



СРПСКО ДРУШТВО ЗА РАЧУНСКУ МЕХАНИКУ  
SERBIAN SOCIETY FOR COMPUTATIONAL MECHANICS

**Serbian Society for Computational Mechanics**



**Bioengineering Research and  
Development Center BioIRC**



**European Community on  
Computational Methods in  
Applied Sciences ECCOMAS**



**Department of  
Technical Sciences  
Serbian Academy of  
Sciences and Arts**



**Faculty of  
Engineering  
University of  
Kragujevac**



**Ministry of  
Education, Science  
and Technological  
Development of  
Republic of Serbia**

**ISBN: 978-86-921243-0-3**

**Session T.1 - 09:00-09:40**  
**Computational Biology**  
**Chair: Marko Živanović**

- T.1.1** - *Mean-Field Approximation of Two Coupled Populations of Excitable Units Modeled by FitzHugh-Nagumo Elements*  
Kristina Todorović, Igor Franović, Nebojša Vasović, Srđan Kostić
- T.1.2** - *microRNA Based Methodology for Early Cancer Detection*  
Marko Živanović, Danijela Cvetković, Nenad Filipović
- T.1.3** - *Computer Driven Bioavailability Analysis of Some Important Compounds Found in Anticancer Herbs*  
Draško Tomić, Miroslav Puškarić, Zlatan Car
- T.1.4** - *Modification of Polysaccharides with Phenols for Hydrogels Formation and Electrospinning*  
Nikolina Popović, Olga Prodanović, Ivana Gađanski, Danijela Cvetković, Marko Živanović, Vladimir Pavlović, Nenad Filipović, Radivoje Prodanović

**Session T.2 - 09:40-10:30**  
**Computational Chemistry (part I)**  
**Chair: Dejan Milenković**

- T.2.1** - *Theoretical Investigation of Antioxidative Activity of Caffeic Acid*  
Izudin Redžepović, Svetlana Marković, Jelena Tošović
- T.2.2** - *QSAR Analysis of Antioxidant Properties of Polyphenols by OH-Related Molecular Descriptors*  
Nenad Raos, Ante Miličević
- T.2.3** - *Antioxidant Activity of the Carboxylate Anions of the Selected Dihydroxybenzoic Acids*  
Jelena Đorović, Svetlana Jeremić, Edina Avdović, Ana Amić, Jasmina M. Dimitrić Marković
- T.2.4** - *Thermodynamics of  $2H^+/2e^-$  Free Radical Scavenging Mechanisms of 3-(4-Hydroxy-3-Methoxyphenyl)Propanoic Acid*  
Ana Amić, Zoran Marković, Jasmina Dimitrić Marković, Svetlana Jeremić, Bono Lučić, Dragan Amić

10:30 - 11:00	Keynote speaker: <b>“Computational Modeling of Long Bone Microstructure and Ultrasonic Evaluation of the Fracture Healing Process”</b> <b>Prof. Dimitrios Fotiadis</b> <i>University of Ioannina, Greece</i>
11:00 - 11:30	Coffee Break
11:30 - 12:00	Keynote speaker: <b>“Theoretical Study of Primary Antioxidant Action Thermodynamics”</b> <b>Prof. Erik Klein</b> <i>Slovak Technical University, Slovakia</i>

calculation show that modern design has better clinical behavior due to lower chronic outward force, better superplastic behavior and higher radial resistive strength. In the paper was comparison results between two stent designs, old design and modern design obtained by optimizing old stent designs.

**M.4.9 - Computational Fluid Dynamics (CFD) Modeling of the Fluid Flow Through Porous Structures - Varun Sharma**

Open cell metallic foam hydrodynamics were studied using computational fluid dynamics (CFD) in view of thermal engineering applications with a major focus on the heat exchanger. Very latest Voronoi tessellation 3D effects based techniques were used for foam creation as well as for the computational domain. Latest analytical formulas were also discussed covering the recent development. For CFD modelling, steady state incompressible laminar flow model was investigated. Finite difference methods based on commercial pre and post processing software was used for iteration solving. Three different inlet velocities 2 m/s, 4 m/s, 6 m/s were chosen to pass through the pore channel. The sole purpose of the investigation was to observe the velocity regime effects under different rate, pressure exertion on the strut length, pressure drop and geometrical influence on the dynamics behavior. Due to highly chaotic behavior, CFD helps us in understanding of the inner pore field. Results showed that with the increase in velocity there is an upsurge in pressure drop under different inlet flow rate. The geometrical parameter is mainly responsible for the fluid behavior.

**Session T.1 - 09:00-09:40  
Computational Biology**

**Chair: Marko Živanović**

**T.1.1 - Mean-Field Approximation of Two Coupled Populations of Excitable Units Modeled by FitzHugh-Nagumo Elements - Kristina Todorović, Igor Franović, Nebojša Vasović, Srđan Kostić**

In this study, the focus lies with the two delay-coupled populations of identical excitable units modeled by the Fitzhugh-Nagumo elements. The analysis on stability and bifurcations in the macroscopic dynamics exhibited by the system of two coupled large populations comprised of  $N$  stochastic excitable units each is performed by studying an approximate system, obtained by replacing each population with the corresponding mean-field model. The aim is to demonstrate that the bifurcations affecting the stability of the stationary state of the original system, governed by a set of  $4N$  stochastic delay-differential equations for the microscopic dynamics, can accurately be

reproduced by a flow containing just four deterministic delay-differential equations which describe the evolution of the mean-field based variables. We show how analytically tractable bifurcations occurring in the approximate model can be used to identify the characteristic mechanisms by which the stationary state is destabilized under different system configurations, like those with symmetrical inter-population couplings.

**T.1.2 - microRNA Based Methodology for Early Cancer Detection - Marko Živanović, Danijela Cvetković, Nenad Filipović**

Nowadays, cancer is increasingly widespread disease. Early diagnosis is very important because it increases the survival rate of patients and if cancer is detected in early stage a complete healing is not negligible. In these circumstances, cancer is becoming a chronic disease. Speaking of detection, numerous tumor markers are followed, including the growing use of detection microRNA. Our methodology is based on precise, fast, accurate and inexpensive detection of microRNAs as tumor markers. We chose the establishment of the methodology for determining the microRNA-21, which can be considered a breast cancer marker.

**T.1.3 - Computer Driven Bioavailability Analysis of Some Important Compounds Found in Anticancer Herbs - Draško Tomić, Miroslav Puškarić, Zlatan Car**

There is a mounting evidence that some herbs can slow down the spread of cancer, and in some cases even cure it. In the Eastern medicines like Chinese and Ayurveda, and in the South America, the evidence for this is present for centuries. Western medicine is slow in adopting this evidence. There are several reasons for that, among them the lack of clinical trials, the chemical complexity of anti-cancer herbs consisting of dozens of compounds like polyphenols, tannins, saponins, quinones etc., and the concern about the safety of their use. In opposite to in-vivo clinical trials, a large number of in-vitro experiments with anti-cancer herbs was performed, showing us that these herbs alone, or in the combination with other herbs, can effectively kill various types of cancer cells. Other experiments have shown that these herbs can enhance the effectiveness of chemotherapy and lessen the side effects of it and the radiotherapy. Moreover, mouse model experiments proved the toxicity of most anti-cancer herbs is below the dosage required for the effective cancer-killing dose. However, in-vivo animal experiments are not so convincing, and in most cases, reasons for that is the poor bioavailability of the herbal compound that fights cancer. Especially in the case when a certain compound is poorly soluble in water, it can hardly reach cancer cells within the body. In vitro and in vivo experiments are costly, last a while, and results are highly dependent on the experimental environment. Besides, there are important ethical questions when using animals in such experiments. For these reasons, we decided to perform the computer driven water solubility analysis of



# **Proceedings**

**The 6th International Congress  
of Serbian Society of Mechanics**

**Tara, June 19-21, 2017**

**Edited by:**

**Mihailo Lazarević  
Damir Madjarević  
Ines Grozdanović  
Nemanja Zorić  
Aleksandar Tomović**

## **The 6th International Congress of Serbian Society of Mechanics**

### **Editors:**

Mihailo P. Lazarević

Damir Madjarević

Ines Grozdanović

Nemanja Zorić

Aleksandar Tomović

### **Circulation**

120 copies

### **Published by**

Serbian Society of Mechanics and

Faculty of Mechanical Engineering,

University of Belgrade, Belgrade

### **Printed by**

Djurdjevdan, Arandjelovac

CIP- Каталогизacija u publikaciji  
Народна библиотека Србије

531/534(082)(0.034.2)

SRPSKO društvo za mehaniku. Međunarodni kongres (6 ; 2017 ; Tara)

Proceedings [Elektronski izvor] / The 6th International Congress of Serbian Society of Mechanics, Tara, June 19-21, 2017 ; edited by Mihailo P. Lazarević ... [et al.]. - Belgrade : Serbian Society of Mechanics : Faculty of Mechanical Engineering, University, 2017 (Arandelovac : Đurđevdan).

- 1 USB fleš memorija ; 9 x 5 cm (u obliku kartice)

Sistemske zahteve: Nisu navedeni. - Nasl. sa naslovne strane dokumenta. - Tiraž 120. - Bibliografija uz svaki rad.

ISBN 978-86-909973-6-7

a) Механика - Зборници

COBISS.SR-ID 237139468

## **M3 Bionengineering**

**M3\_1** *Chair: Miloš Kojić*

*Co-Chair: Miljan Milošević*

M3a: Kristina Todorović, I. Franović, N. Vasović, S. Kostić  
SPONTANEOUS FORMATION OF SYNCHRONIZATION CLUSTERS IN  
NEURONAL POPULATIONS INDUCED BY NOISE AND INTERACTION  
DELAYS

M3b: Miloš Kojić, Miljan Milosević, Vladimir Simić  
CONVECTION–DIFFUSION TRANSPORT MODEL USING COMPOSITE  
SMEARED FINITE ELEMENT

M3c: Andjelka N. Hedrih, Katica (Stevanović) Hedrih  
RESONANCE AS POTENTIAL MECHANISM FOR HOMOLOG  
CHROMOSOMES SEPARATION THROUGH BIOMECHANICAL  
OSCILLATORY MODEL OF MITOTIC SPINDLE

M3d: Miljan Milosević, Milos Kojić, Vladimir Simić  
FIELD OF CORRECTION FACTORS FOR SMEARED FINITE ELEMENT

**M3\_2** *Chair: Nenad Filipović*

*Co-Chair: Velibor Isailović*

M3e: Milica M. Nikolić, Nenad D. Filipović  
APPLICATION OF DPD METHOD ON MODELLING SEMICIRCULAR  
CANALS

M3f: Velibor Isailović, Igor Saveljić, Dalibor Nikolić, Zarko Milosević, Dusan  
Pavlović, Nenad D. Filipović  
EYE TRACKING ALGORITHM AND COMPUTATIONAL MODELING IN  
PREDICTION OF BENIGN PAROXYSMAL POSITIONAL VERTIGO DISEASE

M3g: Nenad Filipović, Velibor Isailović, Žarko Milosević, Dalibor Nikolić, Igor  
Saveljić, Milica Nikolić, Bojana Ćirković-Andjelković, Nikola Jagić, Exarchos  
Themis, Dimitris Fotiadis, Gualtiero Pelosi, Oberdan Parodi  
COMPUTATIONAL MODELING FOR PLAQUE PROGRESSION AND  
FRACTIONAL FLOW RESERVE IN THE CORONARY ARTERIES

Venturi nozzle (Reynolds number in the throat of Venturi vary from  $2.8 \cdot 10^4$  to  $4.2 \cdot 10^4$ ) are presented in the paper. The analysis of two-phase flow in a Venturi nozzle was performed, with a focus on the movement of a vapor phase in a fluid domain. The resulting flow parameters enable determination of the cavitation number and loss coefficient in the nozzle. The results were compared to the relevant experimental results.

M2i: Jela M. Burazer

### NUMERICAL RESEARCH OF ENERGY SEPARATION IN A CYLINDER WAKE

Energy separation is a spontaneous energy redistribution within a fluid flow. As a consequence, there are places with higher and lower values of total temperature in the fluid flow. It is characteristic for many flow geometries. This paper deals with the energy separation in a cylinder wake. Two flow conditions are being considered. In the first one, the velocity in the wake is only deformed, while in the second one a turbulent vortex street is formed and vortices are detaching from the cylinder. Two different solvers from the open source package OpenFOAM are used in order to capture the phenomenon of energy separation. One of these solvers is modified for the purpose of calculation in a particular case of the vortex street flow. The energy equation based on the internal energy present in this solver is replaced by the energy equation written in the form of a total enthalpy. The other solver has been previously tested in the vortex tube flow, and can also capture the energy separation in the wake of the cylinder. In both cylinder wake flow conditions, a two-dimensional computational domain is assumed. The standard k- $\epsilon$  model is used for computations. It is proved that OpenFOAM is capable of capturing the energy separation phenomenon in a proper way in both of the wake flow cases. Good agreement between the experimental results and the ones from computations is obtained in the case of the velocity deformation in the wake flow. Previous research findings are also confirmed in the case of vortex street flow.

## M3 Bionengineering

M3a: Kristina Todorović, I. Franović, N. Vasović, S. Kostić

### SPONTANEOUS FORMATION OF SYNCHRONIZATION CLUSTERS IN NEURONAL POPULATIONS INDUCED BY NOISE AND INTERACTION DELAYS

The spontaneous onset of cluster states is of particular interest to neuroscience [1] for the conjectured role in information encoding, as well as for participating in motor coordination or accompanying some neurological disorders. We explore a new mechanism which rests on the excitable character of neuronal dynamics and mutual adjustment between noise and time delay to yield the self-organization into functional modules within an otherwise unstructured network. The spontaneous formation of clusters of synchronized spiking in a structureless ensemble of equal stochastically perturbed excitable neurons with delayed coupling is demonstrated for the first time in our study [2]. The effect is a consequence of a subtle interplay between interaction delays, noise, and the excitable character of a single neuron.



# **XXXVI Dynamics Days Europe**

Book of Abstracts

**6-10 June Corfu 2016**

## OC.032.Activation process in systems of excitable units with multiple noise sources

10 June 10:00-12:30 (Parallel 4), Session: Chaos/Pattern Formation

We consider the activation process in cases of a single and two interacting units [1], as well as the assembly of class II excitable units [2] influenced by two independent sources of noise, which may be interpreted as external and internal noise. For all three analyzed systems, we determine the most probable activation paths around which the corresponding stochastic trajectories are clustered.

In case of a single unit, the theoretically most important point lies in introducing the terminating boundary set relevant for class II excitability, which can immediately be generalized to scenarios involving two coupled units. We examine how the properties of the activation process depend on the particular type of noise, as well as the linear or nonlinear character of interactions [1].

In case of an assembly, we first apply the mean-field approach to explicitly show that the assembly of excitable units can itself exhibit macroscopic excitable behavior. In order to allow for the comparison between the excitable dynamics of a single unit and an assembly, three distinct formulations of the assembly activation event are introduced. Each formulation treats different aspects of the relevant phenomena, including the threshold-like behavior and the role of coherence of individual spikes [2]. The activation processes of individual units are analyzed in light of the competition between the noise-led and the relaxation-driven dynamics.

We also consider how the statistical features of the activation process, such as the mean time-to-first pulse and the associated coefficient of variation, are influenced by the coaction of two noise sources. An intriguing fact is that the statistical features turn out to be qualitatively analogous for all three formulations of the assembly activation event, whereby these further resemble the results for a single and two interacting units. We demonstrate that such a universal behavior generically derives from the fact that the considered systems undergo a stochastic bifurcation from the stochastically stable fixed point to continuous oscillations [1,2].

[1] Igor Franović, Kristina Todorović, Matjaž Perc, Nebojša Vasović, and Nikola Burić, "Activation process in excitable systems with multiple noise sources: One and two interacting units", *Physical Review E* **92**, 062911 (2015).

[2] Igor Franović, Matjaž Perc, Kristina Todorović, Srdjan Kostić, and Nikola Burić, "Activation process in excitable systems with multiple noise sources: Large number of units", *Physical Review E* **92**, 062912 (2015).

Igor Franović

Scientific Computing Laboratory, Institute of Physics Belgrade, University of Belgrade, Pregrevica 118, 11080 Belgrade  
franovic@ipb.ac.rs

Matjaž Perc

Faculty of Natural Sciences and Mathematics, University of Maribor, Koroška Cesta 160, SI-2000 Maribor, Slovenia  
matjaz.perc@uni-mb.si

Kristina Todorović

Department of Physics and Mathematics, Faculty of Pharmacy, University of Belgrade, Vojvode Stepe 450, 11221 Belgrade, Serbia  
kisi@pharmacy.bg.ac.rs

# XIX Symposium on Condensed Matter Physics



Conference Program

7–11 September 2015  
Belgrade, Serbia



Wednesday, 9 September 2015, Hall 2, 1<sup>st</sup> floor

Surface, Interface and Low-dimensional Physics – Graphene, Nanotubes, Quantum Dots and Contacts, 2D Magnetism (Part II)

**Session Chair: Bosiljka Tadić**

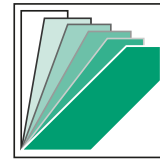
9:00-9:25	<b>Ivanka Milošević</b>	Potential of Helically Coiled Carbon Nanotubes for Sensing Applications
9:25-9:50	<b>Zoran Mišković</b>	Modeling Graphene Interactions with Electrolyte
9:50-10:15	<b>Emmanuele Cappelluti</b>	Strain Engineering in Two-Dimensional Transition-Metal Dichalcogenides
10:15-10:40	<b>Mihajlo Vanević</b>	Electron and Electron-hole Wave Functions in a Driven Quantum Contact
10:40-10:52	<b>Sonja Predin</b>	The Effect of the Trigonal Warping on the Energy and the Entanglement Spectrum of Graphene Bilayers

**Coffee Break**

Statistical Physics of Complex Systems

**Session Chair: Igor Kulić**

11:10-11:35	<b>Leonardo Golubović</b>	Classical and Statistical Mechanics of Celestial Scale Strings: Rotating Space Elevators
11:35-12:00	<b>Bosiljka Tadić</b>	Structure of Noise in Complex Systems Revealed by Multifractal and Graph-Theory Techniques
12:00-12:25	<b>Milan Rajković</b>	Quantifying Self-organization and Complexity in Complex Systems
12:25-12:50	<b>Marija Mitrović Dankulov</b>	Quantitative Study and Modeling of Collective Knowledge Building via Questions and Answers
12:50-13:02	<b>Igor Franović</b>	Mean-field Dynamics of Systems of Delay-coupled Noisy Excitable Units
14:30-20:00	<b>Conference Excursion to Viminacium.</b> The buses depart from Studentski trg (see the map)	



# XXXIV Dynamics Days Europe

8-12 September 2014, University of Bayreuth, Germany

## Book of Abstracts



## Control and Synchronization

CT5.1

Tuesday 17:45 - 19:45, Room H19

### Controlling synchrony in oscillatory networks via act-and-wait algorithm

CT5.1-1

*Kestutis Pyragas and Irmantas Ratas*

### Control of synchronization bistability in oscillatory networks

CT5.1-2

*Irmantas Ratas and Kestutis Pyragas*

### Cross-frequency synchronization of delay-coupled oscillators

CT5.1-3

*Vladimir Klinshov*

### Mean-field treatment of collective motion in systems of delay-coupled stochastic excitable units

CT5.1-4

*Igor Franovic, Kristina Todorovic, Nebojsa Vasovic, and Nikola Buric*

### Dynamically emergent explosive synchronization

CT5.1-5

*Vanesa Avalos-Gaytan, Juan Almendral, and Stefano Boccaletti*

### Robust synchronization analysis by quadratic phase equation

CT5.1-6

*Wataru Kurebayashi, Sho Shirasaka, and Hiroya Nakao*

### Controlling synchrony in oscillatory networks via act-and-wait algorithm

CT5.1-1

*Kestutis Pyragas and Irmantas Ratas*

17:45

Center for Physical Sciences and Technology, A. Gostauto 11, LT-01108 Vilnius, Lithuania  
email: pyragas@pfi.lt

The act-and-wait control algorithm is proposed to suppress synchrony in globally coupled oscillatory networks in the situation when the simultaneous registration and stimulation of the system is not possible. The algorithm involves the periodic repetition of the registration (wait) and stimulation (act) stages, such that in the first stage the mean field of the free system is recorded in a memory and in the second stage the system is stimulated with the recorded signal. A modified version of the algorithm that takes into account the charge-balanced requirement is considered as well. The efficiency of our algorithm is demonstrated analytically and numerically for globally coupled Landau-Stuart oscillators, and synaptically all-to-all coupled FitzHugh-Nagumo as well as Hodgkin-Huxley neurons.

**CT5.1-4 Mean-field treatment of collective motion in systems of delay-coupled stochastic excitable units**  
18:45

Igor Franovic<sup>1</sup>, Kristina Todorovic<sup>2</sup>, Nebojsa Vasovic<sup>3</sup>, and Nikola Buric<sup>1</sup>

<sup>1</sup>Scientific Computing Laboratory, Institute of Physics Beograd-Zemun, Belgrade, Serbia

<sup>2</sup>Department of Physics and Mathematics, Faculty of Pharmacy, University of Belgrade, Belgrade, Serbia

<sup>3</sup>Department of Applied Mathematics, Faculty of Mining and Geology, University of Belgrade, Belgrade, Serbia

email: franovic@ipb.ac.rs

Excitability is a dynamical feature shared by the systems poised close to a bifurcation leading from the stationary state toward the sustained oscillatory motion. Excitable units may generate small or large-amplitude excitations in response to perturbation, showing strong sensitivity to stimulus magnitude within a narrow range of relevant values. Modeling the dynamics of systems of excitable units typically requires one to consider the effects of different forms of noise, which in general act as excitability amplifiers, and further involves the explicit introduction of interaction delays, that may account for the finite signal conduction velocities and/or latency in the unit's responses.

We focus on assemblies made up of type II excitable units represented by the canonical Fitzhugh-Nagumo model, whereby each unit is influenced by the local noise and interaction delays. In mathematical terms, the assembly dynamics is described by a large system of stochastic delay-differential equations (SDDEs). Synchronization between the units' activities may give rise to collective mode/modes, whose onset conforms to the scenario of stochastic bifurcation where the global variables undergo transition from the stochastically stable fixed point to the stochastically stable limit cycle.

Given that the analysis on stability and bifurcations exhibited by the large systems of SDDEs cannot be carried out analytically, we derive the approximate mean-field (MF) model which qualitatively accounts for the stochastic stability of the exact system, as well as the scenarios for the onset and the suppression of the collective mode. In quantitative terms, the MF model can capture the frequency of the induced oscillations. The MF model is based on two relevant approximations, referred to as the Gaussian approximation (GA) and the quasi-independence approximation (QIA) [1]. On one hand, we demonstrate that the given approximations are not universal, in a sense that their precise formulation and the fashion in which their validity is verified have to be adapted to the essential properties of the underlying class of systems, here mainly reflected in the relaxation character of oscillations. On the other hand, it is shown that the noise-induced bistability in the MF model's dynamics may indicate in a self-consistent fashion the parameter domains where the QIA, and therefore the MF model as a whole breaks down. We also point to a scenario where the global bifurcation exhibited by the MF model can be used to predict the onset of the cluster states [2].

It is further made explicit how the application of the MF model may be extended to hierarchical networks made up of populations of excitable units [3]. Taking as an example the case of two populations where the nonlinear coupling function involves the global variables, we confirm the validity of the paradigm by which the approximate system should be built by replacing each population by the appropriate MF model.

[1] I. Franović, K. Todorović, N. Vasović and N. Burić, *Phys. Rev. E* **89** 022926 (2014).

[2] I. Franović, K. Todorović, N. Vasović and N. Burić, *Phys. Rev. Lett.* **108** 094101 (2012).

[3] I. Franović, K. Todorović, N. Vasović and N. Burić, *Phys. Rev. E* **87** 012922 (2013).

Giorgio Lollino  
Daniele Giordan  
Giovanni B. Crosta  
Jordi Corominas  
Rafiq Azzam  
Janusz Wasowski  
Nicola Sciarra *Editors*



# Engineering Geology for Society and Territory – Volume 2

Landslide Processes



 Springer

---

Engineering Geology for Society  
and Territory – Volume 2

---

Giorgio Lollino • Daniele Giordan  
Giovanni B. Crosta  
Jordi Corominas • Rafiq Azzam  
Janusz Wasowski • Nicola Sciarra  
Editors

# Engineering Geology for Society and Territory – Volume 2

Landslide Processes

*Editors*

Giorgio Lollino  
Daniele Giordan  
Institute for Geo-Hydrological Protection  
National Research Council (CNR)  
Turin  
Italy

Rafiq Azzam  
Department of Engineering Geology  
and Hydrogeology  
RWTH Aachen University  
Aachen  
Germany

Giovanni B. Crosta  
Department of Earth and Environmental Science  
University of Milan Bicocca  
Milan  
Italy

Janusz Wasowski  
Institute for Geo-Hydrological Protection  
National Research Council (CNR)  
Bari  
Italy

Jordi Corominas  
Department of Geotechnical Engineering  
and Geosciences  
Universitat Politècnica de Catalunya  
Barcelona  
Spain

Nicola Sciarra  
University G. D'Annunzi Chieti Pescara  
Chieti  
Italy

ISBN 978-3-319-09056-6      ISBN 978-3-319-09057-3 (eBook)  
DOI 10.1007/978-3-319-09057-3  
Springer Cham Heidelberg New York Dordrecht London

Library of Congress Control Number: 2014946956

© Springer International Publishing Switzerland 2015

This work is subject to copyright. All rights are reserved by the Publisher, whether the whole or part of the material is concerned, specifically the rights of translation, reprinting, reuse of illustrations, recitation, broadcasting, reproduction on microfilms or in any other physical way, and transmission or information storage and retrieval, electronic adaptation, computer software, or by similar or dissimilar methodology now known or hereafter developed. Exempted from this legal reservation are brief excerpts in connection with reviews or scholarly analysis or material supplied specifically for the purpose of being entered and executed on a computer system, for exclusive use by the purchaser of the work. Duplication of this publication or parts thereof is permitted only under the provisions of the Copyright Law of the Publisher's location, in its current version, and permission for use must always be obtained from Springer. Permissions for use may be obtained through RightsLink at the Copyright Clearance Center. Violations are liable to prosecution under the respective Copyright Law.

The use of general descriptive names, registered names, trademarks, service marks, etc. in this publication does not imply, even in the absence of a specific statement, that such names are exempt from the relevant protective laws and regulations and therefore free for general use.

While the advice and information in this book are believed to be true and accurate at the date of publication, neither the authors nor the editors nor the publisher can accept any legal responsibility for any errors or omissions that may be made. The publisher makes no warranty, express or implied, with respect to the material contained herein.

*Cover illustration:* Landslide affecting the hill of Ruinas, Oristano, Italy. On February, 2005, the phenomenon invaded the road path and caused difficulties to the traffic. During the emergency, to ensure safety of the road traffic, a particular monitoring and early warning system was deployed. *Photo:* Daniele Giordan.

Printed on acid-free paper

Springer is part of Springer Science+Business Media (www.springer.com)



<b>232</b>	<b>GPS Monitoring of the Scopello (Sicily, Italy) DGSD Phenomenon: Relationships Between Surficial and Deep-Seated Morphodynamics . . . . .</b>	<b>1321</b>
	Valerio Agnesi, Edoardo Rotigliano, Umberto Tammaro, Chiara Cappadonia, Christian Conoscenti, Francesco Obrizzo, Cipriano Di Maggio, Dario Luzio, and Folco Pingue	
<b>233</b>	<b>Ganderberg Landslide Characterization Through Monitoring . . . . .</b>	<b>1327</b>
	Giulia Bossi, Simone Frigerio, Matteo Mantovani, Gianluca Marcato, Luca Schenato, and Alessandro Pasuto	
<b>234</b>	<b>Real-Time Monitoring of Deep-Seated Gravitational Slope Deformation in the Taiwan Mountain Belt . . . . .</b>	<b>1333</b>
	Rou-Fei Chen, Ya-Ju Hsu, Shui-Beih Yu, Kuo-Jen Chang, Ruo-Ying Wu, Yu-Chung Hsieh, and Ching-Wee Lin	
<b>235</b>	<b>Long-Term Continuous Monitoring of a Deep-Seated Compound Rock Slide in the Northern Apennines (Italy) . . . . .</b>	<b>1337</b>
	Alessandro Corsini, Francesco Bonacini, Marco Mulas, Marcello Petitta, Francesco Ronchetti, and Giovanni Truffelli	
<b>Part XX</b>	<b>Mathematical-Numerical Modelling Approaches for Slope Stability Analyses</b>	
<b>236</b>	<b>Use Accelerogram of Real Earthquakes in the Evaluation of the Stress-Strain State of Landslide Slopes in Seismically Active Regions of Ukraine . . . . .</b>	<b>1343</b>
	O. Trofymchuk, I. Kaliukh, K. Silchenko, V. Polevetskiy, V. Berchun, and T. Kalyukh	
<b>237</b>	<b>Reconstruction of the Geotechnical Model Considering Random Parameters Distributions . . . . .</b>	<b>1347</b>
	Calista Monia, Pasculli Antonio and Sciarra Nicola	
<b>238</b>	<b>Complex Dynamics of Landslides with Time Delay Under External Seismic Triggering Effect. . . . .</b>	<b>1353</b>
	Srđan Kostić, Nebojša Vasović, Dragutin Jevremović, Duško Sunarić, Igor Franović, and Kristina Todorović	
<b>239</b>	<b>Artificial Neural Networks and Kriging Method for Slope Geomechanical Characterization . . . . .</b>	<b>1357</b>
	Romina Secci, M. Laura Foddis, Alessandro Mazzella, Augusto Montisci, and Gabriele Uras	
<b>240</b>	<b>Comparative Study of System Reliability Analysis Methods for Soil Slope Stability. . . . .</b>	<b>1363</b>
	Xiao Liu, D.V. Griffiths, and Hui-ming Tang	
<b>241</b>	<b>Simplification of the Stratigraphic Profile in Geotechnical Models of Landslides: An Analysis Through a Stochastic Approach . . . . .</b>	<b>1367</b>
	G. Bossi, L. Borgatti, G. Marcato, and G. Gottardi	

Srđan Kostić, Nebojša Vasović, Dragutin Jevremović,  
Duško Sunarić, Igor Franović, and Kristina Todorović

---

## Abstract

In present paper, model of infinite creeping slope with Dieterich-Ruina rate-and state-dependent friction law is analyzed using methods of nonlinear dynamics. The model is examined under the variation of two parameters: time delay  $t_d$  and initial shear stress  $s_0$ . Time delay describes the memory effect of the sliding surface and it is generally considered as a function of history of sliding. Initial stress parameter is periodically perturbed, corresponding to long duration shear seismic wave, or it could be generated by non-natural sources such as traffic vibrations. The co-action of the observed parameters is estimated for two different regimes of sliding, namely  $\beta < 1$  and  $\beta > 1$ , where  $\beta$  denotes the ratio of long-term to short-term (immediate) stress change. The results of the analysis indicate that the most complex dynamics occurs for  $\beta < 1$ , when a possible Ruelle-Takens-Newhouse route to chaos is observed, with a transition from equilibrium state, through periodic and quasiperiodic motion to deterministic chaos. For  $\beta > 1$ , system exhibits chaotic dynamics for  $t_d = 0.1$  and for  $\delta_s \leq 0.18$ . These results correspond well with the previous experimental observations on clay and siltstone with low clay fraction, indicating that the motion along the sliding surface is velocity-strengthening ( $\beta < 1$ ).

---

## Keywords

Landslides • Friction law • Time delay • Perturbation • Deterministic chaos

---

## 238.1 Introduction

The common analysis of slope stability uses a simple static Coulomb failure criterion, where shear strength depends on the cohesion  $c$  and the angle of internal friction  $\varphi$  (Labuz and Zang 2012). However, this failure model alone does not explain the time-dependent nature of the failure threshold and it holds only for  $V = 0$ . This temporal dependence of friction along a rough sliding surface was firstly observed in rock mass, and it is well described by Dieterich-Ruina rate-and state-dependent friction law (Dieterich 1979; Ruina 1983). Besides these experiments for dry rock joints, Skempton (1985) observed similar behavior of clays in ring shear tests, for much slower sliding rate comparing to the results obtained for the Burridge-Knopoff earthquake model

---

S. Kostić (✉) · N. Vasović · D. Jevremović  
Faculty of Mining and Geology, University of Belgrade, Belgrade,  
Serbia  
e-mail: srdjan.kostic@rgf.bg.ac.rs

D. Sunarić  
Institute for the Development of Water Resources “Jaroslav  
Čermi”, Belgrade, Serbia

I. Franović  
Institute of Physics, University of Belgrade, Belgrade, Serbia

K. Todorović  
Faculty of Pharmacy, University of Belgrade, Belgrade, Serbia

(Carlson and Langer 1989; Erickson et al. 2008). Following these results, Chau (1995) suggested that Dieterich-Ruina friction law with one state variable can be used to model landslides that occur in natural infinite slope along a plane of weak surface, such as a persistent rock joint, a rock joint filled with wet gouge or a soil interface. In present paper, we follow the work of Chau (1995) and investigate the impact of time delay and periodic stress perturbation on landslide dynamics. Time delay describes the memory effect along the sliding surface, which is the feature already pointed out for tectonic faults (Scholz 1998). By assuming the analogy between the landslide faults and tectonic faults (Fleming and Johnson 1989; Gomberg et al. 1995), it is plausible that the time delay is also inherent for the friction coefficient along the sliding surface. On the other hand, the perturbation of initial shear stress could correspond to long duration seismic wave or it could be generated by non-natural sources such as traffic vibrations (Gomberg et al. 1995).

### 238.2 Background of the Original Model

According to Chau (1995), a motion of the single block on an inclined slope could be described by the system of three coupled nonlinear first-order differential equations:

$$\begin{aligned} \frac{dV}{dt} &= g \sin\alpha - \frac{\tau}{\rho h} \\ \frac{d\tau}{dt} &= \frac{d\theta}{dt} + \frac{A}{V} \frac{dV}{dt} \\ \frac{du}{dt} &= V \end{aligned} \tag{238.1}$$

where  $g$  is gravitational constant,  $\alpha$  is the slope angle,  $\rho$  is the mass density,  $\theta$  is state variable,  $h$  is the thickness of the overlying soil,  $\tau$  is the shear strength along the sliding surface,  $V$  and  $u$  are the velocity and displacement of the block, respectively, while  $A$  represents material constant. By introducing the appropriate nondimensional quantities, model (238.1) could be expressed in the following form:

$$\begin{aligned} \frac{ds}{dT} &= -\lambda e^v [s - s_0 - (1 - \beta)v] + \frac{e^{-v}}{\kappa} (\gamma - s) \\ \frac{dv}{dT} &= \frac{e^{-v}}{\kappa} (\gamma - s) \\ \frac{d\delta}{dT} &= e^v \end{aligned} \tag{238.2}$$

where  $s = \tau/A$  (dimensionless stress),  $v = \ln(V/V_0)$  (dimensionless velocity),  $\delta = u/h$  (dimensionless displacement),  $T = V_0 t/h$  (dimensionless time),  $s_0 = \tau_0/A$ ,  $\kappa = \rho V_0^2/A$ ,  $\gamma = \rho g h s \sin\alpha/A$ ,  $\beta = B/A$ ,  $\lambda = h/L$  and  $\theta = \tau - \tau_0 - A \ln(V/V_0)$ . Parameter  $\beta$  represents the key parameter for further

analysis, as a rate of friction stress variation with the change in sliding velocity.

### 238.3 Numerical Analysis

In present analysis, we incorporate time delay  $t_d$  in model (238.2):

$$\begin{aligned} \frac{ds}{dT} &= -\lambda e^v [s(t - t_d) - s_0 - (1 - \beta)v] + \frac{e^{-v}}{\kappa} (\gamma - s) \\ \frac{dv}{dT} &= \frac{e^{-v}}{\kappa} (\gamma - s) \\ \frac{d\delta}{dT} &= e^v \end{aligned} \tag{238.3}$$

where meaning of all terms is the same as in (238.2). Time delay  $t_d$  is introduced only in the shear stress term, since the additional time delays (in other observed parameters) would make the system more stiff in numerical sense, and, thus, it would be harder to capture the main dynamical features. In this way, we also model the impact of the second state variable, introduced previously in the work of Chau (1999).

Moreover, we assume periodic perturbations of the initial shear stress  $s_0$  in the subsequent form:

$$s_0(t) = s_0 + \delta_s \sin(\omega_s t) \tag{238.4}$$

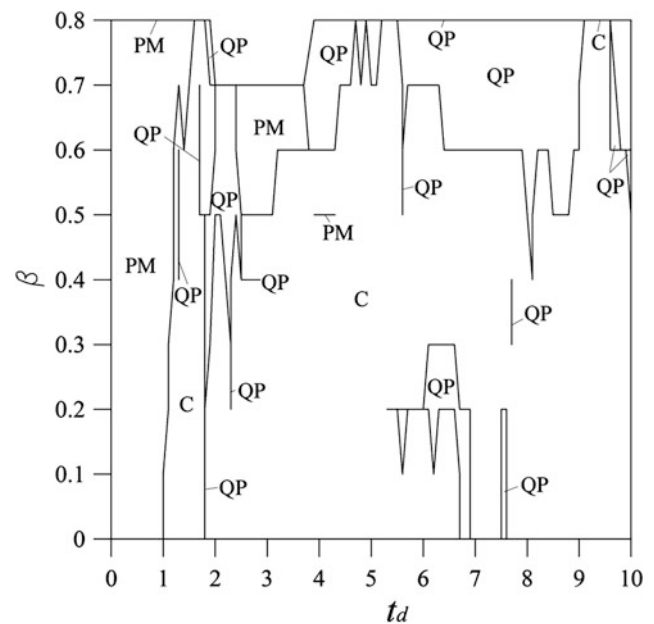


**Fig. 238.1** Parameter domains ( $t_d, \beta$ ) admitting periodic motion (PM), quasiperiodic motion (QP) and deterministic chaos (C), under the variation of  $s_0$ , with  $\delta_s = 0.5$  and  $\omega_s = 0.5$ . Other parameter values are:  $s_0 = 1.0$ ,  $\lambda = 1.5$ ,  $\kappa = 2.0$  and  $\gamma = 1.0$ . Diagram is constructed for step size equal 0.1 for both  $t_d$  and  $\beta$

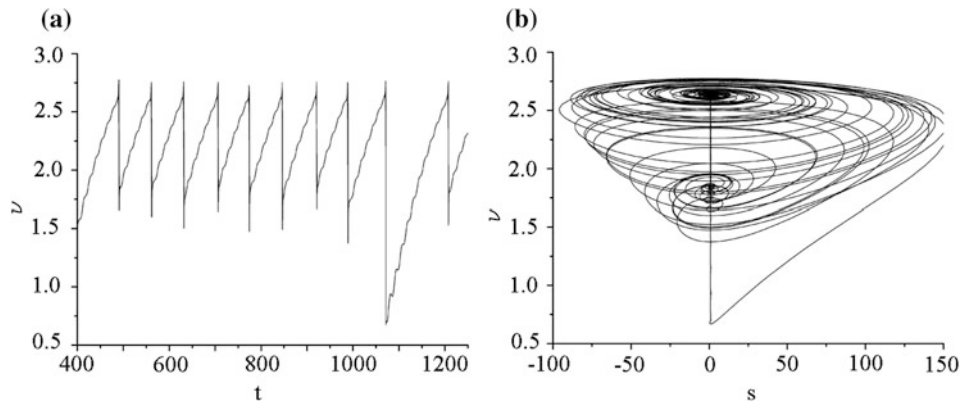


**Fig. 238.2** Time series  $v(t)$  and phase portrait for  $\beta = 1.1$ ,  $t_d = 0.1$ ,  $\delta_s = 0.15$  and  $\omega_s = 0.5$ . Other parameter values are:  $s_0 = 1.0$ ,  $\lambda = 1.5$ ,  $\kappa = 2.0$  and  $\gamma = 1.0$

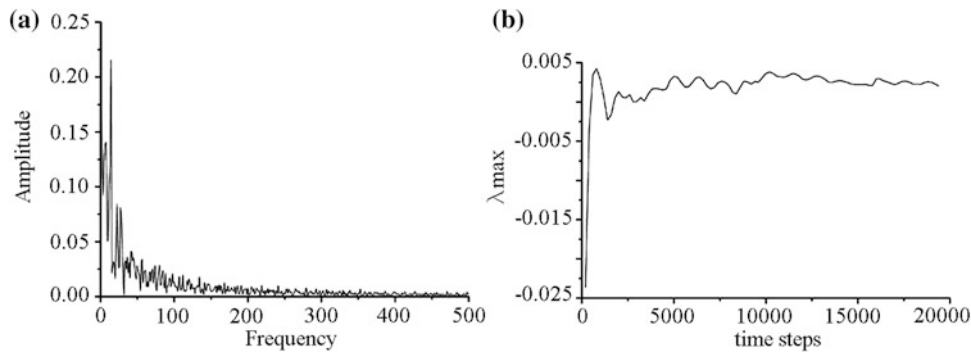


**Fig. 238.3** **a** Continuous broadband noise in Fourier power spectrum confirms chaotic motion of block. **b** Maximal Lyapunov exponent, calculated by using the Wolf’s method (Wolf et al., 1985), converges well to positive value,  $\lambda_{max} = 0.002$

such that  $\delta_s$  and  $\omega_s$  represent the constant oscillation amplitude and the angular frequency, respectively. The former satisfy the constraint  $\delta_s \leq s_0$ , which ensures the model’s consistency as it confines each perturbation term to an appropriate range of values. Equilibrium point for the system (238.3) is obtained by assuming that  $ds/dT = dv/dT = 0$ , while  $d\delta/dT = const$ . Hence, the parameter values at the equilibrium point must satisfy the following conditions:

$$s = \gamma, \quad v = \frac{\gamma - s_0}{1 - \beta}, \quad \delta = e^{\gamma t} \tag{238.5}$$

In present analysis, the initial conditions  $(s, v, \delta)$  are set near the equilibrium point. Regarding the fashion in which the delay-differential equations are numerically solved, the initial function is selected such that its values within the interval  $[-t_d, 0]$  are set by the first equation in (238.3) with  $\lambda = 0$ . The results

of the performed analysis for  $\delta_s = 0.5$  and  $\omega_s = 0.5$  are shown in Fig. 238.1 for  $\beta < 1$  and for  $t_d$  in range  $[0.1-10]$ .

For  $\beta = 1$ , if we take that  $\delta_s = 0.06$ , while the other parameter values are as in Fig. 238.1, the introduction of time delay  $t_d$  slows down the block, and for  $t_d = 0.4$ , the block’s velocity becomes negative (upward motion). Similar behavior is observed for other amplitude values in the range  $[0, 1]$ . As for  $\beta > 1$ , system (238.3) exhibits chaotic dynamics for  $t_d = 0.1$ , if the perturbation amplitude is  $\delta_s \leq 0.18$  (Fig. 238.2), while for  $\delta_s > 0.18$ , block’s velocity is changing periodically in negative domain. Deterministic chaos is further corroborated by broadband noise in Fourier power spectrum and by positive asymptotic value of maximal Lyapunov exponent (Fig. 238.3).

The positive value of maximal Lyapunov exponent is further confirmed by using the method of Rosenstein et al. (1993), shown in Fig. 238.4.

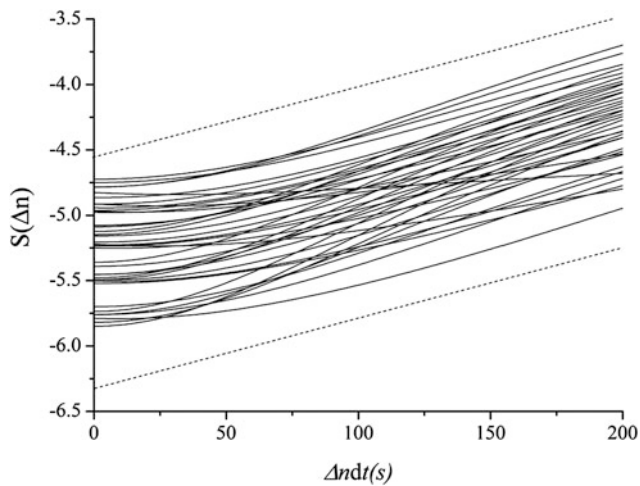


**Fig. 238.4** Maximal Lyapunov exponent for  $v(t)$  in Fig. 238.2a, using the method of Rosenstein et al. (1993).  $S(\Delta n)$  represents the average of the logarithm of the distance of all nearby trajectories to the reference trajectory as a function of the relative time  $\Delta n$ . The results are determined for 1,000 reference points and neighboring distance  $\varepsilon = 0.005\text{--}0.015$ . The obtained value of maximal Lyapunov exponent ( $\lambda_{\max} \approx 0.005$ ) is of the same order of magnitude, as in Fig. 238.3b

### 238.4 Conclusion

The performed analysis showed that the most complex dynamics of motion along the slope is observed for  $\beta < 1$  ( $A - B > 0$ ), meaning that the slip surface is velocity strengthening, which is observed in laboratory conditions for clay and siltstone with low clay fraction (Skempton 1985). In comparison to the original model (238.1), our analysis shows that the instability of motion along the slope could occur even for  $\beta < 1$  with introduced time delay, while Chau (1995) observed the appearance of instable motion only for  $\beta > 1$ , which is, as already stated, the case that is not detected

in laboratory conditions (Skempton 1985). Interesting result is the dual effect of time delay  $t_d$  on the motion of the block, which can render the complex dynamics, and, on the other hand, stabilize the motion of the block, depending on the value of the control parameter  $\beta$ .

**Acknowledgments** This research has been supported by Ministry of Education, Science and Technological development of the Republic of Serbia, Contracts No. 176016, 171015 and 171017.

### References

- Carlson JM, Langer JS (1989) Mechanical model of an earthquake fault. *Phys Rev A* 40:6470–6484
- Chau KT (1995) Landslides modeled as bifurcations of creeping slopes with nonlinear friction law. *Int J Solids Struct* 32:3451–3464
- Chau KT (1999) Onset of natural terrain landslides modeled by linear stability analysis of creeping slopes with a two-state variable friction law. *Int J Numer Anal Methods* 23:1835–1855
- Dieterich JH (1979) Modeling of rock friction—1. Experimental results and constitutive equations. *J Geophys Res* 84:2161–2168
- Erickson B, Birnir B, Lavallee D (2008) A model for aperiodicity in earthquakes. *Nonlinear Proc Geophys* 15:1–12
- Fleming RW, Johnson AM (1989) Structures associated with strike-slip faults that bound landslide elements. *Eng Geol* 27:39–114
- Gomberg J, Bodin P, Savage W, Jackson ME (1995) Landslide faults and tectonic faults, Analogs?—the slumgullion earthflow, Colorado. *Geology* 23:41–44
- Labuz J, Zang A (2012) Mohr-Coulomb failure criterion. *Rock Mech Rock Eng* 45(6):975–979
- Rosenstein MT, Collins JJ, De Luca CJ (1993) A practical method for calculating largest Lyapunov exponents from small data sets. *Physica D* 65:117–134
- Ruina A (1983) Slip instability and state variable friction laws. *J Geophys Res* 88(10):359–370
- Scholz C (1998) Earthquakes and friction laws. *Nature* 391:37–42
- Skempton AW (1985) Residual strength of clays in landslides, folded strata and the laboratory. *Geotechnique* 35:3–18
- Wolf A, Swift J, Swinney H, Vastano J (1985) Determining Lyapunov exponents from a time series. *Physica D* 16:285–317

# Nonlinear Dynamics at the Free University Berlin



## Organization

[Welcome](#)  
[Map & Directions](#)  
[Links](#)  
[Imprint](#)

## Activities

[Publications](#)  
[Projects](#)  
[Cooperations](#)  
[Lectures, Seminars, Conferences](#)  
[Theses](#)  
[Handbook of Dyn. Syst.](#)

## Research Group Nonlinear Dynamics

[Prof. Dr. B. Fiedler](#)

[Prof. Dr. A. Azouani](#)

[Dr. J.-Y. Dai](#)

[PD Dr. S. Liescher](#)

[A. López](#)

[I. González](#)

[Dr. I. Schneider](#)

[Dr. H. Stuke](#)

[Y. Tokuta](#)

[N. Vassena](#)

[PD Dr. Martin Vath](#)

[Former Members](#)

## Research Group Hysteresis Dynamics

[PD Dr. P. Gurevich](#)

[M. Curran](#)

[A. Güngör](#)

Summer 2017

## Oberseminar Nonlinear Dynamics

### Organizers

- [Matthias Wolfrum](#) (WIAS Berlin)
- [Bernold Fiedler](#) (FU Berlin)

### Program

	<p>Juliana Pimentel (UFABC, Brazil)</p>	<p>Permutation characterization for slowly non-dissipative equations.</p>
Apr 25, 2017	<p>We study the longtime behavior of slowly non-dissipative scalar reaction-diffusion equations. By extending known results, we are able to obtain a complete decomposition of the non-compact global attractor and still manage to determine the heteroclinic connections based on the Sturm permutation method.</p> <p><b>Please note that the seminar takes place at 3:15 p.m. at WIAS Berlin, Mohrenstr 39, in Erhard-Schmidt lecture room, 10117 Berlin.</b> Tea/coffee will be at 2:45 p.m. at WIAS as well.</p>	
May 2, 2017	Cancelled	
May 9, 2017	Cancelled	
	<p>Hannes Stuke (Freie Universität Berlin)</p>	<p>Parabolic blow-up in complex time.</p>
May 16, 2017	<p>In my talk I will give an overview of my research on parabolic differential equations and blow-up. Blow-up denotes the phenomenon, when solutions diverge to infinity. By considering complex time we try to establish a connection between two opposed worlds: on the one hand bounded solutions, in particular equilibria and heteroclinic orbits and on the other hand blow-up in equations with entire nonlinearities.</p> <p><b>Please note that the seminar takes place at 3:15 p.m. at WIAS Berlin, Mohrenstr 39, in Erhard-Schmidt lecture room, 10117 Berlin.</b> Tea/coffee will be at 2:45 p.m. at WIAS as well.</p>	
	<p>Pavel Gurevich (Freie Universität Berlin)</p>	<p>A short introduction to machine learning:</p>

		towards (un)certainty quantification.
May 23, 2017	<p>Machine learning is a rapidly developing field that deals with searching for and generating patterns in data. It is nowadays a very broad field encompassing many tasks and methods. In my talk, I will give a short overview, rapidly narrowing my focus towards a particular topic, namely, neural networks and their ability not only to find patterns but also quantify how certain they are in doing so. If time permits, I will conclude with a discussion of our joint work with Hannes Stuke on certainty quantification.</p> <p><b>Please note that the seminar takes place at 3:15 p.m. at WIAS Berlin, Mohrenstr 39, in Erhard-Schmidt lecture room, 10117 Berlin.</b> Tea/coffee will be at 2:45 p.m. at WIAS as well.</p>	
	<p>Phillipo Lappicy (Freie Universität Berlin)</p>	Einstein constraints: a dynamical approach.
May 30, 2017	<p>The Einstein constraint equations describe the space of initial data for the evolution equations, dictating how space should curve within spacetime. Under certain assumptions, the constraints reduce to a scalar quasilinear parabolic equation on the sphere, and nonlinearity being the prescribed scalar curvature of space. We focus on self-similar solutions of Schwarzschild type, which describe the space of initial data of certain black holes, for example.</p> <p>The first main result gives a detailed study of the axially symmetric solutions, since the domain is now one dimensional and nodal properties can be used to describe certain asymptotics of the rescaled self-similar solutions. Such asymptotics describe the possible metrics arising at an event horizon of a black hole, depending on the metric inside the horizon. Those are described by Sturm attractors. In particular, we compute an example for a prescribed scalar curvature.</p> <p>The second main result states a symmetrization property of certain metrics in the event horizon, namely, how the symmetry of the spherical domain can influence the symmetry of solutions.</p> <p><b>Please note that the seminar takes place at 3:15 p.m. in the lecture room 3.13, Hausvogteiplatz 11 A. Please wait at the doorkeeper's Mohrenstrasse 39 (usual location) to get access to the other building.</b></p>	
June 6, 2017	Cancelled	
June 13, 2017	Cancelled	
June 20, 2017	Cancelled	
	<p>Igor Franović (Institute of Physics Belgrade, University of Belgrade)</p>	Bistability, rate oscillations and slow rate fluctuations in networks of noisy neurons with coupling delay

June 27, 2017	<p>Spontaneous activity of cortical neurons is typically characterized as a doubly-stochastic process, underlying two distinct forms of variability. While the local spike-train variability is reflected on the fast timescale, the variability associated with much longer timescales involves macroscopic irregular fluctuations of the firing rate. The latter fluctuations apparently emerge by coherent switching of neurons between the “up” and “down” states of membrane potential, and are believed to play important functional roles. In order to gain qualitative insight into the mechanisms behind such switching phenomena, we consider a random network of rate-based neurons influenced by external and internal noise, as well as the coupling delay. The network behavior is analyzed by deriving the second-order stochastic mean-field model, which describes the network dynamics in terms of the mean-rate and the associated variance. The mean-field model is used to study the stability and bifurcations in the thermodynamic limit, as well as the fluctuations due to the finite-size effect. For the thermodynamic limit, it is established that (i) the network may exhibit coexistence between two stationary levels in a wide range of parameters, whereby the two types of noise affect the levels in a fundamentally different fashion, and (ii) coupling delay may give rise to oscillations of the mean-rate. The slow rate fluctuations are demonstrated to emerge via two distinct scenarios. In the delay-free case, the leading mechanism can be seen as noise-induced transitions between two metastable states, quite reminiscent to fluctuations of a particle in a double-well potential. In the second scenario, which involves the cooperative action of noise and delay, the fluctuations can be interpreted as stochastic mixing between two different oscillatory regimes.</p> <p><b>Please note that the seminar takes place at 3:15 p.m. at WIAS Berlin, Mohrenstr 39, in Erhard-Schmidt lecture room, 10117 Berlin.</b> Tea/coffee will be at 2:45 p.m. at WIAS as well.</p>	
July 4, 2017	<p>Augusto Visintin (Università di Trento)</p> <p><a href="#">Abstract</a></p> <p><b>Please note that the seminar takes place at 3:15 p.m. at WIAS Berlin, Mohrenstr 39, in Erhard-Schmidt lecture room, 10117 Berlin.</b> Tea/coffee will be at 2:45 p.m. at WIAS as well.</p>	<p>Compactness and structural stability of nonlinear flows</p>
July 11, 2017	Cancelled	
July 18, 2017	<p>Jia-Yuan Dai (Freie Universität Berlin)</p> <p>We prove the existence of spiral waves for the complex Ginzburg-Landau equation in the circular and spherical geometries. Instead of applying the shooting method from the literature, we establish a functional approach and adopt global bifurcation analysis to solve the spiral wave elliptic equation. Moreover, we prove the existence of two new patterns: frozen spirals in the circular and spherical geometries and spiral-pairs, that is, spirals with two tips, in the spherical geometry.</p> <p><b>Please note that the seminar takes place at 3:15 p.m. at WIAS Berlin, Mohrenstr 39, in Erhard-Schmidt lecture room, 10117 Berlin.</b> Tea/coffee will be at 2:45 p.m. at WIAS as well.</p>	<p>Spiral Waves in Circular and Spherical Geometries. The Ginzburg-Landau Paradigm</p>



Matthias Wolfrum <wolfrum@wias-berlin.de>

5/3/16 ☆



to me ▾

Dear Igor,

I am looking forward to your visit to Berlin next week. I will be on Monday at WIAS around 9:30.

Do you like to present a talk? we could organize a seminar, if send us a title and abstract in advance.

Regards,

Matthias

---

Igor Franovic <igor.franovic@gmail.com>

📎 5/5/16 ☆



to Matthias ▾

Dear Matthias,

I am also looking forward to my visit to WIAS. Thank you very much for inviting me to hold the seminar. My talk will be entitled "**Mean-field approach for analysis of collective dynamics and activation processes in coupled noisy excitable systems**". As far as the date for the seminar is concerned, any date apart from Monday will be fine. Please let me know whether it will be an hour-long seminar or a shorter one, so that I can adapt the presentation. The abstract of the talk is attached with this letter.

I will come to WIAS on Monday at 9:30, as you have indicated.

Best regards,

Igor

Dear Professor Geier,

thank you very much for the invitation. I will be able to come to the Institute at Adlershof on Thursday at 11. Naturally, I could prepare a small presentation of say 15-20 minutes, just to go over some recent results. Please let me know if that would be sufficient.

I am looking forward to meeting you in Berlin.

Best regards,  
Igor Franović

On 08 Feb 2015 14:02, [alsg@physik.hu-berlin.de](mailto:alsg@physik.hu-berlin.de) wrote:

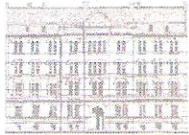
Dear Igor,

I will be have teaching at tuesday and Wednesday. Best day for a meeting would be Thursday.

In case you could come to the Institute of Physics at Berlin-Adlershof at 11 am, you could give a small presentation ??

Please respond,

L. Schimansky-Geier



1839.  
2013.

Универзитет у Београду  
ФИЗИЧКИ ФАКУЛТЕТ

додељује  
Годишњу награду за научни рад



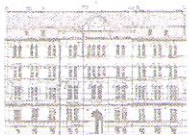
младом истраживачу

*Игору Франовићу*

10. октобар 2013.



Декан Физичког факулета  
Проф. др Јаблан Дојчиловић



1839.  
2013.

University of Belgrade  
FACULTY OF PHYSICS

## AWARDS

### The Annual Prize for Scientific Research



*Igor Franović*  
*Research Assistant*

October 10, 2013



Dean of the Faculty of Physics  
Professor Jablan Dojčilović



SEARCH



MENU

[Home](#) > [Journals](#) > [Chaos, Solitons & Fractals](#) > [Editorial Board](#)[Submit Your Paper](#) [View Articles](#)[Guide for Authors](#) [Abstracting/ Indexing](#)[Track Your Paper](#) [Order Journal](#)[Journal Metrics](#)CiteScore: **1.55** i[More about CiteScore](#)Impact Factor: **1.455** i5-Year Impact Factor: **1.604**iSource Normalized Impact  
per Paper (SNIP): **0.856** iSCImago Journal Rank  
(SJR): **0.530** i [View More on Journal  
Insights](#)[Your Research Data](#)

# Chaos, Solitons & Fractals - Editorial Board

## Co-Editors-in-Chief

### Stefano Boccaletti

Ist. dei Sistemi Complessi, National Research  
Council of Italy (CNR), via Madonna del Piano,  
10, 50019, Florence, Italy



### Maurice Courbage

Theory of Complex Systems, Université Paris  
Diderot (Paris 7), Paris 7, Paris, France



## Special Issue Editor

### Paolo Grigolini

University of North Texas, Denton, Texas, USA



## Editors

Ravindra Amritkar



- Share your research data
- Visualize your data
- Data in Brief co-submission

### Related Links

- Author Stats i
- Researcher Academy
- Author Services
- Try out personalized alert features

### Related Publications

Communications in  
Nonlinear Science and  
Numerical Simulation

Physical Research Laboratory, Ahmedabad, India  
Synchronization Complex networks; Time series analysis;  
Characterization of chaos (fractal dimension,  $f-\alpha$  etc.);  
Extreme events; Nonlinear dynamics in dissipative systems  
and applications

### Christian Beck

Queen Mary, University of London (QMUL),  
London, UK

Dynamical systems; Statistical mechanics;  
Fractals and multifractals; Spatio-temporal  
chaos; Turbulence; Stochastic modelling; Complexity science



### Mauro Bologna

Universidad de Tarapacá, Arica, Chile  
Hydrodynamics; Mathematical physics;  
Fractional calculus; Lévy processes;  
Magnetohydrodynamics



### Mattia Frasca

University of Catania, Catania, Italy  
Control of complex systems; Engineering  
applications of chaos; Nonlinear dynamics and  
chaos; Coupled dynamical systems



### Stefano Galatolo

University of Pisa, Pisa, Italy  
Dynamical systems; Ergodic theory and  
statistical properties; Numerical methods;  
Algorithms



### Alexander E. Hramov

Yuri Gagarin State Technical University of Saratov, Saratov,  
Russian Federation

## Dong-Uk Hwang

National Institute for Materials Science  
(NIMS), Daejeon, The Republic of Korea



## Sarika Jalan

Indian Institute of Technology, Indore, India

## Stefano Lepri

National Research Council of Italy (CNR),  
Florence, Italy  
Nonlinear dynamics and Non-equilibrium  
processes in physics



## Boris Malomed

Tel Aviv University, Tel Aviv, Israel  
Nonlinear waves; nonlinear optics; solitons;  
Bose-Einstein condensates; pattern formation  
in dissipative media; nonlinear lattice dynamics



## Matjaž Perc

University of Maribor, Maribor, Slovenia  
Statistical physics; Complex systems;  
Evolutionary game theory; Cooperation;  
Network science; Data analysis; Cyclic  
dominance; Social systems; Stochastic processes



## Awadhesh Prasad

University of Delhi, Delhi, India  
Low dimensional systems; Forced systems;  
Coupled oscillators: synchronization and  
amplitude death



## Bernardo Spagnolo

University of Palermo, Palermo, Italy



Nonequilibrium Statistical Mechanics for Classical and Quantum Physical Systems, and Physics of Complex Systems in Interdisciplinary applications; Noise-induced phenomena in physical, biological and financial complex systems; Anomalous diffusion and Lévy flights; Transient dynamics in Josephson junctions; Spintronics

### Trong Tuong Truong

University of Cergy-Pontoise, Cergy-Pontoise Cedex, France

Integrable systems - Solitons; Inverse Problems for Imaging - Radon transforms; Quantum Theory - Anyons and anharmonic oscillators



### Sandro Vaienti

Centre de Physique Theorique, Marseille, France

Ergodic theory; Statistical properties of dynamical systems; Decay of correlations and limit theorems; Extreme value theory; Random dynamical systems



### Zhen Wang

Kyushu University, Fukuoka, Japan

Evolutionary game; Prey-predator dynamics; Disease spreading; Behavior epidemiology; Synchronization; Complex network (structure and dynamics); Social dynamics and online social network; System optimization and control; Metapopulation; Climate change research; Routing traffic; Traffic flow; Nonlinear and interdisciplinary physics





## Associate Editors

### Paolo Allegrini

Consiglio Nazionale delle Ricerche (CNR), Pisa,  
Italy

Non-equilibrium statistical mechanics; Linear  
response theory; Stochastic processes and  
modeling; Continuous-time random walks; Scaling; Time-  
series analysis; Applications to life and cognitive sciences



### Wael Bahsoun

Loughborough University, Loughborough, Leicestershire, UK

### Luis Barreira

Instituto Superior Técnico, Lisbon, Portugal

Differential equations; Dynamical systems; Ergodic theory

### Stelios Bekiros

European University Institute, Florence, Italy

Econometrics; Chaotic dynamics; Extreme value theory;  
Machine learning; Bayesian statistics; Wavelets; Kalman  
filtering; DSGE modeling; Behavioral economics; Monetary  
economics; Econophysics; Complex systems

### Ginestra Bianconi

Queen Mary, University of London (QMUL),  
London, UK

Statistical mechanics; Networks; Complex  
systems; Critical phenomena; Disordered  
systems; Inference problems; Spin models; Biological systems;  
Social networks



### Jean-Marie Bilbault

National Center for Scientific Research, Dijon, France

## Anna Carbone

Technical University of Turin, Torino, Italy



## Giuseppe Carbone

Technical University of Bari, Bari, Italy

## Regino Criado

Universidad Rey Juan Carlos, Madrid, Spain  
Complex networks structure and dynamics;  
Complex systems; Social networks; Graph  
theory



## Jorge Milhazes de Freitas

University of Porto, Porto, Portugal  
Ergodic Theory; Extreme Value Theory and applications to  
dynamical systems; Recurrence; Statistical and stochastic  
stability; Decay of correlations; Large deviations; Limiting  
laws; Point processes

## Alexander Dubkov

Lobachevsky State University of Nizhni  
Novgorod, Nizhni Novgorod, Russian  
Federation

Noise-induced phenomena in complex  
dynamical systems Non-equilibrium thermodynamics and  
fluctuation-dissipation relations Anomalous diffusion, Levy  
flights and Levy walks Turbulence, fractals and scaling



## Igor Franović

Center for the Study of Complex Systems, Institute of Physics  
Belgrade, Serbia

## Lucia Valentina Gambuzza

University of Catania, Catania, Italy

**Thomas Gilbert**

Université Libre de Bruxelles (ULB), Brussels, Belgium

**Alexander Kitaev**

Steklov Mathematical Institute, St. Petersburg, Russian Federation

Integrable systems; Ordinary differential equations and special functions

**Claudia Lainscsek**

The Salk Institute for Biological Studies, La Jolla, California, USA

**Xavier Leoncini**

Centre de Physique Theorique, Marseille, France

**Yongyao Li**

Foshan University, Foshan, China

**Sylvain Mangiarotti**

Centre d'Etudes Spatiales de la Biosphère (CESBIO), Toulouse, France; Institut de Recherche pour le Développement (IRD), Marseille, France

Theory of nonlinear dynamical systems and chaos modelling from observational data; Applications to environmental behaviors as observed in situ or from space, with a special focus on biosphere (vegetation, ecology, epidemiology) and hydrosphere (karstic springs, ground water, snow)

**Jan Nagler**

Max Planck Institut (MPI) für Dynamik und Selbstorganisation, Göttingen, Germany  
Stochastic systems, with applications at the interface between physics, biology, sociology



and economics, in particular phase transitions and tipping points, ergodicity breaking and estimation of risk in uncertain environments

### **Andrey Pankratov**

Russian Academy of Sciences, Nizhny  
Novgorod, Russian Federation  
Noise and fluctuations in dynamical systems  
and, in particular, in Josephson electronic  
devices



### **David Papo**

University of Lille 3, Lille, France

### **Paolo Paradisi**

National Research Council of Italy (CNR), Pisa, Italy

### **Tomaz Prosen**

University of Ljubljana, Ljubljana, Slovenia  
Quantum chaos; Many-body quantum dynamics; Open  
quantum systems; Non-equilibrium statistical mechanics and  
transport

### **Bruno Otávio Teixeira**

Universidade Federal de Minas Gerais (UFMG), Belo  
Horizonte, Brazil

### **Davide Valenti**

University of Palermo, Palermo, Italy  
Non-Equilibrium Statistical Mechanics in  
classic and quantum physical systems: -  
stochastic processes and noise induced effects  
in nonlinear systems;- Josephson junctions;- dynamics of  
quantum particles in bistable potentials;- models of  
Population Dynamics with applications to Complex Systems:  
spatio-temporal dynamics of phytoplankton in marine



environment; bacterial growth;- noise effects and stabilizing  
role of fluctuations (volatility) in financial markets  
(Econophysics)

**Claudia Valls**

University of Lisbon, Lisbon, Portugal  
ODEs; Hyperbolicity; Integrability

---

## Editorial Board Members

**Leonid Bunimovich**

Georgia Institute of Technology, Atlanta, Georgia, USA

**Bernard Cazelles**

Ecole Normale Supérieure de Paris, Paris, France

**Mario Chavez**

Hôpital de la Pitié-Salpêtrière, Paris, France

**Pierre Collet**

Centre de Physique Théorique, Palaiseau, France

**Jean-Louis Deneubourg**

Université Libre de Bruxelles (ULB), Bruxelles, Belgium

**Alain Destexhe**

National Center for Scientific Research, Gif-sur-Yvette, France

**Leone Fronzoni**

University of Pisa, Pisa, Italy

**Jesus Gomez-Gardeñes**

University of Zaragoza, Zaragoza, Spain

**Sergey Gonchenko**

Nizhny Novgorod State University, Nizhny Novgorod, Russian Federation

**Kostya Khanin**

University of Toronto, Toronto, Ontario, Canada

**Roberto Livi**

University of Florence, Sesto Fiorentino, Italy

**Francesco Mainardi**

University of Bologna, Bologna, Italy

**Yamir Moreno**

University of Zaragoza, Zaragoza, Spain

**Adilson E. Motter**

Northwestern University, Evanston, Illinois, USA

**Vladimir I. Nekorkin**

Russian Academy of Sciences, Novgorod, Russian Federation

**Francesco Pellicano**

Università di Modena e Reggio Emilia, Modena, Italy

**Yakov B. Pesin**

Pennsylvania State University, University Park, Pennsylvania, USA

**Mikhail Rabinovich**

University of California at San Diego (UCSD) Medical Center, San Diego, California, USA

**Linda Reichl**

University of Texas at Austin, Austin, Texas, USA

**Joerg Schmeling**

Lund University, Lund, Sweden

**Didier Sornette**

Eidgenössische Technische Hochschule (ETH) Zürich, Zurich, Switzerland

**Lev Tsimring**

University of California at San Diego (UCSD), San Diego, California, USA

**Bruce J. West**

Duke University, Durham, North Carolina, USA

**Lai-Sang Young**

New York University, New York, New York, USA

---

**Founding Editor**

**M.S. El Naschie**

## Chaos, Solitons & Fractals

Readers

[View Articles](#)

[Volume/ Issue Alert](#)

[Personalized Recommendations](#)

Authors

[Author Information Pack](#)

[Submit Your Paper](#)

[Track Your Paper](#)

[Early Career Resources](#)

[Support Center](#)

Librarians

[Ordering Information and Dispatch Dates](#)

[Abstracting/ Indexing](#)

Editors

[Publishing Ethics Resource Kit](#)

[Guest Editors](#)

[Support Center](#)

Reviewers

[Reviewer Guidelines](#)

[Log in as Reviewer](#)

[Reviewer Recognition](#)

[Support Center](#)

Advertisers Media Information

Societies

Copyright © 2018 Elsevier B.V.

[Careers](#) - [Terms and Conditions](#) - [Privacy Policy](#)

Cookies are used by this site. To decline or learn more, visit our [Cookies](#) page.







- Folders**
- Inbox (1641)
  - Drafts
  - Sent
  - Junk
  - Trash

**Subject** Please handle this manuscript as an Editor  
**From** Chaos, Solitons & Fractals   
**Sender** eesserver@eesmail.elsevier.com   
**To** igor.franovic@gmail.com , franovic@ipb.ac.rs   
**Reply-To** Chaos, Solitons & Fractals   
**Date** 2018-04-04 17:15

Ms. Ref. No: [REDACTED]  
 Title: [REDACTED]  
 Corresponding author: [REDACTED]  
 Chaos, Solitons & Fractals

Dear Dr. Igor Franović,

I invite you to serve as the handling editor for the above-referenced manuscript. To view the details of this assignment and the PDF of the paper, please log into the Elsevier Editorial System as an editor and then either accept or decline this assignment.

URL: <https://ees.elsevier.com/chaos/>

Your username is [REDACTED]

If you need to retrieve password details, please go to: [http://ees.elsevier.com/CHAOS/automail\\_query.asp](http://ees.elsevier.com/CHAOS/automail_query.asp)

Thank you.

Yours sincerely,

Maurice Courbage  
 Editor-in-Chief  
 Chaos, Solitons & Fractals

\*\*\*\*\*

For further assistance, please visit our customer support site at <http://help.elsevier.com/app/answers/list/p/7923>. Here you can search for solutions on a range of topics, find answers to frequently asked questions and learn more about EES via interactive tutorials. You will also find our 24/7 support contact details should you need any further assistance from one of our customer support representatives.



**Subject** Chaos: [REDACTED] Request to Review  
**From** <cha-edoffice@aip.org>  
**To** <igor.franovic@gmail.com>  
**Cc** <franovic@ipb.ac.rs>  
**Date** 2018-02-20 06:18

Dear Dr. Franovic,

Would you be willing and available to review the below referenced manuscript, which has been submitted for possible publication in Chaos: An Interdisciplinary Journal of Nonlinear Science:

Title: [REDACTED]

Author: [REDACTED]

Regards and thanks,

Prof. Thomas Peacock  
Mechanical Engineering  
MIT

ps If you are unable to provide a review via one of the several options below, I would be most grateful if you can suggest alternative reviewers.

\*\*\*\*

The manuscript's abstract is:

[REDACTED]

I would be extremely grateful for your help in providing a review of the manuscript, in terms of its suitability for the journal, its scientific and technical merit, as well as the quality of its presentation.

If you agree to review this manuscript, I would ask for your comments within four weeks from your acceptance. If you are not available for the review work, but want to refer it to a graduate student or a postdoc researcher, who is under your supervision, please click the ACCEPT link below. The instruction email will be sent to you directly, and you can access the paper from your account in the submission system. After the paper is reviewed, please take the final responsibility, including proofreading and approving the comments, and uploading the finished review through your account.

Alternatively, if you want to refer the review assignment to an experienced, highly-qualified postdoc researcher who is capable of managing the workflow without your supervision, please respond to this email with his/her name and email address and we will reach out to this person directly.

To view the manuscript and accept or decline the reviewer assignment, please go to the following URL:

[REDACTED]

If you have any questions or need more information, feel free to reply to this e-mail.

Thank you for your consideration and support of Chaos: An Interdisciplinary Journal of Nonlinear Science.

Sincerely,

Prof. Thomas Peacock  
Editor  
Chaos

**Subject** CONFIDENTIAL: request to review Scientific Reports manuscript [REDACTED]  
**From** <scientificreports@nature.com>  
**To** <franovic@ipb.ac.rs>  
**Date** 2017-08-11 13:45



Dear Dr. Fnanovic,

Some time ago you kindly refereed for us the original version of the manuscript entitled [REDACTED]

[REDACTED] The manuscript has now been revised in response to the comments provided during review.

We hope you will be willing to look at the revised manuscript – to let us know whether your concerns have been addressed – in which case we would hope to receive your comments within approximately 10 days. If you would like to assist us but require a few extra days to review the manuscript please do not hesitate to contact us.

To accept or decline our request, please use the following link:  
[REDACTED]

Many thanks in advance for your help; I look forward to hearing from you.

Best regards,

Serhiy Yanchuk  
Editorial Board Member  
Scientific Reports

This email has been sent through the Springer Nature Tracking System NY-610A-NPG&MTS

*Confidentiality Statement:*

*This e-mail is confidential and subject to copyright. Any unauthorised use or disclosure of its contents is prohibited. If you have received this email in error please notify our Manuscript Tracking System Helpdesk team at <http://platformsupport.nature.com> .*

*Details of the confidentiality and pre-publicity policy may be found here <http://www.nature.com/authors/policies/confidentiality.html>*

[Privacy Policy](#) | [Update Profile](#)

**Subject** [REDACTED] Review request

**From** <editorial.office@epleters.net>

**To** <franovic@ipb.ac.rs>

**Date** 2017-08-01 10:18



---

• [REDACTED] (~646 KB)

---

Dr. Igor Franovic  
Scientific Computing Laboratory, Center for the Study of Complex Systems  
Institute of Physics Belgrade  
Pregrevica 118  
SER - 11080 Belgrade

Mulhouse, 1 August 2017

REF.: [REDACTED]

[REDACTED]

[REDACTED]

Dear Dr. Franovic,

Please find attached the above manuscript which has been submitted for publication in EPL.

I am writing on behalf of Professor Juergen Kurths, who is the Co-Editor in charge of this manuscript. As an expert in the field, you could help us greatly by reviewing this paper and advise whether this manuscript is suitable for a Letters journal and in particular whether it is novel enough for EPL.

To ensure a rapid schedule of publication, please send your report within two weeks to the Editorial Office preferably via our report form located at:

[REDACTED]

If you feel that you are not an appropriate referee, or if you do not have time, would you please suggest alternative referees or, if possible, pass on the file to a colleague (indicating then his/her name to our secretariat via our on-line form)?

In either case, we kindly ask you to confirm receipt of this message via our on-line form as soon as possible and to let us know whether you are available to referee the paper.

Your report will be transmitted immediately to the Co-Editor, who will make the final decision. Please note that although referee reports may be transmitted to the author, these reports remain anonymous.

We invite you to update your personal data and especially to complete your 'Interests' by clicking on the 'Update account' link.

With many thanks for your cooperation.

Yours sincerely

Mr Frederic Burr  
Staff Editor

Follow EPL on Twitter @epl\_journal

EPL website for authors and referees: <https://www.epleters.net>

\*\*\*\*\*

EPL Editorial Office  
European Physical Society  
6 rue des Freres Lumiere  
F - 68200 Mulhouse

tel/fax: + 33 389 32 94 44 / + 33 389 32 94 49

email: [editorial.office@epleters.net](mailto:editorial.office@epleters.net)

web: <https://www.epleters.net>

\*\*\*\*\*



**Subject** Invitation to review [REDACTED]  
**From** Chaos, Solitons & Fractals <csf@elsevier.com>  
**Sender** <ees.chaos.0.3410cd.bfedff26@eesmail.elsevier.com>  
**To** <igor.franovic@gmail.com>, <franovic@ipb.ac.rs>  
**Date** 2015-09-20 04:18

Ms. Ref. No.: [REDACTED]

Title: [REDACTED]

Chaos, Solitons & Fractals

Dear Dr. Franović,

This is an automated email to remind you that there is a reviewer invitation awaiting your response.

To indicate whether you can complete the review, and to stop these reminders being sent, please do the following:

To **accept** this invitation, please click here:

[Agree to Review](#)

To **decline** this invitation, please click here:

[Decline to Review](#)

On Sep 14, 2015, I sent you the abstract below, which was submitted to Chaos, Solitons & Fractals. I would be most grateful if you could find the time to read this paper and comment on its suitability for publication.

-----

1. Go to this URL: <http://ees.elsevier.com/chaos/>
2. If you need to retrieve password details, please go to: [http://ees.elsevier.com/CHAOS/automail\\_query.asp](http://ees.elsevier.com/CHAOS/automail_query.asp).
3. Click [Reviewer Login]  
This takes you to the Reviewer Main Menu.
4. Click [New Reviewer Invitations]

You can access and download a full version of this manuscript as a PDF file. You can also submit your review here when complete.

If you are unable to review this paper, please suggest alternative referees.

Thank you very much for your time and your assistance.

Yours sincerely,

Ms. Sumantha Alagarsamy

Journal Manager

Chaos, Solitons & Fractals

ABSTRACT:

[REDACTED]

\*\*\*\*\*

For further assistance, please visit our customer support site at <http://help.elsevier.com/app/answers/list/p/7923>. Here you can search for solutions on a range of topics, find answers to frequently asked questions and learn more about EES via interactive tutorials. You will also find our 24/7 support contact details should you need any further assistance from one of our customer support representatives.





**Subject** Invitation to review manuscript [REDACTED] for journal  
**Physics Letters A**

**From** Charles Doering (Physics Letters A) <EvisSupport@elsevier.com>

**To** <franovic@ipb.ac.rs>

**Reply-To** [REDACTED]

**Date** 2016-11-28 00:59

Ref: [REDACTED]

Title: [REDACTED]

Journal: Physics Letters A

Corresponding Author: [REDACTED]

Co-authors: [REDACTED]

Dear Dr. Franovic,

I would like to invite you to review the above-referenced manuscript. To maintain our journal's high standards we need the best reviewers, and given your expertise in this area I would greatly appreciate your contribution.

I hope that this manuscript will be of interest to you. Please use one of the links below to view the manuscript and accept or decline this invitation.

Click [here](#) to access the PDF

Please find the abstract of the manuscript at the end of this email.

If you have any concerns about potential conflicts of interest, please consult the Editor.

If you are willing to review this manuscript, please click on the link below:

[Register to accept](#)

If you accept this invitation, I would appreciate your submitting your review within 21 days.

Please submit your review via EVISE® at: [http://www.evise.com/evise/faces/pages/navigation/NavController.jspx?JRNL\\_ACR=PLA](http://www.evise.com/evise/faces/pages/navigation/NavController.jspx?JRNL_ACR=PLA).

If you cannot review this manuscript, please click on the link below. I would also appreciate your suggestions for alternate reviewers.

[Decline](#)

Kindly note that your review assignment is present in the email address (username) in the 'TO' field of this email. If you have already registered an account in EVISE via a different email address, please let us know before accepting the invitation and we will re-invite you to your registered email address.

I look forward to receiving your response.

Kind regards,

Charles Doering  
Editor  
Physics Letters A

**Abstract:**

[REDACTED]

probe can be applied for system with discontinuities.

### **Free access to ScienceDirect and Scopus**

To assist you with reviewing this manuscript it is our pleasure to offer you 30 days of free access to ScienceDirect and Scopus. Your complimentary access starts from the day you accept this review invitation and will ensure that you can access ScienceDirect and Scopus both from home and via your institute. Just click on 'Go to Review' and then on the 'Go to Scopus' link under the Useful links section on the My Review tab or click [here](#) for more information.

### **Have questions or need assistance?**

For more information on the review process, please visit the [Reviewer Support](#) site.

For further assistance, please visit our [Customer Support](#) site. Here you can search for solutions on a range of topics, find answers to frequently asked questions, and learn more about EVISE® via interactive tutorials. You can also talk 24/5 to our customer support team by phone and 24/7 by live chat and email.

-----  
Copyright © 2016 Elsevier B.V. | [Privacy Policy](#)

Elsevier B.V., Radarweg 29, 1043 NX Amsterdam, The Netherlands, Reg. No. 33156677.



**Subject** Neurocomputing Review Request [REDACTED]  
**From** Neurocomputing <eesserver@eesmail.elsevier.com>  
**Sender** <eesserver@eesmail.elsevier.com>  
**To** <franovic@ipb.ac.rs>  
**Reply-To** Neurocomputing <neurocomputing@xs4all.nl>  
**Date** 2018-03-20 11:36

Dear Dr. Franović,

As editor of Neurocomputing, I would hereby like to ask you the big favor of reviewing the manuscript

[REDACTED]

The abstract is attached below. You can also view it on <https://ees.elsevier.com/neucom/>, where you should login as a Reviewer with

Your username is: [REDACTED]

If you can't remember your password please click the "Send Password" link on the Login page.

Here you can also notify us whether you accept or decline this invitation, view the manuscript once you have accepted to review, and eventually fill in your comments.

If possible, I would welcome receiving your review by 04/17/2018 (mm/dd/yyyy).

To assist you in the reviewing process, I am delighted to offer you full access to Scopus\* for 30 days. With Scopus you can search for related articles, references and papers by the same author. You may also use Scopus for your own purposes at any time during the 30-day period. If you already use Scopus at your institute, having this 30 day full access means that you will also be able to access Scopus from home. Access instructions will follow once you have accepted this invitation to review

\*Scopus is the world's largest abstract and citation database of research information and quality internet sources.

Your help as an expert on neural networks is highly appreciated!

Kind regards,

Professor Zidong Wang  
Editor in Chief

Reviewer Guidelines are now available to help you with your review

[REDACTED]

Please note: Reviews are subject to a confidentiality policy,  
[http://service.elsevier.com/app/answers/detail/a\\_id/14156/supporthub/publishing/](http://service.elsevier.com/app/answers/detail/a_id/14156/supporthub/publishing/)





**Subject** Request for review - WAMOT-[REDACTED]  
**From** Andrew Norris <eesserver@eesmail.elsevier.com>  
**Sender** <eesserver@eesmail.elsevier.com>  
**To** <franovic@ipb.ac.rs>  
**Reply-To** Andrew Norris <norris@rutgers.edu>  
**Date** 2017-04-18 14:33

---

Ms. Ref. No.: WAMOT-[REDACTED]  
Title: [REDACTED]  
Wave Motion

Dear Dr. Franovic,

I would be grateful if you would agree to review the above-mentioned manuscript that has been submitted for publication in Wave Motion. Thank you very much in advance!

The abstract is placed below. To view the complete article, please click on:  
[REDACTED]

If you are willing to review this manuscript, please click on the link below:  
[REDACTED]

If you are NOT able to review this manuscript, please click on the link below. We would appreciate receiving suggestions for alternative reviewers.  
[REDACTED]

Alternatively, you may also register your response by accessing the Elsevier Editorial System for Wave Motion as a REVIEWER using the logon credentials below:

<https://ees.elsevier.com/wamot/>

Your username is: [REDACTED]

If you need to retrieve password details, please go to: [http://ees.elsevier.com/wamot/automail\\_query.asp](http://ees.elsevier.com/wamot/automail_query.asp)

If you accept this invitation, I would be very grateful if you would return your review within 25 days.

You may submit your comments online at the above URL. There you will find spaces for confidential comments to the editor, comments for the author and a report form to be completed.

As a reviewer you are entitled to complimentary access to Scopus and ScienceDirect for 30 days. Full instructions and details will be provided upon accepting this invitation to review.

In addition to accessing our subscriber content, you can also use our Open Access content.

Read more about Open Access here: <http://www.elsevier.com/openaccess>

Upon submission of your review report to the system, you will get access to your personalized Elsevier reviews profile page as well as the possibility of creating a public page listing your reviews across all publishers in just a few steps! See

<http://www.reviewerrecognition.elsevier.com> and <http://www.reviewerpage.com> for more information.

With kind regards,

Kwok W Chow, PhD  
Editorial Board Member  
Wave Motion

Reviewer Guidelines are now available to help you with your review:

<http://www.elsevier.com/wps/find/reviewerhome.reviewers/reviewerguidelines>

ABSTRACT:

[REDACTED]

\*\*\*\*\*  
For further assistance, please visit our customer support site at <http://help.elsevier.com/app/answers/list/p/7923>. Here you can search for solutions on a range of topics, find answers to frequently asked questions and learn more about EES via interactive tutorials. You will also find our 24/7 support contact details should you need any further assistance from one of our customer support representatives

Please note: Reviews are subject to a confidentiality policy,  
[http://service.elsevier.com/app/answers/detail/a\\_id/14156/supporthub/publishing/](http://service.elsevier.com/app/answers/detail/a_id/14156/supporthub/publishing/)

# Web of Science

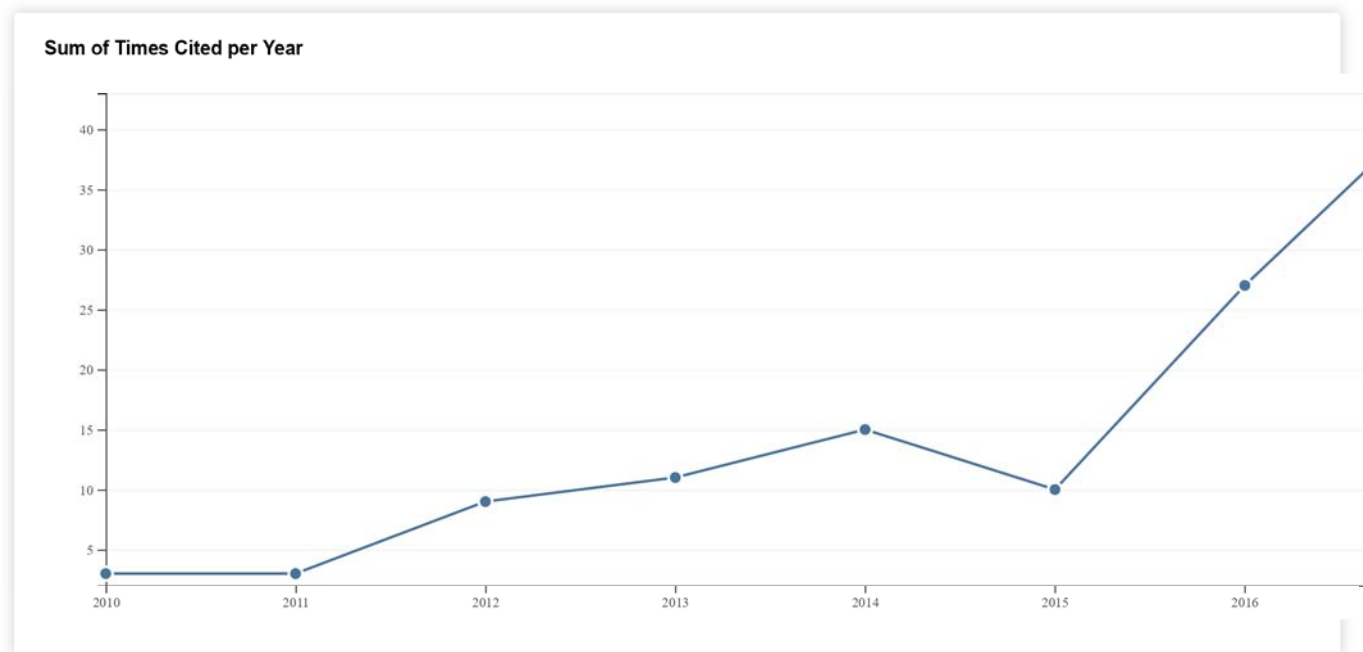
Citation report for **33** results from Web of Science Core Collection between 1996 and 2018

You searched for: **AUTHOR:** (Franovic, I) ...[More](#)

This report reflects citations to source items indexed within Web of Science Core Collection. Perform a Cited Reference Search to include citations to items not indexed within Web of Science Core Collection.

Export Data:

<p><b>Total Publications</b></p> <p><b>33</b></p>	<p><b>h-index</b></p> <p><b>8</b></p> <p>Average citations per item</p> <p><b>4.06</b></p>	<p><b>Sum of Times Cited</b></p> <p><b>134</b></p> <p>Without self citations</p> <p><b>82</b></p>	<p><b>Citing articles</b></p> <p><b>85</b></p> <p>Without self citations</p> <p><b>64</b></p>
---	--	---	---



Sort by: Times Cited | Date |  | Page 1 of 4

	2014	2015	2016	2017	2018	Total	Average Citations per Year
Use the checkboxes to remove individual items from this Citation Report							
<input type="checkbox"/> or restrict to items published between 1996 and 2018 <input type="button" value="Go"/>	15	10	27	42	14	134	14.89
<input type="checkbox"/> 1. <a href="#">Spontaneous Formation of Synchronization Clusters in Homogenous</a>	4	2	2	1	1	14	2.00





*33 records matched your query of the 40,576,688 in the data limits you selected.*

---

© 2018 [CLARIVATE ANALYTICS](#)   [TERMS OF USE](#)   [PRIVACY POLICY](#)   [FEEDBACK](#)

---

### Citing Articles: 14

(from Web of Science Core Collection)

**For:** Spontaneous Formation of Synchronization Clusters in Homogeneous Neuronal Ensembles Induced by Noise ...[More](#)

#### Times Cited Counts

- 15 in All Databases
  - 14 in Web of Science Core Collection
  - 2 in BIOSIS Citation Index
  - 2 in Chinese Science Citation Database
  - 0 data sets in Data Citation Index
  - 0 publication in Data Citation Index
  - 0 in Russian Science Citation Index
  - 0 in SciELO Citation Index
- [View Additional Times Cited Counts](#)

### Refine Results

#### Filter results by:

Open Access (2)

[Refine](#)

#### Publication Years

- 2014 (4)
- 2013 (3)
- 2015 (2)
- 2016 (2)
- 2012 (1)

[more options / values...](#)

[Refine](#)

#### Web of Science Categories

- PHYSICS MATHEMATICAL (8)
- PHYSICS FLUIDS PLASMAS (6)

Sort by: **Date** Times Cited Usage Count

Page of 1

More

Select Page 5K

Save to EndNote online

Add to Marked List

### Create Citation Report

#### Analyze Results

**Times Cited: 0**  
(from Web of Science Core Collection)

**Usage Count**

#### 1. Clustering promotes switching dynamics in networks of noisy neurons

By: Franovic, Igor; Klinshov, Vladimir

CHAOS Volume: 28 Issue: 2 Article Number: 023111  
Published: FEB 2018

[Full Text from Publisher](#)

[View Abstract](#)

**Times Cited: 5**  
(from Web of Science Core Collection)

**Usage Count**

#### 2. Effects of time delays in a mathematical bone model

By: Wang, Li-Fang; Qiu, Kang; Jia, Ya

CHINESE PHYSICS B Volume: 26 Issue: 3 Article Number: 030503  
Published: MAR 2017

[Full Text from Publisher](#)

[View Abstract](#)

**Times Cited: 1**  
(from Web of Science Core Collection)

**Usage Count**

#### 3. Slow rate fluctuations in a network of noisy neurons with coupling delay

By: Franovic, I.; Klinshov, V.

EPL Volume: 116 Issue: 4 Article Number: 48002  
Published: NOV 2016

[Full Text from Publisher](#)

[View Abstract](#)

**Times Cited: 3**  
(from Web of Science Core Collection)

**Usage Count**

#### 4. Earthquake nucleation in a stochastic fault model of globally coupled units with interaction delays

By: Vasovic, Nebojsa; Kostic, Srdan; Franovic, Igor; et al.

COMMUNICATIONS IN NONLINEAR SCIENCE AND NUMERICAL SIMULATION Volume: 38 Pages: 117-129  
Published: SEP 2016

[Full Text from Publisher](#)

[View Abstract](#)

#### 5. Activation process in excitable systems with

**Times Cited: 13**

MATHEMATICS APPLIED (4)  
 MECHANICS (3)  
 PHYSICS MULTIDISCIPLINARY (3)

[more options / values...](#)

[Refine](#)

---

**Document Types** ▼

ARTICLE (14)

[Refine](#)

---

**Organizations-Enhanced** ▼

UNIVERSITY OF BELGRADE (9)  
 EAST CHINA NORMAL UNIVERSITY (2)  
 INST DEV WATER RESOURCES JAROSLAV CERNI (2)  
 INSTITUTE OF APPLIED PHYSICS OF THE RUSSIAN ACADEMY OF SCIENCES (2)  
 RUSSIAN ACADEMY OF SCIENCES (2)

[more options / values...](#)

[Refine](#)

---

**Funding Agencies** ◀

---

**Authors** ◀

---

**Open Access** ◀

---

**View all options**

*For advanced refine options, use*

[Analyze Results](#)

**multiple noise sources: Large number of units**

By: Franovic, Igor; Perc, Matjaz; Todorovic, Kristina; et al.  
**PHYSICAL REVIEW E** Volume: 92 Issue: 6 Article Number: 062912 Published: DEC 14 2015

[Full Text from Publisher](#) [View Abstract](#)

*(from Web of Science Core Collection)*

**Usage Count**

6. **Interplay between internal delays and coherent oscillations in delayed coupled noisy excitable systems**

By: Grozdanovic, Ines; Todorovic, Kristina; Vasovic, Nebojsa; et al.  
**INTERNATIONAL JOURNAL OF NON-LINEAR MECHANICS** Volume: 73 Special Issue: SI Pages: 121-127 Published: JUL 2015

[Full Text from Publisher](#) [View Abstract](#)

**Times Cited: 0**  
*(from Web of Science Core Collection)*

**Usage Count**

7. **A simplified memory network model based on pattern formations**

By: Xu, Kesheng; Zhang, Xiyun; Wang, Chaoqing; et al.  
**SCIENTIFIC REPORTS** Volume: 4 Article Number: 7568 Published: DEC 19 2014

[Free Full Text from Publisher](#) [View Abstract](#)

**Times Cited: 5**  
*(from Web of Science Core Collection)*

**Usage Count**

8. **Stability, coherent spiking and synchronization in noisy excitable systems with coupling and internal delays**

By: Franovic, Igor; Todorovic, Kristina; Vasovic, Nebojsa; et al.  
**COMMUNICATIONS IN NONLINEAR SCIENCE AND NUMERICAL SIMULATION** Volume: 19 Issue: 9 Pages: 3202-3219 Published: SEP 2014

[Full Text from Publisher](#) [View Abstract](#)

**Times Cited: 1**  
*(from Web of Science Core Collection)*

**Usage Count**

9. **Enhanced corticomuscular coherence by external stochastic noise**

By: Trenado, Carlos; Mendez-Balbuena, Ignacio; Manjarrez, Elias; et al.  
**FRONTIERS IN HUMAN NEUROSCIENCE** Volume: 8 Article Number: 325 Published: MAY 20 2014

[Free Full Text from Publisher](#) [View Abstract](#)

**Times Cited: 4**  
*(from Web of Science Core Collection)*

**Usage Count**

10. **Persistence and failure of mean-field approximations adapted to a class of systems of delay-coupled excitable units**

By: Franovic, Igor; Todorovic, Kristina; Vasovic, Nebojsa; et al.  
**PHYSICAL REVIEW E** Volume: 89 Issue: 2 Article Number: 022926 Published: FEB 28 2014

[Full Text from Publisher](#)

**Times Cited: 5**  
*(from Web of Science Core Collection)*

**Usage Count**

[Full Text from Publisher](#)

[View Abstract](#)

11. **Controlling self-sustained spiking activity by adding or removing one network link**

By: Xu, Kesheng; Huang, Wenwen; Li, Baowen; et al.  
 EPL Volume: 102 Issue: 5 Article Number: 50002  
 Published: JUN 2013

**Times Cited: 3**  
 (from Web of Science Core Collection)

**Usage Count**

[Full Text from Publisher](#)

[View Abstract](#)

12. **Role of delay in the mechanism of cluster formation**

By: Singh, Aradhana; Jalan, Sarika; Kurths, Juergen  
 PHYSICAL REVIEW E Volume: 87 Issue: 3 Article  
 Number: 030902 Published: MAR 25 2013

**Times Cited: 11**  
 (from Web of Science Core Collection)

**Usage Count**

[Full Text from Publisher](#)

[View Abstract](#)

13. **Mean-field approximation of two coupled populations of excitable units**

By: Franovic, Igor; Todorovic, Kristina; Vasovic, Nebojsa; et al.  
 PHYSICAL REVIEW E Volume: 87 Issue: 1 Article  
 Number: 012922 Published: JAN 31 2013

**Times Cited: 12**  
 (from Web of Science Core Collection)

**Usage Count**

[Full Text from Publisher](#)

[View Abstract](#)

14. **Cluster synchronization of spiking induced by noise and interaction delays in homogenous neuronal ensembles**

By: Franovic, Igor; Todorovic, Kristina; Vasovic, Nebojsa; et al.  
 CHAOS Volume: 22 Issue: 3 Article Number: 033147  
 Published: SEP 2012

**Times Cited: 8**  
 (from Web of Science Core Collection)

**Usage Count**

[Full Text from Publisher](#)

[View Abstract](#)

Select Page   **5K**


Save to EndNote online 

Add to Marked List

Sort by: **Date** Times Cited Usage Count

Page of 1

More 

Show: 50 per page 

14 records matched your query of the 40,553,433 in the data limits you selected.

### Citing Articles: 13

(from Web of Science Core Collection)

**For:** Activation process in excitable systems with multiple noise source s: One and two interacting units  
[...More](#)

#### Times Cited Counts

- 13 in All Databases
  - 13 in Web of Science Core Collection
  - 1 in BIOSIS Citation Index
  - 0 in Chinese Science Citation Database
  - 0 data sets in Data Citation Index
  - 0 publication in Data Citation Index
  - 0 in Russian Science Citation Index
  - 0 in SciELO Citation Index
- [View Additional Times Cited Counts](#)

### Refine Results

#### Filter results by:

- Highly Cited in Field (2)
- Open Access (1)

[Refine](#)

#### Publication Years

- 2017 (9)
- 2018 (2)
- 2015 (1)
- 2016 (1)

[more options / values...](#)

[Refine](#)

#### Web of Science Categories

Sort by: **Date** Times Cited Usage Count Page of 1

More

Select Page 5K

Save to EndNote online

Add to Marked List

### Create Citation Report

#### Analyze Results

**Times Cited: 0**  
(from Web of Science Core Collection)

**Usage Count**

#### 1. Estimation of biophysical parameters in a neuron model under random fluctuations

By: Upadhyay, Ranjit Kumar; Paul, Chinmoy; Mondal, Argha; et al.

APPLIED MATHEMATICS AND COMPUTATION

Volume: 329 Pages: 364-373 Published: JUL 15 2018

Full Text from Publisher

View Abstract

#### 2. Measuring spike timing distance in the Hindmarsh-Rose neurons

By: Zhu, Jinjie; Liu, Xianbin

COGNITIVE NEURODYNAMICS Volume: 12 Issue: 2

Pages: 225-234 Published: APR 2018

Full Text from Publisher

View Abstract

**Times Cited: 0**  
(from Web of Science Core Collection)

**Usage Count**

#### 3. Electromagnetic induction and radiation-induced abnormality of wave propagation in excitable media

By: Ma, Jun; Wu, Fuqiang; Hayat, Tasawar; et al.

PHYSICA A-STATISTICAL MECHANICS AND ITS APPLICATIONS

Volume: 486 Pages: 508-516

Published: NOV 15 2017

Full Text from Publisher

View Abstract

**Times Cited: 8**  
(from Web of Science Core Collection)

**Usage Count**

#### 4. Parametric wave induces straight drift of spiral waves in excitable medium

By: Deng, Yu; Liu, Bao Yu; Wu, Tong; et al.

EPL Volume: 119 Issue: 5 Article Number: 58002

Published: SEP 2017

Full Text from Publisher

View Abstract

**Times Cited: 0**  
(from Web of Science Core Collection)

**Usage Count**

PHYSICS MATHEMATICAL (5)  
 MATHEMATICS APPLIED (4)  
 PHYSICS FLUIDS PLASMAS (3)  
 PHYSICS MULTIDISCIPLINARY (3)  
 MATHEMATICS INTERDISCIPLINARY APPLICATIONS (2)

[more options / values...](#)

**Refine**

---

**Document Types** ▼

ARTICLE (13)

**Refine**

---

**Organizations-Enhanced** ▼

KUNMING UNIVERSITY OF SCIENCE TECHNOLOGY (3)  
 CHINA UNIVERSITY OF MINING TECHNOLOGY (2)  
 KING ABDULAZIZ UNIVERSITY (2)  
 LANZHOU UNIVERSITY OF TECHNOLOGY (2)  
 NANJING UNIVERSITY OF AERONAUTICS AND ASTRONAUTICS (2)

[more options / values...](#)

**Refine**

---

**Funding Agencies** ◀

---

**Authors** ◀

---

**Open Access** ◀

---

**View all options**

*For advanced refine options, use*

[Analyze Results](#)

5. **Mean-field dynamics of a population of stochastic map neurons**  
 By: Franovic, Igor; Maslennikov, Oleg V.; Bacic, Iva; et al.  
[PHYSICAL REVIEW E](#) Volume: 96 Issue: 1 Article Number: 012226 Published: JUL 27 2017  
 [Full Text from Publisher](#)  [View Abstract](#)
  
6. **Levy noise-induced escape in an excitable system**  
 By: Cai, Rui; Chen, Xiaoli; Duan, Jinqiao; et al.  
[JOURNAL OF STATISTICAL MECHANICS-THEORY AND EXPERIMENT](#) Article Number: 063503  
 Published: JUN 2017  
 [Full Text from Publisher](#)  [View Abstract](#)
  
7. **Crossing the quasi-threshold manifold of a noise-driven excitable system**  
 By: Chen, Zhen; Zhu, Jinjie; Liu, Xianbin  
[PROCEEDINGS OF THE ROYAL SOCIETY A-MATHEMATICAL PHYSICAL AND ENGINEERING SCIENCES](#) Volume: 473 Issue: 2201 Article Number: 20170058 Published: MAY 1 2017  
 [Full Text from Publisher](#)  [View Abstract](#)
  
8. **Synaptic dynamics regulation in response to high frequency stimulation in neuronal networks**  
 By: Su, Fei; Wang, Jiang; Li, Huiyan; et al.  
[COMMUNICATIONS IN NONLINEAR SCIENCE AND NUMERICAL SIMULATION](#) Volume: 55 Pages: 29-41  
 Published: FEB 2017  
 [Full Text from Publisher](#)  [View Abstract](#)
  
9. **Statistics for anti-synchronization of intracellular calcium dynamics**  
 By: Duan, Wei-Long; Zeng, Chunhua  
[APPLIED MATHEMATICS AND COMPUTATION](#) Volume: 293 Pages: 611-616 Published: JAN 15 2017  
 [Full Text from Publisher](#)  [View Abstract](#)
  
10. **Non-Gaussian noises induce transitions in intracellular calcium dynamics**  
 By: Lin, Ling; Duan, Wei-Long  
[CHAOS SOLITONS & FRACTALS](#) Volume: 94 Pages: 63-67 Published: JAN 2017  
 [Full Text from Publisher](#)  [View Abstract](#)

**Times Cited: 0**  
*(from Web of Science Core Collection)*

**Usage Count**

**Times Cited: 0**  
*(from Web of Science Core Collection)*

**Usage Count**

**Times Cited: 0**  
*(from Web of Science Core Collection)*

**Usage Count**

**Times Cited: 0**  
*(from Web of Science Core Collection)*

**Usage Count**

**Times Cited: 5**  
*(from Web of Science Core Collection)*

Highly Cited Paper

**Usage Count**

**Times Cited: 2**  
*(from Web of Science Core Collection)*

**Usage Count**

11. **Signal power amplification of intracellular calcium dynamics with non-Gaussian noises and time delay**

By: Duan, Wei-Long; Zeng, Chunhua  
**APPLIED MATHEMATICS AND COMPUTATION**  
Volume: 292 Pages: 400-405 Published: JAN 1 2017

[Full Text from Publisher](#)

[View Abstract](#)

**Times Cited: 7**  
*(from Web of Science Core Collection)*

Highly Cited Paper

**Usage Count**

12. **Spike-Threshold Variability Originated from Separatrix-Crossing in Neuronal Dynamics**

By: Wang, Longfei; Wang, Hengtong; Yu, Lianchun; et al.  
**SCIENTIFIC REPORTS** Volume: 6 Article Number: 31719  
Published: AUG 22 2016

[Free Full Text from Publisher](#)

[View Abstract](#)

**Times Cited: 1**  
*(from Web of Science Core Collection)*

**Usage Count**

13. **Activation process in excitable systems with multiple noise sources: Large number of units**

By: Franovic, Igor; Perc, Matjaz; Todorovic, Kristina; et al.  
**PHYSICAL REVIEW E** Volume: 92 Issue: 6 Article Number: 062912  
Published: DEC 14 2015

[Full Text from Publisher](#)

[View Abstract](#)

**Times Cited: 13**  
*(from Web of Science Core Collection)*

**Usage Count**

Select Page



▾

Sort by: **Date** Times Cited Usage Count

▾

Show:  ▾

Page of 1

*13 records matched your query of the 40,553,433 in the data limits you selected.*

### Citing Articles: 13

(from Web of Science Core Collection)

**For:** Activation process in excitable systems with multiple noise source s: Large number of units ...[More](#)

#### Times Cited Counts

- 13 in All Databases
  - 13 in Web of Science Core Collection
  - 1 in BIOSIS Citation Index
  - 0 in Chinese Science Citation Database
  - 0 data sets in Data Citation Index
  - 0 publication in Data Citation Index
  - 0 in Russian Science Citation Index
  - 0 in SciELO Citation Index
- [View Additional Times Cited Counts](#)

### Refine Results

#### Filter results by:

- Highly Cited in Field (2)
- Open Access (1)

[Refine](#)

#### Publication Years

- 2017 (8)
- 2018 (3)
- 2015 (1)
- 2016 (1)

[more options / values...](#)

[Refine](#)

#### Web of Science Categories

- MATHEMATICS APPLIED (5)

Sort by: **Date** Times Cited Usage Count

Page of 1

More

Select Page 5K

Save to EndNote online

Add to Marked List

#### Create Citation Report

#### Analyze Results

**Times Cited: 0**  
(from Web of Science Core Collection)

**Usage Count**

#### 1. Estimation of biophysical parameters in a neuron model under random fluctuations

By: Upadhyay, Ranjit Kumar; Paul, Chinmoy; Mondal, Argha; et al.

APPLIED MATHEMATICS AND COMPUTATION

Volume: 329 Pages: 364-373 Published: JUL 15 2018

[Full Text from Publisher](#)

[View Abstract](#)

#### 2. Measuring spike timing distance in the Hindmarsh-Rose neurons

By: Zhu, Jinjie; Liu, Xianbin

COGNITIVE NEURODYNAMICS Volume: 12 Issue: 2

Pages: 225-234 Published: APR 2018

[Full Text from Publisher](#)

[View Abstract](#)

**Times Cited: 0**  
(from Web of Science Core Collection)

**Usage Count**

#### 3. Promotion of cooperation based on swarm intelligence in spatial public goods games

By: Chen, Ya-Shan; Yang, Han-Xin; Guo, Wen-Zhong; et al.

APPLIED MATHEMATICS AND COMPUTATION

Volume: 320 Pages: 614-620 Published: MAR 1 2018

[Full Text from Publisher](#)

[View Abstract](#)

**Times Cited: 0**  
(from Web of Science Core Collection)

**Usage Count**

#### 4. Two types of coherence resonance in an intracellular calcium oscillation system

By: Ma, Juan; Gao, Qingyu

CHEMICAL PHYSICS Volume: 495 Pages: 29-34

Published: SEP 27 2017

[Full Text from Publisher](#)

[View Abstract](#)

**Times Cited: 0**  
(from Web of Science Core Collection)

**Usage Count**



<p>PHYSICS MATHEMATICAL (3) MECHANICS (2) MULTIDISCIPLINARY SCIENCES (2) PHYSICS FLUIDS PLASMAS (2)</p> <p><a href="#">more options / values...</a></p> <p style="text-align: right;"><a href="#">Refine</a></p>	<p>5. <b>Parametric wave induces straight drift of spiral waves in excitable medium</b></p> <p>By: Deng, Yu; Liu, Bao Yu; Wu, Tong; et al. EPL Volume: 119 Issue: 5 Article Number: 58002 Published: SEP 2017</p> <p><input type="checkbox"/> <a href="#">Full Text from Publisher</a></p> <p style="text-align: right;"><input type="checkbox"/> <a href="#">View Abstract</a></p>	<p><b>Times Cited: 0</b> <i>(from Web of Science Core Collection)</i></p> <p><b>Usage Count</b></p>
<p><b>Document Types</b> ▼</p> <p>ARTICLE (13)</p> <p style="text-align: right;"><a href="#">Refine</a></p>	<p>6. <b>Levy noise-induced escape in an excitable system</b></p> <p>By: Cai, Rui; Chen, Xiaoli; Duan, Jinqiao; et al. JOURNAL OF STATISTICAL MECHANICS-THEORY AND EXPERIMENT Article Number: 063503 Published: JUN 2017</p> <p><input type="checkbox"/> <a href="#">Full Text from Publisher</a></p> <p style="text-align: right;"><input type="checkbox"/> <a href="#">View Abstract</a></p>	<p><b>Times Cited: 0</b> <i>(from Web of Science Core Collection)</i></p> <p><b>Usage Count</b></p>
<p><b>Organizations-Enhanced</b> ▼</p> <p>MINIST EDUC (3) CHINA UNIVERSITY OF MINING TECHNOLOGY (2) FUJIAN PROV KEY LAB NETWORK COMP INTELLIGENT IN (2) FUZHOU UNIVERSITY (2) KUNMING UNIVERSITY OF SCIENCE TECHNOLOGY (2)</p> <p><a href="#">more options / values...</a></p> <p style="text-align: right;"><a href="#">Refine</a></p>	<p>7. <b>Crossing the quasi-threshold manifold of a noise-driven excitable system</b></p> <p>By: Chen, Zhen; Zhu, Jinjie; Liu, Xianbin PROCEEDINGS OF THE ROYAL SOCIETY A-MATHEMATICAL PHYSICAL AND ENGINEERING SCIENCES Volume: 473 Issue: 2201 Article Number: 20170058 Published: MAY 1 2017</p> <p><input type="checkbox"/> <a href="#">Full Text from Publisher</a></p> <p style="text-align: right;"><input type="checkbox"/> <a href="#">View Abstract</a></p>	<p><b>Times Cited: 0</b> <i>(from Web of Science Core Collection)</i></p> <p><b>Usage Count</b></p>
<p><b>Funding Agencies</b> ◀</p>	<p>8. <b>Aspiration-induced dormancy promotes cooperation in the spatial Prisoner's Dilemma games</b></p> <p>By: Chen, Ya-Shan; Yang, Han-Xin; Guo, Wen-Zhong PHYSICA A-STATISTICAL MECHANICS AND ITS APPLICATIONS Volume: 469 Pages: 625-630 Published: MAR 1 2017</p> <p><input type="checkbox"/> <a href="#">Full Text from Publisher</a></p> <p style="text-align: right;"><input type="checkbox"/> <a href="#">View Abstract</a></p>	<p><b>Times Cited: 1</b> <i>(from Web of Science Core Collection)</i></p> <p><b>Usage Count</b></p>
<p><b>Authors</b> ◀</p>	<p>9. <b>Synaptic dynamics regulation in response to high frequency stimulation in neuronal networks</b></p> <p>By: Su, Fei; Wang, Jiang; Li, Huiyan; et al. COMMUNICATIONS IN NONLINEAR SCIENCE AND NUMERICAL SIMULATION Volume: 55 Pages: 29-41 Published: FEB 2017</p> <p><input type="checkbox"/> <a href="#">Full Text from Publisher</a></p> <p style="text-align: right;"><input type="checkbox"/> <a href="#">View Abstract</a></p>	<p><b>Times Cited: 0</b> <i>(from Web of Science Core Collection)</i></p> <p><b>Usage Count</b></p>
<p><b>Open Access</b> ◀</p>	<p>10. <b>Statistics for anti-synchronization of intracellular calcium dynamics</b></p> <p>By: Duan, Wei-Long; Zeng, Chunhua APPLIED MATHEMATICS AND COMPUTATION Volume: 293 Pages: 611-616 Published: JAN 15 2017</p> <p><input type="checkbox"/> <a href="#">Full Text from Publisher</a></p> <p style="text-align: right;"><input type="checkbox"/> <a href="#">View Abstract</a></p>	<p><b>Times Cited: 5</b> <i>(from Web of Science Core Collection)</i></p> <p style="text-align: right;"><b>Highly Cited Paper</b></p>
<p><b>View all options</b></p> <p><i>For advanced refine options, use</i></p> <p style="text-align: center;"><input type="button" value="Analyze Results"/></p>		

	Full Text from Publisher	View Abstract	Usage Count
11. <b>Signal power amplification of intracellular calcium dynamics with non-Gaussian noises and time delay</b>	<a href="#">Full Text from Publisher</a>	<a href="#">View Abstract</a>	<b>Times Cited: 7</b> <i>(from Web of Science Core Collection)</i>
By: Duan, Wei-Long; Zeng, Chunhua <b>APPLIED MATHEMATICS AND COMPUTATION</b> Volume: 292 Pages: 400-405 Published: JAN 1 2017			<b>Highly Cited Paper</b>
	<a href="#">Full Text from Publisher</a>	<a href="#">View Abstract</a>	<b>Usage Count</b>
12. <b>Spike-Threshold Variability Originated from Separatrix-Crossing in Neuronal Dynamics</b>			<b>Times Cited: 1</b> <i>(from Web of Science Core Collection)</i>
By: Wang, Longfei; Wang, Hengtong; Yu, Lianchun; et al. <b>SCIENTIFIC REPORTS</b> Volume: 6 Article Number: 31719 Published: AUG 22 2016			<b>Usage Count</b>
	<a href="#">Free Full Text from Publisher</a>	<a href="#">View Abstract</a>	
13. <b>Activation process in excitable systems with multiple noise sources: One and two interacting units</b>			<b>Times Cited: 13</b> <i>(from Web of Science Core Collection)</i>
By: Franovic, Igor; Todorovic, Kristina; Perc, Matjaz; et al. <b>PHYSICAL REVIEW E</b> Volume: 92 Issue: 6 Article Number: 062911 Published: DEC 14 2015			<b>Usage Count</b>
	<a href="#">Full Text from Publisher</a>	<a href="#">View Abstract</a>	

Select Page   **5K**

▾

Sort by: **Date** Times Cited Usage Count Page of 1

▾

Show:  ▾

*13 records matched your query of the 40,553,433 in the data limits you selected.*

## Citing Articles: 12

(from Web of Science Core Collection)

**For:** Mean-field approximation of two coupled populations of excitable units [...More](#)

### Times Cited Counts

- 12 in All Databases
- 12 in Web of Science Core Collection
- 0 in BIOSIS Citation Index
- 0 in Chinese Science Citation Database
- 0 data sets in Data Citation Index
- 0 publication in Data Citation Index
- 0 in Russian Science Citation Index
- 0 in SciELO Citation Index

[View Additional Times Cited Counts](#)

## Refine Results

### Filter results by:

Open Access (1)

[Refine](#)

### Publication Years

- 2014 (3)
- 2015 (3)
- 2016 (3)
- 2017 (2)
- 2018 (1)

[more options / values...](#)

[Refine](#)

### Web of Science Categories

- PHYSICS MATHEMATICAL (9)
- PHYSICS FLUIDS PLASMAS (8)
- MATHEMATICS APPLIED (3)

Sort by: **Date** Times Cited Usage Count

More

Page of 1

Select Page   **5K**

Save to EndNote online

Add to Marked List

### Create Citation Report

### Analyze Results

**Times Cited: 0**  
(from Web of Science Core Collection)

**Usage Count**

#### 1. Clustering promotes switching dynamics in networks of noisy neurons

By: Franovic, Igor; Klinshov, Vladimir

**CHAOS** Volume: 28 Issue: 2 Article Number: 023111  
Published: FEB 2018

#### 2. Mean-field dynamics of a population of stochastic map neurons

By: Franovic, Igor; Maslennikov, Oleg V.; Bacic, Iva; et al.  
**PHYSICAL REVIEW E** Volume: 96 Issue: 1 Article Number: 012226  
Published: JUL 27 2017

**Times Cited: 0**  
(from Web of Science Core Collection)

**Usage Count**

#### 3. Chimeralike states in two distinct groups of identical populations of coupled Stuart-Landau oscillators

By: Premalatha, K.; Chandrasekar, V. K.; Senthilvelan, M.; et al.

**PHYSICAL REVIEW E** Volume: 95 Issue: 2 Article Number: 022208  
Published: FEB 10 2017

**Times Cited: 1**  
(from Web of Science Core Collection)

**Usage Count**

#### 4. Slow rate fluctuations in a network of noisy neurons with coupling delay

By: Franovic, I.; Klinshov, V.

**EPL** Volume: 116 Issue: 4 Article Number: 48002  
Published: NOV 2016

**Times Cited: 1**  
(from Web of Science Core Collection)

**Usage Count**

<p>MATHEMATICS INTERDISCIPLINARY APPLICATIONS (2) MECHANICS (2)</p> <p><a href="#">more options / values...</a></p> <p><a href="#">Refine</a></p>	<p>5. <b>The Space-Clamped Hodgkin-Huxley System with Random Synaptic Input: Inhibition of Spiking by Weak Noise and Analysis with Moment Equations</b></p> <p>By: Tuckwell, Henry C.; Ditlevsen, Susanne <b>NEURAL COMPUTATION</b> Volume: 28 Issue: 10 Pages: 2129-2161 Published: OCT 2016</p> <p><input type="checkbox"/> <a href="#">Full Text from Publisher</a></p> <p><input type="checkbox"/> <a href="#">View Abstract</a></p>	<p><b>Times Cited: 1</b> <i>(from Web of Science Core Collection)</i></p> <p><b>Usage Count</b></p>
<p><b>Document Types</b> ▼</p> <p>ARTICLE (12)</p> <p><a href="#">Refine</a></p>	<p>6. <b>Earthquake nucleation in a stochastic fault model of globally coupled units with interaction delays</b></p> <p>By: Vasovic, Nebojsa; Kostic, Srdan; Franovic, Igor; et al. <b>COMMUNICATIONS IN NONLINEAR SCIENCE AND NUMERICAL SIMULATION</b> Volume: 38 Pages: 117-129 Published: SEP 2016</p> <p><input type="checkbox"/> <a href="#">Full Text from Publisher</a></p> <p><input type="checkbox"/> <a href="#">View Abstract</a></p>	<p><b>Times Cited: 3</b> <i>(from Web of Science Core Collection)</i></p> <p><b>Usage Count</b></p>
<p><b>Organizations-Enhanced</b> ▼</p> <p>UNIVERSITY OF BELGRADE (9) INSTITUTE OF APPLIED PHYSICS OF THE RUSSIAN ACADEMY OF SCIENCES (4) RUSSIAN ACADEMY OF SCIENCES (4) INST DEV WATER RESOURCES JAROSLAV CERNI (2) KING ABDULAZIZ UNIVERSITY (2)</p> <p><a href="#">more options / values...</a></p> <p><a href="#">Refine</a></p>	<p>7. <b>Activation process in excitable systems with multiple noise sources: One and two interacting units</b></p> <p>By: Franovic, Igor; Todorovic, Kristina; Perc, Matjaz; et al. <b>PHYSICAL REVIEW E</b> Volume: 92 Issue: 6 Article Number: 062911 Published: DEC 14 2015</p> <p><input type="checkbox"/> <a href="#">Full Text from Publisher</a></p> <p><input type="checkbox"/> <a href="#">View Abstract</a></p>	<p><b>Times Cited: 13</b> <i>(from Web of Science Core Collection)</i></p> <p><b>Usage Count</b></p>
<p><b>Funding Agencies</b> ◀</p>	<p>8. <b>Activation process in excitable systems with multiple noise sources: Large number of units</b></p> <p>By: Franovic, Igor; Perc, Matjaz; Todorovic, Kristina; et al. <b>PHYSICAL REVIEW E</b> Volume: 92 Issue: 6 Article Number: 062912 Published: DEC 14 2015</p> <p><input type="checkbox"/> <a href="#">Full Text from Publisher</a></p> <p><input type="checkbox"/> <a href="#">View Abstract</a></p>	<p><b>Times Cited: 13</b> <i>(from Web of Science Core Collection)</i></p> <p><b>Usage Count</b></p>
<p><b>Authors</b> ◀</p>	<p>9. <b>Mean-field dynamics of a random neural network with noise</b></p> <p>By: Klinshov, Vladimir; Franovic, Igor <b>PHYSICAL REVIEW E</b> Volume: 92 Issue: 6 Article Number: 062813 Published: DEC 10 2015</p> <p><input type="checkbox"/> <a href="#">Full Text from Publisher</a></p> <p><input type="checkbox"/> <a href="#">View Abstract</a></p>	<p><b>Times Cited: 3</b> <i>(from Web of Science Core Collection)</i></p> <p><b>Usage Count</b></p>
<p><b>Open Access</b> ◀</p>	<p>10. <b>Stability, coherent spiking and synchronization in noisy excitable systems with coupling and internal delays</b></p> <p>By: Franovic, Igor; Todorovic, Kristina; Vasovic, Nebojsa; et al. <b>COMMUNICATIONS IN NONLINEAR SCIENCE AND NUMERICAL SIMULATION</b> Volume: 19 Issue: 9</p>	<p><b>Times Cited: 1</b> <i>(from Web of Science Core Collection)</i></p> <p><b>Usage Count</b></p>
<p><b>View all options</b></p> <p><i>For advanced refine options, use</i></p> <p><input type="button" value="Analyze Results"/></p>		

Pages: 3202-3219 Published: SEP 2014

[Full Text from Publisher](#)

[View Abstract](#)

11. **Cooperative behavior between oscillatory and excitable units: the peculiar role of positive coupling-frequency correlations**

**Times Cited: 8**  
*(from Web of Science Core Collection)*

By: Sonnenschein, Bernard; Peron, Thomas K. D. M.; Rodrigues, Francisco A.; et al.

**Usage Count**

EUROPEAN PHYSICAL JOURNAL B Volume: 87  
Issue: 8 Article Number: 182 Published: AUG 11 2014

[Free Full Text from Publisher](#)

[View Abstract](#)

12. **Persistence and failure of mean-field approximations adapted to a class of systems of delay-coupled excitable units**

**Times Cited: 5**  
*(from Web of Science Core Collection)*

By: Franovic, Igor; Todorovic, Kristina; Vasovic, Nebojsa; et al.

**Usage Count**

PHYSICAL REVIEW E Volume: 89 Issue: 2 Article Number: 022926 Published: FEB 28 2014

[Full Text from Publisher](#)

[View Abstract](#)

Select Page



Save to EndNote online

Add to Marked List

Sort by: **Date** Times Cited Usage Count

Page of 1

More

Show: 50 per page

12 records matched your query of the 40,553,433 in the data limits you selected.

Citing Articles: 11

(from Web of Science Core Collection)

For: Friction memory effect in complex dynamics of earthquake model ...More

Times Cited Counts

- 11 in All Databases
11 in Web of Science Core Collection
1 in BIOSIS Citation Index
0 in Chinese Science Citation Database
0 data sets in Data Citation Index
0 publication in Data Citation Index
0 in Russian Science Citation Index
0 in SciELO Citation Index

View Additional Times Cited Counts

Refine Results

Filter results by:

Open Access (3)

Refine

Publication Years

- 2017 (4)
2014 (3)
2016 (2)
2013 (1)
2018 (1)

more options / values...

Refine

Web of Science Categories

- MECHANICS (5)
ENGINEERING MECHANICAL (4)

Sort by: Date Times Cited Usage Count

Page of 1

More

Select Page



Save to EndNote online

Add to Marked List

Create Citation Report

Analyze Results

Times Cited: 0 (from Web of Science Core Collection)

Usage Count

1. Nonlinear dynamics behind the seismic cycle: One-dimensional phenomenological modeling

By: Kostic, Srdan; Vasovic, Neboja; Todorovic, Kristina; et al.

CHAOS SOLITONS & FRACTALS Volume: 106 Pages: 310-316 Published: JAN 2018

Full Text from Publisher

View Abstract

2. A novel approach with smallest transition matrix for milling stability prediction

By: Huang, Tao; Zhang, Xiaoming; Ding, Han

NONLINEAR DYNAMICS Volume: 90 Issue: 1 Pages: 95-104 Published: OCT 2017

Full Text from Publisher

View Abstract

Times Cited: 0 (from Web of Science Core Collection)

Usage Count

3. Multistable slip of a one-degree-of-freedom spring-slider model in the presence of thermal-pressurized slip-weakening friction and viscosity

By: Wang, Jeen-Hwa

NONLINEAR PROCESSES IN GEOPHYSICS Volume: 24 Issue: 3 Pages: 467-480 Published: AUG 11 2017

Free Full Text from Publisher

View Abstract

Times Cited: 0 (from Web of Science Core Collection)

Usage Count

4. An upper limit for slow-earthquake zones: self-oscillatory behavior through the Hopf bifurcation mechanism from a spring-block model under lubricated surfaces

By: Castellanos-Rodriguez, Valentina; Campos-Canton, Eric; Barboza-Gudino, Rafael; et al.

NONLINEAR PROCESSES IN GEOPHYSICS Volume: 24 Issue: 3 Pages: 419-433 Published: AUG 4 2017

Free Full Text from Publisher

View Abstract

Times Cited: 0 (from Web of Science Core Collection)

Usage Count

PHYSICS MATHEMATICAL (4)  
 MATHEMATICS  
 INTERDISCIPLINARY  
 APPLICATIONS (3)  
 GEOCHEMISTRY GEOPHYSICS  
 (2)

[more options / values...](#)

[Refine](#)

---

**Document Types** ▼

ARTICLE (11)

[Refine](#)

---

**Organizations-Enhanced** ▼

UNIVERSITY OF BELGRADE (6)  
 INST DEV WATER  
 RESOURCES JAROSLAV  
 CERNI (3)  
 INSTITUTE OF APPLIED  
 PHYSICS OF THE RUSSIAN  
 ACADEMY OF SCIENCES (2)  
 RUSSIAN ACADEMY OF  
 SCIENCES (2)  
 UNIVERSITY OF MARIBOR (2)

[more options / values...](#)

[Refine](#)

---

**Funding Agencies** ◀

---

**Authors** ◀

---

**Open Access** ◀

---

**View all options**

*For advanced refine options, use*

[Analyze Results](#)

5. **Dynamics of fault motion in a stochastic spring-slider model with varying neighboring interactions and time-delayed coupling**

By: Kostic, Srdan; Vasovic, Nebojsa; Franovic, Igor; et al.  
**NONLINEAR DYNAMICS** Volume: 87 Issue: 4 Pages:  
 2563-2575 Published: MAR 2017

[Full Text from Publisher](#)

[View Abstract](#)

**Times Cited: 0**  
*(from Web of Science Core Collection)*

**Usage Count**

6. **Phase response curves for models of earthquake fault dynamics**

By: Franovic, Igor; Kostic, Srdjan; Perc, Matjaz; et al.  
**CHAOS** Volume: 26 Issue: 6 Article Number: 063105  
 Published: JUN 2016

[Full Text from Publisher](#)

[View Abstract](#)

**Times Cited: 2**  
*(from Web of Science Core Collection)*

**Usage Count**

7. **Chaotic behavior of earthquakes induced by a nonlinear magma up flow**

By: Pelap, F. B.; Kagho, L. Y.; Fogang, C. F.  
**CHAOS SOLITONS & FRACTALS** Volume: 87 Pages:  
 71-83 Published: JUN 2016

[Full Text from Publisher](#)

[View Abstract](#)

**Times Cited: 1**  
*(from Web of Science Core Collection)*

**Usage Count**

8. **Dynamics of landslide model with time delay and periodic parameter perturbations**

By: Kostic, Srdan; Vasovic, Nebojsa; Franovic, Igor; et al.  
**COMMUNICATIONS IN NONLINEAR SCIENCE AND  
 NUMERICAL SIMULATION** Volume: 19 Issue: 9  
 Pages: 3346-3361 Published: SEP 2014

[Full Text from Publisher](#)

[View Abstract](#)

**Times Cited: 2**  
*(from Web of Science Core Collection)*

**Usage Count**

9. **Complex Dynamics of Spring-Block Earthquake Model Under Periodic Parameter Perturbations**

By: Kostic, Srdan; Vasovic, Nebojsa; Franovic, Igor; et al.  
**JOURNAL OF COMPUTATIONAL AND NONLINEAR  
 DYNAMICS** Volume: 9 Issue: 3 Article Number:  
 031019 Published: JUL 2014

[Full Text from Publisher](#)

[View Abstract](#)

**Times Cited: 1**  
*(from Web of Science Core Collection)*

**Usage Count**

10. **Triggered dynamics in a model of different fault creep regimes**

By: Kostic, Srdan; Franovic, Igor; Perc, Matjaz; et al.  
**SCIENTIFIC REPORTS** Volume: 4 Article Number:  
 5401 Published: JUN 23 2014

[Free Full Text from Publisher](#)

[View Abstract](#)

**Times Cited: 9**  
*(from Web of Science Core Collection)*

**Usage Count**

11. **Dynamic analysis of earthquake phenomena by means of pseudo phase plane**

**Times Cited: 7**  
(from Web of Science Core Collection)

By: Lopes, Antonio M.; Tenreiro Machado, J. A.

**NONLINEAR DYNAMICS** Volume: 74 Issue: 4 Pages: 1191-1202 Published: DEC 2013

**Usage Count**

[Full Text from Publisher](#)

[View Abstract](#)

Select Page

  **5K**

Sort by: **Date** Times Cited Usage Count

Page of 1

Show:

*11 records matched your query of the 40,553,433 in the data limits you selected.*



## Citing Articles: 9

(from Web of Science Core Collection)

**For:** Triggered dynamics in a mode I of different fault creep regimes  
[...More](#)

### Times Cited Counts

- 10 in All Databases
  - 9 in Web of Science Core Collection
  - 0 in BIOSIS Citation Index
  - 0 in Chinese Science Citation Database
  - 0 data sets in Data Citation Index
  - 0 publication in Data Citation Index
  - 1 in Russian Science Citation Index
  - 0 in SciELO Citation Index
- [View Additional Times Cited Counts](#)

## Refine Results

### Filter results by:

Open Access (1)

[Refine](#)

### Publication Years

- 2016 (5)
- 2017 (4)

[more options / values...](#)

[Refine](#)

### Web of Science Categories

- PHYSICS MATHEMATICAL (3)
- MATHEMATICS APPLIED (2)
- MECHANICS (2)
- PHYSICS MULTIDISCIPLINARY (2)
- COMPUTER SCIENCE
- ARTIFICIAL INTELLIGENCE (1)

Sort by: **Date** Times Cited Usage Count

More

Page of 1

Select Page



Save to EndNote online

Add to Marked List

1. **Numerical Modeling Describing the Effects of Heterogeneous Distributions of Asperities on the Quasi-static Evolution of Frictional Slip**

By: Selvadurai, P. A.; Parker, J. M.; Glaser, S. D.  
**ROCK MECHANICS AND ROCK ENGINEERING**  
 Volume: 50 Issue: 12 Pages: 3323-3335 Published: DEC 2017

[View Abstract](#)

### Create Citation Report

#### Analyze Results

**Times Cited: 0**  
 (from Web of Science Core Collection)

**Usage Count**

2. **Event-triggered fault detection for discrete-time Lipschitz nonlinear networked systems in finite-frequency domain**

By: Gu, Ying; Yang, Guang-Hong  
**NEUROCOMPUTING** Volume: 260 Pages: 245-256  
 Published: OCT 18 2017

[View Abstract](#)

**Times Cited: 0**  
 (from Web of Science Core Collection)

**Usage Count**

3. **Dynamics of fault motion in a stochastic spring-slider model with varying neighboring interactions and time-delayed coupling**

By: Kostic, Srdan; Vasovic, Nebojsa; Franovic, Igor; et al.  
**NONLINEAR DYNAMICS** Volume: 87 Issue: 4 Pages: 2563-2575  
 Published: MAR 2017

[View Abstract](#)

**Times Cited: 0**  
 (from Web of Science Core Collection)

**Usage Count**

4. **Influence of prestress and periodic corrugated boundary surfaces on Rayleigh waves in an orthotropic medium over a transversely isotropic dissipative semi-infinite substrate**

By: Gupta, Shishir; Ahmed, Mostaid  
**EUROPEAN PHYSICAL JOURNAL PLUS** Volume: 132  
 Issue: 1 Article Number: 8 Published: JAN 12 2017

**Times Cited: 1**  
 (from Web of Science Core Collection)

**Usage Count**

[more options / values...](#)  
Refine

**Document Types** ▼  
ARTICLE (9)  
Refine

**Organizations-Enhanced** ▼

- RUSSIAN ACADEMY OF SCIENCES (3)
- INST DEV WATER RESOURCES JAROSLAV CERNI (2)
- INSTITUTE OF APPLIED PHYSICS OF THE RUSSIAN ACADEMY OF SCIENCES (2)
- UNIVERSITY OF BELGRADE (2)
- COMMONWEALTH SCIENTIFIC INDUSTRIAL RESEARCH ORGANISATION CSIRO (1)

[more options / values...](#)  
Refine

**Funding Agencies** ◀

**Authors** ◀

**Open Access** ◀

**View all options**

*For advanced refine options, use*

[Analyze Results](#)

[Full Text from Publisher](#)

[View Abstract](#)

5. **Stochastic chaos induced by diffusion processes with identical spectral density but different probability density functions**

**Times Cited: 0**  
*(from Web of Science Core Collection)*

**Usage Count**

By: Lei, Youming; Zheng, Fan  
**CHAOS** Volume: 26 Issue: 12 Article Number: 123111 Published: DEC 2016

[Full Text from Publisher](#)

[View Abstract](#)

6. **Analysis of Dynamics in Multiphysics Modelling of Active Faults**

**Times Cited: 1**  
*(from Web of Science Core Collection)*

**Usage Count**

By: Alevizos, Sotiris; Poulet, Thomas; Veveakis, Manolis; et al.  
**MATHEMATICS** Volume: 4 Issue: 4 Article Number: 57 Published: DEC 2016

[Free Full Text from Publisher](#)

[View Abstract](#)

7. **Phase response curves for models of earthquake fault dynamics**

**Times Cited: 2**  
*(from Web of Science Core Collection)*

**Usage Count**

By: Franovic, Igor; Kostic, Srdjan; Perc, Matjaz; et al.  
**CHAOS** Volume: 26 Issue: 6 Article Number: 063105 Published: JUN 2016

[Full Text from Publisher](#)

[View Abstract](#)

8. **Chaotic behavior of earthquakes induced by a nonlinear magma up flow**

**Times Cited: 1**  
*(from Web of Science Core Collection)*

**Usage Count**

By: Pelap, F. B.; Kagho, L. Y.; Fogang, C. F.  
**CHAOS SOLITONS & FRACTALS** Volume: 87 Pages: 71-83 Published: JUN 2016

[Full Text from Publisher](#)

[View Abstract](#)

9. **Effect of Dynamic Stress State Perturbation on Irreversible Strain Accumulation at Interfaces in Block-Structured Media**

**Times Cited: 15**  
*(from Web of Science Core Collection)*

**Usage Count**

By: Grigoriev, A. S.; Shilko, E. V.; Astafurov, S. V.; et al.  
**PHYSICAL MESOMECHANICS** Volume: 19 Issue: 2 Pages: 136-148 Published: APR 2016

[View Abstract](#)

Select Page   **5K**

[Save to EndNote online](#)

[Add to Marked List](#)

Sort by: **Date** Times Cited Usage Count

More ▼

Show: 50 per page ▼

### Citing Articles: 8

(from Web of Science Core Collection)

**For:** Cluster synchronization of spiking induced by noise and interaction delays in homogenous neuronal network [...More](#)

#### Times Cited Counts

- 8 in All Databases
  - 8 in Web of Science Core Collection
  - 0 in BIOSIS Citation Index
  - 0 in Chinese Science Citation Database
  - 0 data sets in Data Citation Index
  - 0 publication in Data Citation Index
  - 0 in Russian Science Citation Index
  - 0 in SciELO Citation Index
- [View Additional Times Cited Counts](#)

### Refine Results

#### Publication Years

- 2014 (3)
- 2013 (2)
- 2017 (2)
- 2016 (1)

[more options / values...](#)

Refine

#### Web of Science Categories

- PHYSICS MATHEMATICAL (7)
- MATHEMATICS APPLIED (3)
- PHYSICS FLUIDS PLASMAS (3)
- AUTOMATION CONTROL SYSTEMS (1)
- ENGINEERING ELECTRICAL ELECTRONIC (1)

[more options / values...](#)

Refine

Sort by: **Date** | Times Cited | Usage Count | Page 1 of 1

More

Select Page 5K

Save to EndNote online

#### Create Citation Report

#### Analyze Results

- 1. Delay-induced locking in bursting neuronal networks**

By: Zhu, Jinjie; Liu, Xianbin  
[CHAOS](#) Volume: 27 Issue: 8 Article Number: 083114  
 Published: AUG 2017

**Times Cited: 0**  
(from Web of Science Core Collection)

**Usage Count**
  
- 2. Mean-field dynamics of a population of stochastic map neurons**

By: Franovic, Igor; Maslennikov, Oleg V.; Bacic, Iva; et al.  
[PHYSICAL REVIEW E](#) Volume: 96 Issue: 1 Article Number: 012226  
 Published: JUL 27 2017

**Times Cited: 0**  
(from Web of Science Core Collection)

**Usage Count**
  
- 3. Locking induced by distance-dependent delay in neuronal networks**

By: Zhu, Jinjie; Liu, Xianbin  
[PHYSICAL REVIEW E](#) Volume: 94 Issue: 5 Article Number: 052405  
 Published: NOV 14 2016

**Times Cited: 0**  
(from Web of Science Core Collection)

**Usage Count**
  
- 4. Fault tolerant synchronization for a class of complex interconnected neural networks with delay**

By: Wang, Zhanshan; Li, Tieshan; Zhang, Huaguang  
[INTERNATIONAL JOURNAL OF ADAPTIVE CONTROL AND SIGNAL PROCESSING](#) Volume: 28  
 Issue: 10 Pages: 859-881 Published: OCT 2014

**Times Cited: 20**  
(from Web of Science Core Collection)

**Usage Count**
  
- 5. Clustering versus non-clustering phase synchronizations**

**Times Cited: 5**  
(from Web of Science Core Collection)

**Usage Count**

**Document Types** ▼

ARTICLE (7)  
REVIEW (1)

[more options / values...](#)

Refine

---

**Organizations-Enhanced** ▼

NANJING UNIVERSITY OF AERONAUTICS AND ASTRONAUTICS (2)  
UNIVERSITY OF BELGRADE (2)  
BEIHANG UNIVERSITY (1)  
CHINESE ACADEMY OF SCIENCES (1)  
DALIAN MARITIME UNIVERSITY (1)

[more options / values...](#)

Refine

---

**Funding Agencies** ◀

---

**Authors** ◀

---

**Open Access** ◀

---

**View all options**

*For advanced refine options, use*

[Analyze Results](#)

By: Liu, Shuai; Zhan, Meng  
**CHAOS** Volume: 24 Issue: 1 Article Number: 013104  
Published: MAR 2014

Core Collection)  
**Usage Count**

[Full Text from Publisher](#)  [View Abstract](#)

6. **Persistence and failure of mean-field approximations adapted to a class of systems of delay-coupled excitable units**

**Times Cited: 5**  
*(from Web of Science Core Collection)*  
**Usage Count**

By: Franovic, Igor; Todorovic, Kristina; Vasovic, Nebojsa; et al.  
**PHYSICAL REVIEW E** Volume: 89 Issue: 2 Article Number: 022926 Published: FEB 28 2014

[Full Text from Publisher](#)  [View Abstract](#)

7. **Cluster synchronization induced by one-node clusters in networks with asymmetric negative couplings**

**Times Cited: 15**  
*(from Web of Science Core Collection)*  
**Usage Count**

By: Zhang, Jianbao; Ma, Zhongjun; Zhang, Gang  
**CHAOS** Volume: 23 Issue: 4 Article Number: 043128  
Published: DEC 2013

[Full Text from Publisher](#)  [View Abstract](#)

8. **Cooperative dynamics in neuronal networks**

**Times Cited: 31**  
*(from Web of Science Core Collection)*  
**Usage Count**

By: Wang, Qingyun; Zheng, Yanhong; Ma, Jun  
**CHAOS SOLITONS & FRACTALS** Volume: 56 Special Issue: SI Pages: 19-27 Published: NOV 2013

[Full Text from Publisher](#)  [View Abstract](#)

Select Page   **5K**

**Sort by:** Date Times Cited Usage Count Page of 1

▼

Show:  ▼

*8 records matched your query of the 40,553,433 in the data limits you selected.*

Citing Articles: 8

(from Web of Science Core Collection)

For: Phase plane approach to cooperative rhythms in neuron motifs with delayed inhibitory synapses ...More

Times Cited Counts

- 8 in All Databases
8 in Web of Science Core Collection
1 in BIOSIS Citation Index
0 in Chinese Science Citation Database
0 data sets in Data Citation Index
0 publication in Data Citation Index
0 in Russian Science Citation Index
0 in SciELO Citation Index
View Additional Times Cited Counts

Refine Results

Publication Years

- 2012 (4)
2013 (2)
2016 (1)
2017 (1)

more options / values...

Refine

Web of Science Categories

- PHYSICS MATHEMATICAL (6)
PHYSICS MULTIDISCIPLINARY (5)
MATHEMATICS INTERDISCIPLINARY APPLICATIONS (4)
MATHEMATICS APPLIED (1)
MULTIDISCIPLINARY SCIENCES (1)

more options / values...

Refine

Sort by: Date Times Cited Usage Count Page of 1

More

Select Page 5K

Save to EndNote online Add to Marked List

Create Citation Report

Analyze Results

Times Cited: 0 (from Web of Science Core Collection)

Usage Count

1. Mean-field dynamics of a population of stochastic map neurons

By: Franovic, Igor; Maslennikov, Oleg V.; Bacic, Iva; et al. PHYSICAL REVIEW E Volume: 96 Issue: 1 Article Number: 012226 Published: JUL 27 2017

Full Text from Publisher

View Abstract

2. Dependence of inter-neuronal effective connectivity on synchrony dynamics in neuronal network motifs

By: Deng, Bin; Deng, Yun; Yu, Haitao; et al. CHAOS SOLITONS & FRACTALS Volume: 82 Pages: 48-59 Published: JAN 2016

Full Text from Publisher

View Abstract

Times Cited: 2 (from Web of Science Core Collection)

Usage Count

3. Impact of delays on the synchronization transitions of modular neuronal networks with hybrid synapses

By: Liu, Chen; Wang, Jiang; Yu, Haitao; et al. CHAOS Volume: 23 Issue: 3 Article Number: 033121 Published: SEP 2013

Full Text from Publisher

View Abstract

Times Cited: 12 (from Web of Science Core Collection)

Usage Count

4. The effects of time delay on the synchronization transitions in a modular neuronal network with hybrid synapses

By: Liu, Chen; Wang, Jiang; Yu, Haitao; et al. CHAOS SOLITONS & FRACTALS Volume: 47 Pages: 54-65 Published: FEB 2013

Full Text from Publisher

View Abstract

Times Cited: 6 (from Web of Science Core Collection)

Usage Count

**Document Types** ▼

ARTICLE (8)

[Refine](#)

---

**Organizations-Enhanced** ▼

TIANJIN UNIVERSITY (3)  
 UNIVERSITY OF BELGRADE (2)  
 HONG KONG POLYTECHNIC UNIVERSITY (1)  
 HUAZHONG UNIVERSITY OF SCIENCE TECHNOLOGY (1)  
 INSTITUTE OF APPLIED PHYSICS OF THE RUSSIAN ACADEMY OF SCIENCES (1)

[more options / values...](#)

[Refine](#)

---

**Funding Agencies** ◀

---

**Authors** ◀

---

**Open Access** ◀

---

**View all options**

*For advanced refine options, use*

[Analyze Results](#)

5. **Harmonic synchronization model of the mating dengue vector mosquitoes**

By: Yang Nan; Long ZhangCai; Wang Fei  
**CHINESE SCIENCE BULLETIN** Volume: 57 Issue: 31  
 Pages: 4043-4048 Published: NOV 2012

**Times Cited: 0**  
*(from Web of Science Core Collection)*

**Usage Count**

[Full Text from Publisher](#) [View Abstract](#)

6. **The role of neural architecture and the speed of signal propagation in the process of synchronization of bursting neurons**

By: Gosak, Marko; Markovic, Rene; Marhl, Marko  
**PHYSICA A-STATISTICAL MECHANICS AND ITS APPLICATIONS** Volume: 391 Issue: 8 Pages: 2764-2770  
 Published: APR 15 2012

**Times Cited: 14**  
*(from Web of Science Core Collection)*

**Usage Count**

[Full Text from Publisher](#) [View Abstract](#)

7. **Possibilities of introducing different functional circuits on top of a structural neuron triplet: Where do the gains lie?**

By: Franovic, Igor; Miljkovic, Vladimir  
**CHAOS SOLITONS & FRACTALS** Volume: 45 Issue: 4  
 Pages: 527-538 Published: APR 2012

**Times Cited: 1**  
*(from Web of Science Core Collection)*

**Usage Count**

[Full Text from Publisher](#) [View Abstract](#)

8. **Delay-induced diversity of firing behavior and ordered chaotic firing in adaptive neuronal networks**

By: Gong, Yubing; Wang, Li; Xu, Bo  
**CHAOS SOLITONS & FRACTALS** Volume: 45 Issue: 4  
 Pages: 548-553 Published: APR 2012

**Times Cited: 2**  
*(from Web of Science Core Collection)*

**Usage Count**

[Full Text from Publisher](#) [View Abstract](#)

Select Page   **5K**

[Save to EndNote online](#) [Add to Marked List](#)

**Sort by:** Date Times Cited Usage Count

More

Show: 50 per page

Page of 1

*8 records matched your query of the 40,553,433 in the data limits you selected.*

Citing Articles: 7

(from Web of Science Core Collection)

For: Power law behavior related to mutual synchronization of chemicall y coupled map neurons ...More

Times Cited Counts

- 8 in All Databases
7 in Web of Science Core Collection
1 in BIOSIS Citation Index
1 in Chinese Science Citation Database
0 data sets in Data Citation Index
0 publication in Data Citation Index
0 in Russian Science Citation Index
0 in SciELO Citation Index
View Additional Times Cited Counts

Refine Results

Publication Years

- 2011 (2)
2010 (1)
2012 (1)
2013 (1)
2014 (1)

more options / values...

Refine

Web of Science Categories

- PHYSICS MULTIDISCIPLINARY (6)
MATHEMATICS INTERDISCIPLINARY APPLICATIONS (2)
PHYSICS MATHEMATICAL (2)
BIOCHEMICAL RESEARCH METHODS (1)
NEUROSCIENCES (1)

more options / values...

Sort by: Date Times Cited Usage Count

Page of 1

More

Select Page 5K

Save to EndNote online

Add to Marked List

Create Citation Report

Analyze Results

1. Synchronization in network motifs of delay-coupled map-based neurons

By: Sausedo-Solorio, J. M.; Pisarchik, A. N.
EUROPEAN PHYSICAL JOURNAL-SPECIAL TOPICS
Volume: 226 Issue: 9 Pages: 1911-1920 Published: JUN 2017

Full Text from Publisher

View Abstract

Times Cited: 2
(from Web of Science Core Collection)

Usage Count

2. Synchronization of map-based neurons with memory and synaptic delay

By: Sausedo-Solorio, J. M.; Pisarchik, A. N.
PHYSICS LETTERS A Volume: 378 Issue: 30-31
Pages: 2108-2112 Published: JUN 13 2014

Full Text from Publisher

View Abstract

Times Cited: 19
(from Web of Science Core Collection)

Usage Count

3. A brief history of excitable map-based neurons and neural networks

By: Girardi-Schappo, M.; Tragtenberg, M. H. R.; Kinouchi, O.
JOURNAL OF NEUROSCIENCE METHODS Volume: 220 Issue: 2 Special Issue: SI
Pages: 116-130 Published: NOV 15 2013

Full Text from Publisher

View Abstract

Times Cited: 23
(from Web of Science Core Collection)

Usage Count

4. Possibilities of introducing different functional circuits on top of a structural neuron triplet: Where do the gains lie?

By: Franovic, Igor; Miljkovic, Vladimir
CHAOS SOLITONS & FRACTALS Volume: 45 Issue: 4
Pages: 527-538 Published: APR 2012

Full Text from Publisher

View Abstract

Times Cited: 1
(from Web of Science Core Collection)

Usage Count

<p style="text-align: right;"><a href="#">Refine</a></p> <p><b>Document Types</b> ▼</p> <p>ARTICLE (6) REVIEW (1)</p> <p><a href="#">more options / values...</a></p> <p style="text-align: right;"><a href="#">Refine</a></p> <p><b>Organizations-Enhanced</b> ▼</p> <p>UNIVERSITY OF BELGRADE (3) POLYTECHNIC UNIVERSITY OF MADRID (2) UNIVERSIDAD AUTONOMA DEL ESTADO DE HIDALGO (2) CIO CENTRO DE INVESTIGACIONES EN OPTICA A C (1) CTR INVEST OPTIC (1)</p> <p><a href="#">more options / values...</a></p> <p style="text-align: right;"><a href="#">Refine</a></p> <p><b>Funding Agencies</b> ◀</p> <p><b>Authors</b> ◀</p> <p><b>Open Access</b> ◀</p> <p><b>View all options</b></p> <p><i>For advanced refine options, use</i></p> <p><a href="#">Analyze Results</a></p>	<p>5. <b>Map-based models in neuronal dynamics</b></p> <p>By: Ibarz, B.; Casado, J. M.; Sanjuan, M. A. F. <b>PHYSICS REPORTS-REVIEW SECTION OF PHYSICS LETTERS</b> Volume: 501 Issue: 1-2 Pages: 1-74 Published: APR 2011</p> <p><a href="#">Full Text from Publisher</a></p> <p><a href="#">View Abstract</a></p> <p>6. <b>Functional motifs: a novel perspective on burst synchronization and regularization of neurons coupled via delayed inhibitory synapses</b></p> <p>By: Franovic, Igor; Miljkovic, Vladimir <b>CHAOS SOLITONS &amp; FRACTALS</b> Volume: 44 Issue: 1-3 Pages: 122-130 Published: JAN-MAR 2011</p> <p><a href="#">Full Text from Publisher</a></p> <p><a href="#">View Abstract</a></p> <p>7. <b>Phase plane approach to cooperative rhythms in neuron motifs with delayed inhibitory synapses</b></p> <p>By: Franovic, I.; Miljkovic, V. <b>EPL</b> Volume: 92 Issue: 6 Article Number: 68007 Published: DEC 2010</p> <p><a href="#">Full Text from Publisher</a></p> <p><a href="#">View Abstract</a></p>	<p><b>Times Cited: 117</b> <i>(from Web of Science Core Collection)</i></p> <p><b>Usage Count</b></p> <p><b>Times Cited: 4</b> <i>(from Web of Science Core Collection)</i></p> <p><b>Usage Count</b></p> <p><b>Times Cited: 8</b> <i>(from Web of Science Core Collection)</i></p> <p><b>Usage Count</b></p>
	<p>Select Page</p> <p><a href="#">Save to EndNote online</a> <a href="#">Add to Marked List</a></p> <p><a href="#">5K</a></p>	
	<p><b>Sort by:</b> <u>Date</u> Times Cited Usage Count</p> <p>More</p> <p>Show: 50 per page</p>	<p>Page of 1</p>
	<p><i>7 records matched your query of the 40,553,433 in the data limits you selected.</i></p>	



### Citing Articles: 5

(from Web of Science Core Collection)

**For:** Persistence and failure of mean-field approximations adapted to a class of systems of delay-coupled ...[More](#)

#### Times Cited Counts

- 5 in All Databases
  - 5 in Web of Science Core Collection
  - 0 in BIOSIS Citation Index
  - 0 in Chinese Science Citation Database
  - 0 data sets in Data Citation Index
  - 0 publication in Data Citation Index
  - 0 in Russian Science Citation Index
  - 0 in SciELO Citation Index
- [View Additional Times Cited Counts](#)

### Refine Results

#### Filter results by:

Open Access (1)

[Refine](#)

#### Publication Years

- 2015 (2)
- 2014 (1)
- 2016 (1)
- 2017 (1)

[more options / values...](#)

[Refine](#)

#### Web of Science Categories

- PHYSICS FLUIDS PLASMAS (3)
- PHYSICS MATHEMATICAL (3)
- PHYSICS CONDENSED MATTER (1)

Sort by: **Date** Times Cited Usage Count

Page of 1

More

Select Page 5K

Save to EndNote online

Add to Marked List

### Create Citation Report

#### Analyze Results

**Times Cited: 0**  
(from Web of Science Core Collection)

**Usage Count**

#### 1. Mean-field dynamics of a population of stochastic map neurons

By: Franovic, Igor; Maslennikov, Oleg V.; Bacic, Iva; et al.  
[PHYSICAL REVIEW E](#) Volume: 96 Issue: 1 Article Number: 012226 Published: JUL 27 2017

[Full Text from Publisher](#)

[View Abstract](#)

#### 2. Slow rate fluctuations in a network of noisy neurons with coupling delay

By: Franovic, I.; Klinshov, V.  
[EPL](#) Volume: 116 Issue: 4 Article Number: 48002 Published: NOV 2016

[Full Text from Publisher](#)

[View Abstract](#)

**Times Cited: 1**  
(from Web of Science Core Collection)

**Usage Count**

#### 3. Activation process in excitable systems with multiple noise sources: Large number of units

By: Franovic, Igor; Perc, Matjaz; Todorovic, Kristina; et al.  
[PHYSICAL REVIEW E](#) Volume: 92 Issue: 6 Article Number: 062912 Published: DEC 14 2015

[Full Text from Publisher](#)

[View Abstract](#)

**Times Cited: 13**  
(from Web of Science Core Collection)

**Usage Count**

#### 4. Mean-field dynamics of a random neural network with noise

By: Klinshov, Vladimir; Franovic, Igor  
[PHYSICAL REVIEW E](#) Volume: 92 Issue: 6 Article Number: 062813 Published: DEC 10 2015

[Full Text from Publisher](#)

[View Abstract](#)

**Times Cited: 3**  
(from Web of Science Core Collection)

**Usage Count**

#### 5. Cooperative behavior between oscillatory and excitable units: the peculiar role of positive

**Times Cited: 8**  
(from Web of Science Core Collection)

PHYSICS MULTIDISCIPLINARY (1)

[more options / values...](#)

**Refine**

**Document Types** ▼

ARTICLE (5)

**Refine**

**Organizations-Enhanced** ▼

- UNIVERSITY OF BELGRADE (4)
- INSTITUTE OF APPLIED PHYSICS OF THE RUSSIAN ACADEMY OF SCIENCES (3)
- RUSSIAN ACADEMY OF SCIENCES (3)
- BERNSTEIN CTR COMPUTAT NEUROSCI BERLIN (1)
- HUMBOLDT UNIVERSITY OF BERLIN (1)

[more options / values...](#)

**Refine**

**Funding Agencies** ◀

**Authors** ◀

**Open Access** ◀

**View all options**

*For advanced refine options, use*

[Analyze Results](#)

### coupling-frequency correlations

Core Collection)

By: Sonnenschein, Bernard; Peron, Thomas K. D. M.; Rodrigues, Francisco A.; et al.

EUROPEAN PHYSICAL JOURNAL B Volume: 87  
Issue: 8 Article Number: 182 Published: AUG 11 2014

**Usage Count**

[Free Full Text from Publisher](#)

[View Abstract](#)

Select Page   **5K**

▼

[Add to Marked List](#)

**Sort by:** Date Times Cited Usage Count

Page of 1

▼

Show:  ▼

*5 records matched your query of the 40,553,433 in the data limits you selected.*

**Citing Articles: 5***(from Web of Science Core Collection)***For:** Dynamics of simple earthquake model with time delay and variation of friction strength [...More](#)**Times Cited Counts**

5 in All Databases

5 in Web of Science Core Collection

0 in BIOSIS Citation Index

0 in Chinese Science Citation Database

0 data sets in Data Citation Index

0 publication in Data Citation Index

0 in Russian Science Citation Index

0 in SciELO Citation Index

[View Additional Times Cited Counts](#)**Refine Results****Publication Years** ▾

2016 (2)

2018 (2)

2017 (1)

[more options / values...](#)[Refine](#)**Web of Science Categories** ▾

PHYSICS MATHEMATICAL (3)

PHYSICS MULTIDISCIPLINARY (3)

MATHEMATICS INTERDISCIPLINARY APPLICATIONS (2)

MECHANICS (2)

ACOUSTICS (1)

[more options / values...](#)[Refine](#)**Document Types** ▾Sort by: **Date** Times Cited Usage Count

Page

of 1

More ▾

Select Page



Save to EndNote online ▾

Add to Marked List

**Create Citation Report** **Analyze Results****Times Cited: 0***(from Web of Science Core Collection)***Usage Count**1. **Solitary waves in the excitable Burridge-Knopoff model**

By: Morales, J. E.; James, G.; Tonnelier, A.

**WAVE MOTION** Volume: 76 Pages: 103-121

Published: JAN 2018

 [Full Text from Publisher](#)[View Abstract](#)2. **Nonlinear dynamics behind the seismic cycle: One-dimensional phenomenological modeling**

By: Kostic, Srdan; Vasovic, Neboja; Todorovic, Kristina; et al.

**CHAOS SOLITONS & FRACTALS** Volume: 106

Pages: 310-316 Published: JAN 2018

 [Full Text from Publisher](#)[View Abstract](#)**Times Cited: 0***(from Web of Science Core Collection)***Usage Count**3. **Dynamics of fault motion in a stochastic spring-slider model with varying neighboring interactions and time-delayed coupling**

By: Kostic, Srdan; Vasovic, Nebojsa; Franovic, Igor; et al.

**NONLINEAR DYNAMICS** Volume: 87 Issue: 4 Pages:

2563-2575 Published: MAR 2017

 [Full Text from Publisher](#)[View Abstract](#)**Times Cited: 0***(from Web of Science Core Collection)***Usage Count**4. **Phase response curves for models of earthquake fault dynamics**

By: Franovic, Igor; Kostic, Srdjan; Perc, Matjaz; et al.

**CHAOS** Volume: 26 Issue: 6 Article Number: 063105

Published: JUN 2016

 [Full Text from Publisher](#)[View Abstract](#)**Times Cited: 2***(from Web of Science Core Collection)***Usage Count**

ARTICLE (5)

Refine

Organizations-Enhanced

- INST DEV WATER RESOURCES JAROSLAV CERNI (3)
- UNIVERSITY OF BELGRADE (3)
- INSTITUTE OF APPLIED PHYSICS OF THE RUSSIAN ACADEMY OF SCIENCES (2)
- RUSSIAN ACADEMY OF SCIENCES (2)
- HUMBOLDT UNIVERSITY OF BERLIN (1)

more options / values...

Refine

Funding Agencies

Authors

Open Access

View all options

For advanced refine options, use

Analyze Results

5. Chaotic behavior of earthquakes induced by a nonlinear magma up flow

By: Pelap, F. B.; Kagho, L. Y.; Fogang, C. F.

CHAOS SOLITONS & FRACTALS Volume: 87 Pages: 71-83 Published: JUN 2016

Full Text from Publisher

View Abstract

Select Page



Save to EndNote online

Add to Marked List

Times Cited: 1 (from Web of Science Core Collection)

Usage Count

Sort by: Date Times Cited Usage Count

Page of 1

More

Show: 50 per page

5 records matched your query of the 40,553,433 in the data limits you selected.

## Citing Articles: 5

(from Web of Science Core Collection)

**For:** The effects of synaptic time delay on motifs of chemically coupled Rulkov model neurons [...More](#)

### Times Cited Counts

- 5 in All Databases
  - 5 in Web of Science Core Collection
  - 1 in BIOSIS Citation Index
  - 0 in Chinese Science Citation Database
  - 0 data sets in Data Citation Index
  - 0 publication in Data Citation Index
  - 0 in Russian Science Citation Index
  - 0 in SciELO Citation Index
- [View Additional Times Cited Counts](#)

## Refine Results

### Publication Years

- 2013 (2)
- 2011 (1)
- 2016 (1)
- 2017 (1)

[more options / values...](#)

[Refine](#)

### Web of Science Categories

- PHYSICS FLUIDS PLASMAS (3)
- PHYSICS MATHEMATICAL (3)
- BIOCHEMICAL RESEARCH METHODS (1)
- MATHEMATICS APPLIED (1)
- MATHEMATICS INTERDISCIPLINARY APPLICATIONS (1)

[more options / values...](#)

[Refine](#)

Sort by: **Date** Times Cited Usage Count Page of 1

More

Select Page   **5K**

Save to EndNote online

### Create Citation Report

### Analyze Results

**Times Cited: 0**  
(from Web of Science Core Collection)

**Usage Count**

1. **Mean-field dynamics of a population of stochastic map neurons**

By: Franovic, Igor; Maslennikov, Oleg V.; Bacic, Iva; et al.  
[PHYSICAL REVIEW E](#) Volume: 96 Issue: 1 Article Number: 012226 Published: JUL 27 2017

2. **Stability and synchronization of coupled Rulkov map-based neurons with chemical synapses**

By: Hu, Dongpo; Cao, Hongjun  
[COMMUNICATIONS IN NONLINEAR SCIENCE AND NUMERICAL SIMULATION](#) Volume: 35 Pages: 105-122 Published: JUN 2016

**Times Cited: 4**  
(from Web of Science Core Collection)

**Usage Count**

3. **A brief history of excitable map-based neurons and neural networks**

By: Girardi-Schappo, M.; Tragtenberg, M. H. R.; Kinouchi, O.  
[JOURNAL OF NEUROSCIENCE METHODS](#) Volume: 220 Issue: 2 Special Issue: SI Pages: 116-130 Published: NOV 15 2013

**Times Cited: 23**  
(from Web of Science Core Collection)

**Usage Count**

4. **Bursting frequency versus phase synchronization in time-delayed neuron networks**

By: Nordenfelt, Anders; Used, Javier; Sanjuan, Miguel A. F.  
[PHYSICAL REVIEW E](#) Volume: 87 Issue: 5 Article Number: 052903 Published: MAY 9 2013

**Times Cited: 17**  
(from Web of Science Core Collection)

**Usage Count**

**Document Types**

ARTICLE (4)  
REVIEW (1)

[more options / values...](#)

[Refine](#)

**Organizations-Enhanced**

UNIVERSIDAD REY JUAN CARLOS (2)  
BEIJING JIAOTONG UNIVERSITY (1)  
INSTITUTE OF APPLIED PHYSICS OF THE RUSSIAN ACADEMY OF SCIENCES (1)  
NEW YORK UNIVERSITY (1)  
RUSSIAN ACADEMY OF SCIENCES (1)

[more options / values...](#)

[Refine](#)

**Funding Agencies**

**Authors**

**Open Access**

**View all options**

*For advanced refine options, use*

[Analyze Results](#)

5. **Map-based models in neuronal dynamics**

By: Ibarz, B.; Casado, J. M.; Sanjuan, M. A. F.  
**PHYSICS REPORTS-REVIEW SECTION OF PHYSICS LETTERS** Volume: 501 Issue: 1-2 Pages: 1-74 Published: APR 2011

**Times Cited: 117**  
*(from Web of Science Core Collection)*

**Usage Count**

[Full Text from Publisher](#)

[View Abstract](#)

Select Page

5K

[Save to EndNote online](#)

[Add to Marked List](#)

Sort by: **Date** Times Cited Usage Count

Page of 1

More

Show: 50 per page

*5 records matched your query of the 40,553,433 in the data limits you selected.*

Citing Articles: 4

(from Web of Science Core Collection)

For: Functional motifs: a novel perspective on burst synchronization and regularization of neurons couple ...More

Times Cited Counts

- 4 in All Databases
4 in Web of Science Core Collection
0 in BIOSIS Citation Index
0 in Chinese Science Citation Database
0 data sets in Data Citation Index
0 publication in Data Citation Index
0 in Russian Science Citation Index
0 in SciELO Citation Index
View Additional Times Cited Counts

Refine Results

Publication Years

- 2012 (3)
2016 (1)

more options / values...

Refine

Web of Science Categories

- PHYSICS MATHEMATICAL (4)
MATHEMATICS INTERDISCIPLINARY APPLICATIONS (2)
PHYSICS MULTIDISCIPLINARY (2)
MATHEMATICS APPLIED (1)
PHYSICS FLUIDS PLASMAS (1)

more options / values...

Refine

Document Types

Sort by: Date Times Cited Usage Count

Page of 1

More

Select Page



Save to EndNote online

Add to Marked List

Create Citation Report

Analyze Results

Times Cited: 2 (from Web of Science Core Collection)

Usage Count

1. Dependence of inter-neuronal effective connectivity on synchrony dynamics in neuronal network motifs

By: Deng, Bin; Deng, Yun; Yu, Haitao; et al.

CHAOS SOLITONS & FRACTALS Volume: 82 Pages: 48-59 Published: JAN 2016

Full Text from Publisher

View Abstract

2. Cluster synchronization of spiking induced by noise and interaction delays in homogenous neuronal ensembles

By: Franovic, Igor; Todorovic, Kristina; Vasovic, Nebojsa; et al.

CHAOS Volume: 22 Issue: 3 Article Number: 033147 Published: SEP 2012

Full Text from Publisher

View Abstract

Times Cited: 8 (from Web of Science Core Collection)

Usage Count

3. Complex synchronous behavior in interneuronal networks with delayed inhibitory and fast electrical synapses

By: Guo, Daqing; Wang, Qingyun; Perc, Matjaz

PHYSICAL REVIEW E Volume: 85 Issue: 6 Article Number: 061905 Part: 1 Published: JUN 7 2012

Full Text from Publisher

View Abstract

Times Cited: 95 (from Web of Science Core Collection)

Usage Count

4. Possibilities of introducing different functional circuits on top of a structural neuron triplet: Where do the gains lie?

By: Franovic, Igor; Miljkovic, Vladimir

CHAOS SOLITONS & FRACTALS Volume: 45 Issue: 4 Pages: 527-538 Published: APR 2012

Full Text from Publisher

Times Cited: 1 (from Web of Science Core Collection)

Usage Count

### Citing Articles: 3

(from Web of Science Core Collection)

**For:** Earthquake nucleation in a stochastic fault model of globally coupled units with interaction delays  
[...More](#)

#### Times Cited Counts

- 3 in All Databases
  - 3 in Web of Science Core Collection
  - 0 in BIOSIS Citation Index
  - 0 in Chinese Science Citation Database
  - 0 data sets in Data Citation Index
  - 0 publication in Data Citation Index
  - 0 in Russian Science Citation Index
  - 0 in SciELO Citation Index
- [View Additional Times Cited Counts](#)

### Refine Results

#### Publication Years

- 2017 (2)
- 2018 (1)

[more options / values...](#)

Refine

#### Web of Science Categories

- ENGINEERING MECHANICAL (2)
- MECHANICS (2)
- MATHEMATICS INTERDISCIPLINARY APPLICATIONS (1)
- PHYSICS MATHEMATICAL (1)
- PHYSICS MULTIDISCIPLINARY (1)

[more options / values...](#)

Refine

#### Document Types

Sort by: **Date**    Times Cited    Usage Count    Page of 1

More

Select Page      **5K**

Save to EndNote online

Add to Marked List

#### Create Citation Report

 Analyze Results

1. **Nonlinear dynamics behind the seismic cycle: One-dimensional phenomenological modeling**

By: Kostic, Srdan; Vasovic, Neboja; Todorovic, Kristina; et al.

**CHAOS SOLITONS & FRACTALS** Volume: 106  
 Pages: 310-316 Published: JAN 2018

 [Full Text from Publisher](#)

[View Abstract](#)

**Times Cited: 0**  
 (from Web of Science Core Collection)

**Usage Count**

2. **A novel approach with smallest transition matrix for milling stability prediction**

By: Huang, Tao; Zhang, Xiaoming; Ding, Han

**NONLINEAR DYNAMICS** Volume: 90 Issue: 1 Pages: 95-104  
 Published: OCT 2017

 [Full Text from Publisher](#)

[View Abstract](#)

**Times Cited: 0**  
 (from Web of Science Core Collection)

**Usage Count**

3. **Dynamics of fault motion in a stochastic spring-slider model with varying neighboring interactions and time-delayed coupling**

By: Kostic, Srdan; Vasovic, Nebojsa; Franovic, Igor; et al.

**NONLINEAR DYNAMICS** Volume: 87 Issue: 4 Pages: 2563-2575  
 Published: MAR 2017

 [Full Text from Publisher](#)

[View Abstract](#)

**Times Cited: 0**  
 (from Web of Science Core Collection)

**Usage Count**

Select Page      **5K**

Save to EndNote online

Add to Marked List

Sort by: **Date**    Times Cited    Usage Count    Page of 1

More

Show: 50 per page

3 records matched your query of the 40,553,433 in the data limits you selected.



Citing Articles: 3

(from Web of Science Core Collection)

For: Mean-field dynamics of a random neural network with noise ...More

Times Cited Counts

- 3 in All Databases
3 in Web of Science Core Collection
0 in BIOSIS Citation Index
0 in Chinese Science Citation Database
0 data sets in Data Citation Index
0 publication in Data Citation Index
0 in Russian Science Citation Index
0 in SciELO Citation Index

View Additional Times Cited Counts

Refine Results

Publication Years

- 2016 (1)
2017 (1)
2018 (1)

more options / values...

Refine

Web of Science Categories

- PHYSICS MATHEMATICAL (2)
MATHEMATICS APPLIED (1)
PHYSICS FLUIDS PLASMAS (1)
PHYSICS MULTIDISCIPLINARY (1)

more options / values...

Refine

Document Types

- ARTICLE (3)

Sort by: Date Times Cited Usage Count

Page of 1

More

Select Page 5K

Save to EndNote online

Add to Marked List

Create Citation Report

Analyze Results

Times Cited: 0 (from Web of Science Core Collection)

Usage Count

1. Clustering promotes switching dynamics in networks of noisy neurons

By: Franovic, Igor; Klinshov, Vladimir

CHAOS Volume: 28 Issue: 2 Article Number: 023111 Published: FEB 2018

Full Text from Publisher

View Abstract

2. Mean-field dynamics of a population of stochastic map neurons

By: Franovic, Igor; Maslennikov, Oleg V.; Bacic, Iva; et al.

PHYSICAL REVIEW E Volume: 96 Issue: 1 Article Number: 012226 Published: JUL 27 2017

Full Text from Publisher

View Abstract

Times Cited: 0 (from Web of Science Core Collection)

Usage Count

3. Slow rate fluctuations in a network of noisy neurons with coupling delay

By: Franovic, I.; Klinshov, V.

EPL Volume: 116 Issue: 4 Article Number: 48002 Published: NOV 2016

Full Text from Publisher

View Abstract

Times Cited: 1 (from Web of Science Core Collection)

Usage Count

Select Page 5K

Save to EndNote online

Add to Marked List

Sort by: Date Times Cited Usage Count

Page of 1

More

Show: 50 per page

3 records matched your query of the 40,553,433 in the data limits you selected.

Citing Articles: 2 (from Web of Science Core Collection)

For: Percolation transition at growing spatiotemporal fractal patterns in models of mesoscopic neural net ...More

Times Cited Counts

- 3 in All Databases
3 in Web of Science Core Collection
0 in BIOSIS Citation Index
0 in Chinese Science Citation Database
0 data sets in Data Citation Index
0 publication in Data Citation Index
0 in Russian Science Citation Index
0 in SciELO Citation Index
View Additional Times Cited Counts

Refine Results

Publication Years

2010 (2)

Refine

Web of Science Categories

- PHYSICS CONDENSED MATTER (1)
PHYSICS FLUIDS PLASMAS (1)
PHYSICS MATHEMATICAL (1)

more options / values...

Refine

Document Types

ARTICLE (2)

Refine

Organizations-Enhanced

Sort by: Date Times Cited Usage Count

Page of 1

More

Select Page 5K

Save to EndNote online

Add to Marked List

1. Power law behavior related to mutual synchronization of chemically coupled map neurons

By: Franovic, I.; Miljkovic, V. EUROPEAN PHYSICAL JOURNAL B Volume: 76 Issue: 4 Pages: 613-624 Published: AUG 2010

Full Text from Publisher

View Abstract

2. Spatial-temporal dynamics of chaotic behavior in cultured hippocampal networks

By: Chen, Wenjuan; Li, Xiangning; Pu, Jiangbo; et al. PHYSICAL REVIEW E Volume: 81 Issue: 6 Article Number: 061903 Part: 1 Published: JUN 1 2010

Full Text from Publisher

View Abstract

Select Page 5K

Save to EndNote online

Add to Marked List

Sort by: Date Times Cited Usage Count

Page of 1

More

Show: 50 per page

2 records matched your query of the 40,553,433 in the data limits you selected.

Create Citation Report

Analyze Results

Times Cited: 7 (from Web of Science Core Collection)

Usage Count

Times Cited: 2 (from Web of Science Core Collection)

Usage Count

Citing Articles: 2

(from Web of Science Core Collection)

For: Phase response curves for models of earthquake fault dynamics ...More

Times Cited Counts

- 2 in All Databases
2 in Web of Science Core Collection
0 in BIOSIS Citation Index
0 in Chinese Science Citation Database
0 data sets in Data Citation Index
0 publication in Data Citation Index
0 in Russian Science Citation Index
0 in SciELO Citation Index

View Additional Times Cited Counts

Refine Results

Publication Years

2017 (2)

Refine

Web of Science Categories

- COMPUTER SCIENCE
ARTIFICIAL INTELLIGENCE (1)
MATHEMATICS APPLIED (1)
PHYSICS MATHEMATICAL (1)

more options / values...

Refine

Document Types

ARTICLE (2)

Refine

Organizations-Enhanced

CONSIGLIO NAZIONALE DELLE

Sort by: Date Times Cited Usage Count

Page of 1

More

Select Page 5K

Save to EndNote online

Add to Marked List

- 1. Event-triggered fault detection for discrete-time Lipschitz nonlinear networked systems in finite-frequency domain

By: Gu, Ying; Yang, Guang-Hong
NEUROCOMPUTING Volume: 260 Pages: 245-256
Published: OCT 18 2017

Full Text from Publisher

View Abstract

- 2. The remarkable coherence between two Italian far away recording stations points to a role of acoustic emissions from crustal rocks for earthquake analysis

By: Zimatore, Giovanna; Garilli, Gianpaolo; Poscolieri, Maurizio; et al.
CHAOS Volume: 27 Issue: 4 Article Number: 043101
Published: APR 2017

Full Text from Publisher

View Abstract

Select Page 5K

Save to EndNote online

Add to Marked List

Sort by: Date Times Cited Usage Count

Page of 1

More

Show: 50 per page

2 records matched your query of the 40,553,433 in the data limits you selected.

Create Citation Report

Analyze Results

Times Cited: 0 (from Web of Science Core Collection)

Usage Count

Times Cited: 0 (from Web of Science Core Collection)

Usage Count

**Citing Articles: 2**  
(from Web of Science Core Collection)

**For:** Dynamics of landslide model with time delay and periodic parameter perturbations [...More](#)

**Times Cited Counts**

- 2 in All Databases
  - 2 in Web of Science Core Collection
  - 0 in BIOSIS Citation Index
  - 0 in Chinese Science Citation Database
  - 0 data sets in Data Citation Index
  - 0 publication in Data Citation Index
  - 0 in Russian Science Citation Index
  - 0 in SciELO Citation Index
- [View Additional Times Cited Counts](#)

**Refine Results**

**Filter results by:**

Open Access (1)

[Refine](#)

**Publication Years**

- 2016 (1)
- 2017 (1)

[more options / values...](#)

[Refine](#)

**Web of Science Categories**

- GEOCHEMISTRY GEOPHYSICS (1)
- MATHEMATICS APPLIED (1)
- MATHEMATICS INTERDISCIPLINARY APPLICATIONS (1)
- MECHANICS (1)

Sort by: **Date** Times Cited Usage Count Page of 1

More

Select Page 5K

Save to EndNote online

**Create Citation Report**

**Analyze Results**

**Times Cited: 0**  
(from Web of Science Core Collection)

**Usage Count**

1. **A 3D model for rain-induced landslides based on molecular dynamics with fractal and fractional water diffusion**  
  
By: Martelloni, Gianluca; Bagnoli, Franco; Guarino, Alessio  
**COMMUNICATIONS IN NONLINEAR SCIENCE AND NUMERICAL SIMULATION** Volume: 50 Pages: 311-329 Published: SEP 2017

2. **CASE STUDY OF THE TENSOR ANALYSIS OF GROUND DEFORMATIONS EVALUATED FROM GEODETIC MEASUREMENTS IN A LANDSLIDE AREA**  
  
By: Szafarczyk, Anna; Gawalkiewicz, Rafal  
**ACTA GEODYNAMICA ET GEOMATERIALIA** Volume: 13 Issue: 2 Pages: 213-222 Published: 2016

**Times Cited: 1**  
(from Web of Science Core Collection)

**Usage Count**

Select Page 5K

Save to EndNote online

Sort by: **Date** Times Cited Usage Count Page of 1

More

Show:

2 records matched your query of the 40,553,433 in the data limits you selected.

Citing Articles: 1

(from Web of Science Core Collection)

For: Slow rate fluctuations in a net work of noisy neurons with coupling delay ...More

Times Cited Counts

- 1 in All Databases
1 in Web of Science Core Collection
0 in BIOSIS Citation Index
0 in Chinese Science Citation Database
0 data sets in Data Citation Index
0 publication in Data Citation Index
0 in Russian Science Citation Index
0 in SciELO Citation Index

View Additional Times Cited Counts

Refine Results

Publication Years

2018 (1)

Refine

Web of Science Categories

- MATHEMATICS APPLIED (1)
PHYSICS MATHEMATICAL (1)

more options / values...

Refine

Document Types

ARTICLE (1)

Refine

Organizations-Enhanced

- INSTITUTE OF APPLIED PHYSICS OF THE RUSSIAN ACADEMY OF SCIENCES (1)

Sort by: Date Times Cited Usage Count

Page of 1

More

Select Page 5K

Save to EndNote online

Add to Marked List

Create Citation Report

Analyze Results

Times Cited: 0 (from Web of Science Core Collection)

Usage Count

1. Clustering promotes switching dynamics in networks of noisy neurons

By: Franovic, Igor; Klinshov, Vladimir

CHAOS Volume: 28 Issue: 2 Article Number: 023111

Published: FEB 2018

Full Text from Publisher

View Abstract

Select Page 5K

Save to EndNote online

Add to Marked List

Sort by: Date Times Cited Usage Count

Page of 1

More

Show: 50 per page

1 records matched your query of the 40,553,433 in the data limits you selected.

Citing Articles: 1

(from Web of Science Core Collection)

For: Stability, coherent spiking and synchronization in noisy excitable systems with coupling and interna ...More

Times Cited Counts

- 1 in All Databases
1 in Web of Science Core Collection
0 in BIOSIS Citation Index
0 in Chinese Science Citation Database
0 data sets in Data Citation Index
0 publication in Data Citation Index
0 in Russian Science Citation Index
0 in SciELO Citation Index
View Additional Times Cited Counts

Refine Results

Publication Years

2015 (1)

Refine

Web of Science Categories

- ENGINEERING MULTIDISCIPLINARY (1)
MATHEMATICS INTERDISCIPLINARY APPLICATIONS (1)
MECHANICS (1)

more options / values...

Refine

Document Types

ARTICLE (1)

Refine

Sort by: Date Times Cited Usage Count

Page of 1

More

Select Page 5K

Save to EndNote online

Add to Marked List

Create Citation Report

Analyze Results

Times Cited: 3 (from Web of Science Core Collection)

Usage Count

- 1. H-infinity synchronization of coupled delay partial differential systems via nonsingular transformation method

By: Wu, Kai-Ning; Li, Chang-Xi; Wang, Xinsheng; et al. APPLIED MATHEMATICAL MODELLING Volume: 39 Issue: 16 Pages: 4646-4654 Published: AUG 15 2015

Full Text from Publisher

View Abstract

Select Page 5K

Save to EndNote online

Add to Marked List

Sort by: Date Times Cited Usage Count

Page of 1

More

Show: 50 per page

1 records matched your query of the 40,553,433 in the data limits you selected.

Citing Articles: 1

(from Web of Science Core Collection)

For: Complex Dynamics of Spring-Block Earthquake Model Under Periodic Parameter Perturbations ...More

Times Cited Counts

- 1 in All Databases
1 in Web of Science Core Collection
0 in BIOSIS Citation Index
0 in Chinese Science Citation Database
0 data sets in Data Citation Index
0 publication in Data Citation Index
0 in Russian Science Citation Index
0 in SciELO Citation Index
View Additional Times Cited Counts

Refine Results

Publication Years

2016 (1)

Refine

Web of Science Categories

- ENGINEERING MECHANICAL (1)
MECHANICS (1)

more options / values...

Refine

Document Types

ARTICLE (1)

Refine

Organizations-Enhanced

POLYTECHNIC INSTITUTE OF

Sort by: Date Times Cited Usage Count

Page of 1

More

Select Page [Icons] 5K

Save to EndNote online

Add to Marked List

Create Citation Report

Analyze Results

Times Cited: 2 (from Web of Science Core Collection)

Usage Count

1. Entropy Analysis of Industrial Accident Data Series

By: Lopes, Antonio M.; Tenreiro Machado, J. A.

JOURNAL OF COMPUTATIONAL AND NONLINEAR DYNAMICS Volume: 11 Issue: 3 Article Number: 031006 Published: MAY 2016

Full Text from Publisher

View Abstract

Select Page [Icons] 5K

Save to EndNote online

Add to Marked List

Sort by: Date Times Cited Usage Count

Page of 1

More

Show: 50 per page

1 records matched your query of the 40,553,433 in the data limits you selected.

Citing Articles: 1

(from Web of Science Core Collection)

For: Possibilities of introducing different functional circuits on top of a structural neuron triplet: Wh ...More

Times Cited Counts

- 1 in All Databases
1 in Web of Science Core Collection
0 in BIOSIS Citation Index
0 in Chinese Science Citation Database
0 data sets in Data Citation Index
0 publication in Data Citation Index
0 in Russian Science Citation Index
0 in SciELO Citation Index
View Additional Times Cited Counts

Refine Results

Publication Years

2016 (1)

Refine

Web of Science Categories

- MATHEMATICS INTERDISCIPLINARY APPLICATIONS (1)
PHYSICS MATHEMATICAL (1)
PHYSICS MULTIDISCIPLINARY (1)

more options / values...

Refine

Document Types

ARTICLE (1)

Refine

Sort by: Date Times Cited Usage Count

Page of 1

More

Select Page [Icons] 5K

Save to EndNote online

Add to Marked List

Create Citation Report

Analyze Results

1. Dependence of inter-neuronal effective connectivity on synchrony dynamics in neuronal network motifs

By: Deng, Bin; Deng, Yun; Yu, Haitao; et al.

CHAOS SOLITONS & FRACTALS Volume: 82 Pages: 48-59 Published: JAN 2016

Times Cited: 2 (from Web of Science Core Collection)

Usage Count

Full Text from Publisher

View Abstract

Select Page [Icons] 5K

Save to EndNote online

Add to Marked List

Sort by: Date Times Cited Usage Count

Page of 1

More

Show: 50 per page

1 records matched your query of the 40,553,433 in the data limits you selected.



Citing Articles: 1

(from Web of Science Core Collection)

For: Stability, bifurcations, and dynamics of global variables of a system of bursting neurons ...More

Times Cited Counts

- 1 in All Databases
1 in Web of Science Core Collection
0 in BIOSIS Citation Index
0 in Chinese Science Citation Database
0 data sets in Data Citation Index
0 publication in Data Citation Index
0 in Russian Science Citation Index
0 in SciELO Citation Index

View Additional Times Cited Counts

Refine Results

Publication Years

2016 (1)

Refine

Web of Science Categories

- MATHEMATICS APPLIED (1)
PHYSICS MATHEMATICAL (1)

more options / values...

Refine

Document Types

ARTICLE (1)

Refine

Organizations-Enhanced

- SOUTH CHINA UNIVERSITY OF TECHNOLOGY (1)
UNIVERSITY OF CALIFORNIA

Sort by: Date Times Cited Usage Count

Page of 1

More

Select Page 5K

Save to EndNote online

Add to Marked List

Create Citation Report

Analyze Results

Times Cited: 0 (from Web of Science Core Collection)

Usage Count

1. Bifurcation dynamics of the tempered fractional Langevin equation

By: Zeng, Caibin; Yang, Qigui; Chen, YangQuan

CHAOS Volume: 26 Issue: 8 Article Number: 084310

Published: AUG 2016

Full Text from Publisher

View Abstract

Select Page 5K

Save to EndNote online

Add to Marked List

Sort by: Date Times Cited Usage Count

Page of 1

More

Show: 50 per page

1 records matched your query of the 40,553,433 in the data limits you selected.

Citing Articles: 1

(from Web of Science Core Collection)

For: Fractal properties of percolation clusters in Euclidian neural networks ...More

Times Cited Counts

- 1 in All Databases
1 in Web of Science Core Collection
0 in BIOSIS Citation Index
0 in Chinese Science Citation Database
0 data sets in Data Citation Index
0 publication in Data Citation Index
0 in Russian Science Citation Index
0 in SciELO Citation Index
View Additional Times Cited Counts

Refine Results

Publication Years

2017 (1)

Refine

Web of Science Categories

- ENGINEERING ELECTRICAL ELECTRONIC (1)
ENGINEERING MECHANICAL (1)
TRANSPORTATION SCIENCE TECHNOLOGY (1)

more options / values...

Refine

Document Types

PROCEEDINGS PAPER (1)

Refine

Organizations-Enhanced

Sort by: Date Times Cited Usage Count

Page of 1

More

Select Page 5K

Save to EndNote online Add to Marked List

1. Heuristic Algorithm Simulated for of TiO2 Porous Structures

By: Calderon-Segura, Y. Y.; Burlak, G.; Cuevas Arteaga, C.; et al.
Book Group Author(s): IEEE
Conference: IEEE International Conference on Mechatronics, Electronics and Automotive Engineering (ICMEAE) Location: Cuernavaca, MEXICO Date: NOV 21-24, 2017
Sponsor(s): IEEE Joint Chapter Morelos Robot & Automat & Computat Intelligence; Univ Autonoma Estado Morelos; IEEE; Inst Ingn Morelos; Inst Ingn Electronicos Electricos Morelos A C; CIICAq; IEEE VTS
2017 INTERNATIONAL CONFERENCE ON MECHATRONICS, ELECTRONICS AND AUTOMOTIVE ENGINEERING (ICMEAE) Book Series: Proceedings International Conference on Mechatronics Electronics and Automotive Engineering (ICMEAE) Pages: 175-180
Published: 2017

View Abstract

Select Page 5K

Save to EndNote online Add to Marked List

Sort by: Date Times Cited Usage Count

Page of 1

More

Show: 50 per page

1 records matched your query of the 40,553,433 in the data limits you selected.

Create Citation Report

Analyze Results

Times Cited: 0 (from Web of Science Core Collection)

Usage Count

# Clustering promotes switching dynamics in networks of noisy neurons

Igor Franović<sup>1,a)</sup> and Vladimir Klinshov<sup>2,b)</sup>

<sup>1</sup>Scientific Computing Laboratory, Center for the Study of Complex Systems, Institute of Physics Belgrade, University of Belgrade, Pregrevica 118, 11080 Belgrade, Serbia

<sup>2</sup>Institute of Applied Physics of the Russian Academy of Sciences, 46 Ulyanov Street, 603950 Nizhny Novgorod, Russia

(Received 30 November 2017; accepted 26 January 2018; published online 21 February 2018)

Macroscopic variability is an emergent property of neural networks, typically manifested in spontaneous switching between the episodes of elevated neuronal activity and the quiescent episodes. We investigate the conditions that facilitate switching dynamics, focusing on the interplay between the different sources of noise and heterogeneity of the network topology. We consider clustered networks of rate-based neurons subjected to external and intrinsic noise and derive an effective model where the network dynamics is described by a set of coupled second-order stochastic mean-field systems representing each of the clusters. The model provides an insight into the different contributions to effective macroscopic noise and qualitatively indicates the parameter domains where switching dynamics may occur. By analyzing the mean-field model in the thermodynamic limit, we demonstrate that clustering promotes multistability, which gives rise to switching dynamics in a considerably wider parameter region compared to the case of a non-clustered network with sparse random connection topology. *Published by AIP Publishing.* <https://doi.org/10.1063/1.5017822>

The striking feature of neuronal systems is that variability is reflected on two fundamentally different levels. While there is substantial knowledge on microscopic variability associated to spike trains of individual neurons, much less is known about macroscopic variability, which is a form of emergent behavior in neural networks. Macroscopic variability involves considerably longer timescales than the microscopic one, whereby its signature activity consists in slow rate oscillations, reflected in spontaneous alternation between the distinct network states. The latter are typically referred to as the UP and the DOWN states, such that in the UP state, both the firing rates and the synaptic conductances of neurons are elevated relative to the DOWN state. The switching dynamics between the collective states is especially relevant for activity of neocortical pyramidal neurons and is believed to facilitate or mediate different types of learning and memory. In this paper, we investigate the key ingredients behind switching dynamics, focusing on the interplay of different sources of noise and the network topology. In particular, we consider a clustered network of rate-based neurons and derive an effective model which describes its collective activity in terms of coupled second-order stochastic mean-field systems representing the particular clusters. The effective model is used to qualitatively analyze the mechanisms behind the switching dynamics in the non-clustered and clustered networks, comparing the associated parameter domains. For a homogeneous random network, where all neurons comprise a single cluster, switching is found only within a small parameter region in the vicinity of the pitchfork bifurcation, with the underlying mechanism resembling the motion of a noise-driven particle in a double-well potential. We demonstrate that clustering

plays a facilitatory role with respect to switching dynamics, enhancing the network multistability compared to the case of a homogeneous random network.

## I. INTRODUCTION

The fascinating feature of neuronal dynamics is that variability appears in a twofold fashion. For single units, one observes the spike-train variability,<sup>1</sup> reflected in that the same input sequence applied to a given neuron under identical experimental conditions gives rise to different neuronal responses. Apart from the variability on the short timescale, one also encounters variability as an emergent network phenomenon<sup>2-4</sup> associated to much longer timescales.<sup>5</sup> The hallmark of macroscopic variability is irregular slow rate oscillations,<sup>6,7</sup> alternatively called up-down states (UDS),<sup>8-10</sup> which comprise large amplitude, low frequency (0.1–2 Hz) spontaneous fluctuations between the collective UP and DOWN states.<sup>11</sup> These states are characterized by clearly distinct firing rates and synaptic conductances, whereby the UP state involves neurons with depolarized membrane potential, elevated firing rates, and increased synaptic conductances relative to those in the DOWN state.<sup>12-15</sup> Switching is induced by coherent activity of a large number of neurons and has been observed in cortical assemblies *in-vivo* during quiet wakefulness, sleep, and under the influence of anesthetic agents, as well as in certain *in-vitro* preparations.<sup>8,10,16-18</sup> UDS are the prominent form of spontaneous activity of neocortical pyramidal neurons, facilitating coordination of temporal interactions between neocortex and hippocampus,<sup>12,19,20</sup> which is fundamental to several types of learning and memory.<sup>19,21-23</sup>

The issue of the mechanisms that give rise to macroscopic variability as an emergent network phenomenon has remained unresolved, but there are two general directions of

<sup>a)</sup>Electronic mail: franovic@ipb.ac.rs

<sup>b)</sup>Electronic mail: vladimir.klinshov@ipfran.ru

research.<sup>24</sup> One connects the slow rate fluctuations to deterministic networks with balanced massive excitation and inhibition,<sup>4,25,26</sup> which leaves the collective dynamics highly sensitive to fluctuations. The other direction relates slow rate oscillations to bistability or multistability in attractor model networks where alternation between the coexisting states emerges due to noise,<sup>27,28</sup> which acts as the finite-size effect.<sup>29–31</sup> In this paper, we develop the latter framework by examining the interplay of stochastic neuronal dynamics and heterogeneous network topology on the onset and robustness of slow rate oscillations. In particular, we consider a network of rate-based neurons, focusing on how the different sources of noise, combined with the clustered network topology, give rise to slow stochastic fluctuations of the mean-rate. A qualitative insight into the mechanisms behind the slow fluctuations and the associated parameter domains is gained by developing an effective model of network activity, where the collective dynamics is described by coupled stochastic mean-field systems representing each of the clusters. The effective model for the clustered network with *random* inter- and intra-cluster connectivity is derived here for the first time, using the approach which incorporates the Gaussian closure hypothesis.<sup>32–34</sup> As an intermediate result, we determine how the different sources of noise from local dynamics as well as statistical heterogeneity of the connection topology contribute to noise at the macroscopic level. This presents generalization of our previous work, where we have considered bistability and slow fluctuations in a network with simple random connection topology.<sup>30,35</sup>

Investigating the impact of clustered topology on collective dynamics is biologically plausible, given that neural networks with statistically inhomogeneous wiring are inherent to mammalian neocortex,<sup>36,37</sup> where the clustered structures with stronger synapses and increased connection probability make up the so-called cell assemblies. Earlier studies have indicated that clustered connectivity could give rise to bistability or multistability,<sup>4,25,38</sup> potentially allowing for switching dynamics between interacting populations, considered as a likely paradigm for decision-making processes during perception or cognition. In this study, we demonstrate that clustering promotes multistability, thereby substantially enhancing the parameter domain admitting the slow rate fluctuations, as compared to a network with simple random connection topology.

The paper is organized as follows. In Sec. II, we present the key points of the derivation of the effective model for collective dynamics of the clustered network, explicitly demonstrating how the neuronal noise and network heterogeneity contribute to different finite-size effects. In Sec. III, we analyze how the network multistability and switching dynamics are influenced by the clustered topology. It is first indicated that in the absence of clustering, switching occurs in a relatively narrow parameter domain, whereby its mechanism resembles the noise-driven motion of a particle in a double-well potential. Then, we show that by introducing clustering, one enhances the network multistability, which ultimately makes the switching phenomenon considerably more robust. In Sec. IV, we provide a brief summary and discussion of the results obtained.

## II. DERIVATION OF THE MEAN-FIELD MODEL

We consider a network comprising  $N$  neurons arranged into clusters, such that intra-cluster connectivity is larger than the connectivity between neurons from different clusters. The local dynamics of a given neuron  $i$  from cluster  $X$  follows the rate model<sup>30,35,39,40</sup>

$$\frac{dr_{Xi}}{dt} = -\lambda_X r_{Xi} + H(v_{Xi}) + \sqrt{2D_X} \xi_{Xi}(t), \quad (1)$$

where  $\lambda_X$  defines the rate relaxation time,  $\xi_{Xi}(t)$  denotes the intrinsic neuronal noise which typically derives from stochastic opening of ion-gating channels, whereas  $H$  is the nonlinear gain function, whose form will be specified further below. The total input to a neuron  $v_{Xi} = u_{Xi} + I_X + \sqrt{2B_X} \eta_{Xi}(t)$  consists of a synaptic input  $u_{Xi} = \sum_Y \kappa_{YX} \sum_j a_{YXji} r_{Yj}$  and the external bias current  $I_X$ , while fluctuations in the embedding environment are accounted for by synaptic (external) noise  $\eta_{Xi}(t)$ , characterized by  $B_X$ . The coupling scheme is given by the adjacency matrix  $a_{YXji} \in \{0, 1\}$ , with the notation  $a_{YXji}$  referring to the link which projects from neuron  $j$  in cluster  $Y$  to neuron  $i$  from cluster  $X$ . Coupling weights between two clusters or within a single cluster are assumed to be homogeneous, whereby we adopt the scaling  $\kappa_{YX} = K_{YX}/N$ . To improve readability, a summary of the most relevant notation is provided in Table I. Both external and intrinsic fluctuations are represented by Gaussian white noise terms which satisfy  $\langle \langle \xi_{Xi}(t) \xi_{Yj}(t') \rangle \rangle = \langle \langle \eta_{Xi}(t) \eta_{Yj}(t') \rangle \rangle = \delta_{XY} \delta_{ij} \delta(t-t')$  and  $\langle \langle \xi_{Xi}(t) \eta_{Yj}(t') \rangle \rangle = 0$ .

The mean-field model involves a Gaussian closure hypothesis,<sup>32–34,41</sup> such that the collective dynamics of each cluster  $X$  is described by the mean-rate  $R_X$  and the associated variance  $S_X$

$$R_X = \frac{1}{N_X} \sum_i r_{Xi} \equiv \langle r_{Xi} \rangle, \\ S_X = \langle r_{Xi}^2 \rangle - R_X^2, \quad (2)$$

where  $N_X = n_{xN}$  is the size of the cluster  $X$ , whereas  $\langle \cdot \rangle$  refers to averaging over the neurons within the given cluster. The network behavior will be represented in terms of dynamics of interacting mean-field systems, each attributed to the

TABLE I. Summary of notation in Sec. II.

$\lambda_X$	Relaxation time of units in cluster $X$
$D_X$	Intensity of internal noise in cluster $X$
$B_X$	Intensity of external noise in cluster $X$
$I_X$	External current to cluster $X$
$U_X$	Average input to cluster $X$
$N_X \equiv n_{xN}$	Size of cluster $X$
$K_{YX}$	Strength of couplings projecting from cluster $Y$ to cluster $X$
$\kappa_{YX} \equiv K_{YX}/N$	Normalized coupling strength
$a_{YXji}$	Element of adjacency matrix characterizing links projecting from neuron $j$ of cluster $Y$ to neuron $i$ in cluster $X$
$p_{YX}$	Connection probability from cluster $Y$ to cluster $X$
$R_X$	Mean rate of cluster $X$
$S_X$	Rate variance in cluster $X$

particular cluster. Our immediate goal is to derive a second-order stochastic mean-field (macroscopic) model for an arbitrary cluster by appropriately averaging the local (microscopic) neuronal dynamics. To this end, we first introduce an Ansatz regarding the local variables,<sup>30,35</sup> which will ultimately allow us to treat the nonlinear threshold term  $H(v_{Xi})$ . In particular, one assumes that  $r_{Xi}$  may be written as  $r_{Xi} = R_X + \sqrt{S_X}\rho_{Xi}$ ,<sup>42</sup> where  $\rho_{Xi}$  is a set of variables that satisfies  $\langle \rho_{Xi} \rangle = 0$ ,  $\langle \rho_{Xi}^2 \rangle = 1$ , as follows from definition (2). Using the Ansatz, the total input  $v_{Xi}$  to the neuron may be rewritten as  $v_{Xi} = U_X + \delta v_{Xi}$ , where

$$U_X = I_X + \frac{1}{N} \sum_Y K_{YX} p_{YX} N_Y R_Y, \quad (3)$$

$$\delta v_{Xi} = \frac{1}{N} \sum_Y K_{YX} R_Y \nu_{YXi} + \frac{1}{N} \sum_Y K_{YX} \sqrt{S_Y} \sigma_{YXi}. \quad (4)$$

In particular, Eq. (3) presents the assembly-averaged input to cluster  $X$ , with  $p_{Y X}$  denoting the connectedness probability from cluster  $Y$  to cluster  $X$ . The deviation  $\delta v_{Xi}$  from the average input  $U_X$  contains two terms, namely, the “topological” and the “dynamical” one, whereby  $\nu_{YXi} = \sum_j a_{YXji} - p_{YX} N_Y$  accounts for the deviation from the average number of connections  $p_{YX} N_Y$ , and  $\sigma_{YXi} = \sum_j a_{YXji} \rho_{Yj}$  describes the effect of local rate fluctuations. Equations (3) and (4) enable one to expand  $H(v_{Xi})$  about  $U_X$ , which proves crucial for deriving the reduced system for cluster dynamics. In particular, one obtains  $H(v_{Xi}) = H_{0X} + H_{1X} \delta v_{Xi} + H_{2X} \delta v_{Xi}^2$ , where we have introduced notation  $H_{0X} \equiv H(U_X)$ ,  $H_{1X} = \frac{dH}{dv_{Xi}}(U_X)$ ,  $H_{2X} = \frac{1}{2} \frac{d^2 H}{dv_{Xi}^2}(U_X)$ . From the latter expression and the definition of  $R_X$ , one obtains

$$\begin{aligned} \frac{dR_X}{dt} = & -\lambda_X \langle r_{Xi} \rangle + H_{0X} + 2B_X H_{2X} + H_{1X} \langle \Gamma_{1X} \rangle \\ & + H_{2X} \langle \Gamma_{2X} \rangle + \sqrt{2D_X} \langle \zeta_{Xi}(t) \rangle, \end{aligned} \quad (5)$$

with  $\langle \Gamma_{1X} \rangle$  and  $\langle \Gamma_{2X} \rangle$  given by

$$\begin{aligned} \langle \Gamma_{1X} \rangle = & \frac{1}{N} \sum_Y K_{YX} R_Y \langle \nu_{YXi} \rangle + \frac{1}{N} \sum_Y K_{YX} \sqrt{S_Y} \langle \sigma_{YXi} \rangle \\ & + \sqrt{2B_X} \langle \eta_{Xi} \rangle, \end{aligned} \quad (6)$$

$$\begin{aligned} \langle \Gamma_{2X} \rangle = & \frac{1}{N^2} \sum_{YZ} K_{YX} K_{ZX} R_Y R_Z \langle \nu_{YXi} \nu_{ZXi} \rangle \\ & + \frac{1}{N^2} \sum_{YZ} K_{YX} K_{ZX} \sqrt{S_Y S_Z} \langle \sigma_{YXi} \sigma_{ZXi} \rangle \\ & + \frac{2}{N^2} \sum_{YZ} K_{YX} K_{ZX} R_Y \sqrt{S_Z} \langle \nu_{YXi} \sigma_{ZXi} \rangle \\ & + \frac{2\sqrt{2B_X}}{N} \sum_Y K_{YX} R_Y \langle \nu_{YXi} \eta_{Xi}(t) \rangle \\ & + \frac{2\sqrt{2B_X}}{N} \sum_Y K_{YX} \sqrt{S_Y} \langle \sigma_{YXi} \eta_{Xi}(t) \rangle. \end{aligned} \quad (7)$$

In order to calculate the final expression for the cluster mean-rate, one has to estimate the terms containing  $\nu_{Y Xi}$  and  $\sigma_{Y Xi}$  and the associated averages. We have been able to carry this

out in a systematic fashion, assessing the order of each term. Ultimately, the stochastic mean-field model will include stochastic terms as finite-size effects, whereby we neglect the terms whose order is higher than  $\mathcal{O}(1/N)$ . In Subsection II A, we briefly discuss how one may determine the contributions from each term comprising  $\langle \Gamma_{1X} \rangle$  and  $\langle \Gamma_{2X} \rangle$ .

### A. Evaluating the finite-size effects

Let us first address the terms  $\nu_{YXi}$ , which by definition present the deviation from the average number of links  $p_{YX} N_Y$  projecting from cluster  $Y$  to a given node  $i$  of subassembly  $X$ . From the theory of complex networks, it is known that the average over the ensemble of different network configurations, which we denote by  $[\cdot]$ , is  $[\nu_{YXi}] = 0$ , whereas the associated variance is  $[\nu_{YXi}^2] = p_{YX}(1 - p_{YX})N_Y$ . By these arguments, it follows that  $\langle \nu_{YXi} \rangle$  contributes to a constant random parameter dependent on the particular network configuration, which is manifestation of the quenched randomness introduced by fixing the given configuration. The variance of such a term between the different configurations is approximately  $[\langle \nu_{YXi} \rangle^2] = \frac{p_{YX}(1-p_{YX})N_Y}{N_X} \approx \widetilde{p}_{YX} N_Y / N_X$ , where  $\widetilde{p}_{YX} = p_{YX}$  for the sparse connectivity  $p_{YX} \ll 1$  and  $\widetilde{p}_{YX} = 0$  in the limit of strong connectivity  $p \sim 1$ . Note that the division by  $N_X$  comes from the fact that the variance of a sum of independent random variables is equal to the sum of variances of the given variables. The terms  $\langle \nu_{YXi} \nu_{ZXi} \rangle$  may be treated in a similar fashion, though one has to distinguish between the cases  $Y = Z$  and  $Y \neq Z$ . If  $Y = Z$ , one may clearly use the estimate  $[\langle \nu_{YXi}^2 \rangle] = p_{YX}(1 - p_{YX})N_Y \approx p_{YX} N_Y$ , while if  $Y \neq Z$ , the terms  $\langle \nu_{YXi} \nu_{ZXi} \rangle$  contribute to a random constant parameter, whose variance over the ensemble of different network configurations may be evaluated as  $[\langle \nu_{YXi} \nu_{ZXi} \rangle^2] = p_{YX} N_Y p_{ZX} N_Z / N_X$ .

The terms containing  $\sigma_{Y Xi}$  may heuristically be approached as follows. From the definition, it follows that  $\sigma_{YXi} = \sum_j a_{YXji} \rho_{Yj} = \sum_{j \in \mathcal{C}_{YXi}} \rho_{Yj}$ , i.e., the sum runs over the subassembly of neurons from cluster  $Y$  which project to neuron  $i$  from cluster  $X$ . By construction, such subassembly contains a small number of units  $p_{YX} N_Y$ , if the connectivity between clusters  $Y$  and  $X$  is sparse ( $p_{YX} \ll 1$ ). In the limit of strong connectivity ( $p_{YX} \sim 1$ ), one has the sum  $\sigma_{YXi} \approx 0$ , because the departure from the limit case  $p_{Y X} = 1$  due to the subset of neurons that do not project from  $Y$  to  $Xi$  is small. Though one cannot say *a priori* anything regarding the distribution of  $\rho_{Yj}$ , in the first approximation, one may consider them as a set of normally distributed random variables of zero mean and unit variance. This enables us to treat  $\sigma_{Y Xi}$  as a set of normally distributed random variables of zero mean and variance  $p_{YX} N_Y$ . Also note that the correlation  $\sigma_{YXk} \sigma_{YXi} = \sum_{i,j} a_{YXik} a_{YXjl} = p_{YX}^2 N_Y$ , which is small due to smallness of  $p_{YX}$ , such that all the terms  $\sigma_{YXi}$  may be taken as uncorrelated.

The above arguments imply that  $\langle \sigma_{YXi} \rangle$  may be evaluated as effective noisy terms of zero mean and variance  $[\langle \sigma_{YXi} \rangle^2] = (1 - \widetilde{p}_{YX}) N_Y / N_X$ . By the above line of arguments, it may explicitly be shown that the variables  $\sigma_{YXi}^2$  can effectively be

treated as random variables whose mean and variance satisfy  $[\sigma_{YXi}^2] = p_{YX}N_Y$  and  $[\sigma_{YXi}^4] - [\sigma_{YXi}^2]^2 = 2p_{YX}^2N_Y^2$ , respectively.

## B. Equations of the mean-field model

The results from Subsection II A enable us to systematically evaluate the contributions from all the terms on the r.h.s. of (6) and (7). Focussing on (6) first, one finds that the three associated terms give rise to finite-size effects of different nature. In particular, the first term contains an effective random parameter associated to the given network configuration and may be written as  $\frac{1}{N}K_{YX}R_Y\sqrt{p_{YX}N_Y/N_X}\gamma_1$ , where  $\gamma_1$  is a  $\mathcal{N}(0, 1)$  variable. The latter should not be confound with noise, as  $\gamma_1$  can be treated as a random parameter. The second element from the r.h.s. of (6) contributes to pseudo-noise of the order  $\mathcal{O}(1/N)$ , which is given by  $\frac{1}{N}K_{YX}\sqrt{S_Y}\sqrt{p_{YX}N_Y/N_X}\gamma_2(t)$ . One refers to it as pseudo-noise because it fluctuates randomly in time, but does not derive from the actual microscopic noise. The third term on the r.h.s. of (6) presents the sum of local external noises, which gives rise to a genuine macroscopic noise  $\sqrt{2B_X/N_X}\zeta_X(t)$ .

As far as  $\langle \Gamma_{2X} \rangle$  is concerned, the terms containing  $\langle \nu_{YXi}\nu_{ZXi} \rangle$  and  $\langle \sigma_{YXi}\sigma_{ZXi} \rangle$  for  $Y=Z$  together provide the  $\mathcal{O}(1/N)$  deterministic finite-size effect of the form  $\frac{1}{N}K_{YX}^2p_{YX}n_Y(R_Y^2 + S_Y)$ . The remaining contribution from such terms for  $Y=Z$  and  $Y \neq Z$  amounts to random constant parameters and pseudo-noises, respectively, whose intensity is of the order  $\mathcal{O}(N^{-3/2})$  and as such can be neglected. As an illustration, we state that the terms involving  $\langle \nu_{YXi}\nu_{ZXi} \rangle$  for  $Y \neq Z$  may be evaluated as  $\frac{1}{N^2}K_{YX}K_{ZX}R_YR_Z\sqrt{p_{YX}p_{ZX}N_YN_Z/N_X}$ , which is indeed  $\mathcal{O}(N^{-3/2})$ . Finally, averaging over all the terms at the r.h.s. of (7) containing the genuine noises  $\eta_{Xi}(t)$  at the macroscopic level provides stochastic effects of the order  $\mathcal{O}(1/N^2)$ , which can also be neglected within our mean-field model.

Collecting all the results stated so far, one arrives at the following equation for the dynamics of the cluster mean-rate:

$$\begin{aligned} \frac{dR_X}{dt} = & -\lambda_X R_X + H_{0X} + 2B_X H_{2X} \\ & + H_{2X} \sum_Y K_{YX}^2 p_{YX} n_Y (R_Y^2 + S_Y) / N \\ & + \sqrt{\Psi_X} \beta(t) + \sqrt{\Omega_X} \eta, \end{aligned} \quad (8)$$

where the ‘‘macroscopic’’ noise is of intensity  $\Psi_X = \frac{1}{N}(2D_X + 2B_X H_{1X}^2) + \frac{1}{N} H_{1X}^2 \sum_Y K_{YX}^2 p_{YX} \frac{N_Y}{N_X} S_Y$ , and the associated random variable  $\beta(t)$  is Gaussian distributed. The macroscopic noise is made up of three terms which may be interpreted as follows. The two terms in the first bracket represent the contribution from the local intrinsic and external noise translated to macroscopic level, whereby the latter is manifested as multiplicative, rather than the additive noise. The third term is of different character and essentially reflects the impact of local fluctuations in the input provided to each neuron within the cluster. Apart from this, Eq. (8) also contains a random term where  $\eta$  is just a constant random number  $\mathcal{N}(0, 1)$ , whereas the associated intensity is  $\Omega_X = \frac{1}{N} H_{1X}^2 \sum_Y K_{YX}^2 p_{YX} \frac{N_Y}{N_X} R_Y^2$ . Note that the latter factor derives

from the topological ‘‘uncertainty’’ effect related to quenched randomness, in a sense that each particular network realization is characterized by distinct deviations from the average connectivity degree.

Starting from the definition and applying the Itô derivative, one may use analogous methods to obtain the final equation for the variance  $S_X$ . We omit the details of the lengthy calculation, but just state that here we also neglect the deterministic finite-size correction of the order of  $\mathcal{O}(1/N)$ , as well as all the noisy terms and the terms related to uncertainty parameter derived from the particular network realization. The final equation for the variance then becomes

$$\frac{dS_X}{dt} = -2\lambda_X S_X + 2B_X H_{1X}^2 + 2D_X. \quad (9)$$

Equations (8) and (9) make up the second-order stochastic mean-field model describing the collective activity of each cluster within the network. To complete the model, it is necessary to specify the gain function  $H$ . In general, the gain function should meet the requirements that it is zero for sufficiently small input and that it saturates for large enough input, whereas for intermediate input values,  $H$  should just be smooth and monotonous. For convenience of analytical study,<sup>30,35</sup> we adopt the following form of  $H$ :

$$H(Q) = \begin{cases} 0, & Q \leq 0, \\ 3Q^2 - 2Q^3, & 0 < Q < 1, \\ 1, & Q \geq 1. \end{cases} \quad (10)$$

## III. ANALYSIS OF THE MEAN-FIELD MODEL AND SWITCHING DYNAMICS

In order to demonstrate the facilitatory role of clustering on switching dynamics more explicitly, we first investigate how the switching emerges in case of statistically homogeneous random network and then draw comparison to scenario the involving clustered network topology. In both instances, the analysis of the mean-field model in the thermodynamic limit  $N \rightarrow \infty$  is used to gain qualitative insight into the parameter domains supporting coexistence of different stationary states. The latter is a necessary ingredient for the onset of slow rate fluctuations, which emerge due to the finite-size effect. It will be demonstrated that the switching dynamics in clustered and non-clustered networks are based on different mechanisms, which we relate to the finding that clustering promotes network multistability.

### A. Slow rate fluctuations in a non-clustered network

Let us first consider the deterministic dynamics of the non-clustered network with uniform coupling strengths. Given that this case has been analyzed in detail in our previous papers,<sup>30,35</sup> here we provide only a brief summary of the main results.

The network behavior is described by the deterministic part of the system Eqs. (8) and (9), whereby (4) implies that the average input to each neuron amounts to  $U = I + KpR = I + \alpha R$ , with  $\alpha = Kp$  being the connectivity parameter. Note that  $S$  generally affects the  $R$  dynamics only via  $\mathcal{O}(1/N)$

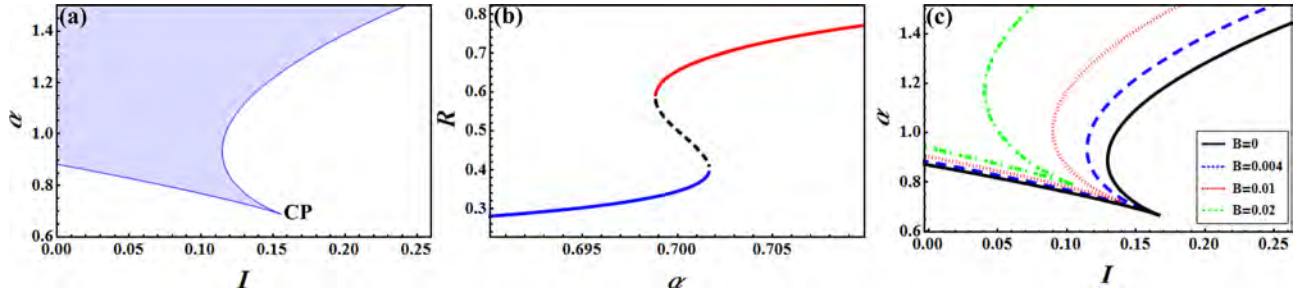


FIG. 1. Analysis of the mean-field model of a non-clustered random network in the thermodynamic limit  $N \rightarrow \infty$ . (a) Bistability domain (highlighted region) in the  $(I - \alpha)$  plane is bounded by two branches of saddle-node bifurcations. The latter meets at the cusp point CP, located at  $(I_p, \alpha_p)$ , where the pitchfork bifurcation occurs. External noise is set to  $B = 0.004$ , whereas  $D = 0.02$ . (b)  $R(\alpha)$  dependence within the bistability tongue ( $I = 0.15, B = 0.004$ ) shows coexistence between the UP and the DOWN state. (c) Shift of bistability domain for increasing  $B \in \{0, 0.004, 0.01, 0.02\}$ .

terms, which contribute to the small deterministic correction term and the macroscopic noise. Thus, in the thermodynamic limit, one may neglect the  $S$  evolution and replace it with the corresponding stationary value  $S_0 = (B_\chi H_1^2 + D)/\lambda$ . For simplicity, we adopt  $\lambda = 1$  in the remainder of the paper. In order to analyze the stability of (8) in the limit  $N \rightarrow \infty$ , it is convenient to rewrite it in terms of the average input  $U$  as<sup>30,35</sup>

$$\frac{dU}{dt} = -2\alpha U^3 + 3\alpha U^2 - 12\alpha B U - U + 6\alpha B + I. \quad (11)$$

Equation (11) always admits at least one stable stationary state. For the given external noise  $B$ , the onset of bistable regime is associated to the pitchfork bifurcation that occurs at  $\alpha_p = 2/(3(1 - 8B))$  and  $I_p = (1 - \alpha_p)/2$ . From this cusp point emanate two branches of saddle-node bifurcations, which outline the bistability “tongue” where the UP and the DOWN states characterized by the high and low mean-rates coexist, cf. Fig. 1(a). In particular, the upper curve corresponds to creation of the UP state, whereas the lower curve coincides with annihilation of the DOWN state. Within the coexistence region, the two stable states are separated by the unstable state, cf. Fig. 1(b), whereby the level of the unstable state decreases with  $\alpha$ . This confines the attraction basin of the DOWN state, facilitating the prevalence of the UP state at higher connectivity. Figure 1(c) further shows that for increasing  $B$ , the bistability domain gets shifted toward larger  $\alpha$ . Note that the change of  $\alpha$  is achieved by increasing the coupling strength  $K$  while the connectedness probability  $p = 0.2$  is kept fixed to conform to the case of sparse random network, which maintains certain biological plausibility.

The mechanism behind switching dynamics in the non-clustered network may be explained by analyzing the finite-size effect and is reminiscent of the noise-driven motion of a

particle in a double-well potential. The analogy lies in the fact that the macroscopic noise, as the finite-size effect, allows for the network mean-rate to jump between the minima of the potential, which correspond to the two stationary levels of the deterministic part of the mean-field model, see the example of  $R(t)$  series in Fig. 2(a). Replacing  $S$  by its stationary value, Eq. (8) for the stochastic dynamics of the mean-rate may be written in term of  $U$  as

$$\frac{dU}{dt} = -\frac{dV}{dU} + \sqrt{\Psi}\xi, \quad (12)$$

where  $V$  presents the potential  $V(U) = \alpha U^4/2 - \alpha U^3 + (6\alpha B + 1/2)U^2 - (6\alpha B + I)U + \mathcal{O}(1/N)$ , whereas the macroscopic noise amounts to  $\Psi = \alpha^2(2 + \alpha^2)[36B U^2(1 - U)^2 + D]/N$ . In the vicinity of the pitchfork bifurcation,  $V$  indeed has the shape of a double-well potential, as illustrated in Fig. 2(b).

The described switching mechanism is generic, in a sense that one expects to observe it close to bifurcation inducing the bistability, but is not robust, given that the physically meaningful switching rates are obtained in the sufficiently small parameter domain about the bifurcation value. Beyond this area, the potential barrier becomes too high for the noise to overcome it, making the switching events extremely unlikely.

In principle, the macroscopic noise  $\Psi(U)$  is multiplicative, which makes finding the analytical expression for the underlying transition rates extremely difficult. Nevertheless, in a first approximation, the setup may be reduced to the classical Kramers problem<sup>43</sup> if  $\Psi$  is replaced by its mean  $\Psi_m$  obtained by averaging over the  $U$  values between the two potential wells. Figure 3(a) illustrates that  $\Psi_m$  may be considered representative for the whole range of  $\Psi(U)$  values,<sup>30</sup> especially given that the macroscopic noise is well bounded

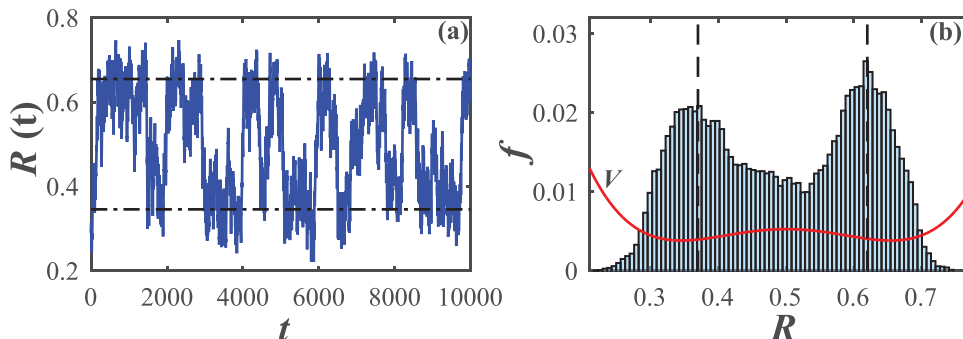


FIG. 2. Slow rate fluctuations illustrated by the  $R(t)$  series in (a) and the associated stationary probability distribution  $f(R)$  in (b). The results are obtained numerically for  $I = 0.15, \alpha = 0.7, B = 0.004, D = 0.02$  and the network size  $N = 400$ . The dashed-dotted lines in (a) indicate the UP and DOWN levels of the corresponding mean-field model in the thermodynamic limit. The solid line in (b) presents the double-well potential  $V$ , cf. Eq. (12).

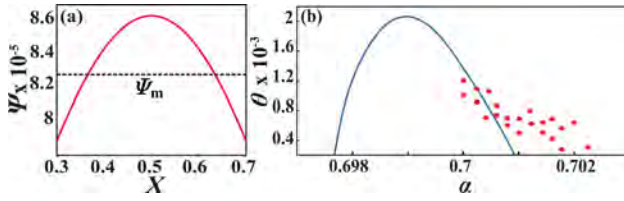


FIG. 3. (a) Macroscopic noise  $\Psi$  as a function of the mean-input  $X$ . The dotted line indicates the average  $\Psi_m$  over the relevant  $X$  range. (b) The solid line shows  $\theta(\alpha)$  dependence obtained for the mean-field model via the Kramers formula (13). Dots denote the switching rates obtained numerically for  $I = 0.15$ ,  $B = 0.004$ ,  $D = 0.02$ , and  $N = 400$ .

within the relevant  $U$  interval. Within this framework, the first passage time between the two wells can be determined via the Kramers formula<sup>44–46</sup>

$$T_{U_{\pm} \rightarrow U_{\mp}} \approx \frac{\pi}{\sqrt{|V''(U_{max})| |V''(U_{\pm})|}} \exp \left[ \frac{V(U_{max}) - V(U_{\pm})}{\Psi_m} \right], \quad (13)$$

where  $U_{\pm}$  refer to the two minima of the double-well potential, whereas  $U_{max}$  denotes the location of its maximum. The total transition rate is then given by  $\theta = 1/(T_{U_{+} \rightarrow U_{-}} + T_{U_{-} \rightarrow U_{+}})$ . For  $\alpha$  values in vicinity of the pitchfork bifurcation, the last expression may be used to compare with the numerical findings, cf. Fig. 3(b). One finds qualitative matching of the prediction derived from the mean-field model and the simulation within two aspects: (i) the region where  $\theta(\alpha)$  is positive corresponds well to the region where the exact system exhibits slow rate fluctuations, and (ii) the order of the predicted  $\theta$  values is the same as the one obtained from simulations.

## B. Switching dynamics in clustered networks

In Subsection III A, we have shown that switching in homogeneous random networks is confined to the parameter domain in close vicinity of the pitchfork bifurcation. The main goal here is to demonstrate that switching in clustered networks is based on the paradigm that clustering promotes networks multistability. The outcome is that the switching phenomenon gains on robustness, in a sense that it can be found for parameter regions where it cannot be observed in statistically homogeneous random networks.

We shall show that sufficiently strong clustering supports multistability by giving rise to network states which do not exist in the non-clustered case. The increased number of network levels derives from the states with broken symmetry, where *subsets of clusters* occupy different levels, lying either in the UP or the DOWN state. By analyzing the mean-field model in the thermodynamic limit, we find that such multistability can be achieved only by varying the connectivity features of the network (topological heterogeneity), rather than by introducing the parameter heterogeneity over the subsets of network clusters. With increased multistability, the stochastic terms contributing to finite-size effect may cause the network to cross to another level just by inducing the switching event within a single cluster. The slow rate oscillations are then naturally supported by the fact that the

impact of the finite-size effect is more pronounced for individual clusters than for the entire network.

Though the system Eqs. (8) and (9) are quite general in a sense that they may be applied to a network comprising an arbitrary number of clusters of arbitrary sizes, for simplicity, we address here the case where the network consists of  $m$  equal clusters of size  $N_c = N/m$ . Clustering algorithm consists in rearranging the links from the homogeneous random network, such that the average connectedness probability  $p = 0.2$  is preserved. We introduce additional clustering parameter  $g$  to characterize topological heterogeneity, cf. Table II for the summary of notation relevant for Sec. III B. Parameter  $g$  presents the ratio between the intra-cluster and cross-cluster connectivity,  $\alpha_{in}$  and  $\alpha_{out}$ , respectively, such that  $\alpha_{in} = g\alpha_{out}$  with  $g > 1$ . Larger  $g$  implies stronger clustering, whereby the limiting case  $g = 1$  describes the non-clustered network, whereas the case  $g \rightarrow \infty$  corresponds to the network of disconnected clusters. One may show that  $\alpha_{in}$  and  $\alpha_{out}$  can be expressed in terms of the connectivity of the original homogeneous network  $\alpha$  as

$$\alpha_{in} = \frac{gm}{m-1+g}\alpha, \quad \alpha_{out} = \frac{m}{m-1+g}\alpha. \quad (14)$$

This allows us to compare the relevant parameter domains between the homogeneous and the clustered networks.

Let us now focus on the scenario where  $l$  clusters occupy state  $R_a$ , and  $m-l$  clusters lie at  $R_b$ . While the homogeneous state has the permutation symmetry  $\Sigma_m$  with respect to exchange of all the cluster indices, the solutions we consider now have a reduced symmetry  $\Sigma_l \otimes \Sigma_{m-l}$ . One may analyze the stability and bifurcations of the corresponding mean-field model in the thermodynamic limit  $N \rightarrow \infty$ , cf. (11). The model is given by

$$\begin{aligned} \frac{dR_a}{dt} &= -2U_a^3(R_a, R_b) + 3U_a^2(R_a, R_b) \\ &\quad + 6B(1 - 2U_a(R_a, R_b)) - R_a \\ \frac{dR_b}{dt} &= -2U_b^3(R_a, R_b) + 3U_b^2(R_a, R_b) \\ &\quad + 6B(1 - 2U_b(R_a, R_b)) - R_b, \end{aligned} \quad (15)$$

where the average input to the two groups of clusters reads

$$\begin{aligned} U_a(R_a, R_b) &= I + \frac{\alpha}{m-1+g} [(g+l-1)R_a + (m-l)R_b], \\ U_b(R_a, R_b) &= I + \frac{\alpha}{m-1+g} [lR_a + (g+m-l-1)R_b]. \end{aligned} \quad (16)$$

As for the non-clustered network, the variances  $S_a$  and  $S_b$  can be substituted by their respective stationary values

TABLE II. Summary of notation in Sec. III B.

$\alpha \equiv Kp$	Connectivity parameter of the homogeneous network
$m$	Total number of clusters
$\alpha_{in}$	Intra-cluster connectivity
$\alpha_{out}$	Inter-cluster connectivity
$g \equiv \alpha_{in}/\alpha_{out}$	Clustering parameter
$\delta \equiv 1/(g-1)$	Inverse clustering parameter



$S_i^* = (B_x H_i^2 + D)/\lambda$ , with  $i \in \{a, b\}$ . Using (16), one may express  $R_a$  and  $R_b$  in terms of  $U_a$  and  $U_b$  via

$$\begin{aligned} R_a &= \frac{U_a - I}{\alpha} + \frac{m - l}{\alpha(g - 1)}(U_a - U_b), \\ R_b &= \frac{U_b - I}{\alpha} + \frac{l}{\alpha(g - 1)}(U_b - U_a). \end{aligned} \tag{17}$$

Inserting the latter expressions into (15), we obtain that the steady states of the mean-field model satisfy

$$\begin{aligned} I - f(U_a) + \delta(m - l)(U_b - U_a) &= 0, \\ I - f(U_b) + \delta l(U_b - U_a) &= 0. \end{aligned} \tag{18}$$

In (18),  $f(U_i)$  is given by  $f(U_i) = 2\alpha U_i^3 - 3\alpha U_i^2 + (1 + 12B\alpha)U_i - 6B\alpha$ , which implies that the terms  $I - f(U_i)$  have exactly the same form as the r.h.s. of (11) for the homogeneous random network. For convenience, we have introduced the inverse clustering parameter  $\delta = (g - 1)^{-1}$ , whereby the limit  $\delta \rightarrow \infty$  corresponds to the non-clustered network, while the case  $\delta \rightarrow 0$  coincides with ultimate clustering, i.e., the scenario where the network comprised effectively independent clusters. The system (18) naturally possesses the symmetry with respect to exchanging  $l$  and  $m - l$  together with  $U_a$  and  $U_b$  ( $l \leftrightarrow m - l, U_a \leftrightarrow U_b$ ).

Our interest lies with the inhomogeneous states where the respective stationary levels of the two groups of clusters are different,  $R_a^* \neq R_b^*$ . The analysis of (18) reveals that apart from the homogeneous states described in Sec. III A, one may indeed find one or two coexisting inhomogeneous states depending on the inverse clustering parameter  $\delta$  under fixed  $(m, l, I, B)$ . While the system (15) and the subsequent Eqs. (16)–(18) can describe a network of arbitrary number of equal clusters, the analysis below is focused on the network of  $m = 5$  clusters. This is chosen as a minimal paradigmatic example, convenient since due to symmetry, the cases  $l = 1$  and  $l = 2$  exhaust all the possible inhomogeneous solutions.

Onset of inhomogeneous states is investigated in detail by constructing the  $\delta - I$  bifurcation diagrams (see Fig. 4). The left and the right plots refer to cases  $l = 1$  and  $l = 2$ , respectively, with the remaining network parameters fixed to  $\alpha = 0.8, B = 0.004$ . For  $\delta$  values less than the level indicated by the red dotted line in Fig. 4(b), there exists an  $I$  interval where two inhomogeneous solutions can coexist, whereas above the given  $\delta$ , one can find only monostable inhomogeneous states.

Note that the region of coexistence between the two inhomogeneous states admits a total of 9 solutions of the mean-field model (15), cf. the notation in Fig. 4(b), whereas in the two domains with a single genuine clustered regime, one finds a total of 7 solutions of the mean-field model. Most of the curves indicated in Fig. 4 correspond to saddle-node bifurcations. In particular, the transitions from regions with 1 to regions with 3 solutions and *vice versa* coincide with creation or annihilation of the homogeneous states already described in Sec. III A. Also, the boundary between regions with 5 and 7 solutions is given by the branches of saddle-node bifurcations which meet at the cusp point where the pitchfork bifurcation occurs. Exceptions to this paradigm are the transitions involving regions with 3 and 5 solutions of the mean-field model. The latter present fold bifurcations of the inhomogeneous states within the symmetry subgroup  $\Sigma_l \otimes \Sigma_{m-l}$ , whereby the emanating branches correspond to an unstable fixed point and a saddle point.

A more detailed picture of the inhomogeneous states and their stability domains relative to homogeneous states may be obtained by analyzing the corresponding  $R(I)$  bifurcation diagrams for fixed  $(m, l, B, \delta, \alpha)$ . The plots in Fig. 5 are provided for  $(\delta, I)$  values supporting the coexistence of two inhomogeneous states. The top and the bottom panels refer to cases  $l = 1$  and  $l = 2$ , respectively. In each panel, the left and the middle plots indicate the states occupied by the groups of  $l$  and  $m - l$  clusters, respectively, whereas the right plot concerns the entire network (left and middle plots superimposed).

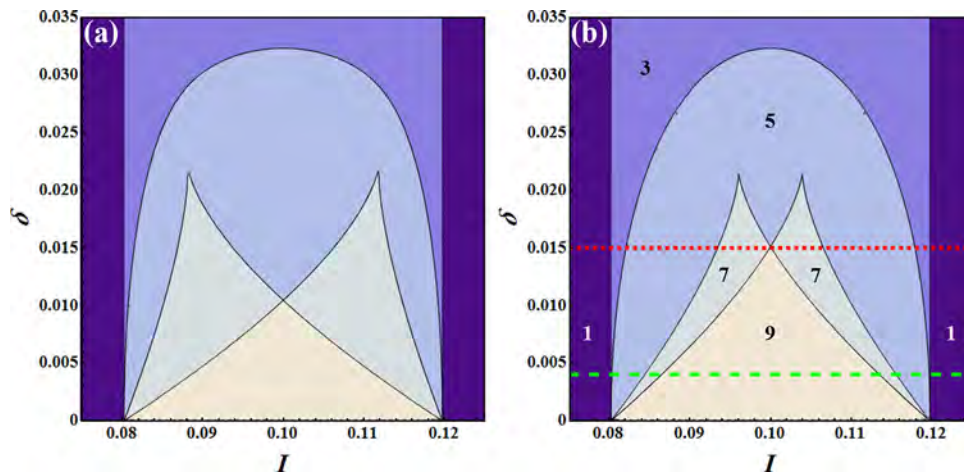


FIG. 4. Bifurcation diagrams  $\delta(I)$  for the inhomogeneous solutions of the mean-field model (15). (a) corresponds to case  $l = 1$ , whereas (b) refers to case  $l = 2$ . In (b), the total number of solutions obtained for the mean-field model within the different parameter domains is indicated. The regions with 1 and 3 solutions admit only homogeneous states, while the region with 5 solutions contains unstable inhomogeneous states. The regions with 7 and 9 solutions facilitate monostable inhomogeneous states and coexistence between the two inhomogeneous states, respectively. The bistability between inhomogeneous states arises only for sufficiently strong clustering below the red dotted line, cf. the bifurcation diagrams in Fig. 5 and Fig. 6 obtained for the  $\delta$  level just above the red line and the  $\delta$  value indicated by the green dashed line, respectively. The remaining network parameters are  $m = 5, B = 0.004, \alpha = 0.8$ .

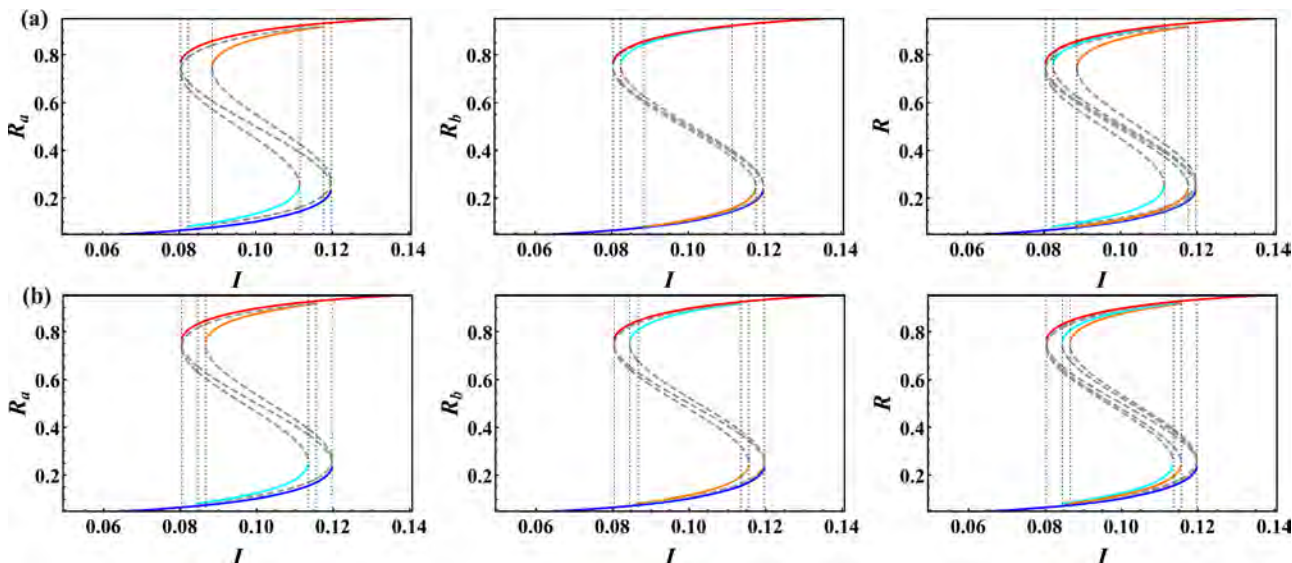


FIG. 5. Bifurcation diagrams  $R(I)$  for strong clustering  $\delta = 0.004$ , cf. the level denoted by the green dashed line in Fig. 4(b). Panels (a) and (b) correspond to cases  $l = 1$  and  $l = 2$ , respectively. The left and middle columns refer to states of particular groups of clusters  $R_a$  and  $R_b$ . The latter are superimposed in the right column to indicate the possible network states. The stable solutions are given by the solid lines, and the unstable branches are shown by the gray dashed lines. The  $R_a$  and  $R_b$  states corresponding to the same solution are presented by the same color. The remaining system parameters are  $m = 5$ ,  $B = 0.004$ ,  $\alpha = 0.8$ .

One clearly distinguishes between the regions where only one inhomogeneous solution is stable (either  $l$  clusters in the DOWN state and  $m - l$  in the UP state or *vice versa*) and the central  $I$  region where two inhomogeneous solutions coexist. For instance, in the bottom panel, coexistence of two inhomogeneous states is found for  $I \in (0.0866, 0.1135)$ , whereas the regions with  $l$  clusters UP or DOWN as the only inhomogeneous solutions are given by  $I \in (0.0845, 0.0866)$  and  $I \in (0.1135, 0.1156)$ . The presentation scheme is such that the solid (dashed) lines indicate the stable (unstable) branches of solutions. Note that the top-most (red solid line) and the bottom-most curves (blue solid line) in both panels

indicate the homogeneous states. In case of inhomogeneous states, the color coding is such that  $R_a$  and  $R_b$  corresponding to the same solution are assigned with the same color. As expected, the stability domains of the inhomogeneous states are smaller than the regions supporting the homogeneous states.

In Fig. 6, the  $R(I)$  bifurcation diagrams for lower clustering (larger  $\delta$ ) are shown, which no longer admits bistability between the inhomogeneous states. The top and the bottom panels again refer to cases  $l = 1$  and  $l = 2$ , respectively. From both panels, one learns that the two  $I$  intervals, where single inhomogeneous solutions exist, are separated by the  $I$  interval

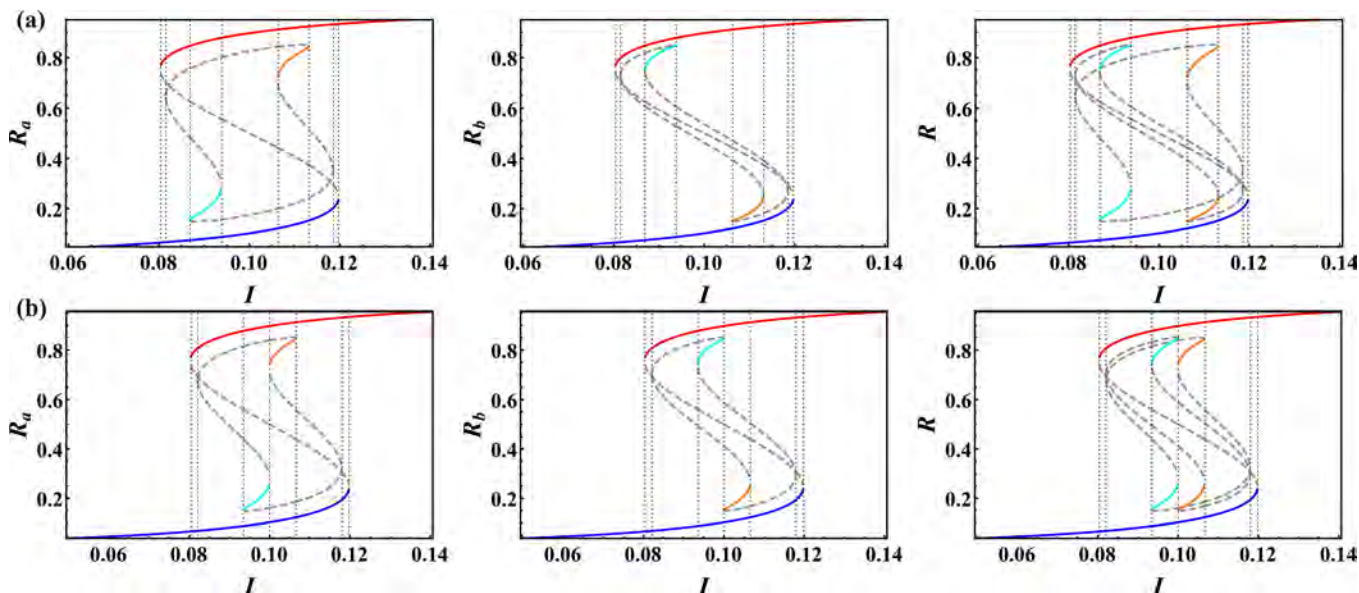


FIG. 6. Bifurcation diagrams  $R(I)$  in case of weak clustering  $\delta = 0.0151$ , the value just above the level indicated by the red dotted line in Fig. 4(b). The top and bottom panels correspond to cases  $l = 1$  and  $l = 2$ , respectively. The presentation style is the same as in Fig. 5. The remaining network parameters are  $m = 5$ ,  $B = 0.004$ ,  $\alpha = 0.8$ .

where only the two homogeneous states are available. A more detailed view of the basins of attraction of the particular states can be obtained by examining the vector fields for the relevant  $I$  values, cf. Fig. 7.

To gain a more general understanding of the multistability of the mean-field model (15), one should note that it is affected by two types of parameters, namely (i) the ones associated to homogeneous network and (ii) those characterizing the clustering. System (18) implies that the case of ultimate clustering ( $\delta = 0$ ) leads to the same type of dynamics as that of a homogeneous network. Consequently, the area of bistability of the homogeneous network corresponds to the maximal multistability of the clustered network: each cluster may either be in the UP or the DOWN state, which yields  $m + 1$  different stable solutions in total. Bistability of the homogeneous network has been addressed in Fig. 1 and has been examined in greater detail in our earlier papers.<sup>30,35</sup>

The main novelty here concerns the impact of the clustering degree and its interplay with  $\alpha, B$ , and  $m$ . As already indicated in Fig. 4, reduction of the clustering degree, i.e., increase of  $\delta$ , leads to gradual extinction of the inhomogeneous states via saddle-node bifurcations. Nevertheless, we have established that the stronger average network connectivity  $\alpha$  allows for the inhomogeneous states to occur at lower clustering, as corroborated by the shift of the relevant  $\delta$  region to higher values when  $\alpha$  is increased under all the other parameters fixed (not shown). Also, one finds that the  $\delta$  region admitting inhomogeneous states reduces under increasing noise  $B$ .

In order to investigate the effect of the number of clusters  $m$ , one may introduce the ratio  $\mu = l/m$  and rewrite Eq. (18) as

$$\begin{aligned} I - f(U_a) + \delta m(1 - \mu)(U_b - U_a) &= 0, \\ I - f(U_b) + \delta m\mu(U_b - U_a) &= 0. \end{aligned} \quad (19)$$

It follows that for the given ration  $\mu$ , the bifurcations in the system depend only on the product  $m\delta$ . The latter implies that the increase in the number of clusters  $m$  leads to the onset of the relevant bifurcations for smaller  $\delta$ . In other words, the more clusters present in the network, the stronger clustering is required to support the same level of multistability.

The analysis on multistability of the clustered network derived from the mean-field model is qualitative in character, but allows one to classify all the network states and gain understanding of the mechanism behind the switching dynamics.

The qualitative character of the predictions is reflected in that the mean-field model becomes the least accurate in vicinity of bifurcations where fluctuations are most pronounced, such that the finite-size effect prevails. Nevertheless, via the mean-field approach, one is also able to compare the effect of certain system parameters on the dynamics of the homogeneous and the clustered network. In particular, we are interested in comparison with respect to parameters  $I$  and  $\alpha$ . For the homogeneous network, one finds the bistability tongue, whereby the switching dynamics occurs in close vicinity of the cusp. Using the model (15), we have constructed analogous  $\delta - I$  bifurcation diagrams for the clustered network with fixed  $\alpha$ . Our goal is to apply these results to explicitly demonstrate that multistability promoted by the clustered topology plays the facilitatory role with respect to switching dynamics. This is easily understood intuitively, as additional multistability induced by clustering implies more network levels distributed less widely. Then, switching between different levels becomes more efficient because it may be achieved just by alternations within individual clusters, and the finite-size effect within the clusters is more pronounced given their smaller size compared to the whole network.

To illustrate the impact of clustering on the onset of slow rate oscillations, we consider an example where the system parameters  $B, I, \alpha$  are fixed to  $B = 0.01, I = 0.0513, \alpha = 0.9$ , respectively. For the given  $B$ , the selected  $(\alpha, I)$  values lie deep within the bistability tongue of the homogeneous random network, viz., far from the cusp point, cf. Figure 1(c). The corresponding time series of the network mean-rate  $R_N(t)$  and the associated stationary probability distribution obtained for the *full* system Eq. (1) are shown in Fig. 8. The latter corroborates that indeed no switching can be observed for the given parameter set in case of the homogeneous network. Nevertheless, for the sufficiently large  $g$  (small  $\delta$ ), the clustered network exhibits strong switching dynamics for the same  $(I, \alpha)$  values, see the results for the *full* system Eq. (1) in Fig. 9. In Fig. 9(a), the sequences from the mean-rate dynamics of individual clusters  $R_i(t)$  and the network rate  $R_N(t)$  are shown, whereas in panel (b), the corresponding probability distributions are provided. Note that the network parameters are selected from the domain supporting maximal multistability, i.e., the region where the mean-field model (15) admits 9 different solutions, allowing for the coexistence of two inhomogeneous states within the same  $\Sigma_l \otimes \Sigma_{m-l}$  symmetry subgroup.

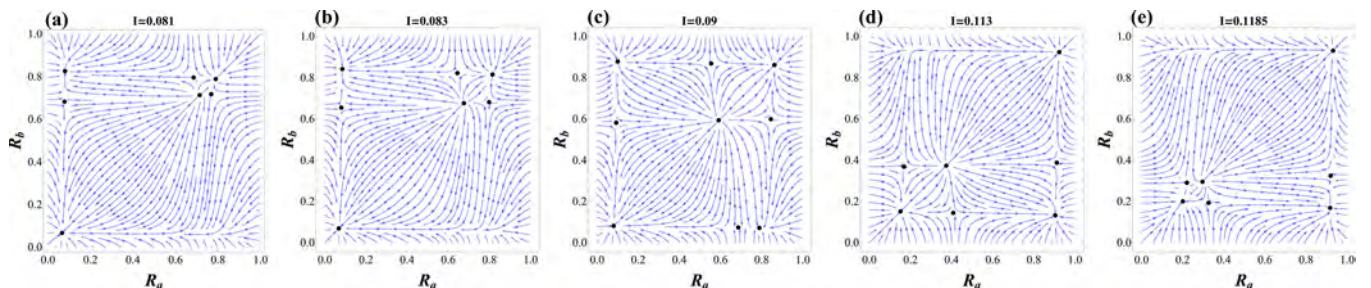


FIG. 7. Vector field plots indicating basins of attraction for the different types solutions of the mean-field model (15) in the  $(R_a, R_b)$  plane. The bias current  $I$  increases systematically from (a)-(e). The plots correspond to the example indicated in Fig. 5(b). The network parameters are  $m = 5, B = 0.004, \delta = 0.004, \alpha = 0.8$ .

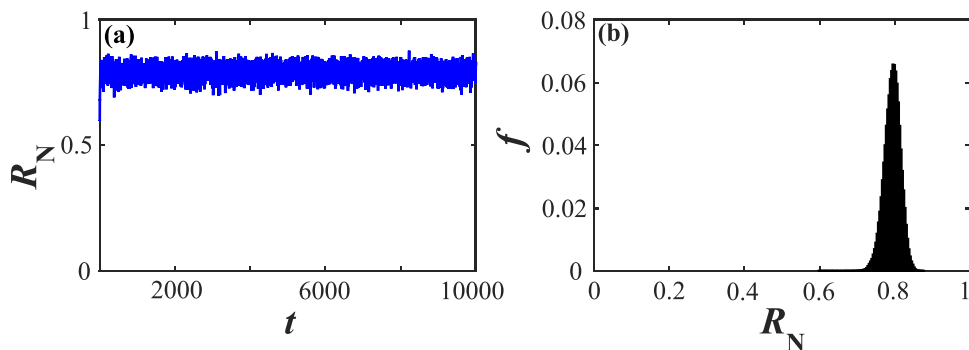


FIG. 8. Absence of switching dynamics for the *non-clustered* network beyond the vicinity of pitchfork bifurcation. In (a), the time trace of the network mean-rate  $R_N(t)$  for the full system (1) is shown, whereas in (b), the corresponding stationary probability distribution  $f(R)$  is provided. The network parameters are  $\alpha = 0.9$ ,  $I = 0.05$ ,  $B = 0.01$ ,  $N = 500$ . Note that the selected  $(\alpha, I)$  values lie within the  $B = 0.01$  bistability tongue, but far from the cusp point, cf. Fig. 1(c).

The results in Figs. 8 and 9 indicate a good qualitative agreement between the dynamics of the full system and the effective model, in a sense that the analysis of the mean-field model can anticipate the parameter values where one may observe the switching dynamics in the full system. Naturally, the levels of the effective model obtained for the clustered network correspond to metastable states of the full system, whereby switching between them occurs due to the finite-size effects.

#### IV. CONCLUSION

In this paper, we have analyzed the interplay of clustered topology and different types of noise on the spontaneous activity of networks of rate-based neurons. Clustered topology appears to be biologically relevant,<sup>4,25,49</sup> as the recent research on the microstructure of cortical networks has indicated that the small clusters of excitatory neurons are significantly over-represented.<sup>36,47</sup> In real neural networks, the clusters may be important as functional units performing certain tasks<sup>48</sup> or may constitute processing units adapted to receiving a certain type of stimuli.<sup>50–52</sup> We have demonstrated that clustering affects the collective dynamics of neural networks in a nontrivial fashion by promoting multistability such that spontaneous slow rate fluctuations gain on robustness.

From the theoretical perspective, our main contribution consists in derivation of the reduced system which describes the network activity in terms of interacting mean-field models representing each of the clusters. Typically, the reduced models address the two limit cases of a globally connected network<sup>32–34</sup> or a network with the random sparse connectivity,<sup>30,35</sup> such that the fluctuations of input between the units are small. The model presented here interpolates between these two scenarios, as the intra-cluster connectivity is strong, whereas the inter-cluster connectivity is weaker. We have identified three types of finite-size effects, including the small deterministic correction term, the macroscopic noise, and the topological uncertainty derived from the fact that each particular network realization features distinct deviations from the average connectivity degree. The macroscopic noise is a multiplicative one and incorporates three different sources of randomness, describing the impact of local neuronal noise on collective activity and the fluctuations in the input received by each of the units. Interestingly, the local intrinsic noise translates to additive macroscopic noise, whereas the microscopic external noise is reflected as multiplicative noise at the macroscopic level.

It has been demonstrated that the mean-field model can be used to qualitatively analyze the spontaneous activity of

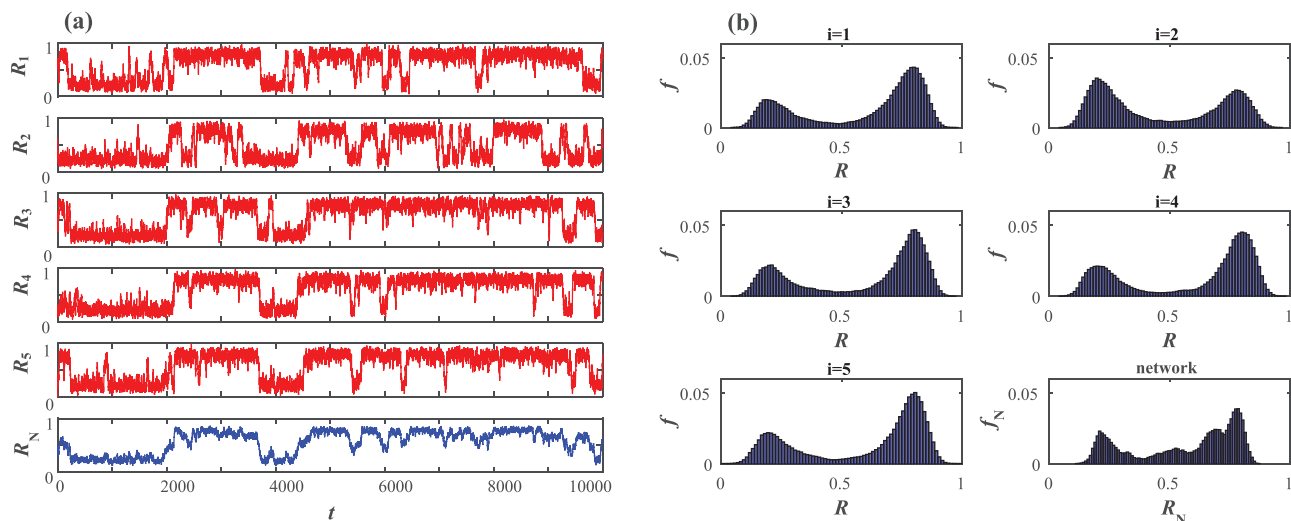


FIG. 9. Example of switching dynamics in the clustered network. Panel (a) shows the time traces of mean-rates of individual clusters  $R_i(t)$ ,  $i \in \{1, \dots, 5\}$  and the network  $R_N(t)$  obtained by simulating the full system (1). In panel (b), the corresponding probability distributions  $f(R)$  for the single clusters and the network are presented. The network parameters are  $m = 5$ ,  $B = 0.01$ ,  $\alpha = 0.9$ ,  $I = 0.0513$ ,  $\delta = 0.01$ ,  $N = 500$ . The fact that clustering promotes multistability allows for the switching dynamics to occur in the much broader  $(I, \alpha)$  domain than for the homogeneous random network, cf. Fig. 1(c) and the time series in Fig. 8.

the clustered network. The mechanism behind slow rate fluctuations has been explained by considering the stability and bifurcations of the mean-field model in the thermodynamic limit. The latter also allowed us to contrast the cases of the non-clustered and clustered network. In the non-clustered network, the crucial ingredient to slow rate fluctuations is that the network parameters lie close to pitchfork bifurcation. The evolution of the mean-rate may then locally be described by the paradigm of noise-driven motion of a particle in a double-well potential, so that its local minima coincide with the UP and DOWN states of the network. Such mechanism is *per se* generic, but lacks robustness, as it is confined to a small vicinity of the pitchfork bifurcation. The key effect of introducing clustering consists in the increased multistability of the network, facilitated by the onset and coexistence of states where different groups of clusters lie in the UP or the DOWN states. This promotes the switching dynamics, making it more efficient in a sense that alternation between the different network levels can be achieved just by changing the states of individual clusters rather than the whole network. Alternations within single clusters are naturally more likely since the finite-size effect associated to macroscopic noise is more pronounced. This way, the switching phenomenon gains on robustness, extending into the parameter domains where it cannot be observed for the non-clustered network.

The importance of clustered topology for macroscopic variability has earlier been indicated for the networks of spiking neurons with *balanced* excitatory-inhibitory input.<sup>4,24,25,53</sup> However, with such local dynamics, slow fluctuations of the mean network activity cannot even be observed for a simple random network topology, which implies that clustering indeed plays the crucial role in inducing the switching behavior. Thus, our results on the rate-based neurons together with the previous work on spiking neurons suggest that promoting of slow rate fluctuations by clustered topology may indeed be a universal phenomenon independent on the particular model of local neuronal dynamics.

In view of the fact that the spontaneous activity of real neurons may indeed be described as a doubly stochastic process,<sup>54–56</sup> combining the fluctuations on short and long timescales, the presented work has been aimed at providing theoretical tools for analysis of macroscopic variability in neural networks and its relation to microscopic dynamics and the network topology. We believe that the same method can be used to analyze the evoked activity of the network, examining the impact of clustering on the network's response to external stimulation. Also, our research so far has been confined to networks of excitatory neurons, but we believe that the same theoretical framework can readily be used to analyze the complex behavior of networks with both excitatory and inhibitory neurons. One expects that the presence of inhibitory subassembly should have a nontrivial impact both to spontaneous and evoked network activities.

## ACKNOWLEDGMENTS

This work was supported by the Ministry of Education, Science and Technological Development of Republic of Serbia

under Project No. 171017 and by the Russian Foundation for Basic Research under Project No. 17-02-00904.

- <sup>1</sup>A. Destexhe, M. Rudolph, and D. Paré, *Nat. Rev. Neurosci.* **4**, 739 (2003).
- <sup>2</sup>M. R. Cohen and A. Kohn, *Nat. Neurosci.* **14**, 811 (2011).
- <sup>3</sup>B. B. Averbeck, P. E. Latham, and A. Pouget, *Nat. Rev. Neurosci.* **7**, 358 (2006).
- <sup>4</sup>A. Litwin-Kumar and B. Doiron, *Nat. Neurosci.* **15**, 1498 (2012).
- <sup>5</sup>M. Smith and A. Kohn, *J. Neurosci.* **28**, 12591 (2008).
- <sup>6</sup>G. Buzsáki, C. A. Anastassiou, and C. Koch, *Nat. Rev. Neurosci.* **13**, 407 (2012).
- <sup>7</sup>G. Buzsáki, *Rhythms of the Brain* (Oxford University Press, Oxford, 2006).
- <sup>8</sup>T. T. G. Hahn, J. M. McFarland, S. Berberich, B. Sakmann, and M. R. Mehta, *Nat. Neurosci.* **15**, 1531 (2012).
- <sup>9</sup>A. Destexhe, D. Contreras, and M. Steriade, *J. Neurosci.* **19**, 4595 (1999); available at <http://www.jneurosci.org/content/19/11/4595>.
- <sup>10</sup>C. C. H. Petersen, T. T. G. Hahn, M. Mehta, A. Grinvald, and B. Sakmann, *Proc. Natl. Acad. Sci. U. S. A.* **100**, 13638 (2003).
- <sup>11</sup>V. V. Vyazovskiy and K. D. Harris, *Nat. Rev. Neurosci.* **14**, 443 (2013).
- <sup>12</sup>T. T. G. Hahn, B. Sakmann, and M. R. Mehta, *Nat. Neurosci.* **9**, 1359 (2006).
- <sup>13</sup>G. Gigante, G. Deco, S. Marom, and P. Del Giudice, *PLoS Comput. Biol.* **11**, e1004547 (2015).
- <sup>14</sup>R. Cossart, D. Aronov, and R. Yuste, *Nature* **423**, 283 (2003).
- <sup>15</sup>R. L. Cowan and C. J. Wilson, *J. Neurophysiol.* **71**, 17 (1994).
- <sup>16</sup>D. Millman, S. Mihalas, A. Kirkwood, and E. Niebur, *Nat. Phys.* **6**, 801 (2010).
- <sup>17</sup>M. Steriade, D. A. McCormick, and T. J. Sejnowski, *Science* **262**, 679 (1993).
- <sup>18</sup>J. Anderson *et al.*, *Nat. Neurosci.* **3**, 617 (2000).
- <sup>19</sup>D. Ji and M. A. Wilson, *Nat. Neurosci.* **10**, 100 (2007).
- <sup>20</sup>Y. Isomura *et al.*, *Neuron* **52**, 871 (2006).
- <sup>21</sup>M. Remondes and E. M. Schuman, *Nature* **431**, 699 (2004).
- <sup>22</sup>S. Diekelmann and J. Born, *Nat. Rev. Neurosci.* **11**, 114 (2010).
- <sup>23</sup>D. Miyamoto, *et al.*, *Science* **352**, 1315 (2016).
- <sup>24</sup>F. Lagzi and S. Rotter, *PLoS ONE* **10**, e0138947 (2015).
- <sup>25</sup>B. Doiron and A. Litwin-Kumar, *Front. Comput. Neurosci.* **8**, 56 (2014).
- <sup>26</sup>M. D. McDonnell and L. M. Ward, *PLoS One* **9**, e88254 (2014).
- <sup>27</sup>M. D. McDonnell and L. M. Ward, *Nat. Rev. Neurosci.* **12**, 415 (2011).
- <sup>28</sup>A. A. Faisal, L. P. J. Selen, and D. M. Wolpert, *Nat. Rev. Neurosci.* **9**, 292 (2008).
- <sup>29</sup>R. Moreno-Bote, J. Rinzler, and N. Rubin, *J. Neurophys.* **98**, 1125 (2007).
- <sup>30</sup>I. Franović and V. Klinshov, *Europhys. Lett.* **116**, 48002 (2016).
- <sup>31</sup>L. Albantakis and G. Deco, *PLoS Comput. Biol.* **7**, e1002086 (2011).
- <sup>32</sup>B. Lindner, J. Garcia-Ojalvo, A. Neiman, and L. Schimansky-Geier, *Phys. Rep.* **392**, 321 (2004).
- <sup>33</sup>M. A. Zaks, X. Sailer, L. Schimansky-Geier, and A. B. Neiman, *Chaos* **15**, 026117 (2005).
- <sup>34</sup>I. Franović, K. Todorović, N. Vasović, and N. Burić, *Phys. Rev. E* **87**, 012922 (2013).
- <sup>35</sup>V. Klinshov and I. Franović, *Phys. Rev. E* **92**, 062813 (2015).
- <sup>36</sup>R. Perin, T. K. Berger, and H. Markram, *Proc. Natl. Acad. Sci. U. S. A.* **108**, 5419 (2011).
- <sup>37</sup>L. Zemanová, C. Zhou, and J. Kurths, *Physica D* **224**, 202 (2006).
- <sup>38</sup>W. Gerstner, W. M. Kistler, R. Naud, and L. Paninski, *Neuronal Dynamics: From Single Neurons to Networks and Models of Cognition* (Cambridge University Press, Cambridge, 2014).
- <sup>39</sup>H. Hasegawa, *Phys. Rev. E* **75**, 051904 (2007).
- <sup>40</sup>R. A. Anderson, S. Musallam, and B. Pesaran, *Curr. Opin. Neurobiol.* **14**, 720 (2004).
- <sup>41</sup>I. Franović, K. Todorović, N. Vasović, and N. Burić, *Phys. Rev. Lett.* **108**, 094101 (2012).
- <sup>42</sup>A. N. Burkitt, *Biol. Cybern.* **95**, 1 (2006).
- <sup>43</sup>V. I. Mel'nikov, *Phys. Rep.* **209**, 1 (1991).
- <sup>44</sup>C. W. Gardiner, *Handbook of Stochastic Methods for Physics, Chemistry and the Natural Sciences* (Springer-Verlag, Berlin, 2004).
- <sup>45</sup>A. Bovier and F. den Hollander, *Metastability, a Potential-Theoretic Approach* (Springer International Publishing, Switzerland, 2015).
- <sup>46</sup>G. A. Pavliotis, *Stochastic Processes and Applications* (Springer, New York, 2014).
- <sup>47</sup>S. Song, P. Sjöström, M. Reigl, S. Nelson, and D. Chklovskii, *PLoS Biol.* **3**, e68 (2005).

- <sup>48</sup>L. Yassin, B. L. Benedetti, J. Jouhanneau, J. A. Wen *et al.*, *Neuron* **68**, 1043 (2010).
- <sup>49</sup>E. L. Lameu, C. A. Batista, A. M. Batista, K. Iarosz, R. L. Viana, S. R. Lopes, and J. Kurths, *Chaos* **22**, 043149 (2012).
- <sup>50</sup>S. B. Hofer, H. Ko, B. Pichler, J. Vogelstein, H. Ros *et al.*, *Nat. Neurosci.* **14**, 1045 (2011).
- <sup>51</sup>H. Ko, S. B. Hofer, B. Pichler, K. A. Buchanan, P. J. Sjöström, and T. D. Mrsic-Flogel, *Nature* **473**, 87 (2011).
- <sup>52</sup>Y. Yoshimura, J. L. M. Dantzker, and E. M. Callaway, *Nature* **433**, 868 (2005).
- <sup>53</sup>G. Deco and E. Hugues, *PLoS Comput. Biol.* **8**, e1002395 (2012).
- <sup>54</sup>M. Churchland and L. Abbott, *Nat. Neurosci.* **15**, 1472 (2012).
- <sup>55</sup>A. Ponce-Alvarez, A. Thiele, T. D. Albright, G. R. Stoner, and G. Deco, *Proc. Natl. Acad. Sci. U. S. A.* **110**, 13162 (2013).
- <sup>56</sup>B. M. Yu, J. P. Cunningham, G. Santhanam, S. I. Ryu, K. V. Shenoy, and M. Sahani, *J. Neurophysiol.* **102**, 614 (2009).



## Nonlinear dynamics behind the seismic cycle: One-dimensional phenomenological modeling



Srdan Kostić<sup>a,\*</sup>, Nebojša Vasović<sup>b</sup>, Kristina Todorović<sup>c</sup>, Igor Franović<sup>d</sup>

<sup>a</sup> Department for Scientific Research and Informatics, Institute for Development of Water Resources “Jaroslav Černi”, Jaroslava Černog 80, Belgrade 11226, Serbia

<sup>b</sup> Department of Applied Mathematics, University of Belgrade Faculty of Mining and Geology, Serbia

<sup>c</sup> Department of Physics and Mathematics, University of Belgrade Faculty of Pharmacy, Serbia

<sup>d</sup> Scientific Computing Lab, University of Belgrade, Institute of Physics, Serbia

### ARTICLE INFO

#### Article history:

Received 12 July 2017

Revised 27 November 2017

Accepted 30 November 2017

#### Keywords:

Spring-block model

Time delay

Rate-and-state dependent friction law

Seismic cycle

### ABSTRACT

In present paper, authors examine the dynamics of a spring-slider model, considered as a phenomenological setup of a geological fault motion. Research is based on an assumption of delayed interaction between the two blocks, which is an idea that dates back to original Burridge–Knopoff model. In contrast to this first model, group of blocks on each side of transmission zone (with delayed interaction) is replaced by a single block. Results obtained indicate predominant impact of the introduced time delay, whose decrease leads to transition from steady state or aseismic creep to seismic regime, where each part of the seismic cycle (co-seismic, post-seismic and inter-seismic) could be recognized. In particular, for coupling strength of order  $10^2$  observed system exhibit inverse Andronov–Hopf bifurcation for very small value of time delay,  $\tau \approx 0.01$ , when long-period ( $T = 12$ ) and high-amplitude oscillations occur. Further increase of time delay, of order  $10^{-1}$ , induces an occurrence of a direct Andronov–Hopf bifurcation, with short-period ( $T = 0.5$ ) oscillations of approximately ten times smaller amplitude. This reduction in time delay could be the consequence of the increase of temperature due to frictional heating, or due to decrease of pressure which follows the sudden movement along the fault. Analysis is conducted for the parameter values consistent with previous laboratory findings and geological observations relevant from the seismological viewpoint.

© 2017 Elsevier Ltd. All rights reserved.

### 1. Introduction

It is generally considered that process of accumulation and release of stress along the seismogenic faults always obeys the same rule: period with no movement along the fault (or with aseismic creep), when the stress is being accumulated, is followed by its sudden release, which could be further succeeded by the partial emission of the remained stored energy. These three periods, formally known as inter-seismic, co-seismic and post-seismic, respectively, constitute a single seismic cycle, which could be manifested at regular time intervals (for the strongest seismic events), or, more likely, occurrence of seismic events appears as a random process following Poisson distribution [1]. From the seismological viewpoint previous studies on properties of a seismic cycle resulted in sufficiently accurate characterization of each of the aforementioned periods. It is well known that inter-seismic deformation indicates depth of the zone that will eventually rupture seismically [2] and

the rate at which stress is accumulating along the fault zone [3]. The very end of this inter-seismic period could be marked by the occurrence of foreshocks as small partial releases of the stored potential energy before the main event. On the other hand, post-seismic deformation is usually driven by the preceding co-seismic stress change [3] and it could be as large as the fault slip during the main seismic event. Observed post-seismic behavior includes poroelastic deformation [4], frictional afterslip [5] and viscoelastic relaxation [6]. Similarly to the inter-seismic period, post-seismic part of the seismic cycle could be marked by the occurrence of aftershocks, as sudden releases of the remaining stored energy with significantly smaller magnitude in comparison to the main seismic event.

From the purely mechanical viewpoint, it is commonly considered that alternation of seismic cycles could be described by irregular stick-slip behavior [7]. For a simple frictional system, like commonly used spring-block model, the occurrence of stick-slip is due to a difference in static and kinetic friction, i.e. once the block starts to slide the friction drops suddenly to a lower level [8]. It is generally considered that surface roughness and normal

\* Corresponding author.

E-mail address: [srdjan.kostic@jcerni.co.rs](mailto:srdjan.kostic@jcerni.co.rs) (S. Kostić).

stress level play main role in “pushing” the spring-block model into stick-slip regime [9]. In present analysis, we analyze only the effect of friction on dynamics of spring-block model, by assuming some small constant value of normal stress which does not significantly affect the dynamics of the model. This could correspond to shallow parts of the Earth’s crust, or parts where horizontal stresses are much higher than vertical ones, due to significant effect of tectonics and surface erosion which reduced the thickness of the overlying layers.

Results of the pioneer work of Burridge and Knopoff [10] on dynamics of a simple spring-block model set a solid base for succeeding laboratory and theoretical research of seismogenic fault motion. The main outcome of their work is that distribution of displacement sums (i.e. earthquake magnitudes) follows two key macroseismological laws: Gutenberg–Richter and Omori–Utsu power law distribution. This finding enabled succeeding researchers a wide specter of additional analyzes, from the purely seismological [11,12], across the tribological [13,14] to purely dynamical [15]. These “dynamical” research are primarily in our focus, since they showed that for a certain parameter range, dynamics of spring-block models exhibit a regular transition between different dynamical regimes, with the eventual occurrence of chaotic dynamics [16,17]. Nevertheless, former studies did not treat the problem of seismic cycle *per se*, except from our previous paper, where we analyzed the impact of transient seismic wave on the dynamics of spring-block model, which resulted in transition between different seismic cycles [18]. One of the goals of the present analysis is to match different dynamical regimes of a spring-block model to appropriate phases of seismic cycles. In particular, the performed analysis should provide answers to the following questions: (1) what are the relevant parameter ranges for which the dynamic of the spring-block model enters the stick-slip regime, (2) what are the main dynamical features of that regime and (3) what does it mean for the real conditions in Earth’s crust. In that way, we will be able to reveal the main controlling mechanism behind the regularity of seismic cycle. One should note that, besides seismology, nonlinear models in general have been successively applied in other areas of natural sciences, as well [19–24].

Besides the analogy with the macroseismological laws, another important outcome of the original work of Burridge and Knopoff concerns a delayed transition of motion among two sets of blocks, indicating possible highly complex dynamical behavior. In particular, they showed that displacement among two boundary group of blocks in an one-dimensional chain is being transmitted with a certain time delay, whose order of unit corresponds to the viscosity of the middle set of blocks. Although this finding opened a lot of possibilities for investigating the cause and consequences of such a feature, it was not taken into consideration in succeeding studies. Effect of time delay was previously only implicitly introduced in friction term [25,26], and between the neighboring blocks in an one-dimensional chain of blocks with rate-dependent friction law [27]. In present paper, we analyze the transition between different seismic cycles considering the delayed interaction among the blocks with a rate- and state-dependent friction law. In contrast to our previous work, delayed interaction is assumed between the blocks exhibiting rate- and state-dependent friction law, which corresponds well to the laboratory observations of rock friction. Also, present analysis is conducted for the values of parameters which are either observed in reality or in laboratory conditions. We consider that this behavior is also relevant from the viewpoint of seismology, since different friction conditions along the fault (e.g. different thickness and physico-mechanical properties of fault gouge, impact of pore fluid, etc.) could cause a delayed transition of motion among different parts of the active seismogenic fault.

To sum up, the main idea of the present study is to determine the main dynamical mechanism by which the fault motion model reaches stick-slip like oscillations, as an appropriate dynamical state of a seismic fault motion which includes the inter-seismic, co-seismic and post-seismic regime. Thereby, dynamics of the relevant model is examined for the parameter values meaningful from the viewpoint of seismology, under the influence of the assumed delayed interaction of variable strength. Introduction of new influential parameters is motivated by the previous laboratory findings, with the aim of modeling the effect of changeable friction properties along the fault. The analysis is conducted using both analytical and numerical methods, former of which involved the application of local bifurcation analysis for the model with constant time delay whose results are corroborated numerically.

## 2. Model development

### 2.1. Original model of fault motion

Our numerical simulations of a spring-block model are based on the system of equations coupled with Dieterich–Ruina rate- and state-dependent friction law [16]:

$$\begin{aligned}\dot{\theta} &= -\left(\frac{v}{L}\right)\left(\theta + B \log\left(\frac{v}{v_0}\right)\right) \\ \dot{u} &= v - v_0 \\ \dot{v} &= \left(-\frac{1}{M}\right)\left(ku + \theta + A \log\left(\frac{v}{v_0}\right)\right)\end{aligned}\quad (1)$$

where parameter  $M$  is the mass of the block and the spring stiffness  $k$  corresponds to the linear elastic properties of the rock mass surrounding the fault [28]. According to Dieterich and Kilgore [29] the parameter  $L$  corresponds to the critical sliding distance necessary to replace the population of asperity contacts. The parameters  $A$  and  $B$  are empirical constants, which depend on material properties. Variables  $u$  and  $v$  represent displacement and velocity, while  $\theta$  denotes the state variable describing the state of the rough surface along which blocks are moving [30]. Parameter  $v_0$  represents the constant background velocity of the upper plate Fig. 1). For convenience, system ((2) is non-dimensionalized by defining the new variables  $\theta'$ ,  $v'$ ,  $u'$  and  $t'$  in the following way:  $\theta = A\theta'$ ,  $v = v_0v'$ ,  $u = Lu'$ ,  $t = (L/v_0)t'$ , after which we return to the use of  $\theta$ ,  $v$ ,  $u$  and  $t$ . This non-dimensionalization puts the system into the following form:

$$\begin{aligned}\dot{\theta} &= -v(\theta + (1 + \varepsilon) \log(v)) \\ \dot{u} &= v - 1 \\ \dot{v} &= -\gamma^2[u + (1/\xi)(\theta + \log(v))]\end{aligned}\quad (2)$$

where  $\varepsilon = (B - A)/A$  measures the sensitivity of the velocity relaxation,  $\xi = (kL)/A$  is the nondimensional spring constant, and  $\gamma = (k/M)^{1/2}(L/v_0)$  is the nondimensional frequency [16]. As it was previously shown [18], a supercritical direct Andronov–Hopf bifurcation curve occurs for the following parameter values  $\varepsilon = 0.27$ ,  $\xi = 0.5$  and  $\gamma = 0.8$ , leading from equilibrium state to regular periodic oscillations.

### 2.2. Fault motion model under study

We analyze the dynamics of two coupled blocks Fig. 1), whose motion is governed by the following system of first-order ordinary



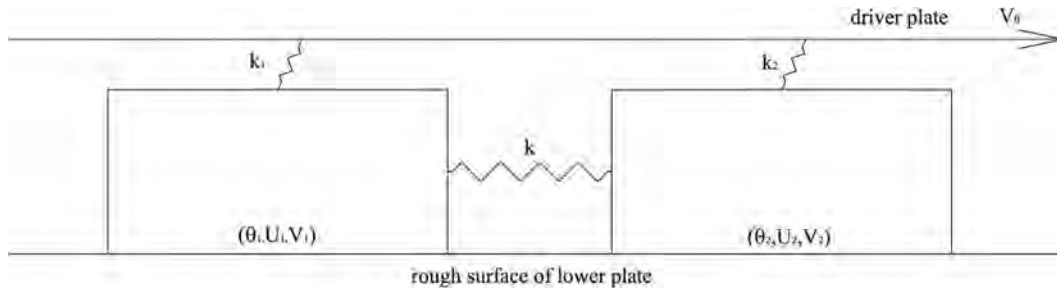


Fig. 1. Setup of the analyzed model.

differential equations, starting from the original system (1):

$$\begin{aligned}\dot{\theta}_1 &= -\left(\frac{V_1}{L_1}\right) \cdot \left(\theta_1 + B_1 \ln\left(\frac{V_1}{V_0}\right)\right) \\ \dot{U}_1 &= V_1 - V_0 \\ \dot{V}_1 &= (-1/M_1)[k_1 U_1 - k(U_2(t - \tau) - U_1(t)) + \theta_1 + A_1 \ln(V_1/V_0)] \\ \dot{\theta}_2 &= -\left(\frac{V_2}{L_2}\right) \cdot \left(\theta_2 + B_2 \ln\left(\frac{V_2}{V_0}\right)\right) \\ \dot{U}_2 &= V_2 - V_0 \\ \dot{V}_2 &= (-1/M_2)[k_2 U_2 - k(U_1(t - \tau) - U_2(t)) + \theta_2 + A_2 \ln(V_2/V_0)]\end{aligned}\quad (3)$$

Here we introduced time delay between the two coupled blocks. In this way, we simulate the original model of Burridge and Knopoff [10], where two blocks actually represent two boundary sets of blocks, and the effect of the middle set of blocks (with different viscosity properties in comparison to other two sets) is replicated by the delayed interaction between the two blocks.

Appropriate non-dimensionalization puts the system (3) into the following form:

$$\begin{aligned}\theta_1 &= -V_1 \cdot (\theta_1 + (1 + \varepsilon_1) \ln V_1) \\ U_1 &= V_1 - 1 \\ V_1 &= \gamma_1^2 \left(-U_1 + c_1(U_2(t - \tau) - U_1(t)) - \left(\frac{1}{\xi_1}\right)(\theta_1 + \ln(V_1))\right) \\ \theta_2 &= -V_2 \cdot (\theta_2 + (1 + \varepsilon_2) \ln V_2) \\ U_2 &= V_2 - 1 \\ V_2 &= \gamma_2^2 \left(-U_2 + c_2(U_1(t - \tau) - U_2(t)) - \left(\frac{1}{\xi_2}\right)(\theta_2 + \ln(V_2))\right)\end{aligned}\quad (4)$$

where  $c_i = k/k_i$ ,  $i = 1, 2$ ;  $\theta_{1new} = \theta_{1old}/A$ ,  $V_{new} = V_{old}/V_0$ ,  $U_{new} = U_{old}/L$ ,  $t_{new} = (L/V_0)t_{old}$ ,  $\varepsilon = (B - A)/A$ ,  $\xi = (kL)/A$ ,  $\gamma = (k/M)^{1/2}(L/V_0)$ . In present paper, we consider that  $\varepsilon_1 = \varepsilon_2 = \varepsilon$ ,  $\gamma_1 = \gamma_2 = \gamma$ ,  $\xi_1 = \xi_2 = \xi$  and  $c_1 = c_2 = c$ .

### 3. Choice of the relevant parameter values

As it is commonly known, dynamics of any system is predominantly controlled by an action of a few control parameters, whose tuning induce corresponding transitions between different dynamical regimes. Thereby, variations of control parameters should be performed within the relevant intervals, i.e. by taking the parameter values which are of interest either from theoretical viewpoint, or which are observed in laboratory conditions or *in situ*.

Original model (2) has three main control parameters that predetermine its dynamics. As it was previously indicated, parameter  $\varepsilon$  denotes the ratio of stress drop and stress increase during the fault motion (Fig. 2). According to the results of previous studies [5], this ratio needs to be positive in order to capture the velocity-weakening behavior, i.e. for  $(B - A) > 0$  one could observe the unsta-

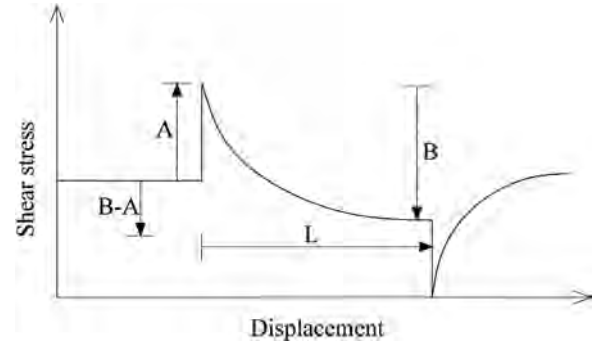


Fig. 2. General scheme of a shear stress variation during the motion of analyzed model shown in Fig. 1.

ble dynamics relevant from the viewpoint of seismology. Previous research showed that this condition is fulfilled at depths in Earth's crust where the most crustal earthquake foci are located, approximately between 5 and 15 km [5]. Below and above this zone, parameter  $\varepsilon$  has negative values, indicating velocity-strengthening behavior, which secures the stable dynamics of fault motion. Regarding the relevant values of parameter  $\varepsilon$ , preceding laboratory findings on friction properties of granite samples (since continental crust is mostly composed of granite) indicated that parameters A and B are of the order of magnitude  $10^{-3}$  [31], with ratio  $(B - A)/A$  in the interval  $[-0.17, 0.36]$ , which indicates that meaningful values of  $\varepsilon$  could be taken from the interval  $[-1, 1]$  (Table 1). One should note that present analysis is constrained only to the dynamics of crustal faults, since fault motion in the subduction zones is under prevailing gravitational influence, which is not examined in this study. It should also be emphasized that in present analysis we observe only the velocity weakening behavior, so negative values of dimensionless stress ratio are not examined.

Parameter  $\xi$  is defined as a function of spring stiffness  $k_L$ , block mass M and stress increase A. Stiffness  $k_L$  is related to the spring by which blocks are attached to the upper moving plate, which according to Brown et al. [32] needs to be much more flexible than spring connecting the blocks (whose stiffness is described by  $k_C$ ), since the distance between the interacting blocks along the fault is much smaller than the dimension of the driving plate. In present analysis if one takes that the value of  $k_C$  is around 1, than parameter  $k_L$  could take values two order of units smaller,  $k_L = 10^{-2}$ . This further means that relevant values of parameter  $c$  ( $k_C/k_L$ ) are of  $10^2$  order of unit. Regarding the block mass, we assume that M takes very small values (order of unit of  $10^{-6}$ ), since, in present analysis, we do not analyze the effect of gravity (normal stress), but dynamic instability is assumed to occur due to effect of friction and delayed interaction. Hence, analysis is conducted for almost massless blocks. When all of these assumptions, constraints and previously obtained results are taken into consideration, one arrives at the relevant values of  $\xi$  of the order of  $10^{-1}$  (Table 1).

**Table 1**  
Relevant parameter values for the analysis.

Parameter	Relevant value from the previous studies (order of unit)	Reference
Stress increase: A	$10.3 - 19.9 \times 10^{-3}$	[25]
Stress drop: B	$12.1 - 20.3 \times 10^{-3}$	[25]
Spring stiffness between the upper plate and the block: $k_L$	$k_L \ll k_C (10^{-2})$	[26]
Critical slip distance: L	$10^{-2}$	[27]
Velocity of the driving plate: $V_0$	1	[16]
Controlling parameters		
Parameter	Relevant value from the previous studies (order of unit)	Adopted interval for present analysis
$\varepsilon = (B-A) / A$	[-0.17,0.36]	[-1,1]
$\xi = k_L \times M/A$	$10^{-1}$	[0,1]
$\gamma = (k_L/M)^{1/2} \times (L/V_0)$	1	[0,2]

Relevant values of parameter  $\gamma$  are determined by taking into the consideration the spring stiffness  $k_L$ , block mass  $M$ , critical slip distance  $L$  and velocity of the upper driving plate  $V_0$ . According to Scholz [33], critical slip distance  $L$  represents a displacement needed to make a transition between the steady-state friction regimes (Fig. 2). Its recommended value is  $10^{-2}$  order of unit. Regarding the velocity of the upper driving plate,  $V_0$ , its relevant value is determined by the stationary solution of system (2), which is  $(\theta, U, V) = (0, 0, 1)$  according to Erickson et al. [16]. Hence, we take  $V_0 = 1$  as a meaningful value of the upper plate velocity. Concerning these appropriate values of  $k_L$ ,  $M$ ,  $L$  and  $V_0$ , one finds that relevant value of  $\gamma$  is of a single order of unit (Table 1).

One should note that the value of time delay is observed in comparison with the oscillation period relevant from the seismological viewpoint. In present paper, authors consider time delay as relevant for those values which are significantly smaller than the corresponding oscillation period. This is in correspondence with the proposal by Burridge and Knopoff, who took time delay significantly smaller for the part of the fault that exhibits viscous slipping rather than the parts that move by fracture.

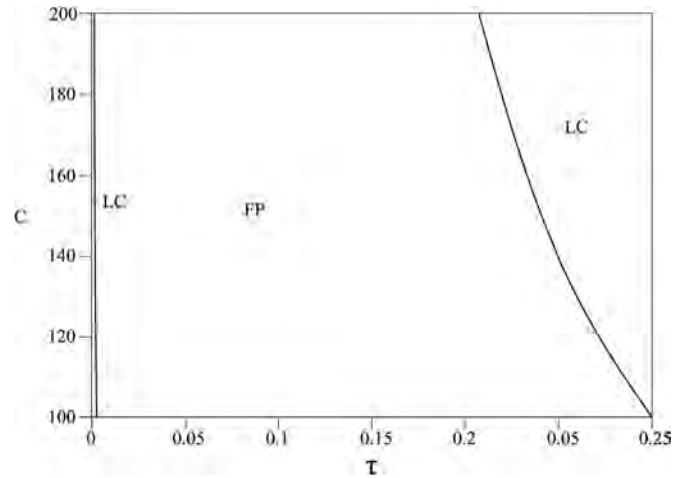
**4. Results**

Regarding the local bifurcation analysis, the considered delay differential equation (DDE) system is treated numerically using DDE BIFTOOL, having the obtained results further corroborated by the Runge-Kutta 4th order numerical method. System (4) has only one stationary solution, namely  $(\theta_1, U_1, V_1, \theta_2, U_2, V_2) = (0, 0, 1, 0, 0, 1)$ , which corresponds to steady sliding. We proceed in the standard way to determine and analyze the characteristic equation of (4) around a stationary solution  $(0, 0, 1, 0, 0, 1)$ . Details of the analysis are given in Appendix.

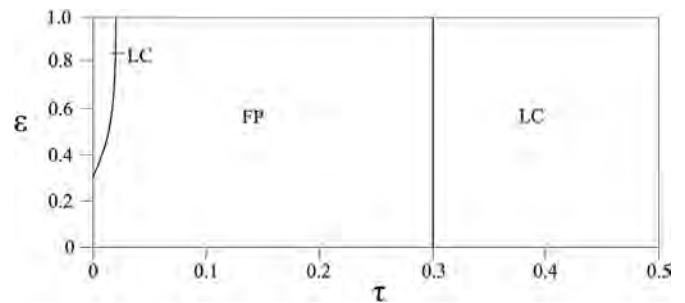
Next we shall analyze the effect of stationary time delay coupled with the influence of coupling strength  $c$  and the main control parameters of the observed system, namely  $\varepsilon$ ,  $\xi$  and  $\gamma$ . All the analyzes were done for the limit cycle as the starting dynamical regime of the initial observed system ( $\tau = 0$ ), which is considered as a co-seismic regime.

Fig. 3 shows the Hopf bifurcation curves in  $\tau$ - $c$  diagram. For the relevant range of values for coupling strength ( $10^2$  order of unit), observed system exhibit inverse Andronov–Hopf bifurcation, from the initial oscillatory regime, with period  $T \approx 12$ , to equilibrium state (fixed point), for very small value of time delay,  $\tau \approx 0.01$ . Increase of time delay, e.g.  $\tau = 0.3$ , for  $c = 100$ , induces an occurrence of a direct Andronov–Hopf bifurcation, with the appearance of regular periodic oscillations, with period  $T = 0.5$ . Regarding the oscillation amplitudes, direct Andronov–Hopf bifurcation triggers approximately ten times smaller displacements.

Effect of the interaction of time delay and dimensionless stress ratio  $\varepsilon$  is given in Fig. 4. As in the previous case, an inverse supercritical Andronov–Hopf bifurcation curve occurs with the in-



**Fig. 3.** Diagram  $\tau(c)$ , for the fixed values of parameters  $\varepsilon = 0.4$ ,  $\xi = 0.5$  and  $\gamma = 0.8$  (limit cycle of the starting system). Andronov–Hopf bifurcation curves denotes the transition from limit cycle (LC) to equilibrium state (EQ) and again to limit cycle (LC). Qualitatively similar diagrams are obtained for other parameter values for the initial conditions near the equilibrium point.



**Fig. 4.** Diagram  $\tau(\varepsilon)$ , for the fixed values of parameters  $c = 100$ ,  $\xi = 0.5$  and  $\gamma = 0.8$  (limit cycle of the starting system). Andronov–Hopf bifurcation curve denotes the transition from the initial limit cycle (LC) across the equilibrium state (EQ) and again to limit cycle (LC). Qualitatively similar diagrams are obtained for other parameter values for the initial conditions near the equilibrium point.

crease of  $\tau$ , introducing the change of dynamical regime from the limit cycle (for the values of  $\varepsilon > 0.27$ ) to equilibrium state, and further again to regular periodic oscillations (for  $\tau > 0.3$ ), with the occurrence of direct bifurcation. Qualitatively similar behavior is observed when  $\tau$  and nondimensional frequency  $\gamma$  are simultaneously varied (Fig. 5). With the increase of time delay, for constant value of  $\gamma$ , both inverse and direct supercritical Andronov–Hopf bifurcation occurs.

In the case when  $\tau$  and  $\xi$  are varied, while other parameters are held fixed for the equilibrium state of the original system (2),

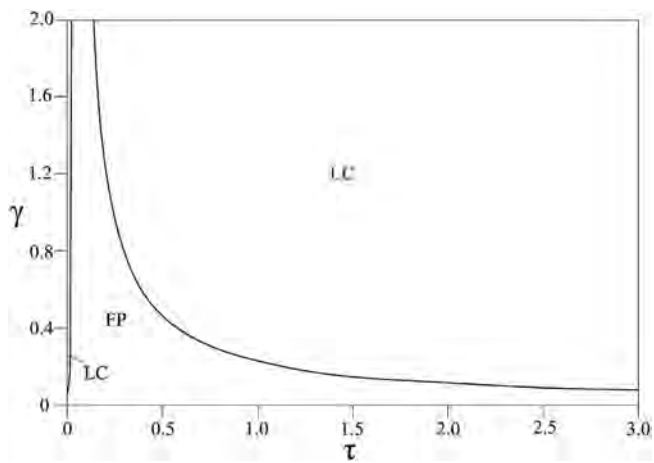


**Fig. 5.** Diagram  $\tau(\gamma)$ , for the fixed values of parameters  $c=100$ ,  $\xi=0.5$  and  $\varepsilon=0.4$  (limit cycle of the starting system). Andronov–Hopf bifurcation curve denotes the transition from equilibrium state (EQ) to limit cycle (LC). Qualitatively similar diagrams are obtained for other parameter values for the initial conditions near the equilibrium point.

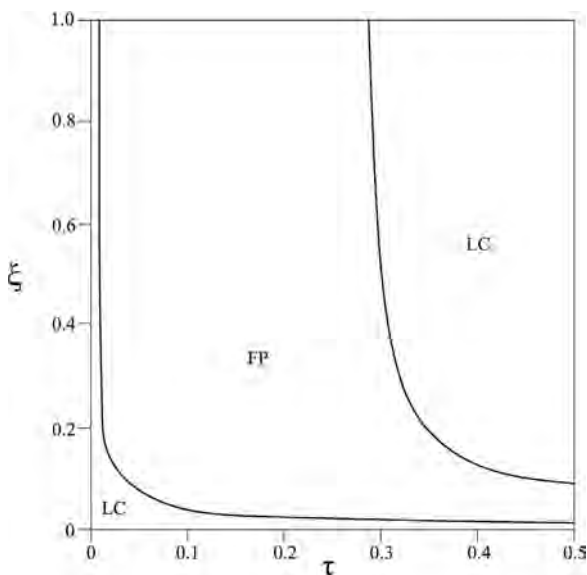


**Fig. 6.** Diagram  $\tau(\xi)$ , for the fixed values of parameters  $c=100$ ,  $\varepsilon=0.4$  and  $\gamma=0.8$  (limit cycle of the starting system). Andronov–Hopf bifurcation curve denotes the transition from the limit cycle (LC) across the equilibrium state (EQ) to limit cycle (LC). Qualitatively similar diagrams are obtained for other parameter values for the initial conditions near the equilibrium point.

there is an Andronov–Hopf bifurcation curve occurs from the equilibrium state to regular periodic oscillations (Fig. 6).

## 5. Discussion

Results of the performed analysis are new and meaningful for both the nonlinear dynamics and seismology. From the viewpoint of nonlinear dynamics, present analysis is relevant from the phenomenological aspect. In particular, the obtained results indicate that by assuming the delayed interaction between the blocks, one can observe two phenomena: inverse and direct Andronov–Hopf bifurcation. It should be emphasized that this feature is observed for the values of time delay about  $4 \times 10^2$  order of unit smaller than the corresponding period of regular oscillations of the starting system (for  $\tau \approx 0$ ).

From the seismological aspect, interpretation could be interesting if one looks in the opposite direction. In particular, if the ex-

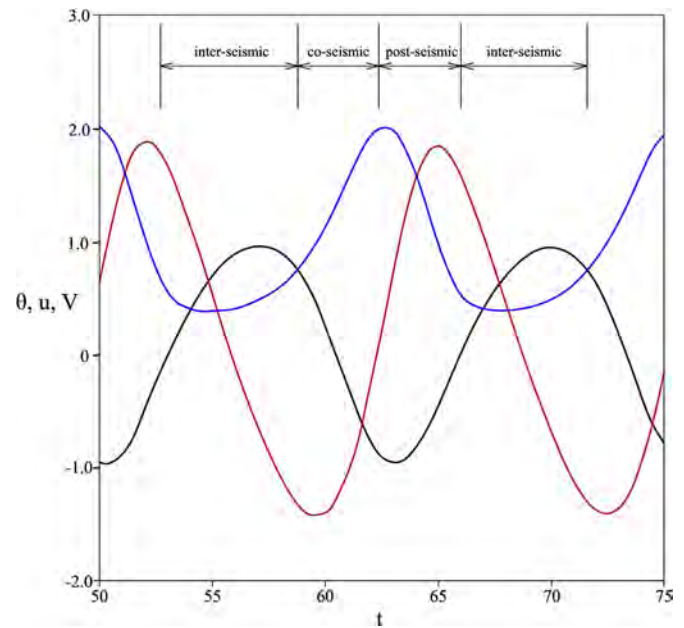


**Fig. 7.** Transition between seismic cycles in oscillatory regime of spring-slider dynamics. Black line denotes the change of friction (state variable), red line is for displacement, while blue line indicates the change of velocity.

istence of delayed interaction among different fault segments is justified, considering different viscous properties of fault gouge, than starting dynamical regime should be with introduced positive value of time delay. This means that the starting system is probably in equilibrium state (fixed point), which is proved to occur with the introduction of time delay. However, further increase of time delay induces the transition to regular periodic oscillations, which certainly could not be considered as the onset of co-seismic regime, for two main reasons. Firstly, frequency of displacements is very high, i.e. oscillation period is approximately 0.5, which is near the value of time delay (0.3), where the bifurcation point occurs. Such large value of time delay could hardly be expected in natural conditions. Secondly, displacement amplitude is about ten times smaller than for the starting system, which is also not likely to happen, since the majority of displacement along the fault takes place during the earthquakes, i.e. in the co-seismic regime. Hence, in order to “force” the examined system with the included time delay to enter the co-seismic regime, one needs to analyze the conditions which lead to the reduction of viscosity effect. Certainly, weaker impact of viscosity is expected in high temperature and low pressure conditions, which are the two conditions usually satisfied during the fault movement. In particular, the unconsolidated angular shaped rock material that constitutes the fault gouge exhibits high friction, which further induces the increase in temperature. Also, during the fault movement, fault itself is released of the pressure generated by the strong tectonic forces acting in opposite directions along the fault. In particular, heat generated during frictional sliding is a substantial component of the energy budget of earthquakes [34,35]. When time delay is significantly small ( $\tau \ll 0.01$ ), fault enters the co-seismic dynamical regime, where regular periodic oscillations have low-frequency (i.e. high period,  $T \approx 12$ ), and rather large amplitude (around 1.2–2.0 in our numerical simulations). Certainly, case with  $\tau=0$  is out of the question, since main assumption of the analysis is that delayed interaction is inherent property of the compound fault.

Once the examined model is in oscillatory regime, one could easily recognize the co-seismic, post-seismic and inter-seismic regime, latter of which represent short-term occurrence (Fig. 7).

One should note that such dynamics, relevant from the viewpoint of seismology, is observed for the parameter values adopted using the previous laboratory findings.

**6. Conclusion**

In present paper, authors examine dynamics of a spring-slider model as a setup of fault movement. Examined model is composed of two blocks with delayed interaction, which mimics delayed interaction among a group of blocks from the original Burridge–Knopoff model. Analysis is conducted for the parameter values relevant from the seismological viewpoint, based on the previous laboratory findings and seismological observations. Main goal of the research was to establish the background dynamics of a seismic cycle, including the transition from steady state or aseismic creep to stick-slip-like seismic regime, with alternation of inter-seismic, co-seismic and post-seismic cycles.

Results of the performed analysis indicate the following. Introduction of small time delay, significantly smaller when compared to the period of oscillatory regime, leads to transition from fixed point (equilibrium state) to periodic oscillations (limit cycle). From the viewpoint of seismology, these findings indicate a key role of the interaction among different parts of a compound fault in generation of seismogenic motion. More closely, effect of viscosity of a fault zone plays a crucial role in transmission of a movement along the fault. From the standpoint of earthquake phenomenology, one could consider regular periodic oscillations as an example of stick-slip like regime, with the successive shifts between the co-seismic regime (increasing velocity branch and decreasing friction), post-seismic regime (decreasing velocity branch and increasing friction) and inter-seismic regime (quasi-stationary velocity branch). On the other hand, some authors could consider the whole oscillatory regime as a representative of a co-seismic fault movement [36].

Another interesting outcome of the present research lies in the specific effect of the main controlling parameters, which were previously indicated as the most relevant for the modeled fault dynamics [16]. Apparently, ratio of stress drop to stress increase (parameter  $\varepsilon$ ), for the range of other parameters' values relevant from the seismological viewpoint and for the assumed delayed interaction as inherent property of fault dynamics, induces the transition from equilibrium state to periodic oscillations. Regarding the effect of other two parameters,  $\gamma$  and  $\xi$ , related to the stiffness of the spring connecting the blocks and the upper driving plate, results obtained imply that a change from steady state or aseismic creep to seismic fault motion occurs with the increase of  $\gamma$  and  $\xi$ . However, these parameters are considered as constants for the observed system, so it is highly unlikely to expect their significant changes during the fault motion. The expected changes of these parameters are either small or these changes are slow from the viewpoint relevant for the duration of seismogenic fault motion.

As for the effect of coupling strength  $c$ , increase of  $c$  for the relevant range of parameter values ( $>10^2$ ) leads to the change of dynamical regime only for rather high values of time delay, which is certainly not expected in the real conditions along the fault zone in the Earth's crust. Hence, in this case, time delay plays again the significant role, in a way that the reduction of time delay could lead to the onset of co-seismic regime.

Concerning the predominant effect of delayed coupling on dynamics of fault motion, further research could include the analysis of time varying delay on fault motion. Such an assumption is justified from the seismological viewpoint, since one could expect changes of friction properties along the fault zone in a reasonable period of time. From the standpoint of nonlinear dynamics, introduction of coupling with variable delay would certainly induce

more complex behavior and, maybe, indicate some new dynamical mechanisms in the background of earthquake nucleation.

**Acknowledgments**

This research was partly supported by the Ministry of Education, Science and Technological Development of the Republic of Serbia (Contract Nos. 176016 and 171017).

**Appendix**

Linearization of the system (4) and substitution  $\theta_1 = A_1 e^{\lambda t}$ ,  $U_1 = B_1 e^{\lambda t}$ ,  $V_1 = C_1 e^{\lambda t}$ ,  $\theta_2 = A_2 e^{\lambda t}$ ,  $U_2 = B_2 e^{\lambda t}$ ,  $V_2 = C_2 e^{\lambda t}$  and with  $U_1(t-\tau) = B_1 e^{\lambda(t-\tau)}$  and  $U_2(t-\tau) = B_2 e^{\lambda(t-\tau)}$  results in a system of algebraic equations for the constants  $A_1$ ,  $B_1$ ,  $C_1$ ,  $A_2$ ,  $B_2$  and  $C_2$ . This system has a nontrivial solution if the following is satisfied:

$$\begin{aligned}
 & -(\lambda + 1) \left[ \lambda \left( \lambda + \gamma_1^2 \left( \frac{1}{\xi_1} \right) \right) \cdot D \right. \\
 & \left. + \gamma_1^2 (1 + c_1) \cdot D + \gamma_1^2 c_1 e^{-\lambda \tau} (\lambda + 1) \gamma_2^2 c_2 e^{-\lambda \tau} \right] \\
 & + \lambda (1 + \varepsilon_1) \gamma_1^2 \left( \frac{1}{\xi_1} \right) \cdot D = 0
 \end{aligned} \tag{1A}$$

where:

$$D = \begin{vmatrix} -(\lambda + 1) & 0 & -(1 + \varepsilon_2) \\ 0 & -\lambda & 1 \\ -\gamma_2^2 \left( \frac{1}{\xi_2} \right) & -\gamma_2^2 (1 + c_2) & -\left( \lambda + \gamma_2^2 \left( \frac{1}{\xi_2} \right) \right) \end{vmatrix}$$

The Eq. (1A) is the characteristic equation of the system (4) and can be written in the following form:

$$\begin{aligned}
 & \left\{ -(\lambda + 1) \left[ \lambda \left( \lambda + \gamma_1^2 \left( \frac{1}{\xi_1} \right) \right) + \gamma_1^2 (1 + c_1) \right] + \lambda (1 + \varepsilon_1) \gamma_1^2 \left( \frac{1}{\xi_1} \right) \right\} \cdot \\
 & D = (\lambda + 1)^2 \gamma_1^2 \gamma_2^2 c_1 c_2 e^{-2\lambda \tau}
 \end{aligned} \tag{2A}$$

in which we substitute  $\lambda = i\omega$  to obtain:

$$\begin{aligned}
 & \frac{\left[ \omega^2 \gamma_1^2 \left( \frac{1}{\xi_1} \right) + \omega^2 - \gamma_1^2 (1 + c_1) \right] + i\omega \left[ \omega^2 - \gamma_1^2 (1 + c_1) - \gamma_1^2 \left( \frac{1}{\xi_1} \right) + (1 + \varepsilon_1) \gamma_1^2 \left( \frac{1}{\xi_1} \right) \right]}{\gamma_1^2 \gamma_2^2 c_1 c_2 [-\omega^2 + 1 + i2\omega]} D = \\
 & = \cos(2\omega\tau) - i \sin(2\omega\tau)
 \end{aligned} \tag{3A}$$

The resulting two equations for the real and imaginary part of (3A) after squaring and adding give an equation for each of the parameters,  $c_1$ ,  $c_2$ ,  $\varepsilon_1$  and  $\varepsilon_2$  in terms of the other parameters,  $\omega$ ,  $\mu$ ,  $\gamma_1$  and  $\gamma_2$ , and after division, an equation for  $\tau$  in terms of the parameters  $\omega$ ,  $\mu$ ,  $\gamma_1$ ,  $\gamma_2$ ,  $\varepsilon_1$ ,  $\varepsilon_2$ ,  $\xi_1$  and  $\xi_2$ . In this way, one obtains parametric representations of the relations between  $\tau$  and the parameters, which correspond to the bifurcation values  $\lambda = i\omega$ . The general form of such relations is illustrated by the following formula for  $\varepsilon_1$  as a function of  $\omega$ :

$$(1 + \varepsilon_1)_{1/2} = - \frac{F \pm \sqrt{F^2 - G^2}}{H} \tag{4A}$$

where F, G and H are abbreviations for the following terms:

$$\begin{aligned}
 F = & \left( \omega \left[ \left( \omega^2 - \gamma_1^2 (1 + c_1) - \gamma_1^2 \left( \frac{1}{\xi_1} \right) \right) B + AD \right] (-\omega^2 + 1) \right. \\
 & \left. - 2 \left[ AB - \omega^2 \left( \omega^2 - \gamma_1^2 (1 + c_1) - \gamma_1^2 \left( \frac{1}{\xi_1} \right) \right) D \right] \right) \cdot \\
 & \omega \gamma_1^2 \left( \frac{1}{\xi_1} \right) \{ B(-\omega^2 + 1) + 2\omega^2 D \} \\
 & + \left( \left( AB - \omega^2 \left( \omega^2 - \gamma_1^2 (1 + c_1) - D \gamma_1^2 \left( \frac{1}{\xi_1} \right) \right) \right) (-\omega^2 + 1) \right. \\
 & \left. + B\omega^2 \left( 2 \left( \omega^2 - \gamma_1^2 (1 + c_1) - \gamma_1^2 \left( \frac{1}{\xi_1} \right) \right) + AD \right) \right)
 \end{aligned}$$

$$\begin{aligned}
G &= \left[ \left( \omega \gamma_1^2 \left( \frac{1}{\xi_1} \right) \{ B(-\omega^2 + 1) + 2\omega^2 D \} \right)^2 \right. \\
&\quad \left. + \left( \omega^2 \gamma_1^2 \left( \frac{1}{\xi_1} \right) \left\{ B \left( 1 + \frac{1}{\mu} \right) - D(-\omega^2 + 1) \right\} \right)^2 \right] \\
&\quad \left[ \left( \left( \omega \left[ \left( \omega^2 - \gamma_1^2 (1 + c_1) - B \gamma_1^2 \left( \frac{1}{\xi_1} \right) \right) + AD \right] (-\omega^2 + 1) \right. \right. \right. \\
&\quad \left. \left. - 2 \left[ AB - D \omega^2 \left( \omega^2 - \gamma_1^2 (1 + c_1) - \gamma_1^2 \left( \frac{1}{\xi_1} \right) \right) \right] \right) \right)^2 + \right. \\
&\quad \left. + \left( \left( AB - \omega^2 \left( \omega^2 - \gamma_1^2 (1 + c_1) - D \gamma_1^2 \left( \frac{1}{\xi_1} \right) \right) \right) \right) (-\omega^2 + 1) \right. \\
&\quad \left. + \omega^2 \left( 2 \left( \omega^2 - \gamma_1^2 (1 + c_1) - B \gamma_1^2 \left( \frac{1}{\xi_1} \right) \right) + AD \right) \right)^2 - \\
&\quad \left. - \left( \left( (-\omega^2 + 1)^2 + 2\omega^2 \right) \left( \gamma_1^2 \gamma_2^2 c_1 c_2 \right) \right)^2 \right] \\
H &= \left( \gamma_1^2 \left( \frac{1}{\xi_1} \right) \omega \{ B(-\omega^2 + 1) + 2\omega^2 D \} \right)^2 \\
&\quad + \left( \omega^2 \gamma_1^2 \left( \frac{1}{\xi_1} \right) \{ 2B - D(-\omega^2 + 1) \} \right)^2 \quad (5A)
\end{aligned}$$

and A, B and D are:

$$\begin{aligned}
A &= \omega^2 \gamma_1^2 \left( \frac{1}{\xi_1} \right) + \omega^2 - \gamma_1^2 (1 + c_1) \\
B &= \omega^2 \cdot \left( \gamma_2^2 \left( \frac{1}{\xi_2} \right) + 1 \right) - \gamma_2^2 (1 + c_2) \\
D &= \omega^2 - \gamma_2^2 (1 + c_2) - \gamma_2^2 \left( \frac{1}{\xi_2} \right) + \gamma_2^2 (1 + \varepsilon_2) \left( \frac{1}{\xi_2} \right)
\end{aligned} \quad (6A)$$

On the other hand, for  $c_1$  as a function of  $\omega$ :

$$(c_1)_{1/2} = \frac{-F \pm \sqrt{F^2 - GH}}{H} \quad (7A)$$

where F, G and H are the same as in (7).

For  $\tau$  as a function of  $\omega$ :

$$\tau = \frac{1}{2\omega} \left\{ \arctan \left( -\frac{J}{K} \right) + k\pi \right\} \quad (8A)$$

where  $k$  is any nonnegative integer such that  $\tau_k \geq 0$ , and J and K are the abbreviations for the following terms:

$$\begin{aligned}
J &= \frac{\omega}{(-\omega^2 + 1)^2 + 4\omega^2} \{ [CB + AD](-\omega^2 + 1) - [2AB - \omega^2 CD] \} \\
K &= \frac{1}{(-\omega^2 + 1)^2 + 4\omega^2} \{ [AB - \omega^2 CD](-\omega^2 + 1) + 2\omega^2 [CB + AD] \}
\end{aligned} \quad (9A)$$

where A, B and D are the same as in (8), and C stands for the following term:

$$C = \omega^2 - \gamma_1^2 (1 + c_1) - \gamma_1^2 \left( \frac{1}{\xi_1} \right) + (1 + \varepsilon_1) \gamma_1^2 \left( \frac{1}{\xi_1} \right). \quad (10A)$$

## References

[1] Ayyub BM, McCuen RH. Probability, statistics and reliability for engineers and scientists. Boca Raton, Florida, USA: CRC Press; 2000. p. 628.  
[2] Ito T, Hashimoto M. Spatiotemporal distribution of interplate coupling in southwest Japan from inversion of geodetic data. *J Geophys Res* 2004;109.  
[3] Thatcher W. The earthquake deformation cycle at the Nankai trough, southwest Japan. *J Geophys Res* 1984;89:3087–101.

[4] Jonsson S, Segall P, Pedersen R, Bjornsson G. Post-earthquake ground movements correlated to pore-pressure transients. *Nature* 2003;424:179–83.  
[5] Scholz CH. Earthquakes and friction laws. *Nature* 1998;391:37–42.  
[6] Hetland EA, Hager BH. Postseismic relaxation across the central Nevada seismic belt. *J Geophys Res* 2003;108. doi:10.1029/2002JB002257.  
[7] Brace WF, Byerlee JD. Stick-slip as a mechanism for earthquakes. *Science* 1966;153(3739):990–2.  
[8] Byerlee JD. The mechanics of stick-slip. *Tectonophysics* 1970;9(5):475–86.  
[9] Gobel THW. Microseismicity, fault structure, & the seismic cycle. University of Southern California; 2013. p. 172.  
[10] Burridge R, Knopoff L. Model and theoretical seismicity. *Bull Seismol Soc Am* 1967;57(3):341–71.  
[11] Winter ME. The plausibility of long-wavelength stress correlation or stress magnitude as a mechanism for precursory seismicity: results from two simple elastic models. *Pure Appl Geophys* 2000;157(11–12):2227–48.  
[12] Mori T, Kawamura H. Spatiotemporal correlations of earthquakes in the continuum limit of the one-dimensional Burridge–Knopoff model. *J Geophys Res* 2008;113(11):B11305.  
[13] Amundsen DS, Scheibert J, Thøgersen K, Trømborg J, Malthe-Sørensen A. 1D model of precursors to frictional stick-slip motion allowing for robust comparison with experiments. *Tribol Lett* 2012;45(2):357–69.  
[14] Ichinose S. Non-equilibrium statistical approach to friction models. *Tribol Int* 2016;93:446–50.  
[15] Ueda Y, Morimoto S, Kakui S, Yamamoto T, Kawamura H. Dynamics of earthquake nucleation process represented by the Burridge–Knopoff model. *Eur Phys J B* 2015;88(9):235.  
[16] Erickson B, Birnir B, Lavalley D. A model for aperiodicity in earthquakes. *Non-linear Process Geophys* 2008;15:1–12.  
[17] Caldeira B, Silva HG, Borges JF, Tlemçani M, Bezzeghoud M. Chaotic behavior of seismic mechanisms: experiment and observation. *Ann Geophys* 2012;55(1):57–62.  
[18] Kostić S, Franović I, Perc M, Vasović N, Todorović K. Triggered dynamics in a model of different creep regimes, 4. *Scientific Reports: Nature Publishing Group*; 2014. p. 5401.  
[19] Valipour M, Asghar Montazar A. An evaluation of SWDC and WinSRFR models to optimize of infiltration parameters in furrow irrigation. *American J Sci Res* 2012;69:128–42.  
[20] Valipour M. Increasing irrigation efficiency by management strategies: cutback and surge irrigation. *ARPN J Agri Biol Sci* 2013;8:35–43.  
[21] Valipour M. Application of new mass transfer formulae for computation of evapotranspiration. *J Appl Water Eng Res* 2014;2:33–46.  
[22] Valipour M. Use of surface water supply index to assessing of water resources management in Colorado and Oregon, US. *Adv Agri Sci Engineering Res* 2013;3:631–40.  
[23] Valipour M, Ali Gholami Defidkouhi M, Raeini Sarjaz M. Selecting the best model to estimate potential evapotranspiration with respect to climate change and magnitudes of extreme events. *Agri Water Manage* 2017;180:50–60.  
[24] Valipour M. Number of required observation data for rainfall forecasting according to the climate conditions. *Am J Sci Res* 2012;74:79–86.  
[25] Kostić S, Franović I, Todorović K, Vasović N. Friction memory effect in complex dynamics of earthquake model. *Nonlinear Dyn* 2013;73(3):1933–43.  
[26] Kostić S, Vasović N, Franović I, Todorović K. Dynamics of simple earthquake model with time delay and variation of friction strength. *Nonlinear Process Geophys* 2013;20:857–65.  
[27] Vasović N, Kostić S, Franović I, Todorović K. Earthquake nucleation in a stochastic fault model of globally coupled units with interaction delays. *Commun Nonlinear Sci Numer Simul* 2016;38:117–29.  
[28] Scholz CH. The mechanics of earthquake and faulting. Cambridge: Cambridge University Press; 2002. p. 504.  
[29] Dieterich JH, Kilgore BD. Direct observation of frictional contacts: new insights for state dependent properties. *Pure Appl Geophys* 1994;143:283–302.  
[30] Clancy I, Corcoran D. State-variable friction for the Burridge–Knopoff model. *Phys Rev E Stat Nonlin Soft Matter Phys* 2009;80:016113.  
[31] Kilgore BD, Blanpied ML, Dieterich JH. Velocity dependent friction of granite over a wide range of conditions. *Geophys Res Lett* 1993;20:903–6.  
[32] Brown SR, Scholz CH, Rundle JB. A simplified spring-block model of earthquakes. *Geophys Res Lett* 1991;18:215–18.  
[33] Scholz CH. The critical slip distance for seismic faulting. *Nature* 1988;336:761–3.  
[34] McGarr A, Fletcher JB, Beeler NM. Attempting to bridge the gap between laboratory and seismic estimates of fracture energy. *Geophys Res Lett* 2004;31:L14606. doi:10.1029/2004GL020091.  
[35] Venkataraman A, Kanamori H. Observational constraints on the fracture energy of subduction zone earthquakes. *J Geophys Res* 2004;109:B05302. doi:10.1019/2003JB002549.  
[36] Vasudevan K, Cavers M, Ware A. Earthquake sequencing: chimera states with Kuramoto model dynamics on directed graphs. *Nonlinear Process Geophys* 2015;22:499–512.

# Disordered configurations of the Glauber model in two-dimensional networks

IVA BAČIĆ<sup>1</sup>, IGOR FRANOVIĆ<sup>1</sup> and MATJAŽ PERC<sup>2,3,4</sup>

<sup>1</sup> *Scientific Computing Laboratory, Center for the Study of Complex Systems, Institute of Physics Belgrade, University of Belgrade - Pregrevica 118, 11080 Belgrade, Serbia*

<sup>2</sup> *Faculty of Natural Sciences and Mathematics, University of Maribor - Koroška cesta 160, SI-2000 Maribor, Slovenia*

<sup>3</sup> *CAMTP – Center for Applied Mathematics and Theoretical Physics, University of Maribor - Mladinska 3, SI-2000 Maribor, Slovenia*

<sup>4</sup> *Complexity Science Hub - Josefstädterstraße 39, A-1080 Vienna, Austria*

received 31 January 2018; accepted 13 February 2018  
published online 28 February 2018

PACS 89.75.Fb – Structures and organization in complex systems  
PACS 89.75.Hc – Networks and genealogical trees

**Abstract** – We analyze the ordering efficiency and the structure of disordered configurations for the zero-temperature Glauber model on Watts-Strogatz networks obtained by rewiring 2D regular square lattices. In the small-world regime, the dynamics fails to reach the ordered state in the thermodynamic limit. Due to the interplay of the perturbed regular topology and the energy neutral stochastic state transitions, the stationary state consists of two intertwined domains, manifested as multiclustered states on the original lattice. Moreover, for intermediate rewiring probabilities, one finds an additional source of disorder due to the low connectivity degree, which gives rise to small isolated droplets of spins. We also examine the ordering process in paradigmatic two-layer networks with heterogeneous rewiring probabilities. Comparing the cases of a multiplex network and the corresponding network with random inter-layer connectivity, we demonstrate that the character of the final state qualitatively depends on the type of inter-layer connections.

Copyright © EPLA, 2018

The interplay of local dynamics and the underlying network topology has been in the focus of research in physics and various interdisciplinary fields [1–3], having recently attracted considerable interest in the context of phase ordering processes [4–6]. The Ising-Glauber model [7] constitutes one of the paradigmatic models for analyzing such processes [8]. While it has been introduced to describe the nonequilibrium dynamical behavior of magnetic systems consisting of a large number of interacting particles, it has since been applied to a variety of other problems, including those in social sciences [9], geology [10], and electrochemistry [11].

Within the Glauber model, the spin variables can assume two discrete values, having the states of nodes evolve according to the local majority rule. The Glauber model was initially defined on a regular lattice [7]. Nevertheless, given that non-lattice topologies including random, scale-free [12] and small-world [13] networks are often better suited to describe real-world systems, the issue of Glauber dynamics on complex networks has been gaining

increasing attention [8,14–16]. Apart from such models, complexity of interactions in many real-world systems may also involve “networks of networks” featuring modular or multilayer architecture [17], the scenarios which have been much less explored in the framework of Glauber dynamics.

Our work addresses two problems of ordering in complex networks: i) the disordered states of the zero-temperature Glauber model on monolayer rewired networks, where we identify two types of disordered configurations, and ii) the ordering process on two-layer rewired networks, where we find that the ordering process is strongly affected by the type of inter-layer connections.

In case of the two-dimensional square lattice, when only interactions between four nearest neighbors are taken into account, see fig. 1(a), the zero-temperature Glauber dynamics is multistable [18]. In particular, the system either reaches the ground state for  $\approx 2/3$  of all the process realizations, or ends up in the frozen striped state with probability  $p_f \approx 1/3$ . Concerning rewired square lattices with coordination number  $\langle k \rangle = 4$ , it has been shown that

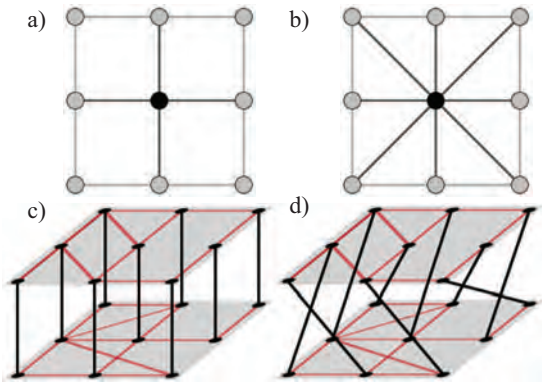


Fig. 1: (Color online) Considered network topologies. Panel (a) shows the scenario of a monolayer network with nearest-neighbor interactions ( $k = 4$ ), whereas panel (b) shows the case where the next-nearest neighbor interactions are also included ( $k = 8$ ). Panel (c) shows results for the multiplex two-layer network, whereas panel (d) shows results when there is random connectivity between the two layers.

the dynamics fails to reach the ground state [15,19], but little is known about the nature of the associated disordered configurations.

Our immediate goals are to understand why the Glauber model on small-world networks fails to reach ground state and to gain insight into the character of the disordered states on rewired networks with  $\langle k \rangle = 4$  and  $\langle k \rangle = 8$ . We also study the ordering process on two-layer rewired networks with  $\langle k \rangle = 4$ , comparing the effects of different types of inter-layer connectivity, including multiplexing, see fig. 1(c), and the scenario with connections distributed between randomly selected pairs of nodes, cf. fig. 1(d).

**Model.** – In the Glauber model, the interactions are usually confined (but not necessarily restricted) to nearest-neighbor units. Incorporating higher-order competing (frustrated) interactions is one of the classical scenarios for the onset of new phases and potentially new types of phase transitions lying outside of Ising universality class. While the ferromagnetic interactions imposed by the model favor parallel alignment of spins, thermal noise prevents the system from reaching the ground state at any nonzero value of temperature. To avoid such stochastic effects which prevent full ordering, we consider systems quenched from an infinitely high temperature to absolute zero, in which spin states are initially uncorrelated and the net magnetization is vanishing. The Hamiltonian of the system is given by  $H = -\sum_{\langle ij \rangle} J_{ij} S_i S_j$  where  $S_i = \pm 1$  are Ising spin variables, the sum  $\langle ij \rangle$  is over pairs of neighbors, and  $J_{ij} > 0$  are ferromagnetic coupling constants, assumed to be uniform in our paper ( $J_{ij} = J$ ). Each pair of parallel neighboring spins contributes  $-J$  to the energy, while the contribution of antiparallel pairs is  $+J$ . Without loss of generality, we set  $J = 1$  in the present study.

The state of the system evolves according to the majority rule applied to spins sequentially selected at random in each time step. This dynamical rule allows only energy

lowering or the energy neutral state transitions. The former correspond to events where the spin variable is updated to the state prevalent in its local neighborhood, while the latter conform to scenario without a local majority, such that the given spin evolves stochastically with both orientations being equally likely.

Watts and Strogatz [13] have introduced an algorithm for generating small-world and random graphs by gradually rewiring a regular lattice. In their model, links from the regular lattice are chosen at random and replaced with new ones until a desired fraction of links  $p$  is rewired. Rewiring effectively introduces shortcuts between distant nodes, thereby drastically reducing the mean shortest path even in the limit  $p \rightarrow 0$ . By increasing the amount of disorder ( $p \rightarrow 1$ ) one obtains a random network with the mean connectivity conserved. Small-world networks are generated by introducing an intermediate level of disorder ( $0 < p \ll 1$ ), and are characterized by the high clustering coefficient and the short average path length. The former implies that neighboring nodes tend to group in well connected clusters, whereas the latter means that an arbitrary distant node can be reached by a small number of intermediate links.

We simulate Glauber dynamics of Ising spins on Watts-Strogatz rewired networks generated from two-dimensional regular  $L \times L$  lattices with periodic boundary conditions. To understand the interplay between topological effects and the local majority dynamical rule, we vary several parameters in addition to  $L$  and the rewiring probability  $p$ , including the mean connectivity degree  $\langle k \rangle$  and the initial magnetization  $m_0$ . As an additional ingredient, we also examine how the ordering process is affected by whether the Glauber dynamical rule allows for stochastic flipping or not. We refer to the rule without stochastic flipping as the modified Glauber rule.

To distinguish the influence of rewiring itself from the effect of connectivity of the network, we compare the results of simulations on networks with  $\langle k \rangle = 4$  and  $\langle k \rangle = 8$  in the small-world regime. We regard the next nearest neighbors as first neighbors in the topological sense by setting all interactions to be of equal strength. Assigning a finite value to the initial magnetization  $m_0 \neq 0$  can be understood as introducing an initial bias toward local state clustering in the network. Modifying the Glauber dynamical rule by allowing state transitions only in the case of a strong local majority allows us to understand the effect of energy neutral processes on ordering in disordered topologies. In this scenario, nodes with an equal number of neighbors in both states are ignored when encountered during a trial rather than having their state determined stochastically. It turns out that the ground state is always reached on regular square lattices when a strong majority is necessary for state transition, *i.e.*, the striped state turns out to be the consequence of energy neutral stochastic flips.

To gain a more comprehensive insight into structure of the disordered configurations, we make a distinction between the domains comprised of topologically connected

nodes in the same state, and the clusters with respect to positions of the nodes on the original regular lattice. The lattice and the graph neighborhoods are always identical for spins placed on regular lattices. However, as the lattice structure is modified such that the links between neighbors are replaced by links to distant nodes, the lattice and the topological neighbors may not necessarily coincide, which results in rich patterns on the lattice. In order to investigate the crossover from frozen striped configurations occurring in regular lattices to disordered states occurring in the rewired lattices, we compare the correlation length  $\xi$  to characteristic graph length measures, namely the radius  $R$ , diameter  $D$  and the mean shortest path  $\langle s \rangle$ . The correlation length is defined as the decay rate of the two-point correlation function  $G(l) = \langle S_i S_j \rangle - \langle S_i \rangle \langle S_j \rangle$  which measures the correlation of states as a function of the Manhattan distance  $l$  between the nodes. Note that  $\xi$  characterizes the competition between topology and dynamics on the state of distant nodes, while  $R$ ,  $D$  and  $\langle s \rangle$  are purely topological measures.

We also address the issue of how connecting two networks of the same size with different rewiring probabilities affects the ordering process. To do so, we compare the results obtained for the two-layer multiplex network ( $N$  bonds connecting nodes of two layers in one-to-one fashion) with the results for the case where the same number of inter-layer connections is distributed between randomly chosen pairs of nodes.

The main quantity of interest is the fraction of configurations that have not reached the ground state (“active configurations”)  $f_a$  after a given simulation time  $T$  as a function of  $p$ . The absolute value of net magnetization  $|m|$  is an order parameter for individual systems:  $|m| = 1$  corresponds to the ground case, whereas  $|m| = 0$  corresponds to the case in which there is an equal number of spins in both states. Thus, we measure the dependence of the final value of the magnetization  $|m_f|$  in disordered configurations on  $p$ . However,  $|m_f|$  contains no information about clustering in the network.

We simulate the dynamics on networks consisting of  $50 \times 50$ ,  $80 \times 80$  and  $150 \times 150$  nodes for fixed values of  $N$ ,  $\langle k \rangle$ ,  $p$  and  $m_0$ . The total number of trials in each particular case is set to 1000. In summary, our numerical algorithm consists of the following steps:

- I) *Regular network initialization.* Construct lattices with  $k = 4$  or  $k = 8$  as in fig. 1.
- II) *Rewiring.* Following the method described in [15], our rewiring process ensures that there are no self-loops or multiple links between pairs of nodes, and that the minimal connectivity degree is 2. Bonds are sequentially selected at random and rewired with probability  $p$  until a desired fraction  $p$  of the total number of bonds is rewired.
- III) *Spin state initialization.* The initial state is set by randomly putting each of the  $N$  spins into one of the

possible states. If the initial magnetization is  $m_0$ , the state of each spin is set to  $+1$  with the probability  $p_{spin} = \frac{1+m_0}{2}$  and to  $-1$  with probability  $1 - p_{spin}$ .

- IV) *Glauber dynamics.* The evolution of the system is governed by the original or the modified (non-stochastic) Glauber dynamical rule, proceeding either until it reaches the ground state or until it fails to do so after a predetermined number of steps. We choose this value to be  $T = 5000N$  (5000 attempted spin flips per node).

In what follows, we first analyze the case of a monolayer Watts-Strogatz network, and then consider the ordering process in paradigmatic two-layer networks with two types of inter-layer connections.

**Monolayer networks.** – Figure 2(a) shows how the fraction of active configurations  $f_a$  depends on  $p$  for Watts-Strogatz networks with local Glauber dynamics following a zero-temperature quench ( $m_0 = 0$ ). The nonlinear dependence of  $f_a$  on  $p$  is observed regardless of  $\langle k \rangle$ , but turns out to be qualitatively different for the cases  $\langle k \rangle = 4$  and  $\langle k \rangle = 8$ . When  $\langle k \rangle = 8$ , with increasing randomness ( $p \gtrsim 0.5$ ), the dynamics leads to almost complete ordering. Nevertheless, when  $\langle k \rangle = 4$ , a finite fraction of configurations fails to reach the ground state in the thermodynamic limit over the whole range of  $p$  values. In the small-world regime, however, the ground state is not reached in the thermodynamic limit in either case. The result that ordering cannot be attained in small worlds when state transitions are governed by Glauber dynamics has been previously demonstrated for rewired rings ( $d = 1$ ) and rewired square lattices ( $d = 2$ ) with  $\langle k \rangle = 4$  [15,19].

One infers that the local neighborhood majority rule with stochastic spin flips cannot lead to an ordered state on graphs with a perturbed regular topology. While the neighborhood from the regular lattice is mostly conserved in the small-world limit,  $R$ ,  $D$  and  $\langle s \rangle$  on the other hand monotonically decrease with  $p$  due to the presence of shortcuts (see fig. 3). Thus, it follows that perturbing the local neighborhood essentially leads to dynamical frustration of the local majority rule. A very small amount of topological disorder is sufficient to induce the critical slowing-down of dynamics, causing the disordered states to appear as deformed stripes on the lattice. Further deformation of the stripes leads to multiclustering on the lattice, which is reflected in the crossover effect [20]. We have established that this effect corresponds to the drop of  $\xi$  below the topological distances. At the same time, the low value of  $\xi$  indicates the absence of long-range ferromagnetic order. The two-point correlation function is found to satisfy an exponential scaling law  $G(l) \propto e^{-\frac{l}{\xi}}$  over the whole range of  $p$ . Furthermore, depending on the  $p$  value, both  $\xi$  and  $R$ ,  $D$  and  $\langle s \rangle$  exhibit different scaling regimes.

In particular, in the small-world regime,  $R$ ,  $D$ ,  $\langle s \rangle$  and  $\xi$  exhibit a power law dependence on  $p$ ,  $r \propto p^{-a}$  with  $r \in \{R, D, \langle s \rangle, \xi\}$  and  $a \in \{a_R, a_D, a_{\langle s \rangle}, a_\xi\}$ . For  $80 \times 80$



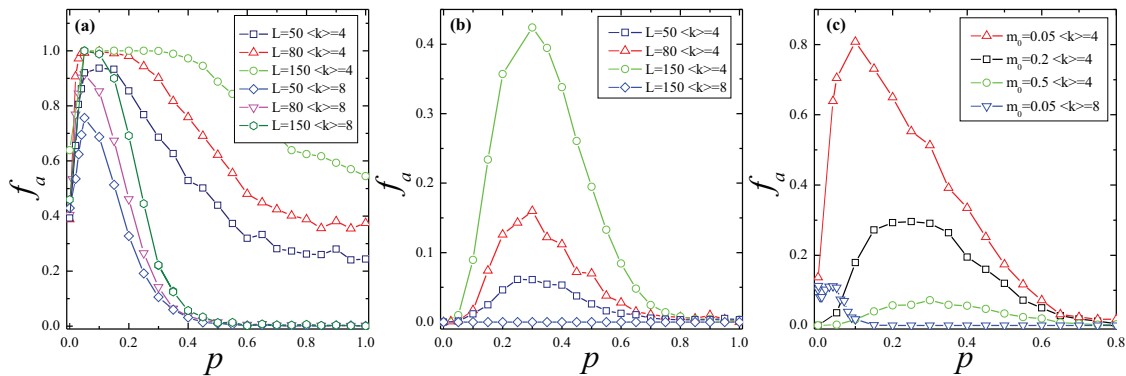


Fig. 2: (Color online) (a) Final fraction of active runs  $f_a$  in terms of rewiring probability  $p$  for the standard Glauber rule with  $m_0 = 0$ . The results are provided for networks with  $\langle k \rangle = 4$  and  $\langle k \rangle = 8$  neighbors and  $L \in \{50, 80, 150\}$ . Note that complete ordering is not observed in the small-world regime  $0 < p \ll 1$  independent of  $\langle k \rangle$ . (b) Impact of modified Glauber rule: for  $\langle k \rangle = 8$ , the system reaches complete ordering (hence only the curve corresponding to  $L = 150$  is shown), whereas for  $\langle k \rangle = 4$ , the frustration effect emerges at intermediate  $p$ , becoming more pronounced with the network size. Panel (c) displays  $f_a$  for systems governed by the standard Glauber rule starting from initial conditions  $m_0 \neq 0$ . The influence of small worldliness is such that it suppresses disorder regardless of  $\langle k \rangle$  with increasing  $m_0$ , while it still promotes disorder at intermediate  $p$  range for  $\langle k \rangle = 4$ .

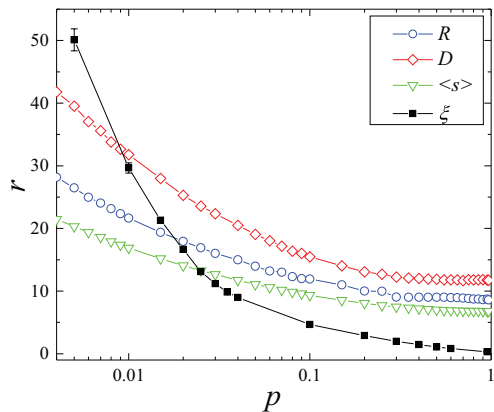


Fig. 3: (Color online) Correlation length  $\xi$  compared to graph distance measures (radius  $R$ , diameter  $D$ , and average path length  $\langle s \rangle$ ) as functions of  $p$ . While  $\xi$  reflects the interplay between the dynamics and the network structure, the remaining quantities characterize purely topological features of the network. Crossing of  $\xi(p)$  with other curves indicates the transition between the dynamics typical for the regular lattices and that for the rewired networks. Note that all four quantities exhibit a power law dependence  $r \propto p^{-a}$  in the  $p$  region approximately coinciding with the small-world regime. The results refer to networks with  $80 \times 80$  nodes and  $\langle k \rangle = 4$ .

networks, the following values for the exponent  $a$  are found:  $a_R = -0.259 \pm 0.004$ ,  $a_D = -0.296 \pm 0.005$ ,  $a_{\langle s \rangle} = -0.25 \pm 0.003$  and  $a_\xi = -0.77 \pm 0.01$ . For larger values of  $p$ , the topological measures do not change significantly with increasing  $p$  indicating that topological effects remain the same after  $\approx 0.5$ . Nevertheless,  $\xi$  decays to zero as  $p \rightarrow 1$ , which implies that the dynamics is sensitive to rewiring over the whole range of  $p$ , as corroborated by the growing number of “clusters” of decreased sizes in disordered configurations for large  $p$ , see fig. 4.

Interestingly, a deeper understanding of the difference in ordering efficiency in terms of  $p$  may be gained by

considering  $f_a$  for configurations governed by the modified Glauber rule. Evidently, the difficulty in attaining order subsides when stochasticity is eliminated from the dynamics in the small-world limit regardless of  $\langle k \rangle$ , see fig. 2(b). In other words, the ground state is reached with probability one if energy-neutral state transitions are not allowed. This always holds for  $\langle k \rangle = 8$ , and also for networks with  $\langle k \rangle = 4$  in the limits  $p \rightarrow 0$  and  $p \rightarrow 1$ . For intermediate  $p$ , ordering remains suppressed to a certain degree.

The next objective is to demonstrate that varying initial magnetization  $m_0$  allows one to interpolate between the influences of dynamics and topology. Figure 2(c) shows  $f_a$  as a function of  $p$  for  $m_0 \neq 0$  under the standard Glauber rule. While initial bias towards local clustering promotes complete ordering for regular networks, the dynamical outcome is different for rewired networks. In case  $\langle k \rangle = 8$ , small values of  $m_0 \neq 0$  significantly increase ordering, whereby the position of the peak of  $f_a(p)$  coincides with the peak value of  $f_a(p)$  at  $m_0 = 0$ . Perturbing the quenched initial state on graphs in the small-world regime increases the prevalence of the ground state. Nevertheless, the peaks of  $f_a(p)$  curves for  $\langle k \rangle = 4$  networks in fig. 2(c) shift toward the peak value from fig. 2(b) as  $m_0$  is increased. A fraction of configurations still fails to reach the ground state for some values of  $p$ , even for high values of  $m_0$ . The shift demonstrates that as the number of stochastic state transitions decreases due to the initial bias in clustering, the dynamical frustration is reduced. Nonetheless, the topological obstructions in networks with low  $\langle k \rangle$  can suppress ordering even for high values of  $m_0$ .

Further insight on this issue can be gained by observing how  $|m_f|$  averaged over active configurations depends on  $p$ , see fig. 5. The initial increase in magnetization corresponds to the divergence of relaxation time in the limit  $p \rightarrow 0$ , *i.e.*, the crossover from large-world to small-world behavior. Expectedly, there is a qualitative difference in

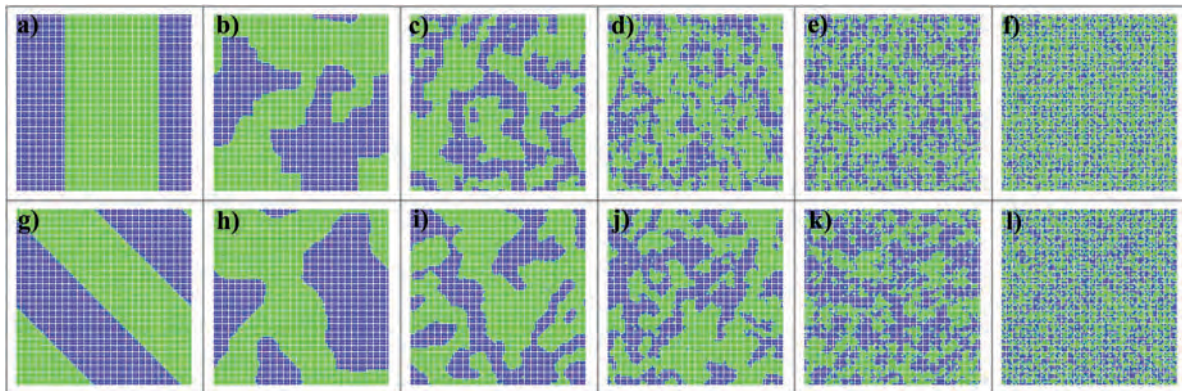


Fig. 4: (Color online) Snapshots of disordered configurations at  $T = T_f$  on the lattice. The top (bottom) row refers to networks with  $\langle k \rangle = 4$  ( $\langle k \rangle = 8$ ). The rewiring probabilities are  $p = 0$  in (a) and (g),  $p = 0.02$  in (b) and (h),  $p = 0.1$  in (c) and (i),  $p = 0.3$  in (d) and (j),  $p = 0.5$  in (e) and (k), as well as  $p = 1$  in (f) and (l). The stripe structure is gradually lost with increasing  $p$ , giving way to the multiclustered states with respect to the original lattice. The number of domains increases with  $p$  as the network topology substantially departs from the lattice one. In terms of the network structure, each of the disordered configurations consists of two connected components. All the results are obtained for networks with  $80 \times 80$  nodes.

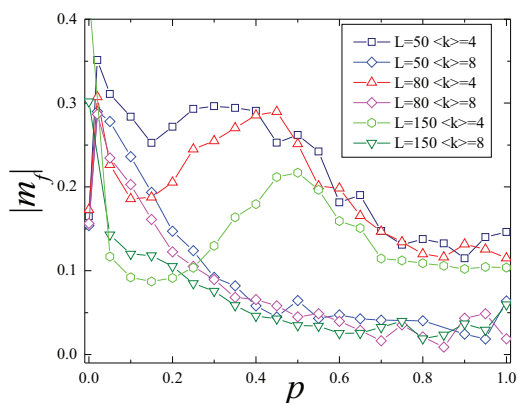


Fig. 5: (Color online) Final magnetization averaged over the ensemble of disordered configurations  $|m_f|$  in dependence of  $p$ . For  $\langle k \rangle = 8$ , one finds approximately equal numbers of nodes in both states as  $p \rightarrow 0$ . For  $\langle k \rangle = 4$ , within the small-world regime,  $|m_f|$  is reduced compared to the regular lattice, while for intermediate  $p$ , the droplet configurations lead to an increase of  $|m_f|$ . The peak of  $|m_f|(p)$  gets shifted because the fraction of active runs is higher at a wider range of  $p$  values for larger networks, cf. fig. 2(a).

the  $|m_f|(p)$  profile for different  $\langle k \rangle$  under increasing  $p$ . The curves for  $\langle k \rangle = 8$  monotonically decrease, indicating that the small number of configurations that does survive converges to a state consisting of a similar number of opposite spins in the limit  $p \rightarrow 1$ . In contrast, the initial decrease in  $|m_f|$  for networks with  $\langle k \rangle = 4$  is followed by the peak at intermediate values of  $p$ , associated to the presence of droplet configurations with  $|m_f| \rightarrow 1$ .

Moreover, we have verified that the disordered configurations in the small-world regime consist of two intertwined topological spin domains of almost similar size with stochastically fluctuating interfaces. An example of such a two-component state for  $p = 0.1$  is provided in fig. 6, whereby the corresponding lattice domain configuration is shown in fig. 4(c). Blinkers that arise as a result of the

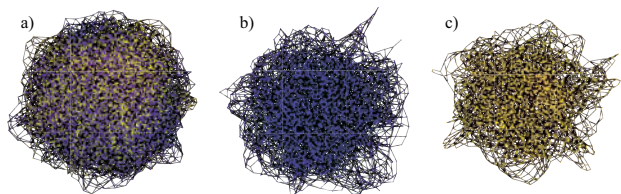


Fig. 6: (Color online) Example of a disordered configuration obtained for the network of size  $80 \times 80$ , with  $\langle k \rangle = 4$  neighbors on average and  $p = 0.1$  rewired links. (a) refers to the full configuration, whereas (b) and (c) show the larger component (3637 nodes) and the smaller component (2763 nodes), respectively. The final magnetization is  $|m_f| \approx 0.14$ . The nodes are separated into two domains of similar size, forming a multi-domain state on the lattice, cf. fig. 5(c).

long-range connections can be present along with stochastic flipping of interfaces on the lattice. Increasing  $p$  corresponds to the formation of domains with decreasing size with respect to the lattice. Several examples of configurations with two topological components for different  $p$  are shown in fig. 4. The number of these domains counted on the lattice grows exponentially with  $p$  (not shown). In the random network limit, as the fraction of links belonging to the original lattice  $1 - p$  decreases, clusters become indistinguishable when observed on the lattice. Topologically, the two-domain configuration is reminiscent of the disordered configurations of the voter model on small-world networks [8,21]. Once the dynamics cannot cause further decrease in energy, the interface length reaches a constant value, as interface diffusion is no longer possible. In this scenario, while a fraction of nodes with even connectivity degrees continues to flip indefinitely with no energy cost, the states of the odd-degree nodes become stationary.

Nevertheless, the disordered configurations associated to the increase of  $f_a$  in fig. 2(b) for  $\langle k \rangle = 4$  are frozen at very high values of  $|m_f|$ , *viz.*  $|m_f| \rightarrow 1$  in

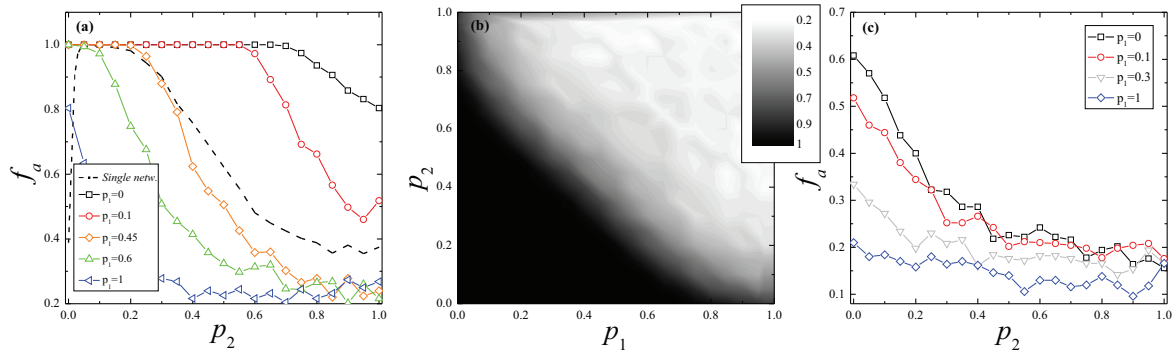


Fig. 7: (Color online) (a) Ordering in two-layer multiplex networks:  $f_a$  for the layer with rewiring probability  $p_1$  (see the legend) in terms of the rewiring probability  $p_2$  of the other layer. For comparison, the results for the single (monolayer) network are indicated by the dashed line. (b)  $f_a$  of a single layer of a multiplex network as a function of  $p_1$  and  $p_2$ . The states of two layers are strongly correlated, but the ordering is completely inhibited in the small-world regime. (c)  $f_a$  of a layer of the network with random inter-layer connectivity. Ordering is significantly improved for all values of  $p$ . All the results are obtained for networks with  $80 \times 80$  nodes and  $\langle k \rangle = 4$ .

the thermodynamic limit, and correspond to *absorbing* states of the network. These configurations result from low connectivity and consist of a tiny fraction of spins isolated in small domains surrounded by the “sea” of nodes of the opposite orientation. In this scenario, nodes with small  $k$  form stable droplets of opposing magnetization which cannot be dynamically influenced by the nodes from the rest of the network, preventing the system from reaching the full order. These droplets may appear on the remnants of the regular lattice, such that their interior consists of nodes connected by links from the regular lattice ( $k = 4$ ), whereas their boundary is mainly comprised of nodes with one removed link ( $k = 3$ ), thereby trapping the “interior” in the same state. Even-degree nodes that appear on the boundaries have more links with nodes within the droplet than with other neighbors, such that their state cannot be changed either. With further rewiring of the lattice, stable droplets may still form as even smaller groups of interconnected nodes with small degrees ( $k = 2$  or  $k = 3$ ), likewise disconnected from the rest of the network. The larger the network, the more likely becomes such a scenario. Also, for larger network sizes, a larger number of droplets may be present, which is the reason why a larger fraction of configurations fails to reach order. This peculiar frustration on the remnants of a regular lattice also accounts for the incomplete ordering of systems governed by the standard Glauber dynamics in rewired networks with  $\langle k \rangle = 4$ , and explains for the difference in the behavior in the limit  $p \rightarrow 1$ . Final configurations in networks with  $\langle k \rangle = 4$  can consist of two large components and a few isolated droplets for  $p$  above the small-world regime, similar to final configurations obtained for  $m_0 \neq 0$ .

**Two-layer networks.** – We now address the ordering process in multilayer networks, focussing on the paradigmatic example of two coupled  $\langle k \rangle = 4$  networks with different rewiring probabilities  $p_1$  and  $p_2$ . By our

algorithm, the individual layers are rewired consecutively, after which  $N$  links are introduced between them, either at random or with the one-to-one correspondence between the layers’ nodes. The simulation is terminated after  $2T$  steps if order is not reached. Note that introducing new links effectively generates a large network with  $\langle k \rangle = 5$  and  $5N$  bonds.

Our findings indicate that both cases lead to highly correlated states of layers, which are simultaneously ordered/disordered and have  $m_{f_1} \approx m_{f_2}$ . For this reason,  $f_a$  of a single layer presents an appropriate quantity to characterize the ordering process. We find that the dependence of  $f_a$  on rewiring probability changes qualitatively depending on the nature of the inter-layer bonds, cf. fig. 7(a) and fig. 7(c). The multiplex configuration turns out to suppress ordering of both networks in the small-world regime, as indicated in fig. 7(a) and fig. 7(b). However, fig. 7(a) shows that ordering efficiency can be increased if at least one of the networks is “sufficiently random”, with a smooth transition taking place at  $0.35 \lesssim p \lesssim 0.45$ . Interestingly, the other scenario, which involves placing the same number of bonds between randomly chosen pairs of nodes from both networks, promotes both ordering and correlation between the layer states. This is corroborated by fig. 7, suggesting that regardless of  $p_1$  and  $p_2$ , ordering in this case is significantly improved compared to that on a single network and the multiplex network.

The curves obtained for multiplex networks resemble the ones obtained for the single network even for  $p$  as large as 0.6, while those obtained for random inter-layer connections are monotonically decreasing as  $p_2$  is increased over the whole range of  $p$ . Even though in both cases networks become correlated in terms of  $m_f$  and ordering, multiplexing seems to preserve the type of dynamics obtained on small-world structures of one network, while introducing random bonds between the layers destroys the small-worldliness effect.

**Conclusions.** – We have analyzed ordering efficiency of the Glauber model of Ising spin kinetics on the Watts-Strogatz networks obtained by rewiring from the two-dimensional square lattices with coordination numbers  $\langle k \rangle = 4$  and  $\langle k \rangle = 8$ . We have extended the previous results concerning the failure of such systems to reach the ground state in the small-world regime  $0 < p \ll 1$ , gaining insight into the associated disordered configurations. The fraction of active configurations exhibits a nonlinear dependence on the rewiring probability. It is interesting that a similar type of dependence has been observed in relation to the synchronization process on small-world networks [22]. It is found that the Glauber dynamics on small-world networks becomes stuck in metastable stationary active configurations, which consist of two intertwined domains of opposite spins, whereby the fraction of nodes on the interfaces flips indefinitely. This effect is manifested as clustering patterns in the lattice representation. The size of domains on the lattice becomes smaller as  $p$  is increased. We have demonstrated that the limiting value of  $p$  at which the number of lattice and topological domains is equal (to two) corresponds to the value where the correlation length  $\xi$  becomes smaller than the average path length in the network.

Our analysis shows that the active configurations in the small-world regime emerge when the perturbed regular topology constrains the number of possible energy lowering processes, while the stochastic energy-neutral spin-flipping processes contribute to dynamical frustration and trap the system in a set of metastable states with the same energy. While the ground state is not accessible because energy lowering processes are not possible, the energy-neutral processes allow for the transitions between states of the same energy. This is similar to what has been reported for Glauber dynamics on 3D regular lattices [23], Glauber dynamics on random graphs [8], and the voter model on small-world networks [21].

We have further demonstrated that there exists a finite probability of finding another type of disordered configuration in networks with low connectivity for intermediate values of  $p$ . These are frozen, almost completely ordered states with a few isolated droplets of opposing magnetization. For  $\langle k \rangle = 8$ , such configurations become unlikely due to the high average connectivity degree in the network, giving way to fully ordered states if  $p$  is sufficiently increased ( $p > 0.5$ ). In networks with  $\langle k \rangle = 4$ , a certain fraction of configurations exists as a combination of these states, especially if an initial bias towards clustering ( $m_0 \neq 0$ ) is introduced.

We have also examined the features of the ordering process in paradigmatic two-layer networks. It has been found that the structure of inter-layer connections strongly affects the ordering process. In particular, multiplexing decreases ordering efficiency in the small-world regime  $0 < p \ll 1$ , but improves it if the rewiring probability in both layers is sufficiently high. Nevertheless, random connectivity between the layers always promotes ordering,

regardless of layer topology. In all the considered scenarios, the layers typically end up in highly correlated states.

We believe that the future research may be directed towards extending our findings on the dynamics of interacting rewired networks. In particular, it could be interesting to modify inter-layer coupling strengths, vary the number of connections between the layers or consider hierarchical networks and networks with a large number of layers.

\* \* \*

This research was supported by the Ministry of Education, Science and Technological Development of Republic of Serbia (Grant 171017) and by the Slovenian Research Agency (Grants J1-7009 and P5-0027).

## REFERENCES

- [1] STROGATZ S., *Nature*, **410** (2001) 268.
- [2] ALBERT R. and BARABÁSI A.-L., *Rev. Mod. Phys.*, **74** (2002) 47.
- [3] BOCCALETTI S., LATORA V., MORENO Y., CHAVEZ M. and HWANG D.-U., *Phys. Rep.*, **424** (2006) 175.
- [4] BRAY A. J., *Adv. Phys.*, **51** (2002) 481.
- [5] CASTELLANO C., *Rev. Mod. Phys.*, **81** (2009) 591.
- [6] PASTOR-SATORRAS R., CASTELLANO C., VAN MIEGHEM P. and VESPIGNANI A., *Rev. Mod. Phys.*, **87** (2015) 925.
- [7] KRAPIVSKY P. L., REDNER S. and BEN-NAIM E., *A Kinetic View of Statistical Physics* (Cambridge University Press, Cambridge) 2010.
- [8] CASTELLANO C., LORETO V., BARRAT A., CECCONI F. and PARISI D., *Phys. Rev. E*, **71** (2005) 066107.
- [9] STAUFFER D., *Am. J. Phys.*, **76** (2008) 470.
- [10] GANGULY J., *Advances in Physical Geochemistry: Diffusion, Atomic Ordering, and Mass Transport* (Springer, New York) 2012.
- [11] BOSCO E., *J. Electroanal. Chem.*, **346** (1993) 433.
- [12] BARABÁSI A.-L. and ALBERT R., *Science*, **286** (1999) 509.
- [13] WATTS D. J. and STROGATZ S. H., *Nature*, **393** (1998) 440.
- [14] CASTELLANO C. and PASTOR-SATORRAS R., *J. Stat. Mech.* (2006) P05001.
- [15] HERRERO C. P., *J. Phys. A: Math. Theor.*, **42** (2009) 415102.
- [16] BAEK Y., HA M. and JEONG H., *Phys. Rev. E*, **85** (2012) 031123.
- [17] BOCCALETTI S. *et al.*, *Phys. Rep.*, **544** (2014) 1.
- [18] SPIRIN V., KRAPIVSKY P. L. and REDNER S., *Phys. Rev. E*, **65** (2001) 016119.
- [19] BOYER D. and MIRAMONTES O., *Phys. Rev. E*, **67** (2003) 035102.
- [20] BARTHÉLÉMY M. and AMARAL L. A. N., *Phys. Rev. Lett.*, **82** (1999) 3180.
- [21] CASTELLANO C., VILONE D. and VESPIGNANI A., *Europhys. Lett.*, **63** (2003) 153.
- [22] GRABOW C., HILL S. M., GROSSKINSKY S. and TIMME M., *Europhys. Lett.*, **90** (2010) 48002.
- [23] SPIRIN V., KRAPIVSKY P. L. and REDNER S., *Phys. Rev. E*, **63** (2001) 036118.

**Mean-field dynamics of a population of stochastic map neurons**Igor Franović,<sup>1,\*</sup> Oleg V. Maslennikov,<sup>2,†</sup> Iva Bačić,<sup>1</sup> and Vladimir I. Nekorkin<sup>2</sup><sup>1</sup>*Scientific Computing Laboratory, Center for the Study of Complex Systems, Institute of Physics Belgrade, University of Belgrade, Pregrevica 118, 11080 Belgrade, Serbia*<sup>2</sup>*Institute of Applied Physics of the Russian Academy of Sciences, 46 Ulyanov Street, 603950 Nizhny Novgorod, Russia*

(Received 6 March 2017; published 27 July 2017)

We analyze the emergent regimes and the stimulus-response relationship of a population of noisy map neurons by means of a mean-field model, derived within the framework of cumulant approach complemented by the Gaussian closure hypothesis. It is demonstrated that the mean-field model can qualitatively account for stability and bifurcations of the exact system, capturing all the generic forms of collective behavior, including macroscopic excitability, subthreshold oscillations, periodic or chaotic spiking, and chaotic bursting dynamics. Apart from qualitative analogies, we find a substantial quantitative agreement between the exact and the approximate system, as reflected in matching of the parameter domains admitting the different dynamical regimes, as well as the characteristic properties of the associated time series. The effective model is further shown to reproduce with sufficient accuracy the phase response curves of the exact system and the assembly's response to external stimulation of finite amplitude and duration.

DOI: [10.1103/PhysRevE.96.012226](https://doi.org/10.1103/PhysRevE.96.012226)**I. INTRODUCTION**

Gaining a comprehensive understanding of the emergent dynamics of neuronal populations and their interactions is a topical issue in neuroscience [1,2]. The acquired neurobiological data corroborate that the operational tasks at different levels of the brain's multiscale hierarchical organization are distributed across anatomically segregated, but functionally integrated, moduli [3–5]. Within theoretical studies, substantial attention have received the phenomena unfolding on the intermediate (mesoscopic) scale [6], whereby the considered models are supposed to reflect the behavior of assemblies comprising microcolumns or cortical columns [7–9]. The mesoscopic dynamics typically consists of oscillations of different frequencies and amplitudes, which may be interspersed by episodes of chaotic or pseudo-chaotic irregular behavior [7]. This can further be modulated via interplay with activity generated at other scales, primarily the stochastic fluctuations from the microscopic level and the slow rhythms derived from the macroscopic structures.

Conceptually, the given phenomena are often addressed by invoking a paradigm where each population exhibiting a collective mode is regarded as a large-scale oscillator, such that the assembly's response to external stimuli, noise, or collective oscillations from afferent populations may be examined using the methods of nonlinear dynamics [10]. The ensuing models of collective motion are developed using different forms of mean-field (MF) approximation, which mainly apply the bottom-up strategy [11] to build reduced and analytically tractable description of population behavior starting from the high-dimensional system of (stochastic) differential equations for the local neuron dynamics. An additional point that makes the mesoscopic circuits particularly suitable for the MF treatment is that the often used assumption on assembly homogeneity approximately holds at this scale

[12]. In terms of fashion by which the population dynamics is statistically characterized, one may classify the effective systems into neural mass or probability density models [8,13]. The former rely on the large coherence approximation and yield the mean-rate dynamics [14], whereas the latter involve the diffusion approximation, providing for the evolution of the assembly-averaged dynamics and the corresponding variance [15,16]. The MF approach and its generalization to spatially extended systems have become a standard tool for analyzing diverse problems in neuroscience and other fields [17–23].

Nevertheless, one should emphasize that the MF analysis has so far exclusively been applied to the class of continuous-time systems, while the effective models for assemblies of coupled maps have been lacking. In particular, the collective motion of spiking or bursting neurons influenced by noise has been extensively studied using different models of coupled discrete systems, such as Rulkov [24–31] or Izhikevich neuron maps [32,33], but this has not been complemented by an appropriate MF theory. The latter has likely been the consequence of inability to implement the Fokker-Planck formalism to discrete-time systems. In the present paper, we obtain for the first time the MF theory for a population of coupled stochastic neuronal maps. The derivation relies on Gaussian approximation, which is introduced within the framework of Gaussian closure hypothesis [34–40].

We apply the MF approach to systematically analyze the emergent behavior and the stimulus-response relationship of a population of stochastic map neurons, where the local dynamics can exhibit a variety of regimes, including excitability, subthreshold oscillations, regular and chaotic spiking or bursting, as well as mixed spiking-bursting oscillations [41–44]. The particular set of issues we address consists in establishing whether and how the MF model can be used to (i) qualitatively analyze the network stability and bifurcations of the exact system associated to emergence of generic collective regimes; (ii) provide adequate quantitative predictions in terms of bifurcation thresholds, and the average interspike intervals or bursting cycles of the exact system; as well as (iii) accurately anticipate the population's response

\*franovic@ipb.ac.rs

†olmaov@ipfran.ru

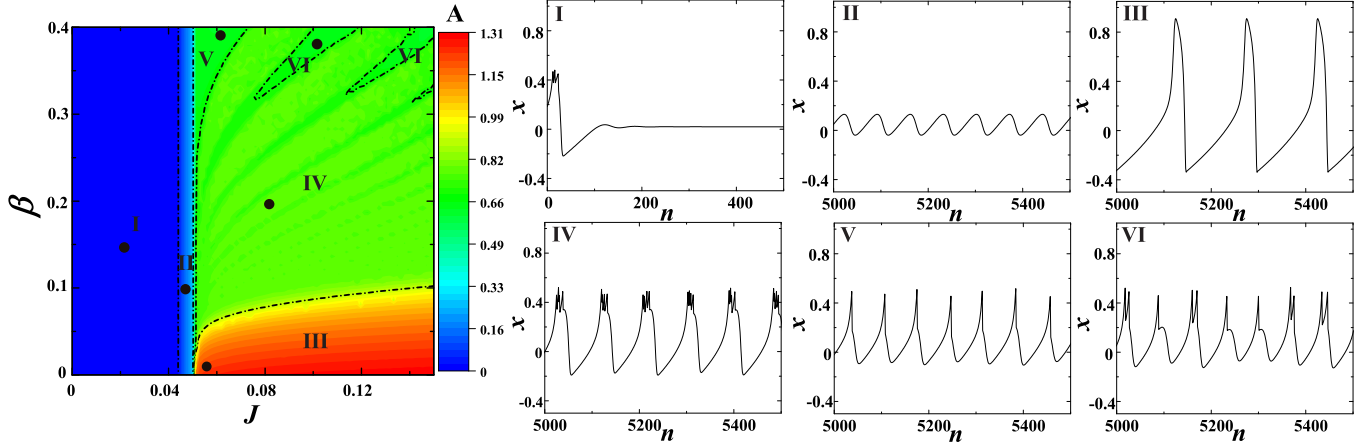


FIG. 1. Dynamical regimes exhibited by model (1). The heat map refers to variation of the amplitude of oscillations  $A$  of the  $x$  time series in the  $J$ - $\beta$  plane. The wave forms shown in subfigures I–VI illustrate the different forms of neuron’s behavior, including excitability (I), subthreshold oscillations (II), regular spiking (III), chaotic bursting (IV), chaotic spiking (V), as well as the mixed spike-burst activity (VI). The dots in the heat map indicate the particular  $(J, \beta)$  values where the representative wave forms are obtained.

to different forms of external stimuli. Within this context, it will be examined whether the effective model is capable of reproducing the properties of noise-activated, noise-induced, and noise-perturbed modes of collective behavior.

The paper is organized as follows. In Sec. II, we make an overview of the local map dynamics and introduce the population model. Section III outlines the ingredients most relevant for the derivation of the MF system, with the remaining technical details left for the Appendix. In Sec. IV, the qualitative and quantitative agreement between the dynamics of the exact and the MF model is illustrated by the appropriate bifurcation diagrams, as well as by comparing the characteristic features of the associated regimes. Section V concerns the assembly’s stimulus-response relationship, first investigating the analogy between the respective phase-response curves (PRCs) of the exact system and the effective model in spiking and bursting regimes and then considering the extent to which the MF model reproduces the population’s response to rectangular pulses of finite amplitude and duration. In Sec. VI, we provide a summary of our main results.

## II. MAP NEURON DYNAMICS AND THE POPULATION MODEL

The dynamics of an isolated neuron conforms to a map model first introduced in Refs. [45,46], which is given by

$$\begin{aligned} x_{n+1} &= x_n + G(x_n) - \beta H(x_n - d) - y_n, \\ y_{n+1} &= y_n + \epsilon(x_n - J), \end{aligned} \quad (1)$$

where  $n$  denotes the iteration step. The variable  $x_n$  qualitatively accounts for the membrane potential, whereas the recovery variable  $y_n$ , whose rate of change is set by a small parameter  $\epsilon = 10^{-2}$ , mimics the behavior of ion-gating channels. The parameters  $a$ ,  $\beta$ , and  $d$  modify the profile of the ensuing oscillations, while  $J$  crucially influences the neural excitability, viz. the transitions from silence to active regimes.

The  $x_n$  evolution features two nonlinear terms, one being a FitzHugh-Nagumo-like cubic nonlinearity

$G(x_n) = x_n(x_n - a)(1 - x_n)$ , which is complemented by a discontinuity term  $-\beta H(x_n - d)$ , where  $H$  stands for the Heaviside step function. The parameters  $a = 0.1$  and  $d = 0.45$  are kept fixed throughout the paper. The impact of discontinuity consists in making the fast subsystem [Eq. (1) with  $\epsilon = 0$ ] a Lorenz-type map within certain parameter domains [46,47], which endows the model with the ability to generate chaotic spike or burst oscillations, otherwise lacking in the FitzHugh-Nagumo type of systems.

Under variation of  $J$  and  $\beta$ , the map (1) may reproduce a rich repertoire of generic regimes displayed by the real neurons, as demonstrated in Fig. 1. In particular, the main frame shows amplitudes of the corresponding  $x$  time series for the given  $(J, \beta)$ , while the remaining subfigures illustrate the characteristic wave forms pertaining to excitable regime (region I), subthreshold oscillations II, regular (III) or chaotic spiking (I), chaotic bursting (V), as well as the mixed chaotic spike-burst activity (VI). Some of the indicated boundaries, such as those involving domains IV, V, and VI should be understood as tentative, since the associated transitions are smooth and therefore difficult to discern.

The detailed phase plane analysis concerning the relevant unstable invariant curves and the mechanisms underlying transitions between the different dynamical regimes can be found in Ref. [48]. Here we briefly mention that under increasing  $J$ , the equilibrium loses stability via the Neimark-Sacker bifurcation, which gives rise to subthreshold oscillations. Note that the latter may be considered an excitable state, in the sense that a strong-enough perturbation can elicit genuine spike, though the phase point does not relax to the equilibrium but rather to a closed invariant curve.

Adopting model (1) for local dynamics, we focus on an assembly of  $N$  stochastic neurons coupled in the all-to-all fashion via electrical synapses (diffusive couplings). Each neuron receives input from the units within the assembly and is further influenced by synaptic noise from the embedding environment. Note that it is quite common in two-dimensional neuron models with sharp separation of characteristic time scales to interpret the stochastic perturbation acting on the fast

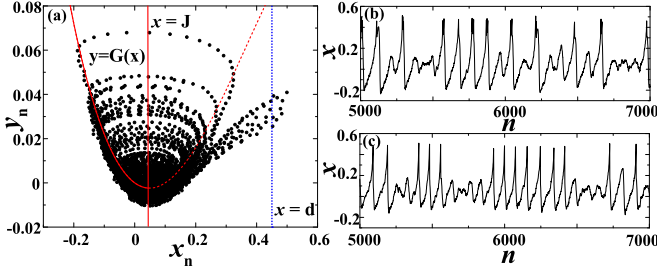


FIG. 2. Impact of noise on a single map neuron in the excitable regime. (a) The mechanism behind noise-induced spiking. The data are obtained for  $J = 0.046$ ,  $\beta = 0.4$ ,  $\sigma = 0.005$ . The equilibrium is deterministically stable given that the line  $x = J$  intersects the invariant curve  $y = G(x)$  below the curve's minimum. (b) The  $x_n$  series corresponding to noise-induced bursting ( $J = 0.042$ ,  $\beta = 0.2$ ,  $\sigma = 0.008$ ), whereas (c) demonstrates stochastic spiking superimposed on subthreshold oscillations ( $J = 0.048$ ,  $\beta = 0.4$ ,  $\sigma = 0.008$ ).

(slow) time scale as synaptic (intrinsic) noise [49–51]. The population activity is then described by the following system:

$$\begin{aligned} x_{i,n+1} &= x_{i,n} + G(x_{i,n}) - \beta H(x_{i,n} - d) - y_{i,n} + I_{i,n}^{\text{syn}}, \\ y_{i,n+1} &= y_{i,n} + \epsilon(x_{i,n} - J), \end{aligned} \quad (2)$$

$$I_{i,n}^{\text{syn}} = I_{i,n}^{\text{coup}} + I_{i,n}^{\text{rand}} = \frac{c}{N} \sum_{j=1, j \neq i}^N (x_{j,n} - x_{i,n}) + \sigma \xi_{i,n},$$

where  $i$  specifies the particular neuron. The synaptic currents  $I_{i,n}^{\text{syn}}$  comprise two types of terms. The diffusive couplings  $I_{i,n}^{\text{coup}}$  are characterized by the strength  $c$ , which is assumed to be uniform over the network and is set to  $c = 1$  in the remainder of the paper. The random inputs  $I_{i,n}^{\text{rand}}$  involve uncorrelated white noise [ $E[\xi_{i,n}] = 0$ ,  $E[\xi_{i,n}\xi_{j,n'}] = \delta_{ij}\delta(n - n')$ ] of intensity  $\sigma$ .

Confined to a single unit, the stochastic component may influence its dynamics either by perturbing the deterministic oscillatory regimes or by inducing oscillations in the excitable regime, cf. Fig. 2(b). The onset of noise-induced spiking or bursting within the parameter domain where the fixed point is deterministically stable (domain  $I$  in Fig. 1) corresponds to a phenomenon of stochastic bifurcation [39,52–55]. The latter are typically described phenomenologically, in a sense that certain time-averaged quantities, such as the asymptotic probability distributions of relevant variables or the associated power spectra, exhibit a qualitative change under variation of noise intensity. For instance, in continuous-time systems, it has been shown that the stochastic Hopf bifurcation from a stochastically stable fixed point to a stochastically stable limit cycle is accompanied by the loss of Gaussian property for the asymptotic distributions of the appropriate variables [56]. At variance with standard deterministic bifurcations, where one clearly observes a critical value of the control parameter, the change of system's behavior in noise-induced transitions is gradual [39]. Note that noise can also play an important part in the  $(J, \beta)$  region II where the deterministic map shows subthreshold oscillations. Here noise can give rise to a form of dynamics reminiscent of mixed-mode oscillations, cf. Fig. 2(c).

So far, models similar to (2) have been applied to address a number of problems associated to collective phenomena in

networks of coupled neurons, including synchronization of electrically coupled units with spike-burst activity [57,58], pattern formation in complex networks with modular architecture [41,42,59], transient cluster activity in evolving dynamical networks [44], as well as the basin stability of synchronization regimes in small-world networks [43]. Within this paper, the collective motion will be described in terms of the global variables  $X_n = \frac{1}{N} \sum_{i=1}^N x_{i,n}$  and  $Y_n = \frac{1}{N} \sum_{i=1}^N y_{i,n}$ .

### III. DERIVATION OF THE MEAN-FIELD MODEL

Considering a MF approximation, our main goal lies in deriving a reduced low-dimensional deterministic set of nonlinear difference equations whose dynamics is qualitatively analogous to the collective motion of the original system (2) composed of  $2N$  coupled stochastic maps. In particular, the MF model should be able to generate all the regimes exhibited by the exact system, qualitatively reproducing the bifurcations that the latter undergoes. Also, applying the effective model, one should be capable of inferring with sufficient accuracy the parameter domains which admit the different collective states of the exact system, with the corresponding time series exhibiting similar characteristic quantitative features. Regarding the explicit effects of noise, the MF model is expected to account for the onset or suppression of different types of collective modes associated to macroscopic spiking or bursting activity, which are mediated by synchronization or desynchronization of individual neuron dynamics, respectively. The synchronization processes may be influenced by noise in a variety of ways, including the scenarios where noise acts as a perturbation to mainly deterministic (and chaotic) local oscillations, or the ones where noise plays a facilitatory role, in the sense that the collective mode emerges via synchronization of noise-induced local dynamics.

Given that we consider a system of discrete-time equations, one cannot adopt the usual method of deriving the MF model via Fokker-Planck formalism [40]. Nevertheless, an analytically tractable MF model may still be built by focusing on the evolution of cumulants [34–36,39], whereby the full density of states is factorized into a series of marginal densities. The advantage of such an approach is that the simplifying approximations aimed at truncating the underlying cumulant series can be introduced in a controlled fashion. Such approximations, stated in a form of closure hypothesis [34], are required due to nonlinearity of the original system, which causes the dynamics of cumulants of the given order to be coupled to those of the higher order.

In our case, the derivation of the effective model incorporates an explicit Gaussian closure hypothesis [34–36,39], by which all the cumulants above second order are assumed to vanish. The collective dynamics is then described by a set of five variables (the first- and second-order cumulants), including

- (i) the means, given by  $m_{x,n} = \lim_{N \rightarrow \infty} \frac{1}{N} \sum_{i=1}^N x_{i,n} \equiv \langle x_{i,n} \rangle$ ,  $m_{y,n} = \lim_{N \rightarrow \infty} \frac{1}{N} \sum_{i=1}^N y_{i,n} \equiv \langle y_{i,n} \rangle$ ;
- (ii) the variances, defined as  $S_{x,n} = \langle x_{i,n}^2 \rangle - \langle x_{i,n} \rangle^2 = \langle x_{i,n}^2 \rangle - m_{x,n}^2$  and  $S_{y,n} = \langle y_{i,n}^2 \rangle - \langle y_{i,n} \rangle^2 = \langle y_{i,n}^2 \rangle - m_{y,n}^2$ ;
- (iii) the covariance  $U_n = \langle x_{i,n} y_{i,n} \rangle - m_{x,n} m_{y,n}$ .

The expressions for higher-order moments  $\langle x_{i,n}^k \rangle$  in terms of the first- and second-order cumulants [60], such as

$$\begin{aligned} \langle x_i^3 \rangle &= m_x^3 + 3m_x S_x \\ \langle x_i^4 \rangle &= m_x^4 + 6m_x^2 S_x + 3S_x^2 \\ \langle x_i^2 y_i \rangle &= m_y S_x + m_y m_x^2 + 2m_x U \\ \langle x_i^3 y_i \rangle &= 3S_x U + 3S_x m_x m_y + 3m_x^2 U + m_y m_x^3 \\ \langle x_i^5 \rangle &= m_x^5 + 15m_x S_x^2 + 10m_x^3 S_x \\ \langle x_i^6 \rangle &= m_x^6 + 15S_x^3 + 15m_x^4 S_x + 45m_x^2 S_x^2, \end{aligned} \quad (3)$$

can be derived using the closure hypothesis.

The Gaussian approximation effectively amounts to an assumption that the relation

$$\lim_{N \rightarrow \infty} \frac{1}{N} \sum_{i=1}^N x_{i,n}^k \approx E[x_{i,n}^k], \quad (4)$$

holds, whereby  $E$  refers to expectation value obtained by averaging over an ensemble of different stochastic realizations. In other words, one supposes that the local variables are independent and are drawn from a normal distribution  $\mathcal{N}(m_x, S_x)$ . We do not know *a priori* whether such an assumption is fulfilled but can only judge on its validity by verifying the correctness of the predictions on the population dynamics provided by the MF model. Also note that the effective model concerns the assembly dynamics in the thermodynamic limit

$N \rightarrow \infty$ . The stochastic terms in this case can be neglected, as one may show them to contribute to finite-size effects which scale as  $1/N$ . This means that the influence of noise in our MF model is felt only via the noise intensity, which assumes the role of an additional bifurcation parameter.

Let us illustrate the main technical points required for the derivation of the MF model. Our focus will lie with a couple of relevant examples, whereas the remaining details are provided in the Appendix. We begin by considering the dynamics of  $m_x$ , which is given by

$$m_{x,n+1} = m_{x,n} - m_{y,n} + \langle G(x_{i,n}) \rangle - \beta \langle H(x_{j,n} - d) \rangle. \quad (5)$$

It is easy to see that there is no contribution from the coupling term. As far as the third term on the right-hand side of Eq. (5) is concerned, using Eq. (3), one arrives at

$$\begin{aligned} \langle G(x_i) \rangle &= \langle -x_i^3 + (1+a)x_i^2 - ax_i \rangle \\ &= G(m_x) + S_x(1+a-3m_x). \end{aligned} \quad (6)$$

In the last expression, we have dropped the time index for simplicity and have introduced the shorthand notation  $G(m_x) \equiv -m_x^3 + (1+a)(m_x^2 + S_x)$ .

The key problem is how to treat the final term in the right-hand side of Eq. (5). Our approach consists in replacing the assembly average by the expectation value ( $\langle H(x_i - d) \rangle \approx E[H(x_i - d)]$ ), obtained by assuming that the local variables at an arbitrary time moment are normally distributed according to  $P(x_i) \sim \mathcal{N}(m_x, S_x)$ . The expectation may then be evaluated as

$$\begin{aligned} E[-\beta \langle H(x_i - d) \rangle] &= \int dx_1 \int dx_2 \dots \int dx_N \left( -\frac{\beta}{N} \sum_i H(x_i - d) \right) p(x_1, x_2, \dots, x_N) \\ &= -\beta \int_{-\infty}^{\infty} dx_1 H(x_1 - d) p(x_1) = -\beta \int_d^{\infty} \frac{1}{\sqrt{2\pi S_x}} e^{-\frac{(x_1 - m_x)^2}{2S_x}} = -\frac{\beta}{2} \left( 1 - \text{Erf} \left[ \frac{d - m_x}{\sqrt{2S_x}} \right] \right), \end{aligned} \quad (7)$$

with the error function  $\text{Erf}(x) = \frac{2}{\sqrt{\pi}} \int_0^x e^{-t^2} dt$ . In the above calculation, we have explicitly used the assumption on the independence of distributions of local variables at any given moment of time.

In a similar fashion, one may consider the  $S_x$  dynamics, which constitutes the most demanding part of the derivation. In particular, proceeding from the  $S_x$  definition, we obtain

$$\begin{aligned} S_{x,n+1} &= \langle x_{i,n+1}^2 \rangle - \langle x_{i,n+1} \rangle^2 \\ &= \langle [(1-c)x_{i,n} + G(x_{i,n}) - \beta H(x_{i,n} - d) - y_{i,n} + \xi_{i,n} + cm_{x,n}]^2 \rangle - [m_{x,n} - m_{y,n} + G(m_{x,n}) + S_{x,n}(1+a-3m_{x,n}) \\ &\quad - \beta \langle H(x_{i,n} - d) \rangle]^2. \end{aligned} \quad (8)$$

As an illustration, let us evaluate one of the terms containing an average over the threshold function:

$$\begin{aligned} -2\beta E[\langle G(x_i) H(x_i - d) \rangle] &= -2\beta \left[ \int dx_1 G(x_1) H(x_1 - d) p(x_1) - \int dx_1 H(x_1 - d) p(x_1) [G(m_x) + S_x(1+a-3m_x)] \right] \\ &\approx -2\beta \left[ \int dx_1 [G(m_x) + G'(m_x)(x_1 - m_x) + \frac{1}{2}G''(m_x)(x_1 - m_x)^2] H(x_1 - d) p(x_1) \right. \\ &\quad \left. - \int dx_1 H(x_1 - d) p(x_1) [G(m_x) + S_x(1+a-3m_x)] \right] = \dots \\ &= -2\beta [(1+a)(m_x + d) - a - 3m_x d] \sqrt{\frac{S_x}{2\pi}} \exp \left[ -\frac{(d - m_x)^2}{2S_x} \right]. \end{aligned} \quad (9)$$

Again, the time indexes have been suppressed to simplify the notation.



Leaving the remaining elements of the derivation for the Appendix, we now state the final equations of the MF model in the thermodynamic limit

$$\begin{aligned}
 m_{x,n+1} &= m_{x,n} - m_{y,n} + G(m_{x,n}) + S_{x,n}(1 + a - 3m_{x,n}) - \frac{\beta}{2} \left( 1 - \text{Erf} \left[ \frac{d - m_{x,n}}{\sqrt{2S_{x,n}}} \right] \right) \\
 m_{y,n+1} &= m_{y,n} + \epsilon(m_{x,n} - J) \\
 S_{x,n+1} &= (1 - c)^2 S_{x,n} + S_{y,n} + \sigma^2 - 2(1 - c)U_n + S_{x,n}(-3m_{x,n}^2 + 2(1 + a)m_{x,n} - a)^2 \\
 &\quad - 2(1 - c)(3m_{x,n}^2 S_{x,n} + 3S_{x,n}^2 - 2(1 + a)m_{x,n} S_{x,n} + aS_{x,n}) + 2(3S_{x,n}U_n + 3m_{x,n}^2 U_n - 2(1 + a)m_{x,n}U_n) \\
 &\quad - 2\beta[(1 + a)(m_{x,n} + d) - a - 3dm_{x,n}] \sqrt{\frac{S_{x,n}}{2\pi}} \exp \left[ -\frac{(d - m_{x,n})^2}{2S_{x,n}} \right] - 2\beta(1 - c) \sqrt{\frac{S_{x,n}}{2\pi}} \exp \left[ -\frac{(d - m_{x,n})^2}{2S_{x,n}} \right] \\
 &\quad + S_{x,n}^2 [36m_{x,n}^2 - 24(1 + a)m_{x,n} + 2(1 + a)^2 + 6a] + 15S_{x,n}^3 \\
 S_{y,n+1} &= S_{y,n} + \epsilon^2 S_{x,n} + 2\epsilon U_n \\
 U_{n+1} &= U_n - (a + c + \epsilon)U_n + \epsilon(1 - c - a)S_{x,n} - S_{y,n} - (U_n + \epsilon S_{x,n})[3S_{x,n} + 3m_{x,n}^2 - 2(1 + a)m_{x,n}] \\
 &\quad - \beta\epsilon \sqrt{\frac{S_{x,n}}{2\pi}} \exp \left[ -\frac{(d - m_{x,n})^2}{2S_{x,n}} \right].
 \end{aligned} \tag{10}$$

#### IV. ANALYSIS OF STABILITY AND BIFURCATIONS

In this section, our goal is to demonstrate the qualitative and quantitative analogies between the dynamics of the exact system and the MF model. To this end, we first examine the succession of macroscopic regimes in the  $J$ - $\beta$  parameter plane for  $\sigma$  fixed at an intermediate value  $\sigma = 0.002$ , see Fig. 3. As in case of a single unit, changing  $J$  is relevant for the system's excitability, viz. the transitions from silent to active regimes, while  $\beta$  influences the wave forms of the active states (spiking, bursting, or mixed spike-bursting activity). The assembly is found to exhibit the collective modes which qualitatively correspond to the dynamics of a single unit illustrated in plates

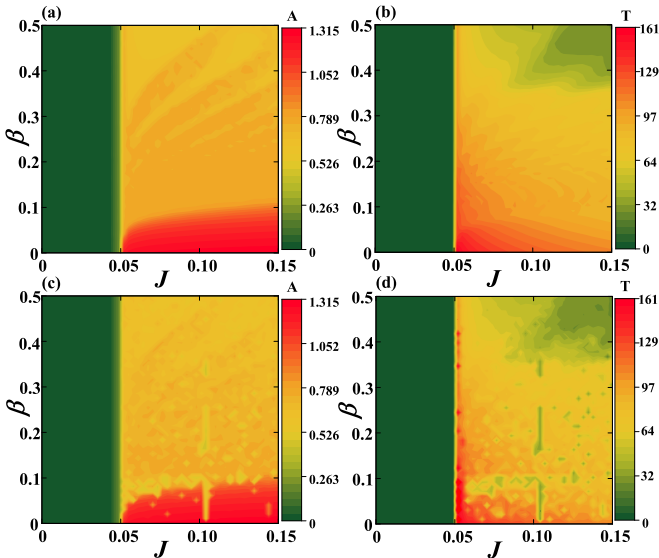


FIG. 3. Heat maps in (a) and (b) show the dependencies  $A(J, \beta)$  and  $T(J, \beta)$  obtained by stochastic averaging for a network of  $N = 100$  neurons, respectively. Panels (c) and (d) illustrate the analogous results for the MF model. The noise intensity in all instances is  $\sigma = 0.001$ .

III and VI of Fig. 1. The heat maps in the left column of Fig. 3 provide a comparison between the oscillation amplitudes  $A$  of the global variable  $X$  (top row) and the MF variable  $m_x$  (bottom row) for the given  $(J, \beta)$ . The right column indicates how well are matched the average interspike interval (or the average bursting cycle)  $T$  of the exact system with the corresponding characteristics of the dynamics of the MF model (A1). In the given instances, exact system comprises an assembly of  $N = 100$  neurons, having obtained  $A$  by averaging over a

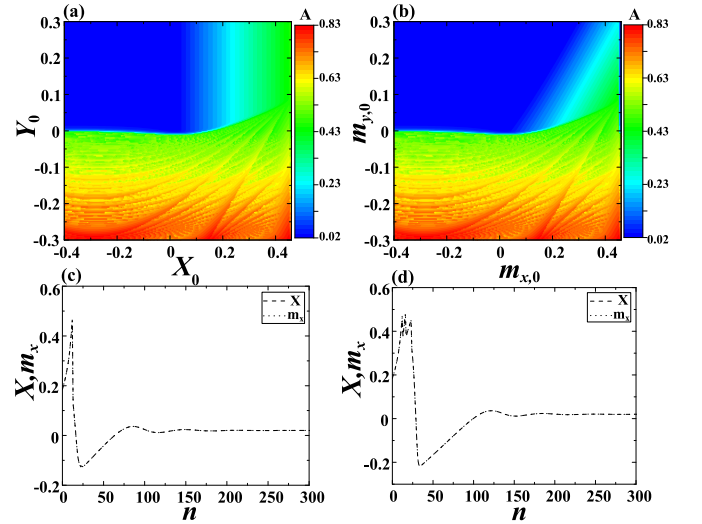


FIG. 4. Macroscopic excitability feature. In (a) and (b) are shown the maximum values of  $X$  and  $m_x$  reached within the time series of the exact and the MF system, starting from the analogous initial conditions  $(X_0, Y_0)$  and  $(m_{x,0}, m_{y,0})$ , respectively. The parameters are  $J = 0.02, \beta = 0.4$ . (c) Illustrates the case where a strong-enough perturbation elicits a single-spike response ( $J = 0.02, \beta = 0.4$ ), whereas (d) corresponds to a bursting response made up of three spikes ( $J = 0.02, \beta = 0.15$ ). In both instances, the time series of the MF model (dotted line) is indistinguishable from that of the exact system (dashed line).

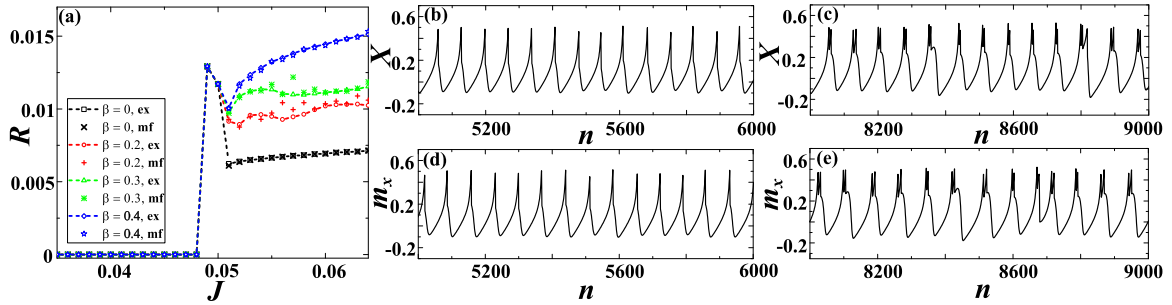


FIG. 5. (a) A family of  $R(J)$  curves over  $\beta$  for a network of size  $N = 100$  under fixed  $\sigma = 0.001$ . Superimposed are the results for the MF model, whereby the symbols  $\times, +, *, \star$  correspond to cases  $\beta = 0, 0.2, 0.3$ , and  $0.4$ , respectively. Panels (b) and (c) illustrate the  $X$  series associated to the spiking and the bursting collective modes. The considered network is made up of  $N = 100$  neurons, with the parameters set to  $J = 0.06, \beta = 0.4, \sigma = 0.001$  in (b), and  $J = 0.08, \beta = 0.2, \sigma = 0.001$  in (c). In (d) and (e) are provided the  $m_x$  series obtained for parameters from (b) and (c).

sufficiently long time series, whereas  $T$  is determined by taking average over an ensemble of 20 different stochastic realizations. With regard to  $T$ , we have selected a convenient threshold  $\theta = 0.2$ , which allows a clear detection of individual spikes and enables one to unambiguously discern the initiation stage of bursts, as required for calculating the length of the bursting cycle.

Let us begin the analysis by focusing on the domain of  $J$  values where the exact system exhibits the stochastically stable equilibrium, while the MF model has a stable stationary state. The stochastic stability physically implies that fluctuations around the deterministic fixed point are typically of the order of noise, though some rare spikes may still be evoked. For  $J$  sufficiently close to the region admitting the sub-threshold oscillations, the population manifests macroscopic excitability. The term “macroscopic” here refers to a form of emergent assembly behavior rather than the characteristic spatial scale. To properly illustrate this feature, we have analyzed the assembly dynamics in the limit  $\sigma = 0$ , cf. Fig. 4. In particular, Figs. 4(a) and 4(b) show the maximum  $X$  and  $m_x$  values reached in the corresponding time series obtained for sets of different initial conditions  $(X_0, Y_0)$  and  $(m_{x,0}, m_{y,0})$ , respectively. The comparison between the two plots clearly corroborates that the boundary defining the domain of spiking response is appropriately anticipated by the MF model. An important remark is that for the given  $J$ , the assembly may exhibit different forms of macroscopic excitability, generating a single spike or a burst of spikes, as dependent on the value of  $\beta$ . This is demonstrated by the time series in Figs. 4(c) and 4(d). The former refers to a one-spike response in case of  $\beta = 0.4$ . For smaller  $\beta$ , one observes responses comprising two or more closely packed spikes, with Fig. 4(d) illustrating a three-spike burst encountered for  $\beta = 0.25$ . Note that the time series of the full system and the MF model are exactly matched in the limit  $\sigma = 0$ .

Next we address the noise-influenced transitions from silence to active regimes observed under increasing  $J$ . To do so, in Fig. 5(a) we have plotted the change of the firing (spiking or bursting) frequency  $R$  for an assembly consisting of  $N = 100$  neurons. The average frequency is determined by considering an ensemble of 20 different stochastic realizations, having  $\sigma$  fixed to the moderate value from Fig. 4. The results from simulations of the full system (2) are compared against

the data obtained for the MF model. In this context, two points should be stressed. First, for moderate  $\sigma$ , note that the firing frequencies of the MF model lie in close agreement to those of the exact system. As a second point, one finds that such quantitative agreement extends to different forms of collective behavior, viz. it holds for different types of transitions from silent to active regimes. As already indicated, the wave forms pertaining to the active states depend on  $\beta$ , such that the associated transitions are mediated by the distinct synchronization processes. For instance, at  $\beta = 0$ , synchronization involves time series of single units that conform to spiking activity of type III from Fig. 1, which are quite resilient to impact of noise. On the other hand, for  $\beta = 0.3$  or  $\beta = 0.4$ , the individual units exhibit chaotic bursting or spiking activity, respectively, such that the underlying synchronization process may be more susceptible to stochastic effects. The typical  $X$  time series illustrating the different collective modes are compared to the corresponding  $m_x$  series in Figs. 5(b)–5(e). The top (bottom) row concerns the data for the exact system (MF model).

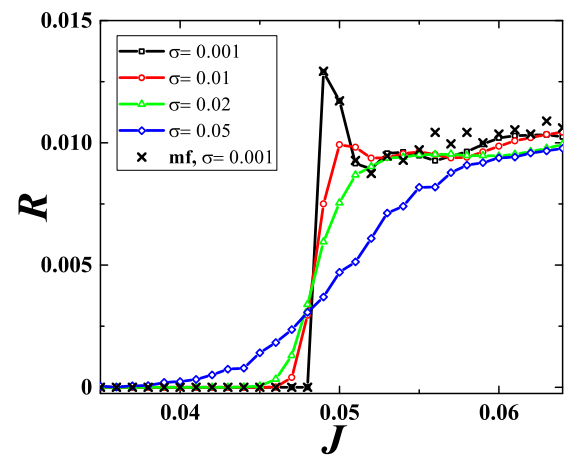


FIG. 6. Family of  $R(J)$  curves over  $\sigma$  obtained for a network of  $N = 100$  neurons under fixed  $\beta = 0.2$ . The different symbols correspond to cases  $\sigma = 0.001$  (squares),  $\sigma = 0.01$  (circles),  $\sigma = 0.02$  (triangles), and  $\sigma = 0.05$  (diamonds). The crosses connected by the dashed line highlight the  $R(J)$  curve for the MF model at  $\sigma = 0.001$ .

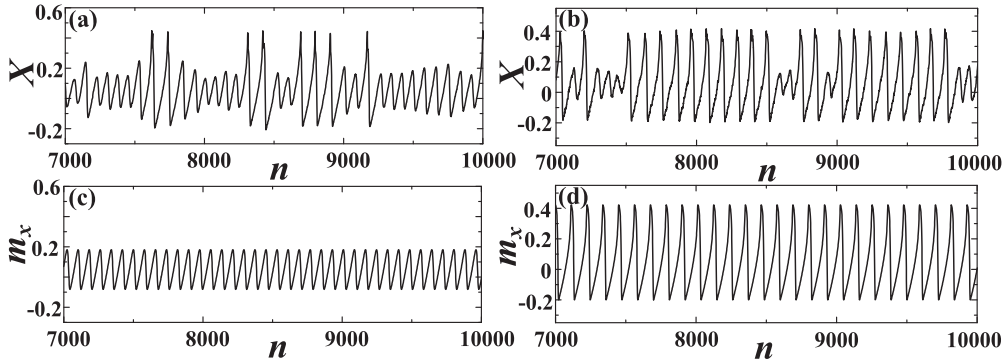


FIG. 7. Noise-induced phenomena within the  $J$  interval in vicinity of the deterministic threshold.  $X$  series in (a) shows the noise-induced spike-bursting activity on top of subthreshold oscillations ( $J = 0.047$ ,  $\beta = 0.2$ ,  $\sigma = 0.02$ ). (b) Illustrates the “skipping” phenomenon where the stochastic effects occasionally suppress the large-amplitude oscillations of the  $X$  variable ( $J = 0.058$ ,  $\beta = 0.2$ ,  $\sigma = 0.01$ ). In (c) and (d) are provided the  $m_x$  series corresponding to parameter sets from (a) and (b), respectively.

In order to investigate more closely the influence of noise for  $J$  interval in vicinity of the transition from silence to active regimes, we examine how the profiles of  $R(J)$  curves change under increasing  $\sigma$ . The results shown in Fig. 6 refer to  $\beta = 0.2$  and a population comprised of  $N = 100$  neurons. As expected, the transition appears quite sharp for moderate noise  $\sigma = 0.001$  but is considerably flattened for larger  $\sigma$ , e.g.,  $\sigma = 0.05$ . The crosses indicate the firing frequencies predicted by the MF model for  $\sigma = 0.001$ .

For larger  $\sigma$ , the MF model fails to reproduce the behavior of the exact system in vicinity of threshold  $J$ , in the sense that it overestimates the maximal  $R$  value, as well as the actual critical  $J$  characterizing the transition. Viewed from another angle, one may infer that for sufficiently large  $\sigma$  and  $J$  below the threshold given by the MF model, the latter fails to capture the impact of synchronization processes taking place between the noise-induced oscillations of individual units. This especially refers to  $J$  interval where the spikes or bursts (depending on the given  $\beta$ ) are superimposed on the background of subthreshold oscillations. An example of such a discrepancy between the behavior of the exact and the effective system is provided in Fig. 7, cf. Fig. 7(a) and Fig. 7(c). Also, for strong  $\sigma$  and  $J$  values above the transition, the firing frequencies anticipated by the effective model are typically higher than those of the exact system (not shown). Within this region, the stochastic effects suppress synchronization between the chaotic oscillations of single neurons, thereby reducing the corresponding  $R$  value. This is not accounted for with sufficient accuracy by the MF system. Note that such suppression of synchronization is reflected in the corresponding  $X$  series by the spike (burst) “skipping” mechanism, where the large-amplitude oscillations are occasionally replaced with subthreshold oscillations. For the associated  $J$  and  $\sigma$  values, such a phenomenon is absent in the dynamics of the effective model, cf. Fig. 7(b) and Fig. 7(d). In both of the scenarios illustrated in Fig. 7, the reason for the failure of MF model is that the Gaussian approximation breaks down due to large stochastic fluctuations.

The fashion in which the validity of the effective model’s predictions deteriorates with increasing  $\sigma$  is made more explicit in Fig. 8, which shows the  $A(J, \sigma)$  and  $T(J, \sigma)$  dependencies for the exact and the approximate system at

fixed  $\beta = 0.4$ . The considered size of the network is  $N = 100$ . Comparison between the respective  $A$  (left column) and  $T$  plots (right column) suggests that the range of  $\sigma$  values where the MF approximation applies is contingent on  $J$ . For instance, in the  $J$  region below the deterministic threshold, one may estimate this range by noting that the effective bifurcation diagram in Fig. 8(a) indicates that noise-induced macroscopic oscillations emerge for  $\sigma \approx 0.003$ . Since this point is not adequately represented by the effective model, cf. Fig. 8(c), one may state that the Gaussian approximation breaks down around  $\sigma \approx 0.003$  within the given  $J$  region. Nevertheless, for  $J$  above the deterministic threshold, the validity of the MF model appears to depend rather strongly on particular  $J$ , with the  $\sigma$  values where the Gaussian approximation effectively fails spanning the range  $\sigma \in (0.002, 0.006)$ .

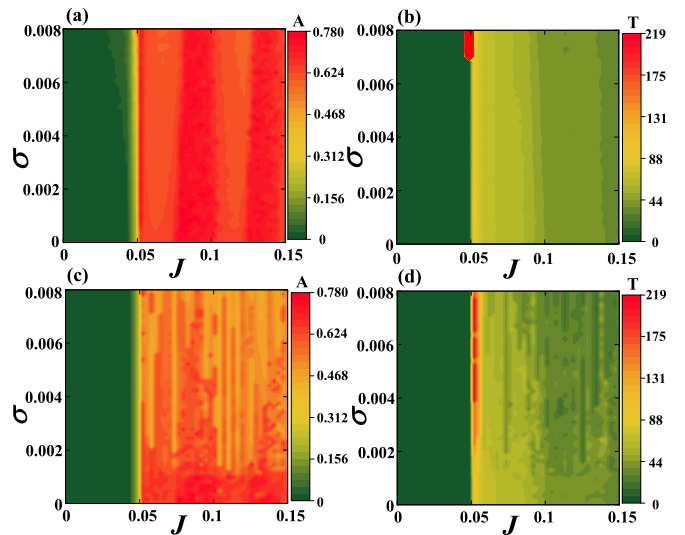


FIG. 8. Panels (a) and (b), respectively, refer to  $A(J, \sigma)$  and  $T(J, \sigma)$  dependencies for the network of  $N = 100$  neurons under fixed  $\beta = 0.4$ . The results in (a) are obtained by averaging over a sufficiently long time series, whereas data in (b) derive from averaging over an ensemble of 20 different stochastic realizations. In (c) and (d) are provided the  $A(J, \sigma)$  and  $T(J, \sigma)$  dependencies determined by numerical simulations of the MF model.

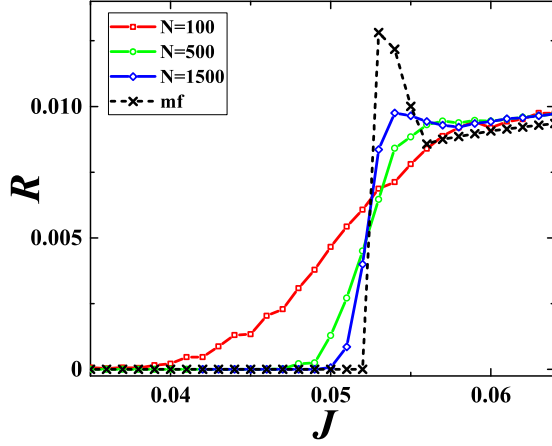


FIG. 9.  $R(J)$  dependencies for increasing  $N$  under fixed  $(\beta, \sigma) = (0.2, 0.05)$ . The squares, circles, and diamonds correspond to cases  $N = 100$ ,  $N = 500$ , and  $N = 1500$ , respectively. The results predicted by the MF model are indicated by crosses connected via dashed line.

So far, we have investigated the impact of noise by comparing the results for the network of size  $N = 100$  to those obtained for the effective system. Nevertheless, within Sec. III, it has already been emphasized that the MF model, deterministic in character, refers to the system's behavior in the thermodynamic limit  $N \rightarrow \infty$ , whereas the explicitly stochastic terms could only be incorporated as finite-size effects. This makes it relevant to examine how the behavior of the exact system within the  $J$  domain around deterministic threshold changes for large and fixed  $\sigma$  under increasing  $N$ . To this end, we have plotted in Fig. 9 the  $R(J)$  curves calculated for  $N = 100$  (squares),  $N = 500$  (circles), and  $N = 1500$  (diamonds) at fixed  $\beta = 0.2, \sigma = 0.05$ . The curve for  $N = 100$  evinces that the given  $\sigma$  value is quite large in a sense of being sufficient to induce collective oscillations within the excitable regime. Apart from the dependencies for the full system, we also show the  $R(J)$  curve associated to the MF model (dashed line with crosses). An interesting point regarding the latter is that the  $J$  threshold for the emergence of the collective mode is shifted toward a larger value compared to the case  $\sigma \approx 0.01$ . While the given transition itself appears quite sharp, the curves corresponding to the exact system approach it with increasing  $N$ , both in terms of the  $J$  threshold and the  $R$  values above the transition. This corroborates that the  $(J, \sigma)$  domain where the Gaussian approximation behind the MF model fails expectedly reduces with the increasing system size.

## V. RESPONSE TO EXTERNAL STIMULI

The aim of this section is to investigate the extent to which the MF model can be used to predict the stimulus-response relationship of an assembly exhibiting different macroscopic regimes, including the excitable state, as well as the spiking and bursting collective modes. Let us first focus on the two latter instances and examine the sensitivity of a population to an external pulse perturbation within the framework of phase resetting theory [61–64]. In order to compare the behavior of the exact system and the effective model, we determine

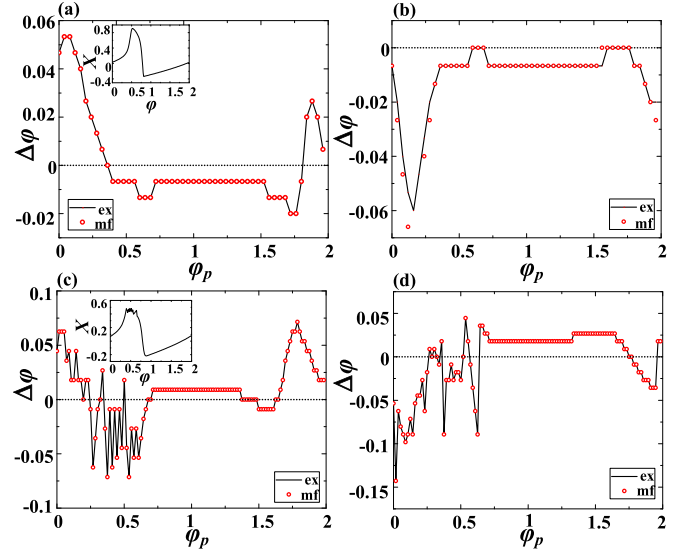


FIG. 10. Assembly phase resetting. Panels (a) and (b) show the PRCs for a population in spiking regime ( $J = 0.055$ ,  $\beta = 0$ ) under excitatory ( $a = 0.008$ ) and inhibitory stimulation ( $a = -0.008$ ), respectively. Results for the exact system ( $N = 500$ ) are indicated by the solid line, whereas the data for the MF model are denoted by circles. The bottom row illustrates the PRCs for an assembly exhibiting macroscopic bursting ( $J = 0.06$ ,  $\beta = 0.1$ ), whereby (c) describes the effect of an excitatory ( $a = 0.01$ ) and (d) of an inhibitory pulse perturbation ( $a = -0.01$ ). The insets in (a) and (c) demonstrate how the phases are assigned to the points within the spiking and bursting cycles, respectively. Phase is expressed in units of  $\pi$ .

the corresponding PRCs, which describe the phase shift  $\Delta\phi$ , induced by the perturbation, in terms of the phase  $\phi_p$  when the perturbation is applied. The considered stimulus has a form of a short pulse current  $I_p = a_p H(n - n_i) H(n - n_f)$ , whose magnitude  $a_p$  and width  $\Delta = n_i - n_f$  are small compared to the amplitude and duration of the spiking (or bursting) cycle  $T_0$ , respectively. In case of the exact system, the same pulse current is delivered to each neuron  $i$ , adding the term  $I_p$  to  $x_i$  dynamics, whereas in the effective model, stimulation is administered via the  $m_x$  variable. The phase  $\phi_p$  is defined in reference to  $T_0$  by  $\phi_p = n_p / T_0$ . The associated phase difference following the reset is calculated as  $\Delta\phi = 1 - T_1 / T_0$ , where  $T_1$  denotes the duration of the perturbed spiking or bursting cycle.

The PRCs characterizing the assembly response in the spiking regime are provided in Fig. 10(a) and Fig. 10(b), whereby the former is obtained under the action of an excitatory ( $a_p > 0$ ), and the latter under the influence of inhibitory stimulation ( $a_p < 0$ ). We stress that, in both instances, the results derived from the effective model, denoted by circles, show excellent agreement with the data for the exact system (solid lines). In qualitative terms, one observes that excitatory stimulation may advance the phase of the spiking cycle if it arrives sufficiently close to the spike but still before the sharp rising stage. However, an excitatory perturbation acting during the spike or within the effective refractory period has a suppression effect, reflected in delaying of the next spike. In contrast to excitatory stimulation, the inhibitory pulse postpones the next firing time if it is introduced within the interval close to the rising stage of spike.

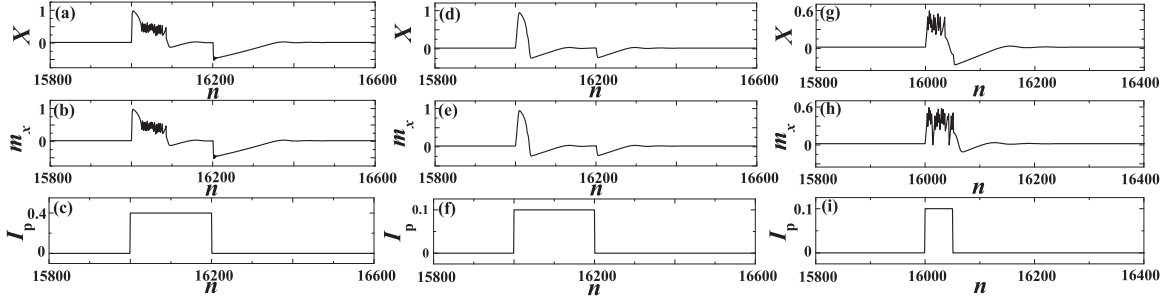


FIG. 11. Stimulus-response relationship in the excitable regime ( $J = 0.02$ ). The top (middle) row refers to the response of the full system (MF model), whereas the bottom row shows the profile of the external stimulation. In panels (a)–(c), the system parameters are  $\beta = 0.4$ ,  $\sigma = 0$ , while the perturbation is characterized by  $a_p = 0.4$ ,  $\Delta = 200$ . Panels (d)–(f) concern the response of an assembly ( $\beta = 0.1$ ,  $\sigma = 0.001$ ) subjected to a rectangular pulse  $a_p = 0.4$ ,  $\Delta = 200$ . Panels (g)–(i) illustrate the response of a population ( $\beta = 0.4$ ,  $\sigma = 0.001$ ) influenced by the external stimulation  $a_p = 0.1$ ,  $\Delta = 50$ . The considered network is of size  $N = 500$ .

The PRCs determined for an assembly exhibiting collective bursting show qualitatively analogous effects to those described so far, see Fig. 10(c) and Fig. 10(d). This especially refers to impact of perturbation delivered sufficiently close to a moment of burst initiation. An apparent difference compared to Fig. 10(a) and Fig. 10(b) emerges during the bursting stage itself, where the associated PRCs expectedly exhibit strong fluctuations. Apart from that, one finds an interesting effect that both the excitatory and the inhibitory stimulation have a facilitatory role, i.e., cause phase advancement during the relaxation stage of the bursting cycle.

For a population in the excitable state, we consider scenarios where the system is influenced by a rectangular pulse perturbation of finite magnitude and duration, in a sense that the latter are comparable to corresponding features of typical spiking or bursting cycles. Note that the selected  $J$  value  $J = 0.02$  lies sufficiently away from the interval admitting the subthreshold oscillations. Again, our objective is to determine whether the MF model correctly anticipates the response of the exact system, now in the presence of small to moderate noise. Some of the illustrative examples concerning the stimulus-response relationship under the finite perturbation are provided in Fig. 11. The top and the middle rows refer to  $X$  and corresponding  $m_x$  time series, respectively, while the bottom row shows the profile of the applied stimulus. We find that in the absence of noise or for sufficiently small  $\sigma$ , the effective model reproduces the evoked behavior of the full system quite accurately. This also refers to some highly complex forms of responses, as corroborated in Figs. 11(a)–11(c), which concern relatively large  $a_p$  and  $\Delta$ . Under increasing  $\sigma$ , the ability of the MF model to predict the dynamics of the exact system gradually reduces but in a fashion that involves a nontrivial dependence on  $\beta$ . In particular, for smaller  $\beta \approx 0.1$ , which would facilitate macroscopic spiking mode for supercritical  $J$ , it turns out that the dynamics of the MF model lies in close agreement to the one of the exact system even for moderate noise  $\sigma = 0.001$ , cf. Figs. 11(d)–11(f). However, for higher  $\beta$ , such an analogy between the responses of the exact and the MF system is lost, see Figs. 11(g)–11(i). Naturally, the validity of the predictions given by the MF model deteriorates if the stimulation amplitude  $a_p$  and the duration  $\Delta$  are large, especially in the presence of non-negligible noise.

## VI. SUMMARY AND DISCUSSION

We have developed an MF approach in order to systematically analyze the emergent dynamics and the input-output relationship of a population of stochastic map neurons. The reduced low-dimensional model has been derived within the framework of Gaussian approximation, formally introduced in a form of a closure hypothesis. In physical terms, such an approximation suggests that the local variables at an arbitrary moment of time are independent and conform to a normal distribution centered about the assembly mean and characterized by the associated assembly variance. Validity of such an approximation cannot be established *a priori*, but has been systematically verified by numerically corroborating that the MF model reproduces the behavior of the exact system with sufficient accuracy.

In particular, we have first demonstrated that the effective model can qualitatively capture all the bifurcations of the exact system leading to the onset of different generic regimes of collective behavior. As far as the quantitative agreement is concerned, we have established substantial matching between the parameter domains admitting the respective dynamical regimes for the exact and the approximate system. Moreover, the typical features of the associated regimes, such as the average interspike interval or the average bursting cycle, exhibit analogous changes with parameter variation and in many parameter domains display numerically similar values.

An important issue has been to explicitly examine how the effects of noise are reflected in the behavior of the MF model. For the noise-perturbed activity, where the sufficiently small noise weakly influences the deterministic attractors of the system, the obtained results indicate that the Gaussian approximation holds. Nevertheless, the physical picture changes in case of noise-induced collective behavior. In particular, for different scenarios of stochastic bifurcations, typically corresponding to transitions from subthreshold oscillations, which involve generalized excitability feature, to spiking or bursting regimes, the exact system undergoes a gradual (smooth) change of collective dynamics, whereas the MF model exhibits a standard deterministic bifurcation with a sharp bifurcation threshold. In such instances, the collective variables of exact system manifest large fluctuations, which

explicitly violate the Gaussian approximation behind the effective model. Note that the loss of Gaussianity property for asymptotic distribution of relevant variables, which accompanies the described stochastic bifurcations, does not imply per se that our Gaussian approximation fails in the supercritical state. This point is evinced by the fact that the dynamics of the effective model shows qualitatively and quantitatively similar features to those of the exact system if the considered parameters lie sufficiently above the stochastic bifurcation. In fact, the Gaussian approximation applied in the derivation of the MF model breaks down only in vicinity of such transitions, where the finite-size effects neglected in Eq. (A1) become most prominent. We have numerically verified the prevalence of finite-size effects in these parameter domains, showing that the change of the appropriate order parameter, such as the spiking frequency, becomes sharper as the size of the neural assembly is increased. Nevertheless, the validity of Gaussian approximation is regained once the system is sufficiently above the bifurcation.

Apart from considering asymptotic dynamics, we have verified that the MF model is capable of capturing the stimulus-response features of the exact system. For short pulse-like perturbations, it has been found that the approximate system reproduces the PRCs of the exact system for both the spiking and bursting regimes of collective activity with high

accuracy. Substantial analogies have also been observed in case of macroscopic excitable regime for scenarios where the assembly is stimulated by rectangular pulse perturbations of finite amplitude and duration.

Having developed a viable MF approach, the present research has set the stage for a more systematic exploration of collective dynamics of assemblies of map neurons by analytical means. We believe that the introduced techniques can be successfully applied for treating the emergent behavior of populations in case of chemically and delay-coupled neurons [41]. Moreover, the method may likely be used to explore the effects of parameter inhomogeneity, as well as to study the impact of complex network topologies [41,43]. Our ultimate goal will be to extend the MF approach to account for collective behavior of interacting populations of map neurons [41,42].

### ACKNOWLEDGMENTS

This work is supported by the Ministry of Education, Science and Technological Development of Republic of Serbia under Project No. 171017 and by the Russian Foundation for Basic Research under Project No. 15-02-04245. Numerical experiments are supported by the Russian Science Foundation under Project No. 14-12-01358.

### APPENDIX

In the following, we provide the remaining details concerning the calculation of the  $S_x$  dynamics, which is the most complex part of the derivation of the effective model. Following some algebra, Eq. (9) can be transformed to

$$\begin{aligned}
S_{x,n+1} = & (1-c)^2 S_{x,n} + S_{y,n} + \sigma^2 - 2(1-c)U_n + \underbrace{(\langle G(x_{i,n})^2 \rangle - \langle G(x_{i,n}) \rangle^2)}_{\text{Var}(G(x_{i,n}))} + 2(1-c)(\langle x_{i,n} G(x_{i,n}) \rangle - m_{x,n} \langle G(x_{i,n}) \rangle) \\
& - 2(\langle y_{i,n} G(x_{i,n}) \rangle - m_{y,n} \langle G(x_{i,n}) \rangle) - 2\beta(1-c)[\langle x_{i,n} H(x_{i,n}-d) \rangle - m_{x,n} \langle H(x_{i,n}-d) \rangle] - 2\beta(\langle G(x_{i,n}) H(x_{i,n}-d) \rangle \\
& - \langle G(x_{i,n}) \rangle \langle H(x_{i,n}-d) \rangle) + \beta^2 \underbrace{(\langle H(x_{i,n}-d)^2 \rangle - \langle H(x_{i,n}-d) \rangle^2)}_{\text{Var}(H(x_{i,n}-d))}. \tag{A1}
\end{aligned}$$

The partial results required for completing the calculation are given by

$$\begin{aligned}
\langle x_i G(x_i) \rangle - m_x \langle G(x_i) \rangle &= G'(m_x) S_x - 3S_x^2 \\
\langle y_i G(x_i) \rangle - m_y \langle G(x_i) \rangle &= -3S_x U_{xy} - 3m_x^2 U_{xy} + 2(1+a)m_x U_{xy}, \tag{A2}
\end{aligned}$$

where  $G'(m_x) \equiv -3m_x^2 + 2(1+a)m_x - a$ . Note that the time indexes have been omitted for simplicity. After some tedious work, it may also be shown that the expression for variance  $\text{Var}(G(x_i))$  reads

$$\text{Var}(G(x_i)) = G'^2(m_x) S_x + S_x^2 [36m_x^2 - 24(1+a)m_x + 2(1+a)^2 + 6a] + 15S_x^3. \tag{A3}$$

Let us now explicitly calculate the terms containing the threshold function. First, we have

$$\begin{aligned}
& -2\beta(1-c)[\langle x_i H(x_i - d) \rangle - \langle x_i \rangle \langle H(x_i - d) \rangle] \\
&= -2\beta(1-c) \left[ \int dx_1 dx_2 \dots dx_N \frac{1}{N} \sum_i x_i H(x_i - d) p(x_1, \dots, x_N) - m_x \int dx_1 dx_2 \dots dx_N \frac{1}{N} \sum_i H(x_i - d) p(x_1, \dots, x_N) \right] = \dots \\
&= -2\beta(1-c) \left[ \int dx_1 (x_1 - m_x) H(x_1 - d) p(x_1) \right] = -2\beta(1-c) \sqrt{\frac{S_x}{2\pi}} \exp \left[ -\frac{(d - m_x)^2}{2S_x} \right]. \tag{A4}
\end{aligned}$$

Note that the second term containing the threshold function has been evaluated in the main text, cf. Eq. (10).

Finally, let us address the term  $\beta^2 \text{Var}[H(x_i - d)]$ , which can be estimated by considering the associated expectation  $\beta^2 \text{Var}[H(x_i - d)] \approx \beta^2 [\langle H(x_i - d)^2 \rangle - \langle H(x_i - d) \rangle^2]$ . Applying the technique introduced in Sec. III, we obtain

$$\begin{aligned} E[\beta^2 H(x_i - d)^2] &= \beta^2 \int dx_1 \int dx_2 \dots \int dx_N \left[ \frac{1}{N^2} \sum_i \sum_j H(x_i - d) H(x_j - d) \right] p(x_1, x_2, \dots, x_N) \\ &= \underbrace{\frac{\beta^2}{N^2} N \int dx_1 H(x_1 - d) p(x_1)}_{N \text{ cases where } i=j} + \underbrace{\frac{\beta^2}{N^2} N(N-1) \int dx_1 \int dx_2 H(x_1 - d) H(x_2 - d) p(x_1) p(x_2)}_{N(N-1) \text{ cases where } i \neq j} \\ &= \frac{\beta^2}{2N} \left[ 1 - \text{Erf} \left( \frac{d - m_x}{\sqrt{2S_x}} \right) \right] + \frac{\beta^2}{4N^2} N(N-1) \left[ 1 - \text{Erf} \left( \frac{d - m_x}{\sqrt{2S_x}} \right) \right]^2. \end{aligned} \quad (\text{A5})$$

Given that  $\beta^2 \langle H(x_i - d) \rangle^2 = \frac{\beta^2}{4} \left[ 1 - \text{Erf} \left( \frac{d - m_x}{\sqrt{2S_x}} \right) \right]^2$ , one arrives at

$$\beta^2 \text{Var}[H(x_i - d)] = \frac{\beta^2}{4N} \left[ 1 - \text{Erf} \left( \frac{d - m_x}{\sqrt{2S_x}} \right) \right] \left[ 1 + \text{Erf} \left( \frac{d - m_x}{\sqrt{2S_x}} \right) \right]. \quad (\text{A6})$$

This shows that the variance of the threshold function ultimately contributes to a finite-size effect which can be neglected in the thermodynamic limit.

- 
- [1] G. Buzsáki, *Rhythms of the Brain* (Oxford University Press, Oxford, 2009).
- [2] A. Destexhe and D. Contreras, *Science* **314**, 85 (2006).
- [3] C. Zhou, L. Zemanová, G. Zamora, C. C. Hilgetag, and J. Kurths, *Phys. Rev. Lett.* **97**, 238103 (2006).
- [4] E. Bullmore and O. Sporns, *Nat. Rev. Neurosci.* **10**, 186 (2009).
- [5] O. Sporns, D. Chialvo, M. Kaiser, and C. C. Hilgetag, *Trends Cogn. Sci.* **8**, 418 (2004).
- [6] W. J. Freeman, *Neurodynamics: An Exploration in Mesoscopic Brain Dynamics* (Springer-Verlag, London, 2000).
- [7] H. Liljenström, *Scholarpedia* **7**, 4601 (2012).
- [8] G. Deco, V. K. Jirsa, P. A. Robinson, M. Breakspear, and K. Friston, *PLoS Comput. Biol.* **4**, e1000092 (2008).
- [9] J. L. P. Velazquez and R. Wennberg, *Coordinated Activity in the Brain: Measurements and Relevance to Brain Function and Behavior* (Springer, New York, 2009).
- [10] Y. Baibolatov, M. Rosenblum, Z. Z. Zhanabaev, M. Kyzgarina, and A. Pikovsky, *Phys. Rev. E* **80**, 046211 (2009).
- [11] W. Gerstner, H. Sprekeler, and G. Deco, *Science* **338**, 60 (2012).
- [12] *Lectures in Supercomputational Neuroscience: Dynamics in Complex Brain Networks*, edited by P. beim Graben, C. Zhou, M. Thiel, and J. Kurths (Springer-Verlag, Berlin, 2008).
- [13] M. Breakspear, *Nat. Neurosci.* **20**, 340 (2017).
- [14] W. J. Freeman, *Mass Action in the Nervous System: Examination of the Neurophysiological Basis of Adaptive Behavior through the EEG* (Academic Press, London, 1975).
- [15] N. Fourcaud and N. Brunel, *Neural Comput.* **14**, 2057 (2002).
- [16] S. El Boustani, and A. Destexhe, *Neural Comput.* **21**, 46 (2009).
- [17] S. E. Folias and P. C. Bressloff, *Phys. Rev. Lett.* **95**, 208107 (2005).
- [18] S. E. Folias and P. C. Bressloff, *SIAM J. Appl. Math.* **65**, 2067 (2005).
- [19] C. R. Laing, W. C. Troy, B. Gutkin, and G. B. Ermentrout, *SIAM J. Appl. Math.* **63**, 62 (2002).
- [20] P. C. Bressloff, *Phys. Rev. E* **82**, 051903 (2010).
- [21] M. A. Buice and J. D. Cowan, *Phys. Rev. E* **75**, 051919 (2007).
- [22] N. Brunel and V. Hakim, *Neural Comput.* **11**, 1621 (1999).
- [23] H. Hasegawa, *Phys. Rev. E* **67**, 041903 (2003).
- [24] N. F. Rulkov, *Phys. Rev. E* **65**, 041922 (2002).
- [25] N. F. Rulkov, I. Timofeev, and M. Bazhenov, *J. Comput. Neurosci.* **17**, 203 (2004).
- [26] D. Q. Wei and X. S. Luo, *Europhys. Lett.* **78**, 68004 (2007).
- [27] Q. Y. Wang, Z. Duan, M. Perc, and G. Chen, *Europhys. Lett.* **83**, 50008 (2008).
- [28] C. A. S. Batista, A. M. Batista, J. A. C. de Pontes, R. L. Viana, and S. R. Lopes, *Phys. Rev. E* **76**, 016218 (2007).
- [29] B. Ibarz, J. M. Casado, and M. A. F. Sanjuán, *Phys. Rep.* **501**, 1 (2011).
- [30] I. Franović and V. Miljković, *Europhys. Lett.* **92**, 68007 (2010).
- [31] I. Franović and V. Miljković, *Commun. Nonlinear Sci. Numer. Simul.* **16**, 623 (2011).
- [32] E. M. Izhikevich, *Neural Comput.* **18**, 245 (2006).
- [33] E. M. Izhikevich and G. M. Edelman, *Proc. Natl. Acad. Sci. U.S.A.* **105**, 3593 (2008).
- [34] B. Lindner, J. Garcia-Ojalvo, A. Neiman, and L. Schimansky-Geier, *Phys. Rep.* **392**, 321 (2004).
- [35] I. Franović, K. Todorović, N. Vasović, and N. Burić, *Phys. Rev. E* **89**, 022926 (2014).
- [36] I. Franović, K. Todorović, N. Vasović, and N. Burić, *Phys. Rev. E* **87**, 012922 (2013).
- [37] I. Franović, K. Todorović, N. Vasović, and N. Burić, *Chaos* **22**, 033147 (2012).
- [38] V. Klinshov and I. Franović, *Phys. Rev. E* **92**, 062813 (2015).
- [39] M. A. Zaks, X. Sailer, L. Schimansky-Geier, and A. B. Neiman, *Chaos* **15**, 026117 (2005).
- [40] B. Sonnenschein, M. A. Zaks, A. B. Neiman, and L. Schimansky-Geier, *Eur. Phys. J. Special Topics* **222**, 2517 (2013).
- [41] O. V. Maslennikov and V. I. Nekorkin, *Phys. Rev. E* **90**, 012901 (2014).

- [42] O. V. Maslennikov, D. V. Kasatkin, N. F. Rulkov, and V. I. Nekorkin, *Phys. Rev. E* **88**, 042907 (2013).
- [43] O. V. Maslennikov, V. I. Nekorkin, and J. Kurths, *Phys. Rev. E* **92**, 042803 (2015).
- [44] O. V. Maslennikov and V. I. Nekorkin, *Commun. Nonlinear Sci. Numer. Simul.* **23**, 10 (2015).
- [45] V. I. Nekorkin and L. V. Vdovin, *Izv. Vyssh. Uchebn. Zaved. Prikladn. Nelinejn. Din.* **15**, 36 (2007).
- [46] M. Courbage, V. I. Nekorkin, and L. V. Vdovin, *Chaos* **17**, 043109 (2007).
- [47] O. V. Maslennikov and V. I. Nekorkin, *Chaos* **23**, 023129 (2013).
- [48] O. V. Maslennikov and V. I. Nekorkin, Map-based approach to problems of spiking neural network dynamics, in *Nonlinear Dynamics and Complexity*, edited by V. Afraimovich, A. C. J. Luo, and X. Fu (Springer International, Switzerland, 2014), pp. 143–161.
- [49] A. Destexhe and M. Rudolph-Lilith, *Neuronal Noise* (Springer, New York, 2012).
- [50] I. A. Khovanov, A. V. Polovinkin, D. G. Luchinsky, and P. V. E. McClintock, *Phys. Rev. E* **87**, 032116 (2013).
- [51] I. Franović, K. Todorović, M. Perc, N. Vasović, and N. Burić, *Phys. Rev. E* **92**, 062911 (2015).
- [52] L. Arnold, *Random Dynamical Systems* (Springer Verlag, Berlin, 1999).
- [53] J. A. Acebrón, A. R. Bulsara, and W.-J. Rappel, *Phys. Rev. E* **69**, 026202 (2004).
- [54] M. Gaudreault, J. M. Berbert, and J. Viñals, *Phys. Rev. E* **83**, 011903 (2011).
- [55] P. Kaluza, C. Strege, and H. Meyer-Ortmanns, *Phys. Rev. E* **82**, 036104 (2010).
- [56] S. Tanabe and K. Pakdaman, *Phys. Rev. E* **63**, 031911 (2001).
- [57] V. I. Nekorkin and O. V. Maslennikov, *Radiophys. Quantum Electron. (Engl. Transl.)* **54**, 56 (2011).
- [58] M. Courbage, O. V. Maslennikov, and V. I. Nekorkin, *Chaos Soliton. Fract.* **45**, 645 (2012).
- [59] O. V. Maslennikov and V. I. Nekorkin, *Radiophys. Quantum Electron. (Engl. Transl.)* **55**, 198 (2012).
- [60] C. W. Gardiner, *Handbook of Stochastic Methods for Physics, Chemistry and the Natural Sciences*, 3rd ed. (Springer-Verlag, Berlin, 2004).
- [61] *Phase Response Curves in Neuroscience: Theory, Experiment, and Analysis*, edited by N. W. Schultheiss, A. A. Prinz, and R. J. Butera (Springer, New York, 2012).
- [62] P. A. Tass, *Phase Resetting in Medicine and Biology: Stochastic Modeling and Data Analysis* (Springer, Berlin, 2007).
- [63] E. M. Izhikevich, *Dynamical Systems in Neuroscience: The Geometry of Excitability and Bursting* (MIT Press, Cambridge, 2007), Chap. 10.
- [64] C. C. Canavier, *Scholarpedia* **1**, 1332 (2006).



# Dynamics of fault motion in a stochastic spring-slider model with varying neighboring interactions and time-delayed coupling

Srđan Kostić · Nebojša Vasović · Igor Franović ·  
Kristina Todorović · Vladimir Klinshov ·  
Vladimir Nekorkin

Received: 9 December 2015 / Accepted: 13 November 2016  
© Springer Science+Business Media Dordrecht 2016

**Abstract** We examine dynamics of a fault motion by analyzing behavior of a spring-slider model composed of 100 blocks where each block is coupled to a varying number of  $2K$  neighboring units ( $1 \leq 2K \leq N$ ,  $N = 100$ ). Dynamics of such model is studied under the effect of delayed interaction, variable coupling strength and random seismic noise. The qualitative analysis of stability and bifurcations is carried out by deriving an approximate deterministic mean-field model, which is demonstrated to accurately capture the dynamics of the original stochastic system. The primary effect concerns the direct supercritical Andronov–Hopf bifurca-

tion, which underlies transition from equilibrium state to periodic oscillations under the variation of coupling delay. Nevertheless, the impact of delayed interactions is shown to depend on the coupling strength and the friction force. In particular, for loosely coupled blocks and low values of friction, observed system does not exhibit any bifurcation, regardless of the assumed noise amplitude in the expected range of values. It is also suggested that a group of blocks with the largest displacements, which exhibit nearly regular periodic oscillations analogous to coseismic motion for system parameters just above the bifurcation curve, can be treated as a representative of an earthquake hypocenter. In this case, the distribution of event magnitudes, defined as a natural logarithm of a sum of squared displacements, is found to correspond well to periodic (characteristic) earthquake model.

S. Kostić (✉)

Department for Scientific Research and Informatics,  
Institute for Development of Water Resources “Jaroslav Černi”,  
Jaroslava Černog 80, Belgrade 11226, Serbia  
e-mail: srdjan.kostic@jcerni.co.rs

N. Vasović

Department of Applied Mathematics and Informatics,  
Faculty of Mining and Geology, University of Belgrade,  
PO Box 162, Belgrade, Serbia

I. Franović

Scientific Computing Lab, Institute of Physics Belgrade,  
University of Belgrade, Pregrevica 118, Belgrade 11080,  
Serbia

K. Todorović

Department of Mathematics and Physics, Faculty of  
Pharmacy, University of Belgrade, Vojvode Stepe 450,  
Belgrade, Serbia

V. Klinshov · V. Nekorkin

Institute of Applied Physics, Russian Academy of Sciences,  
46 Ulyanov Street, Nizhny Novgorod, Russia

**Keywords** Mean-field approximation · Spring-block model · Seismic noise · Time delay · Coupling strength · Periodic earthquake model

## 1 Introduction

From the purely mechanical viewpoint, the dynamics along an active fault could be described by a stick-slip motion of a spring-slider model complemented by an appropriate rate- and (or) state-dependent friction law [1–4]. For such a setup, a sudden drop of shear strength or an increase in block velocity is inter-

preted as an onset of seismic motion, while the magnitude of an event is defined as a natural logarithm of a superthreshold displacement of a block for a simple mono-block model, or a sum of superthreshold displacements of blocks involved in the event in case of a complex multi-block model [5]. The distribution of magnitudes should follow a power-law behavior, viz. the Gutenberg–Richter law, in order for a spring-block model to simulate the real observed fault dynamics. However, mono-block models [6,7] typically do not generate irregular time series of displacements unless some additional ingredients are introduced, including the friction lag [8], transient acceleration changes [9], the seismic noise or some particular forms of parameter perturbation [10]. Nevertheless, irregular distribution of main events is inherent for multi-block models, where a different number of moving blocks may participate in each event. For instance, De Sousa Vieira [6] considered the dynamics of two- and three-block models, having found that the relevant complex behavior is associated with the emergence of deterministic chaos obtained by fine tuning of control parameters. Similarly, Erickson et al. [11] analyzed the dynamics of a one-dimensional Burridge–Knopoff model, showing that it also exhibits both periodic and chaotic motion, whereby the transition to chaos is size dependent. In the present paper, we also examine the dynamics of a multi-block fault model, under the effect of two additional factors that impact the local block dynamics.

In particular, we assume that the main source of dynamical instability in a spring-block system, corresponding to the onset of seismic activity along a real fault, derives from the delayed interaction between the blocks. Introduction of such a delay has first been suggested by Burridge and Knopoff [1], who discussed this type of interaction in their original model comprised of 10 blocks. In their study, the idea has been that the stress transfer between the first and the last few blocks of the array is mediated by a group of central blocks, involving a time delay of the order of the adopted viscous time constant. In our study, this effect is included by explicitly assuming the delayed interaction between the coupled units.

Apart from the inclusion of time delay, we also investigate the effect of the range of interactions on the fault dynamics. In particular, we consider the cases from the nearest-neighbor interactions up to a globally connected assembly of blocks. The intention is to examine whether and how the range of interactions

influences the scenario of transition to seismic motion. This effect is analyzed in the presence of a background seismic noise, which we assume to be the white noise, the point corroborated by the real observed data [12,13] and the previous studies of stick-slip motion [14].

The considered setup of a spring-block model of a fault motion, which involves the effects of coupling delay, the seismic noise as well as  $2K$  nearest-neighbor interactions, is substantially distinct from the limit case of a single block motion discussed in our previous study [8], or the model involving only the nearest-neighbor interactions [15], used to describe the case of a thin isolated plate subjected to a friction force and driven by a shear force. Some previous studies have considered more complex spatiotemporal interactions of blocks [16–18], but without including the effects of delayed interaction and seismic noise. Our aim is to analyze the stability and bifurcations of the fault dynamics under the effect of the two latter factors. To this end, we shall derive a mean-field approximate model for the collective motion of blocks [19–21].

The paper is organized as follows. In Sect. 2, we describe the model of a fault motion comprised of delay-coupled blocks influenced by seismic noise. We also introduce the mean-field approximation of the system's collective dynamics. In Sect. 3 are presented the results of local bifurcation analysis carried out for the approximate system, together with the comparison with the behavior of the starting stochastic system. Section 4 concerns the analysis of magnitude distribution of main events for a group of blocks with the largest displacements. A summary of our main results and directions for further research are provided in Conclusions.

## 2 Model derivation

We consider a system comprised of  $N$  blocks, whereby each block  $i$  interacts with  $2K$  nearest neighbors. Thus, the fault is represented as a one-dimensional array of blocks where a given block  $i$  is coupled to  $K$  of its neighbors on each side. Local dynamics is given by:

$$\begin{aligned} \dot{u}_i &= v_i \\ \dot{v}_i &= -u_i + \Phi(v_i + v_0) - \Phi(v_0) \\ &\quad + \frac{C}{N} \sum_{j \in J} (u_{i+j}(t - \tau) - u_i) + \sqrt{2D} \xi_i(t), \end{aligned} \quad (1)$$

where  $J$  denotes the set of indices  $J = \{-K, \dots, K\} \setminus \{0\}$ . Interaction is characterized by the coupling strength

$C$  and the delay  $\tau$ , which is assumed to be uniform. Parameter  $v_0$  denotes the pulling velocity of the upper moving plate.  $\xi_i(t)$  are independent Gaussian white noise terms, such that  $\langle \xi_i \rangle = 0$ ,  $\langle \xi_i \xi_j \rangle = \delta_{ij}$  holds. In general, seismic noise may derive from various sources, including small-scale faulting, as well as different irregularities and inhomogeneities, but there may also be random perturbations of undefined origin [22, 23]. Note that coherent noise is hardly expected to occur at seismogenic depth, since it typically arises from the reflection of seismic waves, ground rolls or traffic noise. A detailed background regarding model (1) is provided in “Appendix”.

It has to be emphasized that model (1) represents a one-dimensional array of blocks, where blocks at the end of the array are connected to neighboring blocks only on one side.

One should specify the friction force  $\Phi$ , which is in (1) for simplicity given in general form. We assume that  $\Phi$  conforms to a rate-dependent friction law:

$$\Phi(v) = \mu_0 - a \ln(v), \tag{2}$$

where  $\mu_0$  is a steady-state friction (whose values needs to be adequately chosen so as to secure the proper action of friction force) and  $a$  represents a material property which depends on the temperature and pressure conditions. Such dependence of friction on slip rate is qualitatively supported by the recent laboratory findings [24, 25].

In the absence of coupling delay and seismic noise ( $\tau = 0, D = 0$ ), model (1) has a unique stable equilibrium (for the assumed distance between neighboring blocks in initial position of the order of magnitude  $10^{-5}$ ) given by  $(u_i, v_i) = (0, 0)$ .

In principle, the collective dynamics of the multi-block model can be described by introducing the macroscopic variables  $u = \frac{1}{N} \sum_{i=1}^N u_i$ ,  $v = \frac{1}{N} \sum_{i=1}^N v_i$ . In order to be able to analyze dynamics of the starting stochastic model, we need to derive its deterministic approximation, which will qualitatively describe its dynamics, and which will enable conduction of local bifurcation analysis. The method we apply consists in deriving a deterministic mean-field model [26] for the macroscopic behavior of system (1), whereby the noise intensity features as an additional bifurcation parameter. Within such a framework, the collective dynamics is described in terms of the means, viz. the assembly-averaged displacement  $m_u$  and the average velocity  $m_v$ ,

as well as the associated variances and the covariance. The ensuing mean-field model is amenable to local bifurcation analysis and as such may serve to qualitatively describe the stability and bifurcations of the starting stochastic system.

The detailed derivation of the mean-field model is presented in “Appendix”. As discussed there, the mean-field model may be presented as a system of two delay-differential (deterministic) equations describing the evolution of the means:

$$\begin{aligned} \dot{m}_u(t) &= m_v(t) \\ \dot{m}_v(t) &= -m_u(t) + a \ln(v_0) - a \ln(m_v + v_0) \\ &\quad + \frac{1}{2} \frac{D}{(m_v + v_0)} + \frac{2KC}{N} (m_u(t - \tau) - m_u(t)) \end{aligned} \tag{3}$$

In the next section are provided the results of bifurcation analysis for the model (1), together with a brief discussion on the effects of each of the system parameters. The numerical simulations of the starting stochastic system (1) are carried out for the array of  $N = 100$  blocks using the Runge–Kutta fourth-order algorithm with a time step  $\Delta t = 0.001$ .

### 3 Local bifurcation analysis of the mean-field model

Mean-field model (3) has a unique stable stationary solution  $(m_u, m_v) = (\frac{D}{2v_0}, 0)$ . We have performed the stability and bifurcation analysis of model (3) analytically. In particular, system (3) is linearized around the fixed point by assuming that the deviations are of the form  $\delta m_u(t) = A e^{\lambda t}$ ,  $\delta m_v(t) = B e^{\lambda t}$ ,  $\delta m_u(t - \tau) = A e^{\lambda(t - \tau)}$ . This yields a set of algebraic equations for the coefficients  $A$  and  $B$ , whereby the condition for the existence of a nontrivial solution is given by the characteristic equation:

$$\lambda^2 + \frac{\lambda}{v_0} \left( a + \frac{D}{2v_0} \right) + 1 + \frac{2KC}{N} (1 - e^{-\lambda\tau}) = 0. \tag{4}$$

Bifurcations of the stationary state take place for the parameter values where the roots of characteristic equation cross the imaginary axis. Given that  $\lambda = 0$  is not the solution of (4), we look for the pure imaginary roots of the form  $\lambda = i\omega$ , adopting that  $\omega$  is real and positive. Having substituted for  $\lambda$  in (4), one separates the

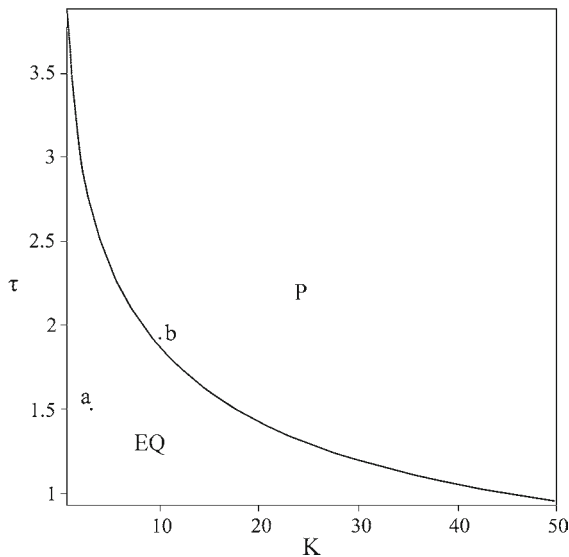


**Fig. 1**  $\tau(K)$  bifurcation curve describing the destabilization of equilibrium in the mean-field model (3) via Andronov–Hopf bifurcation. The remaining system parameters are fixed at  $C = 5$ ,  $D = 0.0001$ ,  $a = 0.1$ ,  $v_0 = 1.2$ . Qualitatively similar diagrams are obtained for other values of  $C$  and  $D$ . *EQ* and *P* denote the equilibrium state and periodic oscillations, respectively. Corresponding time series for mean displacement of systems (1) and (3) at points a and b are provided in Fig. 2

real and the imaginary part and equates them both with zero. After some algebra, we arrive at the expression for the critical coupling delay:

$$\tau = \frac{1}{\omega} \operatorname{arctg} \frac{\frac{\omega}{v_0} \left( a + \frac{D}{2v_0} \right)}{\omega^2 - \left( 1 + \frac{2KC}{N} \right)} \quad (5)$$

Further analysis shows that the mean-field model (3) undergoes Andronov–Hopf bifurcation. Bear in mind that (5) actually defines multiple branches of Hopf bifurcation curves given by  $\tau + j\pi/\omega$ , where  $j = 0, 1, 2, \dots$ . In the present study, we focus only on the first bifurcation curve, since the starting stochastic system (1) above the bifurcation curve exhibits behavior characteristic for strongest earthquakes, as explained further below.

In order to facilitate an easier comparison between the dynamics of the approximate model and the starting stochastic system, which is simulated for  $N = 100$ , we have also fixed  $N = 100$  in (5) and plotted the corresponding  $\tau(K)$  bifurcation curve, see Fig. 1. Naturally, the relevant range of  $K$  values is then  $K \in [1, 50]$ . Also note that the analysis here is confined to values

of coupling delay which are of the order of the oscillation period for the mean-field model (3) just above the bifurcation curve ( $T \approx 3.5$ ).

Qualitative validity of the above results is verified numerically by demonstrating that the starting stochastic system (1) and the mean-field model (3) exhibit qualitatively analogous dynamics, see Fig. 2. From Fig. 2, one may infer that the mean-field model in qualitative sense accurately reproduces the collective behavior of the original model (1). An important point is that we also find a quantitative agreement between the dynamics of the two systems in a sense that the respective oscillation frequencies of the starting stochastic and the approximate system above the bifurcation curve are quite closely matched. The difference in respective amplitudes of periodic motion is negligible, considering the fact that matching of the amplitudes could be found only in cases where the behavior of the mean-field model exhibits similar displacements as the original model comprised of a large number of individual blocks. It could be easily shown that such an outcome can be expected for the multi-block model made up of blocks coupled in the all-to-all fashion.

As shown in Fig. 1, our analysis indicates the occurrence of a supercritical Andronov–Hopf bifurcation from equilibrium state to periodic motion, which is induced by increasing the time delay in interaction among the coupled blocks. For relatively high values of  $\tau$ , bifurcation can arise even in case of very small range of interactions ( $K = 3$ ). Nonetheless, the results obtained also imply that the bifurcation may occur by increasing the number of interacting blocks for a constant value of coupling delay. From the seismological viewpoint, this means that onset of seismic motion could be induced solely by enlarging the active length of a seismogenic fault, provided there is a delayed interaction among different fault segments.

Results shown in Fig. 1 also imply that there is no bifurcation for time delay  $\tau < 0.9$ . In this case, system (1) remains in equilibrium state under increase in  $K$ , viz. coupling more blocks together does not lead to the emergence of the oscillations. From the seismological viewpoint, this means that effect of delayed interaction is essential for occurrence of periodic oscillations, i.e., seismic regime, which will be verified in the subsequent section.

Another interesting point is that for the case when block is coupled only to its nearest neighbors ( $K = 1$ ), there is no bifurcation with the increase in time delay.

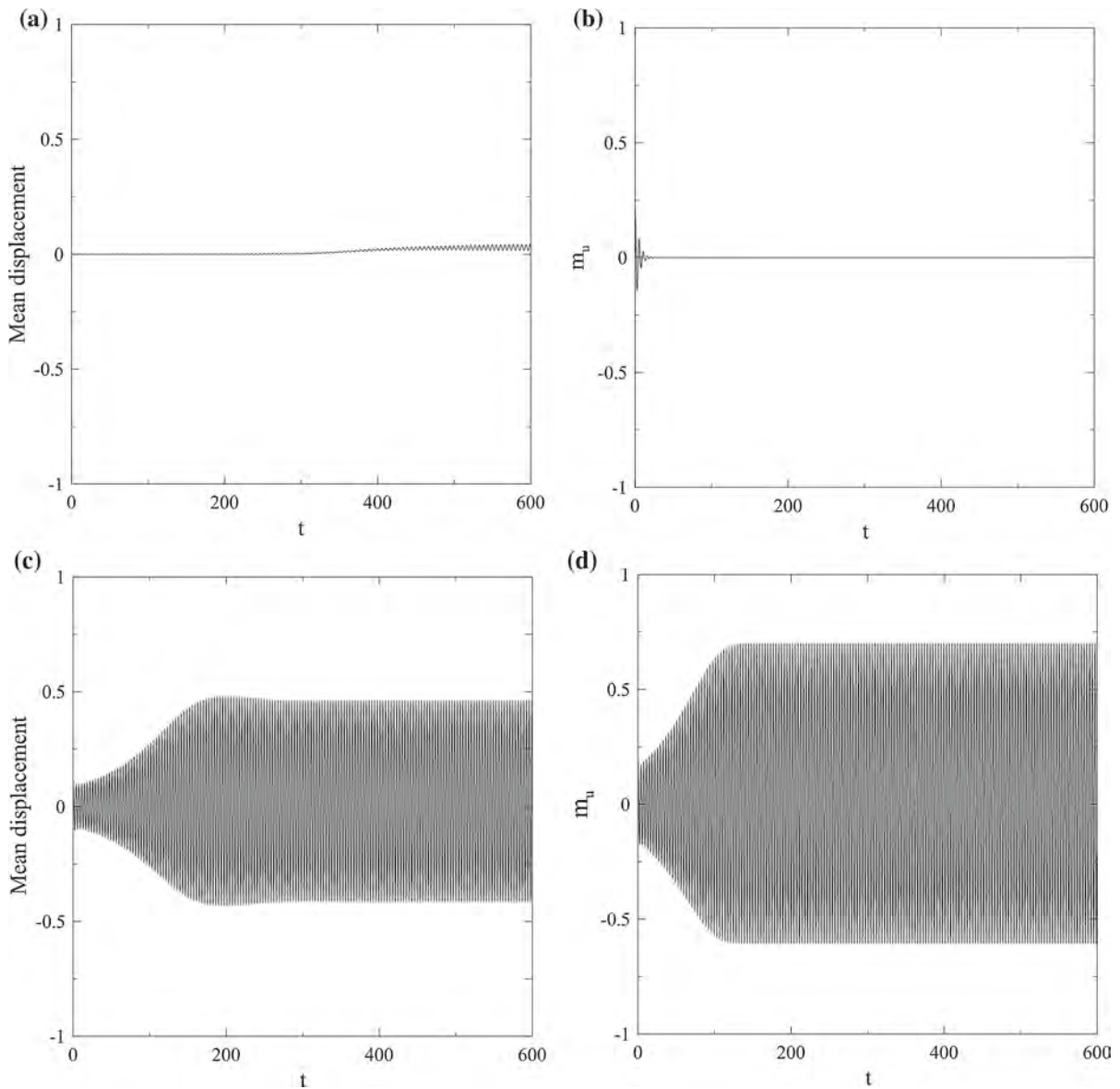


**Fig. 2** Qualitative analogy between the dynamics of the starting stochastic system and the mean-field approximated model. The *left column* shows the time series of mean displacements of blocks for the starting stochastic system, whereas the *right column* refers to the approximated system. The top (*bottom*) row is obtained for parameter values corresponding to point a (point b) in Fig. 1. Initial conditions are set in vicinity of the equi-

librium point. Equilibrium state is illustrated for  $\tau = 1.5$  and  $K = 3$ , while periodic oscillations are illustrated for  $\tau = 1.92$  and  $K = 10$ . Qualitatively similar diagrams of periodic oscillations are obtained for other values of  $K$  and  $\tau$  just above the bifurcation curve. The remaining parameters are fixed at  $C = 5$ ,  $D = 0.0001$ ,  $a = 0.1$ ,  $v_0 = 1.2$

Hence, it turns out that for such simple models, the effect of delayed interaction is negligible.

One should note that previous analysis is conducted for the constant values of parameters  $C$ ,  $D$  and  $a$ . Given

the fact that these parameters could significantly affect the dynamics of fault motion, it is of special interest to analyze how the dynamics of the original system changes under their variation.

### 3.1 Effect of seismic noise

Effect of seismic noise on dynamics of system (1) is negligible for the range of values relevant from the seismological viewpoint, i.e., the common ratio of coseismic slip rate versus seismic noise is in the range  $10^{-2}$ – $10^{-7}$ . Nonetheless, in the context of investigating the noise effects, we have further examined the possibility for the occurrence of stochastic bifurcation in system (1), which conforms to the scenario where the transition to oscillatory motion is induced by increasing the noise intensity.

However, having examined the average amplitudes of a sufficient number of realizations of system (1) below and above the bifurcation curve, we have observed no significant change for values of seismic noise up to 0.1. Thus, the qualitative impact of noise on system dynamics can be considered secondary to that of coupling delay. Also, for relatively high values of seismic noise and for small  $K$ , introduction and increase in time delay does not give rise to bifurcation. In other words, noise may then suppress the onset of the periodic oscillations. For instance, if the level of seismic noise is  $D = 1$ , while the other parameters are fixed as shown in Fig. 1, at least  $K = 6$  is required for the Andronov–Hopf bifurcation to emerge by increasing the time delay. However, from a seismological viewpoint, such a case cannot be expected in real conditions in Earth’s crust, so these phenomena could be interesting solely from the theoretical viewpoint.

### 3.2 Effect of coupling strength

In qualitative terms, the impact of coupling strength  $C$  on dynamics of a spring-block model with time delay is similar to the effect of  $K$ . In particular, bifurcation in the starting stochastic system (1) occurs solely by increasing the coupling strength provided there is interaction delay between the units, see Fig. 3. Also, in analogy with the effect of  $K$ , one finds a delay threshold below which the increase in coupling strength does not induce any dynamical change. Nevertheless, for smaller values of  $C$ , increase of time delay may or may not induce bifurcation, depending on the particular  $K$  value. In other words, for small  $C$ , there exists a threshold  $K$  value below which increase in  $\tau$  cannot give rise to Andronov–Hopf bifurcation. For instance,

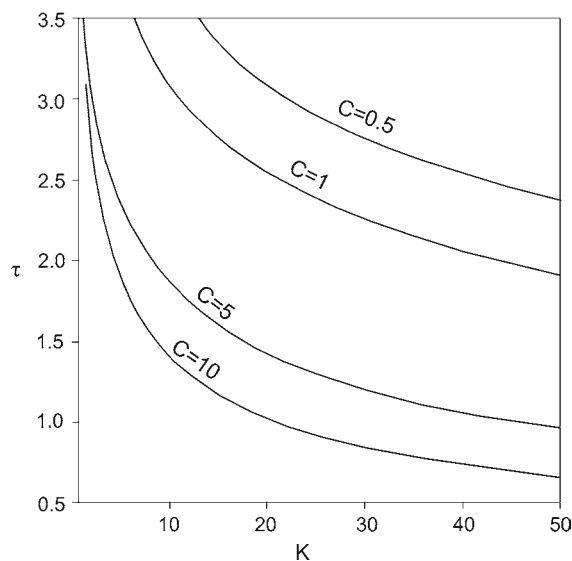


**Fig. 3** Family of  $\tau(K)$  Andronov–Hopf bifurcation curves of the mean-field model (3) for different values of coupling strength  $C$ . The remaining parameters are held constant at  $D = 0.0001$ ,  $a = 0.1$ ,  $v_0 = 1.2$ . Qualitatively similar diagrams are obtained for other values of friction parameter  $a$

when  $C = 0.5$ , each block has to be coupled with at least 15 blocks on each side in order for the system to undergo the Andronov–Hopf bifurcation with the increase in  $\tau$ .

### 3.3 Effect of friction

From the seismological viewpoint, it is interesting to analyze the effect of friction parameter  $a$  on the dynamics of system (1). The results obtained indicate the occurrence of an inverse supercritical Andronov–Hopf bifurcation, induced solely by decreasing the friction (Fig. 4). Such a change of friction is expected in real conditions, because friction usually decreases with the increase in fault motion velocity. Moreover, this suggests that for the fault in equilibrium state, a reduction of friction along the fault zone due to effect of pore water or similar may give rise to bifurcation, provided there are delayed interactions among different parts of a fault, i.e., different fault segments.

## 4 Distribution of main events

The results obtained indicate a transition from equilibrium state to periodic motion may arise by increasing

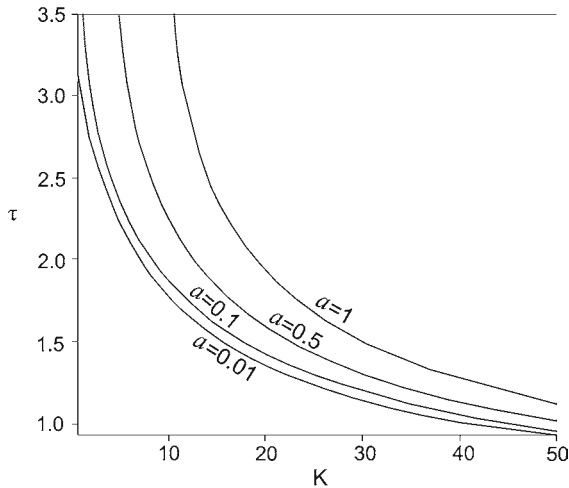


**Fig. 4** Family of  $\tau(K)$  Andronov–Hopf bifurcation curves describing the destabilization of equilibrium of the mean-field model for different values of friction parameter  $a$ . The remaining parameters are fixed at  $D = 0.0001$ ,  $C = 5$ ,  $v_0 = 1.2$ . Qualitatively similar diagrams are obtained for other values of  $C$

the time delay, or due to increase in coupling strength and/or decrease in friction force under the condition that there exists a coupling delay. From the purely seismological viewpoint, if we relate magnitude of a seismic event to displacement of system (1), it appears that regular periodic motion could not be considered as an example of a realistic scenario given that the sequence of earthquakes should obey power-law behavior. In particular, a necessary condition for the Gutenberg–Richter scaling law to be satisfied is that the sequence of seismic events is irregular. Such a dynamical regime could emerge due to effect of seismic noise or the co-effect of seismic noise and some global attractor when the system is near the bifurcation curve, but still in the equilibrium state [27]. However, the results of our analysis here indicate that the sole effect of seismic noise is insufficient to generate high-amplitude irregular oscillations (higher than the noise level, at least). Nonetheless, we have also found no global attractor for different values of initial conditions away from the equilibrium point. In light of these arguments, the interpretation of the results so far requires additional attention. In particular, a better understanding of the relation to actually observed behavior of the real faults may be gained by looking into the dynamics of a group of coupled blocks with the largest displacements in the considered array (1). This group of blocks we take to

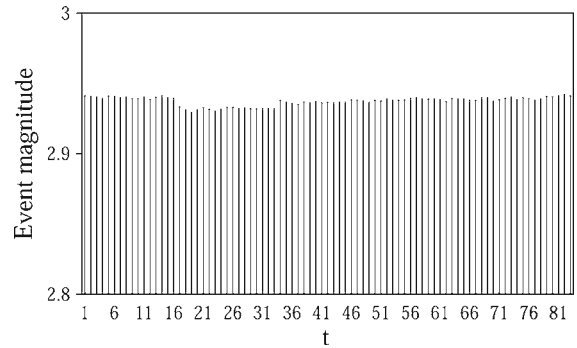


**Fig. 5** Time series of displacement sums for a group of blocks with the largest displacements in the starting stochastic system (1). Initial conditions are set near the equilibrium point. The parameter values are fixed at  $\tau = 1.92$ ,  $K = 10$ ,  $C = 5$ ,  $D = 0.0001$ ,  $a = 0.1$ ,  $v_0 = 1.2$

correspond to a hypocenter of a seismic event. In the present case, magnitude of such an event  $M$  is defined as a natural logarithm of a sum of squares of displacements  $u_i$ :

$$M = \ln \left( \sum_{i=1}^N (u_i)^2 \right) \quad (6)$$

where  $N$  is the number of coupled blocks with the largest displacements in system (1). This definition is similar to the proposal of Kawamura et al. [5], but with a small change regarding the fashion in which the displacement sum is calculated. In particular, we take the sum of squared displacement for each block as a measure of accumulated potential energy released during a single event. This way of calculating the stored potential energy corresponds to our initial assumption on elastic springs connecting the blocks in system (1).

In Fig. 5 is shown the regular sequence of displacement sums for a group of blocks with the largest displacements. Analysis is conducted for the state of system (1) just above the bifurcation curve, as shown in Fig. 2c. These events are regularly spaced, with approximately the same magnitude. Therefore, the proposed model (1) can be regarded as a periodic or characteristic earthquake model [28,29], which has already been observed in the real conditions in the Earth's crust. Indeed, the occurrence of earthquakes with the largest magnitudes along Nankai megathrust or Parkfield section of the San Andreas fault is considered to be nearly periodic [30].

## 5 Conclusions

The main goal of the present study has been to examine the possibility of inducing seismic motion along the real fault in case where fault segments of different sizes are active, under the assumption of a delayed interaction between the fault constituents, and including the impact of background seismic noise. The stability analysis, as well as the qualitative analysis of bifurcations exhibited by the given fault model, is carried out by considering the appropriate mean-field model. In particular, beginning from the original system of  $2N$  coupled stochastic delay-differential equations, we have derived a system comprised of only of two deterministic delay-differential equations for the approximate system.

The dynamics of the starting stochastic and the approximate model are demonstrated to be qualitatively similar. Another important point concerns the quantitative agreement between the two systems, in a sense that the oscillation frequency of the mean-field model matches quite closely the one observed for the stochastic system. Nevertheless, the oscillation amplitudes are the same only in case of globally coupled blocks in the starting stochastic system (1). In other instances, corresponding to smaller  $K$ , the amplitudes of the mean-field model may be up to 1.5 times higher than the amplitudes of periodic oscillations in the system (1), which does not have significant impact on our results from the viewpoint of seismology. In particular, we are only interested in type of oscillations (regular or irregular), while their amplitude is irrelevant, since the models is dimensionless; hence, there is no direct analogy with the real observed earthquake data.

Results of our research indicate that the onset of the oscillations in the starting stochastic system (1), which is shown to qualitatively reflect the seismic motion, can be characterized by the direct supercritical Andronov–Hopf bifurcation of the mean-field model. In the present study, we have focused only on the first bifurcation curve, describing the destabilization of equilibrium, whereas the relevant values of coupling delay have been determined according to the oscillation period of system (1) just above the bifurcation curve.

Regarding the individual effect of the introduced parameters, the main finding is that the transition in system (1) from equilibrium state to periodic oscillations is primarily affected by the coupling delay. However, the impact of the delayed interactions is found to strongly depend on the coupling strength. In particular,

in case of "weak" coupling, the increase in interaction delay cannot generate the transition to limit cycle. In other words, the model comprised of loosely coupled blocks cannot exhibit complex dynamics. A similar effect, though less expressed, is observed for the impact of friction. In particular, for lower values of friction, system (1) can exhibit the transition from equilibrium state to periodic motion for smaller  $K$ . As for the effect of seismic noise, the results obtained imply a less significant role in the dynamics of system (1) for the values consistent with the real observed data (ratio of seismic noise to velocity should be smaller than  $10^{-2}$ ). The impact of strong seismic noise (e.g.,  $D \approx 1.0$ ) is similar to the effect of high values of coupling strength and friction. Apparently, for such a large seismic noise, there is a certain  $K$  threshold above which the system can exhibit Andronov–Hopf bifurcation by increasing the coupling delay.

From the seismological perspective, an important point is that we propose a new definition of an earthquake magnitude for the considered class of spring-block models. In particular, we define magnitude of an event as a natural logarithm of sum of squared displacements for a group of blocks with the largest displacements. Our results indicate that these sequences of events are regular, whereby the distribution of the number of events in dependence of their magnitude corresponds to the occurrence of the strongest (characteristic) earthquakes, as the ones recorded along the Nankai megathrust or Parkfield section of San Andreas fault.

By analyzing dynamics of the group of blocks with largest displacements, we partially captured local dynamics of the real model, which also turned out to be regular, similarly to the mean displacement of the whole array of blocks. Significant deviation from the regular periodic oscillations could be expected for the blocks at the end of the array, which are only coupled to blocks at one side of the "chain." However, dynamics of these blocks is irrelevant from the viewpoint of seismology, since their displacements are quite low and are not connected directly to the earthquake "hypo-center" (i.e., to the group of blocks with the largest displacements).

Though the present analysis provides a clear insight on the role of delayed interaction, seismic noise and coupling strength on the collective dynamics of the multi-block fault model, one should still note that the friction law (2) is assumed in a simplified way, neglecting the potential impact of the state of the contact surface. Moreover, we have analyzed only the case of



a one-dimensional spring-slider model, while in real conditions the fault motion represents a spatiotemporal problem, the point which certainly has to be addressed in future research.

**Acknowledgements** This research has been supported by the Ministry of Education, Science and Technological development of the Republic of Serbia, Contracts No. 176016 and 171017, by the Russian Foundation for Basic research under grants No. 14-02-00042, 15-02-04245 and 15-32-50402, and by the Ministry of Education and Science of the Russian Federation, Agreement No. MK-8460.2016.2.

**Appendix: Model of local block dynamics**

Present research on earthquake fault motion is based on the analysis of a non-dimensional mono-block model, introduced in [6]:

$$\ddot{U}(t) = -U(t) + \Phi(\dot{U}(t)) + v_0 t, \tag{7}$$

where variable  $U$  represents the block displacement,  $\dot{U}$  is the velocity of the block (defined in the standing reference frame),  $\ddot{U}$  is the block acceleration,  $v_0$  is the dimensionless pulling speed and  $t$  is time variable. Friction force  $\Phi$  is assumed to be rate dependent. The unstable equilibrium around which the orbit of a block moves in phase space is given by:

$$U_e(t) = v_0 t + \Phi(v), \tag{8}$$

which is determined by setting  $\ddot{U} = 0$  and  $\dot{U} = v_0$  in (7).

By introducing  $U_1$  and  $U_2$  to denote the displacement and the velocity of a single block, (7) may be rewritten as

$$\begin{aligned} \dot{U}_1(t) &= U_2(t) \\ \dot{U}_2(t) &= -U_1(t) + \Phi(U_2(t)) + v_0 t. \end{aligned} \tag{9}$$

Having applied the coordinate transformation:

$$\begin{aligned} U_{1new}(t) &= U_1 - U_e(t) = U_1(t) - (v_0 t + \Phi(v)), \\ U_{2new}(t) &= U_2(t) - v_0, \end{aligned} \tag{10}$$

and switching back to old notation, one arrives at the following system of equations for the dynamics of a single block:

$$\begin{aligned} \dot{U}_1(t) &= U_2(t) \\ \dot{U}_2(t) &= -U_1(t) + \Phi(U_2(t) + v_0) - \Phi(v_0). \end{aligned} \tag{11}$$

Beginning from (11), one can derive the spring-slider model for  $N$  interconnected blocks given by the system (1) in the main text, cf. Sect. Model derivation.

Derivation of the mean-field approximated model

The mean-field model characterizes the system’s behavior in terms of the means:

$$m_u = \langle u_i \rangle = \frac{1}{N} \sum_i u_i, \quad m_v = \langle v_i \rangle = \sum_i v_i, \tag{12}$$

the associated variances:

$$\begin{aligned} s_u &= \langle \delta u_i^2 \rangle = \langle (u_i - m_u)^2 \rangle = \langle u_i^2 \rangle - m_u^2 \\ s_v &= \langle \delta v_i^2 \rangle = \langle (v_i - m_v)^2 \rangle = \langle v_i^2 \rangle - m_v^2 \end{aligned} \tag{13}$$

and the covariance

$$\begin{aligned} U &= \langle \delta u_i \delta v_i \rangle = \langle (u_i - m_u)(v_i - m_v) \rangle \\ &= \langle u_i v_i \rangle - m_u m_v. \end{aligned} \tag{14}$$

Equations for the evolution of the means may be derived as follows:

$$\begin{aligned} \dot{m}_u &= \frac{1}{N} \sum_i \dot{u}_i = \frac{1}{N} \sum_i v_i = m_v \\ \dot{m}_v &= \frac{1}{N} \sum_i \dot{v}_i \\ &= \frac{1}{N} \sum_i \left\{ -u_i - \Phi(v_0) + \Phi(v_i + v_0) \right. \\ &\quad \left. + \frac{C}{N} \sum_{j \in J} (u_{i+j}(t - \tau) - u_i) + \sqrt{2D} \xi_i(t) \right\} \\ &= -m_u - \Phi(v_0) + \frac{1}{N} \sum_i \Phi(v_i + v_0) \\ &\quad + \frac{1}{N} \sum_i \frac{C}{N} \sum_{j \in J} (u_{i+j}(t - \tau) - u_i). \end{aligned} \tag{15}$$

The third term in equation (15) may be evaluated as follows. In the limit of large  $N$ , one may replace the summation by an appropriate integral  $\frac{1}{N} \sum_i \Phi(v_i + v_0) \rightarrow \int P(v) \Phi(v + v_0) dv$ , where  $P(v)$  is the probability density function. Now if all  $v$  variables are

appropriately Gaussian distributed around  $m_v(t)$ , then  $\Phi(v + v_0)$  may be written as  $\Phi(v + v_0) \approx \Phi(m_v + v_0) + \Phi'(m_v + v_0) \delta v + \frac{1}{2} \Phi''(m_v + v_0) (\delta v)^2$ . In the latter expression,  $\delta v$  denotes the deviation  $\delta v = v - m_v$ . The integral may then be estimated as:

$$\begin{aligned} & \int P(v) \Phi(v + v_0) dv \\ &= \Phi(m_v + v_0) \int P(v) dv + \Phi'(m_v + v_0) \\ & \quad \int P(v) \delta v dv + \frac{1}{2} \Phi''(m_v + v_0) \int P(v) \delta v^2 dv \\ &= \Phi(m_v + v_0) + \frac{1}{2} \Phi''(m_v + v_0) S_v \end{aligned} \quad (16)$$

since, by definition  $\int P(v) dv \equiv 1$ ,  $\int P(v) (v - \langle v \rangle) dv = \langle v \rangle - \langle v \rangle = 0$  and  $\int P(v) (v - \langle v \rangle)^2 dv \equiv S_v$ .

The fourth term in (15) can be handled as follows:

$$\begin{aligned} & \frac{1}{N} \sum_i \frac{C}{N} \sum_{j \in J} (u_{i+j}(t - \tau) - u_i(t)) \\ &= \left\langle \frac{C}{N} \sum_{j \in J} (u_{i+j}(t - \tau) - u_i(t)) \right\rangle \\ &= \frac{2KC}{N} (\langle u_i(t - \tau) \rangle - \langle u_i(t) \rangle) = \\ &= \frac{2KC}{N} (m_u(t - \tau) - m_u(t)). \end{aligned} \quad (17)$$

Proceeding from (15), one then obtains:

$$\begin{aligned} \dot{m}_v &= -m_u - \Phi(v_0) + \Phi(m_v + v_0) \\ & \quad + \frac{1}{2} \Phi''(m_v + v_0) S_v \\ & \quad + \frac{2KC}{N} (m_u(t - \tau) - m_u(t)). \end{aligned} \quad (18)$$

Let us now determine the equations for the dynamics of the variances. From the definition of  $S_u$ , it follows that

$$\begin{aligned} \dot{S}_u &= \langle 2u_i \dot{u}_i \rangle - 2m_u \dot{m}_u = \langle 2u_i v_i \rangle - 2m_u m_v \\ &= 2(U + m_u m_v) - 2m_u m_v = 2U \end{aligned} \quad (19)$$

For  $S_v$ , one finds:

$$\begin{aligned} \dot{S}_v &= \langle 2v_i \dot{v}_i + 2D \rangle - 2m_v \dot{m}_v = \left\langle 2v_i \left( -u_i \right. \right. \\ & \quad \left. \left. - \Phi(v_0) + \Phi(v_i + v_0) \right) \right\rangle \end{aligned}$$

$$\begin{aligned} & \left. + \frac{C}{N} \sum_{j \in J} (u_{i+j}(t - \tau) - u_i) \right\rangle \\ &= -2m_v (-m_u - \Phi(v_0) + \Phi(m_v + v_0) \\ & \quad + \frac{1}{2} \Phi''(m_v + v_0) S_v + \frac{2KC}{N} (m_u(t - \tau) \\ & \quad - m_u(t))) + 2D = -2(U + m_u m_v) \\ & \quad - 2m_v \Phi(v_0) + 2 \langle v_i \Phi(v_i + v_0) \rangle \\ & \quad + \frac{2C}{N} \left\langle v_i \sum_{j \in J} (u_{i+j}(t - \tau) - u_i) \right\rangle \\ & \quad + 2m_u m_v + 2m_v \Phi(v_0) - 2m_v \Phi(m_v + v_0) \\ & \quad - m_v \Phi''(m_v + v_0) S_v - 2m_v \frac{2KC}{N} (m_u(t - \tau) \\ & \quad - m_u(t)) + 2D, \end{aligned} \quad (20)$$

where the term  $\langle 2v_i \dot{v}_i + 2D \rangle$  presents the Itô derivative for the complex function  $v_i^2$  of the stochastic variable  $v_i$ .

The third term in (20) can be estimated in a fashion similar to the second term in (15). In particular, one may write:

$$\begin{aligned} 2 \langle v_i \Phi(v_i + v_0) \rangle &= 2 \langle (m_v + \delta v_i) (\Phi(m_v + v_0) \\ & \quad + \Phi'(m_v + v_0) \delta v_i + \frac{1}{2} \Phi''(m_v + v_0) \delta v_i^2) \rangle \\ &= 2 \langle m_v \Phi(m_v + v_0) + m_v \Phi'(m_v + v_0) \delta v_i \\ & \quad + \frac{1}{2} m_v \Phi''(m_v + v_0) \delta v_i^2 \\ & \quad + \Phi(m_v + v_0) \delta v_i + \Phi'(m_v + v_0) \delta v_i^2 \rangle \\ &= 2 \left( m_v \Phi(m_v + v_0) + \frac{1}{2} m_v \Phi''(m_v + v_0) S_v \right. \\ & \quad \left. + \Phi'(m_v + v_0) S_v \right). \end{aligned} \quad (21)$$

Given that the deviations from the mean are expected to be small, we keep only the terms up to second order in deviations. Also,  $\int m_v \Phi'(m_v) (v - \langle v \rangle) P(v) dv = m_v \Phi'(m_v) (\langle v \rangle - \langle v \rangle) = 0$ .

The fourth term in (20) can be calculated by implementing the quasi-independence approximation:

$$\begin{aligned} & \frac{2C}{N} \left\langle v_i \sum_{j \in J} (u_{i+j}(t - \tau) - u_i) \right\rangle \\ &= \frac{2C}{N} \left\langle \sum_{j \in J} (v_i u_{i+j}(t - \tau) - v_i u_i) \right\rangle \end{aligned}$$

$$\begin{aligned}
 &= \frac{2C}{N} \sum_{j \in J} \langle v_i u_{i+j}(t - \tau) \rangle - \frac{4KC}{N} \langle u_i v_i \rangle \\
 &= \frac{2C}{N} \sum_{j \in J} \langle v_i \rangle \langle u_{i+j}(t - \tau) \rangle \\
 &\quad - \frac{4KC}{N} (U + m_u m_v) \\
 &= \frac{4KC}{N} m_v m_u (t - \tau) - \frac{4KC}{N} (U + m_u m_v). \quad (22)
 \end{aligned}$$

From the strict mathematical viewpoint, one should note that  $\langle v_i(t) u_{i+j}(t - \tau) \rangle = \langle v_i(t) \rangle \langle u_{i+j}(t - \tau) \rangle$  holds only for very large  $\tau$ . This assumption is justified in the present case, since, according to Burridge and Knopoff [1], time delay between the neighboring group of seismically active elements (blocks) should be two orders of magnitude smaller than corresponding time constant for the moving blocks. On the contrary, in the present study, we examine the effect of time delay up to value of  $\tau = 3.5$ , i.e., of the order of the oscillation period for the mean-field model (3) just above the bifurcation curve ( $T \approx 3.5$ ), which is considered to correspond to seismic regime of large events, as previously discussed in Sect. 4.

Inserting (21) and (22) into (20), one arrives at:

$$\dot{S}_v = -2U \left( 1 + \frac{2KC}{N} \right) + 2\Phi'(m_v + v_0) S_v + 2D \quad (23)$$

The equation for the dynamics of the covariance can be obtained as follows:

$$\begin{aligned}
 \dot{U} &= \langle \dot{u}_i v_i \rangle + \langle u_i \dot{v}_i \rangle - \dot{m}_u m_v - m_u \dot{m}_v \\
 &= \langle v_i^2 \rangle + \left\langle u_i \left( -u_i - \Phi(v_0) + \Phi(v_i + v_0) \right. \right. \\
 &\quad \left. \left. + \frac{C}{N} \sum_{j \in J} (u_{i+j}(t - \tau) - u_i) + \sqrt{2D} \xi_i(t) \right) \right\rangle \\
 &\quad - m_v^2 - m_u (-m_u - \Phi(v_0) + \Phi(m_v + v_0)) \\
 &\quad + \frac{1}{2} \Phi''(m_v + v_0) S_v + \frac{2KC}{N} (m_u (t - \tau) \\
 &\quad - m_u(t)) \quad (24)
 \end{aligned}$$

The two terms that have to be considered more carefully are  $\langle u_i \Phi(v_i + v_0) \rangle$  and  $\frac{C}{N} \left\langle u_i \sum_{j \in J} (u_{i+j}(t - \tau) - u_i) \right\rangle$ . As for the former, one may write:

$$\begin{aligned}
 \langle u_i \Phi(v_i + v_0) \rangle &= \left\langle (m_u + \delta u_i) \left( \Phi(m_v + v_0) \right. \right. \\
 &\quad \left. \left. + \Phi'(m_v + v_0) \delta v_i + \frac{1}{2} \Phi''(m_v + v_0) \delta v_i^2 \right) \right\rangle \\
 &= \left\langle m_u \Phi(m_v + v_0) + m_u \Phi'(m_v + v_0) \delta v_i \right. \\
 &\quad \left. + \frac{1}{2} m_u \Phi''(m_v + v_0) \delta v_i^2 \right\rangle + \\
 &\quad + \left\langle \Phi(m_v + v_0) \delta u_i + \Phi'(m_v + v_0) \delta u_i \delta v_i \right. \\
 &\quad \left. + \frac{1}{2} \Phi''(m_v) \delta u_i \delta v_i^2 \right\rangle. \quad (25)
 \end{aligned}$$

In analogy to (21), one has  $\langle m_u \Phi'(m_v + v_0) \delta v_i \rangle = 0$  and  $\langle \Phi(m_v + v_0) \delta u_i \rangle = 0$ , whereas the last term in (25) is assumed to be 0 because we keep only the terms up to second order in deviations.

As for the fifth term in (25), one arrives at  $\langle \Phi'(m_v + v_0) \delta u_i \delta v_i \rangle = \Phi'(m_v + v_0) \langle \delta u_i \delta v_i \rangle = \Phi'(m_v + v_0) \langle (u_i - m_u)(v_i - m_v) \rangle \equiv \Phi'(m_v + v_0) U$ .

Hence, continuing from (25):

$$\begin{aligned}
 \langle u_i \Phi(v_i + v_0) \rangle &= m_u \Phi(m_v + v_0) \\
 &\quad + \frac{1}{2} m_u \Phi''(m_v + v_0) S_v + \Phi'(m_v + v_0) U \quad (26)
 \end{aligned}$$

As for  $\frac{C}{N} \left\langle u_i \sum_{j \in J} (u_{i+j}(t - \tau) - u_i) \right\rangle$ , one may write:

$$\begin{aligned}
 \frac{C}{N} \sum_{j \in J} \langle u_i(t) u_{i+j}(t - \tau) \rangle - \frac{C}{N} \sum_{j \in J} \langle u_i^2 \rangle \\
 &= \frac{C}{N} \sum_{j \in J} \langle u_i \rangle \langle u_{i+j}(t - \tau) \rangle - \frac{2KC}{N} (S_u + m_u^2) \\
 &= \frac{2KC}{N} m_u m_u (t - \tau) - \frac{2KC}{N} (S_u + m_u^2). \quad (27)
 \end{aligned}$$

Finally, proceeding from (24) and incorporating (26) and (27), one obtains:

$$\dot{U} = S_v - S_u \left( 1 + \frac{2KC}{N} \right) + \Phi'(m_v + v_0) U \quad (28)$$

Summarizing all the results so far, the mean-field model for collective dynamics of  $N$  blocks with  $2K$  nearest-neighbor interactions reads:

$$\begin{aligned}
\dot{m}_u &= m_v \\
\dot{m}_v &= -m_u - \Phi(v_0) + \Phi(m_v + v_0) \\
&\quad + \frac{1}{2}\Phi''(m_v + v_0)S_v + \frac{2KC}{N}(m_u(t-\tau) - m_u) \\
\dot{S}_u &= 2U \\
\dot{S}_v &= -2U \left(1 + \frac{2KC}{N}\right) + 2\Phi'(m_v + v_0)S_v + 2D \\
\dot{U} &= S_v - S_u \left(1 + \frac{2KC}{N}\right) + \Phi'(m_v + v_0)U \quad (29)
\end{aligned}$$

In order for these equations to describe a self-consistent system, it is required that the values of variances at the stationary state are nonnegative. This is clearly fulfilled given that  $S_v^{stac} = -\frac{D}{\Phi'(m_v+v_0)}|_{m_v=0} = \frac{Dv_0}{a} \geq 0$  always holds and  $S_u^{stac} = \frac{S_v^{stac}}{1+\frac{2KC}{N}}$ .

System (29) could be further simplified by taking into account only the mean values of displacement and velocity, i.e., by assuming that  $\dot{S}_u(t) = \dot{S}_v(t) = \dot{U}(t) = 0$ . Such an assumption is justified considering very small deviations from the mean displacement and velocity. In other words, changes of mean displacement and velocity are one order of magnitude higher than changes of corresponding variances and covariance. Hence, the variances and the covariance can be replaced by their stationary values. After this, we finally arrive at the following equations for the mean-field approximated model:

$$\begin{aligned}
\dot{m}_u(t) &= m_v(t) \\
\dot{m}_v(t) &= -m_u(t) + a \ln(v_0) - a \ln(m_v + v_0) \\
&\quad + \frac{1}{2} \frac{D}{(m_v + v_0)} + \frac{2KC}{N} (m_u(t-\tau) - m_u(t)) \quad (30)
\end{aligned}$$

The final form of (30) with included rate-dependent friction term is given in the main text as system (3), whereby the friction law is specified by Eq. (2).

## References

- Burridge, R., Knopoff, L.: Model and theoretical seismicity. *Bull. Seismol. Soc. Am.* **57**, 341–371 (1967)
- Dieterich, J.H.: Modeling of rock friction: 1. Experimental results and constitutive equations. *J. Geophys. Res.* **84**, 2161–2168 (1979)
- Ruina, A.: Slip instability and state variable friction laws. *J. Geophys. Res.* **88**(B12), 10359–10370 (1983)
- Carlson, J., Langer, J.: Mechanical model of an earthquake fault. *Phys. Rev. A* **40**, 6470–6484 (1989)
- Kawamura, H., Hatano, T., Kato, N., Biswas, S., Chakrabarti, B.K.: Statistical physics of fracture, friction, and earthquakes. *Rev. Mod. Phys.* **84**(2), 839–884 (2012)
- De Sousa Vieira, M.: Chaos and synchronized chaos in an earthquake model. *Phys. Rev. Lett.* **82**, 201–204 (1999)
- Erickson, B., Birmir, B., Lavallee, D.: A model for aperiodicity in earthquakes. *Nonlinear Process. Geophys.* **15**, 1–12 (2008)
- Kostić, S., Franović, I., Todorović, K., Vasović, N.: Friction memory effect in complex dynamics of earthquake model. *Nonlinear Dyn.* **73**(3), 1933–1943 (2013)
- Kostić, S., Franović, I., Perc, M., Vasović, N., Todorović, K.: Triggered dynamics in a model of different fault creep regimes. *Sci. Rep.* **4**, 5401 (2014)
- Kostić, S., Vasović, N., Franović, I., Todorović, K.: Dynamics of simple earthquake model with time delay and variation of friction strength. *Nonlinear Process. Geophys.* **20**, 857–865 (2013)
- Erickson, B.A., Birmir, B., Lavallée, D.: Periodicity, chaos and localization in a Burridge–Knopoff model of an earthquake with rate-and-state friction. *Geophys. J. Int.* **187**, 178–198 (2011)
- Goudarzi, A., Riahi, M.A.: Seismic coherent and random noise attenuation using the undecimated discrete wavelet transform method with WDGA technique. *J. Geophys. Eng.* **9**, 619–631 (2012)
- Chiu, S.K.: Coherent and random noise attenuation via multichannel singular spectrum analysis in the randomized domain. *Geophys. Prospect.* **61**, 1–9 (2013)
- Pomeau, Y., Le Berre, M.: Critical speed-up versus critical slow-down: a new kind of relaxation oscillation with application to stick-slip phenomena. [arXiv:1107.3331v1](https://arxiv.org/abs/1107.3331v1) (2011)
- Mori, T., Kawamura, H.: Simulation study of spatiotemporal correlations of earthquakes as a stick-slip frictional instability. *Phys. Rev. Lett.* **94**, 058501-1-4 (2005)
- Xia, J., Gould, H., Klein, W., Rundle, J.B.: Near-mean-field behavior in the generalized Burridge–Knopoff earthquake model with variable-range stress transfer. *Phys. Rev. E* **77**, 031132-1-11 (2008)
- Mori, T., Kawamura, H.: Simulation study of earthquakes based on the two-dimensional Burridge–Knopoff model with long-range interactions. *Phys. Rev. E* **77**, 051123-1-16 (2008)
- Varotsos, P.A., Sarlis, N.V., Skordas, E.S., Uyeda, S., Kamogawa, M.: Natural-time analysis of critical phenomena: the case of seismicity. *Europhys. Lett.* **92**, 29002 (2010)
- Lindner, B., Garcia-Ojalvo, J., Neiman, A., Schimansky-Geier, L.: Effects of noise in excitable systems. *Phys. Rep.* **392**, 321 (2004)
- Zaks, M.A., Sailer, X., Schimansky-Geier, L., Neiman, A.B.: Noise induced complexity: from subthreshold oscillations to spiking in coupled excitable systems. *Chaos* **15**, 026117 (2005)
- Klinshov, V., Franović, I.: Mean-field dynamics of a random neural network with noise. *Phys. Rev. E*
- Telford, W.M., Geldart, L.P., Sheriff, R.E.: *Applied Geophysics*, 2nd edn. Cambridge University Press, Cambridge (1990)

23. Ryabov, V.B., Correig, A.M., Urquizu, M., Zaikin, A.A.: Microseism oscillations: from deterministic to noise-driven models. *Chaos Solitons Fract.* **16**, 195–210 (2003)
24. Sone, H., Shimamoto, T.: Frictional resistance of faults during accelerating and decelerating earthquake slip. *Nat. Geosci.* **2**, 705–708 (2009)
25. Lapusta, N.: The roller coaster of fault friction. *Nat. Geosci.* **2**, 676–677 (2009)
26. Burić, N., Ranković, D., Todorović, K., Vasović, N.: Mean field approximation for noisy delay coupled excitable neurons. *Phys. A* **389**, 3956–3964 (2010)
27. Vasović, N., Kostić, S., Franović, I., Todorović, K.: Earthquake nucleation in a stochastic fault model of globally coupled units with interaction delays. *Commun. Nonlinear Sci.* **38**, 117–129 (2016)
28. Shimazaki, K., Nakata, T.: Time-predictable recurrence model for large earthquakes. *Geophys. Res. Lett.* **7**, 279–282 (1980)
29. Kanamori, H.: Earthquake prediction: an overview. *Int. Geophys.* **81**(part B), 1205–1216 (2003)
30. Parsons, T., Console, R., Falcone, G., Muru, M., Yamashina, K.: Comparison of characteristic and Gutenberg–Richter models for time-dependent  $M \geq 7.9$  earthquake probability in the Nankai–Tokai subduction zone, Japan. *Geophys. J. Int.* **190**(3), 1673–1688 (2012)

# Slow rate fluctuations in a network of noisy neurons with coupling delay

I. FRANOVIĆ<sup>1</sup> and V. KLINSHOV<sup>2</sup>

<sup>1</sup> *Scientific Computing Laboratory, Center for the Study of Complex Systems, Institute of Physics Belgrade, University of Belgrade - Pregrevica 118, 11080 Belgrade, Serbia*

<sup>2</sup> *Institute of Applied Physics of the Russian Academy of Sciences - 46 Ulyanov Street, 603950 Nizhny Novgorod, Russia*

received 18 September 2016; accepted in final form 6 December 2016  
published online 28 December 2016

PACS 87.19.1j – Neuronal network dynamics  
PACS 05.40.Ca – Noise  
PACS 02.30.Ks – Delay and functional equations

**Abstract** – We analyze the emergence of slow rate fluctuations and rate oscillations in a model of a random neuronal network, underpinning the individual roles and interplay of external and internal noise, as well as the coupling delay. We use the second-order finite-size mean-field model to gain insight into the relevant parameter domains and the mechanisms behind the phenomena. In the delay-free case, we find an intriguing paradigm for slow stochastic fluctuations between the two stationary states, which is shown to be associated to noise-induced transitions in a double-well potential. While the basic effect of coupling delay consists in inducing oscillations of mean rate, the coaction with external noise is demonstrated to lead to stochastic fluctuations between the different oscillatory regimes.

Copyright © EPLA, 2016

Spontaneous activity of cortical neurons may be characterized as a doubly stochastic process, reflected in a high spike-train variability on a short timescale [1], and *slow* irregular firing rate fluctuations on longer timescales [2,3]. Such slow fluctuations with typical frequencies of  $\sim 0.4$ –2 Hz are recorded via EEG or in measurements of local field potentials as the network-level events [4,5], which comprise “on” episodes of high spiking and synaptic activity interspersed with “off” episodes of relative quiescence [6]. The dynamical substrate behind the associated transitions lies in coherent switching of individual neurons between the supra-threshold depolarized “up” states [7,8] and the hyperpolarized “down” states of membrane potential [9]. Alternation of “up” and “down” states [10–12] is a pervasive phenomenon found in sensory, motor, associative and executive cortical areas during sleep [13], under anesthetized [14] and awake conditions [15], as well as in the case of *in vitro* preparations under different experimental protocols [16–18]. Assuming a number of prominent functional roles, slow rate fluctuations are deemed likely to contribute to cortical response variability [19], and have further been found to mediate certain forms of learning and memory [20–24].

In spite of an extensive experimental account, a comprehensive theoretical insight into the described phenomena is still lacking. In this letter, we report on generic mechanisms behind slow rate fluctuations in large neuronal assemblies by focusing on specific roles and interplay of external and intrinsic neuronal noise [25–27], as well as the coupling delay [28,29]. The individual impact of these three ingredients and their co-effects are investigated in this context for the first time.

Note that the terminology concerning the collective dynamics of the network model is fixed as follows. The term “oscillations of mean rate”, or briefly “rate oscillations”, will be reserved for the delay-induced *regular* oscillations of the mean (assembly-averaged) rate. Nonetheless, the slow fluctuations of the network mean rate that emerge in the presence of noise between the two deterministic attractors, be they the two fixed points (analogues of the “up” and the “down” state in our model), or the two limit cycles, will be referred to as the “slow stochastic fluctuations”. In order to analyze the latter, we derive a second-order stochastic mean-field model for the collective network dynamics. It will be demonstrated that the stability and bifurcation analysis of the effective model can

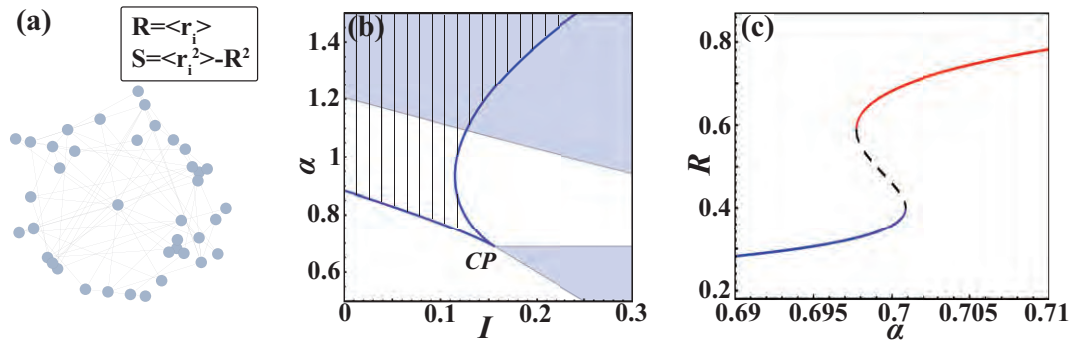


Fig. 1: (Color online) (a) Scheme of a network model. (b) Bifurcation diagram on the  $I$ - $\alpha$  plane obtained for the mean-field model at  $\tau = 0$  and fixed  $B = 0.004$ . The “up” and the “down” states coexist in the hatched region between the two branches of saddle-node bifurcations (solid lines). The latter meet at a cusp point (CP), where the pitchfork bifurcation occurs. Within the shaded domain, the condition  $\omega^2 > 0$  is satisfied, such that the system may undergo Hopf bifurcation for  $\tau > 0$ . (c)  $R(\alpha)$  bifurcation diagram determined analytically for the mean-field model at  $\tau = 0$  and fixed  $B = 0.004$ ,  $I = 0.15$ . The “up” state (red line) and the “down” state (blue line) are separated by the unstable state (dashed line). The system lies in the close vicinity of the cusp point.

be applied to infer the parameter domains relevant for the slow rate fluctuations.

Our use of the mean-field approach can be interpreted in the context of recent research, where the interest has shifted from classical problems treated by deterministic neural field models [30–33] to a corpus of issues related to how fluctuations and correlations affecting individual neurons are translated to a network level, inducing or modifying the different forms of collective behavior [34,35]. Techniques applied to derive *stochastic* mean-field models can broadly be cast in two classes. The “top-down” framework features perturbation techniques, such as system-size expansion or field-theory methods [34,36], whereas the “bottom-up” strategies, implemented by the population density method [37] or the augmented moment approach [38], involve building a macroscopic model from stochastic equations for local processes. Our derivation pertains to the latter category, containing certain novelties which are indicated below.

**Model.** – We consider a population of  $N$  excitatory neurons following a rate-based dynamics given by [39–41]

$$\frac{dr_i}{dt} = -\lambda r_i + \mathcal{H}(\kappa u_{i,\tau} + I + \sqrt{2B}\eta_i) + \sqrt{2D}\xi_i, \quad (1)$$

where unit indices belong to a  $i \in \{1, \dots, N\}$  range, while  $\lambda$  and  $I$  stand for the relaxation rate and the bias current, respectively. Note that  $\kappa$  denotes a normalized coupling coefficient  $\kappa = c/N$ , with  $c$  being the coupling strength. The coupling delay, referred to as  $\tau$ , is assumed to be uniform over the network. Each neuron  $i$  receives from the network an input  $u_{i,\tau} = \sum_j a_{ij} r_{j,\tau}$ , whereby a shorthand notation  $r_{j,\tau} \equiv r_j(t - \tau)$  is introduced for the delayed variables. The interaction topology, specified by the elements of the adjacency matrix  $a_{ij} \in \{0, 1\}$ , conforms to a random network with connectedness probability  $p \sim 0.1$ – $0.2$ , see fig. 1(a). Although recent experiments provide evidence

for nonrandom structure of neural circuits even on microscopic level [42,43], sparse random architecture maintains a degree of biological plausibility [44] and has been adopted as paradigmatic [37,45,46].

The gain function  $\mathcal{H}$  is generally a nonlinear function, which can be explicitly determined for the particular models of spiking neurons [37,46]. The local dynamics is influenced by two independent sources of noise. The external noise  $\eta_i$ , which is attributed intensity  $B$ , is associated to fluctuating synaptic input from the embedding environment, whereas the intrinsic noise  $\xi_i$ , assigned with intensity  $D$ , primarily derives from the stochastic dynamics of ion-channels.

The network dynamics is analyzed via a second-order stochastic mean-field model that incorporates an implicit Gaussian closure hypothesis, in a sense that the mean rate  $R(t) = \frac{1}{N} \sum_i r_i(t)$  and the associated variance  $S(t) = \frac{1}{N} \sum_i r_i(t)^2 - R(t)^2$  are considered sufficient to describe the system’s macroscopic behavior [47–51]. The detailed derivation of the mean-field model in the case of instantaneous couplings ( $\tau = 0$ ) has been carried out in our previous paper [41]. Given that generalization to the case of delayed couplings proceeds in a fashion analogous to [41], here we only summarize the main points and provide the resulting equations.

The key elements in the derivation of  $R$  dynamics include i) the Ansatz that the local variables may be written as  $r_i = R + \sqrt{S}\rho_i$ , where  $\rho_i$  are uncorrelated variables with zero mean and unit variance [52], and ii) the development of the gain function into Taylor series about the average input  $X = cpR + I$  for the neurons within the network. In [41], we have argued that the approximation regarding the character of  $\{\rho_i\}$  holds under two conditions: first, that the distribution of inward connectivity degrees is sufficiently narrow so that the distribution of  $r_i$  is unbiased, and second, that the fraction of shared input between any two neurons is small, which renders their

outputs uncorrelated. Given that the fraction of shared input between any two neurons is  $p$ , and that the coefficient of variation for the number of incoming connections amounts to  $\sqrt{(1-p)/pN}$ , one estimates that the two conditions above will be met if i) the connectivity is small,  $p \ll 1$ , and ii) the network is sufficiently large,  $N \gg 1/p$ . In terms of practical application, in [41] we have further numerically verified that the validity of the mean-field approximation for  $p = 0.2$  (the value kept fixed throughout this Letter) begins to degrade considerably if the network size is smaller than  $N \approx 70$ .

Taking the assembly average of eq. (1) and neglecting the terms  $\mathcal{O}(1/N^2)$ , one ultimately arrives at

$$\frac{dR}{dt} = -\lambda R + H(X_\tau) + \frac{G_\tau}{N} + \sqrt{\frac{\Psi_\tau}{N}} \zeta. \quad (2)$$

In eq. (2), we have used the notation  $H(X_\tau) = \mathcal{H}(X_\tau) + B\mathcal{H}''(X_\tau)$ ,  $G_\tau = c^2\mathcal{H}''(X_\tau) [p(1-p)R_\tau^2 + pS_\tau]$ , and  $\Psi_\tau = 2D + [2B + c^2p^2S_\tau] (\mathcal{H}'(X_\tau))^2$ , where  $\mathcal{H}'(X_\tau) \equiv \frac{d\mathcal{H}}{dX}(X_\tau)$  and  $\mathcal{H}''(X_\tau) \equiv \frac{d^2\mathcal{H}}{dX^2}(X_\tau)$ . The variable  $\zeta$  is a Gaussian white noise that accounts for the joint macroscopic effect of several noisy terms. In particular, the three terms in  $\Psi_\tau$  describe the impact of the internal noise, the external noise, and the so-called network noise, respectively, whereby the latter derives from fluctuations of the neurons' output signals. Note that the indicated noise terms can be grouped together because their sources are independent by construction of the model.

Derivation of dynamics for the variance requires taking the appropriate Itô derivatives, whereby the final result reads

$$\frac{dS}{dt} = -2\lambda S + 2D + 2B(\mathcal{H}'(X))^2. \quad (3)$$

Note that  $S$  affects  $R$  dynamics only via an  $\mathcal{O}(1/N)$  term, cf. eq. (2). For this reason, we can neglect the impact of the terms  $\mathcal{O}(1/N)$  in the evolution of  $S$ .

In the thermodynamic limit  $N \rightarrow \infty$ , the mean-field model comprised of (2) and (3) is completely deterministic, with  $R$  dynamics being independent of  $S$ . For large but finite  $N$ , the finite-size effects become manifest in a twofold fashion. First, a deterministic correction term  $G_\tau/N$  emerges, which only marginally changes the r.h.s. of eq. (2). The more important finite-size effects in eq. (2) are associated to the stochastic term of intensity  $\Psi_\tau/N$ . In what follows, it will be demonstrated that the latter can under certain conditions give rise to slow rate fluctuations.

Our approach will consist in carrying out the stability and bifurcation analysis of the mean-field model in the limit  $N \rightarrow \infty$  in order i) to gain insight into the parameter domains which admit the slow fluctuations of the mean rate in the case  $\tau = 0$ , as well as ii) to outline the regions that facilitate the delay-induced oscillations and the stochastic fluctuations between the different oscillatory regimes for  $\tau > 0$ . Before proceeding, in analogy to [41], we specify the particular form of the gain

function as

$$\mathcal{H}(X) = \begin{cases} 0, & X \leq 0, \\ 3X^2 - 2X^3, & 0 < X < 1, \\ 1, & X \geq 1. \end{cases} \quad (4)$$

**Analysis for thermodynamic limit.** – As indicated above, in the thermodynamic limit the evolution of  $R$  becomes independent of  $S$ . Given the gain function (4), it is convenient to introduce a compound connectivity parameter  $\alpha = cp$  and rewrite (2) in terms of  $X$ , which yields

$$\frac{dX}{dt} = -2\alpha X_\tau^3 + 3\alpha X_\tau^2 - 12\alpha B X_\tau - X + 6\alpha B + I. \quad (5)$$

In the absence of delay, one may show that (5) always admits at least one stable stationary state. For fixed  $B$ ,  $X$  dynamics undergoes a codimension-2 pitchfork bifurcation at  $\alpha_p = 2/[3(1-8B)]$  and  $I_p = (1-\alpha_p)/2$ , where two stable fixed points emerge separated by an unstable one, cf. fig. 1(b) and fig. 1(c). The incipient bistable regime involves the coexistence of the states of higher and lower  $R$ , which one may refer to as the “up” and the “down” state, respectively. Figure 1(b) indicates that  $(I_p, \alpha_p)$  is actually a cusp point, *viz.* the locus where two saddle-node bifurcation curves meet. Thus, for  $\alpha < \alpha_p$ , the mean-field model has a unique stable fixed point, whereas for  $\alpha > \alpha_p$ , it exhibits bistability within a “bistability tongue”. The latter is delineated by the saddle-node bifurcations where the “up” state is born or the “down” state is annihilated. Increasing  $\alpha$  in the tongue area reduces  $R$  of the unstable state. This has the effect of constricting the attraction basin of the “down” state, such that the “up” state becomes a prevailing feature.

In the presence of coupling delay, eq. (5) is found to undergo Hopf bifurcation for  $\tau = \frac{1}{\omega} \arctan(-\omega)$ , where  $\omega^2 = [6\alpha(X_0^2 - X_0 + 2B)]^2 - 1$ , with  $X_0$  denoting the fixed-point solution. The condition  $\omega^2 > 0$  can be used to determine the parameter regions admitting such a scenario, cf. the shaded domain in fig. 1(b). Note that enhancing  $\tau$  may give rise to Hopf bifurcation regardless of whether the delay-free system is monostable or bistable for the given parameter set  $(\alpha, B, I)$ . The bifurcation diagram in fig. 2 refers to the case where the delay-free system is monostable, whereas fig. 3(a) concerns the bistable case. In the latter instance, we find that only the “up” state may undergo Hopf bifurcation, which results in a coexistence of the “down” state and the limit cycle.

For both the scenarios above, we have verified that the exact system displays the behavior qualitatively analogous to that of the mean-field model, see fig. 3(b). An important point is that the mean-field model correctly anticipates not only the stationary states, but also the creation of stable limit cycles, which we interpret as the onset of mean rate oscillations. Interestingly, Hopf bifurcation is not the only mechanism giving rise to rate oscillations. In particular, an increase of  $\tau$  may as well lead to global fold-cycle bifurcations, where a stable and a saddle cycle are born. As a corollary, one finds windows of *bistable rate*



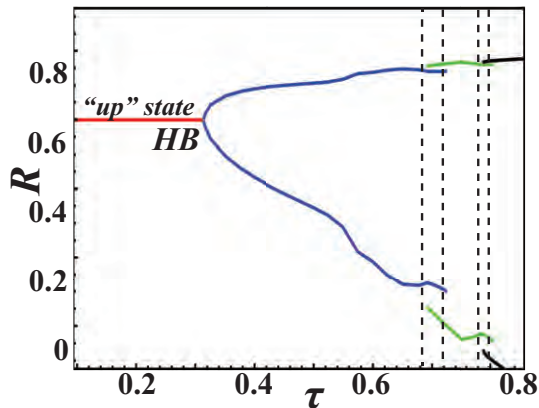


Fig. 2: (Color online) Bifurcation diagram  $R(\tau)$  numerically obtained for the mean-field model under the parameter set  $I = 0.03$ ,  $B = 0.001$ ,  $\alpha = 2.165$ ,  $N = 400$ . The horizontal line corresponds to the “up” state, which is destabilized via Hopf bifurcation (HB). The oscillatory solutions above HB are represented by the corresponding amplitudes. Within the two  $\tau$  intervals indicated by the dashed lines, the mean-field model exhibits bistability between the two limit cycles, which is associated to the occurrence of fold-cycle bifurcations.

*oscillations* with different amplitudes, cf. the two intervals indicated by the dashed lines in fig. 2. Note that in the interval around  $\tau \approx 0.7$ , the saddle cycle acts as a separatrix between the cycle created via Hopf bifurcation and the stable cycle emerging from the fold-cycle bifurcation, whereby the latter has a larger amplitude. The bistability windows terminate in a scenario involving the inverse fold-cycle bifurcation, where the stable cycle with a smaller amplitude vanishes by colliding with the saddle cycle. Below we show that the mean-field model provides meaningful insights even for such complex dynamical regimes.

**Slow rate fluctuations.** – Having analyzed the mean-field model in the limit  $N \rightarrow \infty$ , one is able to anticipate the parameter regions where the exact system is likely to exhibit slow stochastic fluctuations of mean rate. Such a nontrivial behavior can be expected in the domains promoting bistable dynamics for the thermodynamic limit.

Let us first consider the case  $\tau = 0$ . Here, the mechanism behind slow rate fluctuations may be explained by invoking the paradigm of a noise-driven particle fluctuating between the minima of a double-well potential. In the domains where the mean-field model possesses two stable stationary states for  $N \rightarrow \infty$ , each of them may be associated to a minimum of the potential, while the separatrix provides for the barrier. The noisy term emerging for finite  $N$  can then facilitate transitions between the wells.

In order to obtain the form of the potential guiding the system dynamics, we use the adiabatic approximation, which consists in replacing  $S$  by its stationary value  $S_0 = D + B(\mathcal{H}'(X))^2$  given by (3). Substituting this in (2) and rewriting the latter in terms of  $X$ , one obtains

$$\frac{dX}{dt} = -\frac{dV}{dX} + \sqrt{\Phi}\zeta. \quad (6)$$

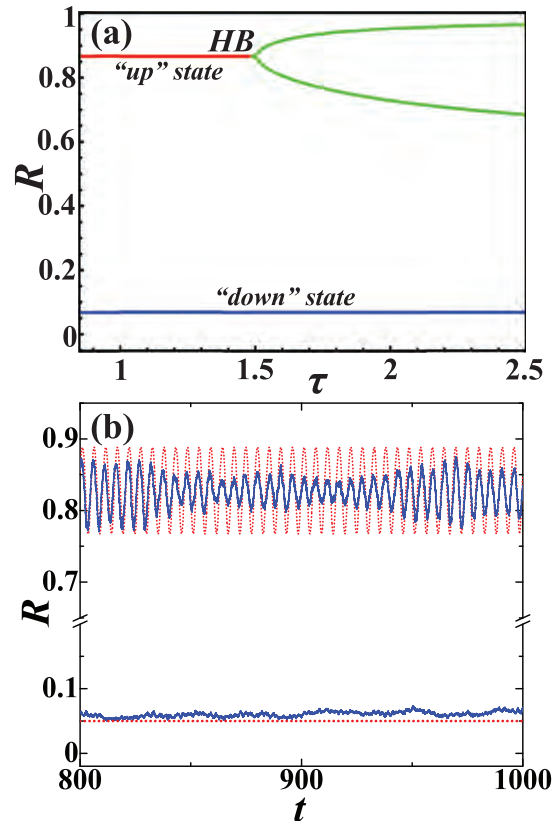


Fig. 3: (Color online) (a) Bifurcation diagram  $R(\tau)$  numerically obtained for the mean-field model under the parameter set  $I = 0.06$ ,  $\alpha = 1.3$ ,  $B = 0.002$ . The horizontal lines denote the levels of the “down” (blue line) and the “up” state (red line), whereby the latter undergoes Hopf bifurcation (HB) at  $\tau = 1.495$ . The oscillatory solutions above HB are represented by the associated amplitudes (green lines). (b)  $R(t)$  series of the exact system (blue solid lines) and the mean-field model (red dotted lines) illustrate a bistable regime involving the coexistence of the oscillatory solution and the “down” state. The results are obtained for  $\tau = 1.9$  and  $N = 400$ , with the remaining parameters being the same as in (a).

Here,  $V(X) = \alpha X^4/2 - \alpha X^3 + (6\alpha B + 1)X^2 - (6\alpha B + I)X + \mathcal{O}(1/N)$ , whereas the macroscopic noise is given by  $\Phi = \alpha^2(2 + \alpha^2) [36BX^2(1 - X)^2 + D]/N$ . The potential  $V(X)$  has a double-well form above the pitchfork bifurcation. Note that the switching between the minima of  $V(X)$  should unfold in a sufficiently close vicinity of the pitchfork bifurcation, because too far above it, the barrier becomes too high for the noisy term to overcome it.

As expected, we have found slow rate fluctuations by numerical simulations of the exact system within the indicated parameter region. There, the typical  $X(t)$  series, such as the one in fig. 4(a), can be described as alternations between the “up” and the “down” state of the mean-field model. This is corroborated by the bimodal form of the probability distribution  $f(X)$  obtained from the  $X(t)$  series, cf. fig. 4(b). The corresponding  $V(X)$  is plotted in the same figure in order to illustrate that the coordinates

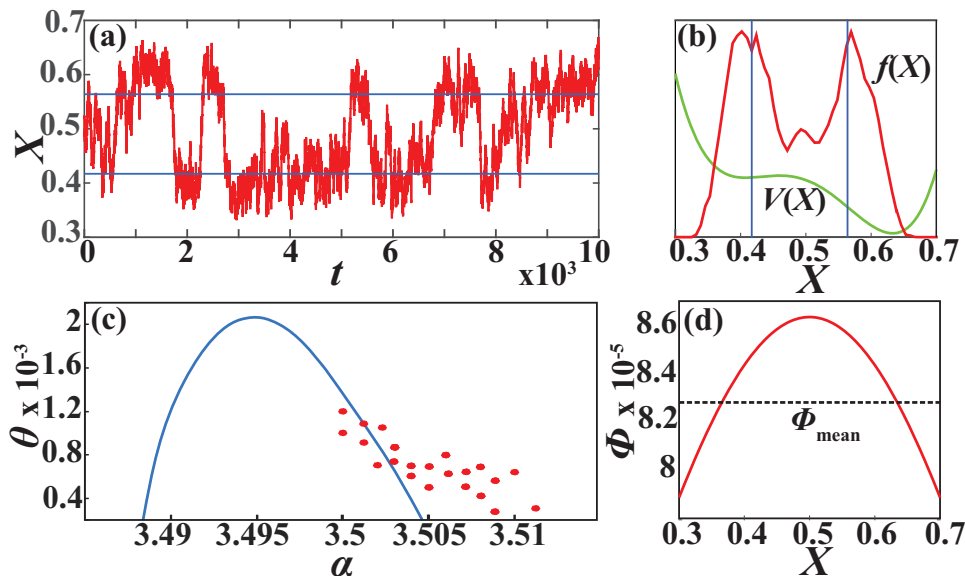


Fig. 4: (Color online) (a) Slow rate fluctuations in the  $X(t)$  series of a network of  $N = 400$  neurons with parameters  $B = 0.004$ ,  $D = 0.02$ ,  $\alpha = 0.7$ ,  $I = 0.1505$ . The latter are the same as in fig. 1(c). Horizontal lines indicate the levels associated to “up” and “down” states of the mean-field model. (b)  $V(X)$  denotes the potential for the mean-field model, whereas  $f(X)$  presents the histogram obtained from the  $X(t)$  series from (a). (c) The solid line and the dots refer, respectively, to the dependences  $\theta(\alpha)$  obtained analytically for the mean-field model and numerically for the exact system. (d)  $\Phi(X)$  determined analytically for the mean-field model (6). The network parameters in (b)–(d) are adopted from (a).

of  $f(X)$  maxima approximately coincide with the location of wells of  $V(X)$ .

The slow rate fluctuations are observed in a confined parameter region, as shown in fig. 4(c). The dots indicate the numerically determined transition rate  $\theta$  for the exact system as a function of the coupling parameter  $\alpha$ . Using the mean-field model, one is further able to estimate  $\theta$  analytically. In this context, first note that the noise intensity in eq. (6) depends on  $X$ , which implies that  $V(X)$  has a fluctuating barrier. Nevertheless, in a first approximation, the problem may be reduced to the scenario with a stationary barrier. To justify this, we have plotted in fig. 4(d) the dependence  $\Phi(X)$  for the parameter set from fig. 4(a). One learns that  $\Phi$  is bounded for  $X$  values between the wells, such that the average value  $\Phi_{mean}$  can be taken as representative. Since the noise intensity is sufficiently small compared to the barrier height, the mean first-passage time from one well to the other may be estimated by the Kramers formula [53,54],

$$T_{X_{\pm} \rightarrow X_{\mp}} \approx \frac{\pi}{\sqrt{|V''(X_u)|V''(X_{\pm})}} \exp \left[ \frac{V(X_u) - V(X_{\pm})}{\Phi_{mean}} \right]. \quad (7)$$

Here,  $X_-$  (“down” state) and  $X_+$  (“up” state) refer to coordinates of minima of  $V(X)$ , whereas  $X_u$  is the location of its maximum. The total transition rate  $\theta$  is then given by  $\theta = 1/(T_{X_+ \rightarrow X_-} + T_{X_- \rightarrow X_+})$ . The solid line in fig. 4(c) shows the dependence  $\theta(\alpha)$  obtained for the mean-field model by applying the described approximation. Note that the indicated  $\alpha$  interval where  $\theta$  is positive lies quite close to the one where the exact system exhibits

rate fluctuations. Moreover, the  $\theta$  values estimated analytically are of the same order as those observed numerically, which further evinces that the mean-field model predicts the behavior of the exact system in a satisfactory fashion. The point that their matching is only qualitative reflects the fact that the mean-field model becomes less accurate in the vicinity of the pitchfork bifurcation [41].

The mean-field model can also account for the mechanism behind more intricate slow rate fluctuations observed in the presence of coupling delays ( $\tau > 0$ ). In particular, it allows one to predict the occurrence of stochastic switching between the different oscillatory solutions. These transitions take place in the parameter domain where the mean-field model possesses two coexisting stable oscillatory solutions for  $N \rightarrow \infty$ , cf. fig. 2. An example of such solutions is illustrated in fig. 5(a) for  $\tau = 0.7$  and the remaining parameters fixed as in fig. 2. Note that the oscillations of larger (smaller) amplitude correspond to a limit cycle born via a global fold-cycle (Hopf) bifurcation. For the given parameter set, we find that the exact system displays large fluctuations of mean rate, cf. fig. 5(b). These fluctuations may be interpreted as noise-induced switching between the two oscillatory solutions.

Nevertheless, one also observes that the matching between the dynamics of the mean-field model and the exact system is qualitative, but rather lacks the quantitative character. In particular, the amplitudes of the two solutions found for the mean-field model are quite close, whereas the characteristic amplitudes of the two oscillatory regimes involved in slow stochastic fluctuations for

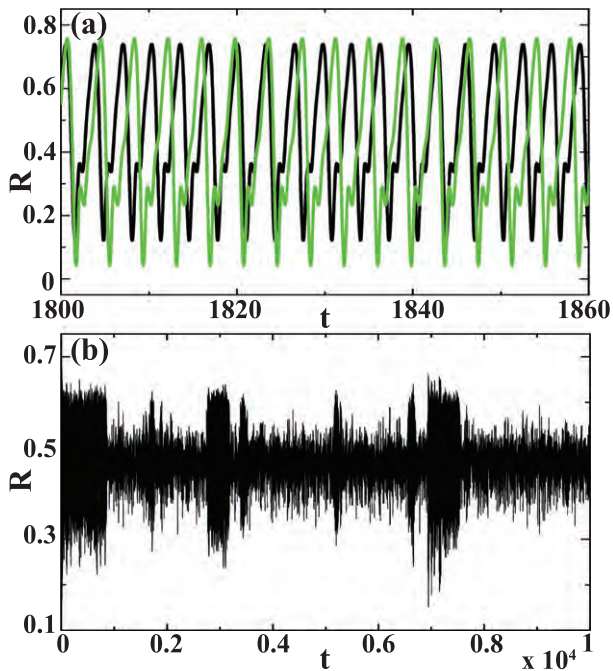


Fig. 5: (Color online) (a) Bistable dynamics of the mean-field model characterized by the coexistence of two limit cycles. The cycle with larger amplitude (green line) is born via the fold-cycle bifurcation, whereas the solution of smaller amplitude (black line) derives from the Hopf bifurcation. The delay is set to  $\tau = 0.7$ , while the rest of parameters are as in fig. 2. (b)  $R(t)$  series for the network of  $N = 400$  neurons shows slow stochastic fluctuations for the parameter set from (a).

the exact system are much further apart, cf. fig. 5(a) and fig. 5(b). This discrepancy derives from the general fact that the system becomes quite sensitive to small perturbations in the vicinity of a bifurcation, which severely affects the validity of the effective model. In this case, the role of such small perturbations is assumed by the finite-size effects. Note that we have already shown in [41] that the finite-size effect grows so large in the vicinity of a pitchfork bifurcation that one cannot use simple linearization to estimate it. We suspect that essentially the same scenario occurs here as the system in fig. 5 lies close to a fold-cycle bifurcation.

**Discussion.** – We have demonstrated how the individual and combined effects of different noise terms and coupling delay give rise to slow fluctuations of mean rate in a random neural network. It has been shown that the generic mechanisms and the underlying statistical features can be qualitatively accounted for by looking into the appropriate second-order stochastic mean-field model. In the delay-free case, the basic scenario behind slow rate fluctuations may be characterized as noise-driven transitions of a particle in a double-well potential. In the thermodynamic limit, the mean-field model displays bistability between the “up” and the “down” state, whereas the finite-size effect consists in introducing a noise term that induces transitions between the metastable states. Apart from

anticipating the parameter domains that promote rate fluctuations, the analysis of the mean-field model has allowed us to estimate the associated transition rates.

Our results further indicate that introducing coupling delays into the network model facilitates the emergence of mean rate oscillations. An interesting finding is that the cooperative action of noise and delay may lead to slow fluctuations that can be interpreted as stochastic mixing between two different oscillatory regimes. The predictions of the mean-field model remain qualitatively valid even for such unexpected scenarios.

It is relevant to estimate how the typical durations of “up” and “down” states from our simulations compare to lifetimes of such states in biological networks, which are established to comprise a range from several hundred ms up to  $\sim 2$  s [12]. In order to do so, we take into account that the time constant  $\tau_m = 1/\lambda$  should be of the order of 1 ms [55,56], from where one may infer that a time unit in eq. (1) roughly corresponds to  $\sim 10^{-3}$  s. Thus, when translated to real time units, the residence times observed in fig. 4(c) span the range of about 800–2000 ms, which approximately coincide with a biologically plausible range.

So far, two alternative scenarios have been suggested in modeling studies to explain for the occurrence of rate fluctuations, emphasizing either the impact of synaptic plasticity or the network topology. By the first scenario, cycling of “up” and “down” states is promoted by a mechanism based on short-term synaptic depression [57,58], whereby the extinction of “up” state is triggered by the activity-dependent self-inhibition. By the other scenario, slow rate fluctuations emerge in balanced excitatory-inhibitory networks [45,59,60], if the latter embed clustered subnetworks [2]. In principle, an analogous form of behavior can also be recovered for balanced networks in the vicinity of transition to chaos [61]. At variance with our approach, prior studies have not explicitly addressed the influence of noise, either in the onset of the rate fluctuations or the underlying statistics. Also, the previous research does not refer to the effects of coupling delay.

An important open question is whether and how more complex network topologies would affect the robustness of rate fluctuations. In our setup with random topology, the effect is relatively sensitive to parameter values. However, given the recent report that the macroscopic rate fluctuations are robust in balanced networks with embedded clusters [2], we have begun to develop a mean-field model for networks with an excitation-inhibition balance and clustered architecture. We believe that the mean-field approach will allow us to gain a deeper understanding of the relation between the network structure and the slow rate fluctuations.

\*\*\*

This work is supported by the Ministry of Education, Science and Technological Development of Republic of Serbia under project No. 171017, by the Russian Foundation for Basic Research within Grants Nos. 14-02-00042

and 15-02-04245, and by the Ministry of Education and Science of the Russian Federation, Agreement No. MK-8460.2016.2.

## REFERENCES

- [1] DESTEXHE A., RUDOLPH M. and PARÉ D., *Nat. Rev. Neurosci.*, **4** (2003) 739.
- [2] LITWIN-KUMAR A. and DOIRON B., *Nat. Neurosci.*, **15** (2012) 1498.
- [3] CHURCHLAND M. M. *et al.*, *Nat. Neurosci.*, **13** (2010) 369.
- [4] BUZSÁKI G., *Rhythms of the Brain* (Oxford University Press, Oxford) 2006.
- [5] BUZSÁKI G., ANASTASSIOU C. A. and KOCH C., *Nat. Rev. Neurosci.*, **13** (2012) 407.
- [6] VYAZOVSKIY V. V. and HARRIS K. D., *Nat. Rev. Neurosci.*, **14** (2013) 443.
- [7] HAHN T. T. G., SAKMANN B. and MEHTA M. R., *Nat. Neurosci.*, **9** (2006) 1359.
- [8] GIGANTE G., DECO G., MAROM S. and DEL GIUDICE P., *PLoS Comput. Biol.*, **11** (2015) e1004547.
- [9] COWAN R. L. and WILSON C. J., *J. Neurophysiol.*, **71** (1994) 17.
- [10] MILLMAN D., MIHALAS S., KIRKWOOD A. and NIEBUR E., *Nat. Phys.*, **6** (2010) 801.
- [11] MCCORMICK D. A., MCGINLEY M. J. and SALKOFF D. B., *Curr. Opin. Neurobiol.*, **31** (2015) 133.
- [12] HAHN T. T. G. *et al.*, *Nat. Neurosci.*, **15** (2012) 1531.
- [13] STERIADE M., MCCORMICK D. A. and SEJNOWSKI T. J., *Science*, **262** (1993) 679.
- [14] ANDERSON J. *et al.*, *Nat. Neurosci.*, **3** (2000) 617.
- [15] PETERSEN C. C. H. *et al.*, *Proc. Nat. Acad. Sci. U.S.A.*, **100** (2003) 13638.
- [16] COSSART R., ARONOV D. and YUSTE R., *Nature*, **423** (2003) 283.
- [17] SANCHEZ-VIVES M. V. and MCCORMICK D. A., *Nat. Neurosci.*, **3** (2000) 1027.
- [18] SHU Y., HASENSTAUB A. and MCCORMICK D. A., *Nature*, **423** (2003) 288.
- [19] GHORBANI M., MEHTA M., BRUINSMAN R. and LEVINE A. J., *Phys. Rev. E*, **85** (2012) 021908.
- [20] JI D. and WILSON M. A., *Nat. Neurosci.*, **10** (2007) 100.
- [21] MARSHALL L., HELGADÓTTIR H., MÖLLE M. and BORN J., *Nature*, **444** (2006) 610.
- [22] DIEKELMANN S. and BORN J., *Nat. Rev. Neurosci.*, **11** (2010) 114.
- [23] HEIB D. P. J. *et al.*, *PLoS ONE*, **8** (2013) e82049.
- [24] MIYAMOTO D. *et al.*, *Science*, **352** (2016) 1315.
- [25] McDONNELL M. D. and WARD L. M., *Nat. Rev. Neurosci.*, **12** (2011) 415.
- [26] FAISAL A. A., SELEN L. P. J. and WOLPERT D. M., *Nat. Rev. Neurosci.*, **9** (2008) 292.
- [27] ANISHCHENKO V. S., ASTAKHOV V., NEIMAN A., VADIVASOVA T. and SCHIMANSKY-GEIER L., *Nonlinear Dynamics of Chaotic and Stochastic Systems* (Springer, Berlin, Heidelberg) 2007.
- [28] PIKOVSKY A., ZAIKIN A. and DE LA CASA M. A., *Phys. Rev. Lett.*, **88** (2002) 050601.
- [29] SCHÖLL E., HILLER G., HÖVEL P. and DAHLEM M. A., *Philos. Trans. R. Soc. A*, **367** (2009) 1079.
- [30] FOLIAS S. E. and BRESSLOFF P. C., *Phys. Rev. Lett.*, **95** (2005) 208107.
- [31] PINTO D. J. and ERMENTROUT G. B., *SIAM J. Appl. Math.*, **62** (2001) 206.
- [32] LAING C. R., TROY W. C., GUTKIN B. and ERMENTROUT G. B., *SIAM J. Appl. Math.*, **63** (2002) 62.
- [33] JIRSA V. K. and HAKEN H., *Physica D*, **99** (1997) 503.
- [34] BRESSLOFF P. C., *SIAM J. Appl. Math.*, **70** (2009) 1488.
- [35] BRESSLOFF P. C., *Phys. Rev. E*, **82** (2010) 051903.
- [36] BUICE M. A. and COWAN J. D., *Phys. Rev. E*, **75** (2007) 051919.
- [37] BRUNEL N. and HAKIM V., *Neural Comput.*, **11** (1999) 1621.
- [38] HASEGAWA H., *Phys. Rev. E*, **67** (2003) 041903.
- [39] HASEGAWA H., *Phys. Rev. E*, **75** (2007) 051904.
- [40] ANDERSON R. A., MUSALLAM S. and PESARAN B., *Curr. Opin. Neurobiol.*, **14** (2004) 720.
- [41] KLINSHOV V. and FRANOVIĆ I., *Phys. Rev. E*, **92** (2015) 062813.
- [42] SONG S. *et al.*, *PLoS Biol.*, **3** (2005) e68.
- [43] KLINSHOV V., TERAMAE J.-N., NEKORKIN V. and FUKAI T., *PLoS ONE*, **9** (2014) e94292.
- [44] LUCK J. M. and MEHTA A., *Phys. Rev. E*, **90** (2014) 032709.
- [45] VAN VREESWIJK C. and SOMPOLINSKY H., *Neural Comput.*, **10** (1998) 1321.
- [46] LY C. and TRANCHINA D., *Neural Comput.*, **19** (2007) 2032.
- [47] FRANOVIĆ I., TODOROVIĆ K., VASOVIĆ N. and BURIĆ N., *Phys. Rev. E*, **89** (2014) 022926.
- [48] FRANOVIĆ I., TODOROVIĆ K., VASOVIĆ N. and BURIĆ N., *Phys. Rev. E*, **87** (2013) 012922.
- [49] FRANOVIĆ I., TODOROVIĆ K., VASOVIĆ N. and BURIĆ N., *Phys. Rev. Lett.*, **108** (2012) 094101.
- [50] LINDNER B., GARCIA-OJALVO J., NEIMAN A. and SCHIMANSKY-GEIER L., *Phys. Rep.*, **392** (2004) 321.
- [51] ZAKS M. A., SAILER X., SCHIMANSKY-GEIER L. and NEIMAN A. B., *Chaos*, **15** (2005) 026117.
- [52] BURKITT A. N., *Biol. Cybern.*, **95** (2006) 1.
- [53] GARDINER C. W., *Handbook of Stochastic Methods for Physics, Chemistry and the Natural Sciences* (Springer-Verlag, Berlin) 2004.
- [54] PAVLIOTIS G. A., *Stochastic Processes and Applications* (Springer, New York) 2014.
- [55] GERSTNER W. and KISTLER W. M., *Spiking Neuron Models: Single Neurons, Populations, Plasticity* (Cambridge University Press, New York) 2004.
- [56] GERSTNER W., KISTLER W. M., NAUD R. and PANINSKI L., *Neuronal Dynamics: From Single Neurons to Networks and Models of Cognition* (Cambridge University Press, Cambridge) 2014.
- [57] HOLCMAN D. and TSODYKS M., *PLoS Comput. Biol.*, **2** (2006) 174.
- [58] MEJAS J. F., KAPPEN H. J. and TORRES J. J., *PLoS ONE*, **5** (2010) e13651.
- [59] VOGELS T. P. and ABBOTT L. F., *J. Neurosci.*, **25** (2005) 10786.
- [60] ROSENBAUM R. and DOIRON B., *Phys. Rev. X*, **4** (2014) 021039.
- [61] KADMON J. and SOMPOLINSKY H., *Phys. Rev. X*, **5** (2015) 041030.

## Phase response curves for models of earthquake fault dynamics

Igor Franović,<sup>1,a)</sup> Srdjan Kostić,<sup>2</sup> Matjaž Perc,<sup>3,4</sup> Vladimir Klinshov,<sup>5</sup> Vladimir Nekorkin,<sup>5,6</sup> and Jürgen Kurths<sup>5,7,8</sup>

<sup>1</sup>Scientific Computing Laboratory, Institute of Physics Belgrade, University of Belgrade, Pregrevica 118, 11080 Belgrade, Serbia

<sup>2</sup>Institute for the Development of Water Resources “Jaroslav Černi,” Jaroslava Černog 80, 11226 Belgrade, Serbia

<sup>3</sup>Faculty of Natural Sciences and Mathematics, University of Maribor, Koroška cesta 160, SI-2000 Maribor, Slovenia

<sup>4</sup>CAMTP—Center for Applied Mathematics and Theoretical Physics, University of Maribor, Krekova 2, SI-2000 Maribor, Slovenia

<sup>5</sup>Institute of Applied Physics of the Russian Academy of Sciences, 46 Ulyanov Street, 603950 Nizhny Novgorod, Russia

<sup>6</sup>University of Nizhny Novgorod, 23 Prospekt Gagarina, 603950 Nizhny Novgorod, Russia

<sup>7</sup>Potsdam Institute for Climate Impact Research, 14412 Potsdam, Germany

<sup>8</sup>Institute of Physics, Humboldt University Berlin, 12489 Berlin, Germany

(Received 15 February 2016; accepted 25 May 2016; published online 10 June 2016)

We systematically study effects of external perturbations on models describing earthquake fault dynamics. The latter are based on the framework of the Burridge-Knopoff spring-block system, including the cases of a simple mono-block fault, as well as the paradigmatic complex faults made up of two identical or distinct blocks. The blocks exhibit relaxation oscillations, which are representative for the stick-slip behavior typical for earthquake dynamics. Our analysis is carried out by determining the phase response curves of first and second order. For a mono-block fault, we consider the impact of a single and two successive pulse perturbations, further demonstrating how the profile of phase response curves depends on the fault parameters. For a homogeneous two-block fault, our focus is on the scenario where each of the blocks is influenced by a single pulse, whereas for heterogeneous faults, we analyze how the response of the system depends on whether the stimulus is applied to the block having a shorter or a longer oscillation period. *Published by AIP Publishing.* [<http://dx.doi.org/10.1063/1.4953471>]

Earthquakes are conceptually considered as frictional instabilities occurring on preexisting tectonic faults. The fault dynamics is often represented by the class of spring-slider block models incorporating different forms of constitutive friction laws. Such models can qualitatively account for the relevant regimes of fault dynamics, including the aseismic creep motion or the stick-slip motion, which is a signature for earthquakes. The research involving these models has so far mainly aspired to gain insight into the scaling laws and the occurrence of characteristic events, as well as to elucidate the relation between small and large earthquakes. Here, we adopt a considerably different approach. Our intention is not to characterize the statistical properties of the underlying time series or to assess the earthquake hazard, but rather to analyze a representative class of fault models from the perspective of nonlinear dynamics theory. Being strongly nonlinear systems, the considered models of earthquake faults are expected to display a number of intricate features, including high sensitivity to external perturbation, whereby the response may qualitatively depend on different system parameters, as well as the fault complexity. In the present paper, the theory of phase response curves is applied for the first time to systematically examine the sensitivity of fault dynamics in the stick-slip regime to external

perturbation. We consider the cases of a simple mono-block and paradigmatic two-block complex faults. Perturbations made up of single or two consecutive pulses are found to affect the fault dynamics in a nontrivial fashion, being able to advance or delay the earthquake cycle or even give rise to long-term effects.

### I. INTRODUCTION

By a basic phenomenological description, earthquakes are regarded as large-scale recurring mechanical failure events,<sup>1</sup> characterized by seismic cycles composed of a comparably long quasi-static stage of tectonic stress build-up and an abrupt dynamical rupture stage, associated with a rapid release of the accumulated strain. Earthquakes occur as dynamical instabilities on preexisting crustal faults and are caused by the motion of tectonic plates, which is fundamentally influenced by the elastic properties of the crust and the frictional features of the fault.<sup>2,3</sup> In dynamical terms, the complexity in earthquake-related behavior derives from the coaction of intrinsic nonlinearity, dominated by friction, and the external driving. Typically, the physical background behind inter-plate earthquakes involves a fault segment, represented by a mass block or an assembly of blocks, which loaded by one tectonic plate and under the frictional

<sup>a)</sup>Electronic mail: franovic@ipb.ac.rs

resistance of the other plate exhibits a stick-slip behavior,<sup>1,2</sup> the type of motion paradigmatic for earthquake dynamics.<sup>2,4,5</sup> In different physical models, the friction terms attain quite a complex form and are expressed by appropriate “constitutive laws.”<sup>2,3,6</sup>

Apart from scale-invariant statistical features, reflected in several well-known empirical scaling laws, some earthquakes exhibit characteristic features, manifested as “characteristic earthquakes” with well-defined time or energy scales.<sup>2,3,7</sup> In the former case, the fault fails in a pseudo-periodic time series, such that its dynamics is reminiscent of a relaxation oscillator. The pertaining oscillations may naturally be sensitive to external perturbations, which can be derived from different kinds of additional forcing whose duration and magnitude are small compared to the tectonic load. In general, if the perturbation is sufficiently small, it does not influence the amplitude of oscillations, but it may considerably affect the phase. In conceptual terms, and especially from the seismological point of view, it becomes relevant to determine whether and how the phase of stick-slip oscillations, and thereby the characteristic event itself, is retarded or advanced by such perturbations.

In the present paper, we consider the sensitivity to external perturbation of the models of a simple mono-block fault and a paradigmatic two-block complex fault, which display relaxation oscillations with the signature stick-slip property. The models are formulated within the Burridge-Knopoff framework of coupled spring-block systems<sup>8–11</sup> and incorporate the Dieterich-Ruina rate- and state-dependent friction law.<sup>12–14</sup> The qualitative analysis will be focused on determining the first- and second-order phase response curves (phase resetting curves, *PRCs*) for these models,<sup>15–19</sup> which to our knowledge is the first time that such an approach is applied in the context of earthquake fault dynamics, despite the fact that the formalism related to phase description of nonlinear oscillators has already been invoked.<sup>2,20–23</sup> So far, the *PRCs* have often been used as a tool to study the system’s response to stimuli, as well as the units’ ability to synchronize in the fields of neuroscience<sup>24–27</sup> and the general theory of coupled phase oscillators.<sup>28–31</sup>

The main corpus of issues we address here includes (i) the sensitivity of a simple monoblock fault to external perturbation, (ii) the influence of system parameters on the profile of *PRCs*, (iii) the effect of two-pulse perturbations and the deviation from the superposition principle due to multidimensionality of the model, as well as (iv) the responses of compound faults, either homogeneous or heterogeneous, to external perturbation. Apart from considering the first-order *PRCs*, our interest will also lie with the second-order *PRCs* because their nontrivial behavior may indicate a potential long-term effect of external perturbation on the duration of an earthquake cycle. The research agenda has a systematic character precisely given the fact that this type of analysis has not been carried out before for models of fault dynamics.

As already mentioned, the pseudo-periodic recurrence times have primarily been associated with large characteristic earthquakes.<sup>23,32–36</sup> By one scenario, the latter involve breaking of the most part of or the entire seismogenic zone,<sup>2,3,41,42</sup> whereas by the other scenario they emerge due

to breaking of similar sections of complex faults.<sup>2,37</sup> Well-known examples are earthquakes in the Nankaido region (Japan), the northern, the southern, and Parkfield sections of the San Andreas Fault,<sup>38</sup> and several regions in China.<sup>39,40</sup> Apart from these large characteristic earthquakes, the description of fault dynamics in terms of relaxation oscillator models may further be justified for certain small repeating earthquakes,<sup>43</sup> as corroborated by the recent proxy data.<sup>44</sup> One should note that many of the relevant models of fault dynamics may yield periodic sequences of events or series with a strong periodic component. For instance, such behavior has been found for the one- and two-dimensional versions of the Burridge-Knopoff model,<sup>10,11,45,46</sup> as well as in case of the Olami-Feder-Christensen model.<sup>47</sup> It has also been indicated that models of coupled relaxation oscillators displaying the stick-slip dynamics may account for a phase-locking mechanism behind earthquake clusters. The latter conform to rupture patterns where the main events occur in groups comprising nearby or distributed faults with similar characteristic periods.<sup>20,21,48</sup>

The paper is organized as follows. In Sec. II, we introduce the models of a simple fault and a two-block complex fault, summarizing the results of bifurcation analysis and explaining the physical background and possible regimes of system behavior. Section III concerns the monoblock fault, considering the scenarios where the fault is subjected to a single or two successive excitations. In the latter case, we demonstrate a nonlinear effect which occurs for systems whose dimension is larger than 1 and consists in a deviation from the superposition principle for two subsequent perturbations. It is also discussed how sensitivity to perturbation depends on the system parameters. Section IV provides our results for the first- and second-order phase response curves in cases of the homogeneous and the heterogeneous two-block complex fault. For homogeneous fault, we analyze how the system responds in case where each of the blocks is perturbed, but the perturbations arrive with a certain phase lag. For the heterogeneous fault, it is examined how the system response changes depending on whether the block with a shorter or longer oscillation period is perturbed. Section V contains a brief summary of our results.

## II. MODEL OF FAULT DYNAMICS

Within the family of spring-block models, the fault dynamics is represented by elastically interacting mass blocks sliding over a rough surface, whereby each block is elastically coupled to a rigid loader plate that moves at a constant velocity, see Fig. 1. In terms of seismological interpretation, it is the interface between the slider blocks and the rough surface that can be considered as an analogue for a one-dimensional earthquake fault,<sup>49</sup> and one is interested in describing the sliders’ slip and the associated slip velocity relative to the loader plate. The model comprising a single block accounts for a simple fault, whereas models containing multiple blocks refer to multi-segment (complex) faults. In the present paper, we study the cases of a simple fault and the paradigmatic two-block complex fault, made up of homogeneous or heterogeneous blocks. The block dynamics is

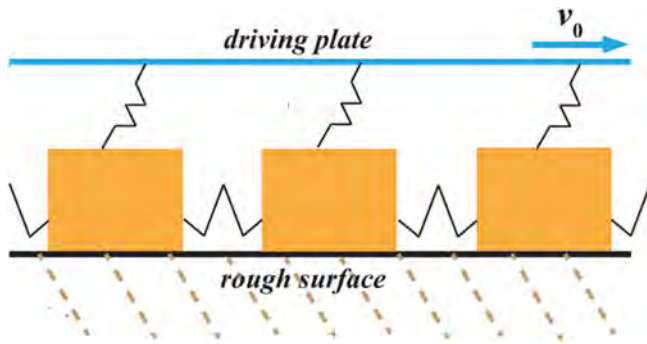


FIG. 1. Schematic representation of the spring-block model of earthquake fault dynamics. The blocks interact via elastic springs, and each block is further elastically coupled to the loader plate which moves at a constant velocity  $v_0$ . The blocks slide over a rough surface, whereby the friction at their interface is typically described by complex constitutive laws.

provided by a version of the Burridge-Knopoff model supplied by the Dieterich-Ruina rate- and state-dependent friction law.<sup>50–54</sup> Note that the selection of friction law is an important point for the models where friction enters as a force term. The early friction laws included effects of slip-weakening (reduction of friction strength during sliding) and rate-weakening (reduction in frictional force which accompanies the increase in slip velocity),<sup>12</sup> but the former could not fully explain for the relationship between the static and dynamic friction, while the experimental data have further shown that friction could not be a function dependent only on velocity.<sup>6</sup> The Dieterich-Ruina law<sup>12–14</sup> resolves these issues by introducing an additional state variable, which may be attributed a microscopic interpretation, associating it to the average life time of asperity contacts at the interface between the blocks and the rough surface.<sup>2</sup>

Without specifying the details of the derivation, which can be found in Refs. 50 and 51, here we provide the final non-dimensional form of equations for the dynamics of a single block

$$\begin{aligned} \frac{d\theta}{dt} &= -v(\theta + (1 + \epsilon)\ln v) \\ \frac{du}{dt} &= v - 1 \\ \frac{dv}{dt} &= -\gamma^2(u + (1/\xi)(\theta + \ln v)). \end{aligned} \quad (1)$$

In the above equation,  $\theta$  represents the state variable, whereas  $u$  denotes the slip (relative to the driver plate) and  $v$  is the associated slip velocity. The strong nonlinearity of (1) is due to the friction term, which involves a logarithm dependence on the velocity. The parameters  $\xi$  and  $\gamma$  are the non-dimensional spring constant and the non-dimensional frequency, respectively. The spring stiffness qualitatively accounts for the elastic properties of the medium where the fault is embedded.<sup>2</sup> The parameter  $\epsilon$  essentially measures the sensitivity of the block's velocity relaxation. This interpretation derives from the point that  $\epsilon$  may be expressed via two additional stress parameters related to the velocity dependence on the friction stress  $\tau$ . In particular,  $\epsilon$  is given by the ratio  $\epsilon = (B - A)/A$ ,<sup>50,51</sup> where  $A$  presents the direct

velocity dependence  $A = \frac{\partial \tau}{\partial \ln(v)}$ , while  $A - B = \frac{\partial \tau_{ss}}{\partial \ln(v_{ss})}$  is the velocity dependence for the steady state,<sup>12,14</sup> when the slider moves at a constant velocity  $v_{ss}$ . In other words,  $\epsilon$  is determined by the ratio of stress dropped during the earthquake to the stress increase that accompanies a sudden change in the block velocity. Note that we consider only positive values of  $B - A$  ( $\epsilon > 0$ ), which from a micro-mechanical point of view corresponds to the velocity-weakening effect.<sup>6</sup> Compared to real fault conditions,  $A$  and  $B$  describe material properties that depend on pressure, temperature, and sliding velocity.<sup>2</sup> These arguments suggest that  $\epsilon$  is the parameter most specific to detailed dynamics of particular faults. In terms of a qualitative comparison to real earthquake faults, it has been established that the relevant range of values for the parameters  $\epsilon$ ,  $\xi$ , and  $\gamma$  is  $\epsilon \in (1, 3.5)$ ,  $\xi \approx 0.5$ ,  $\gamma \in (10^3 - 10^{12})$ .<sup>13,50,55</sup>

System (1) has a stationary state  $(\theta, u, v) = (0, 0, 1)$  which corresponds to sliding at a uniform velocity equal to that of the loader plate, such that the block exhibits no slip relative to the plate. For certain parameter values, the system undergoes a direct supercritical Hopf bifurcation which gives rise to an oscillatory solution. The corresponding bifurcation curves  $\xi(\epsilon)$  obtained for fixed  $\gamma$  and  $\gamma(\epsilon)$  under fixed  $\xi$  are shown in Figs. 2(a) and 2(b). Note that these curves are determined analytically by considering the pure imaginary roots of the characteristic equation  $\lambda^3 - \lambda^2(\frac{\gamma^2}{\xi} - 1) - \lambda\gamma^2(1 - \frac{\xi}{\gamma}) - \gamma^2 = 0$  for system (1). Immediately above the bifurcation curves, system (1) displays harmonic oscillations, cf. Fig. 2(c), which may be appropriate to describe pre-seismic and post-seismic creep regimes.<sup>52</sup> Nevertheless, the regime of relaxation oscillations, which we are interested in, can be found sufficiently away from criticality, see Fig. 2(d). Such relaxation oscillations can be considered as dynamical counterpart of the stick-slip behavior paradigmatic for earthquake motion. In the quasi-static stage of stress accumulation (the “stick” stage), the block is effectively stuck on the rough surface, so that the relative slip to the driver plate decreases at a constant rate as the driver plate first catches up and then even surpasses the block. Once the pulling force overcomes the static friction withholding the block, one arrives at the onset of the slip stage. At this point, the block's velocity increases sharply, such that the slider shoots forward again, which gives rise to a new seismic cycle.

Apart from the monoblock fault, we also consider the case of a two-component fault, where the dynamics of blocks is given by

$$\begin{aligned} \frac{d\theta_i}{dt} &= -v_i(\theta_i + (1 + \epsilon_i)\ln v_i) \\ \frac{du_i}{dt} &= v_i - 1 \\ \frac{dv_i}{dt} &= \gamma_i^2(c(u_i - u_j) + u_i + (1/\xi_i)(\theta_i + \ln v_i)), \end{aligned} \quad (2)$$

with  $i, j \in \{1, 2\}$ ,  $i \neq j$ . The interactions are characterized by the coupling strength  $c$ . We intend to analyze the sensitivity to perturbation of the homogeneous two block fault ( $\epsilon_1 = \epsilon_2$ ,  $\xi_1 = \xi_2$ ,  $\gamma_1 = \gamma_2$ ), as well as the heterogeneous complex fault. Consistent with the arguments regarding the system parameters, heterogeneity will be confined to the

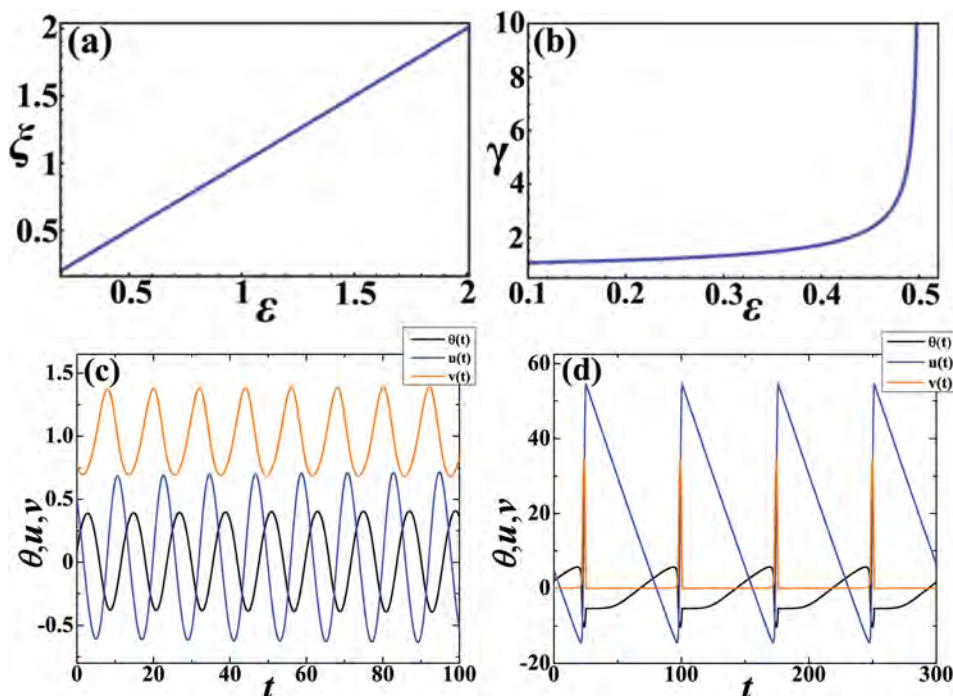


FIG. 2. Bifurcation diagrams and characteristic regimes of motion for the system (1). In (a) is shown the Hopf bifurcation curve  $\xi(\epsilon)$  obtained for fixed  $\gamma = 1000$ . In (b) is presented the Hopf bifurcation curve  $\gamma(\epsilon)$  determined for fixed  $\xi = 0.5$ . (c) and (d) illustrate the dynamics associated with the creep regime (harmonic oscillations) and the stick-slip regime (relaxation oscillations), respectively. (c) is obtained for the parameter set  $(\epsilon, \xi, \gamma) = (0.3, 0.5, 0.8)$ , whereas the parameters in (d) are  $(\epsilon, \xi, \gamma) = (1.45, 0.5, 1000)$ .

case of two blocks with disparate  $\epsilon$ ,  $\epsilon_1 \neq \epsilon_2$ , which results in distinct periods of the respective stick-slip oscillations. Both for the homogeneous and the heterogeneous two-segment faults, we take the coupling strength  $c$  sufficiently weak so that the interaction does not perturb the respective oscillation cycles of the blocks.

A remark is required regarding the numerical treatment of models (1) and (2). In particular, the underlying systems of ordinary differential equations (ODEs) are stiff, in a sense that within the relevant parameter domain, an exceedingly small iteration step is required to maintain the numerical stability of the typical explicit integration schemes, such as the Runge-Kutta method. The stiffness feature derives from the fact that the system involves characteristic time scales of substantially different order, and becomes stronger as  $\gamma$  is increased. Note that the step size is limited more severely by the stability rather than the accuracy requirement of the integration methods. In order to resolve these issues, we have implemented the solver based on the Rosenbrock method, which is specifically adapted to stiff systems. Unless stated otherwise, the parameter set used for the block dynamics throughout the paper is  $(\epsilon, \xi, \gamma) = (1.45, 0.5, 1000)$ .

### III. PRCs FOR THE MONOBLOCK FAULT

#### A. Theoretical background

Phase response curve is an inherent feature of an arbitrary oscillator, which reflects its sensitivity to a brief (pulse-like) stimulus. *PRC* is given by the dependence of the phase shift, induced by a perturbation, as a function of the oscillation phase at which the perturbation has occurred. The effect of phase resetting due to pulse perturbation may formally be treated as follows. We first consider a one-dimensional oscillator, described only by a continuously increasing phase

variable  $\phi$  that evolves as  $\dot{\phi} = \omega$ . Then the system's phase just after a pulse stimulus of strength  $\kappa$  arrived at the moment  $t_p$  can be written as<sup>18,26</sup>

$$\phi_+(t_p) = \phi(t_p) + \kappa Z(\phi, \kappa), \tag{3}$$

where  $Z(\phi, \kappa)$  stands for the *PRC*. In a more general case, periodic oscillations are characterized by a limit-cycle attractor  $X_0(t)$  in an  $N$ -dimensional phase space. Nevertheless, the notion of isochrones<sup>76,77</sup> still allows one to consider a phase space representation of the form  $(\mathbf{a}, \phi)$ , where  $\mathbf{a}$  is an  $(N - 1)$  dimensional "amplitude," and  $\phi$  is the regular phase variable obeying  $\dot{\phi} = \omega$ .<sup>26</sup> Without loss of generality, one may assume that the "amplitude" vanishes on the limit cycle ( $\mathbf{a} = 0$ ). In this setup, if a kick is introduced at the moment  $t_p$ , the reset of the state  $(\mathbf{a}, \phi)$  just after  $t_p$  may be expressed as<sup>26</sup>

$$\begin{aligned} \mathbf{a}_+(t_p) &= \mathbf{a}(t_p) + \kappa A(\mathbf{a}(t_p), \phi(t_p), \kappa) = \kappa A(0, \phi(t_p), \kappa) \\ \phi_+(t_p) &= \phi(t_p) + \kappa \Phi(\mathbf{a}(t_p), \phi(t_p), \kappa) \\ &= \phi(t_p) + \kappa Z(\phi(t_p), \kappa). \end{aligned} \tag{4}$$

The above equations take into account that the initial state lies on the limit cycle ( $\mathbf{a} = 0$ ), such that  $\Phi(0, \phi, \kappa) = Z(\phi, \kappa)$  holds. In terms of application, *PRCs* were first introduced in the study of oscillations in biological systems, including cardiac cells, fireflies populations, and especially neural networks.<sup>56-63</sup> Within these fields, as well the general theory of coupled phase oscillators, the method has facilitated an analysis of the units' interaction properties, including stability, synchronization, or clustering. The concept of *PRCs* allows one to reduce complex models of oscillators to simple phase models which still reflect important features of the original oscillators, viz., the point that the effect of perturbation depends on the dynamical state of the oscillator. In



its representation as a phase oscillator, each oscillator possesses a characteristic *PRC* that can be computed numerically or measured experimentally.<sup>64–68</sup>

Let us now address the details relevant for obtaining the *PRCs* in case of our models of earthquake fault dynamics. In a general multidimensional system, the kick may be applied to any of the system variables. Here, a perturbation is added to the second equation of the system (1) or (2), which is the most plausible choice, because it may be interpreted as a small variation at the loading point. The corresponding equation then takes the form  $\frac{du}{dt} = v - 1 + f(t)$ , where  $f(t)$  is the perturbation term. In real faults, such perturbations may derive from various natural and artificial sources, including rock break, pressure fluctuations, or crack vibration due to the movement of magma and volcanic gases,<sup>69</sup> sudden stress drops,<sup>70,71</sup> drilling and blasting in underground mining activities,<sup>72,73</sup> as well as microearthquakes due to hydraulic fracturing or deep injection of waste fluids.<sup>74</sup>

In order to determine the *PRCs*, one does not have to carry out an explicit phase reduction of the underlying systems, but may rather focus on the occurrence of characteristic events. The latter are associated to large spikes of block's velocity and are representative of earthquakes within the given models. Then, the *PRCs* may effectively be determined in complete analogy to the method typically used for systems of spiking neurons. In particular, the impact of a perturbation is such that it locally changes the oscillation period of a system from the default value  $T_0$  (period in the absence of perturbation) to a different value  $T_1$ , see Fig. 3. One may use this to numerically determine the phase shift  $\Delta\phi$  by measuring the relative change of the period<sup>17,18,26,67,75</sup>

$$\Delta\phi(\phi) = \frac{T_0 - T_1}{T_0}. \quad (5)$$

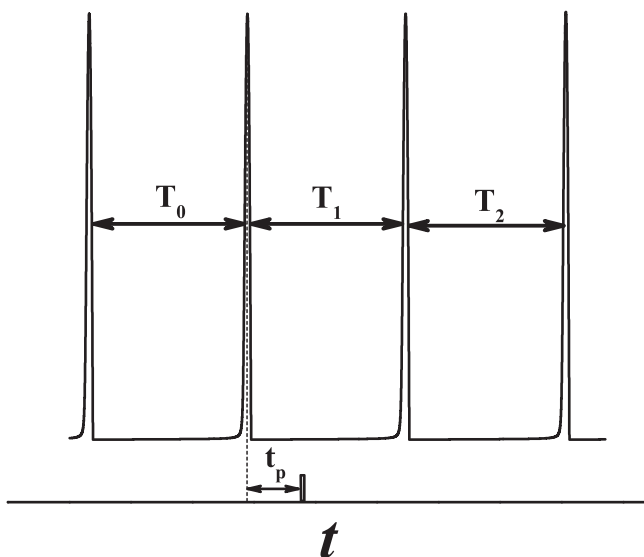


FIG. 3. Illustration of the method used to determine the *PRCs*. The method is based on measuring the perturbation induced changes in oscillation periods of cycles where the pulse perturbation arrived (first-order *PRC*) and the next oscillation cycle (second-order *PRC*).  $T_0$  denotes the default oscillation period,  $T_1$  is the duration of the oscillation cycle influenced by the pulse at phase  $\phi = t_p/T_0$ , whereas  $T_2$  is the duration of the subsequent cycle.

The phase shift  $\Delta\phi$  plotted as a function of the phase  $\phi$  when a perturbation has kicked in is precisely the *PRC*. If  $T_1 < T_0$ , the stimulus advances the cycle and *vice versa*. The change of period of the oscillation cycle where a perturbation has occurred defines the first-order *PRC*. Perturbations may also affect the duration of the next oscillation cycle  $T_2$ , which corresponds to the second-order *PRC*, where the phase shift is given by

$$\Delta\phi^{(2)}(\phi) = \frac{T_0 - T_2}{T_0}. \quad (6)$$

In the seismological context, the second-order *PRC* may be interpreted as qualitatively accounting for a long-term effect of an external perturbation to the pertaining fault dynamics, bearing in mind that the interseismic periods typically comprise very long time scales.

By implementing the described method, we determine the first- and second-order *PRCs* for different models of fault dynamics. Apart from a single pulse perturbation, we also consider scenarios where two subsequent pulses are introduced within a given oscillation cycle. The details regarding the validity of the superposition principle in this case will be discussed in Sec. III C.

The form of the perturbation involves the standard  $\alpha$  function  $f(t) = C * [(-1/t_f) * \exp(-(t - t_p)/t_f) + (1/t_r) * \exp(-(t - t_p)/t_r)] \Theta(t - t_p)$ , whereby the Heaviside  $\Theta$  function is used for shifting along the time-axis. Naturally, the rise and decline characteristic times  $t_r$  and  $t_f$  are selected so that the perturbation maintains a narrow profile compared to the oscillation period ( $t_r = 0.15, t_f = 0.4$ ), whereas  $C$  should be kept sufficiently small so that the perturbation does not affect the amplitude of the underlying oscillations ( $C = 5$ ). A brief remark regarding the explicit form of perturbation is in order. In view of actual fault dynamics, the perturbation form involving the step-like time dependence may be more realistic.<sup>78–80</sup> Nevertheless, within the *PRC* framework, it is well established that the profile of *PRCs* is not qualitatively affected by the particular form of perturbation. In terms of application of the *PRC* theory, the only relevant aspects concern the above conditions on the magnitude and duration of perturbation.

Note that in all the considered instances, zero phase is assigned to the maximum amplitude of the  $u$  variable, which is in the seismological interpretation a natural choice, because it corresponds to the occurrence of the characteristic event (earthquake).

## B. *PRCs* for a single pulse perturbation

In this subsection, we numerically determine the single-pulse *PRCs* for a simple mono-block fault in the stick-slip regime, and then consider how the *PRC* profiles are affected by variation of the fault parameters.

The profiles of the first- and second-order *PRCs* are provided in Fig. 4. Note that in all the figures throughout the paper, the phase values are expressed in units of  $\pi$ . An important point regarding Fig. 4 is that the first-order *PRC* shows a phase advancement only in a narrow phase interval, centered at some small time distance after the earthquake. (Recall that the earthquake event is assigned with  $\phi = 0$ .)

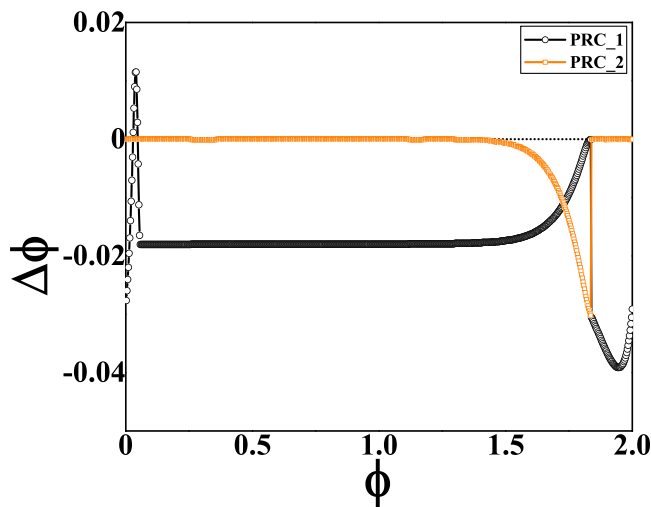


FIG. 4. *PRCs* of the first (black circles) and second order (orange squares) for a monoblock fault in the stick-slip regime. The system parameters are  $(\epsilon, \xi, \gamma) = (1.45, 0.5, 1000)$ .

Nevertheless, the external stimulus introduced at all the other points of the oscillation cycle has a retardation effect, viz., it delays the next characteristic event. The change of sensitivity to a perturbation is expectedly found close to the end of the seismic cycle. In that phase domain, the delay effect is weaker, but the perturbation still cannot advance the cycle. We have verified that the characteristic profile of the *PRC* does not change under variation of the perturbation amplitude within the relevant range of values.

As one may have expected, the second order *PRC* corroborates that the perturbation typically has a negligible impact on the duration of the next seismic cycle. Nevertheless, an interesting point concerns the existence of a long-term retardation effect for  $\phi \approx 1.8\pi$ . Note that this pronounced delay effect occurs precisely in the phase domain where the first-order *PRCs* show a reduced retardation.

Let us now examine how robust are the obtained *PRC* profiles against variation of the fault parameters. It has already been explained that the parameters  $\xi$  and  $\gamma$  are less specific to particular faults, so that the impact of their variation may be of less significance compared to the effect of changing  $\epsilon$ , which is highly specific to particular faults. Still, we note that the *PRC* profiles from Fig. 4 turn out to be generic, i.e., they remain qualitatively unaffected by changing  $\xi$  or  $\gamma$  for fixed  $\epsilon$ . The effects of varying  $\epsilon$  under fixed  $\xi$  and  $\gamma$  are demonstrated in Figs. 5(a) and 5(b). These figures refer to phase shifts corresponding to first- and second-order *PRCs*, respectively, whereby  $\epsilon$  attains values from the seismologically relevant range  $\epsilon \in (1, 3)$ , while  $\xi$  and  $\gamma$  are fixed at values from Fig. 4. Naturally, the parameters of pulse perturbation are the same as in Fig. 4.

Concerning the first-order *PRC*, the effect of advancing the seismic cycle by a perturbation introduced within a preferred time interval just after the earthquake is maintained for most of the considered  $\epsilon$  values, but is downgraded with increasing  $\epsilon$ . In fact, one also finds a critical  $\epsilon$  value above which there is no phase advance, cf. Fig. 5(a). The other interesting effect, which consists in a reduced phase delay if the perturbation occurs close to the end of the seismic cycle,

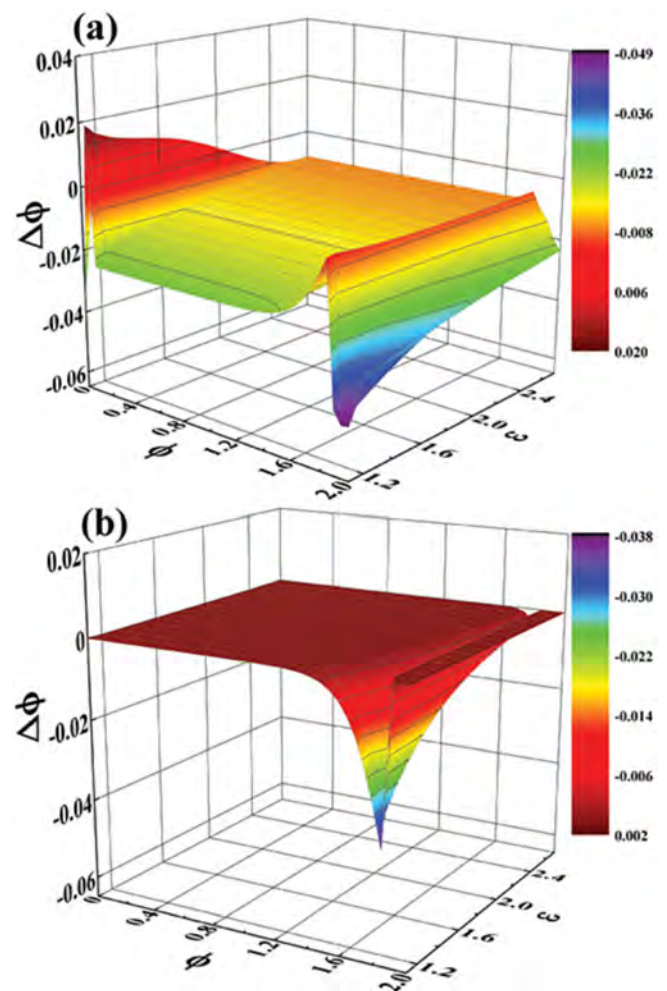


FIG. 5. (a) and (b), respectively, show the families of first- and second-order *PRCs*  $\Delta\phi(\phi, \epsilon)$  for a monoblock fault under variation of  $\epsilon$ . The remaining fault parameters are fixed at  $\xi = 0.5, \gamma = 1000$ .

appears unaffected by variation of  $\epsilon$ . Also, the delay effect characteristic for the most of phase domain is less pronounced with increasing  $\epsilon$ . Therefore, the profile of the first-order *PRC* in general becomes more flat as  $\epsilon$  is enhanced. A similar statement holds in case of the second-order *PRC*. In fact, Fig. 5(b) clearly shows that the pronounced delay effect for the perturbation occurring by the end of the oscillation cycle is gradually lost with  $\epsilon$ .

### C. Two-pulse *PRCs* for a monoblock fault

In this subsection, we consider the response of a monoblock fault in the regime of stick-slip oscillations to two successive pulse perturbations. The first pulse acts at the phase  $\phi_1$  of the oscillation cycle, whereas the other pulse is applied at a phase  $\phi_2$ . Note that the perturbation parameters in both instances are taken to be the same. The occurrence of multiple perturbations during a single oscillation cycle may be attributed to a number of different phenomena, both natural and artificial. Apart from analyzing the pertaining first- and second-order *PRCs*, we also make a remark on the validity of the superposition principle, which assumes the linear summation of phase shifts that result from two successive small perturbations.

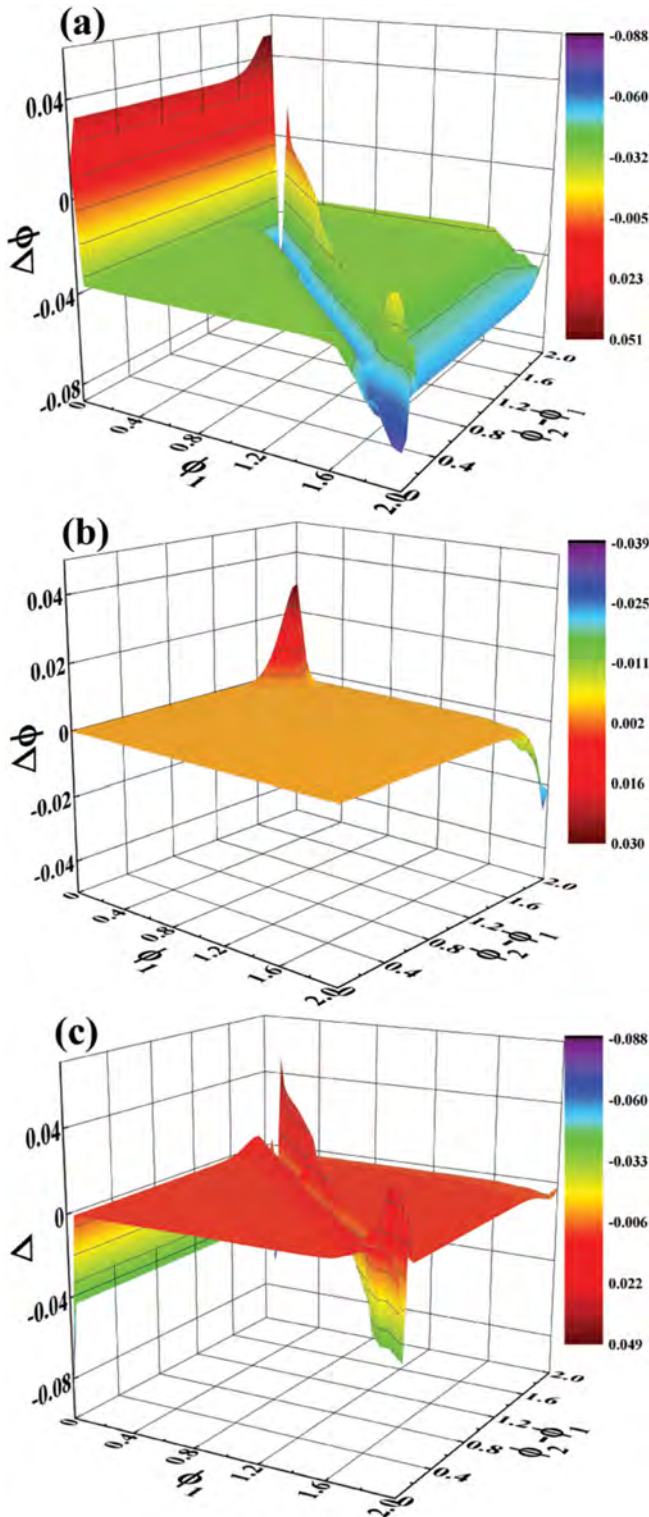


FIG. 6. (a) and (b), respectively, show the *PRCs* of first and second order when a mono-block fault is subjected to two successive pulse perturbations. The first perturbation is introduced at the phase  $\phi_1$ , and the second one is applied with the phase difference  $\phi_2 - \phi_1$ . (c) illustrates the dependence of the deviation from the superposition principle  $\Delta$  on  $\phi_1$  and  $\phi_2 - \phi_1$ . The fault parameters are  $\epsilon = 1.45$ ,  $\xi = 0.5$ ,  $\gamma = 1000$ .

The first-order *PRC* is illustrated in Fig. 6(a). Note that the term *PRC* is preserved for simplicity, though the plot actually shows the dependence of a phase reset in terms of  $\phi_1$  and  $\phi_2 - \phi_1$ . The same terminology is applied when

describing the analogous three-dimensional plots in the remaining part of the paper. Regarding Fig. 6(a), two points on advancing the phase of the seismic cycle stand out. First, if the initial pulse is applied in a narrow interval sufficiently close to the last seismic event ( $\phi = 0$ ), the fault’s phase is substantially advanced, irrespective of the precise point when the second perturbation occurs. Also note that the advancing effect of two pulses is significantly stronger than that of a single pulse, cf. Fig. 4. The second point refers to the domain of  $\phi_1$  values away from the characteristic event. There, the earlier arrival of the first perturbation typically requires a late arrival of the second perturbation in order to cause a substantial phase advancement. However, for sufficiently large  $\phi_1$ , the phase of seismic cycle is advanced only within a narrow interval of preferred  $\phi_2$  values, such that the second pulse arrives in a relatively close succession to the first one. Outside of the  $(\phi_1, \phi_2)$  domains mentioned above, the impact of two successive pulse perturbations is such that they delay the next characteristic event, viz., the perturbations have a stabilizing effect on the fault.

In case of the second-order *PRC*, see Fig. 6(b), one notes a sizeable long-term effect if the first pulse arrives early (small  $\phi_1$ ), and the second pulse is introduced sufficiently late within the given cycle (large  $\phi_2 - \phi_1$ ). It is interesting that the long-term effect may lead either to fault destabilization (advanced phase of oscillation) or fault stabilization (delayed phase of oscillation), which depends sensitively on the phase of the second pulse. Note that we interpret phase advancement (retardation) of the seismic cycle as destabilization (stabilization) of the fault because its next characteristic event is precipitated (postponed) by the perturbation. The presence of both types of behavior is quite distinct from the case of a single pulse perturbation, cf. Fig. 4(b), where the only pronounced effect consists in delaying the next oscillation cycle.

Let us now address the deviation from the superposition principle, which is a nonlinear effect that generally occurs for oscillators with more than one degree of freedom. If the superposition principle were to hold, the phase shift caused by two successive pulses would be given by the sum of the two corresponding *PRCs*, as in case of one-dimensional oscillators. Nevertheless, the actual total phase shift caused by the two pulses in systems with dimension larger than 1 does not coincide with the linear sum of two *PRCs* and may be derived using the formalism from the beginning of this section. In particular, after the first pulse introduced at the moment  $t_p$ , the system is reset to the state given in (4). Just before the second pulse, which arrives at the moment  $t_p + \Delta t$ , the system’s state is  $\phi(t_p + \Delta t) = \phi_+(t_p) + \omega\Delta t$ ,  $\mathbf{a}(t_p + \Delta t) = \Lambda^{\Delta t}(t_p)\mathbf{a}_+(t_p) = \Lambda^{\Delta t}(t_p)\mathbf{a}(0, \phi(t_p), \kappa)$ , where  $\Lambda^{\Delta t}$  is the appropriate evolution operator for the amplitude. Just after the second pulse, the system’s phase is reset to  $\phi_+(t_p + \Delta t) = \phi(t_p + \Delta t) + \kappa\Phi(\mathbf{a}(t_p + \Delta t), \phi(t_p + \Delta t), \kappa)$ , such that the total phase shift induced by the two successive pulses amounts to<sup>26</sup>

$$\Delta\phi = \kappa Z(\phi(t_p), \kappa) + \kappa\Phi(\mathbf{a}(t_p + \Delta t), \phi(t_p + \Delta t), \kappa). \quad (7)$$

An important point is that (7) involves the reset function  $\Phi$  which depends on the system’s amplitude. The presence of

such dependence has been demonstrated to be the reason behind the deviation from the superposition principle for oscillators with more than one degree of freedom. Comparing (7) with the two-pulse *PRC* for a one-dimensional oscillator, one may obtain an explicit expression for the deviation from the superposition principle. In particular, the total phase shift due to two successive pulses for a one-dimensional oscillator is given by  $\delta\phi = \kappa Z(\phi(t_p), \kappa) + \kappa Z(\phi(t_p) + \omega\Delta t + \kappa Z(\phi(t_p), \kappa), \kappa)$ , such that the correction term  $\Delta = \Delta\phi - \delta\phi$  is equal to

$$\begin{aligned} \Delta &= \kappa\Phi(\Lambda^{\Delta t}\kappa A(0, \phi(t_p), \kappa), \mathbf{a}(t_p), \phi(t_p)) \\ &+ \omega\Delta t + \kappa Z(\phi(t_p), \kappa), \kappa) - \kappa Z(\phi(t_p) \\ &+ \omega\Delta t + \kappa Z(\phi(t_p), \kappa), \kappa). \end{aligned} \quad (8)$$

We have numerically determined the correction term  $\Delta$  for the fault dynamics described in (1). The plot illustrated in Fig. 6(c) indicates that the deviation from the superposition principle is most pronounced in the  $(\phi_1, \phi_2)$  domains which admit the advance of phase of the oscillation cycle. In other words, these are the parameter domains where the nonlinear character of system (1) is manifested the most.

#### IV. PHASE RESPONSE OF COMPLEX FAULTS

This section concerns the behavior of complex faults, which may in general consist of multiple segments with different elastic and frictional properties. The focus lies with the paradigmatic case of a complex fault made up of two blocks. We first analyze the sensitivity to a perturbation for the homogeneous fault composed of identical blocks, and then consider the heterogeneous fault, where the blocks are characterized by distinct  $\epsilon$  values.

##### A. *PRCs* for the fault composed of two identical blocks

For the homogeneous complex fault, we analyze the scenario where the perturbation on block 1 acts at phase  $\phi_1$  of its oscillation cycle, whereas block 2 receives a kick with the phase difference  $\phi_2 - \phi_1 > 0$ . The form of perturbation on both blocks is assumed to be identical.

The first- and second-order *PRCs* for the appropriate version of system (2) are illustrated in Fig. 7. The respective phase shifts are denoted by  $\Delta\phi_{ij}$ , where the first index refers to the particular block, and the second index points to the first/second order of the phase response. It is interesting to

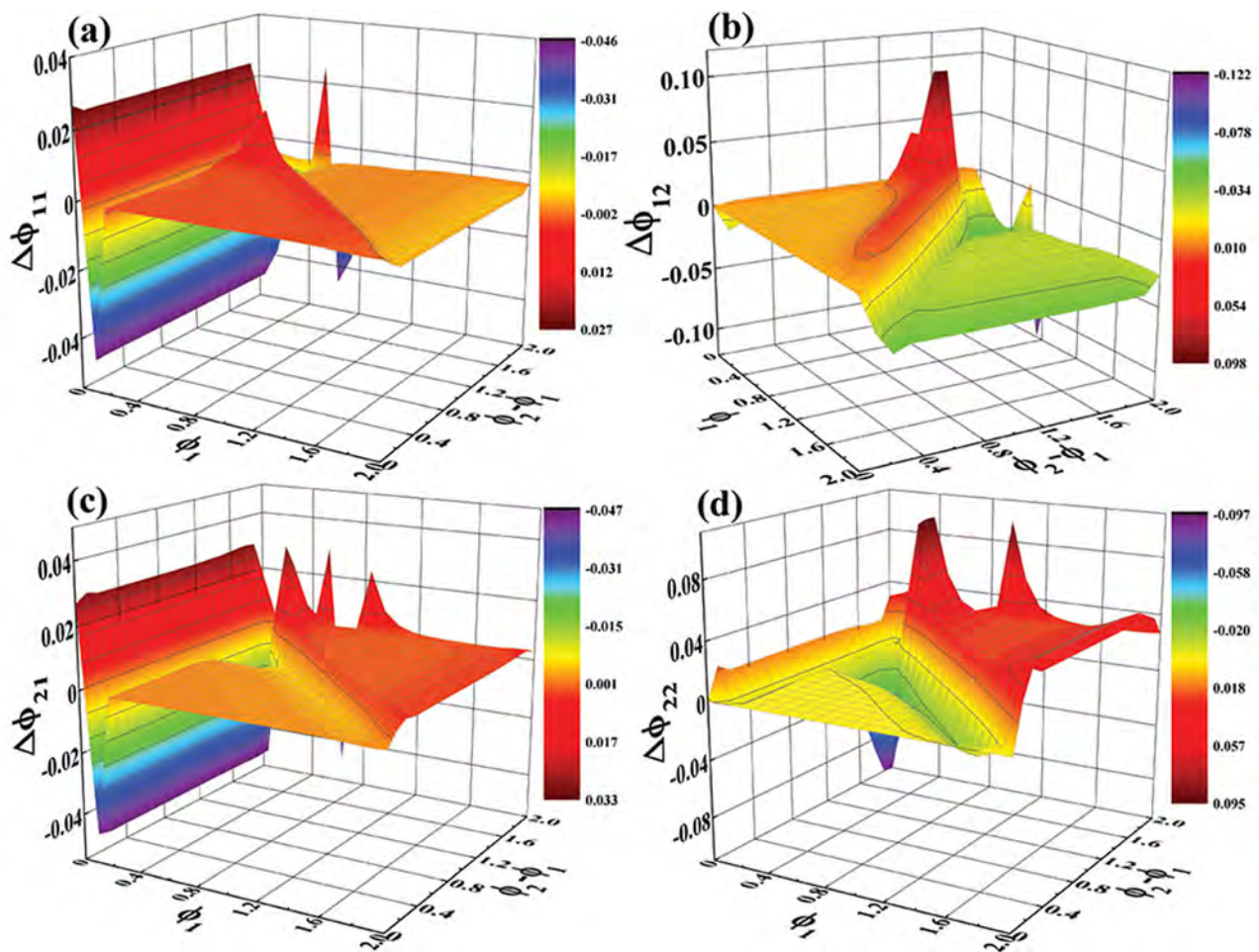


FIG. 7. The top (bottom) row shows the phase responses of the first (left column) and second order (right column) for block 1 (2) in dependence of  $\phi_1$  and  $\phi_2 - \phi_1$ . The blocks are assumed to be identical, and are characterized by parameters  $\epsilon = 1.45, \zeta = 0.5, \gamma = 1000$ . The interaction strength  $c = 0.1$  lies well below the critical bifurcation value and warrants that the periodic oscillations on the coupled blocks are not substantially different from those in the uncoupled case.

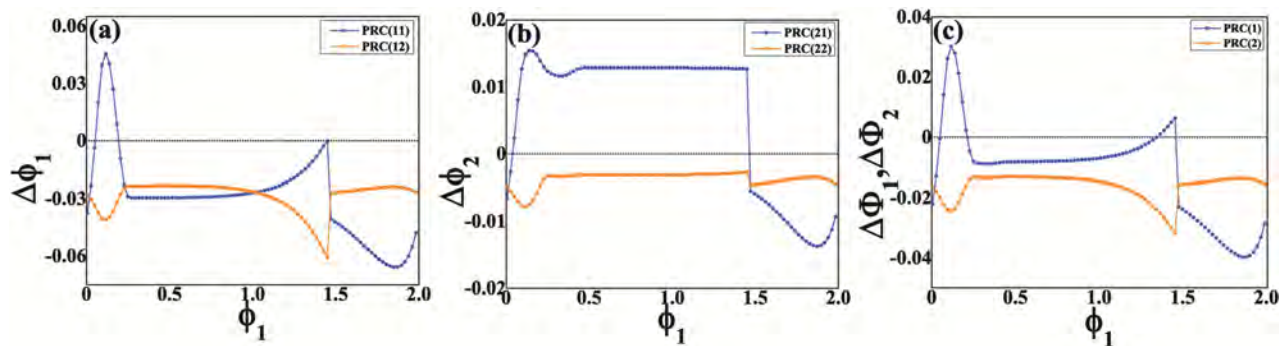


FIG. 8. Scenario where pulse perturbation is introduced to the block with shorter oscillation period. In (a) are shown the first- (blue circles) and second-order *PRCs* (orange squares) for block 1, which is subjected to pulse perturbation. (b) illustrates the first- and second-order *PRCs* for block 2 which is influenced by perturbation only via interaction with block 1. (c) provides an indication on the average phase response  $\Delta\Phi_i$ ,  $i \in \{1, 2\}$  for the total system, viz., the complex fault, whereby index  $i$  refers to the first- or second-order dependence. The block parameters kept fixed are  $\xi = 0.5$ ,  $\gamma = 1000$ , whereas  $\epsilon$  values on particular blocks are  $\epsilon_1 = 1.4$  and  $\epsilon_2 = 2$ .

compare the first-order *PRCs* in Figs. 7(a) and 7(c), because this indicates how the interaction affects the response of individual blocks. In particular, the phase of both blocks is significantly advanced if the first block is stimulated immediately after the characteristic event. In this case, a perturbation of the first block induces a strong destabilization effect on the dynamics of the second block, irrespective of when the second block is perturbed. Just beyond the described region of  $\phi_1$  values, one encounters a narrow domain where the external stimuli delay the cycles of both blocks. Nevertheless, the most interesting point concerns the differences between  $\Delta\phi_{11}$  and  $\Delta\phi_{21}$  dependences. We find that  $\Delta\phi_{21}$  shows a much larger  $(\phi_1, \phi_2)$  domain where the phase of the cycle is strongly advanced compared to  $\Delta\phi_{11}$ . This point corroborates that the dynamics of block 2 is substantially affected by the perturbation of block 1 conveyed via the interaction term. In fact, within the indicated  $(\phi_1, \phi_2)$  domain, the destabilization effect on block 2 is amplified by the coaction of two pulses, reflected in an indirect influence of a perturbation applied to the first block, and a direct impact of the subsequent pulse. Note that the destabilization effect on block 2 is more pronounced if the perturbation on block 1 arrives by the end of its oscillation cycle.

As far as the second order *PRCs* are concerned, Figs. 7(b) and 7(d) both show quite large  $(\phi_1, \phi_2)$  domains of substantial phase advancement and phase retardation. These long-term effects are caused by the interaction between the blocks. Note that for the same  $(\phi_1, \phi_2)$  values, the long-term effects on two blocks are of different nature. In particular, stabilization (phase delay) of one block is accompanied by a destabilization (phase advancement) of the other block.

## B. *PRCs* for the two-block inhomogeneous fault

In this subsection, we examine the *PRCs* of an inhomogeneous fault made up of two blocks with disparate  $\epsilon$  values. The latter are selected so that the respective oscillation periods of coupled units are quite distinct,  $T_1 \approx 51$  vs  $T_2 \approx 77$ . Two different cases are considered: in the first instance, the perturbation is applied only to the block with the shorter oscillation period (here block 1), whereas in the second instance, the block with the longer oscillation period is stimulated (here

block 2). The simulations are carried out in such a way that at the moment when the stimulus arrives to one block, the other block always has the same phase.

The results for the first scenario (perturbation applied to block 1 at phase  $\phi_1$ ) are illustrated in Fig. 8, whereby Figs. 8(a) and 8(b) refer to first- and second-order responses of blocks 1 and 2, respectively. Note that Fig. 8(c) shows the average responses  $\Delta\Phi_i = (\Delta\phi_{1,i} + \Delta\phi_{2,i})/2$  for the total system (complex fault), where  $i \in \{1, 2\}$  stands for the first- or second-order response.

As to be expected, for block 1, the first- and second-order *PRCs* are qualitatively similar to that of an uncoupled block, cf. Fig. 4(a). As far as block 2 is concerned, note that Fig. 8(b) shows the dependence  $\Delta\phi_2(\phi_1)$ , which is obtained for a fixed value of the phase of the second block. In other words, a perturbation is applied at different phases of the cycle of block 1, whereas block 2 at the moment of pulse arrival to block 1 always lies at a certain fixed phase  $\phi_2$ . The first-order response of block 2 implies that the interaction may play an important role in destabilization of the fault. In particular, a perturbation acting on the block with a shorter oscillation period (block 1) is found to substantially advance the phase of the block with the longer oscillation period (block 2) for a broad interval of  $\phi_1$  values. Note that Fig. 8(c) implies that the average response of the two-block system is dominated by the behavior of block 1 where the perturbation is actually applied.

Now let us consider the case of an inhomogeneous two-block fault model where the block characterized by the longer oscillation period (block 2) is perturbed. In analogy to the case above, a perturbation is applied at different phases of the cycle of block 2, whereas block 1 at the moment of pulse arrival to block 2 always has a fixed phase value  $\phi_1$ . The first-order responses of the blocks are shown in Fig. 9(a), whereas Fig. 9(b) refers to the second-order responses. The average first- and second-order response of the complex two-block fault is provided in Fig. 9(c).

At variance with the scenario considered in Fig. 8, the first-order *PRC* for the kicked block now shows two phase intervals which admit an advancement of the seismic cycle, one closely after the characteristic event ( $\phi_2 \approx 0.1\pi$ ), and the other located by the end of the seismic cycle ( $\phi_2 \approx 1.5$ ).

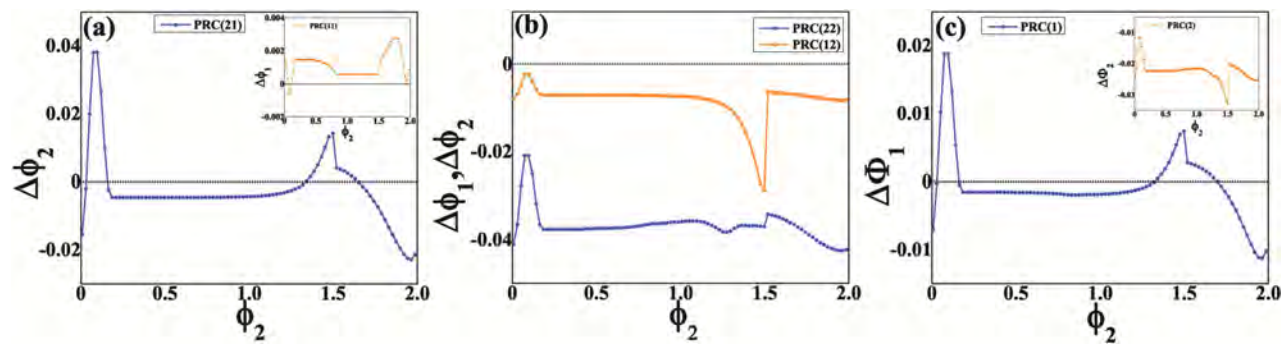


FIG. 9. Scenario where pulse perturbation acts on the block with longer oscillation period. The main frame and inset in (a) shows the first-order *PRC* for block 2 and block 1, respectively. In (b) are shown the second-order *PRCs*, whereby the blue circles (orange squares) are reserved for block 2 (block 1). The main frame and the inset in (c) illustrate the average first- and second-order phase response for the complex fault, respectively. The block parameters are the same as in Fig. 8.

Nevertheless, an important qualitative finding on the first-order response of block 1 is that for almost all  $\phi_2$ , the perturbation on block 2 advances the oscillation cycle on block 1. The analogous effect of phase advance has already been seen in Fig. 8(b), but not in such a broad domain of perturbation phases. As far as the total system is concerned, the first-order response is mostly influenced by the behavior of the block explicitly affected by the perturbation, whereas the leading delay effect in the second-order response derives from the other block, cf. Fig. 9(c).

## V. SUMMARY

In this paper, we have used the framework of *PRCs* to analyze effects of external perturbations in basic models of earthquake fault dynamics. To our knowledge, such an analysis has not been applied earlier in this field, but has been successfully implemented in the fields of neuroscience and the general theory of systems of coupled phase oscillators. The considered models qualitatively reproduce the stick-slip behavior typical for earthquake motion. Nevertheless, the very notion that the fault dynamics resembles to a relaxation oscillator cannot hold in general, but may be considered as a first approximation to behavior of faults which exhibit characteristic earthquakes with a well-defined recurrence period and low variability (the comparably small coefficient of variation for the timing of the events). Within the proposed concept, external perturbations can influence the duration of the seismic cycle where they have occurred, and may also result in long-term effects, reflected in a change of the subsequent oscillation period. These two points are qualitatively illustrated by the profiles of the obtained first and second-order *PRCs*, respectively. The impact of perturbations can be interpreted as either stabilizing or destabilizing to fault dynamics, in a sense that the external stimuli may either advance the phase of the seismic cycle, thereby precipitating the next characteristic event, or may delay the cycle, thus postponing the next large event.

Our study has been concerned with the models of a simple mono-block fault, as well as paradigmatic examples of complex faults involving two identical or distinct blocks. For a mono-block fault, we have examined how the underlying dynamics is affected by a single or two successive pulse

perturbations. In the former case, it is found that external stimuli typically delay the phase of the given oscillation cycle. The exception to this behavior is provided by the stimuli arriving within a narrow interval just after the characteristic event, which result in advancing the phase of the seismic cycle. The second-order *PRCs* indicate an interesting delaying long-term effect for pulses that arrive by the end of the given cycle, which is likely associated with a strong logarithmic nonlinearity of the underlying model. The obtained *PRC* profiles are shown to be relatively robust to variation of fault parameters. The fault dynamics under the influence of two successive pulses is more complex and involves two different mechanisms that may give rise to phase advancement. One mechanism is dominated by the first pulse and is completely analogous to what is found in case of a single perturbation, but the other mechanism is qualitatively distinct and requires that the pulses arrive with a specific phase difference.

For a homogeneous two-block fault, we have considered the scenario where each block is affected by a single pulse perturbation. This is realized by selecting a block which is always perturbed before the other block. The first-order *PRCs* indicate that the most likely outcome is fault destabilization, viz., the advance of oscillation phase at both blocks. Such a behavior is contributed by the interaction between the blocks. The second-order *PRCs* reveal highly complex long-term effects, which may be stabilizing or destabilizing to fault dynamics, depending on the times of pulse arrivals. It is interesting that the long-term effects on the blocks can be asymmetric, in a sense that the cycle of one block is advanced, whereas the cycle of the other block is delayed.

For a heterogeneous two-block fault, we have examined scenarios where the block with a shorter or a longer oscillation period receives a single pulse perturbation. In both instances, the simulations are carried out in such a way that at the moment when the stimulus arrives to one block, the other block always has the same phase. An interesting point concerns the advance of phase displayed by the first-order *PRCs* of the respective blocks that are not subjected to pulse perturbation. It turns out that the effect of perturbation conveyed via interaction between the blocks is non-negligible, and its impact on the block that has not received the pulse perturbation is found to be typically destabilizing.

One should caution that the results obtained here cannot be considered within the context of earthquake hazard assessment, nor can immediately be tied to studies of the earthquake triggering effect.<sup>52,70,81</sup> In reference to the latter point, an interesting issue would be to examine the sensitivity of faults to a stronger perturbation that may affect the amplitude of oscillations. An elaborate investigation of a potential relation between responses of a fault to small perturbation, relevant to the *PRC* theory, and the sensitivity to finite perturbations possibly associated to triggering effect should be an important topic for a future study. Regarding the possible application of the current results, one notes that at variance with the case of a monoblock fault, the *PRCs* for heterogeneous two-block fault exhibit phase advancement for perturbation acting at the later stages of the cycle, cf. Figs. 8(b) and 8(c), as well as Figs. 9(a) and 9(c). At both instances, the advance of phase cycle is found for the block with the longer oscillation period and for the total phase of the compound fault, both in cases where the given block is directly perturbed or when the perturbation is transferred via interaction with the other block. It is reasonable to suggest that the perturbation destabilizing the fault in such a fashion gives rise to a clock advance effect which may be seen as a paradigm for studying the appearance of aftershocks.<sup>82</sup>

It would be interesting to determine how generic are the results obtained, i.e., whether the *PRC* profiles found here can be corroborated for other models of earthquake fault dynamics involving different approximations, containing more complex fault structure and featuring distinct friction laws. In a broader perspective, one wonders whether it would be possible to classify different models of fault dynamics in a fashion similar to what has been done in other fields, e.g., for the neuron models where class I excitability is dominated by phase-advance dynamics, whereas class II excitability has both the regimes of phase advance and delay.<sup>17,18</sup>

## ACKNOWLEDGMENTS

This research was supported by the Ministry of Education, Science and Technological Development of the Republic of Serbia (project Nos. ON171017 and OI1611005 to IF, and project No. ON17176016 to SK), the Slovenian Research Agency (Grant Nos. P5-0027 and J1-7009 to MP), the DFG/FAPESP (Grant IRTG 1740/TRP 2011/50151-0 to JK), the Russian Foundation for Basic Research (Grant Nos. 15-32-50402 and 15-02-04245 to VN, Grant 14-02-00042 to VK), the Government of the Russian Federation (Agreement No. 14.Z50.31.0033 to VK, VN and JK) and the Ministry of Education and Science of the Russian Federation (Agreement No. MK-8460.2016.2 to VK). The numerical simulations were run on the PARADOX supercomputing facility at the Scientific Computing Laboratory of the Institute of Physics Belgrade.

<sup>1</sup>H. Kawamura, T. Hatano, N. Kato, S. Biswas, and B. K. Chakrabarti, *Rev. Mod. Phys.* **84**, 839 (2012).

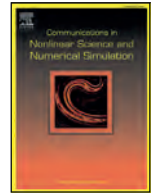
<sup>2</sup>C. H. Scholz, *The Mechanics of Earthquakes and Faulting*, 2nd ed. (Cambridge University Press, New York, 2002).

<sup>3</sup>*Earthquake Seismology: Treatise on Geophysics*, 1st ed., edited by H. Kanamori (Elsevier, Amsterdam, 2009), Vol. 4.

- <sup>4</sup>W. F. Brace and J. D. Byerlee, *Science* **153**, 990 (1966).
- <sup>5</sup>N. M. Beeler, D. L. Lockner, and S. H. Hickman, *Bull. Seismol. Soc. Am.* **91**, 1797 (2001).
- <sup>6</sup>C. Marone, *Annu. Rev. Earth Planet Sci.* **26**, 643 (1998).
- <sup>7</sup>*Modeling Critical and Catastrophic Phenomena in Geoscience*, edited by P. Bhattacharyya and B. Chakrabarti (Springer, Berlin, Heidelberg, 2006).
- <sup>8</sup>R. Burridge and L. Knopoff, *Bull. Seismol. Soc. Am.* **57**, 341 (1967); available online <http://www.bssaonline.org/content/57/3/341.abstract>.
- <sup>9</sup>J. M. Carlson and J. S. Langer, *Phys. Rev. Lett.* **62**, 2632 (1989).
- <sup>10</sup>J. M. Carlson and J. S. Langer, *J. Geophys. Res.* **96**, 4255, doi:10.1029/90JB02474 (1991).
- <sup>11</sup>J. M. Carlson, *Phys. Rev. A* **44**, 6226 (1991).
- <sup>12</sup>A. Ruina, *J. Geophys. Res.* **88**, 10359, doi:10.1029/JB088iB12p10359 (1983).
- <sup>13</sup>J. R. Rice and S. T. Tse, *J. Geophys. Res.* **91**, 521, doi:10.1029/JB091iB01p00521 (1986).
- <sup>14</sup>J. R. Rice, N. Lapusta, and K. Ranjith, *J. Mech. Phys. Solids* **49**, 1865 (2001).
- <sup>15</sup>Y. Kuramoto, *Chemical Oscillations, Waves, and Turbulence* (Dover, Mineola, New York, 2003).
- <sup>16</sup>A. T. Winfree, *The Geometry of Biological Time* (Springer, Berlin, 1980).
- <sup>17</sup>P. A. Tass, *Phase Resetting in Medicine and Biology: Stochastic Modeling and Data Analysis* (Springer, Berlin, Heidelberg, 2007).
- <sup>18</sup>*Phase Response Curves in Neuroscience: Theory, Experiment, and Analysis*, edited by N. W. Schultheiss, A. A. Prinz, and R. J. Butera (Springer, New York, 2012).
- <sup>19</sup>C. C. Canavier, *Scholarpedia* **1**, 1332 (2006).
- <sup>20</sup>C. H. Scholz, *B. Seismol. Soc. Am.* **100**, 901 (2010).
- <sup>21</sup>N. Sugiura, T. Hori, and Y. Kawamura, *Nonlinear Processes Geophys.* **21**, 251 (2014).
- <sup>22</sup>O. Lursmanashvili, T. Paatashvili, and L. Gheonjian, in *Synchronization and Triggering: from Fracture to Earthquake Processes*, edited by V. de Rubéis, Z. Czechowski, and R. Teisseyre (Springer-Verlag, Berlin-Heidelberg, 2010).
- <sup>23</sup>K. Vasudevan, M. Cavers, and A. Ware, *Nonlinear Processes Geophys.* **22**, 499 (2015).
- <sup>24</sup>J. L. Perez Velazquez, R. F. Galán, L. Garcia Dominguez, Y. Leshchenko, S. Lo, J. Belkas, and R. Guevara Erra, *Phys. Rev. E* **76**, 061912 (2007).
- <sup>25</sup>T. Tatenno and H. P. C. Robinson, *Biophys. J.* **92**, 683 (2007).
- <sup>26</sup>G. P. Krishnan, M. Bazhenov, and A. Pikovsky, *Phys. Rev. E* **88**, 042902 (2013).
- <sup>27</sup>S. Achuthan and C. C. Canavier, *J. Neurosci.* **29**, 5218 (2009).
- <sup>28</sup>Y. Kawamura, H. Nakao, K. Arai, H. Kori, and Y. Kuramoto, *Phys. Rev. Lett.* **101**, 024101 (2008).
- <sup>29</sup>H. Kori, Y. Kawamura, H. Nakao, K. Arai, and Y. Kuramoto, *Phys. Rev. E* **80**, 036207 (2009).
- <sup>30</sup>T.-W. Ko and G. B. Ermentrout, *Phys. Rev. E* **79**, 016211 (2009).
- <sup>31</sup>Z. Levnjajić and A. Pikovsky, *Phys. Rev. E* **82**, 056202 (2010).
- <sup>32</sup>S. G. Wesnousky, *Bull. Seismol. Soc. Am.* **84**, 1940 (1994); available at <http://www.bssaonline.org/content/84/6/1940.abstract>.
- <sup>33</sup>K. Sieh, *Proc. Natl. Acad. Sci. U. S. A.* **93**, 3764 (1996).
- <sup>34</sup>P. Tapponnier, F. J. Ryerson, J. Van der Woerd, A. S. Mriaux, and C. Lasserre, *C. R. Acad. Sci., Ser. IIa: Earth Planet. Sci.* **333**, 483 (2001).
- <sup>35</sup>S. P. Nishenko and R. Buland, *Bull. Seismol. Soc. Am.* **77**, 1382 (1987); available at <http://www.bssaonline.org/content/77/4/1382.abstract>.
- <sup>36</sup>T. Parsons, *Geophys. Res. Lett.* **35**, L21301, doi:10.1029/2008GL035887 (2008).
- <sup>37</sup>L. Benedetti *et al.*, *J. Geophys. Res. Solid Earth* **118**, 4948 (2013).
- <sup>38</sup>K. M. Scharer, G. P. Biasi, R. J. Weldon, and T. E. Fumal, *Geology* **38**, 555 (2010).
- <sup>39</sup>Y. Klinger, M. Etchebes, P. Tapponnier, and C. Narteau, *Nat. Geosci.* **4**, 389 (2011).
- <sup>40</sup>L. Haibing, J. Van der Woerd, P. Tapponnier, Y. Klinger, Q. Xuexiang, Y. Jingsuia, and Z. Yintang, *Earth Planet. Sci. Lett.* **237**, 285 (2005).
- <sup>41</sup>L. R. Sykes and W. Menke, *B. Seismol. Soc. Am.* **96**, 1569 (2006).
- <sup>42</sup>K. Ishibashi, *Ann. Geophys.* **47**, 339 (2004).
- <sup>43</sup>T. Matsuzawa, T. Igarashi, and A. Hasegawa, *Geophys. Res. Lett.* **29**, 1543, doi:10.1029/2001GL014632 (2002).
- <sup>44</sup>R. M. Nadeau and T. V. McEvilly, *Bull. Seismol. Soc. Am.* **87**, 1463 (1997); available at <http://bssa.geoscienceworld.org/content/87/6/1463>.
- <sup>45</sup>T. Mori and H. Kawamura, *Phys. Rev. Lett.* **94**, 058501 (2005).
- <sup>46</sup>T. Mori and H. Kawamura, *J. Geophys. Res.* **111**, B07302, doi:10.1029/2005JB003942 (2006).
- <sup>47</sup>T. Kotani, H. Yoshino, and H. Kawamura, *Phys. Rev. E* **77**, 010102(R) (2008).
- <sup>48</sup>C. G. Sammis and S. W. Smith, *Tectonophysics* **589**, 167 (2013).
- <sup>49</sup>J. M. Carlson, J. S. Langer, B. E. Shaw, and C. Tang, *Phys. Rev. A* **44**, 884 (1991).

- <sup>50</sup>B. Erickson, B. Birnir, and D. Lavallée, *Nonlinear Processes Geophys.* **15**, 1 (2008).
- <sup>51</sup>B. Erickson, B. Birnir, and D. Lavallée, *Geophys. J. Int.* **187**, 178 (2011).
- <sup>52</sup>S. Kostić, I. Franović, M. Perc, N. Vasović, and K. Todorović, *Sci. Rep.* **4**, 5401 (2014).
- <sup>53</sup>S. Kostić, N. Vasović, I. Franović, and K. Todorović, *Nonlinear Processes Geophys.* **20**, 857 (2013).
- <sup>54</sup>S. Kostić, I. Franović, K. Todorović, and N. Vasović, *Nonlinear Dyn.* **73**, 1933 (2013).
- <sup>55</sup>M. L. Blanpied, C. J. Marone, D. A. Lockner, J. D. Byerlee, and D. P. King, *J. Geo. Res.* **103**, 9691 (1998).
- <sup>56</sup>R. E. Mirollo and S. H. Strogatz, *SIAM J. Appl. Math.* **50**, 1645 (1990).
- <sup>57</sup>G. B. Ermentrout and N. Kopell, *J. Math. Biol.* **29**, 195 (1991).
- <sup>58</sup>Y. Kuramoto, *Physica D* **50**, 15 (1991).
- <sup>59</sup>S. Bottani, *Phys. Rev. Lett.* **74**, 4189 (1995).
- <sup>60</sup>L. Glass, *Nature* **410**, 277 (2001).
- <sup>61</sup>L. Glass, Y. Nagai, K. Hall, M. Talajic, and S. Nattel, *Phys. Rev. E* **65**, 1 (2002).
- <sup>62</sup>V. V. Klinshov and V. I. Nekorkin, *Chaos Soliton. Fract.* **44**, 98 (2011).
- <sup>63</sup>V. V. Klinshov and V. I. Nekorkin, *Phys.-Usp.* **56**, 1217 (2013).
- <sup>64</sup>G. B. Ermentrout, *Neural Comput.* **8**, 979–1001 (1996).
- <sup>65</sup>G. B. Ermentrout, I. I. Beverlin Bryce, T. Troyer, and T. Netoff, *J. Comput. Neurosci.* **31**, 185–197 (2011).
- <sup>66</sup>R. F. Galán, G. B. Ermentrout, and N. N. Urban, *Phys. Rev. Lett.* **94**, 158101 (2005).
- <sup>67</sup>V. V. Klinshov, D. S. Shchapin, and V. I. Nekorkin, *Phys. Rev. E* **90**, 042923 (2014).
- <sup>68</sup>I. S. Proskurkin, A. I. Lavrova, and V. K. Vanag, *Chaos* **25**, 064601 (2015).
- <sup>69</sup>B. A. Chouet, *Nature* **380**, 309 (1996).
- <sup>70</sup>M. E. Belardinelli, A. Bizzarri, and M. Cocco, *J. Geo. Res.* **108**, 2135, doi:10.1029/2002JB001779 (2003).
- <sup>71</sup>H. Perfettini, J. Schmittbuhl, and A. Cochard, *J. Geo. Res.* **108**, 2409, doi:10.1029/2002JB001804 (2003).
- <sup>72</sup>W. Lu, J. Yang, P. Yan, M. Chen, C. Zhou, Y. Luo, and L. Jin, *Int. J. Rock Mech. Min. Sci.* **53**, 129 (2012).
- <sup>73</sup>F. Mulargia and A. Bizzarri, *Sci. Rep.* **4**, 6100 (2014).
- <sup>74</sup>W. L. Ellsworth, *Science* **341**, 1225942 (2013).
- <sup>75</sup>G. B. Ermentrout and D. H. Terman, *Mathematical Foundations of Neuroscience* (Springer, New York, 2010).
- <sup>76</sup>J. Guckenheimer, *J. Math. Biol.* **1**, 259 (1975).
- <sup>77</sup>J. T. C. Schwabedal and A. Pikovsky, *Phys. Rev. Lett.* **110**, 204102 (2013).
- <sup>78</sup>R. S. Stein, *Nature* **402**, 605 (1999).
- <sup>79</sup>M. Dragoni and A. Piombo, *Nonlinear Processes Geophys.* **18**, 431 (2011).
- <sup>80</sup>M. Dragoni and A. Piombo, *Pure Appl. Geophys.* **172**, 2571 (2015).
- <sup>81</sup>A. M. Freed, *Annu. Rev. Earth Planet. Sci.* **33**, 335 (2005).
- <sup>82</sup>K. R. Felzer and E. E. Brodsky, *Nature* **441**, 735 (2006).





# Earthquake nucleation in a stochastic fault model of globally coupled units with interaction delays



Nebojša Vasović<sup>a</sup>, Srđan Kostić<sup>b,\*</sup>, Igor Franović<sup>c</sup>, Kristina Todorović<sup>d</sup>

<sup>a</sup> Department of Applied Mathematics, Faculty of Mining and Geology, University of Belgrade, Serbia

<sup>b</sup> Institute for Development of Water Resources "Jaroslav Černi", Jaroslava Černog 80, 11226 Belgrade, Serbia

<sup>c</sup> Scientific Computing Lab, Institute of Physics, University of Belgrade, Serbia

<sup>d</sup> Department of Physics and Mathematics, Faculty of Pharmacy, University of Belgrade, Serbia

## ARTICLE INFO

### Article history:

Received 6 March 2015

Revised 9 December 2015

Accepted 7 February 2016

Available online 26 February 2016

### Keywords:

Time delay

Seismic noise

Bifurcation

Bistability

## ABSTRACT

In present paper we analyze dynamics of fault motion by considering delayed interaction of 100 all-to-all coupled blocks with rate-dependent friction law in presence of random seismic noise. Such a model sufficiently well describes a real fault motion, whose prevailing stochastic nature is implied by surrogate data analysis of available GPS measurements of active fault movement. Interaction of blocks in an analyzed model is studied as a function of time delay, observed both for dynamics of individual faults and phenomenological models. Analyzed model is examined as a system of all-to-all coupled blocks according to typical assumption of compound faults as complex of globally coupled segments. We apply numerical methods to show that there are local bifurcations from equilibrium state to periodic oscillations, with an occurrence of irregular aperiodic behavior when initial conditions are set away from the equilibrium point. Such a behavior indicates a possible existence of a bi-stable dynamical regime, due to effect of the introduced seismic noise or the existence of global attractor. The latter assumption is additionally confirmed by analyzing the corresponding mean-field approximated model. In this bi-stable regime, distribution of event magnitudes follows Gutenberg–Richter power law with satisfying statistical accuracy, including the b-value within the real observed range.

© 2016 Elsevier B.V. All rights reserved.

## 1. Introduction

Burridge–Knopoff (BK) model is commonly recognized as a phenomenological model of earthquake fault motion. Since the original experiment of Burridge and Knopoff [1], an array of interconnected blocks driving along the rough surface has been used to mimic the seismic movement along a fault, whose dynamics was repeatedly proved to obey Gutenberg–Richter and Omori–Utsu law [1–7]. Two different models are typically analyzed in this case: discrete one-dimensional or two-dimensional BK model and cellular automata version, initially proposed by Olami et al. [8]. Both of these models are equally used in observing the qualitative features of seismic fault motion [9–12]. Except for the seismic features arising from the specific friction law at the contact of blocks and rough surface of the lower plate [1,13–15] and from the viewpoint of statistical physics [16], BK model and its different variants have been studied from the viewpoint of nonlinear dynamics. Practically, dynamical instabilities in BK model have been studied mainly for single- and two-block models. Apparently, symmetric two-block models can produce spatially asymmetric dynamics [17]. On the other hand, asymmetric models, e.g. with different

\* Corresponding author. Tel.: +381 642848406.

E-mail address: [srdjan.kostic@jcerni.co.rs](mailto:srdjan.kostic@jcerni.co.rs) (S. Kostić).

friction forces on each block, exhibit deterministic chaos for certain parameter ranges [18]. Field et al. [19] analyzed an electronic analog of a two-block mechanical system, and found very rich dynamics as a function of coupling strength. Indeed, their results indicate that the circuit exhibits alternating regions of periodic and chaotic behavior as coupling strength is varied. Galvanetto [20] studied the two-block BK model and showed that several periodic, quasi-periodic and chaotic attractors can coexist in this simple system. Erickson et al. [21] analyzed dynamics of one-block BK model with Dieterich–Ruina friction law and found that system undergoes a Hopf bifurcation to a periodic orbit, which then undergoes a period doubling cascade into a strange attractor. Similarly, the same authors [22] analyzed the dynamics of one-dimensional BK model, and showed that it also exhibits both periodic and chaotic motions, but with the size-dependent system's transition to chaos. Within this research, we also analyze behavior of one-dimensional BK model from the viewpoint of nonlinear dynamics.

One should note that all of these previous studies on the dynamics of BK model analyzed the motion of an array of blocks as a deterministic system, without any stochastic variable. However, if we take into account the fact that the real observed fault motion is stochastic by nature, the starting BK model becomes stochastic, which further excludes the possible occurrence of deterministic chaos. Such a stochasticity naturally arises due to existence of random uncorrelated seismic noise, which originates from small-scale faulting, different irregularities and inhomogeneities or it is of undefined origin [23,24]. For this reason, in present paper we analyze dynamics of BK model in presence of random noise. Nevertheless, it is necessary to emphasize that coherent noise is hardly expected to occur at the seismogenic depth, since it typically arises from the reflection of seismic waves, ground rolls, traffic noise, etc.

Besides the neglected effect of seismic noise on dynamics of fault motion, preceding research on this topic included only the nearest-neighbor coupling in BK model, with only few studies on variable range interaction, primarily from the viewpoint of statistical physics [7,12]. However, long-range interactions are also observed in natural conditions. If we take San Andreas fault system as an example, Sanders [25] suggested that deformation of the northern part of San Jacinto fault zone affects the deformation on the Mojave segment of the San Andreas fault zone, due to geometric continuity of these two fault zones near their intersection. In particular, San Jacinto zone exhibits a seismic cycle every 150 years, which is similar to 132 years of seismic cycle for Mojave segment of San Andreas zone, which could imply that the concentrated stress increase along San Jacinto zone could help induce rupture of the Mojave segment on a similar time scale. If we follow the same reasoning as in Sanders [25], due to geometric continuity among adjacent parts of different segments of San Andreas fault, we could assume that deformation along one fault segment affects deformation along other parts of the same fault, since Johnson and Segall [26] reported that recurrence time of the northern part of San Andreas fault is in the range 188–315 years, close to 132 years for Mojave segment. Now, if we take a look at great earthquakes recorded along the San Andreas fault, namely M7.7 from 1680 in Salton Trough, M7.9 from 1857 in Fort Tejon and M7.8 from 1906 in San Francisco, we could conclude there is an average recurrence period of approximately 150 years between large earthquakes along a single fault. This fact is presumed to confirm two basic assumptions: (1) that all segments of the same fault are indeed in interaction (case of globally coupled units) and (2) that there is a certain delayed effect in their interaction. One should note that, from the viewpoint of nonlinear dynamics, global coupling of blocks represents the limit case of coupling, which is commonly observed in systems with large number of units, like ensembles of neurons [27]. As for the introduced delayed interaction, it could also occur due to assumption of long-range interaction among the units in the observed system, which further implies long-term or memory effect [28]. Practically, if we consider that motion of a single block can represent a seismic event, than it is obvious that such an earthquake would strongly and directly influence the next event, and then the next event again would affect its next one and so on. In other words, movement of a single block or cluster of blocks at time  $t$  depends on some preceding motion of connecting blocks at some previous time  $t - \tau$ . Such an effect is also found to exist in the original work of Burridge and Knopoff [1], who showed that there is a delayed interaction among cluster of blocks, with the intensity of time delay determined by the viscous properties along the specified fault segment. This effect is also qualitatively incorporated in our model by including time delay  $\tau$  in the connections among blocks of the observed system.

To resume, in present paper we analyze the dynamics of an array of blocks, by assuming all-to-all coupling between them, with a time delay in their interaction and in the presence of seismic noise. Although having real and experimental backgrounds, such a model has not been analyzed so far in previous studies. Our main goal is to examine the qualitative changes of dynamics in a proposed spring-slider model, and to try to explain its origin, with only a phenomenological analogy with the real observed data.

## 2. Direct evidence of stochastic fault motion

Mechanism of fault motion has been mainly modeled as a deterministic process [for a review, see 16]. Indeed, most deterministic models provide sufficiently accurate results for a phenomenological description of fault motion and earthquake nucleation. This is probably the reason why stochastic models have not been examined so far in this context. Also, there is a lack of direct experimental evidence confirming the stochastic nature of fault motion. Therefore, we firstly investigate the possible stochastic dynamics of fault motion on the basis of experimental data. Since fault motion at seismogenic depths is not accessible for a direct observation, our analysis is based on in situ measurements of ground deformation near active faults, whose dynamics is assumed to sufficiently well mimic the real fault motion. For this purpose, we examine displacement data recorded at 20 different GPS stations, uniformly distributed along the active segments of San Andreas transform fault, as it is shown in Fig. 1 [29]. Analysis was performed using the surrogate data testing of the null hypothesis that data are independent random numbers drawn from some fixed but unknown distribution [30]. Our aim was to achieve a

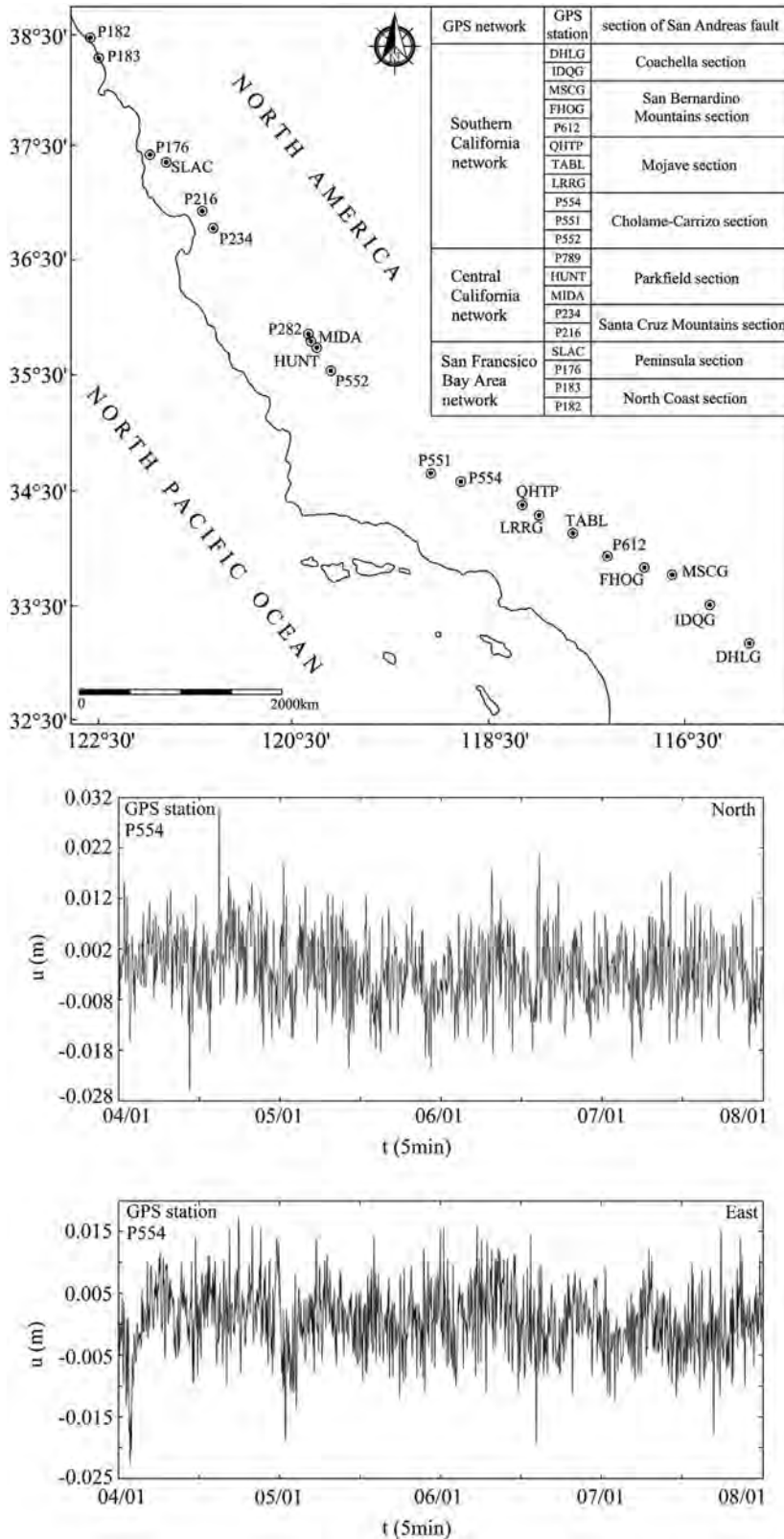


**Fig. 1.** Uniformly distributed GPS stations along a San Andreas fault, whose measurements are examined in present paper (upper panel). Example of recorded north (middle panel) and east (lower panel) horizontal crustal deformation in the period 04/01/2015–08/01/2015 at a GPS station P554. Qualitatively similar time series are recorded at other GPS stations.

significance level of  $\alpha = 0.95$  when confirming or rejecting a null hypothesis, which means that for a single-sided test we have to generate  $[1/(1-\alpha)] - 1$  surrogates for the original data. Therefore, 19 surrogates are generated by randomly shuffling the data (without repetition), thus yielding surrogates with exactly the same distribution yet independent construction. Surrogates are generated using Matlab toolkit MATS [31]. In order to test the null hypothesis, zeroth-order prediction error is calculated for the original recording ( $\gamma_0$ ) and for each of the 19 generated surrogates ( $\gamma$ ) according to the algorithm suggested by Kantz and Schreiber [32]. If  $\gamma_0 < \gamma$ , then a null hypothesis can be rejected. On the other hand, if  $\gamma_0 > \gamma$  at any instance of the test, we could not reject null hypothesis. Prediction errors were calculated by embedding each time series into the phase space with embedding dimension  $m \in [1,5]$  and embedding delay  $\tau \in [1,5]$ . In particular, embedding dimension was determined using the symplectic geometry method [33], while mutual information method [34] was applied for embedding delay. Neighbors for prediction were sought among those points that were inside 5% of the maximal distance to the reference, excluding the effect of in-time neighbors.

Results of the performed analysis indicate that temporal changes of crustal deformation in horizontal direction belong to a class of random temporally uncorrelated series. Apparently, zeroth-order prediction error for the original data  $\gamma_0$  for all the examined GPS measurements is well within the prediction error of the randomly shuffled series  $\gamma$  irrespective of prediction step  $n$  for all generated surrogates, except for the first few prediction steps, which we consider as a transient feature (Fig. 2). Relying on these results, further analysis is conducted by assuming that such behavior arises from the effect of incoherent seismic noise, modeled as independent Wiener process.

### 3. Model setup

In present paper, earthquake fault motion is examined by analysis of dimensionless spring-slider model with  $N$  units, whose dynamics is described by the following set of stochastic delay differential equations (SDDEs):

$$\begin{aligned} \dot{U}_{1i}(t) &= U_{2i}(t) \\ dU_{2i}(t) &= \left\{ -U_{1i}(t) + \Phi(U_{2i} + \nu) - \Phi(\nu) + \frac{K}{N} \sum_{j=1}^N [U_{1j}(t - \tau) - U_{1i}(t)] \right\} dt + \sqrt{2D} dW_i, \end{aligned} \quad (1)$$

where  $U_{1i}$  and  $U_{2i}$  represent displacement and velocity of the  $i$ th block, respectively,  $K$  is constant of spring connecting the blocks,  $\Phi$  stands for the friction force,  $\tau$  is time delay and  $\nu$  is a nondimensional pulling background velocity. Terms  $\sqrt{2D}dW_i$  represent stochastic increments of independent Wiener process, i.e.  $dW_i$  satisfy:

$$E(dW_i) = 0, \quad E(dW_i dW_j) = \delta_{ij} dt \quad (2)$$

where  $E()$  denotes the expectation over many realizations of the stochastic process and  $D$  is intensity of additive local noise. Each of  $i = 1, 2, \dots, N$  units in (1) is coupled with each other unit. In present case, we examine system of 100 units ( $N = 100$ ). In present analysis, values of time delay  $\tau$  and coupling strength  $K$  are chosen to be equal for all the blocks in system (1), which is the limit case of homogeneous conditions along the fault. Also, equal values of coupling strength and time delay could be observed as mean values of these parameters in a multi-block system.

One should note that friction force  $\Phi$  in (1) is given in general form due to simplicity. In particular, it is assumed to be only rate-dependent:

$$\Phi(V) = -(\mu_0 + a \ln(V)), \quad (3)$$

where  $V$  is the general notion for the friction arguments in (1). This type of friction resembles of the friction force already proposed by Scholz [35], only without the state dependent term, which is incorporated in (1) by introducing the time delay  $\tau$ . In (3),  $\mu_0$  is a steady-state friction (whose value could be assumed arbitrarily large in order to secure the proper action of friction force), while  $a$  represent a material property which depends on different temperature and pressure conditions. Such prominent dependence of friction on slip rate is qualitatively supported by the recent laboratory findings, which indicate more complex nature of fault friction, but still strongly dependent on slip rate [36,37]. One should note that Eq. (1) is derived according to the previously proposed model [38]. Details of derivation are given in the Appendix.

From the viewpoint of nonlinear dynamics, detailed mathematical model of fault motion (1) involves an extremely large system of nonlinear stochastic delay differential equations (SDDEs), making its analysis impossible without more or less severe approximations. In order to be able to analyze dynamics of system (1), we need to derive its deterministic approximation, which will sufficiently accurately describe its dynamics, and will enable local bifurcation analysis. It is our goal to study some aspects of an approximation determined by only five deterministic delay differential equations (DDEs) of a fault motion model described by many-component SDDEs. For this purpose, we apply the method of mean-field approximation, which is based on a set of approximations that replace a many component system by a simpler system described by a small number of average macroscopic properties [39]. The attempts at providing a reduced description instead of using the complete set of equations for every constituent of the population have a particularly long history within neuroscience [40–43]. Similar approach has also been applied in the area of seismology, primarily for analyzing the dynamics of earthquake fault models, such as cellular automata or spring-slider model. For instance, Dahmen et al. [44] analyzed a heterogeneous fault system as an array of discrete cells in a two-dimensional plane, with elastic coupling between cells in the mean-field approximation. Results of their research imply that calculated exponents for the power-law earthquake distributions and the

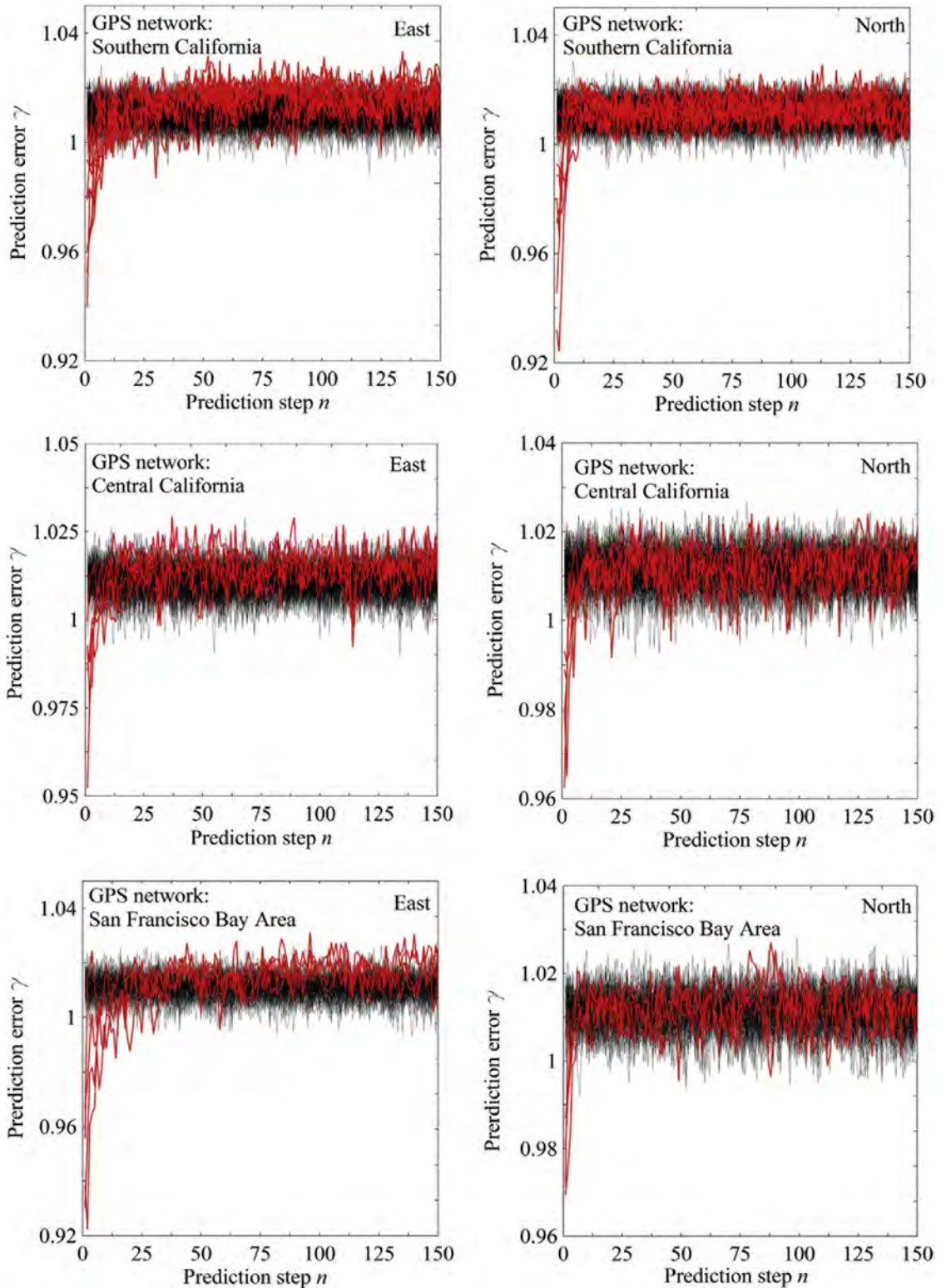


**Fig. 2.** Surrogate data test for the null hypothesis that data are independent random numbers drawn from some fixed but unknown distribution. Black lines indicate zeroth-order prediction errors for the surrogates ( $\gamma$ ), while red lines denote prediction errors for the original recordings ( $\gamma_0$ ) as a function of prediction steps  $n$ . Results in left and right panels pertain to the measurements in horizontal north and east direction, respectively, for all recording stations belonging to the specified GPS networks. It is clear that except for the first few prediction steps,  $\gamma_0$  is well within distribution of  $\gamma$ , which makes it impossible to reject the null hypothesis. (For interpretation of the references to color in this figure legend, the reader is referred to the web version of this article.)

divergence of the cutoff length scale for the mean-field model can be expected to apply to models with realistic interactions, with possible logarithmic corrections. As for the spring-slider models, Xia et al. [7] found a mean-field spinodal critical point in a BK model with long-range stress transfer between the blocks as in the long-range cellular automata models. Moreover, some previous studies [45,46] indicated that natural earthquake fault systems are effectively ergodic and mean-field for significant periods of time.

Within present research, method of mean-field approximation gave the final approximated model (1) in the following form:

$$\begin{aligned}
 \dot{m}_{U_1}(t) &= m_{U_2}(t), \\
 \dot{m}_{U_2}(t) &= -m_{U_1}(t) + a \ln \nu - a \ln (m_{U_2} + \nu) + \frac{a}{2} \frac{1}{(m_{U_2} + \nu)^2} s_{U_2} + \frac{a}{4} \frac{1}{(m_{U_2} + \nu)^4} 3s_{U_2}^2 + \\
 &\quad + K[m_{U_1}(t - \tau) - m_{U_1}(t)], \\
 \frac{1}{2} \dot{s}_{U_1}(t) &= s_{U_1} U_2 \\
 \frac{1}{2} \dot{s}_{U_2}(t) &= s_{U_2} \left[ -\frac{a}{(m_{U_2} + \nu)} - \frac{a}{(m_{U_2} + \nu)^3} s_{U_2} \right] - (K + 1) s_{U_1} U_2 + D, \\
 \dot{s}_{U_1} U_2 &= -s_{U_1} U_2 \left[ \frac{a}{(m_{U_2} + \nu)} + \frac{a}{(m_{U_2} + \nu)^3} s_{U_2} \right] - (K + 1) s_{U_1} + s_{U_2}(t)
 \end{aligned} \tag{4}$$

Detailed derivation of model (4) is given in the Appendix. Further on, we shall proceed with a standard local bifurcation analysis of the system (4) in the vicinity of the equilibrium point.

#### 4. Local bifurcation analysis

Local bifurcation analysis of the approximated model (4) is conducted numerically using DDE-BIFTOOL in Matlab, which comprises a collection of adaptable Matlab routines suitable for the numerical bifurcation analysis of systems of DDEs [47]. The obtained results indicate a transition from equilibrium state to periodic oscillations for certain parameter values, as it is shown in Fig. 3. These dynamical states for mean-field model (4), i.e. 5 deterministic equations (left panel at Fig. 4) correspond well to the behavior of the starting system (1), i.e. 200 stochastic equations (right panel at Fig. 4). In particular,

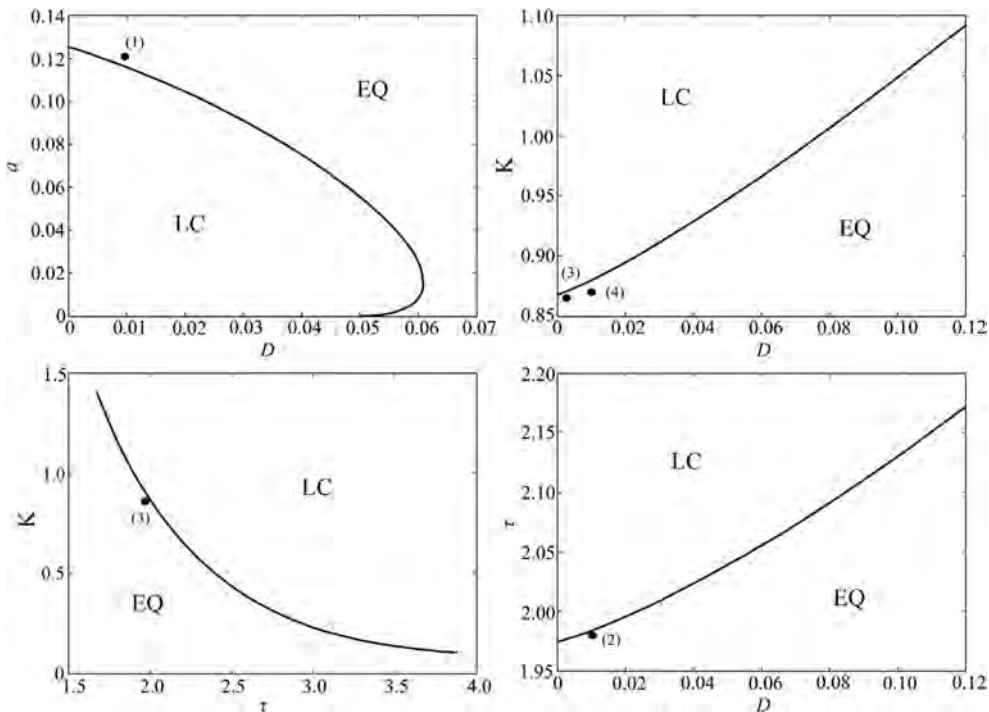


**Fig. 3.** Parameter domains ( $a,D$ ), ( $K,D$ ), ( $K,\tau$ ) and ( $\tau,D$ ) admitting equilibrium state (EQ) or periodic oscillations (LC) of the mean-field approximated model (4). For a given parameter domain, other parameters are held constant at the following values:  $K = 0.9$ ,  $\nu = 1.2$ ,  $D = 0.001$ ,  $\tau = 2$ ,  $a = 0.1$ . Starting system (1), due to stochastic effect of included seismic noise in both cases exhibit fluctuations, which are smaller than assumed noise amplitude in EQ region, and are periodic with nearly constant amplitude in LC region. Points (1)–(4) denote the cases for which the event distribution is determined and shown in Fig. 6.

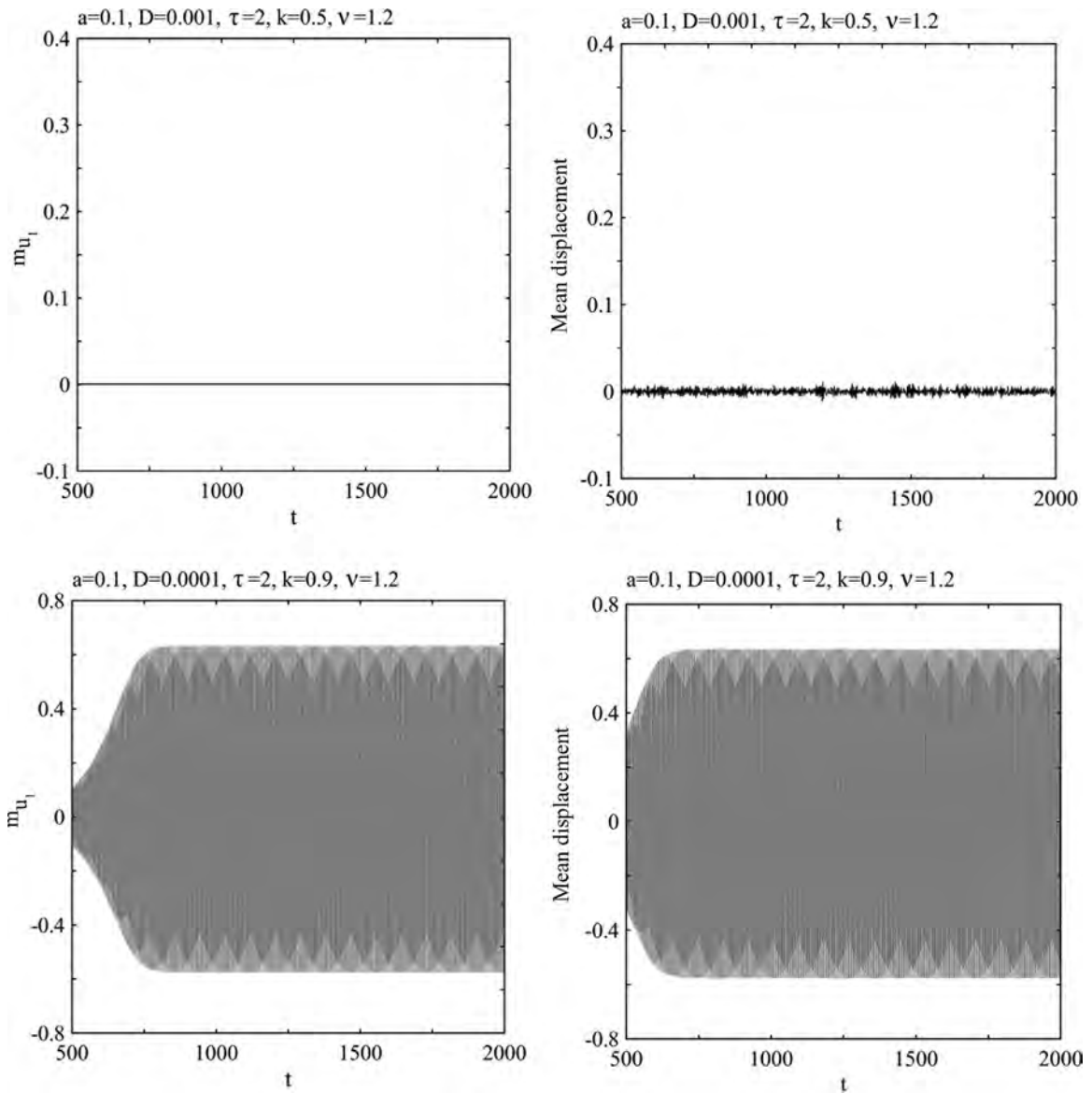


**Fig. 4.** Time series of approximated mean-field displacements (left panels) and corresponding mean displacements of 100 blocks (right panels). Parameter values are conveniently chosen for equilibrium state and periodic oscillations. It is clear that mean-field model (4) in a sufficiently accurate way describes dynamics of the starting model (1), marking in that way expected position of stochastic bifurcation curves for the starting system (1). Frequency of oscillations for both the starting stochastic model and its mean-field approximation is the same ( $f=0.33$ ).

performed numerical analysis showed that qualitatively similar dynamics is observed for both the starting stochastic system of  $N$  blocks (1) and its mean-field approximation (4). One should note that in Fig. 4 we only show time series of a mean displacement for the starting system (1) and mean-field approximated model (4), since displacement magnitude is directly proportional to earthquake magnitude. Corresponding time series for mean velocity of systems (1) and (4) are qualitatively similar. Also, it should be emphasized that negative values of displacement and velocity are the consequence of the coordinate transformation, where the system is constantly moving around the stationary value  $v = 1.2$ . It should be noted that for cases  $U_2 < 0$ , friction force acts in opposite direction, i.e. in both cases (positive and negative values of velocity), it opposes the displacement of the block.

Equilibrium state for the starting model (1) is represented by small fluctuations around the constant zero value of a mean-field approximated displacement for a mean-fied model (4). On the other hand, when bifurcation curve is crossed (e.g. in diagram  $K-\tau$ ), oscillation frequencies are the same for both the starting model (1) and approximated system (4), while amplitude could be slightly different due to effect of the introduced random seismic noise in the stochastic model (1). It should be noted that equilibrium state and periodic oscillations are clearly captured only in  $K-\tau$  diagram. Bifurcation

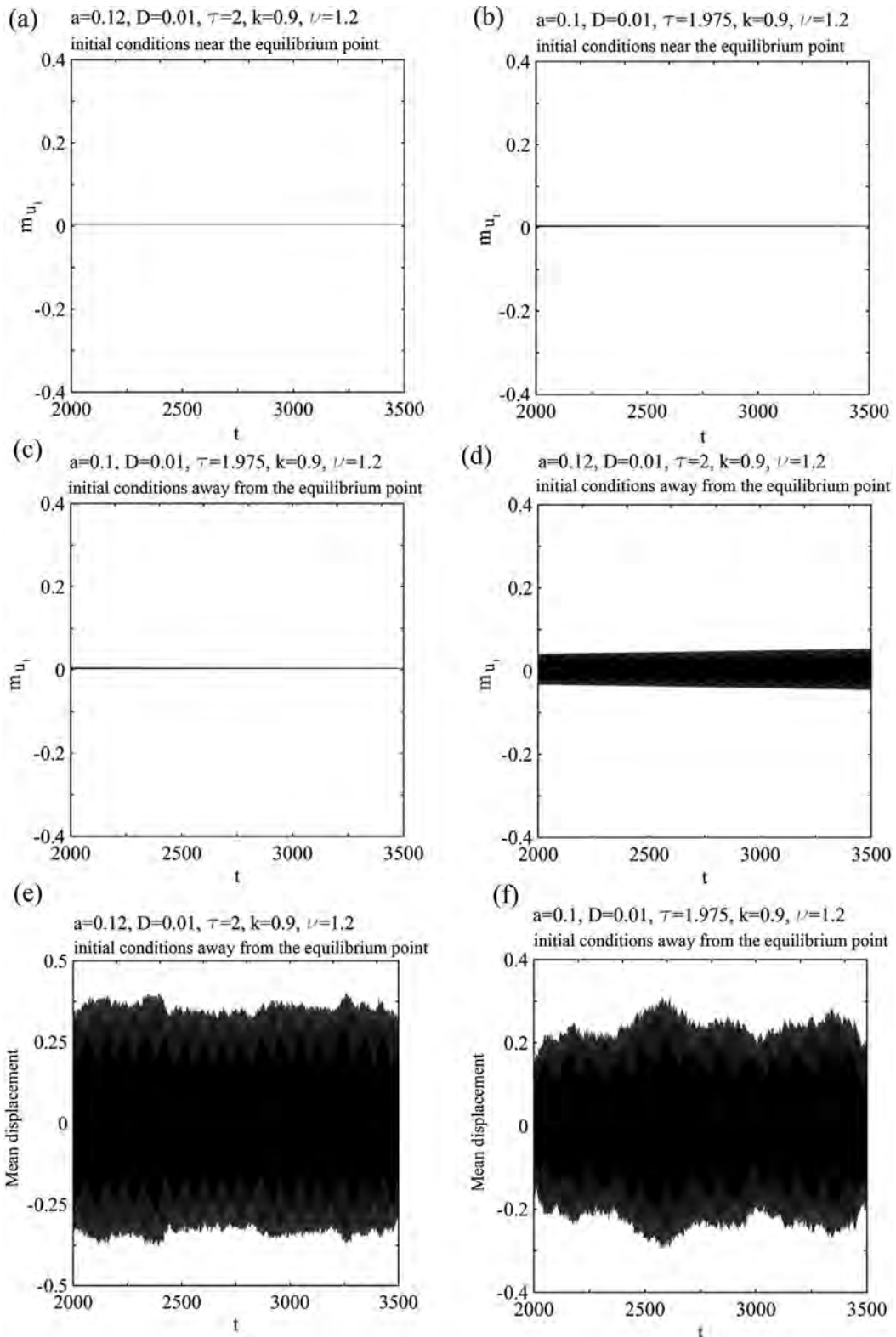


**Fig. 5.** (a–d) Time series of mean-field displacement in an approximated model (4) for initial conditions away from and near the equilibrium point and for different values of material property  $a$  and time delay  $\tau$  prior the bifurcation. (e, f) Time series of mean displacement of 100 blocks in a starting non-approximated system (1) for initial conditions away from the equilibrium point and for different values of material property  $a$  and time delay  $\tau$  prior the bifurcation. Qualitatively similar time series for starting system (1) are obtained for the same parameter values, but for initial conditions near the equilibrium point.



curves in other diagrams, where parameters  $a$ ,  $\tau$  and  $K$  are given as function of  $D$ , are captured only for the mean-field approximated model (4). These bifurcations in the real starting model (1) are captured only as significantly higher fluctuations of stochastic system when bifurcation curve is crossed.

In this way, we confirmed that mean-field approximated model (1) describes the dynamics of the starting model (1) accurately enough, so the obtained bifurcation curves in general correspond to bifurcations of the original system. From the seismological viewpoint, different dynamical states correspond to different regimes of aseismic motion, i.e. equilibrium state corresponds to the state when there is no movement along the fault or steady sliding along the fault in the original system (1A), while the periodic oscillatory motion denotes the aseismic creep along the fault, which is well documented in real conditions in the Earth’s crust [48,49].

One should note that a more detailed analysis of the observed dynamics imply the following. In dependence on initial conditions, for parameter values prior to bifurcation, mean-field approximated model (4) could be in EQ regime or within

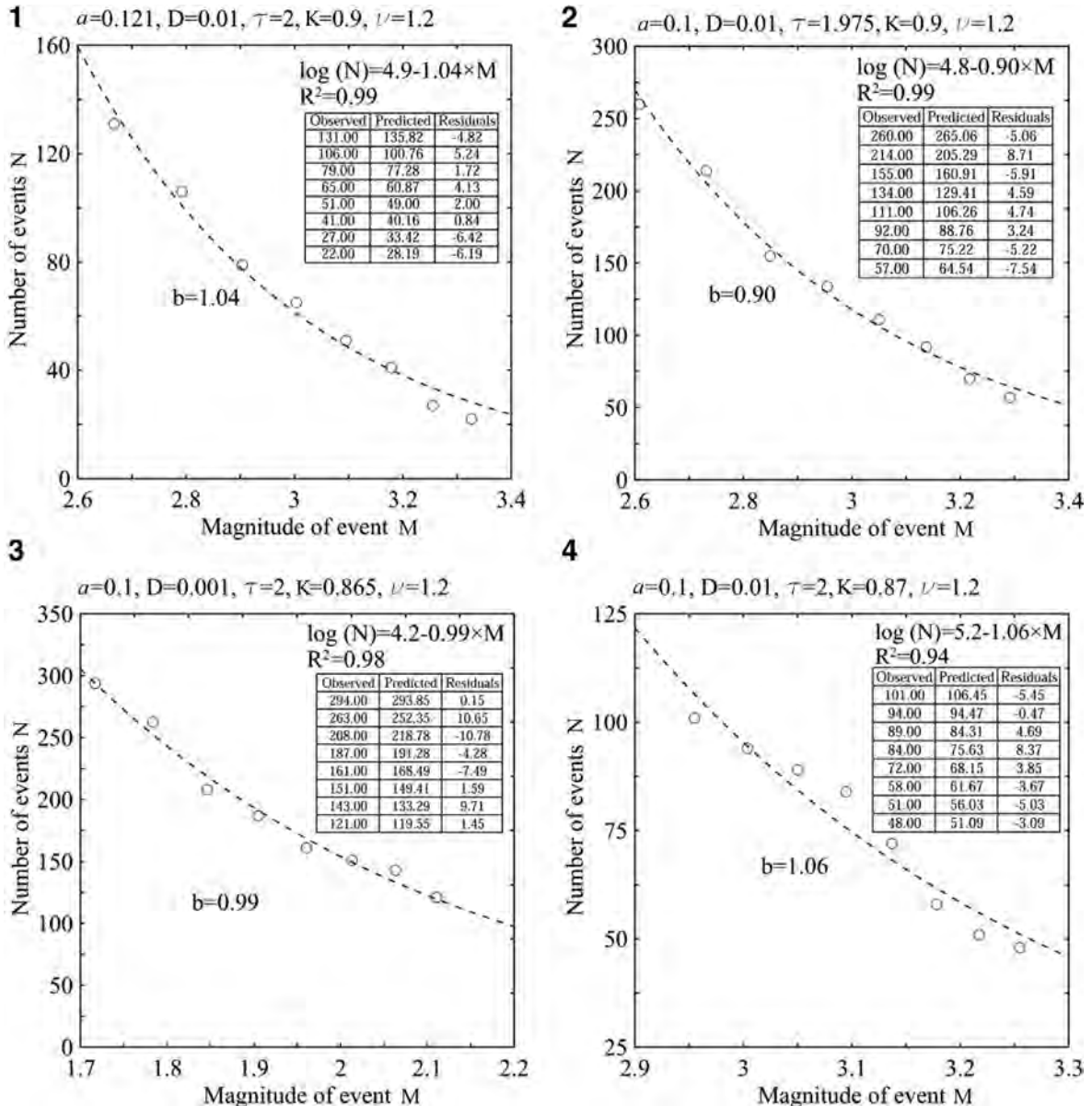


**Fig. 6.** Examples of power-law behavior of system (1) away from the equilibrium point in a bi-stable regime near the bifurcation curves, for the points (1)–(4) in Fig. 3. It is clear that for different parameter values magnitude–frequency distribution follows the Gutenberg–Richter law with satisfying statistical accuracy, while the corresponding  $b$ -value is in the range of real observed data. The lower cut-off was chosen so as to exclude displacements below or equal to the introduced seismic noise, as well as displacement for which event magnitude  $M=0$ . Furthermore, for each example, ratio of velocity sums of all blocks to the introduced noise level is at least  $10^2$ , which qualitatively corresponds to the real observed values.

a so-called “bi-stable regime”. When initial conditions are set near the equilibrium point, mean-field model (4) is in EQ regime, regardless of the parameter values (before the bifurcation occurs, Fig. 5a and b). On the other hand, if initial conditions are set away from the equilibrium point, mean-field model (4) could be in EQ regime (Fig. 5c) or could exhibit oscillatory behavior due to effect of global bifurcation depending on the parameter values prior to local bifurcation (Fig. 5d). In a starting stochastic system of  $N$  blocks (1), impact of global bifurcation reveals in high amplitude fluctuations above the introduced noise level (Fig. 5f). However, such fluctuations in system (1) could also arise due to sole effect of the introduced random seismic noise (Fig. 5e), if the system (4) is close enough to bifurcation curve, regardless of the initial conditions.

In summary, on the basis of the conducted bifurcation analysis, two main conclusions could be drawn. First of all, mean-field model (4) sufficiently well describes dynamics of the starting model (1), which is indicated by qualitatively the same dynamical behavior below and above the obtained bifurcation curves. Secondly, irregular behavior of the starting model (1) imply two possible scenarios: either the effect of introduced noise induces the possible occurrence of stochastic bifurcation or there exists another basin of attraction of some global attractor in parallel to basin of attraction of the equilibrium point.

## 5. Macroseismic implications

From the viewpoint of seismology, performed bifurcation analysis indicates that earthquakes could be expected to occur only in a bi-stable dynamical regime in the vicinity of a bifurcation curve provided that initial conditions along the fault are far from the equilibrium state (the case of active fault). In particular, irregular oscillations with amplitude higher than assumed noise level arise only for this regime, as an effect of either the introduced noise or the global attractor. Small fluctuations of system (1) well below the bifurcation curve, which correspond to equilibrium state, cannot be treated as relevant for real seismic events, since their amplitudes are significantly lower than the introduced noise level. On the other hand, regular periodic oscillations of the starting system (1) above the bifurcation curve could hardly be expected to occur in real conditions, since regular periodic recurrence of seismic events has rarely been observed along a single fault. In particular, periodic occurrence of earthquakes is captured in the real conditions only for the strongest earthquakes at certain locations in the Earth’s crust, like Nankai seismic area [50]. Nevertheless, if we take into account all earthquakes recorded in a single area, than their occurrence will certainly be aperiodic. Therefore, we could treat periodic oscillations also as an example of aseismic creep, which is more frequent case in the reality [48,49].

In order to verify that a starting model (1) in a bi-stable dynamical regime exhibits dynamics which is relevant for the real observed seismicity, we analyze the statistical distribution of events for different time series of displacement sums near the bifurcation curves (Fig. 6). In this case, magnitude of an event is typically defined as a natural logarithm of displacement sums for all blocks [16], while an event is defined as a peak (local maximum) of mean displacement of system (1) above a certain threshold. Introduced noise level is conveniently chosen so as to obtain results which are comparable with the real observed data. In particular, for the lower cut-off we chose those sums whose magnitude is equal to  $M=0$ , excluding in that way very weak earthquakes which are induced only by small displacements along the observed fault. Also, average ratio of velocity sums to the introduced noise is at least  $10^2$ , which is typically reported as a lower threshold for this ratio in real conditions.

Performed statistical analysis indicated that distribution of observed event magnitudes for a certain time range, neglecting the transients, follows the Gutenberg–Richter power law with satisfying statistical accuracy (high values of  $R^2$  and low residual sum of squares) and with the  $b$ -value in the range [0.90–1.06], which corresponds well to the real observed data.

## 6. Conclusion

In present paper, we analyzed stochastic model of fault motion with included effect of seismic noise and time delay. Introduction of seismic noise was justified by surrogate data analysis of ground deformation near San Andreas fault system, which showed that fault movement could be treated as a random process, probably due to the impact of incoherent seismic noise. On the other hand, delayed interaction of blocks within a fault system was also found in the original work of Burridge and Knopoff [1] and it was implied by the real observed data.

Dynamics of starting model, which consists of 100 blocks, is examined using mean-field approach, which enabled us to detect the possible occurrence of deterministic bifurcations. In particular, instead of 200 stochastic delay differential equations, mean-field approach provided five delay differential equations, which sufficiently accurately describe the behavior of the starting system. The obtained results indicate that a bifurcation from equilibrium point to limit cycle occurs for a certain parameter range. Long-period aperiodic irregular oscillations also arise, either due to the introduced seismic noise or they occur under the impact of some global attractor. Either way, these long-period oscillations are shown to obey power-law behavior, with the parameter values which are comparable to the real observed data.

If one compares the performed research and obtained results with the previous studies on the same topic, several novelties could be singled out. First of all, seismic noise and delayed interaction among different fault segments (interacting blocks of the model), as existing natural factors, are for the first time introduced in the examined model. Secondly, method of mean-field approximation is for the first time applied in the analysis of dynamics of a spring-block model, providing sufficiently accurate results. Moreover, it is shown for the first time that irregular mean displacement of a whole fault near the transition from equilibrium state (EQ regime) to aseismic creep (LC regime) could occur either due to sole effect of

seismic noise or under the impact of seismic noise in the presence of local and global attractor. This is contrast with previous studies, which commonly claimed that irregular displacement of a fault, i.e. seismic motion, represents an example of deterministic chaos [21,22,38].

In conclusion, performed research set a solid base for future studies for two main reasons. Firstly, it is shown that stochastic model of fault motion is justified from the viewpoint of seismology, relying on the results of real observed data and surrogate data testing. Secondly, irregular oscillations near the bifurcation curve, which resemble of stick-slip motion, are confirmed to obey power-law behavior. On the basis of these main results, further research should focus on interaction of blocks within the model, by comparing individual and collective behavior. Moreover, interaction of blocks in a two-dimensional plane would certainly bring new dynamical features which could have significant implications from seismological viewpoint.

**Acknowledgments**

This research has been partly supported by the Ministry of Education, Science and Technological development of the Republic of Serbia, Contract nos. 171015 and 176016.

**Appendix**

*Model derivation*

Present research on earthquake fault motion is based on the analysis of non-dimensional mono-block model, originally suggested in [38]:

$$\ddot{U}(t) = -U(t) + \Phi(\dot{U}(t)) + vt, \tag{1A}$$

where variable  $U$  represents the block displacement,  $\dot{U}$  is the velocity of the block (defined in the standing reference frame),  $\ddot{U}$  is the block acceleration,  $v$  is dimensionless pulling speed, and  $t$  is time variable. Friction force  $\Phi$  is assumed to be only rate-dependent. The unstable equilibrium around which the orbits of block move in phase space is given in the following way:

$$U_e(t) = vt + \Phi(v), \tag{2A}$$

which is determined by setting  $\ddot{U} = 0$  and  $\dot{U} = v$  in (1A).

From (1A), one can write:

$$\begin{aligned} \dot{U}_1(t) &= U_2(t) \\ \dot{U}_2(t) &= -U_1(t) + \Phi(U_2(t)) + vt, \end{aligned} \tag{3A}$$

where  $U_1$  and  $U_2$  denote displacement and velocity of a single block, respectively.

Using the following coordinate transformation:

$$\begin{aligned} U_{1new}(t) &= U_1 - U_e(t) = U_1(t) - (vt + \Phi(v)), \\ U_{2new}(t) &= U_2(t) - v, \end{aligned} \tag{4A}$$

after which we return to old notation, one could get the following system of equation for the motion of a single block:

$$\begin{aligned} \dot{U}_1(t) &= U_2(t) \\ \dot{U}_2(t) &= -U_1(t) + \Phi(U_2(t) + v) - \Phi(v). \end{aligned} \tag{5A}$$

Starting from (5A) one can derive the spring-slider model of  $N$  interconnected blocks given as system of Eq. (1) in Section 3.

*Mean-field approximation*

By deriving the Taylor expansion of  $\Phi(U_2(t) + v)$  in the vicinity of the mean values  $(\langle U_1 \rangle, \langle U_2 \rangle) = (\lim_{N \rightarrow \infty} \frac{1}{N} \sum_{i=1}^N U_{1i}(t), \lim_{N \rightarrow \infty} \frac{1}{N} \sum_{i=1}^N U_{2i}(t)) = (m_{U_1}, m_{U_2})$  system (1), in the thermodynamic limit, for  $N \rightarrow \infty$ , becomes:

$$\begin{aligned} dU_{1i}(t) &= U_{2i}(t)dt \\ dU_{2i}(t) &= \{-U_{1i}(t) + \Phi(m_{U_2} + v) - \Phi(v) + \frac{1}{1!}[\Phi'(m_{U_2} + v)][U_2(t) - m_{U_2}] + \\ &\quad + \frac{1}{2!}[\Phi''(m_{U_2} + v)][U_2(t) - m_{U_2}]^2 + \frac{1}{3!}[\Phi'''(m_{U_2} + v)][U_2(t) - m_{U_2}]^3 + \\ &\quad + \frac{1}{4!}[\Phi^{(4)}(m_{U_2} + v)][U_2(t) - m_{U_2}]^4 + K[m_{U_1}(t - \tau) - U_1(t)]\}dt + \sqrt{2D}dW_i. \end{aligned} \tag{1B}$$

In order to derive mean-field approximate dynamical equations for starting system (1) in the main text, we shall first suppose that: (a) dynamics is such that the distributions of  $U_{1i}$  and  $U_{2i}$  are Gaussian and (b) for large  $N$  the average over local random variables is given by the expectation with respect to the corresponding distribution, as in [39]. In the limit  $N \rightarrow \infty$ , the last assumption is expected to become equality, implied by the strong law of large numbers [51]. In the mean-field approach it is commonly assumed that (b) is approximately true even for finite but large  $N$  despite the non-zero interaction between the local random variables. The first assumption should be expected to be true when the noise intensity is small, i.e.  $D \ll 1$  [52,53]. With these assumptions the system (1B) of  $N$  SDEs can be reduced to five DDEs for the macroscopic variables  $m_{U_1}(t)$ ,  $m_{U_2}(t)$  and the second order cumulants.

Following the procedure from Burić et al. [39], starting system (1B) of  $N$  SDEs is reduced to the system of only five deterministic DDEs for the global variables and global centered moments:

$$m_{U_1}(t) = \langle U_1(t) \rangle, \quad m_{U_2}(t) = \langle U_2(t) \rangle, \quad s_{U_1}(t) = \langle n_{U_1}^2(t) \rangle, \quad s_{U_2}(t) = \langle n_{U_2}^2(t) \rangle, \quad s_{U_1 U_2}(t) = \langle n_{U_2} \cdot n_{U_1} \rangle, \quad (2B)$$

where  $n_{U_j}(t) = m_{U_j}(t) - U_{ji}(t)$ ,  $j = 1, 2$ .

The final mean-field approximated model with the general form of friction term  $\Phi$  is given in the following way:

$$\begin{aligned} \dot{m}_{U_1}(t) &= m_{U_2}(t), \\ \dot{m}_{U_2}(t) &= -m_{U_1}(t) + \Phi(m_{U_2} + \nu) - \Phi(\nu) + \frac{1}{2} [\Phi''(m_{U_2} + \nu)] s_{U_2} + \frac{1}{24} [\Phi^{(4)}(m_{U_2} + \nu)] 3s_{U_2}^2 + \\ &\quad + K[m_{U_1}(t - \tau) - m_{U_1}(t)], \\ \frac{1}{2} \dot{s}_{U_1}(t) &= s_{U_1 U_2} \\ \frac{1}{2} \dot{s}_{U_2}(t) &= s_{U_2} \left[ \Phi'(m_{U_2} + \nu) + \frac{1}{2} \Phi'''(m_{U_2} + \nu) s_{U_2} \right] - (K + 1) s_{U_1 U_2} + D, \\ \dot{s}_{U_1 U_2} &= s_{U_1 U_2} \left[ \Phi'(m_{U_2} + \nu) + \frac{1}{2} \Phi'''(m_{U_2} + \nu) s_{U_2} \right] - (K + 1) s_{U_1} + s_{U_2}(t) \end{aligned} \quad (3B)$$

The final form of (3B) with included rate-dependent friction term is given in the main text as system (4).

## References

- [1] Burridge R, Knopoff L. Model and theoretical seismicity. *B Seismol Soc Am* 1967;57:341–71.
- [2] Carlson J, Langer J. Mechanical model of an earthquake fault. *Phys Rev A* 1989;40:6470–84.
- [3] Carlson JM, Langer JS, Shaw BE, Tang C. Intrinsic properties of a Burridge–Knopoff model of an earthquake fault. *Phys Rev A* 1991;44:884–97.
- [4] Schmittbuhl J, Vilotte J, Roux S. A dissipation-based analysis of an earthquake fault model. *J Geophys Res* 1996;101:27,741–64.
- [5] Hainzl S, Zoller G, Kurths J. Self-organized criticality model for earthquakes: quiescence, foreshocks and aftershocks. *Int J Bifurc Chaos* 1999;9:2249–55.
- [6] Mori T, Kawamura H. Simulation study of spatiotemporal correlations of earthquakes as a stick-slip frictional instability. *Phys Rev Lett* 2005;94:058501–1–4.
- [7] Xia J, Gould H, Klein W, Rundle JB. Near-mean-field behavior in the generalized Burridge–Knopoff earthquake model with variable-range stress transfer. *Phys Rev E* 2008;77:031132–1–11.
- [8] Olami Z, Feder HJS, Christensen K. Self-organized criticality in a continuous, nonconservative cellular automaton modeling earthquakes. *Phys Rev Lett* 1992;68:1244–7.
- [9] Knopoff L, Landoni JA, Abinante MS. Dynamical model of an earthquake fault with localization. *Phys Rev A* 1992;46:7445–9.
- [10] Jonsson T, Marinossos SF. Scaling and correlation functions in a model of a two-dimensional earthquake fault. *Phys Scr* 1998;58:282–8.
- [11] De Sousa Vieira M. Self-organized criticality in a bulk-driven one-dimensional deterministic system. *Physica A* 2004;344:737–42.
- [12] Mori T, Kawamura H. Simulation study of earthquakes based on the two-dimensional Burridge–Knopoff model with long-range interactions. *Phys Rev E* 2008;77:051123–1–051123–16.
- [13] Dieterich JH. Modeling of rock friction: 1; experimental results and constitutive equations. *J Geophys Res* 1979;84:2161–95.
- [14] Ruina A. Slip instability and state variable friction laws. *J Geophys Res* 1983;88:10359–70.
- [15] Perrin G, Rice JR, Zheng G. Self-healing slip pulse on a frictional surface. *J Mech Phys Solids* 1995;43:1461–95.
- [16] Kawamura H, Hatano T, Kato N, Biswas S, Chakrabarti BK. Statistical physics of fracture, friction, and earthquakes. *Rev Mod Phys* 2012;84:2839–84.
- [17] Nussbaum J, Ruina A. A two degree-of-freedom earthquake model with static/dynamic friction. *Pure Appl Geophys* 1987;5:629–56.
- [18] Huang J, Turcotte DL. Chaotic seismic faulting with a mass-spring model and velocity-weakening friction. *Pure Appl Geophys* 1992;138:569–89.
- [19] Field S, Venturi N, Nori F. Marginal stability and chaos in coupled faults modeled by nonlinear circuits. *Phys Rev Lett* 1995;74:74–8.
- [20] Galvanetto U. Some remarks on the two-block symmetric Burridge–Knopoff model. *Phys Lett A* 2002;293:251–9.
- [21] Erickson B, Birnir B, Lavalée D. A model for aperiodicity in earthquakes. *Nonlinear Proc Geophys* 2008;15:1–12.
- [22] Erickson BA, Birnir B, Lavalée D. Periodicity, chaos and localization in a Burridge–Knopoff model of an earthquake with rate-and-state friction. *Geophys J Int* 2011;187:178–98.
- [23] Telford WM, Geldart LP, Sheriff RE. Applied geophysics. 2nd ed. Cambridge: Cambridge University Press; 1990.
- [24] Ryabov VB, Correig AM, Urquiza M, Zaikin AA. Microseism oscillations: from deterministic to noise-driven models. *Chaos Solitons Fractals* 2003;16:195–210.
- [25] Sanders CO. Interaction of the San Jacinto and San Andreas fault zones, southern California: triggered earthquake migration and coupled recurrence intervals. *Science* 1993;260:973–6.
- [26] Johnson KM, Segall P. Viscoelastic earthquake cycle models with deep stress-driven creep along the San Andreas fault system. *J Geophys Res* 2004;109:B10403–1–19.
- [27] Franović I, Todorović K, Vasović N, Burić N. Spontaneous formation of synchronization clusters in homogenous neuronal ensembles induced by noise and interaction delays. *Phys Rev Lett* 2012;108:094101.
- [28] Wang JH. Memory effect in  $M \geq 7$  earthquakes of Taiwan. *J Seismol* 2014;18:467–80.
- [29] USGS website: <http://earthquake.usgs.gov/monitoring/gps/>. [accessed 10.01.15].
- [30] Perc M, Green AK, Jane Dixon C, Marhl M. Establishing the stochastic nature of intracellular calcium oscillations from experimental data. *Biophys Chem* 2008;132:33–8.

- [31] Kugiumtzi D, Tsimpiris A. Measures of analysis of time series (MATS): a MATLAB toolkit for computation of multiple measures on time series data bases. *J Stat Softw* 2010;33:1–30.
- [32] Kantz H, Schreiber T. *Nonlinear time series analysis*. Cambridge: Cambridge University Press; 2004.
- [33] Lei M, Wang Z, Feng Z. A method of embedding dimension estimation based on symplectic geometry. *Phys Lett A* 2002;303:179–89.
- [34] Fraser A, Swinney H. Independent coordinates for strange attractors from mutual information. *Phys Rev A* 1986;33:1134–40.
- [35] Scholz CH. Earthquakes and friction laws. *Nature* 1998;391:37–42.
- [36] Sone H, Shimamoto T. Frictional resistance of faults during accelerating and decelerating earthquake slip. *Nat Geosci* 2009;2:705–8.
- [37] Lapusta N. The roller coaster of fault friction. *Nat Geosci* 2009;2:676–7.
- [38] De Sousa Vieira M. Chaos and synchronized chaos in an earthquake model. *Phys Rev Lett* 1999;82:201–4.
- [39] Burić N, Ranković D, Todorović K, Vasović N. Mean field approximation for noisy delay coupled excitable neurons. *Physica A* 2010;389:3956–64.
- [40] Hasegawa H. Stochastic bifurcation in FitzHugh–Nagumo ensembles subjected to additive and/or multiplicative noises. *Physica D* 2008;237:137–55.
- [41] Lindner B, Garcia-Ojalvob J, Neimand A, Schimansky-Geiere L. Effects of noise in excitable systems. *Phys Rep* 2004;392:321–4.
- [42] Stefanescu RA, Jirsa VK. A low dimensional description of globally coupled heterogeneous neural networks of excitatory and inhibitory neurons. *PLoS Biol* 2008;4:1–17.
- [43] Franović I, Todorović K, Vasović N, Burić N. Mean-field approximation of two coupled populations of excitable units. *Phys Rev E* 2013;87:012922–1–13.
- [44] Dahmen K, Ertas D, Ben-Zion Y. Gutenberg–Richter and characteristic earthquake behavior in simple mean-field models of heterogeneous faults. *Phys Rev E* 2008;78:1494–501.
- [45] Ferguson CD, Klein W, Rundle JB. Spinodals, scaling, and ergodicity in a threshold model with long-range stress transfer. *Phys Rev E* 1999;60:1359–74.
- [46] Tiampo KF, Rundle JB, Klein W, Holliday J, Sa Martins JS, Ferguson CD. Ergodicity in natural earthquake fault networks. *Phys Rev E* 2007;75:066107–1–066107–16.
- [47] Engelborghs K, Luzyanina T, Samaey G. *DDE-BIFTOOL v. 2.00: a Matlab package for bifurcation analysis of delay differential equations*. Leuven, Belgium: Department of Computer Science, K.U. Leuven; 2000.
- [48] Galehouse J, Lienkaemper J. Inferences drawn from two decades of alignment array measurements of creep on faults in the San Francisco Bay Region. *Bull Seismol Soc Am* 2003;93:2415–33.
- [49] Lienkaemper JJ, McFarland FS, Simpson RW, Bilham RG, Ponce DA, Boatwright JJ, et al. Long-term creep rates on the Hayward fault: evidence for controls on the size and frequency of large earthquakes. *Bull Seismol Soc Am* 2012;102:31–41.
- [50] Parsons T, Console R, Falcone G, Muru M, Yamashina K. Comparison of characteristic and Gutenberg–Richter models for time-dependent  $M \geq 7.9$  earthquake probability in the Nankai–Tokai subduction zone, Japan. *Geophys J Int* 2012;190:1673–88.
- [51] Arnold L. *Random dynamical systems*. Berlin: Springer-Verlag; 1998.
- [52] Tanabe S, Pakdaman K. Dynamics of moments of FitzHugh–Nagumo neuronal models and stochastic bifurcations. *Phys Rev E* 2001;63:031911.
- [53] Zaks MA, Siler X, Schimansky-Geier L, Neiman AB. Noise induced complexity: from subthreshold oscillations to spiking in coupled excitable systems. *Chaos* 2005;15:026117.

**Mean-field dynamics of a random neural network with noise**Vladimir Klinshov<sup>1,\*</sup> and Igor Franović<sup>2,†</sup><sup>1</sup>*Institute of Applied Physics of the Russian Academy of Sciences, 46 Ulyanov Street, 603950 Nizhny Novgorod, Russia*<sup>2</sup>*Scientific Computing Laboratory, Institute of Physics Belgrade, University of Belgrade, Pregrevica 118, 11080 Belgrade, Serbia*

(Received 8 July 2015; revised manuscript received 9 October 2015; published 10 December 2015)

We consider a network of randomly coupled rate-based neurons influenced by external and internal noise. We derive a second-order stochastic mean-field model for the network dynamics and use it to analyze the stability and bifurcations in the thermodynamic limit, as well as to study the fluctuations due to the finite-size effect. It is demonstrated that the two types of noise have substantially different impact on the network dynamics. While both sources of noise give rise to stochastic fluctuations in the case of the finite-size network, only the external noise affects the stationary activity levels of the network in the thermodynamic limit. We compare the theoretical predictions with the direct simulation results and show that they agree for large enough network sizes and for parameter domains sufficiently away from bifurcations.

DOI: [10.1103/PhysRevE.92.062813](https://doi.org/10.1103/PhysRevE.92.062813)

PACS number(s): 89.75.Fb, 05.40.Ca, 87.19.lj

**I. INTRODUCTION**

The different stages of information processing in large neural systems comprise multiple characteristic spatial and temporal scales. While the *in-vivo* recordings of single neurons indicate considerable subthreshold fluctuations and highly variable spike trains [1–3], the macroscopic measurements have revealed reliable and structured activity in many cortical areas [4]. Accounting for these two results is an outstanding theoretical issue, which requires one to develop analytically tractable models capable of capturing the functional organization and integration of single unit dynamics at different levels of complexity. This is typically resolved by invoking the mean-field approach to describe the coarse-grained activity and interactions of neural populations. Given the often used assumption on population homogeneity, the approach is from the biological view most appropriate for intermediate-scale (mesoscopic) assemblies, such as cortical columns [5,6]. The latter assemblies incorporate on one hand a sufficiently large number of neurons for the averaging effects to occur, but on the other hand, are small enough to support the homogeneity assumption.

The mean-field approach has so far been implemented to network structures as well as spatially extended neural systems, with the pertaining models classified as activity-based or voltage-based depending on the type of the state variable [6,7]. The seminal works of Wilson and Cowan [8,9], as well as Amari [10], employed the heuristic continuum limit, providing the description of the temporal coarse-grained dynamics in neural fields. Though deterministic in nature, such models recovered a number of highly relevant dynamical regimes including multistability [8–10], large-scale oscillations [4,11,12], stationary pulses or bumps [10,13,14], traveling fronts and pulses [15–17], and spiral waves [18], as well as spatially localized oscillations [19,20]. Nevertheless, given the aim to reconcile observations of highly variable local neuron activity and the substantially reliable activity patterns at the macroscopic scale, the key point emerging in

recent research on mean-field models has been to account for the higher-order statistics [21–24]. Conceptually, the goal has become to demonstrate how the fluctuations and correlations from the single unit level translate to and are manifested at the assembly level.

In general, the physical background of variability of single units may be related either to noise or the balanced recurrent excitatory and inhibitory inputs [25–27]. Our interest lies with the former scenario. In neural systems, noise may derive from a number of extrinsic and/or intrinsic sources [28–32]. The external noise is mainly due to random inputs arriving from a large number of afferent neurons (synaptic noise), whereas the internal noise is primarily linked to random opening of a finite number of ion channels (ion-channel noise). In the present paper, we consider a network of randomly connected units, where the local dynamics follows a rate model and is affected both by the internal and the external noise. Using the Gaussian closure hypothesis [33–35], we will derive the stochastic mean-field model characterizing the macroscopic network activity in terms of the mean rate and the associated variance.

The issue of how noise from the single unit level translates to noise at the macroscopic scale is highly nontrivial. So far, the stochastic mean-field models have been constructed either via the top-down or the bottom-up approaches. In the top-down approach, the details of the local neuron dynamics are neglected, which typically leads to phenomenological stochastic neural field models. These are based either on Langevin version of the deterministic equations, having introduced some form of spatiotemporal white noise [36,37], or on treating the neural field equations as the thermodynamic limit of the underlying master equation [7,22,38]. In the latter case, extensions of the deterministic mean-field model have been obtained by perturbation techniques, such as the system-size expansion [21,39], or via the field-theory methods, viz. the path integral formalism [40,41]. The bottom-up construction of stochastic mean-field models has primarily concerned networks of integrate-and-fire neurons with two types of interaction topology, the global coupling scheme [42], or the sparse connectivity [43,44]. Within the framework of population density method [43–47], such networks have been shown to display the asynchronous state despite the fact that

\*vladimir.klinshov@ipfran.ru

†franovic@ipb.ac.rs

the local firing conforms to Poissonian process. Under such conditions, the collective dynamics has been described by an effective mean-field rate equation with a characteristic gain function. Nevertheless, the point that the asynchronous state is stable only in the thermodynamic limit has indicated that the finite-size effects [48–50] may yield qualitatively novel phenomena and contribute as an additional source of intrinsic noise at the network level.

Apart from considering the networks of spiking neurons, the bottom-up approaches to stochastic mean-field models have pursued the second line of research featuring local rate dynamics [51–53]. This is consistent with the long standing debate on the precise temporal codes vs rate codes as the main principles of information encoding in neural systems [54,55]. The importance of rate code has been confirmed for a number of motor and sensory areas [56,57], whereby the potential advantage of the population rate code may lie in the lesser vulnerability to noise. For the class of models built on the rate-based neurons, Hasegawa has introduced the augmented moment approach [51,52,58] to analyze the mean-field dynamics of globally coupled finite-size populations where the units are subjected to additive and multiplicative noise. While we also consider the rate-based neurons, our model is distinct in that it accounts for the effects arising from the random network topology. Also, the issue of how the effects of noise acting on single units are manifested at the assembly level is addressed in a more elaborate fashion, accounting for the origin of multiplicative noise in the mean-field dynamics.

The paper is organized as follows. In Sec. II, we introduce the rate model of local activity and apply the Gaussian closure hypothesis to derive the stochastic mean-field equations for the finite-size population of randomly connected units. Section III concerns the stability analysis of the introduced mean-field model in the thermodynamic limit, where noise intensities act as additional system parameters. Apart from demonstrating the emergence of macroscopic bistable behavior, it is also shown how temporary changing of the level of noise may be used to control the network state in a hysteresislike scenario. In Sec. IV we discuss the finite-size effects and determine the magnitude of fluctuations around the stationary states from the thermodynamic limit. Section V provides a brief summary of the results obtained.

## II. DERIVATION OF THE MEAN-FIELD MODEL

We consider a network of  $N$  excitatory neurons. The local activity is described in terms of firing rates  $r_i, i \in [1, N]$ , whose dynamics is given by

$$\frac{dr_i}{dt} = -\lambda r_i(t) + \mathcal{H}(\kappa u_i(t) + I + \sqrt{2B}\zeta_i(t)) + \sqrt{2D}\xi_i(t). \quad (1)$$

In the last equation,  $\lambda$  denotes the relaxation characterizing the inertness of units,  $\mathcal{H}(u)$  is the gain function and  $\kappa = c/N$  stands for the coupling coefficient, and  $I$  is the external current which is taken to be constant. The above form of rate model is considered paradigmatic [51,56], and a substantial amount of theoretical work has been carried out to analytically obtain the particular transfer functions for a range of spiking neuron models [44,59,60].

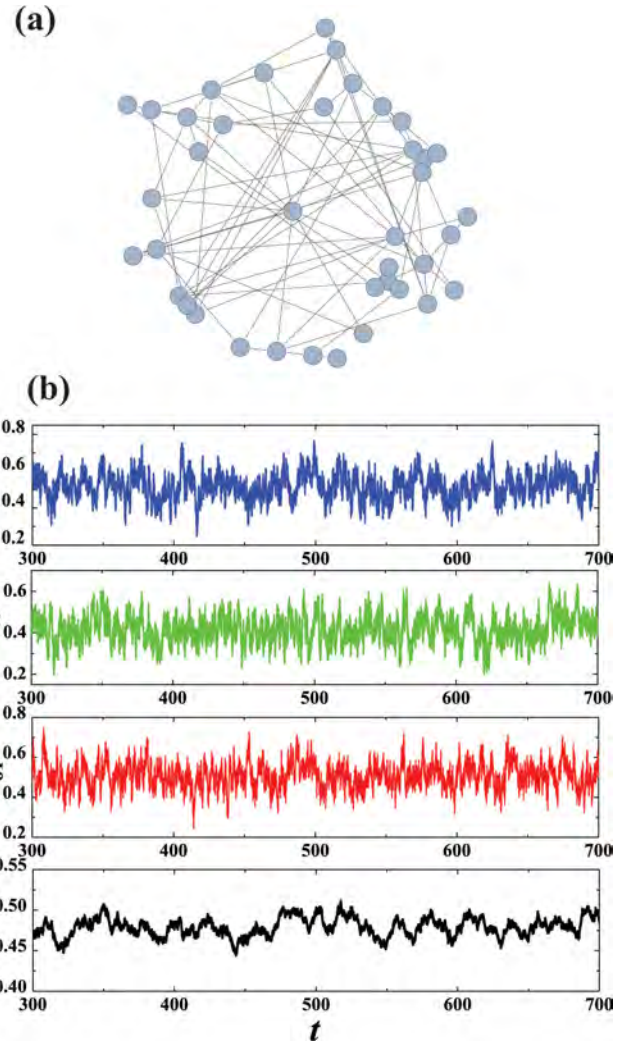


FIG. 1. (Color online) Illustration of the network topology and the typical network activity. (a) A sample configuration of an Erdős-Rényi network for  $N = 40$  and  $p = 0.1$ . (b) Typical time series  $r_i(t)$  of three arbitrary units (first three rows) are compared to the time series of the mean rate  $R(t)$  (bottom row). Note that the fluctuations of the mean rate are much smaller than those for the local variables. The system parameters are  $N = 300$ ,  $p = 0.2$ ,  $c = 3$ ,  $B = 0.002$ ,  $D = 0.0005$ , and  $I = 0.21$ .

Each unit is influenced by the external (synaptic) white noise  $\xi_i(t)$  and the internal (ion-channel) white noise  $\zeta_i(t)$ , whose respective intensities are  $B$  and  $D$ . The external and internal noise sources are assumed to be independent, whereas the random perturbations acting on different units are uncorrelated. The input  $u_i$  which the neuron  $i$  receives from the rest of the network is specified by

$$u_i(t) = \sum_j a_{ij} r_j(t), \quad (2)$$

where  $a_{ij} \in \{0, 1\}$  denote the elements of the adjacency matrix. Throughout the paper, it is assumed that the interaction topology is random, conforming to the Erdős-Rényi type of network; see Fig. 1(a).

TABLE I. Summary of the introduced notation.

$\lambda$	Relaxation time of units
$c$	Coupling strength
$\kappa \equiv c/N$	Normalized coupling strength
$I$	External current
$D$	Intensity of internal noise
$B$	Intensity of external noise
$p$	Connection probability
$\alpha \equiv cp$	Connectivity parameter
$n$	Mean number of connections per unit
$R$	Mean (assembly-averaged) rate
$S$	Rate variance

In the remaining part of this section, we derive the mean-field model for the collective dynamics of the network given by the system (1) and (2). Our approach is essentially based on the well-known quasi-independence and Gaussian approximations [35], and leads to the second-order mean-field model of the macroscopic dynamics. In other words, we use the moment approach with the Gaussian closure hypothesis. The collective behavior is then described in terms of the mean (assembly-averaged) rate and the associated variance,

$$R(t) = \langle r_i \rangle \equiv \frac{1}{N} \sum_i r_i, \quad (3)$$

$$S(t) = \langle [r_i(t) - R(t)]^2 \rangle = \langle r_i(t)^2 \rangle - R(t)^2.$$

One naturally expects that the fluctuations of the mean rate will be comparably smaller than the fluctuations for the local variables; see the sample series in Fig. 1(b). This point will be confirmed during the derivation of the mean-field equations. In order to make the reading easier, a summary of the most relevant notation used throughout the paper is provided in Table I.

Before proceeding to the analytical part, let us explicitly state the approximations relevant for the derivation of the mean-field model. The first one concerns the requirement that the random variables  $r_i(t)$  at any moment  $t$  and for sufficiently large  $N$  satisfy  $\langle r_i \rangle \approx [r_i(t)]$ , where  $[\cdot]$  denotes the expectation over the different stochastic realizations. The mathematical background of this approximation lies in the strong law of large numbers, which states that the sample average  $Y_N = N^{-1} \sum_{i=1}^N y_i$  of  $N$  independently and identically distributed random variables  $y_i$  will almost surely converge to the expectation  $[y_i]$  for  $N \rightarrow \infty$ . The form of convergence for large, but finite  $N$  is specified by the central limit theorem. In physical terms, the outputs of neurons  $r_i$  can be considered unbiased if the distribution of the number of incoming connections (connectivity degrees) over the population is sufficiently narrow.

The second approximation is in a sense implicit for the validity of the first one, and consists in the requirement that the correlation between the outputs of neurons is negligible:  $[r_i(t)r_j(t)] = [r_i(t)][r_j(t)]$ . This is reasonably satisfied when the units share a small fraction of common input from the network [43,61]. Recall that we consider random Erdős-Rényi networks where the probability of connection between two neurons equals constant value  $p$ . For such networks, the fraction of the shared input for two neurons is  $p$ , while

the coefficient of variation for the number of incoming connections equals  $\sqrt{(1-p)/pN}$ . Both values are small for  $N \gg pN \gg 1$ . Thus, in large sparsely connected random networks the approximations for the mean-field approach should be fulfilled. This provided, one can represent the output of each neuron as

$$r_i = R + \sqrt{S}\rho_i, \quad (4)$$

where  $\rho_i$  are uncorrelated variables with zero mean and unit intensity; cf. [62,63].

Proceeding to the derivation of the mean-field model, let us for simplicity first introduce the notation  $x_i = \kappa u_i + I + \sqrt{2B}\zeta_i$  for the total input to the  $i$ th neuron. Using (4), the latter can be written as

$$x_i = X + kv_i R + \kappa\sqrt{S} \sum_j a_{ij}\rho_j + \sqrt{2B}\zeta_i, \quad (5)$$

where  $n_i = \sum_j a_{ij}$  denotes the number of incoming connections to the  $i$ th neuron,  $n = \langle n_i \rangle = pN$  is the mean number of connections,  $v_i = n_i - n$ , and  $X = \kappa n R + I$ . The deviations  $v_i$  are of the order of  $\sqrt{pN}$ , and the independence of the variables  $\rho_i$  implies  $\sum_j a_{ij}\rho_j \sim \sqrt{n}$ . Therefore, the second and the third term in the righthand side of (5) are of the order of  $1/\sqrt{N}$ , i.e., are small. If the external noise  $B$  is weak as well, the function  $\mathcal{H}(x_i)$  can be expanded into the Taylor series around  $X$ :

$$\begin{aligned} \mathcal{H}(x_i) &\approx \mathcal{H}(X) + \mathcal{H}'(X)(x_i - X) + \frac{1}{2}\mathcal{H}''(X)(x_i - X)^2 \\ &= H_0 + \kappa H_1 v_i R + H_2(\kappa^2 v_i^2 R^2 + \kappa^2 S n_i + 2B) \\ &\quad + (H_1 + 2\kappa H_2 v_i R) \left( \kappa\sqrt{S} \sum_j a_{ij}\rho_j + \sqrt{2B}\zeta_i \right). \end{aligned} \quad (6)$$

In the last expression, we have introduced the notation  $H_0 = \mathcal{H}(X)$ ,  $H_1 = \mathcal{H}'(X)$ , and  $H_2 = \frac{1}{2}\mathcal{H}''(X)$ . Note that the products of noisy terms are replaced by the respective means:  $\rho_i \rho_j = \delta_{ij}$ ,  $\zeta_i \zeta_j = \delta_{ij}$ , and  $\rho_i \zeta_j = 0$ .

Inserting (6) into (1), one arrives at the equation for the local rates

$$\frac{dr_i}{dt} = -\lambda r_i + h_i + \gamma_i \sum_j a_{ij}\rho_j + \beta_i \zeta_i + \sqrt{2D}\xi_i, \quad (7)$$

where  $h_i = H_0 + \kappa H_1 R v_i + H_2(\kappa^2 v_i^2 R^2 + \kappa^2 S n_i + 2B)$ ,  $\gamma_i = (H_1 + 2\kappa H_2 v_i R)\kappa\sqrt{S}$ , and  $\beta_i = (H_1 + 2\kappa H_2 v_i R)\sqrt{2B}$ . Taking the population average of the equation for microscopic dynamics (7), we obtain the following for mean (macroscopic) rate  $R$ :

$$\begin{aligned} \frac{dR}{dt} &= -\lambda R + H(R) + \frac{1}{N} \sum_{i,j} \gamma_i a_{ij}\rho_j \\ &\quad + \frac{1}{N} \sum_i \beta_i \zeta_i + \frac{\sqrt{2D}}{N} \sum_i \xi_i, \end{aligned} \quad (8)$$

where  $H(R) = \langle h_i \rangle = H_0 + H_2(\kappa^2 M_2 R^2 + \kappa^2 S n + 2B)$ , and  $M_2 = \langle v_i^2 \rangle = p(1-p)N$  is the second central moment of the connectivity degree distribution.



Note that Eq. (8) effectively includes three noisy terms. Apart from the external and the internal noise, there is also the “network noise” due to variability in connectivity degrees. To estimate the network noise, let us first rewrite the corresponding term as  $\frac{1}{N} \sum_{i,j} \gamma_i a_{ij} \rho_j = \sum_j \rho_j \frac{1}{N} \sum_i \gamma_i a_{ij} = \sum_j \rho_j \langle \gamma_i a_{ij} \rangle$ . Since  $\gamma_i$  and  $a_{ij}$  are not correlated,  $\langle \gamma_i a_{ij} \rangle \approx p \langle \gamma_i \rangle$  holds. Taking this into account, the sum of noisy terms in (8) can be rewritten as  $\xi_R = \frac{1}{N} \sum_i (cpH_1 \sqrt{S} \rho_i + \beta_i \zeta_i + \sqrt{2D} \xi_i)$ , which is equivalent to white noise with the intensity  $2\Psi/N$ , where

$$2\Psi = H_1^2 c^2 p^2 S + 2BH_1^2 + 2D. \quad (9)$$

In the last expression, the terms of the order of  $1/N^2$  have been neglected.

Now let us derive the equation for the variance  $S$ . Taking the appropriate Itô derivatives, one obtains

$$\frac{dS}{dt} = \left\langle 2r_i \frac{dr_i}{dt} + \gamma_i^2 n_i + \beta_i^2 + 2D \right\rangle - 2R \frac{dR}{dt} - 2\Psi/N.$$

It can readily be shown that the noisy terms completely cancel each other. Using the assumption that the outputs  $\rho_i$  are not correlated to the connectivity  $v_i$ , one arrives at the following equation for the variance:

$$\begin{aligned} \frac{dS}{dt} &= 2D + 2BH_1^2 - 2\lambda S + \frac{1}{N} 8p(1-p)BH_2^2 c^2 R^2 \\ &\quad - \frac{1}{N} p(1-p)H_1^2 c^2 S. \end{aligned} \quad (10)$$

Taking into account (8), (9), and (10), the stochastic mean-field model for the finite-size random network of rate-based neurons reads

$$\begin{aligned} \frac{dR}{dt} &= -\lambda R + H_0 + 2H_2 B + \frac{c^2 H_2}{N} (p(1-p)R^2 + pS) \\ &\quad + \sqrt{\frac{1}{N} (H_1^2 c^2 p^2 S + 2BH_1^2 + 2D)} \eta, \end{aligned} \quad (11)$$

$$\begin{aligned} \frac{dS}{dt} &= 2D + 2BH_1^2 + \frac{1}{N} 8p(1-p)BH_2^2 c^2 R^2 \\ &\quad - \left( 2\lambda + \frac{1}{N} p(1-p)H_1^2 c^2 \right) S. \end{aligned} \quad (12)$$

Before proceeding with the stability and bifurcation analysis, a brief remark is required regarding the numerical treatment of system (1), and the ensuing dynamics for the assembly average. In particular, the transfer function involves an argument with the stochastic term corresponding to external noise, which cannot be resolved unless some approximation is introduced. During the derivation of the mean-field model, we have expanded the transfer function  $H(x_i)$  to Taylor series up to second order around the assembly-averaged input  $X$ , having verified that each of the terms contributing the deviation of the input  $x_i$ , received by an arbitrary unit  $i$ , from  $X$  is small. The expansion up to second order may effectively be interpreted as Gaussian approximation for the distribution of  $H(x_i)$  over the assembly. When numerically integrating the system, one cannot hold that such an approximation holds *a priori*. It has to be explicitly verified that the distribution of  $H(x_i)$  is indeed Gaussian for the considered range of

neuronal and network parameters. To this end, before running the simulations, we have calculated the distributions of the function  $H(x + \sqrt{2B}\zeta)$  for various  $x$  and evinced that their skewness and excess kurtosis are small, consistent with the Gaussian requirement. This allowed us to replace the term  $H(x + \sqrt{2B}\zeta)$  by a Gaussian process with the same mean and variance.

### III. ANALYSIS OF STABILITY AND BIFURCATIONS IN THE THERMODYNAMIC LIMIT

In this section, we analyze the stability and bifurcations of the mean-field model (11) and (12) in the thermodynamic limit  $N \rightarrow \infty$ . Under such conditions, the stochastic term in (11) can be neglected, so that the network dynamics effectively becomes deterministic. The influence of noise is reduced to respective noise intensities  $B$  and  $D$ , which may be regarded as additional system parameters. For simplicity, let us further set  $\lambda = 1$  and consider the activation function  $\mathcal{H}(x)$  of the form

$$\mathcal{H}(x) = \begin{cases} 0, & x \leq 0, \\ 3x^2 - 2x^3, & 0 < x < 1, \\ 1, & x \geq 1. \end{cases} \quad (13)$$

Consistent with the notation introduced above, cf. (6), one has  $H_0 = 3X^2 - 2X^3$ , while the first- and second-order derivatives are  $H_1 = 6X - 6X^2$ ,  $H_2 = 6 - 12X$  for  $0 < X < 1$ .

The dynamics of variance  $S$  in the thermodynamic limit is governed by the equation

$$\frac{dS}{dt} = 2D + 2BH_1^2 - 2S. \quad (14)$$

Following relaxation, the variance reaches the stationary value

$$S_0 = D + BH_1^2. \quad (15)$$

Further note that the dynamics of the mean rate  $R$ , given by (11), becomes

$$\frac{dR}{dt} = -R + H_0 + 2H_2 B, \quad (16)$$

which is independent on the variance  $S$ . Taking into account that  $X = \alpha R + I$ , where  $\alpha = cp$ , one can rewrite (16) as

$$\begin{aligned} \frac{dX}{dt} &= F(X) = -2\alpha X^3 + 3\alpha X^2 - (12\alpha B + 1)X \\ &\quad + 6\alpha B + I. \end{aligned} \quad (17)$$

The analysis of (17) indicates that it always exhibits at least one stable stationary state. For the parameter values given by

$$\alpha = \alpha_0 = \frac{2}{3(1-8B)}, \quad I = I_0 = \frac{1-\alpha_0}{2}, \quad (18)$$

Eq. (17) undergoes pitchfork bifurcation where two stable steady states are created separated by an unstable one. The stable states correspond to two distinct values of the mean firing rate which we further refer to as the “low” and the “high” state. For strong enough coupling  $\alpha > \alpha_0$ , the high (low) state emerges via the saddle-node bifurcation, which occurs at the parameter value

$$I = \frac{1-\alpha}{2} \mp \frac{2}{3\sqrt{3}} \left( \frac{\alpha}{\alpha_0} - 1 \right)^{3/2}, \quad (19)$$

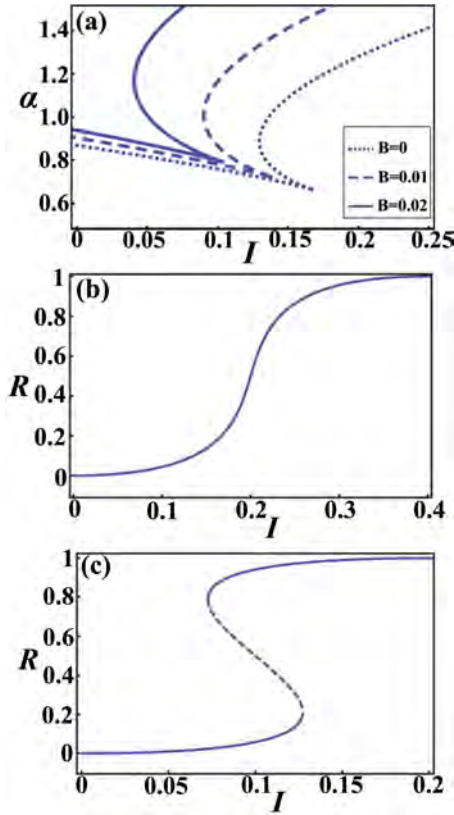


FIG. 2. (Color online) (a) Two-parameter bifurcation diagram of the network in the thermodynamic limit. The lines show saddle-node bifurcations in the  $I - \alpha$  plane for three different values of  $B$ . (b) One-parameter bifurcation diagram showing the dependence of the mean rate  $R$  against the bias current  $I$  for  $B = 0$ ,  $\alpha = 0.6$ . (c) The analogous bifurcation diagram as in (b) is displayed for  $\alpha = 0.8$ . The solid lines indicate the stable branches, whereas the dashed line refers to the unstable branch.

where the minus sign corresponds to the high, and plus to the low state. For  $I$  between these two values, the high and the low states coexist, such that the network is in a bistable regime. The two-dimensional bifurcation diagram in Fig. 2(a) shows the curves (19) for different values of  $B$ . One can see that the two curves form a “tongue” inside which the network is bistable. Figures 2(b) and 2(c) display the one-dimensional bifurcation diagrams for parameter values outside and within the bistability tongue, respectively.

We note the interesting role played by the intensity of external noise  $B$ . It is found to influence the position of the bistability region, shifting it “upwards” toward the domain of stronger couplings. This observation instigated an idea of the potential network control mechanism via the noise intensity. In order to illustrate this mechanism, we have analyzed in more detail how the network dynamics depends on  $B$ . To this end, one can solve the equation  $F(X) = 0$  with respect to  $B$  and obtain the following expression:

$$B = \frac{1}{24} \left( \left( 3 - \frac{2}{\alpha} \right) - 4 \left( X - \frac{1}{2} \right)^2 + \frac{2I-1}{X - \frac{1}{2}} + 1 \right). \quad (20)$$

For  $I > \frac{1}{2}(1 - \alpha)$ , the corresponding one-dimensional bifurcation diagram is provided in Fig. 3(a). The dependence  $X(B)$  is single valued for  $B > B_0$ , where  $B_0 = \frac{1}{24} \left( \left( 3 - \frac{2}{\alpha} \right) - 3 \left( \frac{2I-1}{\alpha} + 1 \right)^{2/3} \right)$ . For such  $B$ , only the high state of the network exists. For  $B = B_0$ , the saddle-node bifurcation takes place, whereby the low state is born. The latter state is found for  $B < B_0$ . Since only positive values of  $B$  are physically meaningful, the low state branch exist only for  $B_0 > 0$ , which is equivalent to the condition

$$\alpha > \frac{2}{3} \text{ and } \frac{1}{2}(1 - \alpha) < I < \frac{1}{2}(1 - \alpha) + \frac{(\alpha - 2/3)^{3/2}}{\alpha^{1/2}}. \quad (21)$$

For  $\alpha$  and  $I$  satisfying (21), the network is bistable for  $B < B_0$  and exhibits only the high state for  $B > B_0$ . Therefore, a pulselike increase of  $B$  may switch the network from the low to the high state via the hysteresis scenario.

This effect is illustrated in Fig. 3(b), which shows the network dynamics before, during, and after the pulselike change of the external noise  $B$ . Prior to strengthening, the external noise level is  $B = 10^{-3}$ , such that the network is bistable and is settled in the low lying state. As soon as the external noise intensity is temporarily increased to  $B = 5 \times 10^{-3}$ , the low state vanishes, and the network switches to the high state. When  $B$  regains the initial value, Eq. (17) admits a bistable regime again, but the network remains in the high state. Thus the temporary increase of  $B$  has caused the network to switch from the low state to the high state.

Note that, for  $I < \frac{1}{2}(1 - \alpha)$ , the inverse scenario is possible, where the network can switch from the high state to the low state by a pulselike increase of the external noise. An example for such a scenario is illustrated in Figs. 3(c) and 3(d).

Interestingly enough, the external noise has an effect not only on the stationary states of the network, but is found to influence its transient dynamics as well. The transient dynamics is important when the external input changes and the network has to track this change and adapt to its rate accordingly. In this scenario, short response time of a network is naturally considered as advantageous [64]. Our analysis shows that under certain conditions, introduction of the external noise may sufficiently reduce the response time. To understand this, let us consider the situation when the input  $I$  switches from some value  $I_1$  to the new value  $I_2$ . For simplicity, we assume that the other parameters are set so that the network is always monostable. Then, the network will evolve from the previous stationary state  $X_1$  to the new one  $X_2$ . According to (17), the rate  $\Gamma$  of the system convergence to  $X_2$  is determined by the absolute value of the derivative  $F'(X_2)$ :

$$\Gamma = -F'(X_2) = -6\alpha X_2^2 + 6\alpha X_2 + 12\alpha B + 1. \quad (22)$$

Thus strengthening of the external noise  $B$  increases the rate  $\Gamma$  and speeds up the network response. This finding is corroborated by numerical simulations illustrated in Fig. 4. Here, two networks are considered: the first one without the external noise ( $B = 0$ , blue curve), and the second one with noise ( $B = 0.01$ , red curve). The values of the other parameters are given in the caption to the figure. For both cases, the input  $I$  changes its value at the moment  $t = 0$  so that the stationary value of  $X$  changes from  $X_1 = 0.25$  to  $X_2 = 0.5$ .

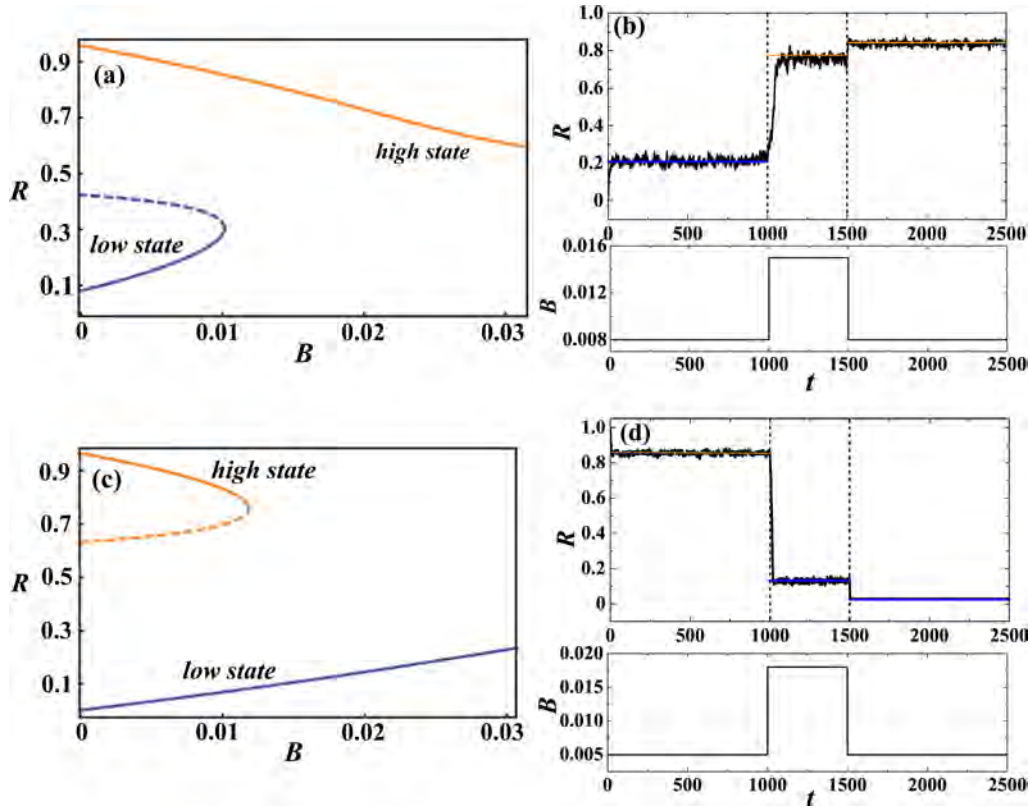


FIG. 3. (Color online) (a) One-parameter bifurcation diagram illustrating the dependence  $R(B)$  for  $\alpha = 0.8$ ,  $I = 0.11$ . The solid lines indicate the stable branches of steady-state solutions, whereas the dashed line stands for the unstable branch. (b) The dynamics of the network under temporary increase of external noise:  $B = 0.004$  for  $t < 1000$  and  $t > 1500$ , and  $B = 0.015$  for  $t \in [1500; 2000]$ . The black thick line refers to numerical results, whereas the thin solid lines indicate the theoretically obtained stable activity levels for the corresponding time intervals. Panels (c) and (d) illustrate the switching scenario from the high state to the low state by the temporary increase of  $B$ . The network parameters are  $\alpha = 0.9$ ,  $I = 0.02$ , whereas  $B$  values are  $B = 0.005$  for  $t < 1000$  and  $t > 1500$  and  $B = 0.018$  for  $t \in [1500; 2000]$ . The presentation style is analogous to that from (a) and (b). The network size in simulations is  $N = 300$ .

The estimate (22) then gives  $\Gamma = 0.025$  without noise and  $\Gamma = 0.103$  with noise, which implies a fourfold speedup of the network response. Note that the numerical results show satisfactory agreement with the theoretical predictions.

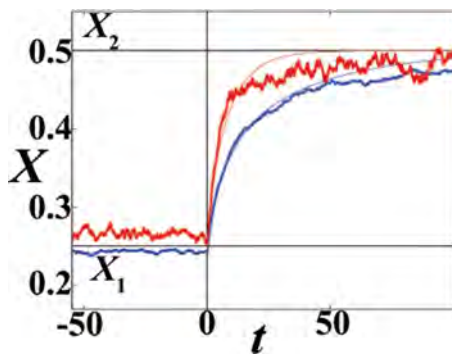


FIG. 4. (Color online) Dependence of the transient dynamics of the network on  $B$ . The change of external input occurs at  $t = 0$ . The response of the network for  $B = 0$  is shown by the blue (light gray) lines, and for  $B = 0.01$  by the red (dark gray) lines. The remaining network parameters are  $N = 400$ ,  $\alpha = 0.65$ , and  $D = 0.001$ . The thick lines represent the numerical results, whereas the thin lines denote the theoretical estimates.

#### IV. FINITE-SIZE EFFECTS

In this section we analyze the influence of the finite-size effects in case where the network is large but finite, viz.  $N \gg 1$ . Then, the noise term in (11) can no longer be considered zero, and can give rise to stochastic fluctuations of the mean rate around the values obtained for the thermodynamical limit.

To study the magnitude of fluctuations, let us rewrite (11) as follows:

$$\frac{dX}{dt} = F(X) + \frac{1}{N}G(X, S) + \frac{1}{\sqrt{N}}\sqrt{2\Psi(X, S)}\eta. \quad (23)$$

For large  $N$ , the variables  $X$  and  $S$  are close to the respective values  $X_0$  and  $S_0$  from the thermodynamic limit, whereby  $X_0$  is defined by the condition  $F(X_0) = 0$ , and  $S_0$  by (15). Since the fluctuations  $x = X - X_0$  are small, one can linearize (23) and obtain

$$\frac{dx}{dt} = F'(X_0)x + \frac{1}{N}G(X_0, S_0) + \frac{1}{\sqrt{N}}\sqrt{2\Psi(X_0, S_0)}\eta. \quad (24)$$

Since the state is stable in the thermodynamic limit,  $F'(X_0) < 0$  applies. The steady state's displacement due to the finite-size

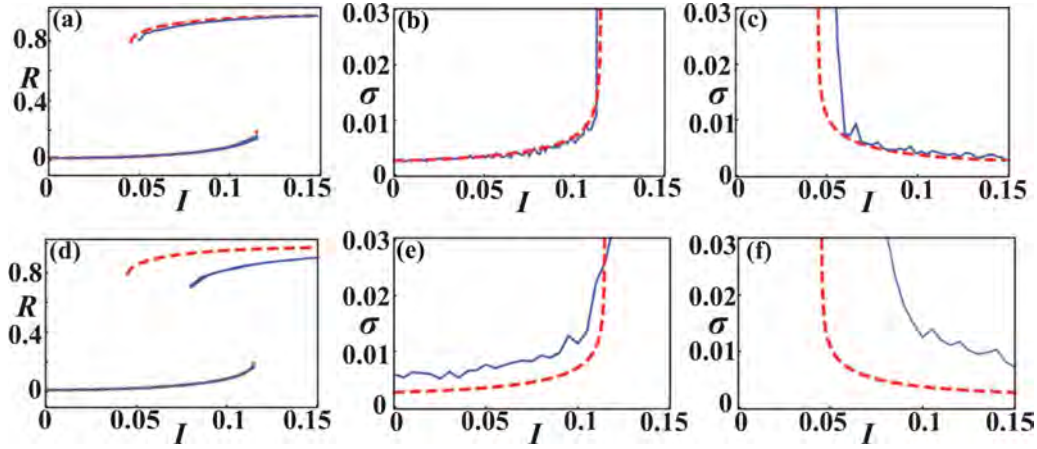


FIG. 5. (Color online) (a) One-parameter bifurcation diagram illustrating the dependence of the stationary mean rate  $R$  vs the bias current  $I$ . Blue solid lines indicate the values observed after the transient, while red dashed lines show the theoretical predictions for the stable levels. (b) and (c) The variance of the mean rate  $\sigma = \sqrt{[\delta X^2]}$ . The solid line denotes the numerical results, whereas the dashed line stands for the approximate model. The parameter values are  $N = 400$ ,  $p = 0.2$ ,  $c = 4.2$ , and  $B = D = 0.002$ . The second row is intended to illustrate the breakdown of theory at smaller network sizes. The presentation style is the same as in the upper row, but the size of the exact system is  $N = 70$ . Panels (d), (e), and (f) show that the stationary mean rate, as well as the associated variance, substantially depart from what is predicted by the approximate model.

effect equals

$$x_0 = \frac{G(X_0, S_0)}{-NF'(X_0)} = \frac{H_2(\mu(X_0 - I)^2 + \alpha^2 p(D + BH_1^2))}{Np^2(12\alpha B + 1 - \alpha H_1)}. \quad (25)$$

This deviation is of the order of  $1/N$ , while the random fluctuations of  $X$  due to noise are of the order of  $1/\sqrt{N}$ . This allows one to neglect the second term in (24) and obtain the following expression for the variance of  $X$  over stochastic realizations:

$$[x^2] = \frac{2\Psi(X_0, S_0)}{-2NF'(X_0)} = \frac{(D + BH_1^2)(2 + \alpha^2 H_1^2)}{2N(12\alpha B + 1 - \alpha H_1)}. \quad (26)$$

The expressions (25) and (26) both contain  $F'(X_0)$  in the denominator. When the value of  $F'(X_0)$  becomes small, the two formulas lose validity since the linearization of (23) is no longer adequate. Note that such a scenario corresponds to the parameter domain near the saddle-node bifurcations of the system in the thermodynamic limit.

In order to verify the validity and the accuracy of the developed mean-field approach, we have performed direct simulations of the network (1) and compared the results with the predictions of the theory. We find that for  $B < 0.01$ ,  $D < 0.01$ , and  $N > 100$  the theory holds quite well in most of the cases: the mean rate of the network is typically predicted with the accuracy no less than 5%. The theory's validity reduces for the values of  $R$  close to zero and unity since the second derivative  $H_2$  has discontinuity at these points.

The comparison between the numerical and the theoretical results is provided in Fig. 5. The intention is to first consider a sufficiently large network  $N = 400$ , where the mean-field treatment is expected to hold; see Fig. 5(a). In particular, for each parameter value, the network is simulated for the period  $T = 200$  starting from 10 different randomly chosen initial conditions. After the transient  $T_{tr} = 50$ , all the observed mean rates  $R$  were saved and plotted versus the corresponding

parameter value. The theoretical prediction for the mean is superimposed on this plot (see the dashed lines). To check the predictions for the magnitude of the stochastic fluctuations, we have further plotted together the observed variance and the estimate (26); cf. Figs. 5(b) and 5(c). Since the network is bistable in a certain parameter interval, the results are plotted separately for the low and the high branches. As expected, the theory becomes inadequate close to the points where the branches vanish through the saddle-node bifurcations. In the rest of the parameter interval the theoretical estimate is quite precise.

The second row in Fig. 5 illustrates the breakdown of theory for smaller system sizes. As an example, we consider the case  $N = 70$ . Note that the upper branch of the mean rates substantially deviates from the theoretical prediction. One also finds that the magnitude of stochastic fluctuations are much larger than what is anticipated by the approximate model, because the assumptions behind (26) no longer hold.

Note that the influence of the system finite size on the value of the variance  $S$  amounts only to its small change, which is of the order  $1/N$ . Namely, the stationary value of the variance for large  $N$  equals

$$S = S_0 + \frac{p(1-p)c^2}{2N} (B(8H^2R^2 - H_1^2) - DH_1^2). \quad (27)$$

## V. SUMMARY AND DISCUSSION

In this paper, we have considered a network of rate-based neurons with random connectivity and two types of noise. In order to study the macroscopic dynamics of the network, we have developed the second-order mean-field approach which incorporates the Gaussian closure hypothesis. The dynamics of the large, but finite network is described in terms of the assembly averaged firing rate and the associated variance, whose evolution is given by the system (11) and (12). The

main approximations relevant to the derivation of the model are that the outputs of the units are unbiased and uncorrelated. The analysis shows that these assumptions are valid for large networks with random sparse connectivity. In fact, such type of connectivity renders correlation between the outputs of units small, which is the point relevant for our derivation.

In the context of neuroscience, random networks are often considered as the simplest model of connectivity of neural circuits [43,44,61,64,65]. On the other hand, most of the research so far dedicated to mean-field approach for stochastic systems has addressed the scenario of a fully connected network [23,33,34,51–53]. However, recent experimental data provides evidence that the organization of synaptic connections in brain is nontrivial and differs drastically from both of the above models [66–69]. The structure of neural networks appears to be inhomogeneous, in a sense that most of the connections are random and sparse, but some units are also organized into densely connected clusters [70,71].

Such clusters have already been established to play an important information-processing role in the cortex [72–75]. Within a broader research agenda, the results gained here for the case of random networks, if incorporated together with the previous work on fully connected networks, may ultimately allow us to derive the mean-field model appropriate for clustered networks.

In terms of research goals, most of the early studies applying the mean-field approach have been focused on explaining the mechanisms behind the spontaneous activity characterized by irregular firing of neurons at low rates, typically found in a living cortex or living hippocampus. Apart from gaining insight into the genesis and the self-sustaining property of these chaotic states, the aim has also been to explain why populations of highly nonlinear units display linear responses to external drive, reacting on time scales faster than the characteristic time scale of a single unit. The emergence of relevant cooperative states has been linked to several different ingredients, including the features of the unit's threshold function, the network connection topology, and the scaling of synaptic strengths. In particular, for a fully connected network of rate-based units with random asymmetrical couplings similar to spin glasses, the onset of chaos has been associated to the gain parameter of the threshold function [76]. For networks comprised of binary neuronlike units, the most important finding has concerned the existence of a chaotic balanced state, where variability is achieved by the balance of excitatory and inhibitory inputs, each being much larger than the unit's threshold [61,64]. Necessary conditions for maintaining such a regime include random and sparse connectivity, as well as comparably strong synapses. Under similar conditions the networks of integrate-and-fire neurons have been found to support a bistable regime between the spontaneous activity, uncorrelated with the received stimuli, and the “working memory” states, strongly correlated with the “learned” stimuli [77,78]. Further research have revealed importance of the weight distribution in random networks of integrate-and-fire neurons and its essential role for the spike-based communication [65].

At variance with the above models, which typically do not consider at all or provide only a limited account of the effects of noise, the central issue of research in recent years has become the point of how noise from the level of single units

is translated to and reflected in the macroscopic-scale behavior. The present study aims to contribute to this line of research, and our main results can be summarized as follows. In the thermodynamic limit, the network dynamics is deterministic in nature. We have determined the stationary levels of the network activity, showing that for strong enough coupling [ $\alpha > \alpha_0$ ; see Eq. (18)] the network exhibits bistable regime, characterized by coexistence of the low and the high stable states. In terms of how noise from microscopic dynamics effectively impacts the collective behavior, our most important finding is that the external and the internal noise play essentially different roles in the mean-field dynamics. In particular, in the thermodynamic limit, the internal noise does not influence the macroscopic dynamics at all, while the external noise changes the position and the number of stable levels. We have demonstrated that this feature can be used to control the network dynamics via external noise in a hysteresislike scenario, as illustrated in Fig. 3. We have also shown that the external noise influences the transient dynamics of a network, at certain instances being able to speed up its response to the change of external drive.

The developed theory has also allowed us to consider the finite-size effects on the network dynamics. The corresponding approximate model for large but finite networks effectively involves three sources of noisy behavior. Apart from the internal and external noises, which manifest as the additive and multiplicative noise at the macroscopic level, we identify an additional term that derives from heterogeneity in the units' connectivity degrees. We have found that the finite-size effects are twofold and consist in (i) displacement of the stationary levels and (ii) in giving rise to stochastic fluctuations of the mean rate. Since the change of the stationary values of  $R$  and  $S$  is of the order of  $1/N$ , the most important are the stochastic fluctuations which have the magnitude of the order of  $1/\sqrt{N}$ . It has also been explicitly demonstrated that the developed approach provides a satisfactory estimate of the magnitude of the fluctuations for the parameter domain sufficiently away from the bifurcations.

We suspect that novel interesting effects may arise in sufficient vicinity of the pitchfork bifurcation, where the network possesses two stable activity levels that are relatively close to each other. In this case, the derivatives  $F'(X_0)$  are close to zero for both states, and the estimate provided by Eq. (26) indicates large fluctuations of the mean rate. If one approaches close enough to the bifurcation, the magnitude of fluctuations may become of the order of the distance between the levels, which is likely to induce stochastic “switching” between the low and the high state. This phenomenon may be associated to high variability of firing rates often observed in neural networks and recently connected to clustering of synaptic connections [71]. However, linearization of Eq. (23) in this case is no longer adequate, such that the full nonlinear equations (11) and (12) should be studied to capture the potential phenomenon of stochastic switchings. This will be one of the main goals for our future research.

#### ACKNOWLEDGMENTS

This work was supported in part by the Russian Foundation for Basic Research (Grant No. 14-02-00042) and the Ministry of Education and Science of the Republic of Serbia

under Project No. 171017. The authors would like to thank Professor Nikola Burić and Professor Vladimir Nekorkin

for valuable discussions during the different stages of the research.

- 
- [1] W. R. Softky and C. Koch, *J. Neurosci.* **13**, 334 (1993).
- [2] M. Steriade, I. Timofeev, and F. Grenier, *J. Neurophysiol.* **85**, 1969 (2001).
- [3] A. Destexhe, M. Rudolph, and D. Paré, *Nat. Rev. Neurosci.* **4**, 739 (2003).
- [4] G. Buzsáki, *Rhythms of the Brain* (Oxford University Press, New York, 2006).
- [5] V. B. Mountcastle, *Brain* **120**, 701 (1997).
- [6] *Lectures in Supercomputational Neuroscience: Dynamics in Complex Brain Networks*, edited by P. beim Graben, C. Zhou, M. Thiel, and J. Kurths (Springer-Verlag, Berlin, 2008).
- [7] *Neural Fields, Theory and Applications*, edited by S. Coombes, P. beim Graben, R. Potthast, and J. Wright (Springer-Verlag, Berlin, 2014).
- [8] H. R. Wilson and J. D. Cowan, *Biophys. J.* **12**, 1 (1972).
- [9] H. R. Wilson and J. D. Cowan, *Kybernetik* **13**, 55 (1973).
- [10] S. Amari, *Biol. Cybern.* **27**, 77 (1977).
- [11] P. A. Robinson, C. J. Rennie, J. J. Wright, H. Bahramali, E. Gordon, and D. L. Rowe, *Phys. Rev. E* **63**, 021903 (2001).
- [12] V. K. Jirsa and H. Haken, *Physica D* **99**, 503 (1997).
- [13] C. R. Laing and C. C. Chow, *Neural Comput.* **13**, 1473 (2001).
- [14] C. R. Laing, W. C. Troy, B. Gutkin, and G. B. Ermentrout, *SIAM J. Appl. Math.* **63**, 62 (2002).
- [15] D. J. Pinto and G. B. Ermentrout, *SIAM J. Appl. Math.* **62**, 206 (2001).
- [16] S. E. Folias and P. C. Bressloff, *SIAM J. Appl. Math.* **65**, 2067 (2005).
- [17] M. Enculescu and M. Bestehorn, *Phys. Rev. E* **67**, 041904 (2003).
- [18] C. R. Laing, *SIAM J. Appl. Dyn. Syst.* **4**, 588 (2005).
- [19] S. E. Folias and P. C. Bressloff, *Phys. Rev. Lett.* **95**, 208107 (2005).
- [20] M. R. Owen, C. R. Laing, and S. Coombes, *New J. Phys.* **9**, 378 (2007).
- [21] P. C. Bressloff, *SIAM J. Appl. Math.* **70**, 1488 (2009).
- [22] P. C. Bressloff, *Phys. Rev. E* **82**, 051903 (2010).
- [23] J. Touboul, *Physica D* **241**, 1223 (2012).
- [24] J. D. Touboul and G. B. Ermentrout, *J. Comput. Neurosci.* **31**, 453 (2011).
- [25] A. Renart, R. Moreno-Bote, X. J. Wang, and N. Parga, *Neural Comput.* **19**, 1 (2007).
- [26] R. Moreno-Bote and N. Parga, *Phys. Rev. Lett.* **96**, 028101 (2006).
- [27] R. Rosenbaum and B. Doiron, *Phys. Rev. X* **4**, 021039 (2014).
- [28] A. A. Faisal, L. P. J. Selen, and D. M. Wolpert, *Nat. Rev. Neurosci.* **9**, 292 (2008).
- [29] M. D. McDonnell and L. M. Ward, *Nat. Rev. Neurosci.* **12**, 415 (2011).
- [30] V. S. Anishchenko, V. Astakhov, A. Neiman, T. Vadivasova, and L. Schimansky-Geier, *Nonlinear Dynamics of Chaotic and Stochastic Systems: Tutorial and Modern Developments* (Springer-Verlag, Berlin, 2007).
- [31] B. Hauschildt, N. B. Janson, A. Balanov, and E. Schöll, *Phys. Rev. E* **74**, 051906 (2006).
- [32] N. B. Janson, A. G. Balanov, and E. Schöll, in *Handbook of Chaos Control*, 2nd ed., edited by E. Schöll and H. G. Schuster (Wiley, New York, 2008), pp. 221–273.
- [33] B. Lindner, J. Garcia-Ojalvo, A. Neiman, and L. Schimansky-Geier, *Phys. Rep.* **392**, 321 (2004).
- [34] I. Franović, K. Todorović, N. Vasović, and N. Burić, *Phys. Rev. E* **87**, 012922 (2013).
- [35] I. Franović, K. Todorović, N. Vasović, and N. Burić, *Phys. Rev. E* **89**, 022926 (2014).
- [36] A. Hutt, A. Longtin, and L. Schimansky-Geier, *Physica D* **237**, 755 (2008).
- [37] O. Faugeras, J. Touboul, and B. Cessac, *Front. Comput. Neurosci.* **3**, 1 (2009).
- [38] S. E. Boustani and A. Destexhe, *Neural Comput.* **21**, 46 (2009).
- [39] N. G. Van Kampen, *Stochastic Processes in Physics and Chemistry* (North-Holland, Amsterdam, 1992).
- [40] M. A. Buice and J. D. Cowan, *Phys. Rev. E* **75**, 051919 (2007).
- [41] M. Buice, J. D. Cowan, and C. C. Chow, *Neural Comput.* **22**, 377 (2010).
- [42] W. Gerstner and J. L. van Hemmen, *Phys. Rev. Lett.* **71**, 312 (1993).
- [43] N. Brunel and V. Hakim, *Neural Comput.* **11**, 1621 (1999).
- [44] N. Brunel, *J. Comput. Neurosci.* **8**, 183 (2000).
- [45] L. F. Abbott and C. van Vreeswijk, *Phys. Rev. E* **48**, 1483 (1993).
- [46] D. Nykamp and D. Tranchina, *J. Comput. Neurosci.* **8**, 19 (2000).
- [47] C. Ly and D. Tranchina, *Neural Comput.* **19**, 2032 (2007).
- [48] H. Soula and C. C. Chow, *Neural Comput.* **19**, 3262 (2007).
- [49] I. Ginzburg and H. Sompolinsky, *Phys. Rev. E* **50**, 3171 (1994).
- [50] C. Meyer and C. van Vreeswijk, *Neural Comput.* **14**, 369 (2002).
- [51] H. Hasegawa, *Phys. Rev. E* **75**, 051904 (2007).
- [52] H. Hasegawa, in *Neuronal Network Research Horizons*, edited by M. L. Weiss (Nova Science Publishers, New York, 2007), pp. 61–98.
- [53] H. Hasegawa, *Physica A* **388**, 499 (2009).
- [54] W. M. Ursey and R. C. Reid, *Annu. Rev. Physiol.* **61**, 435 (1999).
- [55] R. C. deCharms and A. Zador, *Annu. Rev. Neurosci.* **23**, 613 (2000).
- [56] R. A. Anderson, S. Musallam, and B. Pesaran, *Curr. Opin. Neurobiol.* **14**, 720 (2004).
- [57] J. K. Chapin, K. A. Moxon, R. S. Markowitz, and M. A. L. Nicolelis, *Nat. Neurosci.* **2**, 664 (1999).
- [58] H. Hasegawa, *Phys. Rev. E* **67**, 041903 (2003).
- [59] N. Fourcaud and N. Brunel, *Neural Comput.* **14**, 2057 (2002).
- [60] O. Shriki, D. Hansel, and H. Sompolinsky, *Neural Comput.* **15**, 1809 (2003).
- [61] C. van Vreeswijk and H. Sompolinsky, *Neural Comput.* **10**, 1321 (1998).
- [62] H. C. Tuckwell, *Introduction to Theoretical Neurobiology* (Cambridge University Press, Cambridge, UK, 1998).
- [63] A. N. Burkitt, *Biol. Cybern.* **95**, 1 (2006).
- [64] C. van Vreeswijk and H. Sompolinsky, *Science* **274**, 1724 (1996).
- [65] J.-N. Teramae, Y. Tsubo, and T. Fukai, *Sci. Rep.* **2**, 485 (2012).
- [66] H. Markram, *Cereb. Cortex* **7**, 523 (1997).

- [67] S. Song, P. J. Sjöström, M. Reigl, S. Nelson, and D. B. Chklovskii, *PLoS Biol.* **3**, e68 (2005).
- [68] S. Lefort, C. Tamm, J.-C. F. Sarria, and C. C. H. Petersen, *Neuron* **61**, 301 (2009).
- [69] R. Perin, T. K. Berger, and H. Markram, *Proc. Natl. Acad. Sci. USA* **108**, 5419 (2011).
- [70] V. V. Klinshov, J. Teramae, V. I. Nekorkin, and T. Fukai, *PLoS One* **9**, e94292 (2014).
- [71] A. Litwin-Kumar and B. Doiron, *Nat. Neurosci.* **15**, 1498 (2012).
- [72] C. Zhou, L. Zemanova, G. Zamora, C. C. Hilgetag, and J. Kurths, *Phys. Rev. Lett.* **97**, 238103 (2006).
- [73] H. Ko, L. Cossell, C. Baragli, J. Antolik, C. Clopath, S. B. Hofer, and T. D. Mrsic-Flogel, *Nature (London)* **473**, 87 (2011).
- [74] Y. Yoshimura, J. L. M. Dantzker, and E. M. Callaway, *Nature (London)* **433**, 868 (2005).
- [75] L. Yassin, B. L. Benedetti, J. S. Jouhanneau, J. A. Wen, J. F. Poulet, and A. L. Barth, *Neuron* **68**, 1043 (2010).
- [76] H. Sompolinsky, A. Crisanti, and H. J. Sommers, *Phys. Rev. Lett.* **61**, 259 (1988).
- [77] D. J. Amit and N. Brunel, *Netw., Comput. Neural Syst.* **8**, 373 (1997).
- [78] D. J. Amit and N. Brunel, *Cereb. Cortex* **7**, 237 (1997).

**Activation process in excitable systems with multiple noise sources: Large number of units**Igor Franović,<sup>1,\*</sup> Matjaž Perc,<sup>2,3,†</sup> Kristina Todorović,<sup>4</sup> Srdjan Kostić,<sup>5</sup> and Nikola Burić<sup>6,‡</sup><sup>1</sup>*Scientific Computing Laboratory, Institute of Physics, University of Belgrade, P. O. Box 68, 11080 Beograd-Zemun, Serbia*<sup>2</sup>*Faculty of Natural Sciences and Mathematics, University of Maribor, Koroška Cesta 160, SI-2000 Maribor, Slovenia*<sup>3</sup>*Department of Physics, Faculty of Sciences, King Abdulaziz University, Jeddah, Saudi Arabia*<sup>4</sup>*Department of Physics and Mathematics, Faculty of Pharmacy, University of Belgrade, Vojvode Stepe 450, Belgrade, Serbia*<sup>5</sup>*Institute for the Development of Water Resources "Jaroslav Černi," Jaroslava Černog 80, 11226 Belgrade, Serbia*<sup>6</sup>*Scientific Computing Laboratory, Institute of Physics, University of Beograd, P. O. Box 68, 11080 Beograd-Zemun, Serbia*

(Received 19 June 2014; revised manuscript received 10 June 2015; published 14 December 2015)

We study the activation process in large assemblies of type II excitable units whose dynamics is influenced by two independent noise terms. The mean-field approach is applied to explicitly demonstrate that the assembly of excitable units can itself exhibit macroscopic excitable behavior. In order to facilitate the comparison between the excitable dynamics of a single unit and an assembly, we introduce three distinct formulations of the assembly activation event. Each formulation treats different aspects of the relevant phenomena, including the thresholdlike behavior and the role of coherence of individual spikes. Statistical properties of the assembly activation process, such as the mean time-to-first pulse and the associated coefficient of variation, are found to be qualitatively analogous for all three formulations, as well as to resemble the results for a single unit. These analogies are shown to derive from the fact that global variables undergo a stochastic bifurcation from the stochastically stable fixed point to continuous oscillations. Local activation processes are analyzed in the light of the competition between the noise-led and the relaxation-driven dynamics. We also briefly report on a system-size antiresonant effect displayed by the mean time-to-first pulse.

DOI: [10.1103/PhysRevE.92.062912](https://doi.org/10.1103/PhysRevE.92.062912)

PACS number(s): 05.45.Xt, 02.30.Ks

**I. INTRODUCTION**

For the wealth of local and intriguing collective phenomena displayed, the large assemblies comprised of excitable units have now been appreciated as a distinct class of dynamical systems. In terms of theory, the fundamental issue for understanding these systems is whether their macroscopic dynamics itself exhibits excitable behavior. The other important issue naturally concerns the relation between such macroscopic excitability and noise. So far, stochastic effects have been identified as a major factor contributing to the collective behavior of systems of excitable units [1–12].

In this paper, we study large assemblies consisting of noisy type II excitable elements, which are represented by the canonical Fitzhugh-Nagumo (FHN) model. Conceptually, our focus will lie with two main points: (i) demonstrating that an assembly made up of excitable units can itself be considered a macroscopic excitable element and (ii) identifying the analogies and pointing out the differences between the excitable behaviors of a single unit and an assembly.

Note that point (i), at least to our knowledge, has not been treated explicitly so far. In particular, the main obstacle for analytically approaching this issue is that the macroscopic dynamics of an assembly of stochastic FHN units cannot be expressed in a closed form via the global variables, which would otherwise make up a standard and the desired form of describing the collective motion. Some alternative forms of analysis are not available due to complexity of the corresponding Fokker-Planck equation that assumes an

integrodifferential form. In order to resolve this and explicitly demonstrate the excitability feature at the assembly level, we use an approach that relies on the mean-field (MF) approximate model of the assembly's collective motion. In several recent papers, the MF model has already proven successful in the analysis of systems described by large sets of stochastic (delay) differential equations, in particular when treating stability of the stationary state, as well as the scenarios for the onset and the suppression of the collective mode [13–15].

Analysis on point (ii) can be carried out at two levels, one focused on the phenomenology involved and the other concerning the statistical properties of the corresponding noise-driven activation processes. In terms of phenomenology, the excitability feature refers to capability of systems to generate spiking (pulselike) responses or small-amplitude excitations, which are separated by some form of threshold. For a single unit, the large-amplitude response is composed of the activation and the relaxation stages, such that the former is strongly influenced by noise, whereas the latter is typically deterministic and maintains a stereotype profile in a broad range of noise values. Among else, the stereotype character of pulse implies that its amplitude and width are independent on the form of perturbation applied.

The stated arguments on the notion of excitability should naturally hold in case of an assembly as well. Nevertheless, what may differ are the details related to the assembly's thresholdlike behavior, which by itself stands out as a highly nontrivial issue. Another point of difference concerns the local mechanisms by which excitations of units within a population are elicited. In particular, each unit may be evoked to emit a pulse either by noise or via the interaction terms. Adhering to the formulation of an activation event for an excitable unit stated in our previous paper [16], the latter point does not merely imply that the activation processes

\*franovic@ipb.ac.rs

†matjaz.perc@uni-mb.si

‡ Corresponding author: buric@ipb.ac.rs



of individual units cannot be considered independent, as if they were driven by uncorrelated random perturbations, but more significantly indicates that the activation process of an arbitrary unit may be influenced by the relaxation processes of other units. The third point one should stress concerns the process of spike emission at the assembly level. In particular, having accepted the description of collective motion in terms of global variables, one should also bear in mind that their amplitude is affected by coherence of individual spikes, such that the increased coherence implies larger amplitude of the relevant macroscopic variable. By such a concept, evoking a large-amplitude excitation requires that the spikes for a sufficient fraction of individual units become coherent. Analyzing coaction of activation and relaxation processes for individual elements, as well as the role of spike coherence with respect to assembly pulse emission, present intricate issues, absent if small groups of units are considered.

Apart from phenomenological aspects, the comparative analysis of excitable behaviors of a unit and an assembly will address the respective noise-driven activation processes. In analogy to our paper on a single excitable unit and two interacting excitable units [16], we associate the term activation solely to the assembly's large-amplitude excitation. In principle, the definition of assembly activation problem should incorporate appropriate boundary conditions, which provide a clear-cut distinction between the small- and the large-amplitude excitations. Nevertheless, while a single most adequate and relevant definition for the activation problem may be given in cases of an excitable unit or a pair of units [16], the specific character of global variables, or rather the fact that their amplitudes depend on coherence of individual spikes, prevents us from establishing such a formulation in case of an assembly of excitable elements. Instead, we introduce three alternative formulations of the assembly activation event which emphasize different aspects of the relevant phenomena. Their merit will depend on the aims of the particular study of assembly dynamics and the fashion in which one can adapt them to potential applications.

Two of the formulations rest on the standard description of collective motion in terms of global variables and are intended precisely at examining the analogy between the excitable behaviors of a single unit and an assembly. In particular, one formulation is consistent the threshold boundary approach for a FHN unit (terminating boundary condition given by a threshold  $x$  value), whereas the other derives from characteristic boundary approach (terminating boundary conditions given by an appropriate boundary set). Nevertheless, for comparison we also adopt a formulation where the assembly activation is treated as a compound event, composed of *only* first-pulse responses of a sufficient fraction of participant units, regardless of whether the emitted spikes are coherent. The implications of the three formulations are analyzed in terms of statistical properties of the corresponding activation events, characterized by the dependencies of the time-to-first pulse emission (TFP) and the related coefficient of variation on noise.

The paper is organized as follows. Section II provides the background on the applied model. Section III addresses the details of the assembly's excitable behavior, including the analysis carried out on the deterministic MF approximation. Section IV lays out the three formulations of the

assembly activation event. Section V contains the detailed numerical analysis on the statistical properties of activation events conforming to the three adopted formulations. We also consider the qualitative explanation for the bimodal or unimodal distributions of local activation events typical for certain domains of noise intensities. Section VD concerns the effects related to system size, including the "antiresonance" found for the mean TFPs at fixed noise intensities. Section VI provides a brief summary of our main points.

## II. DETAILS OF THE APPLIED MODEL

As a paradigm for analyzing collective excitable behavior, we consider an assembly comprised of FHN units. The dynamics of an arbitrary unit  $i$  is given by

$$dx_i = (x_i - x_i^3/3 - y_i)dt + \frac{c}{N} \sum_{j=1}^N (x_j - x_i)dt + \sqrt{2D_1}dW_1^i$$

$$dy_i = \epsilon(x_i + b)dt + \sqrt{2D_2}dW_2^i, i = 1, \dots, N, \quad (1)$$

where  $b$  and  $\epsilon$  are the intrinsic unit parameters, while  $c$  denotes the coupling strength. The units are assumed to be identical and are connected in the all-to-all fashion. Parameter  $\epsilon$  is set to a small value  $\epsilon = 0.05$ , which warrants that the characteristic time scales for  $x_i$  and  $y_i$  evolution are sharply separated. Being type II excitable means that the units are poised close to transition toward oscillatory state via the Hopf bifurcation [2]. The bifurcation parameter  $b$  is set to 1.05, the value just below critical threshold. Excitability feature of a single FHN unit has been extensively analyzed [1,2,17], and an overview can also be found in our preceding paper [16]. At variance with the latter, the perturbation here may either arrive from the interaction terms or may be caused by random fluctuations due to two independent sources of noise. Motivated by the possible interpretation in the field of neuroscience [17,18], we adopt the convention by which the stochastic terms in the fast (slow) variables are referred to as external noise  $D_1$  (internal noise  $D_2$ ). Note that  $dW_k^i, k \in \{1,2\}, i = 1, \dots, N$  denote stochastic increments of independent Wiener processes whose averages and correlations satisfy  $\langle dW_k^i \rangle = 0$ ,  $\langle dW_k^i dW_l^j \rangle = dt \delta_{kl} \delta_{ij}$ .

In order to gain insight into the assembly's collective dynamics, one may first carry out the bifurcation analysis of the deterministic (noiseless) version of system (1). For  $N$  sufficiently large so the terms  $\mathcal{O}[(c/N)^2]$  and of higher order can be neglected, the characteristic equation describing the stability of equilibrium  $(x_1, y_1, x_2, y_2, \dots, x_N, y_N) = (-b, -b + b^3/3, -b, -b + b^3/3, \dots, -b, -b + b^3/3)$  is given by an approximate expression

$$(\lambda^2 - (1 - b^2)\lambda + \epsilon)(\lambda^2 - (1 - b^2 - c)\lambda + \epsilon)^{N-1} = 0. \quad (2)$$

Since  $b = 1.05$  is kept fixed, it follows that the equilibrium may become unstable only via the direct supercritical Hopf bifurcation controlled by  $c$ . Nonetheless, the critical  $c$  value is  $c^* = 1 - b^2 < 0$ , which implies that the positive coupling strengths do not affect the stability of equilibrium. In the present paper, we only consider the subcritical values  $c > 0$ , such that the system (1) always lies in the excitable regime.

As for the impact of stochastic fluctuations on the asymptotic collective dynamics, it is known that the noise intensity

may act as a control parameter in excitable media, giving rise to three generic regimes of macroscopic behavior [3]. In particular, when noise is systematically increased, the dynamics of global variables undergoes a sequence of transitions, first exhibiting the stochastically stable equilibrium and then the stochastically stable limit cycle, and eventually it decays into disordered behavior. This sequence may be explained as follows. In the approximately stationary state, at any given moment, most of the units lie in the vicinity of equilibrium, whereas the relatively rare excursions due to weak noise or the interaction terms remain incoherent. Therefore, the macroscopic variables only marginally differ from equilibrium values of single elements. At some point, the increase of noise induces more or less coherent oscillations of units which are easy to synchronize. This conforms to the onset of the collective mode according to the scenario of stochastic bifurcation [19–22]. In the supercritical state, the global variables follow a limit cycle attractor whose profile is similar to that of relaxation oscillations of individual units. Once the noise intensity becomes strong enough to overcome the effect of couplings, the disordered regime sets in. The spiking frequency of units remains high, but their activity desynchronizes. Since the majority of units at any moment are refractory, global variables display irregular oscillations with a quenched amplitude.

From our perspective, the conceptually most important transition is the one associated to occurrence of noise-induced collective oscillations. This phenomenon is relevant for the activation process because it indicates the loss of stochastic stability for the fixed point. In other words, under increasing noise, the attractive ability of the fixed point gradually reduces and is eventually lost, which naturally affects how the phase point escapes the vicinity of equilibrium. Note that the above sequence of states has previously been verified in case of an assembly of FHN elements driven by internal noise. We have found that the similar sequence persists if the units are influenced by external noise, though the individual activities become more difficult to synchronize, rendering the amplitude of collective oscillations comparably smaller than the one emerging under internal noise.

### III. EXCITABLE BEHAVIOR AT THE ASSEMBLY LEVEL

Having summarized the points relevant for the deterministic part of dynamics described by (1), we turn to characterization of the assembly's excitability feature. The standard approach to collective motion is to introduce the macroscopic variables  $X(t) = \langle x_i(t) \rangle = \frac{1}{N} \sum_{i=1}^N x_i(t)$  and  $Y(t) = \langle y_i(t) \rangle = \frac{1}{N} \sum_{i=1}^N y_i(t)$ , whereby the aim typically lies in establishing some form of analogy between the dynamics of single units and an assembly. The latter would be especially relevant for examining the issue of excitability at the assembly level. Nevertheless, it is evident that the compound effect of nonlinear terms prevents the whole assembly to evolve in a fashion analogous to that of a single unit, which would occur only if  $\langle x_i^3 \rangle = \langle x_i \rangle^3$  were to hold. Therefore, the collective dynamics in principle cannot be expressed in a closed form via the global variables. The other potential approaches to analysis of macroscopic excitable behavior are

severely limited by the difficulties associated to Fokker-Plank formalism, where the equation for the one-particle density  $P(x, y, t)$  acquires a complex integrodifferential form  $\frac{\partial}{\partial t} P = - \frac{\partial}{\partial x} [x(1-c) - \frac{x^3}{3} - y + c \int x_1 P(x_1, y_1, t) dx_1 dy_1] P - \frac{\partial}{\partial y} \epsilon(x + b) P + D_1 \frac{\partial^2 P}{\partial x^2} + D_2 \frac{\partial^2 P}{\partial y^2}$ .

The arguments above imply that one is required to introduce approximations for collective dynamics corresponding to the *deterministic* part of system (1) in order to analyze the assembly excitability feature and the associated thresholdlike behavior. In the following, we consider two approximate models of collective motion, distinguished by the fashion in which the effect of interaction terms is resolved. The first model holds if the interaction terms vanish or can be neglected. Note that this condition is satisfied if the initial conditions for all the units are identical or lie close to each other. Since the evolution of the system is deterministic and the coupling is diffusive, such a selection of initial conditions facilitates that the whole assembly acts as a macroscopic excitable element. The evolution of global variables is then given by the equations analogous to those for a single unit,

$$\begin{aligned} dX &= (X - X^3/3 - Y)dt \\ dY &= \epsilon(X + b)dt. \end{aligned} \quad (3)$$

The details regarding the excitability feature of such a system are well established [17]. In particular, recall that its threshold behavior is associated to the “ghost separatrix,” a thin layer composed of canardlike trajectories that foliate around the maximum of the fast-variable nullcline, whereby the spread increases with the characteristic scale separation ratio  $\epsilon$ .

Let us now consider a more sophisticated approximation that takes into account the net effect of the interaction terms. The analytical framework suitable for demonstrating the assembly excitability feature in this more general case is provided by the mean-field approach. Before laying out the details, we make an overview of the ingredients crucial for the derivation of the MF model, as well as the results achieved so far on treating the systems of large sets of stochastic- (delay) differential equations. In principle, deriving the MF model involves a number of nontrivial elements, and it ultimately leads to a deterministic system amenable to standard bifurcation analysis, where noise intensity may act as a bifurcation parameter. The MF method combines the cumulant approach with Gaussian approximation, according to which all the cumulants above second order are assumed to vanish. The latter is intended as a closure hypothesis, which is necessary due to presence of nonlinear terms in the exact system (1). Thus, starting from the original system which in general comprises  $kN$  (delay) differential equations, where  $k$  is the number of local degrees of freedom, one ends up with a set of  $k(k+3)/2$  deterministic (delayed) equations describing the evolution of the means, as well as the appropriate variances and the covariances.

As for the main results achieved thus far, the MF method has already been applied in analyzing the stability of assemblies of (delay-) coupled excitable elements, as well as the scenarios for the onset and the suppression of the collective mode. In particular, the bifurcations displayed by the MF model can qualitatively account for the stochastic bifurcations which the

exact system undergoes [1,4,5,13,14,23–25]. It has also been shown that the MF model can provide accurate quantitative predictions, reflected in a close agreement between the oscillation period of the MF model and the average oscillation period of the exact system [13,14]. Furthermore, the MF approach has proven successful in the analysis on stability and the onset or suppression of the collective mode in case of interacting assemblies, thereby indicating a potential extension to modular networks [14]. We stress that the approximations behind the MF model used here, called the Gaussian approximation and the quasi-independence approximation, have been analyzed in detail, not only in terms of precise formulations and adaptation for the systems of class II excitable units but also with respect to parameter domains that warrant their validity [15]. In this context, an important finding is that the dynamics of the MF model can indicate in a self-consistent fashion the parameter domains where the MF approximations break down.

The MF model corresponding to (1) involves five equations describing the evolution of the means  $m_x(t) = E[x_i(t)]$ ,  $m_y(t) = E[y_i(t)]$ , the variances  $s_x(t) = E[x_i(t) - \langle x_i(t) \rangle]^2$ ,  $s_y(t) = E[y_i(t) - \langle y_i(t) \rangle]^2$ , and the covariance  $u(t) = E[(x_i(t) - \langle x_i(t) \rangle)[y_i(t) - \langle y_i(t) \rangle]$ . Note that  $E(\cdot)$  denotes expectations over an ensemble of different stochastic realizations. The detailed derivation of the MF model may be found in Refs. [13,14], whereas here we just state the final result:

$$\begin{aligned} \dot{m}_x &= m_x - m_x(t)^3/3 - s_x m_x - m_y, \\ \dot{m}_y &= \epsilon(m_x + b), \\ \dot{s}_x &= 2s_x(1 - m_x^2 - s_x - c) - 2u + 2D_1 \\ \dot{s}_y &= 2\epsilon u + 2D_2, \\ \dot{u} &= u(1 - m_x^2 - s_x - c) + \epsilon s_x - s_y. \end{aligned} \quad (4)$$

As already indicated, the influence of stochastic terms is expressed through the noise intensities  $D_1$  and  $D_2$ .

Nevertheless, in order to make the analogies between the excitable behaviors of a single FHN unit and an assembly explicit, one should arrive at the system describing the collective motion by two equations. The latter would allow one to apply the phase plane analysis derived from the framework of singular perturbation theory. This is achieved by introducing an additional “adiabatic” approximation [1], which consists in assuming that the relaxation of second-order moments is much faster than that of the first-order ones. This is not a crude approximation given that the initial conditions of units in the exact system are set to be identical (coinciding with the deterministic fixed point), especially if the noise intensities are not too large. Having replaced the fast variables with the stationary values, one obtains the following system for the dynamics of the means:

$$\begin{aligned} \frac{dm_x}{dt} &= F(m_x, m_y) = m_x - \frac{1}{3}m_x^3 - m_y - \frac{m_x}{2}(1 - c) \\ &\quad - m_x^2 + \sqrt{(1 - c - m_x^2)^2 + 4(D_1 + D_2/\epsilon)} \\ \frac{dm_y}{dt} &= G(m_x, m_y) = \epsilon(m_x + b). \end{aligned} \quad (5)$$

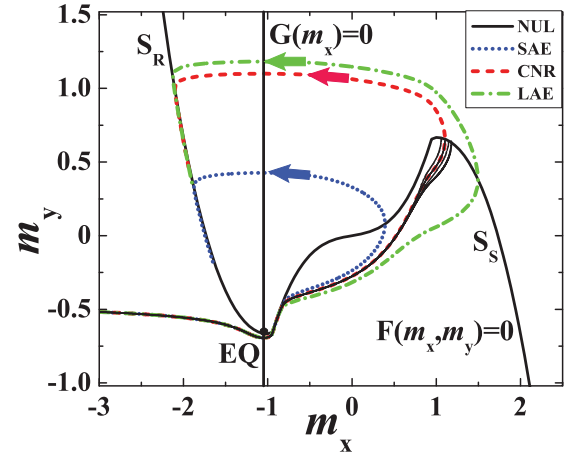


FIG. 1. (Color online) Characterization of the assembly excitable behavior via the phase plane analysis of the corresponding MF model (5). The equilibrium (EQ) lies at the intersection of the nullclines  $F(m_x, m_y) = 0$  and  $G(m_x) = 0$ . The  $m_x$  nullcline is composed of three branches, whereby the spiking and the refractory branches  $S_S$  and  $S_R$  are attractive. For finite  $\epsilon$ , the boundary between the sets of initial conditions that lead to small- or large-amplitude excitations, SAE and LAE, respectively, foliates into a thin layer of canardlike trajectories (CNR), which we refer to as the “ghost separatrix” (solid black lines). The trajectories belonging to the boundary layer are obtained by fixing the  $m_x$  initial condition to a particular value  $m_{x,0} = -3$ , while sweeping over  $m_{y,0}$ . The fact that a difference in  $m_{y,0}$  of the order of  $10^{-18}$  evokes a different type of response corroborates extreme sensitivity to initial conditions in vicinity of the ghost separatrix. The results shown refer to case  $\epsilon = 0.07, b = 1.05$ .

An apparent advantage of (5) is that one may extend the results of phase plane analysis to assembly dynamics, thereby gaining insight into whether and how the excitability feature is manifested at the level of global variables.

The main point is that the system (5) displays class II excitable behavior, which provides an indication that the collection of excitable FHN units described by (1) itself constitutes a macroscopic excitable system. The  $m_x$  and  $m_y$  nullclines, as well as an illustration of how the two marginally different initial conditions give rise to small- or large-amplitude responses, are provided in Fig. 1. Note that the results are obtained for system (5) under  $D_1 = D_2 = 0$ . The  $m_x$  nullcline again consists of three branches, such that in the singular limit  $\epsilon \rightarrow 0$  the spiking branch  $S_S$  and the refractory branch  $S_R$  are attractive, whereas the middle branch is unstable. Compared to the case of single unit, the profile of the middle branch is changed and includes a flexion point, which may be attributed to the compound effect of interaction between the units. The two types of population response to perturbation, or rather the associated thresholdlike behavior, imply the existence of a soft boundary between the corresponding initial conditions.

Carrying out the analysis analogous to that for a single unit, described in brief in the caption of Fig. 1, one may show that the boundary is again given by a thin layer of system trajectories which foliate around the maximum of the  $m_x$  nullcline. The relevant segments of such trajectories are indicated in Fig. 1 by the black solid lines. What is found is quite reminiscent to the

“ghost separatrix” in case of a single excitable unit [17]. The foliation here also becomes more pronounced with increasing  $\epsilon$ . Compared to those for a single unit [17], the trajectories that make up the boundary layer are seen to converge further away from the maximum, mainly because the unstable branch in case of an assembly involves a flexion point. Also, the numerical evidence suggests that the mean-field variables, and therefore the collective dynamics of the assembly, shows greater sensitivity to initial conditions compared to that of a single unit. This conclusion follows from the fact that under analogous parameter values, obtaining the trajectories that belong to boundary set requires a higher numerical precision in case of the MF model than for a single unit, cf. [16] and Fig. 1.

Note that in Sec. V we use the MF model to gain insight into the stochastic stability of equilibrium of the exact system or rather the latter’s sensitivity to random perturbations. This point will be crucial for explaining how the form of the  $\tau(D_1, D_2)$  dependence is related to the stochastic bifurcation leading from the stochastically stable fixed point to continuous oscillations.

#### IV. ALTERNATIVE FORMULATIONS OF ASSEMBLY ACTIVATION PROBLEM

As announced in the Introduction, we consider three alternative formulations of the activation problem, which are associated to different definitions of the assembly activation event. Since the conceptual aspects of a large assembly’s activation problem have not been treated so far, one cannot *a priori* hold any formulation preferred over the others. Thus, the implications of each of the formulations will be qualitatively analyzed and then compared. Note that the physical picture laid out here is distinct from the cases of a single and two coupled excitable units treated in our previous paper [16], where we have been able to provide a unique adequate formulation of the activation event, which allows an immediate generalization from a single unit to a two-unit setup. To properly address the issue of assembly activation, one should invoke a couple of remarks from that study.

First, the activation problem we consider is associated to pulse emission and as such cannot be viewed as an extension of a typical escape problem. Note that the latter would require a genuine saddle structure at the terminating boundary [26], which implies coexistence between two attractors, whereas in our problem the fixed point is the only relevant, and often the unique, attractor. In terms of specifying the terminating boundary, an important point has been to replace the somewhat arbitrary notion of “threshold” for pulse emission by the relevant boundary set consistent with the underlying structure of the phase space. Finally, in the case of two units, we have argued that the definition of an activation event where the phase points of each unit are supposed to reach the appropriate terminating boundary is preferred over any formulation involving the two-unit averages  $[x_1(t) + x_2(t)]/2$  and  $[y_1(t) + y_2(t)]/2$ . This applies because the averages contain additional information on synchronization of units, which are secondary to the two-unit activation process. Nevertheless, such an approach can only be maintained for small groups of units. For larger assemblies, it is of interest to state the activation problem in terms of global variables, since they

present a standard tool for describing collective motion, both theoretically and in applications.

The point which makes the case of large populations intriguing concerns the underlying mechanisms of activation. In particular, the processes on local and global levels are not influenced only by noise but also by the relaxation of units. The arguments above further suggest that an elaborate study on analogies and differences between the statistical properties of activation process in small groups of units and the large assemblies would be in order. Therefore, our approach is on one hand to retain the formulation of the assembly activation problem inherited from the two-unit case where the global variables are not considered and, on the other hand, to introduce two additional formulations that explicitly refer to dynamics of global variables. These three formulations are specified as follows.

*Formulation 1. The assembly activation event occurs when more than a half of participant units have emitted their first pulses.* According to this, assembly activation is perceived as a compound event made up of local activation events. For the local events we adopt the definition provided in our previous paper [16]: The activation path of a single excitable unit influenced by noise emanates from the deterministic fixed point and terminates at the boundary set coinciding with the spiking branch of the limit cycle which would exist in the corresponding supercritical state. In the present context, the terminating boundary set can with sufficient accuracy be approximated by the spiking branch of the cubic nullcline for a noninteracting unit. Motivation behind formulation 1 draws in part from certain applications, especially in the field of neuroscience, where population response to external stimuli typically engages a certain fraction of units rather than the entire assembly [27–32]. From the qualitative perspective, demanding any reasonable macroscopic fraction other than a half of units to be activated makes as good a choice as any, because the main statistical properties of the ensuing activation process will remain similar. In a sense, formulation 1 can be interpreted as an extension of the definition introduced for a two-unit activation event in our previous paper [16].

*Formulation 2. The assembly activation event occurs if the global variable  $X(t)$  crosses the predefined threshold  $X_0[X(t) > X_0, X'(t) > 0]$ .* Unlike the case of a single unit [16,17], the formulation involving an explicit threshold is justified for the global variable because its amplitude depends on coherence of spikes of single units. The latter point introduces ambiguities when attempting to analyze the assembly thresholdlike behavior. In other words, for a single unit, it is not difficult to distinguish between the small- and large-amplitude responses, given that the amplitude of superthreshold excitations is stereotypical. However, in case of an assembly, one is able to understand the associated thresholdlike behavior only in terms of the approximate MF model, cf. Sec. III, but cannot provide clear-cut criteria in terms of global variables of the exact system, especially if coherence of units’ activities for the given parameter set is weak. This point will be further explained when discussing formulation 3, while here we just mention that noise domains may be found where formulation 2 is more or less suitable. Compared to formulation 1, formulation 2 is conceptually distinct because the assembly activation events can be affected by multiple spikes of individual units.

The potential consequences of selecting particular threshold values  $X_0$  will be discussed in the next section.

*Formulation 3.* The assembly activation event occurs once the phase point associated to global variables reaches the appropriate terminating boundary set, defined in analogy to a single unit case. This formulation involves an implicit assumption that the thresholdlike behavior of an assembly is qualitatively similar to that of individual units. As indicated in Sec. III, if the condition  $\langle x_i^3(t) \rangle \approx \langle x_i(t) \rangle^3$  is fulfilled, then the dynamics of global variables can be approximated by the equations analogous to that of a single unit. Consistent with this approximation, the collective motion of finite assemblies in presence of noise may be described by [3,33]

$$\begin{aligned} dX &= (X - X^3/3 - Y)dt + \sqrt{\frac{2D_1}{N}}dW_1 \\ dY &= \epsilon(X + b)dt + \sqrt{\frac{2D_2}{N}}dW_2. \end{aligned} \quad (6)$$

As a corollary, one may use the phase plane analysis and describe the assembly first-pulse emission in terms of motion of phase point  $(X, Y)$  to the spiking branch of the corresponding  $X$  nullcline, which is then naturally considered the relevant terminating boundary set for the assembly activation problem. Nevertheless, the given physical picture is valid only if the fluctuations of individual units are small enough for the above condition to apply, which ultimately depends on the noise intensities.

An important note on formulation 3 is that *coherence* between spikes (approximate matching of spike times) of a large fraction of individual units is required to elicit an assembly activation event, viz. the first-pulse emission for the global variables. For this point, let us make additional remarks on the issues of terminating boundary conditions and the role of spike coherence in the assembly activation process. First, there is no principle difference in the dynamics underlying activation scenarios for three formulations of the assembly activation event. The differences in statistical features, which will be discussed in the next section, are caused by the selection of terminating boundary conditions. This is made explicit in Fig. 2, where a *single* stochastic orbit for  $(X, Y)$  is used to illustrate the difference between formulations 2 and 3. According to formulation 2, the assembly has emitted a pulse once  $X$  crosses a certain threshold (segment of the trajectory indicated by the dashed red line), while formulation 3 requires that the phase point reaches the spiking branch of the  $X$  nullcline (segment of the trajectory indicated by the solid black line). Thus, considering the very same stochastic trajectory for  $(X, Y)$ , the assembly activation event conforming to formulation 2 would have happened earlier than the one satisfying formulation 3. Nevertheless, both of the considered sections of the  $(X, Y)$  orbit correspond to large excitations far above the stochastic fluctuations in vicinity of equilibrium. In fact, which excitation should be considered an activation event effectively depends on the scope of the study. In this context, formulation 2 is more adapted to practical applications, whereas formulation 3 has a more theoretical background.

Comparing Fig. 1 and Fig. 2, one should point out that the latter captures certain fine details on collective dynamics that cannot be reflected in the former. This is because the physical

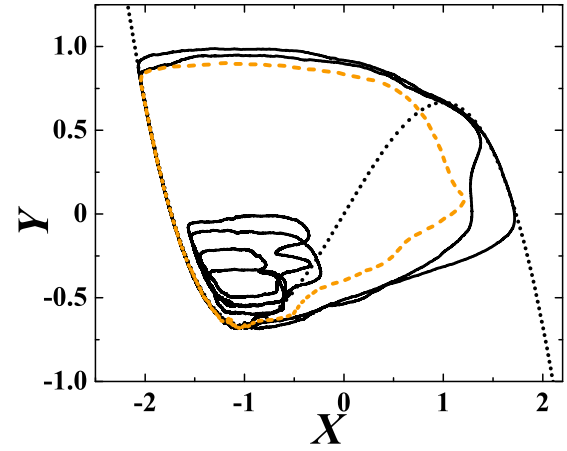


FIG. 2. (Color online) Illustration of differences between formulations 2 and 3. For certain  $(D_1, D_2)$ , the assembly thresholdlike behavior is difficult to resolve because the amplitude of large fluctuations is not stereotypical. The presented  $(X, Y)$  orbit is obtained for a *single* stochastic realization under parameter set  $D_1 = 0.0004, D_2 = 0.0008, c = 0.1, N = 50$ . The bold dotted line indicates the  $X$  nullcline consistent with the approximate system (6). Apart from small-amplitude excitations that remain in close vicinity of deterministic fixed point, one also finds substantially larger excitations far above the stochastic fluctuations around the “stable state,” where the phase point may either fall short of the spiking branch of the  $X$  nullcline (segment of trajectory shown by the orange dashed line) or may actually reach it (segment indicated by the solid black line). The former instance conforms to an activation event by formulation 2 but does not comply with formulation 3. The criteria as to which large excitation is considered an assembly activation ultimately depends on the scope of the particular study.

background of Fig. 1 lies in the approximate MF model, where the stochastic fluctuation effects above the second order are averaged out. In other words, the behavior of the exact system in Fig. 2 is associated with large fluctuations, which can no longer be described by the MF model.

## V. STATISTICAL PROPERTIES OF ACTIVATION PROCESS

### A. Mean TFPs and TFP variability

The statistical properties of the assembly activation process influenced by external and internal local noise are characterized by the mean TFP  $\tau(D_1, D_2)$  and the associated coefficient of variation  $R(D_1, D_2)$  [34–36]. Both quantities involve averaging over an ensemble of different stochastic realizations. In particular, the mean TFP is given by  $\tau(D_1, D_2) = \langle \tau_k \rangle = \frac{1}{n_r} \sum_{k=1}^{n_r} \tau_k(D_1, D_2)$ , where  $n_r$  denotes the number of realizations, while the expression for the coefficient of variation reads  $R(D_1, D_2) = \frac{\sqrt{\langle \tau_k^2 \rangle - \langle \tau_k \rangle^2}}{\langle \tau_k \rangle}$ . Since  $R$  is variation of TFPs normalized by the mean, its smaller values indicate a better clustering of individual TFPs around  $\tau$  [37]. Note that the numerical simulations are carried out via Heun integration scheme with the fixed time step  $\delta t = 0.002$ . The results for the mean TFPs and the variances are obtained by averaging over an ensemble of at least 300 different stochastic realizations of the activation process. For each realization, the initial conditions

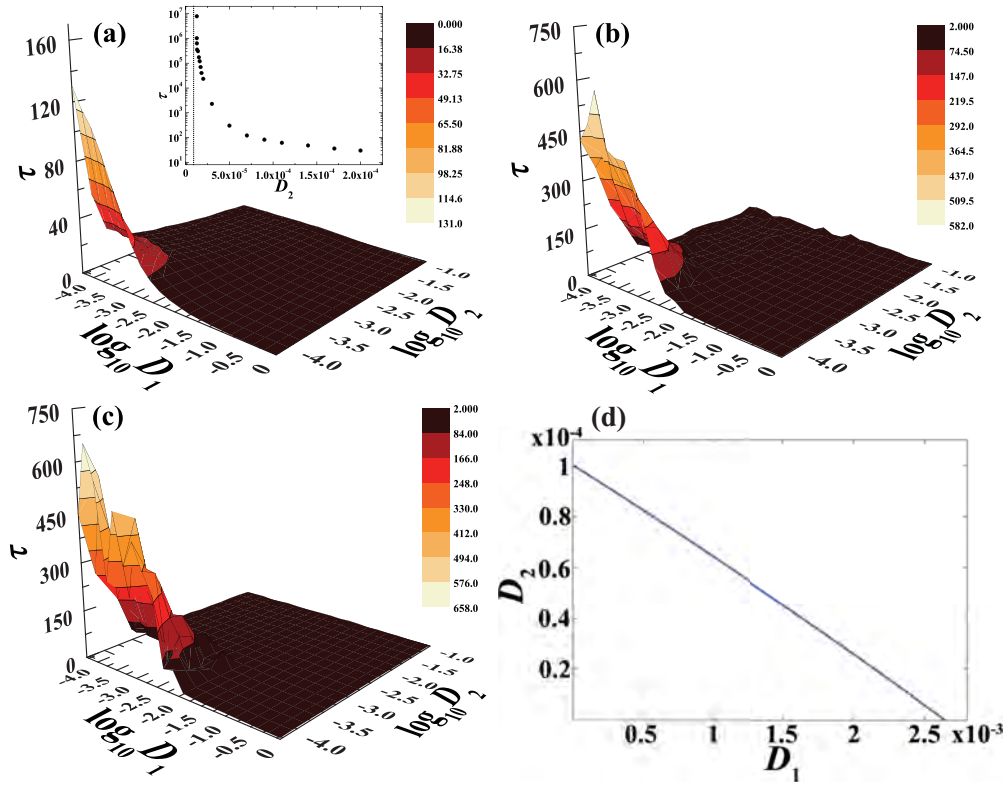


FIG. 3. (Color online) Mean TFPs for the assembly activation process and the role of stochastic bifurcation. Panels (a), (b), and (c) show  $\tau(D_1, D_2)$  dependencies for formulations 1–3 of the activation event, respectively. Results are obtained for  $c = 0.1$  and the assembly size  $N = 100$ , whereby the stochastic average is taken over an ensemble of 300 different activation paths. The inset in (a) illustrates exponential divergence of  $\tau(D_2)$  for fixed  $D_1 = 10^{-5}$  as one approaches  $D_2^* \approx 1.25 \times 10^{-5}$  (the value indicated by the dotted line). The qualitative similarity between the  $\tau(D_1, D_2)$  dependencies in (a), (b), and (c) is associated to stochastic bifurcation underlying transition to continuous oscillations. The corresponding bifurcation curve  $D_2(D_1)$ , determined by analyzing MF model (5), is shown in (d).

for all units are identical and are given by the deterministic fixed point of system (1).

The fields  $\tau(D_1, D_2)$  corresponding to formulations 1–3 of the assembly activation event are plotted in Figs. 3(a), 3(b), and 3(c), respectively. Note that all three dependencies exhibit *qualitatively* similar behavior, whereby one can clearly discern the domain of large mean TFPs and the plateau region. We find that these analogies derive from the fact that the profile of  $\tau(D_1, D_2)$  dependencies in each of the instances is crucially influenced by the stochastic bifurcation. The latter corresponds to the noise-induced transition from the stochastically stable fixed point to continuous oscillations. It is intuitively clear that the stochastic bifurcation should be associated to boundary between the two characteristic forms of  $\tau$  behavior, because above the bifurcation the fixed point loses its attractive power, which makes it easier for noise to induce large-amplitude fluctuations. Also, once the attractive power of the fixed point is lost, any further increase of noise cannot induce qualitatively novel effects. This fact accounts for the existence of the large plateau region in the  $\tau(D_1, D_2)$  dependence. As already indicated, we may gain insight into stochastic bifurcation by carrying out bifurcation analysis on the MF counterpart (5) of the exact system. In particular, it is demonstrated that the MF model undergoes direct supercritical Hopf bifurcation which qualitatively reflects the stochastic bifurcation of the exact system. The Hopf bifurcation curve  $D_2(D_1)$  obtained for the MF model at fixed  $c = 0.1$  is shown in Fig. 3(d).

Note that for small  $(D_1, D_2)$  the mean TFPs grow extremely large. This is explicitly illustrated in the inset of Fig. 3(a), which shows that  $\tau(D_2)$  (for fixed small  $D_1$ ) exponentially diverges as a certain value of noise intensity  $D_2^*$  is approached. The latter point clearly demonstrates the existence of potential barrier associated to the assembly's activation process. The lower boundary on noise intensities that facilitate activation is the largest for formulation 3 and decreases for formulations 2 and 1. The reason behind such a behavior will be considered below.

In quantitative terms, the  $\tau$  dependencies for formulations 1–3 manifestly differ in the regime subcritical relative to stochastic bifurcation. In particular, Fig. 3 shows that the corresponding  $\tau$  values for the same noise intensities are typically ordered as  $\tau_1 < \tau_2 < \tau_3$ . This may be explained by looking into the role played by the spike coherence between the individual units in the respective assembly activation processes. Let us focus first on the adjustment between the local time series  $x_i(t)$  prior to assembly activation, see Fig. 4. Naturally, the early spikes of single units will be the least coherent because the firing is driven by noise, and the effect of diffusive coupling in bringing their firing times closer is weakly felt. As the time passes, the impact of coupling on units' dynamics is felt more strongly, which gradually leads to a *buildup of spike coherence* within the assembly. In other words, firing of individual units will become more coherent (more spikes fall within a relatively narrow time window)

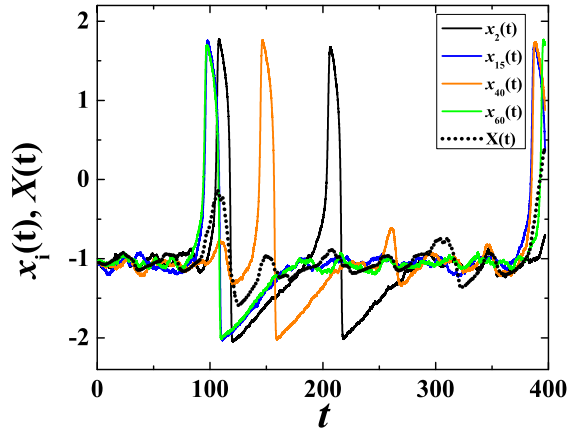


FIG. 4. (Color online) Buildup of spike coherence prior to assembly activation event. The data concern a *single* stochastic realization of the assembly activation event consistent with formulation 2 ( $X_0 = 0.4$ ). The dotted line shows the  $X(t)$  dependence, whereas the solid lines refer to the appropriate time series of individual units  $x_i(t)$ . The system parameters are  $D_1 = 0.0001365$ ,  $D_2 = 0.0001$ ,  $c = 0.1$ ,  $N = 100$ .

as the result of interactions. With time, such approximate synchronization may comprise an increasing number of units, depending on the  $c$  value.

Now we consider how this reflects to assembly activation for different formulations of the activation event. Formulation 1 requires only that more than half of units have emitted their first spikes, imposing no demand for their coherence. In line with the above arguments, satisfying such a requirement will take the least amount of time, which means that the pertaining  $\tau$  will be smaller compared to mean TFPs for formulations 2 and 3 under the same parameter set. Formulations 2 and 3 concern the global variables and thereby do require a certain level of spike coherence within the assembly. Formulation 3 imposes a more strict condition, so its fulfillment is associated to the largest level of spike coherence. Achieving a larger level of spike coherence takes more time, so in the subcritical regime TFPs for formulation 3 will necessarily be larger than those for formulation 2. It is also apparent that the assembly activation will necessarily be induced by the first spikes of single units only for formulation 1, whereas activation by formulations 2 and 3 is bound to be contributed by latter spikes of individual units. Above the stochastic bifurcation, coherence of spikes between the units is naturally achieved, such that the assembly activation for all three formulations is contributed by the first spikes of units. This is the reason why the mean TFPs for  $(D_1, D_2)$  above the bifurcation have similar values for all three formulations of the activation event.

Before proceeding, we make a brief remark on certain details related to formulation 2 of the activation event. As indicated in Sec. IV, it has to be verified whether the results on statistical properties of the activation process depend on the particular value of the threshold  $X_0$ . We have established that for any reasonable selection, viz. the  $X_0$  values lying sufficiently above the amplitude of stochastic fluctuations around the fixed point, the corresponding dependencies  $\tau(D_1, D_2)$  maintain qualitatively similar profile. This holds for  $X_0$  values within the range  $X_0 \in [-0.1, 1.3]$ . Considering

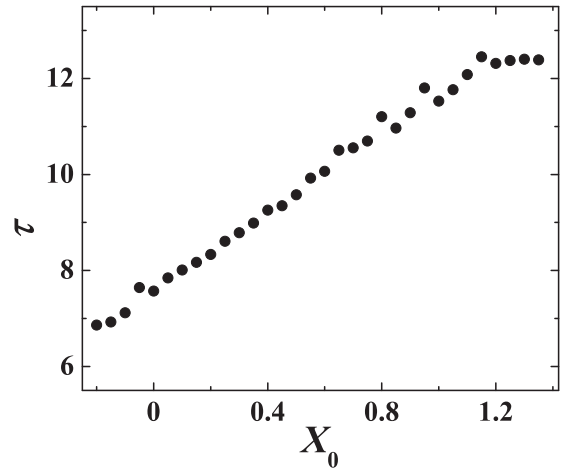


FIG. 5. Impact of different  $X_0$  on the results for formulation 2 of activation event. The example provided illustrates the form of  $\tau(X_0)$  dependence typical in a broad range of  $(D_1, D_2, c, N)$  values. One finds similar behavior for all the other statistical quantities considered. The particular data are obtained for  $D_1 = 0.0207018$ ,  $D_2 = 0.00101739$ ,  $c = 0.1$ ,  $N = 100$ , with the stochastic averaging carried out over an ensemble of 500 different activation paths. The results imply that the statistical properties of activation process derived from formulation 2 are qualitatively independent of  $X_0$ .

$\tau$  values as an example, we have shown that  $\tau(X_0)$  for arbitrary  $(D_1, D_2)$  monotonously increases until reaching saturation around  $X_0 \approx 1.2$ , see Fig. 5. The analogous conclusions regarding the qualitative independence of the results on  $X_0$  have been confirmed for all the other statistical properties of the activation process.

Let us now examine the impact of two different noise sources on the behavior of  $R$  in view of the different formulations of the assembly activation event. The three characteristic setups we consider are as follows. Figure 6(a) refers to  $R(D_1)$  dependence for the fixed very small  $D_2$ , whereas in Fig. 6(b) is shown the  $R(D_2)$  dependence for the fixed very small  $D_1$ . Finally, Fig. 6(c) illustrates the behavior of  $R(D_1)$  when  $D_2$  is fixed at an intermediate value. Comparing Fig. 6(a) and Fig. 6(b), it stands out that formulation 1, on one hand, and formulations 2 and 3, on the other hand, yield substantially different  $R$  dependencies both below and above the stochastic bifurcation, cf. Fig. 3(d). Below the bifurcation, the respectively smaller  $R$  values obtained under formulation 1 indicate that the corresponding activation process is more homogeneous compared to processes conforming to formulations 2 and 3. Furthermore, under formulations 2 and 3, the fluctuations around the mean TFP expectedly increase in the noise domain that gives rise to stochastic bifurcation. The large  $R$  values found there indicate strong irregularity of firing times over an ensemble of different stochastic realizations, cf. the peaks in Fig. 7(a) and Fig. 7(b). Sufficiently above the bifurcation, the  $R$  values decrease for all three formulations. Nevertheless, in the stochastically supercritical state, the physical picture regarding the three formulations is in a sense reversed compared to the subcritical state. The deviations from the mean TFP with  $D_1$  are the largest for the activation process conforming to formulation 1, whereas  $R$  values for

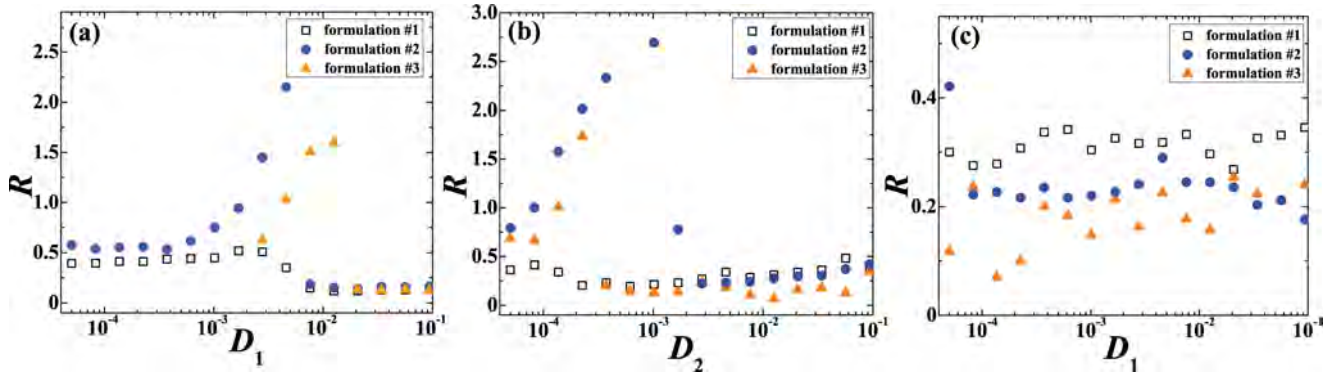


FIG. 6. (Color online) Impact of two noise sources on variability of assembly activation process. The  $R$  values corresponding to formulations 1–3 of the activation event are represented by open squares, solid circles, and open triangles, respectively. In (a) is provided the  $R(D_1)$  dependence for fixed  $D_2 = 0.00005$ , whereas (b) shows the  $R(D_2)$  behavior at fixed  $D_1 = 0.00062$ . Panel (c) refers to  $R(D_1)$  dependence for  $D_2 = 0.00459$ . The noise values kept fixed in (a) and (b) are small, such that the system undergoes stochastic bifurcation under variation of  $D_1$  in (a) and  $D_2$  in (b). The  $D_2$  value in (c) is supercritical relative to stochastic bifurcation. The remaining system parameters are  $c = 0.1, N = 100$ .

formulations 2 and 3 are smaller and fairly insensitive to noise increase, at least for sufficient  $D_1$ . An interesting remark is that by adhering to formulation 1, as opposed to formulations 2 and 3, the coefficient of variation never crosses 1, the value characteristic for the exponential distribution of events. It is

well known that the latter distribution is consistent with the Poisson process [36,38].

Additional information on  $R$  behavior can be gained by comparing the TFP distributions of activation events over an ensemble of different stochastic realizations for  $(D_1, D_2)$  representative of the domains below or above the stochastic bifurcation (not shown). The main point concerns how likely are the deviations biased toward the shorter or longer activation times for an ensemble of realizations. Below the bifurcation, the ensemble of events under formulations 2 and 3 typically splits into fractions with short or very long TFPs. Though the former fraction is considerably larger, the long events still strongly influence the mean TFP. The partition into two fractions persists under formulation 1, though the difference in duration between the two characteristic types of events is considerably reduced. The distribution of TFPs is then found to be bimodal, showing two relatively even peaks. These points are consistent with the differences displayed by the three  $R(D_1, D_2)$  dependencies in Fig. 6 in the stochastically subcritical state. Nevertheless, above the bifurcation, qualitatively similar behavior for all three formulations of activation event is recovered. As expected, the TFPs follow a unimodal distribution centered around the short events, whereby a longer tail becomes visible for formulation 1 if  $D_1$  is increased. The latter accounts for the rise of  $R$  with  $D_1$  in Fig. 6(c).

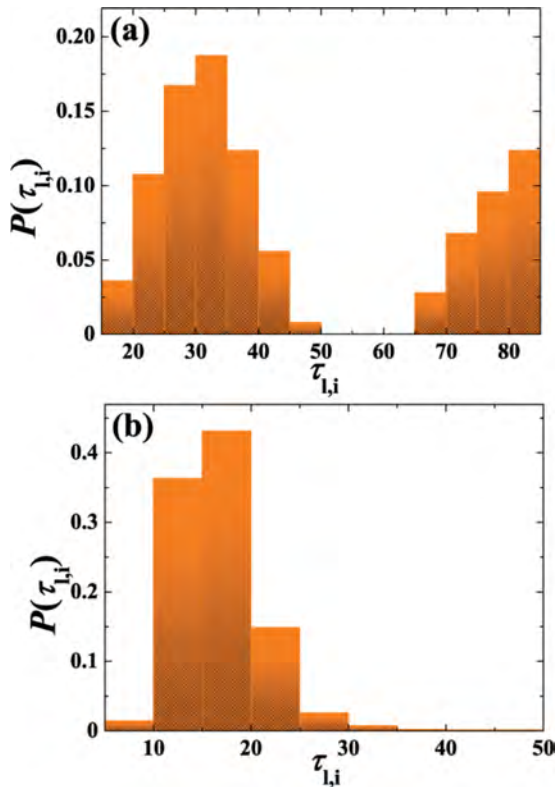


FIG. 7. (Color online) Focus on local activation processes. Panels (a) and (b) show typical distributions  $P(\tau_{1,i})$  of individual unit TFPs  $\tau_{1,i}$  for a single realization of the assembly activation process at  $(D_1, D_2)$  below and above the stochastic bifurcation, respectively. In the subcritical state, one finds two excitation waves, the first being induced by noise, whereas the other is due to relaxation of units. In the supercritical state, the units are primarily elicited by noise. The system parameters are  $D_1 = 0., D_2 = 0.00009, c = 0.1, N = 300$  in (a) and  $D_1 = 0.0002, D_2 = 0.00025, c = 0.1, N = 300$  in (b).

## B. Distribution of single units' TFPs

Having analyzed the properties of collective activation process for an ensemble of different stochastic realizations at fixed  $(D_1, D_2)$ , we now consider the dynamics of local activation processes for a *single* realization of an *assembly* event. In particular, we focus on how the TFPs of *individual* units are distributed for noise domains below or above the stochastic bifurcation. As for the underlying mechanism, an interesting point is to examine the contribution of noise-induced local activation events relative to the ones elicited by the relaxation processes of other units. We find that the typical profiles of the distribution of individual TFPs below and above the stochastic bifurcation differ considerably, as illustrated in Fig. 7(a) and Fig. 7(b), respectively. Note that the qualitatively



analogous results are obtained if one compares the corresponding distributions of individual TFPs for all units over an ensemble of different stochastic realizations (not shown).

The bimodal distribution in Fig. 7(a) suggests the existence of two “waves” of local excitation. While the first wave (short TFPs) is elicited by noise, the second wave is evoked by relaxation of the units that have already emitted the spike (such stimuli are conveyed via the interaction terms). This physical picture is reminiscent of the one obtained when determining the phase response curve of an assembly of oscillators subjected to random perturbations [39]. Note that the smallest TFPs are around 20 a.u., which is about the length of the spike excitation loop, i.e., the duration of the typical relaxation process. This indicates the existence of activation barrier associated to first pulse emission process of single units. Apart from the time scales involved, a remark should also be added regarding the sizes of waves, viz. the fractions of units participating the waves. The sizes are found to depend on  $D_1$ ,  $D_2$ , and  $c$ , whereby the stronger  $c$  expectedly amplifies the secondary wave. One would further expect the secondary wave to be substantially influenced by the topology of interactions within the network.

Above the stochastic bifurcation, the local activation events no longer maintain the two-wave-like form, see Fig. 7(b). Instead, the typical distribution of single unit TFPs becomes unimodal, with some differences observed for the cases of intermediate versus large noise intensities. In particular, in the latter case the peak is more pronounced than in the former, whereby the distribution profile itself may be fitted to a Lorentzian-like form. The very fact that the distribution of local TFPs is unimodal in the stochastically supercritical state implies that the activation of single units is almost exclusively driven by noise. Nonetheless, the point that the TFPs are typically of the order of the excitation loop suggests the lack of activation barrier in the first pulse emission processes of single units.

### C. Activation mechanisms below and above stochastic bifurcation

While discussing  $\tau(D_1, D_2)$  behavior in Fig. 3, it has already been established that below the stochastic bifurcation, the assembly activation process under formulations 2 and 3 is not primarily affected by the first pulses of individual units but is more likely contributed to by the latter spikes. In these cases, we have identified gradual coherence buildup between individual spikes as the mechanism underlying assembly activation. Nevertheless, results in Fig. 7(b) suggest that a potentially different scenario of assembly activation is typical above the stochastic bifurcation. Therefore, our next goal is to explicitly demonstrate the distinction between the mechanisms guiding the assembly activation below or above the stochastic bifurcation. To this end, we numerically determine the most probable trajectories for the first pulse emission process in the  $(X, Y)$  configuration space and analyze the differences between the typical paths obtained for  $(D_1, D_2)$  below or above the stochastic bifurcation, cf. Fig. 8. The trajectories presented conform to formulation 2 of the assembly activation event with the fixed threshold value  $X_0 = 0.3$ .

The details of the applied numerical method are as follows. For the given  $(D_1, D_2)$ , we consider the ensemble of

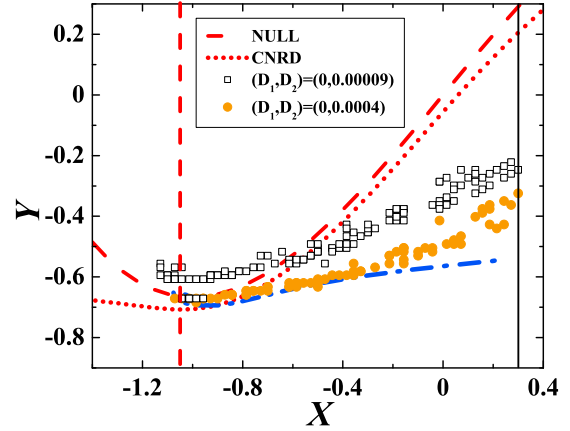


FIG. 8. (Color online) Most probable activation paths for the global variables  $(X, Y)$  under formulation 2 of the activation event. The two illustrated profiles are typical for noise domains below (empty squares) and above (filled circles) the stochastic bifurcation. The shown paths refer to particular noise intensities  $(D_1, D_2) = (0, 0.00009)$  and  $(D_1, D_2) = (0, 0.0004)$ , respectively. Note that the assembly’s maximum likelihood trajectories correspond to the peak of the histogram obtained for an ensemble of different stochastic realizations as a function of time. The paths for the assembly are compared against the one for the approximate model (6) (“macroscopic FHN unit”). The nullclines (NULL) of this model are presented by the dashed lines, whereas the canardlike trajectory (CNRD) is denoted by the dotted line. The trajectory generated by the effective Hamiltonian system associated with (6) is given by the dash-dotted line. The solid line indicates the threshold  $X_0 = 0.3$ . The results for the assembly refer to system size  $N = 100$  and are obtained by averaging over a 1000 different stochastic realizations of the first pulse emission process.

fluctuation paths that start at moment  $t_i$  from the deterministic fixed point  $(X_{eq}, Y_{eq})$  and reach the terminating boundary defined by the threshold  $X_0$ , cf. the solid line in Fig. 8. At  $t_i$ , all the individual units are prepared to the same initial conditions, i.e.,  $(x(t_i), y(t_i)) = (X_{eq}, Y_{eq})$ . The terminating time  $t_f$ , as well as  $Y(t_f)$  are left unspecified. For the described ensemble, we consider statistics of the  $(X(t), Y(t))$  position of trajectories as a function of time  $t_i < t < t_f$  preceding the arrival to  $X_0 = 0.3$ . Naturally, the recorded trajectories may have quite distinct  $t_f$  times. The proper statistical quantity to characterize such an assembly of paths in configuration space is the prehistory probability density, first introduced in Ref. [40] and successfully applied many times since [41]. The former can effectively be obtained if the time when each stochastic realization terminates is set to  $t = 0$ , such that the behavior of the process during the initiation of the pulse is observed by looking backward in time. The appropriate prehistory probability distribution is then defined as  $H(X, Y, t)dXdY = Pr[X(t) \in (X, X + dX), Y(t) \in (Y, Y + dY) | X(t_f) = X_0, X(t_i) = X_{eq}, Y(t_i) = Y_{eq}, t_i < t < t_f, X < X_0]$ . The most probable path for the first pulse emission process is determined by collecting the points  $(X_m(t), Y_m(t))$  that correspond to the maximum of  $H(X, Y, t)$  at the given  $t$ .

In Fig. 8, the most probable activation paths typical for the noise domains below (above) the stochastic bifurcation are indicated by the empty squares (filled circles). In order

to explain the differences between the presented paths, it is useful to invoke the approximate model (6), which effectively assumes that all the units are strongly synchronized. In other words, that model refers to a scenario where the assembly acts as a macroscopic FHN unit. The dashed lines in Fig. 8 denote the nullclines of (6). Further, since the latter has the form analogous to the dynamics of a single FHN unit, we may borrow from our previous paper [16] the results obtained for such a setup. In particular, we plot the canardlike trajectory belonging to the “ghost separatrix” [17], cf. the dotted line in Fig. 8, as well as the trajectory generated by the system of effective Hamiltonian equations associated to (6) as discussed in our previous paper [16] (see the dash-dotted line in Fig. 8). Note that the most probable activation paths for a single FHN unit are only sensitive to the external or internal character of noise but not to the particular noise intensities [16,17].

For the trajectory corresponding to the noise domain below the stochastic bifurcation (empty squares) one finds that the approximate model (6) does not apply. From the latter point, one further infers that the units are not coherent during the initial part of the first pulse emission process, which is consistent with the already described scenario of a gradual buildup of spike coherence. The mechanism of first pulse emission differs for the noise domain above the stochastic bifurcation. Recall that the stochastic bifurcation underlies transition to noise-induced oscillations, which are facilitated by the (stochastic) synchronization of individual units. With this in mind, it is expected that the corresponding most probable first pulse emission trajectory (filled circles) will conform much better to physical picture behind model (6). In the initial part of the activation trajectory, there is (stochastic) synchronization between the units of the assembly, such that the assembly’s activation path indeed fits well to the path given by the “macroscopic FHN unit” model (6). Note that the deviation from the path corresponding to (6) is observed in the latter part of the assembly activation trajectory. This is a natural consequence of the fact that the spike times of single units in the assembly are synchronized *approximately* but are not exactly matched. Thus, the effect of noise in the latter part of activation trajectory is felt more strongly for an assembly than in case of the effectively single FHN unit model (6). As expected, the described physical picture on the supercritical state breaks down if the noise intensity is too large.

#### D. Mean TFP antiresonance as a system-size effect

In this subsection, we briefly report on a system-size effect which discriminates between the different formulations of the assembly activation event. In particular, the effect is observed when applying formulations 2 and 3 which concern the dynamics of global variables, but is absent for formulation 1 that refers to local activation events. The system-size effect consists of the appearance of an antiresonant peak in the dependence of mean TFP with  $N$  for the fixed parameter set  $(D_1, D_2, c)$ . The term antiresonance is applied in a sense that, under variation of  $N$ , the mean TFPs exhibit a maximum for the particular size of the assembly. Note that the effect is found for  $(D_1, D_2)$  values both below and above the stochastic bifurcation but is substantially more pronounced in the stochastically subcritical

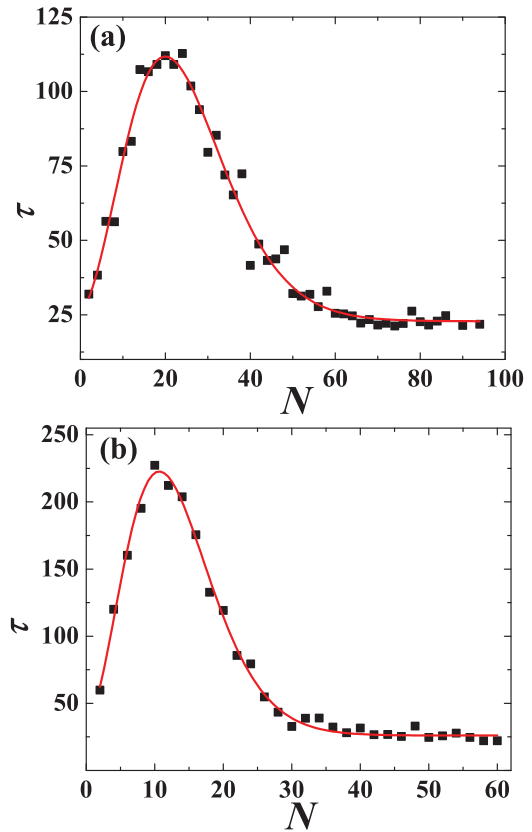


FIG. 9. (Color online) Focus on the antiresonant system-size effect for  $\tau$ . Panels (a) and (b) illustrate the  $\tau(N)$  dependencies typical for subcritical noise intensities, whereby (a) conforms to formulation 2 and (b) to formulation 3 of the assembly activation event. Both plots are obtained for the same set of parameter values  $(D_1, D_2, c) = (0.0001365, 0.0002255, 0.1)$ , with the threshold in (a) fixed to  $X_0 = 0.4$ . The stochastic averaging at each point has been carried out over an ensemble of 1000 different activation paths.

state. As an illustration, in Figs. 9(a) and 9(b) the  $\tau(N)$  dependencies are shown corresponding to formulations 2 and 3, respectively, whereby the noise intensities are typical for the domain below the stochastic bifurcation. Apart from the fact that the formulation 1 does not admit similar behavior, it also yields  $\tau(N)$  dependence that exhibits only a weak decline with  $N$ . As already indicated, under formulations 2 and 3 the antiresonant effect persists above the stochastic bifurcation. Nevertheless, the  $\tau(N)$  maximum in this domain reduces with noise and further shifts to smaller  $N$ . For a comprehensive understanding of the described antiresonant system-size effect, one would have to carry out an elaborate analysis on a number of issues independent on the present study. The focus should primarily lie with the mechanisms contributing the long activation events, including the details on how the competition between the noise- and relaxation-induced local activation processes is affected by the system size.

## VI. SUMMARY

The present study has been aimed at characterizing the excitable behavior and the noise-influenced activation process of an assembly of class II excitable units whereby each

unit is subjected to external and internal noise. The analysis is an extension of our previous work [16] concerning the activation processes for a single and two interacting FHN elements. In conceptual terms, three points can be regarded as most relevant ones. First, we have explicitly demonstrated that an assembly of excitable FHN units may itself exhibit macroscopic excitable behavior. As a second point, we have established the qualitative analogy between the statistical properties of the noise-driven activation processes for a single FHN unit and an assembly. Finally, it has been shown that depending on the noise intensities, two qualitatively distinct local mechanisms may have prevailing effect on the assembly activation process.

The first point has been achieved by implementing the appropriate MF approach, which ultimately yields the approximate model (5). As in case of a single FHN unit, the threshold-like dynamics separating the assembly's spiking responses from the small-amplitude excitations has been linked to the ghost separatrix. An additional result is that compared to excitable dynamics of a single FHN unit for the analogous parameter set, the dynamics of the assembly exhibits larger sensitivity to initial conditions in vicinity of the ghost separatrix.

As for the second point, establishing the qualitative analogy in statistical properties of the activation processes of a single unit and an assembly is a nontrivial result that could not be expected *a priori*. To facilitate the comparison between the respective activation processes, we have introduced three alternative formulations of the assembly activation event, each emphasizing different aspects of collective dynamics. Formulation 1 deliberately makes no mention of global variables, such that the effects of coherence of individual units' spikes are left aside. At variance with this, formulations 2 and 3 are stated in terms of global variables, such that the former involves an explicit scalar threshold for the spiking response, whereas the latter incorporates an appropriate terminating boundary set analogous to the one we adopted for a single and two interacting FHN units [16].

The analysis on statistical properties of assembly activation process has been carried out by determining the  $\tau(D_1, D_2)$  and  $R(D_1, D_2)$  dependencies for the three alternative formulations of the activation event. All three formulations yield qualitatively analogous results for the mean TFPs, but certain quantitative differences are manifested in the subcritical regime. These differences are due to microscopic mechanisms behind the assembly activation and concern the role of spike coherence in the onset of activation event. In particular, the activation processes under formulations 2 and 3 are mediated by the gradual buildup of spike coherence, whereas in case of formulation 1 spike coherence is not relevant.

We have further found that the statistical properties associated to macroscopic excitable behavior qualitatively resemble those for a single unit [16]. The observed qualitative similarity, both with respect to three formulations of the assembly activation event and compared to the case of a single FHN unit, has been tied to stochastic bifurcation that underlies transition from the stochastically stable fixed point to continuous oscillations. The stochastic bifurcation has been analyzed within the framework of the MF model (5), demonstrating that the latter undergoes Hopf bifurcation for

the noise intensities that qualitatively coincide with those that give rise to stochastic bifurcation of the exact system. The stochastic bifurcation has been shown to account for the transition between the  $(D_1, D_2)$  domains admitting large mean TFPs and the plateau region.

As for our third main point, the analysis of the mechanisms behind the local activation processes has revealed substantial differences between the stochastically subcritical and the supercritical state. In the former case, two excitation waves may be discerned: The first is elicited by noise, whereas the second wave is due to relaxation of units, viz. is evoked by the interaction terms. For this scenario, one is able to confirm the existence of a potential barrier associated to single unit activation. At variance with this, above the stochastic bifurcation, the local activation processes are strongly influenced by noise.

The respective roles of noise and interaction terms in the mechanisms leading to assembly activation have further been examined by considering the most probable activation paths characteristic for the noise domains below and above the stochastic bifurcation. The analysis is based on comparing the results for the assembly to the appropriate most probable activation path of the approximate model (6). The latter model assumes strong synchronization between the units, effectively describing the assembly as a macroscopic FHN unit. For the subcritical state, the analysis corroborates the gradual buildup of spike coherence as the leading mechanism behind the assembly activation. This mechanism is naturally influenced by the interaction terms. Nevertheless, above the stochastic bifurcation, noise facilitates stochastic synchronization between the units, rendering the interaction terms negligible. In this scenario, the assembly activation process may indeed be compared to that of the approximate model (6).

In terms of details specific for the assembly excitable behavior, an interesting finding concerns a system-size effect, which consists in the appearance of an antiresonant peak in the  $\tau(N)$  dependence under fixed  $(D_1, D_2)$ . While  $\tau(N)$  displays a maximum for arbitrary noise intensities, the maximum is still substantially more pronounced below than above the stochastic bifurcation.

Apart from providing insights into the assembly activation process, the present study has raised a number of novel issues. For example, the future research may include a systematic study on the mechanisms behind the reported system-size effect or could focus on the impact of connection topology on the activation process. Another relevant point would be to consider whether the qualitative aspects of behavior found here are paradigmatic, i.e., whether they persist if the assembly is built of type I instead of type II excitable units.

## ACKNOWLEDGMENTS

This work was supported by the Ministry of Education, Science and Technological Development of the Republic of Serbia, under Project Nos. 171017 and 176016. M.P. acknowledges support from the Slovenian Research Agency (Grant No. P5-0027) and from the Deanship of Scientific Research, King Abdulaziz University (Grant No. 76-130-35-HiCi).

- [1] B. Lindner, J. Garcia-Ojalvo, A. Neiman, and L. Schimansky-Geier, *Phys. Rep.* **392**, 321 (2004).
- [2] E. M. Izhikevich, *Dynamical Systems in Neuroscience: The Geometry of Excitability and Bursting* (MIT Press, Cambridge MA, 2007).
- [3] P. Kaluza, C. Strege, and H. Meyer-Ortmanns, *Phys. Rev. E* **82**, 036104 (2010).
- [4] M. A. Zaks, A. B. Neiman, S. Feistel, and L. Schimansky-Geier, *Phys. Rev. E* **68**, 066206 (2003).
- [5] M. A. Zaks, X. Sailer, L. Schimansky-Geier, and A. B. Neiman, *CHAOS* **15**, 026117 (2005).
- [6] C. J. Tessone, A. Sciré, R. Toral, and P. Colet, *Phys. Rev. E* **75**, 016203 (2007).
- [7] I. Franović, K. Todorović, N. Vasović, and N. Burić, *Phys. Rev. Lett.* **108**, 094101 (2012).
- [8] P. Gong, H. Steel, P. Robinson, and Y. Qi, *Phys. Rev. E* **88**, 042821 (2013).
- [9] X. Liao, Q. Xia, Y. Qian, L. Zhang, G. Hu, and Y. Mi, *Phys. Rev. E* **83**, 056204 (2011).
- [10] H. Nakao and A. S. Mikhailov, *Nat. Phys.* **6**, 544 (2010).
- [11] S. Sinha, J. Saramäki, and K. Kaski, *Phys. Rev. E* **76**, 015101(R) (2007).
- [12] Y. Qian, X. Huang, G. Hu, and X. Liao, *Phys. Rev. E* **81**, 036101 (2010).
- [13] N. Burić, D. Ranković, K. Todorović, and N. Vasović, *Physica A* **389**, 3956 (2010).
- [14] I. Franović, K. Todorović, N. Vasović, and N. Burić, *Phys. Rev. E* **87**, 012922 (2013).
- [15] I. Franović, K. Todorović, N. Vasović, and N. Burić, *Phys. Rev. E* **89**, 022926 (2014).
- [16] I. Franović, K. Todorović, M. Perc, N. Vasović, and N. Burić, *Phys. Rev. E* **92**, 062911 (2015).
- [17] I. A. Khovanov, A. V. Polovinkin, D. G. Luchinsky, and P. V. E. McClintock, *Phys. Rev. E* **87**, 032116 (2013).
- [18] A. Destexhe and M. Rudolph-Lilith, *Neuronal Noise* (New York, Springer, 2012).
- [19] L. Arnold, *Random Dynamical Systems* (Springer Verlag, Berlin, 1999).
- [20] M. Gaudreault, F. Lépine, and J. Viñals, *Phys. Rev. E* **80**, 061920 (2009).
- [21] M. Gaudreault, J. M. Berbert, and J. Viñals, *Phys. Rev. E* **83**, 011903 (2011).
- [22] J. A. Acebrón, A. R. Bulsara, and W.-J. Rappel, *Phys. Rev. E* **69**, 026202 (2004).
- [23] B. Sonnenschein, T. K. DM. Peron, F. A. Rodrigues, J. Kurths, and L. Schimansky-Geier, *Eur. Phys. J. B* **87**, 182 (2014).
- [24] B. Sonnenschein and L. Schimansky-Geier, *Phys. Rev. E* **88**, 052111 (2013).
- [25] B. Sonnenschein, M. A. Zaks, A. B. Neiman, and L. Schimansky-Geier, *Eur. Phys. J. Spec. Top.* **222**, 2517 (2013).
- [26] S. Beri, R. Mannella, D. G. Luchinsky, A. N. Silchenko, and P. V. E. McClintock, *Phys. Rev. E* **72**, 036131 (2005).
- [27] A. L. Barth and J. F. A. Poulet, *Trends Neurosci.* **35**, 345 (2012).
- [28] T. Hromádka, M. R. DeWeese, and A. M. Zador, *PLoS Biol.* **6**, e16 (2008).
- [29] J. N. D. Kerr, C. P. J. de Kock, D. S. Greenberg, R. M. Bruno, B. Sakmann, and F. Helmchen, *J. Neurosci.* **27**, 13316 (2007).
- [30] A. Vazdarjanova and J. F. Guzowski, *J. Neurosci.* **24**, 6489 (2004).
- [31] *Handbook of Brain Theory and Neural Networks*, 2nd ed., edited by M. A. Arbib (MIT, Cambridge, MA, 2003).
- [32] N. Brunel and V. Hakim, *Neural Comput.* **11**, 1621 (1999).
- [33] R. C. Toral, C. R. Mirasso, and J. D. Gunton, *Europhys. Lett.* **61**, 162 (2003).
- [34] E. V. Pankratova, A. V. Polovinkin, and B. Spagnolo, *Phys. Lett. A* **344**, 43 (2005).
- [35] E. V. Pankratova, A. V. Polovinkin, and E. Mosekilde, *Eur. Phys. J. B* **45**, 391 (2005).
- [36] R. C. Hilborn and R. J. Erwin, *Phys. Rev. E* **72**, 031112 (2005).
- [37] A. S. Pikovsky and J. Kurths, *Phys. Rev. Lett.* **78**, 775 (1997).
- [38] P. Dayan and L. F. Abbott, *Theoretical Neuroscience: Computational and Mathematical Modeling of Neural Systems* (MIT Press, Cambridge, MA, 2001).
- [39] Z. Levnajić and A. Pikovsky, *Phys. Rev. E* **82**, 056202 (2010).
- [40] M. I. Dykman, P. V. E. McClintock, V. N. Smelyanski, N. D. Stein, and N. G. Stocks, *Phys. Rev. Lett.* **68**, 2718 (1992).
- [41] J. M. Newby, P. C. Bressloff, and J. P. Keener, *Phys. Rev. Lett.* **111**, 128101 (2013).

**Activation process in excitable systems with multiple noise sources: One and two interacting units**Igor Franović,<sup>1,\*</sup> Kristina Todorović,<sup>2</sup> Matjaž Perc,<sup>3,4,†</sup> Nebojša Vasović,<sup>5</sup> and Nikola Burić<sup>6,‡</sup><sup>1</sup>*Scientific Computing Laboratory, Institute of Physics, University of Belgrade, P. O. Box 68, 11080 Beograd-Zemun, Serbia*<sup>2</sup>*Department of Physics and Mathematics, Faculty of Pharmacy, University of Belgrade, Vojvode Stepe 450, Belgrade, Serbia*<sup>3</sup>*Faculty of Natural Sciences and Mathematics, University of Maribor, Koroška Cesta 160, SI-2000 Maribor, Slovenia*<sup>4</sup>*Department of Physics, Faculty of Sciences, King Abdulaziz University, Jeddah, Saudi Arabia*<sup>5</sup>*Department of Applied Mathematics, Faculty of Mining and Geology, University of Belgrade, P. O. Box 162, Belgrade, Serbia*<sup>6</sup>*Scientific Computing Laboratory, Institute of Physics, University of Beograd, P. O. Box 68, 11080 Beograd-Zemun, Serbia*

(Received 19 June 2014; revised manuscript received 22 September 2015; published 14 December 2015)

We consider the coaction of two distinct noise sources on the activation process of a single excitable unit and two interacting excitable units, which are mathematically described by the Fitzhugh-Nagumo equations. We determine the most probable activation paths around which the corresponding stochastic trajectories are clustered. The key point lies in introducing appropriate boundary conditions that are relevant for a class II excitable unit, which can be immediately generalized also to scenarios involving two coupled units. We analyze the effects of the two noise sources on the statistical features of the activation process, in particular demonstrating how these are modified due to the linear or nonlinear form of interactions. Universal properties of the activation process are qualitatively discussed in the light of a stochastic bifurcation that underlies the transition from a stochastically stable fixed point to continuous oscillations.

DOI: [10.1103/PhysRevE.92.062911](https://doi.org/10.1103/PhysRevE.92.062911)

PACS number(s): 05.45.Xt, 02.30.Ks

**I. INTRODUCTION**

Excitability is a dynamical feature shared by nonlinear systems that lie in the vicinity of the bifurcation underlying the transition from the stationary state toward sustained periodic activity [1]. Study of models where stochastic excitable dynamics is crucial for shaping local or collective behavior is a rapidly developing field, gaining relevance in terms of theory as well as for offering qualitative insights into a variety of biological [1–3] and inorganic systems [4–6].

Excitability is manifested in the existence of a narrow range of stimuli magnitudes where marginally different perturbations may cause the system to generate two qualitatively distinct types of responses. While smaller perturbations give rise to small-amplitude (linear) responses, the slightly larger perturbations may elicit pulselike, large-amplitude excitation loops. The latter are composed of activation and relaxation stages, whereby the spike profile remains independent of the form of applied perturbation. If one interprets perturbation in terms of setting the particular initial conditions, then the excitability feature is reflected in the point that the system shows strong sensitivity to initial conditions within a small domain of relevant values. Consequently, behavior of excitable systems is heavily susceptible to noise [7], whose influence may at least in part be understood as excitability amplification.

Given the strong likelihood of encountering systems which are influenced by combined action of variations in the environment and the fluctuations of the internal parameters, it is justified to analyze models where different sources of noise affect the dynamics of multiple variables. This point, together with the fact that the existence of pulselike excitations requires a flow with dimension no less than two [8], suggests

that the system with two variables, each subjected to stochastic perturbation, may be considered a paradigmatic setup. For example, two sharply separated characteristic time scales and two sources of noise acting independently on the fast and the slow variable are relevant ingredients for the description of a typical neuron [9,10] or laser dynamics [4]. For neurons, stochastic term affecting the fast variable may account for synaptic noise due to random arrival of spikes from a large number of afferents, whereas the stochastic component in the slow variable dynamics may be seen as internal noise, associated to thermal fluctuations in the opening of the ion-gating channels. Consistent with this, we refer to stochastic term added to the dynamics of the fast (slow) variable as external (internal) noise.

From the theoretical viewpoint, a comprehensive insight into the noise-driven activation process is fundamental for understanding excitability. The problem we focus on concerns the activation process in a single excitable Fitzhugh-Nagumo (FHN) element or two coupled excitable FHN elements driven by two independent sources of noise. The main reason for considering the FHN model lies in its generic character, viz. the fact that it is canonical for class II excitable systems, which involve an almost continuous transition between the small- and the large-amplitude excitations. For conceptual reasons and in view of potential applications, only the spiking responses are relevant and of interest to us. It follows that the formulation of activation event has to be adapted to class II excitable systems, such that it satisfies two criteria: (i) it should warrant a clear-cut distinction of the spiking response from the small-amplitude excitation and (ii) it should allow an immediate generalization from the case of a single unit to that of two interacting units. We stress that in order to meet both criteria, it is crucial to introduce an appropriate terminating boundary set for the activation problem, as demonstrated in the paper.

Note that the term *activation* is inherited from but not used in the same sense as in a typical escape problem [7,11–14]. To

\*franovic@ipb.ac.rs

†matjaz.perc@uni-mb.si

‡Corresponding author: buric@ipb.ac.rs

explain the differences, one first invokes a general remark that for excitable systems, two possible types of response derive from the proximity to bifurcation rather than the bistable dynamics, so the thresholdlike behavior is not associated to a genuine separatrix (saddle structure) but rests on the coaction of nonlinearity and the sharp separation between the system's characteristic time scales. Thus, resolving the origin and character of thresholdlike behavior for excitable elements may be linked to an unstable fixed point or, as in case of a FHN unit, to a quasiseparatrix ("ghost separatrix") [15]. This apparently differs from the typical escape problem scenario.

Another important point is that we tie the activation exclusively to spiking response, so the event where the phase point reaches the quasiseparatrix *per se* is insufficient to count as activation. In other words, crossing the quasiseparatrix does not present a discriminative condition between the small- and the large-amplitude excitations. This is why we introduce novel terminating boundary conditions rather than just consider an extension of the escape problem to excitable systems [15]. One should also point out that our approach conceptually differs from the earlier work concerning noisy excitable neurons [16,17], where the terminating boundary does not constitute a set, but rather a unique boundary point, introduced as an arbitrary threshold independent on the structure of phase space.

We analyze the activation problem from two angles, one by determining the most probable activation paths (MPAPs) and the other by examining the statistical features of the activation process. An important result consists in determining the MPAPs for a single and two coupled units under different ratios of external versus internal noise  $D_1/D_2$ . In the case of two units, the topology of the obtained trajectories is shown to qualitatively depend on the form of coupling. The statistics of a single- and two-unit activation processes is characterized by examining how the time-to-first-pulse (TFP)  $\tau$  averaged over different stochastic realizations and the associated coefficient of variation  $R$  depend on noise. Both  $\tau(D_1, D_2)$  and  $R(D_1, D_2)$  are found to display universal behavior for all considered setups, whereby the transition between two of the observed  $\tau$  regimes is associated to the fact that a unit undergoes stochastic bifurcation induced by  $D_1$  and  $D_2$ . For two units, the form of coupling is shown to have a nontrivial effect on correlation of the individual mean TFPs, which we relate to synchronization properties of the time series for the given parameter set.

The paper is organized as follows. In Sec. II, we present the details of the model, focusing on the thresholdlike behavior of a single unit and the results of bifurcation analysis for the coupled units. Section III concerns the case of a single unit subjected to external and internal noise. Having laid out the details of the method used to determine the MPAPs, cf. Sec. III A, we examine how the topological features of the MPAPs depend on the pertaining noise intensities. Apart from relating the properties of  $\tau(D_1, D_2)$  dependence to the onset of stochastic bifurcation from the stochastically stable fixed point to the stochastically stable limit cycle, we also introduce an approximation to explicitly demonstrate that  $D_1$  and  $D_2$  make substantially different impact on the mean TFPs. Section IV contains the results for two units interacting via the linear or nonlinear couplings. It is analyzed how the different form of coupling affects the profile of the respective MPAPs, the

stochastic bifurcation as well as the correlation of single unit mean TFPs. Section V provides a summary of the main results.

## II. BACKGROUND ON THE APPLIED MODEL

### A. Dynamics of a single excitable unit

As a paradigm for excitable systems, we consider the FHN model, so the dynamics of a single unit is given by

$$\begin{aligned} dx &= f_x(x, y) = [x - x^3/3 - y]dt + \sqrt{2D_1}dW_1 \\ dy &= f_y(x, y) = \epsilon(x + b)dt + \sqrt{2D_2}dW_2. \end{aligned} \quad (1)$$

The model is canonical for the type II excitability class, meaning that the equilibrium lies in the vicinity of the direct supercritical Hopf bifurcation. The latter is controlled by the excitability parameter  $b$ , whereby the critical value is  $|b| = 1$ . For  $|b| > 1$ , the system possesses a unique stable equilibrium  $(x_{\text{eq}}, y_{\text{eq}}) = (-b, -b + b^3/3)$ , whereas for  $|b| < 1$  the oscillatory state sets in. Given the symmetry of the system (1), the analysis may be confined to case  $b > 0$  without loss of generality. The unit in the subcritical state displays excitable behavior if  $b$  is kept close to the bifurcation threshold. In this paper, we fix  $b = 1.05$ .

The other important ingredient of the model is the sharp separation between the characteristic time scales of the activator and the recovery variable. The fast-slow dynamics is facilitated by setting  $\epsilon$  to a small value ( $\epsilon = 0.05$ ). So far, the FHN model has been applied in describing the dynamics of electrochemical reactions [18] and cardiac cells [3] but is best known for its role in the field of neuroscience [1,7]. In the latter context, the fast variable may be viewed as analogous to the neuron membrane potential, whereas the action of the slow variable may qualitatively be compared to that of  $K^+$  ion-gating channels [1]. Regarding the impact of random perturbations, we are interested into how the activation of units is shaped by two independent sources of noise. In Eq. (1), the stochastic effects are represented by the Wiener processes whose increments satisfy  $\langle dW_i \rangle = 0$  and  $\langle dW_i dW_j \rangle = dt\delta_{ij}$  for  $i, j \in 1, 2$ . The dynamics of an excitable unit may be summarized as follows. In the absence of perturbation, the selected parameter values are such that the system lies at equilibrium. Kicked by the perturbation, the unit may either display a small amplitude response, whereby the phase point rapidly decays back to equilibrium, or may exhibit a large excursion, settling to equilibrium only after the phase point has traversed the orbit corresponding to a complete oscillation cycle.

For the proper statement of our problem, it is important to first consider the geometric interpretation of the unit's dynamics. Two particular issues are addressed, one related to the existence and the structure of the boundary between the initial conditions resulting in small- or large-amplitude responses, whereas the other concerns the distinction between the roles of  $D_1$  and  $D_2$  in triggering the pulse emission. Regarding the first point, we summarize the results on the deterministic (noiseless) version of the system (1) obtained by the method of phase plane analysis, which rests on the singular perturbation theory. In the limit  $\epsilon \rightarrow 0$ , (1) turns into a one-dimensional system  $\dot{x} = f_x(x, y)$  under the constraint  $\dot{y} = 0$ , meaning that  $y$  may be viewed as a fixed parameter.

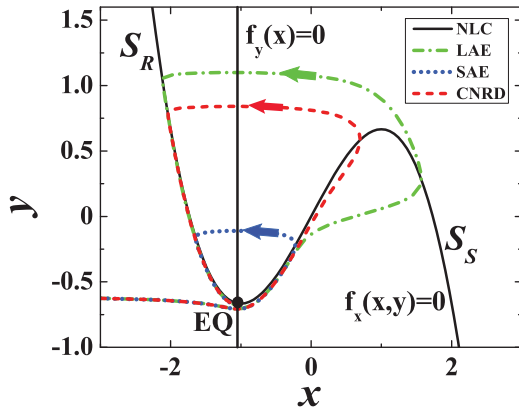


FIG. 1. (Color online) Phase plane analysis for a FHN excitable unit. Equilibrium (EQ) lies at the intersection of the nullclines  $f_x(x, y) = 0$  and  $f_y(x) = 0$ . The  $x$  nullcline comprises three branches. In the singular limit  $\epsilon \rightarrow 0$ , the spiking branch  $S_S$  and the refractory branch  $S_R$  are attractive, whereas the orbit separating the initial conditions that lead to small- or large-amplitude excitations, SAE and LAE, respectively, contains the middle unstable branch. For finite  $\epsilon$ , the boundary between the two sets of initial conditions foliates into a thin layer of canardlike trajectories (CNRD) referred to as “ghost separatrix.” Illustrated trajectories are obtained by fixing the  $x$  initial condition to  $x_0 = -3$ , whereas  $y_0$  is varied. Extreme sensitivity to initial conditions in vicinity of ghost separatrix is corroborated by the fact that a difference in  $y_0$  of the order of  $10^{-14}$  gives rise to a different form of excitation. The parameters of FHN model are fixed to  $\epsilon = 0.05, b = 1.05$ .

For small but finite  $\epsilon$ ,  $x$  quickly relaxes to the value given by  $f_x(x, y) = 0$ , the condition outlining the curve referred to as the  $x$  (cubic) nullcline or the slow manifold, see Fig. 1. The  $x$  nullcline is composed of three branches, whose stability features derive from the singular limit  $\epsilon \rightarrow 0$ . While the refractory  $S_R$  and the spiking branch  $S_S$  may then be regarded as attractors, the middle branch is unstable and is a part of separatrix between the attractive branches. The key point is that for small but finite  $\epsilon$  the structure of the boundary and the related threshold behavior is mostly inherited from the singular limit. The distinction is that finite  $\epsilon$  induces foliation of the boundary around the maximum of the  $x$  nullcline. What has explicitly been shown by the so-called blow-up method [19] is that the boundary between the initial conditions leading to  $S_S$  or  $S_R$  is not given by a single line but rather by a thin layer made up of an infinite family of canardlike trajectories of system (1). The latter further implies that the boundary constitutes an invariant set. Boundary layer may still be perceived as a single line, a kind of “ghost separatrix” [15], because at distances  $d \gg \epsilon$  from the fold point  $(1, 2/3)$ , all the constituent trajectories become virtually indistinguishable.

As for the qualitative interpretation of the effects of noise, it is evident that the noise term added to the slow-variable dynamics may shift the position of the  $y$  nullcline. In other words, internal noise is capable of translating the fixed point from the stable refractory to the unstable (middle) branch of the  $x$  nullcline, which temporarily switches the system from the excitable state to the oscillatory state. While the impact of  $D_2$  can be understood by geometric analysis, there is no analogous interpretation in case of  $D_1$ .

## B. Dynamics of a couple of excitable units

In case of a pair of coupled units, we consider two distinct setups, one where the units interact via the symmetrical linear couplings and the other involving couplings given by the nonlinear thresholdlike function.

The dynamics of a couple of FHN units interacting via linear couplings is given by

$$\begin{aligned} dx_i &= [x_i - x_i^3/3 - y_i]dt + \sqrt{2D_1}dW_1^i + c[x_i - x_j]dt \\ dy_i &= \epsilon(x_i + b)dt + \sqrt{2D_2}dW_2^i, \end{aligned} \quad (2)$$

where  $i, j \in \{1, 2\}, i \neq j$  specify the individual units. The random perturbations are such that the terms acting on different elements are supposed to be uncorrelated  $\langle dW_k^i dW_l^j \rangle = 0, k, l \in 1, 2$ . Regarding the system parameters, note that the units are assumed to be identical (same  $b$  and  $\epsilon$ ), while the symmetrical couplings are characterized by the coupling strength  $c$ . To see how the unit’s excitability feature is modified in the presence of interaction, we make a brief summary of the results of the bifurcation analysis carried out on the noise-free version of the system (2). The first remark is that the equilibrium is located at  $(x_1, y_1, x_2, y_2) = (-b, -b + b^3/3, -b, -b + b^3/3)$ , whereby its stability is determined by the two pairs of complex conjugate characteristic exponents which satisfy  $\mu_{1,2} = [1 - b^2 + 2c \pm \sqrt{(1 - b^2 + 2c)^2 - 4\epsilon}]/2$  and  $\mu_{3,4} = [1 - b^2 \pm \sqrt{(1 - b^2)^2 - 4\epsilon}]/2$ . Given that the single unit parameters are kept fixed, the local stability of equilibrium is changed under variation of the coupling strength. In particular, it may be demonstrated that the system undergoes a direct supercritical Hopf bifurcation at the critical value  $c_{H,L} = (b^2 - 1)/2$ . At this point, the stability of equilibrium is lost and the units are no longer in the excitable regime. However, we stress that the complete picture on the system dynamics cannot be gained from the local bifurcation analysis alone, because even before the excitability feature is lost (for  $c = c_{H,L}$ ), it is modified due to a global fold-cycle bifurcation which occurs at  $c_{FC} < c_{H,L}$ . Thus, under increasing  $c$  the system exhibits three types of characteristic behavior: (i) the “proper” excitable regime for  $c < c_{FC}$ , (ii) the regime of “generalized excitability” for  $c \in (c_{FC}, c_{H,L})$ , and (iii) the oscillatory state at  $c > c_{H,L}$ . The case (ii) involves coexistence between the fixed point and the large limit cycle, whose basins of attraction are separated by the stable manifold of the saddle cycle. In strict terms, such a scenario does not conform to Izhikevich’s definition of excitability, because instead of relaxing to equilibrium after the large excursion, the system displays continuous oscillations. Nevertheless, some authors consider such a behavior as excitable or excitable-like, and one should also note that the oscillation orbit may still pass quite close to equilibrium, depending on the position, size, and manifold structure of the saddle cycle. Note that above  $c_{H,L}$ , the large limit cycle created in the global event survives as the only attractor, because the incipient cycle born via Hopf bifurcation grows only until colliding with the preexisting saddle cycle, such that the two get annihilated in the inverse fold-cycle bifurcation. In other words, the properties of the limit cycle attractor both below and above  $c_{H,L}$  are determined by the global bifurcation.

Having summarized the results of the bifurcation analysis for the setup involving two units coupled via linear function, we turn to the scenario where the units subjected to external and internal noise interact in a nonlinear fashion. The dynamics of the units then obeys

$$\begin{aligned} dx_i &= [x_i - x_i^3/3 - y_i]dt + \sqrt{2D_1}dW_1^i + c \arctan(x_j + b)dt \\ dy_i &= \epsilon(x_i + b)dt + \sqrt{2D_2}dW_2^i. \end{aligned} \quad (3)$$

The interaction terms have a form of a thresholdlike function, whose argument is defined relative to the corresponding unit's equilibrium  $x_j - x_{j,\text{EQ}} = x_j + b$ . This way, the impact of the state  $x_j$  is felt more strongly if it lies further away from the equilibrium. The stability of the equilibrium is determined by the four roots of the characteristic equation, which appear as two pairs of complex conjugates  $\mu_{1,2} = [1 - b^2 + c \pm \sqrt{(1 - b^2 + c)^2 - 4\epsilon}]/2$ ,  $\mu_{3,4} = [1 - b^2 - c \pm \sqrt{(1 - b^2 - c)^2 - 4\epsilon}]/2$ . Again, it may be shown that the system (3) undergoes a direct supercritical Hopf bifurcation at  $c_{H,\text{NL}} = b^2 - 1$ . Note that we confine the analysis to the case  $c > 0$ . Unlike the setup based on the linear coupling, here one does not encounter the global bifurcation controlled by  $c$ . In other words, the equilibrium is stable and the units are in excitable regime for  $c < c_{H,\text{NL}}$ , whereas the system is in oscillatory state for  $c > c_{H,\text{NL}}$ .

### III. ACTIVATION PROCESS IN AN EXCITABLE UNIT DRIVEN BY EXTERNAL AND INTERNAL NOISE

In the following subsection we introduce the numerical method applied to determine the MPAPs. The method is illustrated in case of a single FHN unit, but it can readily carry over to the process of first pulse emission for two interacting units. In Secs. III B and IV A, the topological features of the pertaining trajectories will be analyzed in reference to stochastic bifurcation, viz. for noise intensities substantially below, near, or above the critical domain of  $(D_1, D_2)$  values. While the main focus lies with the MPAPs explicitly obtained from stochastic simulations, the extended discussion will also concern the trajectories generated as solutions of the effective Hamiltonian equations under boundary conditions relevant for the process of first pulse emission. We stress that the use of such equations is distinct from the standard Hamiltonian approach which yields optimal trajectories in a typical escape problem or the generalization of an escape problem to an excitable FHN unit. In order to set up the discussion carried out in Secs. III B and IV A, the following subsection addresses the precise role of these effective equations and the ensuing trajectories.

#### A. Method applied to determine the MPAPs

The problem of obtaining the MPAPs for excitable units in general comprises two issues. One issue concerns how the terminating boundary conditions are specified, whereas the other relates to the particular details of the method. A common ingredient in previous approaches to analysis of activation process in excitable units has been to draw an analogy to motion of a particle in a one-dimensional potential perturbed by noise. Reduction to a one-dimensional problem naturally utilizes the decomposition of the system dynamics to fast

and slow motions. Though such approximate methods are not intended to trace the unit's most likely activation paths, the use of Fokker-Planck formalism still allows one to gain insight into certain statistical features of the activation process, including the mean activation time and its variance [11,20]. Nevertheless, an inherent drawback consists in the lack of ability to account for the simultaneous influence of perturbations added to both the slow and the fast component. In conceptual terms, the key problem lies in the fashion by which the escape from the stationary state is precisely defined. In particular, instead of associating the terminating boundary to the structure of the system's phase space, the activation event is considered a crossing of a predefined threshold, typically coinciding with the fold point at the minimum of the slow manifold. Compared to such methods, the approach we apply is preferred because (i) it introduces a unique definition of the activation path consistent with the structure of the phase space, (ii) one may consider the coaction of random perturbations added to both the fast and the slow subsystem, and (iii) one is able to explicitly determine the MPAPs around which the different stochastic realizations are clustered.

Before proceeding to the details of the numerical method implemented for calculation of the MPAPs, let us specify the boundary conditions relevant for the problem of first pulse emission in case of an excitable FHN unit. In particular, for the noise-driven system (1), we consider the stochastic fluctuation paths in configuration space  $(x, y)$  that emanate from the deterministic fixed point  $(x_{\text{eq}}, y_{\text{eq}}) = (-b, -b + b^3/3)$  and terminate at the spiking branch of the cubic  $[(x)]$  nullcline. The given selection of the terminating boundary set derives from the fact that the spiking branch of the cubic nullcline defines the spike profile for the deterministic limit cycle in the superthreshold regime  $b \lesssim 1$ , while the analogous point holds for the noise-induced oscillations in the excitable regime  $b \gtrsim 1$ . In these terms, it has been verified that the profiles of spikes for an arbitrary combination of relevant  $(D_1, D_2)$  values can be approximated with sufficient accuracy by the orbit corresponding to the deterministic limit cycle characterizing the supercritical state. Note that the terminating boundary set we introduce is distinct from the one in Ref. [15], where a conceptually distinct problem has been considered. In particular, the aim in that paper has been to extend the standard escape problem to the case of an excitable FHN unit, which has been achieved by fixing the "ghost separatrix" as the terminating boundary set. The advantage of the boundary conditions we have adopted is that they can readily be generalized to the case of two interacting excitable units. In another paper, we shall further demonstrate that the relevance of a proper problem formulation which warrants that the small-amplitude response and the spiking response are clearly distinguished, as well as the related selection of the appropriate terminating boundary conditions, is even more pronounced when analyzing the noise-driven first pulse emission process for an assembly of excitable units [21].

The details of the numerical method applied to determine the MPAPs are as follows. For the given  $(D_1, D_2)$ , we consider an ensemble of fluctuation paths  $(x(t), y(t))$  which start from the deterministic fixed point  $(x_{\text{eq}}, y_{\text{eq}})$  at moment  $t_i$  and satisfy the above-stated terminating boundary conditions. The terminating time  $t_f$ , as well as the associated coordinates



$(x(t_f), y(t_f))$ , are left unspecified. For the described ensemble, we study the statistics of the  $(x(t), y(t))$  position of trajectories as a function of time  $t_i < t < t_f$  preceding the arrival to the terminating boundary set. In general, the idea is to sample the different stochastic realizations of activation trajectories in order to determine histograms of the path history reaching the terminating boundary set. Naturally, the recorded trajectories are characterized by the different  $t_f$  times. Thus, the proper approach to characterize the statistics of the paths in configuration space is to consider the prehistory probability density [22], which concerns the distribution of paths ending at the specified boundary set. To obtain the former, one effectively sets the time when each stochastic realization terminates to  $t = 0$ , such that the behavior of the process during the initiation of the pulse is observed by looking backward in time. This approach has been introduced in Ref. [22] and has been applied a number of times since [23]. The prehistory probability distribution is defined as

$$H(x, y, t) dx dy = \Pr[x(t) \in (x, x+dx), y(t) \in (y, y+dy) | x_b(t_f), y_b(t_f), x(t_i) = x_{\text{eq}}, y(t_i) = y_{\text{eq}}, t_i < t < t_f, x < x_b(t_f), y < y_b(t_f)]. \quad (4)$$

The most probable path for the first pulse emission process is determined by collecting the points  $(x_m(t), y_m(t))$  which correspond to the maximum of  $H(x, y, t)$  at any given moment  $t$ . In other words, the MPAP for the given  $(D_1, D_2)$  by definition coincides with the peak of  $H$  as a function of time. In practice, the numerical method used to determine the prehistory probability density has involved dividing the  $(x, y)$  phase space into a grid of  $70 \times 70$  cells of length  $\Delta x = 0.048$  and width  $\Delta y = 0.09$ . Throughout the paper, the numerical integration of the appropriate set of stochastic equations is carried out by the Heun algorithm with the time step  $\delta t = 0.002$ , whereas the averaging is performed over an ensemble of 5000 different stochastic realizations of the first pulse emission process.

In order to provide qualitative guidelines for an extended discussion, the MPAPs determined via the above described method for different setups and the different domains of noise intensities will be compared to trajectories obtained by integrating the set of effective Hamiltonian equations under boundary conditions relevant for the problem of first pulse emission. One recalls that in case of a typical escape problem, the Hamiltonian theory formulated in the extended variable-momentum state space may be used to explicitly obtain the optimal trajectories which coincide with the MPAP, whereby such trajectories are determined by the minimum of action, introduced as an effective cost function. In Ref. [15], such an approach has been implemented for an extension of the escape problem to an excitable FHN unit, having considered the ghost separatrix as the terminating boundary. Due to fundamentally different terminating boundary conditions, one cannot apply the Hamiltonian theory *per se* for the problem of first pulse emission, as we explain in more detail further below. Therefore, our approach cannot be interpreted in the genuine context of or be referred to as an extension of the Hamiltonian theory. In fact, the Hamiltonian system we consider should be interpreted as a set of effective equations integrated for relevant boundary conditions, whereby a particular trajectory is singled

out according to a certain predefined recipe. Our current goal is not to provide a systematic theory but only to point out to striking similarity between the numerically obtained MPAPs for the process of first pulse emission and the trajectories generated by the set of effective Hamiltonian equations. This can be considered a preliminary stage of a study which may ultimately lead to derivation of an appropriate theory for the process of first pulse emission, whose basis would take into account certain aspects of the standard Hamiltonian formalism.

In the remainder of this subsection, we briefly consider the main elements of the Hamiltonian approach, whose detailed description may be found in Ref. [24], and clarify the differences emerging in case of the first pulse emission process. Within the Hamiltonian formalism, the optimal trajectories for a noise-driven escape process are obtained by variation-like approach which minimizes the appropriately defined ‘‘cost functional’’ [25,26]  $\bar{S}(\mathcal{J}, t)$  along the set of possible activation trajectories  $\mathcal{J}$  between the two fixed boundaries. In particular, the probability for noise to induce the  $x_i \mapsto x_f$  transition is given by  $p(x_f | x_i) = \int_{\mathcal{J}} P[\mathcal{J}] d\{\mathcal{J}\}$ , such that  $d\{\mathcal{J}\}$  denotes integration along all the paths  $\{\mathcal{J} = \{x_1, \dots, x_N\}\}$  connecting  $x_i$  and  $x_f$ . Each path is weighted by the probability  $P[\mathcal{J}] \propto \exp[-\frac{S(x_1, \dots, x_N)}{D}]$ , where  $S$  is the cost function for the particular path. When  $D$  is small, the largest contribution to  $p(x_f | x_i)$  comes from the path with the minimal cost function  $S_{\min} = \min\{S_{\mathcal{J}} | \mathcal{J} = \{x_1, \dots, x_N\}\}$ . In other words, small noise rarely gives rise to transition events, but once they occur, all the other orbits are suppressed in favor of the one corresponding to the minimal cost function. The transition probability then takes the asymptotic form

$$p(x_f | x_i) = z \exp\left[\frac{-S_{\min}}{D}\right], \quad x_1 \equiv x_i, \quad x_N \equiv x_f, \quad (5)$$

whereby the prefactor  $z$  is associated to ‘‘degeneracy’’ of the minimum or rather the number of trajectories close to the one given by  $S_{\min}$  [24].

The form of  $\bar{S}$  is selected so to reflect on one hand the impact of noise, whereas on the other hand to explicitly incorporate the constraints between the variables and the stochastic terms which derive from the equations of motion. The necessary conditions for the minimum of such a constraint problem can then be treated by the Lagrange multiplier technique. Ultimately, one arrives at a set of equations that may be interpreted as a Hamiltonian system, where the Lagrange multiplier  $\lambda$  enact the momenta conjugate to the system variables. In particular, for system (1), the corresponding Hamiltonian set including the generalized momenta is given by

$$\begin{aligned} \frac{dx}{dt} &= x - x^3/3 - y + r_x p_x \\ \frac{dy}{dt} &= \epsilon(x + b) + r_y p_y \\ \frac{dp_x}{dt} &= -(1 - x^2)p_x - \epsilon p_y \\ \frac{dp_y}{dt} &= p_x, \end{aligned} \quad (6)$$

where  $p_x$  and  $p_y$  are the components of the momentum, while  $r_x$  and  $r_y$  represent the scaled noise intensities. By the latter notation,  $D_1$  and  $D_2$  are conveniently expressed in

terms of a single amplitude  $D$  ( $D_1 = r_x D$  and  $D_2 = r_y D$ ). System (6) has the Wentzel-Freidlin Hamiltonian [27]  $H = p_x(x - x^3/3 - y) + p_y\epsilon(x + b) + \frac{r_x}{2}p_x^2 + \frac{r_y}{2}p_y^2$ , whereas the trajectories connecting the initial state  $i$  and final state  $f$  are characterized by the action  $S = \int_{t_i}^{t_f} dt \frac{1}{2}(r_x p_x^2 + r_y p_y^2)$ . At variance with system (1), the fixed point of the system (6),  $(x_0, y_0, p_{x,0}, p_{y,0}) = (-b, -b + b^3/3, 0, 0)$ , is unstable for  $b > 1$ , which is corroborated by the positive real part of the characteristic exponents  $\mu_{1,2} = \frac{-(1-b^2) \pm \sqrt{(1-b^2)^2 - 4\epsilon}}{2}$ .

Conceptually, the Hamiltonian formalism is typically applied to escape problems, where the stable equilibrium coexists with a certain saddle state, most often the saddle cycle [24]. The aim is then to obtain the heteroclinic trajectory in the extended space, which emanates from the unstable manifold of the fixed point at  $t \rightarrow -\infty$  and reaches the stable manifold of the saddle cycle asymptotically at  $t \rightarrow \infty$ , as well as tangentially ( $\mathbf{p} \rightarrow 0$ ) for  $t \rightarrow 0$ . In principle, depending on  $\mathbf{p}$ , the dynamics in the extended space may also support the trajectories that do not settle at, but run across, the cycle, as well as the trajectories that are repelled by the cycle, thus being reflected back to initial state. In Ref. [15], an extension of the escape problem to a single FHN unit has been considered by utilizing the threshold-like behavior to construct the “ghost” manifold (a separatrix in the asymptotic limit  $\epsilon \rightarrow 0$ ), which plays the role of a saddle structure. For such a scenario, the Hamiltonian approach yields the optimal trajectory connecting the unstable manifold of the fixed point to the stable manifold of the ghost separatrix.

Compared to this, the problem of first pulse emission fundamentally differs because one should look for trajectories that cross the ghost separatrix, *viz.* leave the basin of attraction of the fixed point. While the action surface in vicinity of the basin boundary should have one clearly defined global minimum, the physical picture near the spiking branch of the  $x$  nullcline typically involves multiple local minima of the action surface. A deeper theoretical analysis of these issues is beyond the scope of the current paper. The point we make here is as follows. Let us consider the trajectories that correspond to local minima of the action surface and adopt as a rule to select the solution that has the smallest momentum at the terminating boundary. Then, for different system configurations, the comparison of the MPAPs numerically obtained from an ensemble of stochastic realizations reveals significant similarity to the respective trajectories generated by the set of effective Hamiltonian equations.

In terms of numerical treatment, obtaining the relevant trajectories from the effective system (6) comprises a boundary value problem. At the initial moment  $t_i$ , the coordinates  $(x(t_i), y(t_i), p_x(t_i), p_y(t_i))$  lying on the unstable manifold of the fixed point are specified according to the method provided in Ref. [24], which connects the coordinates in the configuration space with the components of the momentum. By this method, it follows that the initial coordinates in the extended space can be parameterized via a single angular variable  $\phi \in (0, 2\pi)$ . The different trajectories are then obtained by sampling 1000 equally spaced initial conditions that cover the entire range of  $\phi$  values. The moment of arriving at the second boundary  $t_s$ , as well as the coordinates  $(x(t_s), y(t_s), p_x(t_s), p_y(t_s))$ , are not explicitly specified. In effect, we apply a shooting approach

that involves a set of different trajectories with particular initial conditions, whereby all the trajectories terminate at the spiking branch of the cubic nullcline. System (6) is integrated by a standard solver implementing the fourth-order Runge-Kutta routine. The cost function  $S$  is calculated along each of the trajectories, and we single out the trajectory that corresponds to a local minimum having the smallest value of angular momentum at the terminating boundary (typically of the order of  $10^{-4}$  or less). Note that the analogous numerical approach is applied in case of two interacting units. The only difference is that the initial conditions are parameterized in terms of three angular variables, instead of a single angular variable.

## B. Examples of MPAPs and the method’s persistence under increasing noise

We systematically examined how the MPAPs change under variation of the ratio of external versus internal noise intensity  $r_x/r_y$ . It has been established that the MPAP profiles are not sensitive to gradual changes over the whole range of  $r_x/r_y$  values. In particular, when slowly increasing  $r_x/r_y$ , the trajectories are found to either exhibit barely visible changes in shape or to converge to each other once the “ghost separatrix” is crossed. Therefore, in qualitative terms one may single out three characteristic forms of solutions, corresponding to cases  $(r_x, r_y) = (1, 0)$ ,  $(r_x, r_y) = (0, 1)$  and  $(r_x, r_y) = (1, 1)$ , which can be held representative for the problem of first pulse emission. In other words, the topological features of MPAPs are primarily sensitive to whether a particular noise source or both sources are present in the system (1).

The other point one has to consider is the impact of the noise intensity  $D$ . Naturally, the physical picture described above is maintained for sufficiently small  $D$ . The analysis provided in Sec. III D will show that the term “sufficiently small”  $D$  effectively implies that the system lies sufficiently away from the stochastic bifurcation underlying transition from stochastically stable fixed point to the noise-induced oscillations. Above the stochastic bifurcation, the attractive power of the fixed point is no longer felt, such that the noise can move the phase point away from equilibrium without an opposing force. Thus, if one focuses on MPAPs for any of the three characteristic  $r_x/r_y$  ratios, the impact of noise will become substantial as one approaches the stochastic bifurcation and will become overwhelming above the stochastic bifurcation. Note that for large  $D$ , the MPAPs determined via the method introduced in Sec. III A lose physical meaning, because the fluctuations over an ensemble of stochastic realizations grow too large to be accurately described by the maximums of the prehistory probability density  $H(x, y, t)$ . The influence of noise is reflected in the increase of the skewness and the kurtosis of the distribution of system’s variables for different stochastic realizations at arbitrary  $t$ .

Let us now consider some examples of MPAPs in order to corroborate the points stated above. First we illustrate the validity of the method used to obtain the MPAPs, see Fig. 2(a). The figure refers to the case  $(r_x, r_y) = (0, 1)$  for  $D = 0.00003$ , the noise value substantially below the stochastic bifurcation. By taking 10 arbitrary realizations of the first pulse emission process, it is shown that the stochastic realizations indeed cluster around the MPAP, indicated by the open circles. We

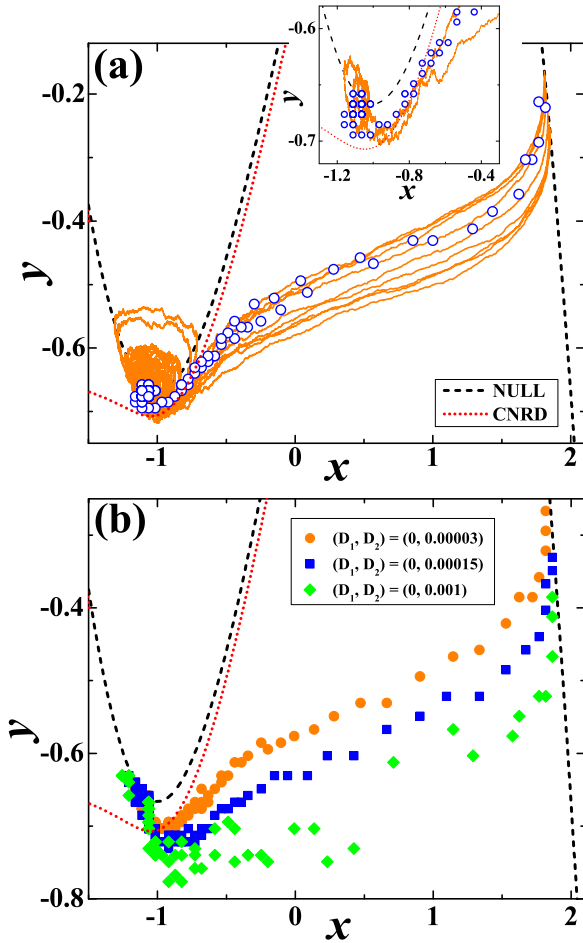


FIG. 2. (Color online) MPAPs for an excitable FHN unit. (a) The main frame shows that the activation paths for different stochastic realizations (solid lines) cluster around the MPAP (open blue circles). The ratio of external vs internal noise intensities is  $r_x : r_y = 0 : 1$ , whereas the noise intensity is  $D = 0.00003$ . The  $x$  nullcline (NULL) and the canardlike trajectory (CNRD) pertaining the ghost separatrix are shown by the dashed and the dotted lines, respectively. Inset: The enlarged view of the region of phase space before the CNRD. In (b) is illustrated how the MPAP profile changes under increasing  $D$  for the fixed ratio  $r_x : r_y = 0 : 1$ . The MPAPs shown correspond to  $D = 0.00003$  (circles),  $D = 0.00015$  (squares), and  $D = 0.001$  (diamonds). These noise intensities lie substantially below, in vicinity and above the stochastic bifurcation, respectively.

have observed that the distribution of  $(x, y)$  values at fixed  $t$  for different stochastic realization is narrow around the terminating boundary and broadens towards the initiation point. With increasing noise intensity  $D$ , the changes in the shape of the MPAPs become clearly visible around  $D \approx 0.00015$ , the value close to the onset of stochastic bifurcation, cf. Fig. 2(b). The effect of noise is felt particularly strong in the region of phase space before the ghost-separatrix, which is indicated by the dotted line. An interesting point is that the larger noise may also have an inhibitory effect on the process of first pulse emission, in the sense that the phase point which has already crossed the ghost separatrix may still diffuse back to the basin of attraction of the fixed point.

We further highlight how the topological properties of MPAPs depend on the characteristic ratio  $r_x/r_y$ . As announced

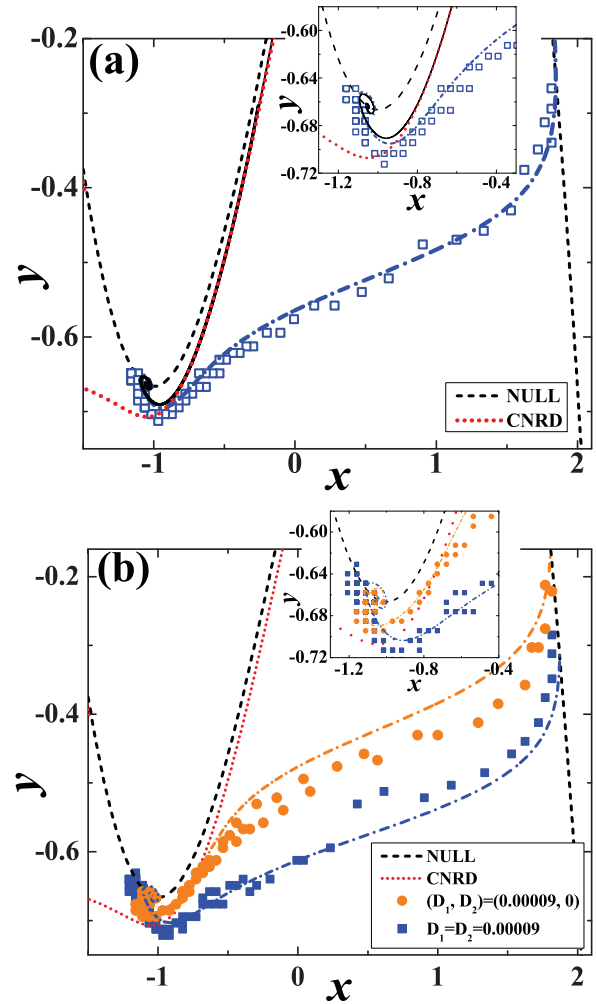


FIG. 3. (Color online) Extended analysis of MPAPs. Panel (a) is intended to illustrate the difference between the first pulse emission problem and the generalized escape problem for a FHN unit. The setup and the style of presentation are the same as in Fig. 2(a), but two additional curves are presented. The solid black line approaching the CNRD indicates the optimal trajectory obtained for the escape problem via the standard Hamiltonian approach, whereas the dash-dotted line denotes the trajectory generated by the system (6) according to the recipe described in Sec. III A. Panel (b) shows the MPAPs for  $r_x : r_y = 1 : 0$  (circles) and  $r_x : r_y = 1 : 1$  (squares), together with the corresponding trajectories (dash-dotted lines) generated by the system (6). In both instances, the noise intensity is  $D = 0.00009$ .

earlier, the discussion is put into a broader perspective by comparing the MPAPs to the trajectories generated by the effective Hamiltonian system (6) according to the prescription provided in Sec. III A. Taking the case  $r_x : r_y = 0 : 1$  as an example, we first demonstrate how the problem of first pulse emission differs from the extension of the escape problem to an excitable FHN unit addressed in Ref. [15]. Apart from the ghost separatrix, denoted by the dotted line, Fig. 3(a) also shows the optimal trajectory for the escape problem obtained using the standard Hamiltonian formalism. The latter trajectory is indicated by the solid line which approaches, but does not cross, the ghost separatrix, because the optimal

escape path cannot intersect the system's manifold. The MPAP numerically determined for the process of first pulse emission is represented by the open squares. The particular MPAP is obtained for small, but finite, noise  $D$ . Such  $D$  values may actually be referred to as intermediate, because, on one hand, they lie below the critical domain giving rise to stochastic bifurcation, but, on the other hand, they cannot be considered as asymptotically small noise ( $D \rightarrow 0$ ) where the theory of large fluctuations would naturally apply. It can be seen that the initial part of the MPAP matches very closely the optimal trajectory calculated by the standard Hamiltonian formalism but also departs from it well before reaching the ghost separatrix. Nevertheless, an interesting finding is that the trajectory generated from the effective system (6), cf. the thick solid line that crosses the ghost separatrix, matches quite closely the MPAP along the entire trajectory relevant for the process of first pulse emission. This point suggests that a theory using certain aspects of the standard Hamiltonian approach could potentially be derived to characterize the first pulse emission process.

Figure 3(b) is intended to compare the MPAPs for the two remaining characteristic  $r_x/r_y$  ratios at  $D$  values substantially below the stochastic bifurcation. As expected, the respective trajectories show significant differences well before crossing the ghost separatrix. The trajectories generated by the effective Hamiltonian equations in the fashion described in Sec. III A again seem to closely match the MPAPs obtained by averaging over the ensemble of stochastic realizations. The profile of the escape paths in vicinity of equilibrium in Fig. 3(b) suggests that the noise-induced linearization [28,29] takes place in the presence of the external noise. In particular, the latter is found to smear the effect of nonlinearity, such that the thresholdlike behavior becomes smoother.

### C. An insight into the activation processes driven by external or internal noise

Before proceeding to numerical results regarding the statistical properties of the activation process, let us briefly consider the conceptual differences between the cases where noise influences the dynamics on the fast ( $D_1 > 0, D_2 = 0$ ) or the slow characteristic time scale ( $D_1 = 0, D_2 > 0$ ). Note that the “mean activation times” obtained from approximations introduced here are not intended to be compared quantitatively with the actual stochastic averages from Sec. III D but are rather aimed at gaining qualitative insight into the distinct mechanisms by which the two noise sources affect the activation process. To this end, we use the standard approach which consists in reducing the original dynamics, given by (1) with  $D_1$  or  $D_2$  set to zero, to an appropriate Langevin equation of the form  $dz = -U'(z)dt + \sqrt{2D}dW(t)$ , where  $U(z)$  denotes the effective potential.

If only  $D_1$  is present, one may conveniently exploit the sharp separation between the two characteristic time scales. The analysis is confined solely to the fast variable subsystem, which is first rewritten as

$$dx = -\frac{\partial U(x,y)}{\partial x}dt + \sqrt{2D_1}dW, \quad (7)$$

with  $U(x,y) = -\frac{1}{2}x^2 + \frac{1}{12}x^4 + xy$ . In the last expression for  $U$ ,  $y$  may simply be seen as a parameter, because the evolution of the  $y$  variable takes place on a time scale much slower than that of the  $x$  variable [30]. Another useful point is that  $U$  has the form of a double-well potential. Its two local minima, as well as the local maximum, correspond to  $x$  values which are the roots of the equation for the  $x$  nullcline  $x - \frac{1}{3}x^3 - y = 0$ . In particular, the local minima are given by the solutions  $x_1$  and  $x_3$  lying on the refractory and the spiking branch, respectively, while the local maximum coincides with the  $x_2$  solution on the unstable branch of the  $x$  nullcline [ $x_1(y) < x_2(y) < x_3(y)$ ]. Then the activation process may be interpreted as a jump from the well at the refractory branch to the one at the spiking branch, whereby the phase point has to overcome the potential barrier provided by the local maximum.

Given that  $U$  has a double-well shape, the escape time for a particle to jump from  $x_1(y)$  to a point near  $x_3(y)$  can be approximated by the well-known Kramers formula [31–33]  $T = \frac{2\pi}{\sqrt{|U''(x_2)|U''(x_1)}} e^{\{[U(x_2)-U(x_1)]/D_1\}}$ . In our case, one may fix the  $y = -2/3$  value, which corresponds to the minimum of the cubic nullcline. Having determined the appropriate  $x_1(-1)$  and  $x_2(-1)$ , we have obtained the dependence  $T(D_1)$  shown by the dashed line in Fig. 4. Naturally, given the crudeness of the introduced approximations, both in terms of system dynamics and the boundary conditions, the obtained  $T$  values should not be compared to the mean activation times for our activation problem.

The scenario where only  $D_2$  is present cannot be approached the same way as above, because  $y$  can no longer be treated as a parameter. Still, one may implement the adiabatic elimination of the fast variable to find the effective potential that influences the  $y$  dynamics. Though the roots of the equation describing the slow manifold  $y = x - \frac{1}{3}x^3$  may be used explicitly, the drawback is that such solutions are not easily handled analytically. In order to keep the

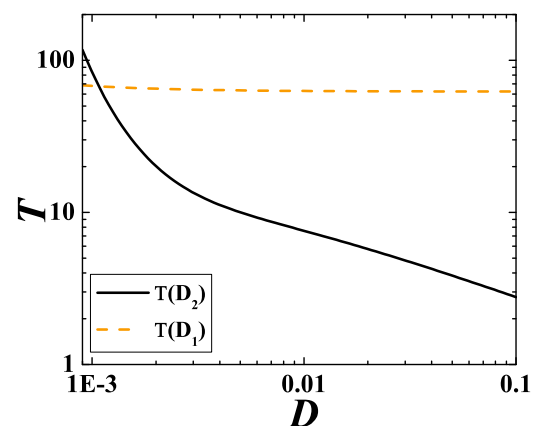


FIG. 4. (Color online) Assessing the impact of two distinct noise sources on the activation process of a single FHN unit. The curves refer to approximate dependencies of “activation times”  $T$  on  $D_1$  (dashed line) and  $D_2$  (solid line). Note that the introduced approximations are crude, so the results can only be considered in a qualitative fashion. Still, the two curves accurately predict that the activation process led by  $D_2$  is comparably faster than the one led by  $D_1$ .

subsequent form of effective potential analytically tractable, it is more convenient to approximate the relation between  $y$  and  $x$  in vicinity of the minimum of the cubic nullcline by a simple relation  $y(x) = y_m + \frac{1}{2}k(x - x_m)^2$ , where  $(x_m, y_m) = (-1, -2/3)$  refer to coordinates of the minimum. In other words, in proximity of the minimum, the cubic dependence has been replaced by a quadratic approximation. Note that  $k = -2x_m$  is determined by taking the second derivative of the equation for the  $x$  nullcline. From the expression for  $y(x)$ , one readily finds that  $x = x_m \pm \sqrt{y - y_m}$ , whereby the plus sign solution is relevant for our activation problem. It follows that the equation for the dynamics of  $y$  may be written as

$$dy = \epsilon(x_m + \sqrt{y - y_m} + b)dt + \sqrt{2D_2}dW, \quad (8)$$

such that the corresponding effective potential reads  $U = \epsilon(x_m + b)y + \frac{2}{3}\epsilon(y - y_m)^{3/2}$ .

Given that  $U$  is not a double-well potential, one cannot use the Kramers-like equation for the mean first-exit time. Instead, it is appropriate to use the general form

$$T = \frac{1}{D_2} \int_i^a du e^{U(u)/D_2} \int_r^u dv e^{-U(v)/D_2}, \quad (9)$$

derived from the Fokker-Planck approximation to a problem involving a single absorbing boundary  $a$  and a single reflecting boundary  $r$  [31–33]. Note that  $i$  in one of the integration limits refers to the injection point (initial location), which in our activation problem corresponds to the deterministic fixed point  $(x_{\text{eq}}, y_{\text{eq}}) = (-b, -b + b^3/3)$ . Regarding the reflecting boundary, it has often been found that the final results are not affected by its particular value [11,31], so  $r$  may readily be set to  $r \rightarrow -\infty$  to simplify the calculations. As for the absorbing boundary, it generally concerns the terminating point of the activation path and remains a free parameter that cannot be known *a priori*. Nevertheless, we may use the results for the MPAP solutions from Sec. III B and simply read the necessary coordinates of the terminating point ( $y = -0.308$ ), which illustrates the complementary nature of the methods applied. Note that the integrals such as the ones in Eq. (9) are typically resolved by introducing convenient approximations. In the particular case, we have used the approximate solution provided in Ref. [11]. The obtained curve  $T(D_2)$  is shown by the solid line in Fig. 4.

It has already explained that the results in Fig. 4 cannot be considered reliable in quantitative sense given the crudeness of the approximations involved. Still, certain qualitative insight have been gained. For instance, the analysis above indicates that the activation processes led by  $D_1$  or  $D_2$  have two considerably distinct backgrounds, whereby only the mechanism of the former may be interpreted in analogy to a jump over the barrier that separates two potential wells. Further, the curves in Fig. 4 turn out to be consistent with the general trend for a single FHN unit demonstrated in the next subsection, according to which the activation is more easily excited by  $D_2$  than  $D_1$ .

#### D. Statistical features of the activation process

The statistics of activation events is characterized in terms of the mean TFP  $\tau(D_1, D_2)$  and the associated coefficient of variation  $R(D_1, D_2)$ . The former is an average of TFPs for different stochastic realizations  $\tau(D_1, D_2) = \frac{1}{n_r} \sum_{i=1}^{n_r} \tau_i(D_1, D_2)$ .

The stochastic paths taken into account satisfy the specified boundary conditions, such that the trajectories emanate from the deterministic fixed point and terminate at the spiking branch of the cubic nullcline. The coefficient of variation is defined as the normalized variation of activation times [34]

$$R(D_1, D_2) = \frac{\sqrt{\langle \tau_i^2 \rangle - \langle \tau_i \rangle^2}}{\langle \tau_i \rangle}, \quad (10)$$

where  $\langle \cdot \rangle$  refers to averaging over an ensemble of stochastic realizations. Quantity  $R$  is intended to describe the regularity of the activation process, in the sense that the smaller  $R$  indicates that the TFPs deviate less from the mean value. Note that numerical simulations for all the considered setups are carried out by implementing the Euler integration scheme with the fixed time step  $\delta t = 0.002$ , having verified that no changes occur for smaller  $\delta t$ . All the results for the mean TFPs and the associated variances are obtained by averaging over an ensemble of 5000 different stochastic realizations of the activation process. In each realization, the initial conditions of a unit coincide with the deterministic fixed point.

The fields  $\tau(D_1, D_2)$  and  $R(D_1, D_2)$  for a single excitable unit are plotted in Figs. 5(a) and 5(b), respectively. The obtained profiles indicate that the mean TFPs are more sensitive to variation of  $D_1$ , whereas  $R$  shows strong dependence on  $D_2$ . Regarding the mean TFPs, one may distinguish three characteristic regimes, including (i) long TFPs, encountered for small  $D_1$  and  $D_2$ ; (ii) the plateau region, comprising intermediate  $D_1$  and intermediate to large  $D_2$  values; as well as (iii) short TFPs, found for large  $D_1$  irrespective of  $D_2$ .

Given that the considered stochastic process is influenced by two sources of noise, one finds that the transitions between the different regimes are gradual rather than sharp, whereby the “boundaries” are naturally smeared due to action of noise. Nevertheless, in terms of theory, it is reasonable and well justified to discuss the physical background giving rise to transitions between the different regimes. What we postulate is that the transition between the domains (i) and (ii) may qualitatively be accounted for by the fact that the excitable unit undergoes stochastic bifurcation induced by  $D_1$  and  $D_2$ . Note that the phenomenological stochastic bifurcation [35–38] we refer to corresponds to the noise-induced transition from the stochastically stable fixed point (stationary probability distribution  $P(x, y)$  focused around the fixed point) to the stochastically stable limit cycle (stationary probability distribution  $P(x, y)$  showing non-negligible contribution for  $(x, y)$  values along the spiking and the refractory branches of the  $x$  nullcline). Intuitively, one understands that the fixed point can be considered stochastically stable if the amplitude of fluctuations around the fixed point is of the order of noise intensity. By the same token, one may perceive a limit cycle as stochastically stable if the general structure involving two branches of the  $x$  nullcline (the spiking and the refractory branch) is preserved under the action of noise.

In support of associating the transition between the domains of large TFPs and the plateau region with the stochastic bifurcation, one may invoke the qualitative argument that, above the bifurcation, the attractive power of the fixed point is effectively no longer felt, in the sense that noise can drive the phase point away from equilibrium without meeting a

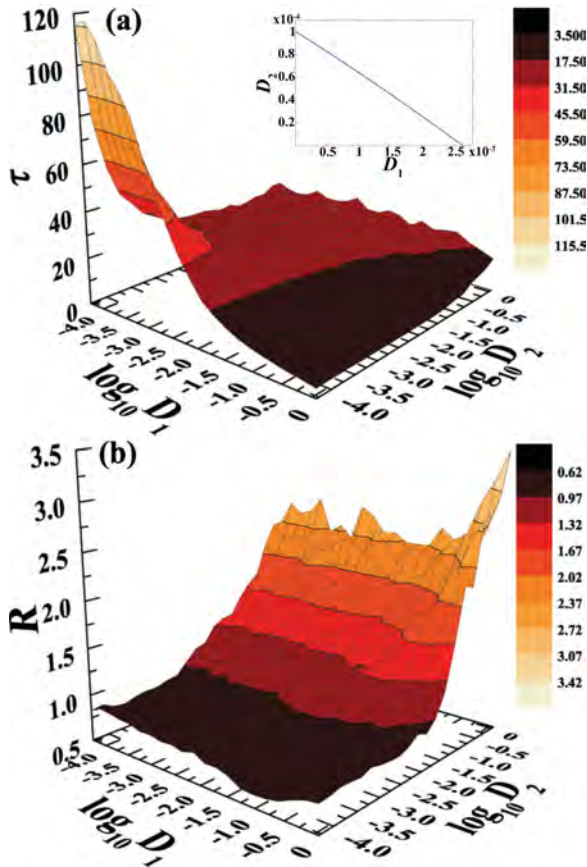


FIG. 5. (Color online) Statistical features of activation process influenced by  $D_1$  and  $D_2$ . In (a) is displayed how the mean TFPs  $\tau$  averaged over an ensemble of different stochastic realizations depend on  $D_1$  and  $D_2$ , whereas (b) concerns the associated coefficient of variation  $R(D_1, D_2)$ .  $\tau(D_1, D_2)$  exhibits three characteristic regimes of behavior, whereby the transition from the large values to the plateau region is found to qualitatively correspond to stochastic bifurcation from the stochastically stable fixed point to continuous oscillations. An indication on the noise intensities that give rise to stochastic bifurcation is provided in the inset of (a). The latter shows bifurcation curve  $D_2(D_1)$  obtained for the approximate model (11) of the original stochastic system (1).

strong opposing force. At the level of mean TFPs, this should be reflected as follows. Below the stochastic bifurcation, the mean TFPs are expected to be longer, while above the bifurcation they should substantially reduce and also become fairly insensitive to further increase of noise. In other words, once the fixed point becomes stochastically unstable, the gross effect of noise is the same because the fixed point holds no attractive power to resist its action.

Having established that the boundary between the domain of long TFPs and the plateau region in Fig. 5(a) should coincide with the  $(D_1, D_2)$  values that give rise to stochastic bifurcation, our next goal is to try to obtain these values analytically. To do so, we derive a deterministic model based on Gaussian approximation of the original system (1). According to Gaussian approximation, all the cumulants above the second order are assumed to vanish [39–41]. One is ultimately left with a set of five equations describing the dynamics of the first moments

$m_x(t) = E[x(t)]$  and  $m_y = E[y(t)]$ , the variances  $s_x(t) = E\{[x(t) - m_x(t)]^2\}$  and  $s_y(t) = E\{[y(t) - m_y(t)]^2\}$ , as well as the covariance  $u(t) = E\{[x(t) - m_x(t)][y(t) - m_y(t)]\}$ :

$$\begin{aligned} \dot{m}_x &= m_x - \frac{1}{3}m_x^3 - m_x s_x - m_y \\ \dot{m}_y &= \epsilon(m_x + b) \\ \dot{s}_x &= 2s_x(1 - m_x^2 - s_x) - 2u + 2D_1 \\ \dot{s}_y &= 2\epsilon u + 2D_2 \\ \dot{u} &= u(1 - m_x^2 - s_x) + \epsilon s_x - s_y. \end{aligned} \quad (11)$$

Note that the impact of noise in Eq. (11) is described only by the respective intensities  $D_1$  and  $D_2$ , which can then be treated as bifurcation parameters. In particular, the bifurcation analysis shows that the approximate model (11) displays direct supercritical Hopf bifurcation, which qualitatively accounts for the stochastic bifurcation exhibited by the excitable unit (1). The obtained bifurcation curve  $D_2(D_1)$ , plotted in the inset of Fig. 5(a), qualitatively characterizes the stochastic bifurcation exhibited by the excitable unit, and thereby accounts for the transition from the large values of mean TFPs to the plateau region.

Better understanding of the nature of the activation process behind the  $\tau$  and  $R$  dependencies from Figs. 5(a) and 5(b) may be gained by examining how the distribution of TFPs over an ensemble of different stochastic realizations changes under variation of  $D_1$  and  $D_2$ . Let us note first that even for a typical escape problem, such an issue has rarely been addressed in the literature and is difficult to approach analytically. In particular, for the distribution of first exit times in a typical escape problem, the only rigorous result so far has been found within the framework of large fluctuations theory [42]. It states that for the *sufficiently small* noise intensity, the distribution of the first exit times *asymptotically* acquires exponential form. If interpolated to the case of an excitable FHN unit, one should expect the latter statement to apply regardless of whether noise is added solely to the fast or the slow variable. Still, note that the mentioned result could concern only the extension of the escape problem to excitable systems, where the terminating boundary set would be given by the “ghost separatrix.” Recall that we have already explained the conceptual difference between such a problem and the activation problem we consider, where the focus exclusively lies with the spiking response of an excitable unit.

The characteristic examples illustrated in Fig. 6 suggest that the activation process dominated by  $D_2$  gives rise to the exponential distribution of TFPs, whereas the distributions generated by the prevailing  $D_1$  conform to Lorentzian-like profile with the cutoff at small TFP values. Regarding the former, one should emphasize that the exponential distribution of the interevent intervals is typically associated with the Poisson process [43], and it is indeed not unexpected to find an excitable unit under small amount of noise to act as a Poisson generator [11]. Nevertheless, an interesting finding is that the activation events led by  $D_1$  seem to be derived from some process other than the Poissonian, though the asymptotic distribution of TFPs is still exponential. Note that the qualitative distinction between the average effects of  $D_1$  and  $D_2$  has already been commented on in Sec. II A. The

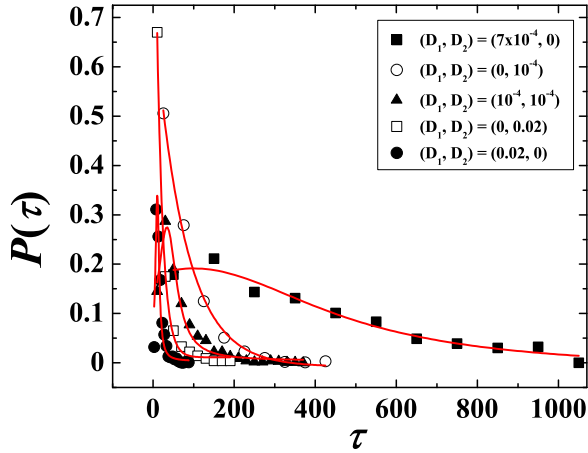


FIG. 6. (Color online) Impact of  $D_1$  and  $D_2$  on the distribution of TFPs  $P(\tau)$  obtained for an ensemble of different stochastic realizations.  $D_2$  alone typically gives rise to an exponential distribution of TFPs, which is consistent with the Poisson process. Under prevailing  $D_1$ , the distributions are found to conform to a unimodal, Lorentzian-like profile. The displayed examples refer to cases  $D_1 = 0.0007, D_2 = 0$  (solid squares);  $D_1 = 0.0001, D_2 = 0.0001$  (solid triangles);  $D_1 = 0.02, D_2 = 0$  (solid circles);  $D_1 = 0, D_2 = 0.0001$  (empty circles); and  $D_1 = 0, D_2 = 0.02$  (empty squares).

remark on the two distribution types holds if the leading noise term is much stronger than the remaining one. Nevertheless, while the validity of this statement is maintained even under substantial increase of  $D_1$  as the leading term, the analogous point for  $D_2$  applies up to a certain value, as explained below.

For  $(D_1, D_2)$  corresponding to the plateau from Fig. 5(a), one generally encounters the exponential distribution of TFPs or some of its modifications. In this context, note that the increase of  $R$  in Fig. 5(b) remains fairly slow, if it appears at all, for  $D_2$  values that warrant  $R < 1$ , but becomes steep once  $R$  passes 1 around  $D_2 \sim 10^{-2}$ . The approximate boundary at  $R = 1$  coincides with the coefficient of variation one obtains for the exponential distribution of TFPs. It is further found that the sufficiently large  $D_2$  values where  $R > 1$  give rise to a peculiar regime where the ensemble of activation events splits in two sharply distinct classes, such that the one with the small TFPs dominates, but the contribution from the events with large TFPs is non-negligible. The examples of stochastic activation paths for large  $D_2$ , including those with long TFPs, where the phase point rebounds onto the refractory branch of the  $x$  nullcline before the transition to spiking branch is triggered, are already provided in Fig. 3(b). Note that the intention there has been to illustrate the setup for which the analytical method of calculating the MPAPs fails.

#### IV. CASE OF TWO UNITS: MPAPS AND STATISTICAL PROPERTIES OF THE ACTIVATION PROCESS

In this section, we investigate how the form of coupling affects the first pulse emission process for two units subjected to external and internal noise. The first subsection is focused on the MPAPs obtained for the setups with linear or nonlinear

interactions, whereas the second subsection concerns the statistical features of the activation process.

##### A. Dependence of MPAPs on the form of coupling

The MPAPs are obtained by the numerical method presented in Sec. III A. Nevertheless, before proceeding with the results, we first consider what counts as a two-unit activation event by providing the appropriate boundary conditions. In terms of the initial conditions, the activation paths of units described by (2) or (3) begin at the equilibrium  $(x_{1,\text{eq}}, y_{1,\text{eq}}, x_{2,\text{eq}}, y_{2,\text{eq}}) = (-b, -b + b^3/3, -b, -b + b^3/3)$ . The terminating boundary conditions are specified in such a way that the phase points of *both* units should reach the spiking branch of their respective  $x_i$  nullclines. This definition implies that the time-to-first pulse for a couple of units is determined by the slower-firing unit. Note that the profile of the spiking branch for a coupled unit is quite similar to that of a single unit, which can readily be verified. In particular, for the given unit one may approximate the  $x$  coordinate of the other unit within the coupling term by its value at the deterministic fixed point, around which the actual values fluctuate for most of the time.

Regarding the coupling strengths, note that we are interested only in  $c$  values that are subcritical with respect to Hopf bifurcation, viz.  $c$  is always set so the deterministic versions of (2) or (3) admit the locally stable fixed point. This is consistent with the goal to examine the *noise-driven* first pulse emission process and the fashion in which it is modified by the presence of coupling. The fact that the  $c$  values are subcritical also implies that, in the deterministic case, the large excitation of one unit (initial conditions far from equilibrium) cannot induce a spiking response of the other unit which lies at equilibrium. One should point out that the adopted formulation of the activation problem for two units is by far more appropriate than the alternatives, including the one cast in terms of the average variables  $(x_1 + x_2)/2$  and  $(y_1 + y_2)/2$ . Without stating the details, we note that the latter approach would have several drawbacks. On one hand, the dynamics associated to synchronization would smear the physical picture relevant for the activation problem, whereas, on the other hand, there would be no immediate generalization from the case of a single unit to the setups with two units.

Now let us focus on the scenario where two excitable units interact via linear couplings. The symmetry of interactions is reflected in the point that the MPAP trajectories are identical for both units. This is corroborated in Fig. 7(a), which shows as an example the respective MPAPs of the two units (solid and open squares) for the characteristic ratio  $r_x : r_y = 1 : 1$  at small  $D$  substantially below the stochastic bifurcation. Several realizations of the first pulse emission process are plotted to demonstrate the clustering around the MPAP. The approximate matching between the units' most likely trajectories is found to persist for all  $(r_x, r_y)$  characteristic setups. The changes of the MPAP profile under increasing noise intensity  $D$  are illustrated in the inset of Fig. 7(a). It has already been mentioned that, depending on  $c$ , the units coupled in a linear fashion may display two different regimes where the fixed point is stable. These regimes have been referred to as excitability

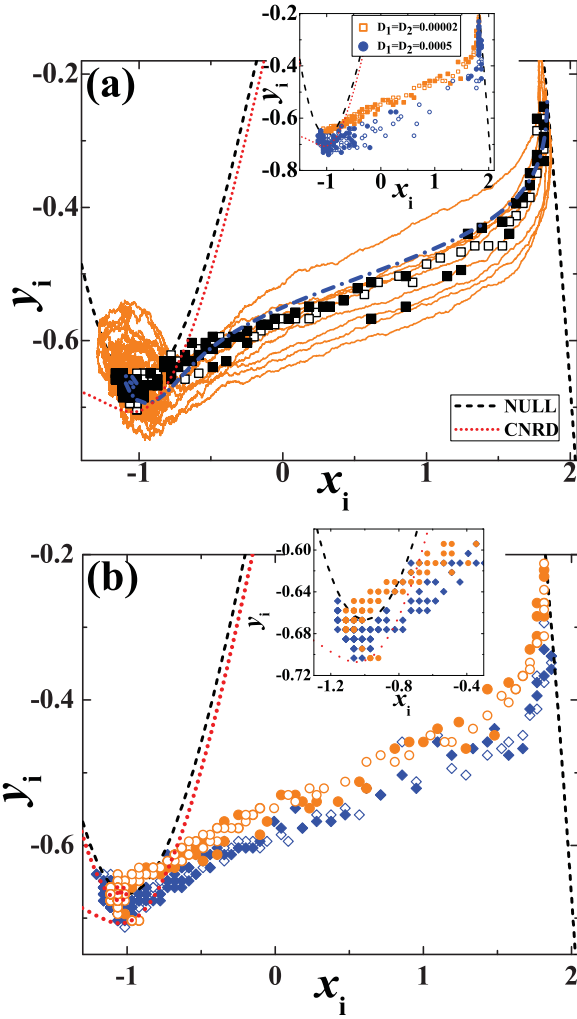


FIG. 7. (Color online) MPAPs for two coupled units. In (a) are displayed the MPAPs for two units (open and solid squares) interacting via linear couplings of subcritical strength  $c = 0.04$ . The solid lines denote 10 sample paths corresponding to the process of first pulse emission. The results are obtained for  $r_x : r_y = 1 : 1$  and  $D = 0.00005$ . The dash-dotted line indicates the trajectory generated by the extended system (12). In the inset are shown the MPAPs for the same characteristic ratio and noise intensities  $D = 0.00002$  (squares) and  $D = 0.0005$  (circles). Panel (b) provides a comparison between the MPAPs obtained for linear (open and solid circles) and nonlinear interactions (open and solid diamonds). In the latter case, the subcritical coupling strength is  $c = 0.07$ , while the noise parameters are the same as in (a). In the inset is shown the enlarged view of the portion of phase space before the CNRD.

proper and generalized excitability, whereby the latter involves coexistence between the stable fixed point and the stable limit cycle created in a global fold-cycle bifurcation. Comparing the cases where  $c$  is sub- or supercritical with respect to global bifurcation, we have established that for small but finite  $D$  the profile of MPAPs for all three characteristic ratios  $r_x/r_y$  does not appear to show significant differences.

As in case of a single unit, we make a brief remark regarding the trajectories generated by the effective set of Hamiltonian equations. Compared to (6), the equations for the dynamics of the extended system are modified to include the interaction

terms

$$\begin{aligned} \frac{dx_i}{dt} &= x_i - x_i^3/3 - y_i + r_x p_{x,i} + c(x_i - x_j) \\ \frac{dy_i}{dt} &= \epsilon(x_i + b) + r_y p_{y,i} \\ \frac{dp_{x,i}}{dt} &= -(1 - x_i^2)p_{x,i} - \epsilon p_{y,i} + c p_{x,j} \\ \frac{dp_{y,i}}{dt} &= p_{x,i}, \end{aligned} \quad (12)$$

whereby  $i, j \in \{1, 2\}, i \neq j$  denote the units' indices. The numerical treatment of the above system again involves integration for the initial conditions set on the unstable manifold of the saddle point. In particular, in configuration subspace one chooses the initial values  $(x_i, y_i)$  that lie on a four-dimensional sphere of a very small radius, which encloses the deterministic fixed point  $(x_{1,\text{eq}}, y_{1,\text{eq}}, x_{2,\text{eq}}, y_{2,\text{eq}})$ . Naturally, the points located on a four-dimensional sphere are parametrized with three independent angular variables. The initial values of the generalized momenta are then obtained using the prescription provided in Ref. [24]. An interesting finding is that the trajectories of the extended system, selected by the rule described in Sec. III A, again closely match the numerically obtained MPAPs, cf. the dotted line in Fig. 7(a). This striking similarity further evinces that the theory in the spirit of the Hamiltonian approach may potentially be derived for the problem of first pulse emission.

An issue that needs to be addressed is whether and how sensitive the topological features of the MPAPs are with respect to the linear or nonlinear form of coupling. The comparison is facilitated in Fig. 7(b), where the corresponding MPAPs for the scenarios with linear (circles) and nonlinear interactions (diamonds) are plotted together. The data shown are obtained for the same  $D_1$  and  $D_2$ , whereas the coupling strengths are analogous in terms of distance from the Hopf bifurcation. The trajectories corresponding to the different units for the same system configuration are distinguished by the solid and open symbols. Note that in case of nonlinear interactions, there is no symmetry to warrant that the respective MPAPs of the two units would be identical for arbitrary values of external and internal noise. It turns out that the MPAPs are approximately identical for intermediate  $D$  sufficiently below the stochastic bifurcation. Nevertheless, we have also found that the spread of the MPAPs in case of nonlinear couplings increases with  $D$ . As for the effects of linear versus nonlinear interactions, one observes significant differences in the profiles of MPAPs within the initiation region, which is shown enlarged in the inset of Fig. 7(b). Also note that the MPAPs of the interacting units substantially depart from what is found in case of a single unit, cf. Figs. 2 and 3.

## B. Statistical properties of the activation process for coupled units

Here we consider two types of numerical results, one referring to the two-unit activation events and the other concerning the correlation between the activation events on individual units. Recall that the ‘‘compound’’ activation event



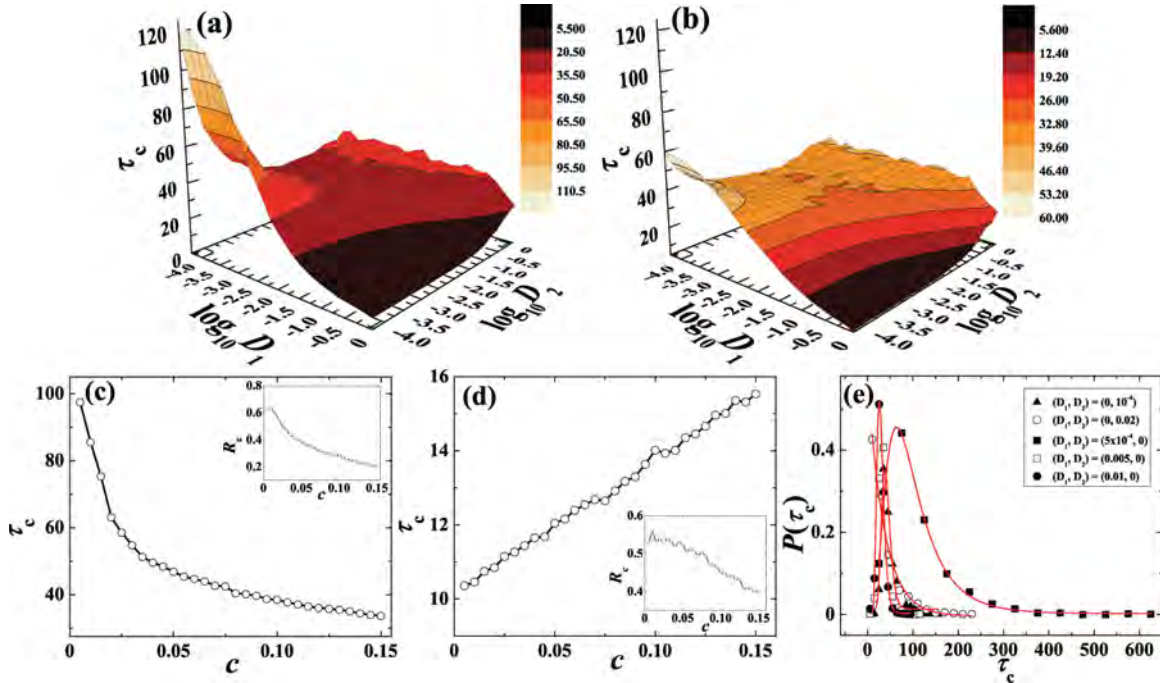


FIG. 8. (Color online) Statistical properties of activation process for two units interacting via linear couplings. Panels (a) and (b) refer to mean TFPs  $\tau_c(D_1, D_2)$  in a strongly subcritical ( $c = 0.01$ ) and a weakly subcritical regime ( $c = 0.04$ ), respectively. Note that the definition of the two-unit activation event requires that the phase points of both units have reached the appropriate terminating boundary set. Panels (c) and (d) show how  $\tau_c$  (main frames) and  $R_c$  (insets) behave under increasing  $c$ . The noise intensities  $(D_1, D_2) = (0.00014, 0.0008)$  fixed in (c) are representative for the domain of large TFPs from (a), whereas (d) is obtained for  $(D_1, D_2) = (0.154, 0.0002)$ , the values corresponding to the plateau region in (a). In panel (e) is demonstrated how the distributions of TFPs over different stochastic realizations vary with  $D_1$  and  $D_2$ . Note that the unimodal distribution profile is preferred over the exponential form. The data are obtained for  $D_1 = 0, D_2 = 0.0001$  (solid triangles);  $D_1 = 0.0005, D_2 = 0$  (solid squares);  $D_1 = 0.01, D_2 = 0$  (solid circles);  $D_1 = 0, D_2 = 0.02$  (empty circles); and  $D_1 = 0.005, D_2 = 0$  (empty squares).

for a couple of units requires that the phase points of both units have reached the spiking branch of the appropriate  $x_i$  nullcline, consistent with the definition adopted in Sec. IV A. Adhering to this, we have calculated the mean TFPs  $\tau_c(D_1, D_2)$  and the associated coefficients of variation  $R_c(D_1, D_2)$  for the scenarios with the linear or the nonlinear couplings, further examining how the results are changed under variation of  $c$ . Though  $c$  is always selected to lie below the Hopf threshold, in the latter context one may still distinguish between the strongly and the weakly subcritical regimes.

In terms of whether the mere form of coupling affects the statistical features of the activation process, it may be shown that the fields  $\tau_c$  and  $R_c$  exhibit qualitatively analogous dependencies for the linear and the nonlinear interactions. It is further found that the behavior of mean TFPs is in several aspects different to that of a single unit, whereas the corresponding coefficient of variation  $R_c$  is only marginally dependent on  $c$ , displaying the “universal” behavior qualitatively similar to the one in Fig. 5(b). As an example of how the properties of activation process change with  $c$ , in Figs. 8(a) and 8(b) are illustrated the respective fields  $\tau_c(D_1, D_2)$  for the strongly and weakly subcritical regimes in case of the linear coupling. Both plots corroborate the existence of the three typical regimes already indicated in reference to Fig. 5(a), though one no longer speaks of stochastic bifurcation in vicinity of the Hopf bifurcation controlled by  $b$  but rather of the one induced by the coupling strength.

Nevertheless, several differences due to presence of coupling should be noted. First, as  $c$  is increased, the mean TFPs for small noise intensities (below the stochastic bifurcation) become shorter, see Fig. 8(c). Also, at small noise intensities the activation times  $\tau_c$  of the couple are reduced when compared to the case of a single unit. However, for intermediate  $D_1$  and  $D_2$  corresponding to the plateau region, the mean TFPs for the pair are larger than those found for a single unit. More importantly, the average activation times in this region seem to increase as  $c$  rises, see Fig. 8(d). One may in fact discern a general trend that the differences between the three characteristic regions are gradually washed out as  $c$  is enhanced, which is manifested even more once  $c$  is supercritical. This is to be expected in the latter case, given that the activation process then becomes primarily deterministic, viz. it is only perturbed by the noise terms. Note that in all the three characteristic regimes the corresponding coefficients of variation are seen to reduce with  $c$ , cf. the insets in Figs. 8(c) and 8(d). The final remark on the impact of coupling is that the region with small mean TFPs apparently decreases with  $c$ .

We have further examined how the distribution of activation events over different stochastic realizations depends on the form and strength of coupling. One may state that the general conclusions reached in case of a single unit, cf. Fig. 6, persist for the activation events of coupled units, though the physical picture is more perturbed for the scenario with the linear than the nonlinear interactions. Recall that for a single unit, only

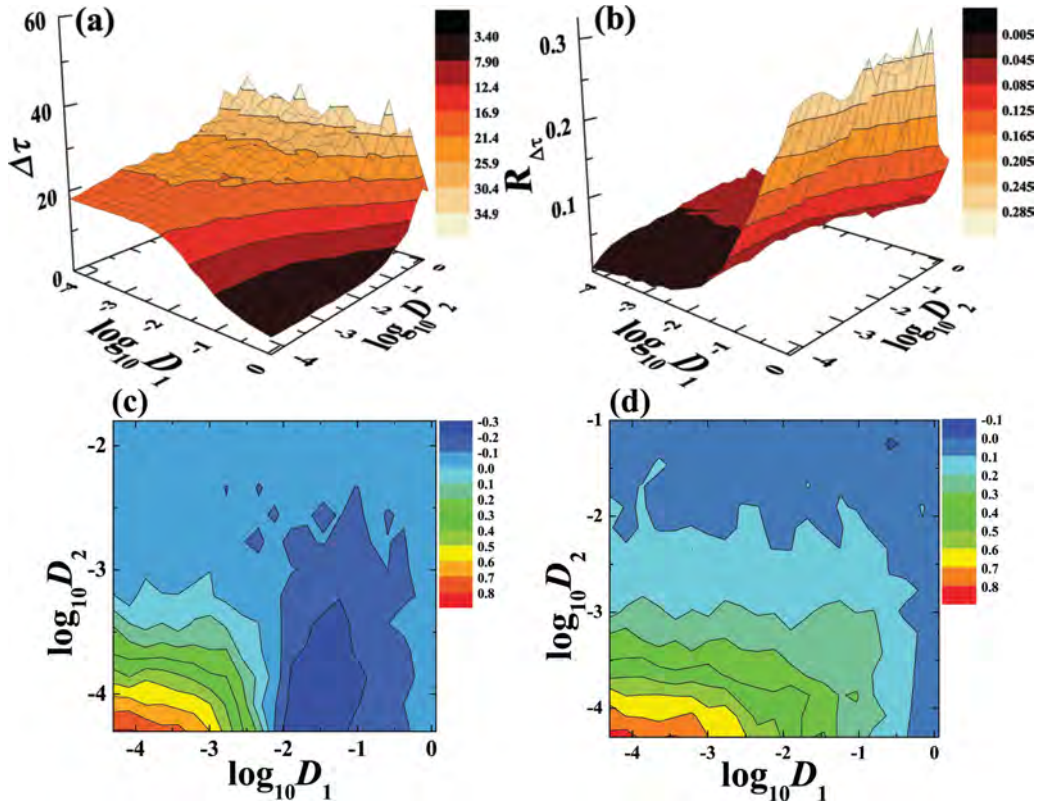


FIG. 9. (Color online) Relationship between TFPs of individual units making up the pair. In panels (a) and (b) are plotted the differences in mean TFPs  $\Delta\tau(D_1, D_2)$  and the associated coefficients of variation  $R_{\Delta\tau}(D_1, D_2)$ , respectively. The data are obtained for the linear couplings of strength  $c = 0.04$ , and similar results are found for the setup with nonlinear interactions. Panels (c) and (d) show the correlation coefficients  $\rho(D_1, D_2)$  between the TFPs for the different stochastic realizations in cases of linear ( $c = 0.04$ ) and nonlinear interactions ( $c = 0.06$ ), respectively.

the external noise has been found to induce deviations from the typical exponential distribution of events. For the scenario involving the nonlinear coupling, there may be more noise domains admitting some distribution other than exponential, but the latter still constitutes the prevailing form of behavior. However, under linear interactions, it turns out that both  $D_1$  and  $D_2$  may give rise to a form of TFP distribution completely absent in case of a single unit. The particular form is unimodal and is numerically best approximated by the lognormal profile, cf. Fig. 8(e). One cannot suspect on the type of activation process producing such a distribution, though the explanation on why it is different from both the scenarios with a single unit and two units interacting in a nonlinear fashion likely has to take into account the existence of global bifurcation [44].

As far as the effects of coupling strength are concerned, the TFP distributions typically become narrower as  $c$  approaches the critical value, viz. the tail at longer activation times is reduced compared to an uncoupled unit for the same  $(D_1, D_2)$ . This point holds independent of the linear or nonlinear form of coupling. Thus, one may state that the impact of stronger coupling is expectedly reflected in the decrease of fraction of the longer individual activation events.

The final point we address concerns the relation between the individual activation processes on the units making up the pair. This issue may be approached from two angles, either by examining the mean difference in the single unit TFPs or by analyzing the correlation between the individual

activation events. On the former point, we introduce a measure of coherence between the individual activation events averaged over an ensemble of  $n_r$  different stochastic realizations,  $\Delta\tau = \frac{1}{n_r} \sum_{k=1}^{n_r} |\tau_{k,1} - \tau_{k,2}|$ , as well as the associated coefficient of variation  $R_{\Delta\tau}$ .  $\Delta\tau(D_1, D_2)$  is intended to describe the net effect of how much the interaction is able to enforce matching between the activation times of noise-driven units. To understand the relevance of this, one should recall that the coherence of the first units' responses is an issue quite distinct from that of asymptotic synchronization between the spiking series.

In Figs. 9(a) and 9(b) are plotted the dependencies  $\Delta\tau(D_1, D_2)$  and  $R_{\Delta\tau}(D_1, D_2)$  for the case of two units interacting via linear couplings, but qualitatively similar results are found for the nonlinear interactions as well. From Fig. 9(a) one learns of a general tendency for the mean difference to increase with the internal noise. For smaller fixed  $D_2$ , the spread of individual TFPs reduces under the action of external noise, but such an effect is lost once  $D_2$  overwhelms the system dynamics. Note that for large internal noise  $\Delta\tau$  becomes comparable to  $\tau_c$  for the coupled units, which suggests a typical scenario where the activation process of one unit is rapid, whereas the pulse emission of the other unit is substantially delayed. Naturally, for the  $(D_1, D_2)$  domain supporting small  $\tau_c$ , the  $\Delta\tau$  dependence tells us that both the units emit pulses virtually at the same time. Regarding Fig. 9(b), the gross effect is that the variation of the difference of single unit TFPs shows

a steep increase above some “threshold” external noise, whose value becomes larger as  $D_2$  is enhanced. Similar dependence is found for the nonlinear interactions, but with the reverse roles of  $D_1$  and  $D_2$ .

Next we examine the correlation of individual activation times for units comprising the pair. The correlation is quantified by the correlation coefficient between the times-to-first-pulses of single units  $\rho = \frac{\langle \tau_{k,1} \tau_{k,2} \rangle - \langle \tau_{k,1} \rangle \langle \tau_{k,2} \rangle}{\sqrt{\langle \tau_{k,1}^2 \rangle - \langle \tau_{k,1} \rangle^2} \sqrt{\langle \tau_{k,2}^2 \rangle - \langle \tau_{k,2} \rangle^2}}$ , where the angled brackets denote averaging over an ensemble of different stochastic realizations. The fields  $\rho(D_1, D_2)$  for the setups with the linear and nonlinear interactions are shown in Figs. 9(c) and 9(d), respectively. A common ingredient in both cases is that there exists a certain value of  $D_2$ , above which the noise effects prevail. There the first-time pulses are neither correlated nor anticorrelated, viz. the correlation coefficient lies around zero. However, for smaller  $D_2$ , the correlation between the individual activation events substantially depends on the form of coupling. For linear interactions, small  $D_1$  then facilitates strong correlation, whereas for larger  $D_1$  the TFPs become significantly anticorrelated. On the other hand, for the nonlinear couplings  $\rho$  displays a more homogeneous dependence on  $D_1$  and  $D_2$ . In fact, the correlation is strong for small noise intensities, and it reduces with the increase of both  $D_1$  and  $D_2$ , whereby the rate of decline depends more on  $D_2$  than  $D_1$ .

As an interesting remark for future study, we indicate a potential link between the form of correlation of the single unit TFPs and the synchronization state of the stochastic units’ time series [45–52] under the given parameter set. In particular, note that in case of linear interactions the time series of two units display a constant phase shift for small  $D_1$ , which coincides with the domain where the TFPs are correlated. Nonetheless, the time series show phase slips and amplitude fluctuations for larger  $D_1$ , where the activation times are uncorrelated or anticorrelated. In a similar fashion, for the nonlinear coupling one typically encounters in-phase synchronization, at least for sufficiently small  $D_1$ , precisely where the TFPs are correlated. These arguments suggest that the approximately constant phase shift in the ensuing time series should imply a strong correlation between the TFPs of individual units. In other words, the ordering effect of coupling can make an impact on the activation processes of units in a fashion similar to what is found for long time asymptotic processes, such as synchronization between the unit’s time series.

## V. CONCLUSIONS

We have analyzed the noise-driven first-pulse emission process for a single and two interacting type II excitable units where both the fast and the slow variable are influenced by stochastic perturbations. Our results concern two main issues: (i) determining the MPAPs around which the stochastic activation paths are clustered and (ii) examining in detail the effects of two different noise sources on the statistical features of the activation process, further demonstrating how the statistics is modified due to linear or nonlinear form of interactions. For both issues, we have highlighted the impact of stochastic bifurcation, which underlies the transition from stochastically stable fixed point to stochastically stable limit cycle.

Since the study is focused on the process of first-pulse emission, one of the requirements has been to provide a clear-cut distinction between the spiking responses and the small-amplitude excitations. This has been achieved by introducing an appropriate terminating boundary set, given by the spiking branch of the cubic nullcline. Note that our problem setup differs from the earlier numerical studies on pulse triggering, which have introduced the terminating boundary as a fixed threshold [16,17], as well as the recent study on a single FHN unit [15], where the ghost separatrix has been used as a terminating boundary within the generalized escape problem. The advantages of our approach lie in that the terminating boundary is analytically tractable, while the adopted formulation further facilitates an immediate generalization of the activation problem from the case of a single unit to different scenarios with two interacting units. The differences in the event statistics between the three mentioned problem setups may depend on the system parameters  $b$  and  $\epsilon$ , as well as the noise intensities.

Regarding point (i), it has been established that the topological features of the MPAPs qualitatively depend on which type of noise affects the system dynamics. This has been demonstrated by examining the MPAPs obtained for three characteristic ratios of external versus internal noise, reflecting the scenarios where a particular noise source or both sources are present. For the fixed characteristic ratio, the MPAP profiles change under increasing noise intensity. The changes become apparent as one approaches the noise values that give rise to stochastic bifurcation. In case of two coupled units, we have shown that the topology of MPAPs is substantially affected by the linear or nonlinear form of interactions. For the linear couplings, the respective MPAPs of the two units are identical, whereby the solution lies comparably close to that of an uncoupled unit under the analogous parameter set. For the nonlinear couplings, the MPAPs of two units may become visibly asymmetrical, depending on the noise intensity. While discussing the topological features of the MPAPs, we have also indicated a somewhat surprising numerical finding that the trajectories of the effective set of Hamiltonian equations selected according to a given predefined rule may show striking similarity to the MPAP profiles for scenarios involving both a single and two coupled FHN units. This observation requires a more elaborate study and suggests that a systematic theory possibly adopting certain elements of the standard Hamiltonian approach to escape problems may potentially be derived for the problem of first pulse emission.

Concerning point (ii), the statistical properties of the first-pulse emission process have been characterized by the dependencies of the mean TFPs and the associated coefficients of variation on  $D_1$  and  $D_2$ . Note that the previous work on FHN model has focused on statistics of first exit times in presence of a single noise source [11,16,17], which has typically led to the well-known Kramers result [31] or its modifications [11]. Compared to our approach, the treatment in Refs. [16,17] is simplified in terms of definition of the considered quantities and with respect to the terminating boundary conditions. An important novel result is that  $\tau$  and  $R$  show nearly universal dependence on  $D_1$  and  $D_2$  for a single unit, as well as for two interacting units. In particular, the mean TFPs are found to display three characteristic regimes, whereby the transition

from the domain of large  $\tau$  values to the plateau region can qualitatively be attributed to the stochastic bifurcation. We have determined the noise intensities that give rise to stochastic bifurcation by introducing the model (11) based on a Gaussian approximation for the dynamics of a stochastic FHN unit. By carrying out the bifurcation analysis of the approximate model, we have obtained the Hopf bifurcation curve  $D_2(D_1)$  which qualitatively outlines the stochastic bifurcation of the exact system. In case of two units, the impact of stochastic bifurcation has been found to depend on the form of coupling.

We have further examined the distributions of TFPs over an ensemble of different stochastic realizations under fixed  $(D_1, D_2)$ . So far, little has been known about the profile of corresponding distributions even for a typical escape problem. In fact, the only available analytical result, derived from the theory of large fluctuations, indicates that the exit time distribution for the escape problem asymptotically acquires exponential form [42]. However, the problem of first pulse emission conceptually differs from the typical escape problem, whereas the noise intensities we consider are small but finite. Still, in case of a single unit, we find exponential distribution of TFPs under prevailing  $D_2$ , which is consistent with the Poissonian process. However, the activation process dominated by  $D_1$  yields a different distribution which shows a unimodal, Lorentzian-like profile. For the interacting units, the profile of TFP distribution is further influenced by the form of coupling.

Apart from the TFP distribution, the form of coupling affects the correlation of individual activation events in a nontrivial fashion. As a qualitative explanation, in Sec. IV B we have suggested a link between the correlation of individual activation events and the synchronization features of the time series for the given parameter set. In this context, the future research should set the ground for potential application of the theory of large fluctuations to the research of stochastic synchronization in excitable systems.

This study has shown how the analysis of activation process may be extended from a single excitable unit to different instances of two interacting units. In a forthcoming paper [21], our goal will be to examine the noise-driven first pulse emission process in an assembly of excitable units, focusing on whether such an assembly may be considered a macroscopic excitable element, and, if so, what may be the analogies and differences compared to the excitable behavior of a single unit.

#### ACKNOWLEDGMENTS

This work was supported by the Ministry of Education, Science and Technological Development of the Republic of Serbia, under Project No. 171017. M.P. acknowledges support from the Slovenian Research Agency (Grant No. P5-0027) and from the Deanship of Scientific Research, King Abdulaziz University (Grant No. 76-130-35-HiCi).

- 
- [1] E. M. Izhikevich, *Dynamical Systems in Neuroscience: The Geometry of Excitability and Bursting* (MIT Press, Cambridge MA, 2007).
- [2] J. White, J. Rubinstein, and A. Kay, *Trends Neurosci.* **23**, 131 (2000).
- [3] W.-Y. Chiang, P.-Y. Lai, and C. K. Chan, *Phys. Rev. Lett.* **106**, 254102 (2011).
- [4] A. M. Yacomotti, P. Monnier, F. Raineri, B. B. Bakir, C. Seassal, R. Raj, and J. A. Levenson, *Phys. Rev. Lett.* **97**, 143904 (2006).
- [5] M. A. Larotonda, A. Hnilo, J. M. Mendez, and A. M. Yacomotti, *Phys. Rev. A* **65**, 033812 (2002).
- [6] M. Brunstein, A. M. Yacomotti, I. Sagnes, F. Raineri, L. Bigot, and A. Levenson, *Phys. Rev. A* **85**, 031803 (2012).
- [7] B. Lindner, J. Garcia-Ojalvo, A. Neiman, and L. Schimansky-Geier, *Phys. Rep.* **392**, 321 (2004).
- [8] S. Wiggins, *Introduction to Applied Nonlinear Dynamical Systems and Chaos*, 2nd ed. (Springer, New York, 2000).
- [9] A. Destexhe and M. Rudolph-Lilith, *Neuronal Noise* (Springer, New York, 2012).
- [10] J. W. Shuai and P. Jung, *Phys. Rev. Lett.* **88**, 068102 (2002).
- [11] R. C. Hilborn and R. J. Erwin, *Phys. Rev. E* **72**, 031112 (2005).
- [12] R. S. Maier and D. L. Stein, *Phys. Rev. Lett.* **69**, 3691 (1992).
- [13] R. S. Maier and D. L. Stein, *J. Stat. Phys.* **83**, 291 (1996).
- [14] M. I. Dykman, D. G. Luchinsky, P. V. E. McClintock, and V. N. Smelyanskiy, *Phys. Rev. Lett.* **77**, 5229 (1996).
- [15] I. A. Khovanov, A. V. Polovinkin, D. G. Luchinsky, and P. V. E. McClintock, *Phys. Rev. E* **87**, 032116 (2013).
- [16] E. V. Pankratova, A. V. Polovinkin, and B. Spagnolo, *Phys. Lett. A* **344**, 43 (2005).
- [17] E. V. Pankratova, A. V. Polovinkin, and E. Mosekilde, *Eur. Phys. J. B* **45**, 391 (2005).
- [18] S. Kadar, J. Wang, and K. Showalter, *Nature* **391**, 770 (1998).
- [19] M. Krupa and P. Szmolyan, *SIAM J. Math. Anal.* **33**, 286 (2001).
- [20] I. Bashkirtseva and L. Ryashko, *Phys. Rev. E* **83**, 061109 (2011).
- [21] I. Franović, M. Perc, K. Todorović, S. Kostić, and N. Burić, *Phys. Rev. E* **92**, 062912 (2015).
- [22] M. I. Dykman, P. V. E. McClintock, V. N. Smelyanski, N. D. Stein, and N. G. Stocks, *Phys. Rev. Lett.* **68**, 2718 (1992).
- [23] J. M. Newby, P. C. Bressloff, and J. P. Keener, *Phys. Rev. Lett.* **111**, 128101 (2013).
- [24] S. Beri, R. Mannella, D. G. Luchinsky, A. N. Silchenko, and P. V. E. McClintock, *Phys. Rev. E* **72**, 036131 (2005).
- [25] V. N. Smelyanskiy, M. I. Dykman, and B. Golding, *Phys. Rev. Lett.* **82**, 3193 (1999).
- [26] R. S. Maier and D. L. Stein, *Phys. Rev. Lett.* **86**, 3942 (2001).
- [27] M. I. Freidlin and A. D. Wentzell, *Random Perturbations of Dynamical Systems*, 3rd ed. (Springer-Verlag, Berlin, 2012).
- [28] N. G. Stocks, N. D. Stein, H. E. Short, R. Mannella, D. G. Luchinsky, and P. V. E. McClintock, in *Fluctuations and Order: The New Synthesis* (Springer, Berlin, 1996), pp. 53–67.
- [29] E. Hunsberger, M. Scott, and C. Eliasmith, *Neural Comput.* **26**, 1600 (2014).
- [30] R. E. Lee DeVille, E. Vanden-Eijnden, and C. B. Muratov, *Phys. Rev. E* **72**, 031105 (2005).
- [31] C. W. Gardiner, *Handbook of Stochastic Methods for Physics, Chemistry and the Natural Sciences*, 3rd ed. (Springer-Verlag, Berlin, 2004).

- [32] H. Risken, *The Fokker-Planck Equation*, 2nd ed. (Springer-Verlag, Berlin, 1989).
- [33] W. Paul and J. Baschnagel, *Stochastic Processes: From Physics to Finance*, 2nd ed. (Springer, Heidelberg, 2013).
- [34] A. S. Pikovsky and J. Kurths, *Phys. Rev. Lett.* **78**, 775 (1997).
- [35] L. Arnold, *Random Dynamical Systems* (Springer Verlag, Berlin, 1999).
- [36] J. A. Acebrón, A. R. Bulsara, and W.-J. Rappel, *Phys. Rev. E* **69**, 026202 (2004).
- [37] M. Gaudreault, F. Lépine, and J. Viñals, *Phys. Rev. E* **80**, 061920 (2009).
- [38] M. Gaudreault, J. M. Berbert, and J. Viñals, *Phys. Rev. E* **83**, 011903 (2011).
- [39] S. Tanabe and K. Pakdaman, *Phys. Rev. E* **63**, 031911 (2001).
- [40] I. Franović, K. Todorović, N. Vasović, and N. Burić, *Phys. Rev. E* **87**, 012922 (2013).
- [41] N. Burić, D. Ranković, K. Todorović, and N. Vasović, *Physica A* **389**, 3956 (2010).
- [42] M. V. Day, *J. Math. Anal. Appl.* **147**, 134 (1983).
- [43] P. Dayan and L. F. Abbott, *Theoretical Neuroscience: Computational and Mathematical Modeling of Neural Systems* (MIT Press, Cambridge, MA, 2001).
- [44] C. Laing and G. J. Lord (eds.), *Stochastic Methods in Neuroscience* (Oxford University Press, New York, 2010).
- [45] A. Balanov, N. Janson, D. Postnov, and O. Sosnovtseva, *Synchronization: From Simple to Complex* (Springer-Verlag, Berlin, 2009), pp. 239–258.
- [46] S. K. Han, T. G. Yim, D. E. Postnov, and O. V. Sosnovtseva, *Phys. Rev. Lett.* **83**, 1771 (1999).
- [47] C. Zhou, J. Kurths, and B. Hu, *Phys. Rev. E* **67**, 030101(R) (2003).
- [48] A. Neiman, *Phys. Rev. E* **49**, 3484 (1994).
- [49] B. Hu and C. Zhou, *Phys. Rev. E* **63**, 026201 (2001).
- [50] H. Henry and H. Levine, *Phys. Rev. E* **68**, 031914 (2003).
- [51] M. Perc, *Phys. Rev. E* **72**, 016207 (2005).
- [52] M. Perc, *Phys. Rev. E* **76**, 066203 (2007).



## OPEN

## Triggered dynamics in a model of different fault creep regimes

## SUBJECT AREAS:

GEOPHYSICS

NONLINEAR PHENOMENA

STATISTICAL PHYSICS

Srđan Kostić<sup>1</sup>, Igor Franović<sup>2</sup>, Matjaž Perc<sup>3,6</sup>, Nebojša Vasović<sup>4</sup> & Kristina Todorović<sup>5</sup>

<sup>1</sup>Department of Geology, University of Belgrade, Faculty of Mining and Geology, Serbia, <sup>2</sup>Scientific Computing Lab., Institute of Physics, University of Belgrade, PO Box 68, 11080 Beograd-Zemun, Serbia, <sup>3</sup>Department of Physics, Faculty of Natural Sciences and Mathematics, University of Maribor, Slovenia, <sup>4</sup>Department of Applied Mathematics, University of Belgrade, Faculty of Mining and Geology, Serbia, <sup>5</sup>Department of Physics and Mathematics, University of Belgrade, Faculty of Pharmacy, Serbia, <sup>6</sup>Faculty of Science, King Abdulaziz University, Jeddah, Saudi Arabia.

Received  
3 March 2014Accepted  
3 June 2014Published  
23 June 2014

Correspondence and requests for materials should be addressed to M.P. (matjaz.perc@uni-mb.si)

The study is focused on the effect of transient external force induced by a passing seismic wave on fault motion in different creep regimes. Displacement along the fault is represented by the movement of a spring-block model, whereby the uniform and oscillatory motion correspond to the fault dynamics in post-seismic and inter-seismic creep regime, respectively. The effect of the external force is introduced as a change of block acceleration in the form of a sine wave scaled by an exponential pulse. Model dynamics is examined for variable parameters of the induced acceleration changes in reference to periodic oscillations of the unperturbed system above the supercritical Hopf bifurcation curve. The analysis indicates the occurrence of weak irregular oscillations if external force acts in the post-seismic creep regime. When fault motion is exposed to external force in the inter-seismic creep regime, one finds the transition to quasiperiodic- or chaos-like motion, which we attribute to the precursory creep regime and seismic motion, respectively. If the triggered acceleration changes are of longer duration, a reverse transition from inter-seismic to post-seismic creep regime is detected on a larger time scale.

Fault creep investigation lies in the focus of earthquake hazard assessment, since creeping is often regarded as a possible indication of a pending earthquake magnitude<sup>1</sup>. Although fault creep is typically slow (<30 mm/yr), the probability of generating large earthquakes along the creeping faults is generally lower, primarily because the slip area in the future earthquake is smaller along the fault that creeps<sup>2</sup>. An alternative explanation of such reduced earthquake possibility along the creeping faults lies in the fact that the slow slippage may partially relieve stress buildup along the faults, thereby decreasing the magnitude of the next seismic event.

Creep motion refers to aseismic slip lasting over several decades between the major earthquakes<sup>3</sup>. According to the temporal distance between the preceding and the pending earthquake, i.e. depending on the phase of an earthquake cycle, several creep regimes are typically observed. Post-seismic creep regime is observed immediately after the seismic motion ceases and is commonly considered as a short period of a few years or decades after the last earthquake. Nevertheless, inter-seismic period is regarded as a period of slow accumulation of elastic strain that coincides with frictional locking of a fault between earthquakes, which may last from decades to thousands of years<sup>4</sup>. The third stage of fault creeping is denoted as a precursory creep regime, typically encountered before a seismic event. Transitions between the different creep regimes occur due to increased accumulation of stress along the fault, eventually leading to the onset of seismic motion. Another reason for switching between the different stages of fault slip lies in the external impact of near or distant earthquakes, which primarily trigger the static and dynamic stress variations along the fault<sup>5</sup>. Instantaneous triggering is typically observed when the external force originated from the passing seismic wave acts along the fault which approaches the end of an earthquake cycle<sup>6–8</sup>. Apart from this instantaneous triggering effect, some locations experience a delayed onset of motion along the fault, which occurs due to a variety of time-dependent stress transfer mechanisms, including the viscous relaxation, poroelastic rebound and afterslip, or could be caused by reductions in fault friction, as predicted by the rate and state constitutive relations<sup>7,9</sup>. These dynamic stress changes may also be responsible for the occurrence of an aftershock sequence just after the mainshock<sup>10</sup>. All these effects could promote a transition between the creep regimes, which may sometimes involve the skipping of the succeeding stage of fault motion, leading eventually to the earthquake nucleation.

Issue of dynamic triggering has been the subject of an extensive research, focusing on one hand on the analysis of the induced seismic events in situ, and on the investigation of the dynamics of spring-slider models from the aspect of a possible advance of an earthquake cycle, on the other hand. The former relies on the recorded evidence of earthquakes which occurred after the large seismic events, including the ones detected in Yellowstone National



Park after the 1992 M7.3 Landers earthquake<sup>11</sup>, the seismic events in southeastern California after the 2002 M7.9 Denali earthquake<sup>12</sup> or the earthquakes in Greece following the 1999 M7.4 Izmit earthquake<sup>6</sup>. As far as the analysis of phenomenological models is concerned, Gombert et al.<sup>13</sup> have shown using a simple massless spring-slider system that the transients hasten the time of earthquakes that ultimately would have happened due to the constant background loading alone. Perfettini et al.<sup>14</sup> extended the work of Gombert et al.<sup>13</sup> by studying the effect of pulses and wave packets in a 2-D continuous quasi-dynamic fault model coupled with Dieterich-Ruina friction law under the variations of both shear and normal stress. Their analysis indicates that dynamic triggering by seismic waves can occur only in the areas of higher pore pressures or along the faults at the end of their earthquake cycle. Du et al.<sup>15</sup> used the same sine wave transient load, as in Gombert et al.<sup>13</sup> and Perfettini et al.<sup>14</sup>, and applied it as a forcing function to the spring-slider system. It has been found that certain types of transient loads can trigger the next anticipated creep events, which then occur either shortly after the transient load ends or with a time delay. This has also been shown by Belardinelli et al.<sup>16</sup>, who analyzed a spring-slider model including inertia, in order to examine the dependence of triggering delays on different system conditions and constitutive parameters. According to their results, the static stress change can advance as well as delay an induced instability depending on its sign, whereas the dynamic stress pulse can only promote a nearly instantaneous failure, though under condition that its amplitude is positive and large enough with respect to the direct effect of friction.

However, despite the notable amount of research on the effects of dynamic triggering on the motion of spring-slider models and in situ, there is no evidence whether the passing seismic wave can induce transitions between the different slip regimes, which is the issue addressed in detail in present paper. The performed analysis is based on the dynamics of spring-slider model coupled with the Dieterich-Ruina friction law, which is assumed to qualitatively describe aseismic displacement along the fault. The impact of a passing seismic wave is mathematically described by a sine wave scaled by an exponential pulse, as already suggested in Gombert et al.<sup>13</sup> and Perfettini et al.<sup>14</sup>. However, in contrast to the previous studies, we assume that the acceleration changes of the block attain such a wave form.

It is important to underline that the analysis of the mono-block model, as a crude picture of the fault slip, is limited in two ways. On one hand, there is a lack of knowledge on the initial state of the fault, both in terms of stress state and the geometrical features, whereas on the other hand, there is insufficient understanding of the governing laws that describe the dissipative physico-chemical mechanisms presumably occurring during a fault motion<sup>17–19</sup>. However, in the present study we deliberately adopt the simplest model in order to qualitatively understand the concept of dynamic triggering, without considering the possible complications that arise from the spatial heterogeneities and geometrical complexity of fault structures handled in the extended fault models.

One should be aware of the fact that the performed research is purely phenomenological, in a sense that the intention is to capture the main mechanisms of fault dynamics under the effect of an external force induced by a passing seismic wave, without setting the goal to solve the complex geological and tectonic relations in the Earth's crust. The objective of the analysis is not to identify the nature of the triggered seismicity, but rather to examine whether it is possible to generate the transition between the different slip regimes and, eventually, induce a seismic motion, only by perturbing the block's acceleration, reflecting, in that way, the effect of a transient seismic wave. In effect, the presented analysis is intended to determine which creep regime is most sensitive to external perturbation.

## Results

In the present paper, we start from the assumption that motion along a single fault could be described by a mono-block spring-slider model coupled with the Dieterich-Ruina rate- and state-dependent friction law, as first proposed in Erickson et al.<sup>20</sup>:

$$\begin{aligned}\dot{\theta} &= -\left(\frac{V}{L}\right)\left(\theta + B \log\left(\frac{V}{V_0}\right)\right) \\ \dot{U} &= V - V_0 \\ \dot{V} &= \left(-\frac{1}{M}\right)\left(kU + \theta + A \log\left(\frac{V}{V_0}\right)\right)\end{aligned}\quad (1)$$

where parameter  $M$  denotes the mass of the block and the spring stiffness  $k$  corresponds to the linear elastic properties of the rock mass surrounding the fault<sup>21</sup>. This physical system is analogous to a single fault patch of fixed dimensions that ruptures in an elastic medium<sup>22</sup>. According to Dieterich and Kilgore<sup>23</sup> parameter  $L$  corresponds to the critical sliding distance necessary to replace the population of asperity contacts. The parameters  $A$  and  $B$  are empirical constants, which depend on the properties of material. Ruina<sup>24</sup> suggested that parameter  $A$  quantifies the direct velocity dependence ("direct effect"), while  $(A - B)$  is a measure of the steady-state velocity dependence. For convenience, system (1) is non-dimensionalized by defining the new variables  $\theta'$ ,  $V'$ ,  $U'$  and  $t'$  in the following way:  $\theta = A\theta'$ ,  $V = V_0V'$ ,  $U = LU'$ ,  $t = (L/V_0)t'$ . The nondimensional system, once we return to the original notation, takes the following form:

$$\begin{aligned}\dot{\theta} &= -V(\theta + (1 + \varepsilon) \log(V)) \\ \dot{U} &= V - 1 \\ \dot{V} &= -\gamma^2[U + (1/\xi)(\theta + \log(V))]\end{aligned}\quad (2)$$

where  $\varepsilon = (B - A)/A$  measures the sensitivity of velocity relaxation,  $\xi = (kL)/A$  is the nondimensional spring constant, and  $\gamma = \sqrt{(k/M)}(L/V_0)$  is the nondimensional frequency<sup>20</sup>.

System (2) represents a fault slip model coupled with the Dieterich-Ruina friction law, so unless it is perturbed, it only describes different types of creep regimes. The dynamics of system (2) for different values of control parameters ( $\varepsilon$ ,  $\xi$ ,  $\gamma$ ) is analyzed in section Methods.

Our focus lies with the analysis of the dynamics of system (2) under the effect of external periodic force, which is induced by a passing seismic wave and which directly affects the acceleration of the block in a form of seismic train oscillation:

$$\dot{V}(t) = A \sin\left(\frac{2\pi t}{T}\right) e^{\left\{\frac{(t-t_0)}{t_w}\right\}^n}.\quad (3)$$

In the above expression,  $A$  denotes the maximum amplitude of the induced change,  $T$  is the wave period,  $t_0$  is the moment for which the perturbation amplitude reaches its maximum value,  $t_w$  is the half width of the induced perturbation, and  $n$  represents an integer that controls the rise-time<sup>14</sup>. This acceleration change consists of a pulse like envelope inside which oscillations of period  $T$  occur. In other words, the effect of a transient external force is simulated using a sine wave of period  $T$ , scaled by an exponential pulse with amplitude  $A$  and width  $2t_w$ . By introducing the transient wave (3) in the observed system (2) we obtain:

$$\begin{aligned}\dot{\theta} &= -V(\theta + (1 + \varepsilon) \log(V)) \\ \dot{U} &= V - 1 \\ \dot{V} &= -\gamma^2[U + (1/\xi)(\theta + \log(V))] + A \sin\left(\frac{2\pi t}{T}\right) e^{\left\{\frac{(t-t_0)}{t_w}\right\}^n}\end{aligned}\quad (4)$$



The effect of different types of external force is reflected in dependence on period  $T$ . In terms of real earthquakes, more rapidly varying (short-period) transient changes of block acceleration could correspond to the effect of closer, smaller earthquakes, while more slowly varying (long-period) transient changes might describe larger, more remote earthquakes<sup>13</sup>.

Note that we do not consider the effect of a passing seismic wave in reference to the phase of the seismic cycle, simply because our model, for the particular parameter values, does not exhibit stick-slip motion, which is regarded as a typical seismic movement. On the contrary, the adopted fault slip model (2) describes creeping along faults, with an earthquake arising once the block starts to move in an irregular chaotic-like fashion. This way, we are able to observe the possible transitions between the different aseismic and seismic slip regimes under the impact of a triggering external force produced by the passing seismic wave from near or distant earthquakes. Concerning this, throughout the study, the parameters of perturbation are set as follows. Analysis is performed for the transient acceleration changes of different half-duration  $t_w \in (3, 100)$  and different period  $T \in (3, 20)$ , in comparison to the frequency of periodic oscillation of the unperturbed system (2) just above the bifurcation curve ( $T_0 \approx 12$ ). Regarding the time for which the amplitude of the induced change reaches its maximum value, we assume a value of  $t_0 = 1000$ , which is sufficiently larger than the time required for the dynamics of the unperturbed system (2) to stabilize on the limit cycle just above the bifurcation curve. Value of parameter  $n$ , which controls the rise-time, is set to 16, as already proposed in Perfettini et al.<sup>14</sup>.

The amplitude of the acceleration change,  $A = 0.6$ , is selected by drawing comparison to the amplitude of oscillations exhibited by system (2) just above the bifurcation curve. In the present paper, we consider the amplitudes that are equal, slightly larger or smaller (two times in both cases) than the amplitude of periodic oscillation of the unperturbed system. Note that the oscillations of the unperturbed system (2) just above the bifurcation curve do not represent an example of a seismic cycle, but only another mode of creep motion. Hence, the amplitude of oscillatory motion does not have an immediate physical interpretation and we consider it unrelated to the seismic events.

**Transient triggering in the post-seismic creep regime.** Under the assumption that a passing seismic wave acts along a fault in the post-seismic creep regime, analysis of block's dynamics is performed for the parameter values below the bifurcation curve ( $\varepsilon = 0.2$ ,  $\xi = 0.5$ ,  $\gamma = 0.8$ ), where the motion of the block is uniform.

For the brief short-period transient changes, represented by the case  $t_w = 3$  and  $T = 3$ , the induced dynamics of the perturbed system (4) shows only a somewhat higher sharp first amplitude response, without irregular oscillations. Qualitatively similar effect is found for the brief long-period acceleration changes. Nevertheless, the transient switch to periodic oscillations is observed for the longer high-frequency changes, which can be regarded as a temporary transition to the inter-seismic creep regime.

For the longer low-frequency acceleration changes, represented by the case  $t_w = 100$  and  $T = 20$ , one encounters weakly irregular oscillations, cf. Figure 1. The irregular character of oscillations is corroborated by the broadband noise in the corresponding Fourier power spectrum (Figure 2a). Given the irregularity of the observed motion, this type of triggered effect could be considered an instance of immediate (instantaneous) earthquake triggering. However, note that the question of qualifying certain transient motion as transient chaos (or, at least, chaos-like behavior) should in principle be treated by determining the finite-time Lyapunov exponent<sup>25</sup>. Here we determine the largest Lyapunov exponent for the time series showing the sufficiently long transient according to the general method of Wolf et al.<sup>26</sup>, whereby the standard procedure is complemented by carrying out the additional averaging over a set of different initial conditions

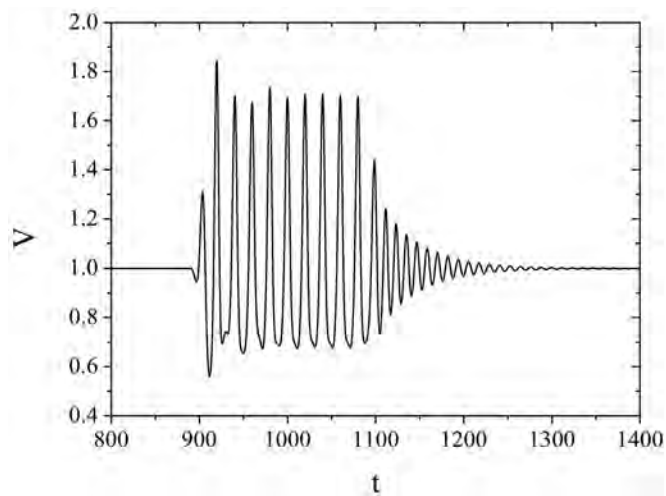


**Figure 1 | Evolution of variable  $V$  for  $\varepsilon = 0.2$ ,  $\xi = 0.5$  and  $\gamma = 0.8$  under the influence of the low-frequency acceleration change ( $T = 20$ ) with longer duration ( $t_w = 100$ ). The remaining parameter values are:  $A = 0.6$ ,  $t_0 = 1000$  and  $n = 16$ . Note that the velocity and time are considered as non-dimensional quantities.**

(Figure 2b). The convergence condition is satisfied in a sense that the approximately stationary values of the largest Lyapunov exponents are reached on the time scale ( $t \approx 30$ ) significantly smaller than the transient length ( $t \approx 100$ ). The maximal Lyapunov exponents determined for the different initial conditions are found to converge well to positive values in the range  $4.1 - 7.4 \times 10^{-2}$ .

Qualitatively similar phenomena are observed in case of larger perturbation amplitudes ( $A = 1.2$ ), whereas the impact of smaller amplitudes ( $A = 0.3$ ) is marginal.

**Transient triggering in the inter-seismic creep regime.** In this case, the analysis is performed for the parameter values just above the bifurcation curve ( $\varepsilon = 0.3$ ,  $\xi = 0.5$ ,  $\gamma = 0.8$ ), where the motion of the block is oscillatory.

In case of a brief short-period change, for  $t_w = 3$  and  $T = 3$ , the system (4) reacts through a sharp first response with a slightly higher amplitude, then displaying a slower convergence to the limit cycle relative to the unperturbed motion. Note that this is similar to the case where the system (2) lies in the steady state post-seismic regime. The qualitatively analogous effect occurs for the long-period transient changes ( $T = 20$ ) of short duration.

However, if the induced acceleration changes are longer ( $t_w = 100$ ) and high-frequency ( $T = 3$ ), the quasiperiodic-like motion with modulated amplitude steps in. We interpret this as a transition to a new precursory creep regime, see Figure 3a. Quasiperiodicity on a torus is corroborated by the presence of two incommensurate frequencies in the corresponding Fourier power spectrum (Figure 3b).

If we now assume longer low-frequency changes ( $t_w = 100$  and  $T = 20$ ), irregular oscillations are found, which correspond to transient seismic motion along the fault, see Figure 4a. Broadband noise in Fourier power spectrum indicates chaos-like behavior (Figure 4b), which is further verified by the positive value of maximal Lyapunov exponent for the different initial conditions (Figure 5).

Another interesting dynamical feature is seen if the amplitude of the induced change is varied during the inter-seismic creep regime. If the high-frequency changes of acceleration attain a larger amplitude ( $A = 1.2$ ), only a short interval of quasiperiodic-like motion is observed, much shorter in comparison to the case shown in Figure 3 where  $A = 0.6$ . From Figure 6 one reads that the duration of the quasiperiodic-like motion is about four times shorter ( $t \approx 50$ ) compared to the case with the smaller amplitude in Figure 3 ( $t \approx 200$ ). Furthermore, apart from the short quasiperiodic-like motion,



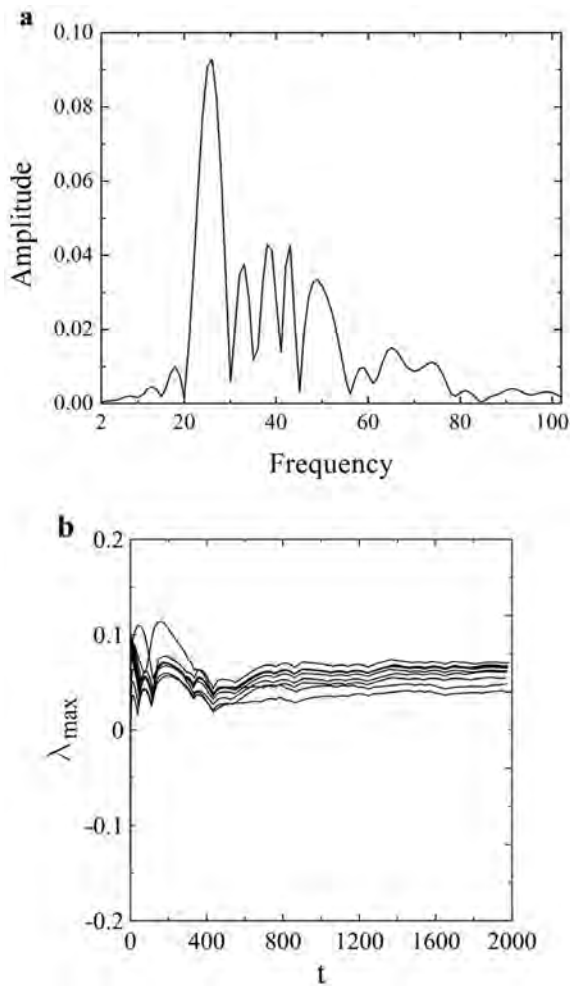


**Figure 2** | (a) The continuous broadband noise in the Fourier power spectrum for the time series in Figure 1 indicates that the system exhibits a relatively weak chaotic behavior. (b) Calculation of the maximal Lyapunov exponent involves the additional averaging over a set of different initial conditions, whereby  $\theta$ ,  $U$ ,  $V$  belong to the respective ranges  $\theta \in [0.01, 0.05]$ ,  $U \in [0.01, 0.05]$ ,  $V \in [0.95, 1.05]$ . The results are obtained by adapting the method of Wolf et al.<sup>26</sup>. Maximal Lyapunov exponents are seen to converge well to the positive values in the range  $\lambda_{\max} = 4.1 - 7.4 \times 10^{-2}$ . Note that time  $t$  is expressed in the units of iteration steps.

there is a temporary transition to post-seismic creep regime, with much slower convergence to the stable limit cycle. Nevertheless, if the low-frequent transient changes acquire the larger amplitude, say  $A = 1.2$ , no significant dynamical phenomena can be reported.

In case when the induced brief high-frequent acceleration changes are of low amplitude ( $A = 0.3$ ), the system (4) is found to respond with a sharp amplitude peak, after which it converges rapidly to a stable limit cycle. Similar effect is observed in case of low-frequent acceleration changes, when only small alterations of oscillation amplitude occur without any transition to another creep regime or to seismic motion.

In the last stage of the analysis, concerning the large values of perturbation amplitude, an effect of duration of transient change was examined by varying the parameter  $t_w$ . It turns out that if a higher amplitude ( $A = 1.2$ ) is assumed for both the high-frequent and the low-frequent transient, acting in inter-seismic creep regime, longer acceleration changes ( $t_w = 800$ ) further induce a switch to uniform motion, i.e. from inter-seismic to post-seismic creep regime, on a much longer time scales before system itself converges again to stable limit cycle. In case of post-seismic creep regime, long-term

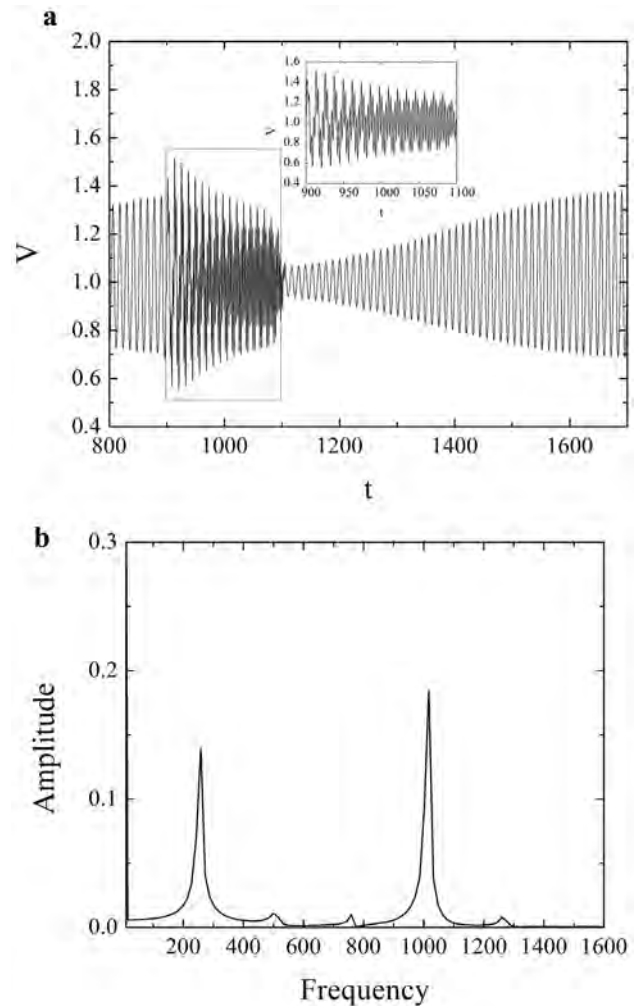


**Figure 3** | (a) Evolution of variable  $V$  for  $\varepsilon = 0.3$ ,  $\zeta = 0.5$  and  $\gamma = 0.8$  induced by the short-period acceleration change ( $T = 3$ ) with longer duration ( $t_w = 100$ ). The remaining parameters are set to:  $A = 0.6$ ,  $t_0 = 1000$  and  $n = 16$ . The rectangular frame indicates the quasiperiodic-like transient part of the time series, whose blowup is displayed in the inset. Note that the velocity and time are given as non-dimensional quantities; (b) Two incommensurate frequencies in the Fourier power spectrum for the time series in Figure (a) indicate the onset of the quasiperiodic-like motion.

transients ( $t_w = 800$ ) of higher amplitude ( $A = 1.2$ ) result only in a temporary transition to inter-seismic creep regime (i.e. oscillatory motion).

## Discussion

In the present paper, we have analyzed the effect of a transient periodic external force induced by a passing transient wave on the dynamics of the spring-slider model. The effect of a transient force is introduced to describe the dynamic triggering impact of nearby or distant earthquakes. The considered single-block model, incorporating the Dieterich-Ruina friction law between the block and the rough surface of the lower plate, is supposed to reproduce creep along the fault. The analysis of the original model (2) indicates that the transition from equilibrium state to stable periodic motion occurs via the direct supercritical Hopf bifurcation for certain values of the control parameters. The influence of a transient external force has been examined for two distinct states along the fault: uniform creep mode, represented by the steady state of the block, and the oscillatory creep mode, corresponding to the stable periodic motion of the block.

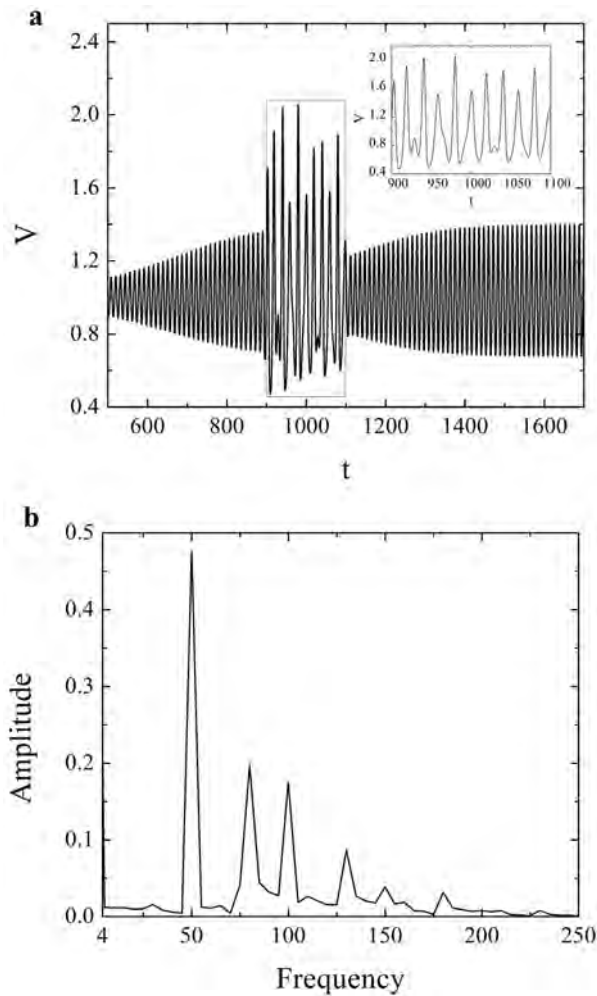


**Figure 4** | (a) Evolution of variable  $V(t)$  for  $\varepsilon = 0.3$ ,  $\zeta = 0.5$  and  $\gamma = 0.8$  and for low-frequency induced acceleration change ( $T = 20$ ) with longer duration ( $t_w = 100$ ). The remaining parameters are set to:  $A = 0.6$ ,  $t_0 = 1000$  and  $n = 16$ . The rectangular frame indicates the irregular (chaos-like) transient part of the time series, which is shown enlarged in the inset. Note that the velocity and time are given as non-dimensional quantities; (b) Continuous broadband noise in Fourier power spectrum for time series in Figure (a) implies a possible chaos-like behavior of the system.

These two states are interpreted to conform to the post-seismic and inter-seismic creep regimes of fault motion, respectively. The impact of the external force due to passing seismic waves is modeled through a change of block's acceleration, whose parameters are set with respect to the periodic oscillations of the unperturbed system (2) just above the bifurcation curve. These oscillations are characterized by the amplitude  $A_0 = 0.6$  and the period  $T_0 \approx 12$ . In this context, we have considered the short-period ( $T < 12$ ) and long-period ( $T > 12$ ) acceleration changes of different duration  $t_w \in (3, 100)$ . It is assumed that the brief short-period transient changes might correspond to closer, smaller earthquakes, while longer, low-frequency transients could represent the effect of larger, more remote earthquakes<sup>13</sup>.

Under the assumption that a passing seismic wave propagates along the fault, dynamics of system (4) reveals the following picture. If the induced acceleration changes are short, system (4) exhibits only the sharp and slightly higher amplitude response, with a slower convergence to an equilibrium state in the uniform creep mode, or a faster convergence to a stable limit cycle, when it comes to oscillatory creep mode. In case when the generated change is of longer duration ( $t_w = 100$ ), different dynamical features are observed,

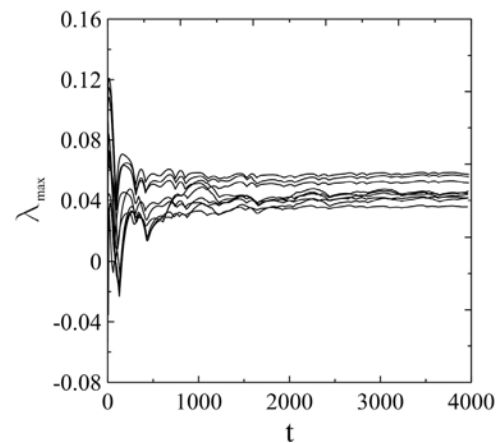


**Figure 5** | Calculation of the maximal Lyapunov exponent. The point that it is calculated for a transient irregular sequence requires one to perform additional averaging over a set of different initial conditions, whereby  $\theta$ ,  $U$ ,  $V$  belong to the respective ranges  $\theta \in [0.01, 0.05]$ ,  $U \in [0.01, 0.05]$ ,  $V \in [0.95, 1.05]$ . The results are obtained by adapting the method of Wolf et al.<sup>26</sup>. Maximal Lyapunov exponents are found to converge well to positive values in the range  $3.6 - 5.7 \times 10^{-2}$ . Note that time  $t$  is expressed in the units of iteration steps.

depending on the frequency of the perturbation of acceleration. A high-frequency acceleration changes in the inter-seismic creep-regime further lead to quasiperiodic-like dynamics, which is assumed to correspond to a precursory creep regime. However, long-period changes of acceleration in both post-seismic and inter-seismic creep regimes invoke irregular oscillations or chaos-like behavior, which can be treated as an onset of the seismic motion. Taking this into account, one may conclude that the longer low-frequency transients could excite a seismic motion even if the fault is in a stable uniform creep regime. Such type of triggering, analogous to the onset of earthquakes within the regions with low triggering threshold, has been observed in the case of series of earthquakes in Greece following the  $M_w 7.4$  Izmit earthquake<sup>6</sup>. These findings are also consistent with the

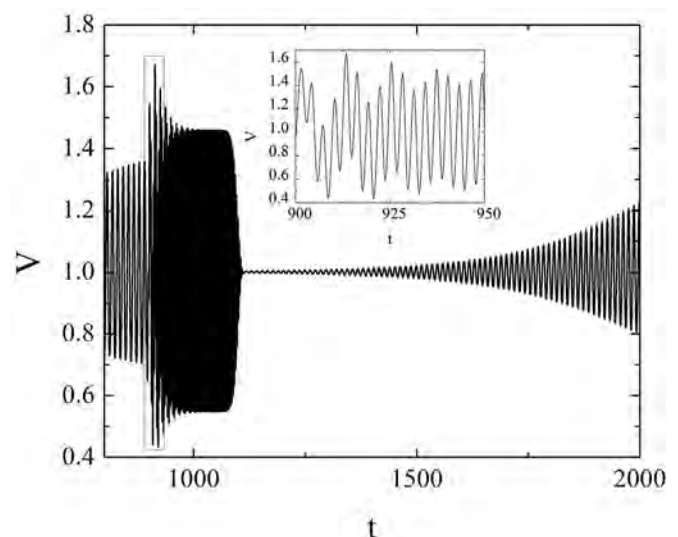


**Figure 6** | Temporal evolution of variable  $V$  for  $(\varepsilon, \zeta, \gamma) = (0.3, 0.5, 0.8)$  when the system is subjected to a short-period acceleration change ( $T = 3$ ). Other parameters are set to:  $A = 1.2$ ,  $t_w = 100$ ,  $t_0 = 1000$  and  $n = 16$ . The rectangular window indicates the time sequence with transient irregular motion, which is shown enlarged in the inset. Note that the velocity and time are expressed in nondimensional units.



results of Brodsky and Prejean<sup>27</sup>, who determined that long-period waves are more effective at generating local seismicity than the short-period waves of comparable amplitude. This analysis covered the records of 12 regional and teleseismic events recorded at Long Valley Caldera.

If one assumes considerably longer acceleration changes (e.g.  $t_w = 800$ ), the only significant dynamical effect arises in the case of inter-seismic creep regime for high-amplitude transients. Apparently, it turns out that such long-term changes further induce a temporary transition from oscillatory to uniform motion, i.e. from an inter-seismic to post-seismic creep regime, after which the system converges to a stable limit cycle. A possible explanation of such a transition from oscillatory creep mode to uniform creep mode could be found in the properties of the fault gouge and the “maturity” of the fault. San Andreas fault system, for example, did not experience significant triggering by the Landers earthquake, due to its thicker and more deformed fault gouge that requires greater stress change to induce a rupture<sup>7</sup>.

The performed analysis has confirmed the occurrence of immediate or instantaneous dynamic triggering effect of a passing seismic wave, which has already been observed in situ following Landers<sup>11</sup>, Denali<sup>12</sup> and Izmit earthquake<sup>6</sup>. A background mechanism for such an event is in relation with the immediate Coulomb-type failure<sup>7</sup>. In the present case, it is determined that the long-period transients, which are assumed to correspond to the effect of distant earthquakes, have the strongest impact on the fault motion, leading to irregular chaos-like behavior, i.e. to the onset of seismic motion. Nevertheless, the high-frequency transients, presumably originating from the nearby earthquakes, further induce a transition to quasiperiodic-like motion, which is recognized as a third, precursory creep regime that typically occurs just before the seismic motion commences. This effect is analogous to the dynamics of the spring-slider model with time delay, where the Ruelle-Takens-Newhouse route to chaos<sup>28</sup> may be found.

Our analysis indicates that the amplitude of the induced acceleration change probably represents one of the most important influential parameters when evaluating the triggering effect of a passing transient wave. Apparently, the dynamics of system (4) under high-amplitude acceleration changes exhibits only the onset of periodic oscillatory motion of higher amplitude, after which the system converges to equilibrium state or a stable limit cycle. When such transients occur in the post-seismic regime, they further generate a short transition to inter-seismic regime, with slow convergence to an equilibrium state. Nevertheless, the low-amplitude variations have no significant impact on the dynamics of system (4). However, one should be aware of the fact that previous studies revealed that even very small dynamic changes (down to  $3 \times 10^{-9}$ ) could trigger faults that are sufficiently near failure<sup>29,30</sup>. Here we underline again that our model represents only the fault creeping that is relatively stable with respect to the short-lived perturbations in loading conditions and that the dynamics of this model does not exhibit transient or asymptotic instability without the external perturbation of sufficiently high amplitude.

Note that the performed analysis did not reveal the occurrence of a delayed triggering, which is typically observed under the real conditions in the Earth’s crust. This is reminiscent to the earlier work of Gomberg et al.<sup>13,31</sup>, where it is indicated that, at least with respect to rate-and-state friction, the transient dynamic stresses could not explain the delay triggering. This is also consistent with Scholz<sup>32</sup>, who suggested that the direct effect of friction, as well as the finite size and duration of nucleation, prevent earthquakes from being triggered by the high-frequency stress oscillations, such as those generated by the passing seismic waves. Similar conclusions are also reached in Belardinelli et al.<sup>16</sup>, who found that a dynamic stress pulse is able to promote a nearly instantaneous failure, but cannot induce delayed triggering. In our setup, the main reason for the absence of

delayed triggering lies in the properties of the chosen model itself, since it does not display irregular motion without the effect of external perturbation. All these arguments suggest that the delayed triggering requires an additional mechanism, such as the one that could lead to a time-dependent increase in the pore pressure. This way, the effective normal stress would be reduced, which is likely to eventually result in triggering of earthquake<sup>7,11</sup>.

One should point out that the presented analysis is non-dimensional, meaning that it only qualitatively captures the basic dynamical mechanism behind the triggering impact of the external signal to the fault motion. In this context, the applied model cannot be expected to capture the full complexity of seismic motion and the impact of the external signal. Further, it is not possible to make quantitative interpretations or predictions. However, what this model does provide is a framework for understanding how the transition between different creep regimes or triggered seismicity may be caused by seismic waves induced by near or distant earthquakes.

Future research could include the analysis of the stochastic effects of seismic noise on the dynamics of the presented model. Moreover, it would be interesting to examine the dual effect of both the additive and the multiplicative noise, with the included external signal, in order to verify whether some longer or even permanent instabilities are possible within the analyzed system. Incorporating another important natural ingredient, the seismic noise, in the analysis, would in qualitative terms make the model closer to the actual conditions observed in the Earth’s crust.

## Methods

The system of first-order ordinary differential equations (2) has a unique stable stationary solution  $(\theta, U, V) = (0, 0, 1)$ , which corresponds to the steady sliding of the block. Hence, by this model, the fault is in a state of constant motion, which makes it more sensitive to the impact of dynamic triggering rather than the static stress changes. Under the real conditions in the Earth’s crust, such a fault motion could correspond to some plate boundary segments, like an Eastern California shear zone, where the average repeat time of fault seismic motion is of the order of thousands of years<sup>7</sup>.

To analyze the dynamics of system (2) around the stationary solution  $(0,0,1)$ , we numerically integrate the system (2) using the Runge-Kutta fourth order method for the different values of the parameter set  $(\varepsilon, \zeta, \gamma)$ . The analysis on stability of the autonomous system (2) under variation of  $\varepsilon$  or  $\zeta$  indicates a transition from equilibrium to periodic motion (obtained by increasing  $\varepsilon$  above  $\varepsilon = 0.27$ ) and vice versa (obtained by reducing  $\zeta$  below  $\zeta = 0.49$ ). At each instance, the parameters held constant attain values which admit the stable equilibrium ( $\varepsilon = 0.2$ ,  $\zeta = 0.5$  and  $\gamma = 0.8$ ). If both control parameters are varied in the  $(\varepsilon, \zeta)$  parameter plane, the equilibrium goes unstable through the direct supercritical Hopf bifurcation, where a new stable limit cycle is created.

In the present paper, we make an interpolation that the different stages of block motion separated by the supercritical Hopf bifurcation curve correspond to the different creeping regimes along the fault. In particular, the uniform motion of the block is treated as a model of fault slip in the post-seismic creep regime (i.e. after-slip), just after the last seismic event has occurred. Nevertheless, the periodic oscillatory motion is considered as corresponding to the displacement along the fault in the inter-seismic creep regime. This refers to the more “mature” faults during the period of slow accumulation of elastic strain that coincides with the frictional locking of a fault between the earthquakes. Consistent with the two assumptions above and taking into account the absence of the coseismic stick-slip motion in the applied model, the periodic oscillations just above the Hopf bifurcation curve cannot be interpreted as an alternation between the slow interseismic phase and the coseismic stage<sup>19</sup>. On the contrary, the model (2) only describes the different stages of the creeping aseismic displacement along the fault, whereas the onset of transient quasiperiodic-like and irregular chaos-like motion occurs only under the effect of external perturbation. The two latter types of motion are assumed to correspond to the precursory creep regime and the seismic motion, respectively. In this context, the presented approach differs significantly from the standard seismological method, which assumes that the dynamic instability arises when the sliding velocity exceeds some pre-defined threshold value<sup>33–36</sup>. Our approach consists in analyzing the motion of a spring-slider model by the methods of nonlinear dynamics and chaos theory. The main aim is to understand the key mechanisms which govern the transition between the different creep regimes, with the ultimate goal to determine whether the onset of seismic motion is possible under the effect of external dynamic triggering.

As for the impact of a passing seismic wave, we have followed the general approach of Gomberg et al.<sup>13</sup> and Perfettini et al.<sup>14</sup>, where a passing seismic wave is described by a simple function in the form of a sine wave scaled by an exponential pulse. Nonetheless, we do not consider explicitly the form of the ensuing seismic wave, but only its effects on the dynamics of acceleration. Hence, in contrast to previous



studies<sup>19</sup>, one does not assume that the sliding acceleration is negligible, which implies a faster evolution of the fault in both the post-seismic and the inter-seismic creep regimes.

- Bakun, W. H. & Lindh, A. G. The Parkfield, California, earthquake prediction experiment. *Science* **229**, 619–624 (1985).
- Field, E. H. A summary of previous working groups on California earthquake probabilities. *Bull. Seismol. Soc. Am.* **97**, 1033–1053 (2007).
- Lienkaemper, J. J., Borchardt, G. & Lisowski, M. Historic Creep Rate and Potential for Seismic Slip Along the Hayward Fault, California. *J. Geophys. Res.* **96**, 18261–18283 (1991).
- Wei, M. *Observations and Modeling of Shallow Fault Creep along the San Andreas Fault System*. PhD thesis, University of California, San Diego, 204 p. (2011).
- Kanamori, H. & Brodsky, E. E. 2004. The physics of earthquakes. *Rep. Prog. Phys.* **67**, 1429–1496.
- Brodsky, E. E., Karakostas, V. & Kanamori, H. A new observation of dynamically triggered regional seismicity: Earthquakes in Greece following the August, 1999 Izmit, Turkey earthquake. *Geophys. Res. Lett.* **27**, 2741–2744 (2000).
- Freed, A. M. Earthquake triggering by static, dynamic, and post-seismic stress transfer. *Annu. Rev. Earth Planet. Sci.* **33**, 335–367 (2005).
- Shelly, D. R., Peng, Z., Hill, D. P. & Aiken, C. Triggered creep as a possible mechanism for delayed dynamic triggering of tremor and earthquakes. *Nature Geosci. Lett.* **4**, 384–388 (2011).
- Brodsky, E. Long-range triggered earthquakes that continue after the wave train passes. *Geophys. Res. Lett.* **33**, L15313 (2006).
- Felzer, K. R. & Brodsky, E. E. Decay of aftershock density with distance indicates triggering by dynamic stresses. *Nature* **441**, 735–738 (2006).
- Hill, D. P. *et al.* Seismicity remotely triggered by the magnitude 7.3 Landers, California, earthquake. *Science* **260**, 1617–1623 (1993).
- Prejean *et al.* Observations of remotely triggered seismicity on the United States West Coast following the M7.9 Denali Fault earthquake. *Bull. Seismol. Soc. Am.* **94**, 348–359 (2004).
- Gomberg, J., Blanpied, M. L. & Beeler, N. M. Transient triggering of near and distant earthquakes. *Bull. Seismol. Soc. Am.* **87**, 294–309 (1997).
- Perfettini, H., Schmittbuhl, J. & Cochard, A. Shear and normal load perturbations on a two-dimensional continuous fault: 2. Dynamic triggering. *J. Geophys. Res.* **108**, B9, 2409-1-16 (2003).
- Du, W.-X., Sykes, L. R., Shaw, B. E. & Scholz, C. H. Triggered aseismic fault slip from nearby earthquakes, static or dynamic effect? *J. Geophys. Res.* **108**, B2, 2131 (2003).
- Belardinelli, M. E., Bizzarri, A. & Cocco, M. Earthquake triggering by static and dynamic stress changes. *J. Geophys. Res.* **108**, 2135 (2003).
- Bizzarri, A. What does control earthquake ruptures and dynamic faulting? A review of different competing mechanisms. *Pure Appl. Geophys.* **166**, 741–776 (2009).
- Bizzarri, A. On the deterministic description of earthquakes. *Reviews of Geophysics* **49**, RG3002 (2011).
- Bizzarri, A. What can physical source models tell us about the recurrence time of earthquakes? *Earth-Science Reviews* **115**, 304–318 (2012).
- Erickson, B., Birnir, B. & Lavallee, D. A model for aperiodicity in earthquakes. *Nonlinear Proc. Geoph.* **15**, 1–12 (2008).
- Scholz, C. H. *The Mechanics of Earthquakes and Faulting*. Cambridge University Press, Cambridge, 504 p. (2002).
- Dieterich, J. H. Earthquake nucleation of faults with rate-and state-dependent strength. *Tectonophysics* **211**, 115–134 (1992).
- Dieterich, J. H. & Kilgore, B. D. Direct observation of frictional contacts: new insights for state dependent properties. *Pure Appl. Geophys.* **143**, 283–302 (1994).
- Ruina, A. L. Slip instability and state variable friction laws. *J. Geophys. Res.* **88**, 10359–10370 (1983).
- Stefański, K., Buszko, K. & Piecyk, K. Transient chaos measurements using finite-time Lyapunov exponents. *Chaos* **20**, 033117-1-13 (2010).
- Wolf, A., Swift, J., Swinney, H. & Vastano, J. Determining Lyapunov exponents from a time series. *Physica D* **16**, 285–317 (1985).
- Brodsky, E. E. & Prejean, S. G. New constraints on mechanisms of remotely triggered seismicity at Long Valley Caldera. *J. Geophys. Res.* **110**, B04302 (2005).
- Kostić, S., Franović, I., Todorović, K. & Vasović, N. Friction memory effect in complex dynamics of earthquake model. *Nonlinear Dynam.* **73**, 1933–1943 (2013).
- Van Der Elst, N. J. & Brodsky, E. E. Connecting near-field and far-field earthquake triggering to dynamic strain. *J. Geophys. Res.* **115**, B07311 (2010).
- Van Der Elst, N. J. *The effect of seismic waves on earthquake nucleation and fault strength*. University of California, Santa Cruz, PhD dissertation, 210 p (2012).
- Gomberg, J., Beeler, N. M., Blanpied, M. L. & Bodin, P. Earthquake triggering by transient and static deformations. *J. Geophys. Res.* **103**, B10, 24411–24426 (1998).
- Scholz, C. H. Earthquakes and friction laws. *Nature* **391**, 37–42 (1998).
- Day, S. M., Dalguer, L. A., Lapusta, N. & Liu, Y. Comparison of finite difference and boundary integral solutions to three-dimensional spontaneous rupture. *J. Geophys. Res.* **110**, B12307 (2005).
- Bizzarri, A. & Belardinelli, M. E. Modelling instantaneous dynamic triggering in a 3-D fault system: application to the 2000 June South Iceland seismic sequence. *Geophys. J. Int.* **173**, 906–921 (2008).
- Rubin, A. M. & Ampuero, J.-P. Earthquake nucleation on (aging) rate and state faults. *J. Geophys. Res.* **110**, B11312 (2005).
- Bizzarri, A. & Spudich, P. Effects of supershear rupture speed on the high frequency content of S waves investigated using spontaneous dynamic rupture models and isochrone theory. *J. Geophys. Res.* **113**, B05304 (2008).

## Author contributions

S.K., I.F., M.P., N.V. and K.T. designed and performed the research as well as wrote the paper.

## Additional information

**Competing financial interests:** The authors declare no competing financial interests.

**How to cite this article:** Kostić, S., Franović, I., Perc, M., Vasović, N. & Todorović, K. Triggered dynamics in a model of different fault creep regimes. *Sci. Rep.* **4**, 5401; DOI:10.1038/srep05401 (2014).



This work is licensed under a Creative Commons Attribution 4.0 International License. The images or other third party material in this article are included in the article's Creative Commons license, unless indicated otherwise in the credit line; if the material is not included under the Creative Commons license, users will need to obtain permission from the license holder in order to reproduce the material. To view a copy of this license, visit <http://creativecommons.org/licenses/by/4.0/>

# Complex Dynamics of Spring-Block Earthquake Model Under Periodic Parameter Perturbations

**Srdan Kostić<sup>1</sup>**

Department of Geology,  
University of Belgrade Faculty  
of Mining and Geology,  
Dušina 7,  
Belgrade 11000 Serbia  
e-mail: srdjan.kostic@rgf.bg.ac.rs

**Nebojša Vasović**

Department of Applied Mathematics,  
University of Belgrade Faculty  
of Mining and Geology,  
Dušina 7,  
Belgrade 11000 Serbia  
e-mail: nebojsa.vasovic@rgf.bg.ac.rs

**Igor Franović**

Department of Theoretical Mechanics,  
Statistical Physics, and Electrodynamics,  
University of Belgrade Faculty of Physics,  
Studentski Trg 12,  
Belgrade 11000 Serbia  
e-mail: igor.franovic@gmail.com

**Kristina Todorović**

Department of Physics and Mathematics,  
University of Belgrade Faculty of Pharmacy,  
Vojvode Stepe 450,  
Belgrade 11000 Serbia  
e-mail: kisi@pharmacy.bg.ac.rs

*A simple model of earthquake nucleation that may account for the onset of chaotic dynamics is proposed and analyzed. It represents a generalization of the Burridge–Knopoff single-block model with Dieterich–Ruina’s rate- and state-dependent friction law. It is demonstrated that deterministic chaos may emerge when some of the parameters are assumed to undergo small oscillations about their equilibrium values. Implementing the standard numerical methods from the theory of dynamical systems, the analysis is carried out for the cases having one or two periodically variable parameters, such that the appropriate bifurcation diagrams, phase portraits, power spectra, and the Lyapunov exponents are obtained. The results of analysis indicate two different scenarios to chaos. On one side, the Ruelle–Takens–Newhouse route to chaos is observed for the cases of limit amplitude perturbations. On the other side, when the angular frequency is assumed constant for the value near the periodic motion of the block in an unperturbed case, variation of oscillation amplitudes probably gives rise to global bifurcations, with immediate occurrence of chaotic behavior. Further analysis shows that chaotic behavior emerges only for small oscillation frequencies and higher perturbation amplitudes when two perturbed parameters are brought into play. If higher oscillation frequencies are assumed, no bifurcation occurs, and the system under study exhibits only the periodic motion. In contrast to the previous research, the onset of chaos is observed for much smaller values of the stress ratio parameter. In other words, even the relatively small perturbations of the control parameters could lead to deterministic chaos and, thus, to instabilities and earthquakes. [DOI: 10.1115/1.4026259]*

*Keywords:* spring-block model, coupled oscillations, spring constant, stress ratio, deterministic chaos

## 1 Introduction

Understanding the development and initial stages of an earthquake rupture is a major goal of earthquake science. Some researchers suggest that the nucleation process, specifically the size of the nucleation zone, is related to the ultimate size of the resulting earthquake [1–3], while others support the view that the size of the nucleation zone is unrelated to the final magnitude of an earthquake [4,5]. However, the influence of the nucleation mechanism on the final impact of an earthquake certainly exists, so the modeling of this phenomenon could lead to new insights on the nature of earthquakes. A common approach in the description of seismic sources is their approximation by a model of equivalent forces that correspond to the linear wave equations, neglecting nonlinear effects in the source area [6–8]. Equivalent forces are defined as the forces that produce displacements at a given point that are identical to those from the real forces acting at the source. Nevertheless, this body-force equivalent is a formal concept and it is necessary to relate its characteristics to the real earthquake source. Today, it is commonly accepted that vast majority of shallow tectonic earthquakes arise from faulting instabilities [9]. However, since the earthquake origin is not accessible to direct observation, the research in this area is conducted either by studying the recorded time series, propagation of seismic waves through the Earth’s interior, or by simulating the earthquakes in laboratory conditions.

In this paper, we succeed the suggestion of Brace and Byerlee [10], that stick-slip occurring in laboratory experiments on rock friction may be significant under shallow crustal conditions and that it can be regarded as a possible source of earthquakes.

Following the idea of Brace and Byerlee [10], Burridge and Knopoff [11] proposed a spring-block model, which is today recognized as a common model for the earthquake nucleation mechanism [12–14]. In the present paper, the Burridge–Knopoff (BK) model consists of only one block (Fig. 1), attached through a harmonic spring to a driving plate, which causes the block to move in a stick-slip fashion along the rough surface of the lower plate [15,16]. In the context of seismology, this spring-block model can be understood as a representation for earthquake motion [17–21].

The main nonlinearity of this system comes from the friction between the block and the rough surface of the lower plate. Concerning this, some specific constitutive laws for rock friction have been developed based on laboratory studies. These laws have been successfully used to explain various aspects of stable and unstable sliding between elastic solids as observed in the laboratory [22,23]. In the present paper, we use the Dieterich–Ruina rate- and state-dependent friction law [24].

Though the simulations of the BK model have led to much insight, one should still be mindful about its character, which is, especially in the elementary configuration, closer to that of a toy model than the realistic representation of the fault dynamics. The model’s realism has been contested for a number of reasons that generally fall into two categories, one related to the basic setup and the other concerned with the friction laws applied [25]. With respect to the former, some of the strongest criticisms refer to a lack of mechanisms by which the seismic energy is radiated or

<sup>1</sup>Corresponding author.

Contributed by the Design Engineering Division of ASME for publication in the JOURNAL OF COMPUTATIONAL AND NONLINEAR DYNAMICS. Manuscript received June 10, 2013; final manuscript received December 11, 2013; published online March 13, 2014. Assoc. Editor: Ahmet S. Yigit.

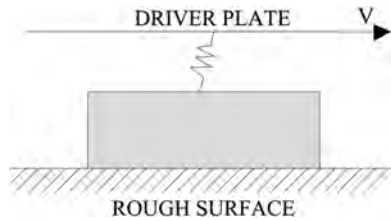


**Fig. 1** The Burridge–Knopoff block and spring model, represented by a slider coupled through a spring to a loader plate, which moves with velocity  $V$

dissipated. Apart from that, attention has also been directed to the absence of the long-range stress transfer and the possibility that the displayed complexity of the small events may be an artifact related to the lack of the continuum limit. As for the Dieterich–Ruina friction law, a drawback lies in that it is valid only for aseismic slip velocities but fails within the range of the seismic ones [26]. The intention here is not to address the specific issues outlined above but rather to point out how there may be some effects and influences whose inclusion into the original model may prove beneficial in qualitative terms. The latter expectation also draws on some of the advantages of the BK model, one of them being that the impact of the introduced variables and parameters is easily tractable. Proceeding in this spirit, the aim is to isolate some potentially novel mechanisms that may contribute to the emergence of chaotic dynamics in the monoblock setup. In particular, we propose a mechanism related to some external effects, like dynamic triggering from distant earthquake or vibrations caused by some artificial source.

In the present paper, we analyze a system of equations proposed by Madariaga, already used in Refs. [20,27], under the assumption that nondimensional stress change ratio and spring constant exhibit simple sinusoidal time dependence. The aim of the research is to show whether this kind of perturbation would generate complex dynamics, giving rise to the onset of deterministic chaos. Moreover, our idea was to determine whether the onset of chaos is also possible in the single-block model, only by coupling two sinusoidal oscillators, which is a common theoretical approach frequently used in the area of nonlinear dynamics.

It has to be emphasized that even though seismic waves do not generate such idealistic perturbations, they are of interest because of their simple shape and because a real wave pattern results in a superposition of such periodic waves. These idealistic perturbations also set the basis for a more complex periodic perturbation in a form of a sine wave scaled by a Gaussian pulse [28]. Similar

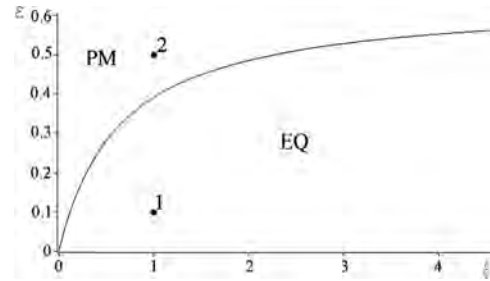


**Fig. 3** Attractors of the system (3) (or (4) with  $\delta_l = 0$ ) in parameter plane  $\varepsilon$ – $\xi$ . The remaining parameters are held fixed at values admitting the equilibrium point, as in Fig. 2. Corresponding time series and phase portraits for points 1 and 2 are shown in Fig. 4. EQ and PM are abbreviations for equilibrium state and periodic motion, respectively.

research was already performed by Perfettini et al. [29], except that they assumed a simplified pulselike stress change. Also, this kind of analysis with sinusoidal parameter perturbations was previously applied in the area of immunology, where periodic variation of a system’s parameters is ascribed to some external perturbations [30].

The purpose of this paper is to provide a minimal, yet sufficient, model of fault dynamics that may give rise to chaotic behavior. One may appreciate the simplicity tied to such an approach, given that a couple of possible mechanisms are laid out that are easy to incorporate as subtle modifications to the original Burridge–Knopoff model with the well-known Dieterich–Ruina’s rate- and state-dependent friction law. An important point is that the considered setups do not presuppose a compound fault structure but rather build on the simplest possible monoblock arrangement. It turns out that the inclusion of minor perturbations to the system parameters may be all that it takes for the system to exhibit robust chaotic dynamics. One cannot rule out the possibility that similar mechanisms operating alone or in synergy with the ones stated above may partially contribute to the occurrence of chaotic dynamics on real faults.

The scheme of the paper is as follows. In Sec. 2, we describe the original model in detail, while the modified model is presented in Sec. 3. Section 4 provides the main results, with detailed analysis of the system’s dynamics when either one or both parameters are perturbed. The obtained complex dynamical behavior is confirmed by calculating the Fourier power spectrum and the largest Lyapunov exponent. Concluding remarks are given in Sec. 5 with suggestions for further research.

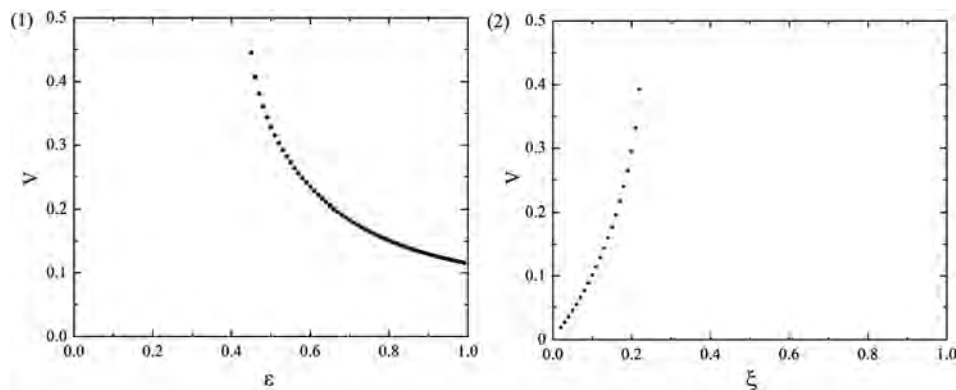


**Fig. 2** Bifurcations of the system (2) (or (3) if  $\delta_l = 0$  is set) under the variation of one of the parameters  $\varepsilon$  (1) and  $\xi$  (2). Orbital diagram is constructed for the section with plane  $\theta = 1$ , and calculation step 0.01, showing the asymptotic dynamics after  $8 \times 10^6$  time units. At each instance, the parameters held constant are awarded values that admit the equilibrium point,  $\varepsilon = 0.2$ ,  $\xi = 0.6$ , and  $\gamma = 0.8$ .

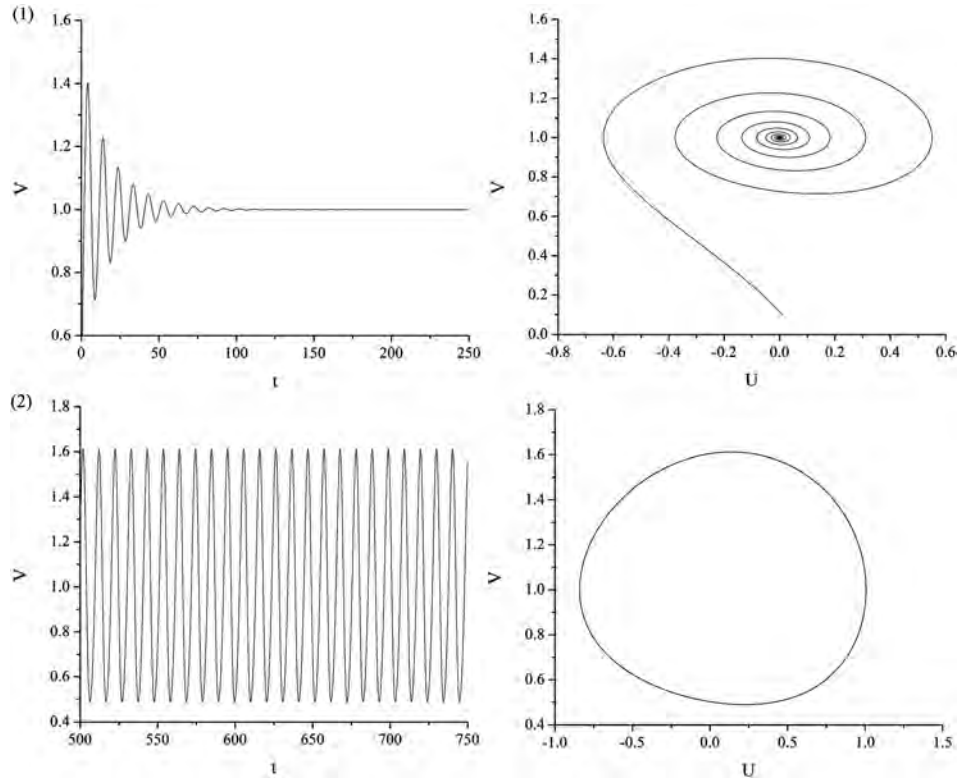


**Fig. 4** Temporal evolution of variable  $V$  and the appropriate phase portraits for: (1)  $\varepsilon = 0.1$ ,  $\zeta = 1.0$ , and  $\gamma = 0.8$  (equilibrium state); (2)  $\varepsilon = 0.5$ ,  $\zeta = 1$ , and  $\gamma = 0.8$  (periodic motion)

## 2 Background of the Original Model

The present analysis on complex dynamics of a spring-block model is based on the system of equations proposed by Madariaga [20]. These equations of motion coupled with the Dieterich–Ruina rate- and state-dependent friction law are originally given by

$$\begin{aligned} \dot{\theta} &= -\left(\frac{V}{L}\right) \left(\theta + B \log\left(\frac{V}{V_0}\right)\right) \\ \dot{U} &= V - V_0 \\ \dot{V} &= \left(-\frac{1}{M}\right) \left(kU + \theta + A \log\left(\frac{V}{V_0}\right)\right) \end{aligned} \quad (1)$$

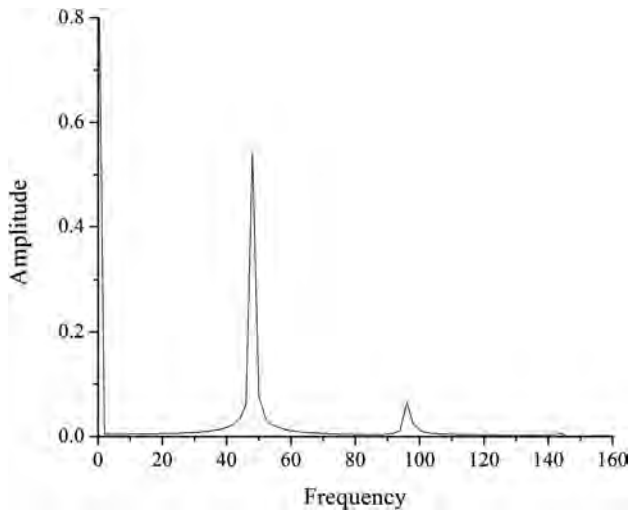


**Fig. 5** Single peak in power spectrum indicates the oscillatory behavior of the model. Parameter values are the same as in Fig. 4(2).

where parameter  $M$  is the mass of the block and the spring stiffness  $k$  corresponds to the linear elastic properties of the rock mass surrounding the fault [18]. According to Dieterich and Kilgore [31] the parameter  $L$  corresponds to the critical sliding distance necessary to replace the population of asperity contacts. The parameters  $A$  and  $B$  are empirical constants, which depend on material properties. According to Ref. [32], parameter  $A$  measures the direct velocity dependence (“direct effect”) while  $(A-B)$  is a measure of the steady-state velocity dependence. For convenience,

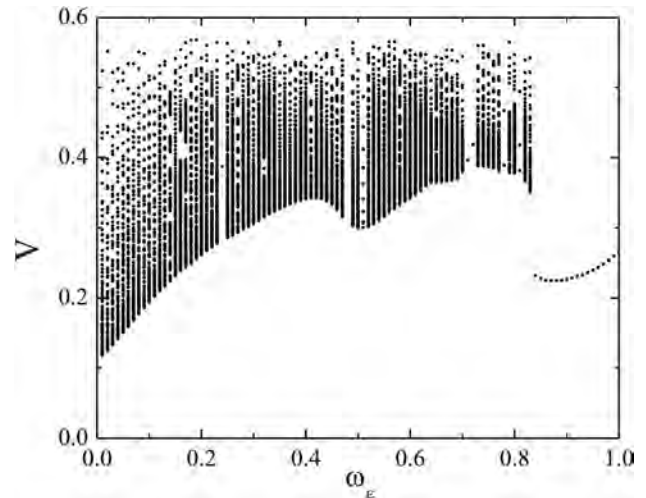


**Fig. 6** Bifurcations of the system (3) under the variation of the parameter  $\varepsilon$ . Orbital diagram is constructed for the section with plane  $\theta = 1$ , and calculation step  $\omega_\varepsilon = 0.01$ , showing the asymptotic dynamics after  $8 \times 10^6$  time units. At each instance, the parameters held constant are awarded the values near the equilibrium point but admitting the limit cycle,  $\varepsilon = 0.4$  ( $\delta_\varepsilon = 0.4$ ),  $\zeta = 0.5$ , and  $\gamma = 0.8$ . Corresponding time series and phase portraits for periodic and chaotic motion are shown in Fig. 7.

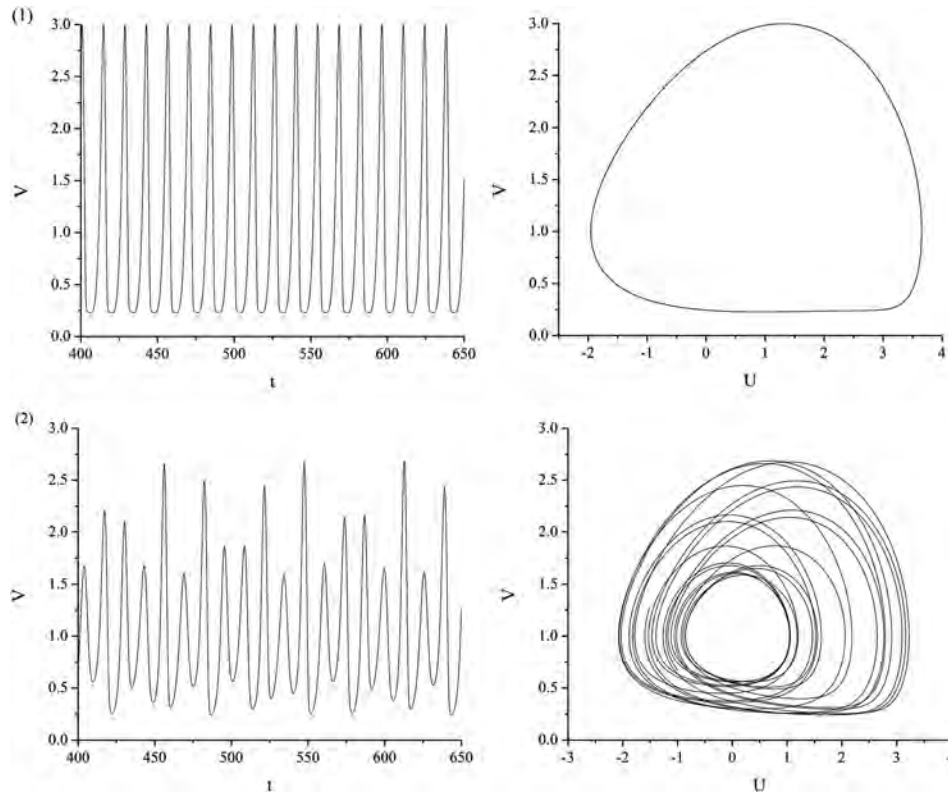


**Fig. 7** Temporal evolution of variable  $V$  and the appropriate phase portraits for: (1)  $\omega_c = 0.9$  (periodic motion); (2)  $\omega_c = 0.2$  (deterministic chaos). At each instance, the parameters held constant are awarded the values near the equilibrium point, but admitting the limit cycle,  $\varepsilon = 0.4$  ( $\delta_\varepsilon = 0.4$ ),  $\xi = 0.5$ , and  $\gamma = 0.8$ .

system (2) is nondimensionalized by defining the new variables  $\theta'$ ,  $V'$ ,  $U'$ , and  $t'$  in the following way:  $\theta = A\theta'$ ,  $V = V_0V'$ ,  $U = LU'$ ,  $t = (L/V_0)t'$ , after which we return to the use of  $\theta$ ,  $V$ ,  $U$ , and  $t$ . This nondimensionalization puts the system into the following form

$$\begin{aligned} \dot{\theta} &= -V(\theta + (1 + \varepsilon) \log(V)) \\ \dot{U} &= U - 1 \\ \dot{V} &= -\gamma^2[U + (1/\xi)(\theta + \log(V))] \end{aligned} \quad (2)$$

where  $\varepsilon = (B-A)/A$  measures the sensitivity of the velocity relaxation,  $\xi = (kL)/A$  is the nondimensional spring constant, and  $\gamma = (k/M)^{1/2}(L/V_0)$  is the nondimensional frequency [20].

### 3 Extended Model With Periodically Perturbed Parameters

In the present paper, the dynamics of a single-block model are analyzed by assuming the time-dependent character of  $\varepsilon$  and  $\xi$  in the following way:

$$\begin{aligned} \dot{\theta} &= -V[\theta + (1 + \varepsilon(t)) \log V] \\ \dot{U} &= U - 1 \\ \dot{V} &= -\gamma^2[U + (1/\xi(t))(\theta + \log V)] \end{aligned} \quad (3)$$

where  $\varepsilon(t)$  and  $\xi(t)$  are positive periodic functions of time:

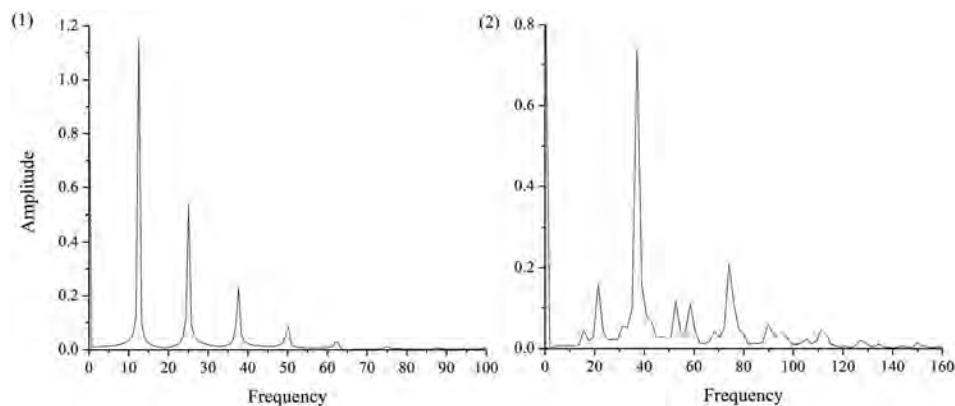


**Fig. 8** (1) Fourier power spectrum of periodic motion (first peak is for fundamental frequency, other peaks represent harmonics); (2) the broadband noise in the Fourier power spectrum indicates the onset of deterministic chaos. Parameter values are the same as in Figs. 7(1) and 7(2), respectively.



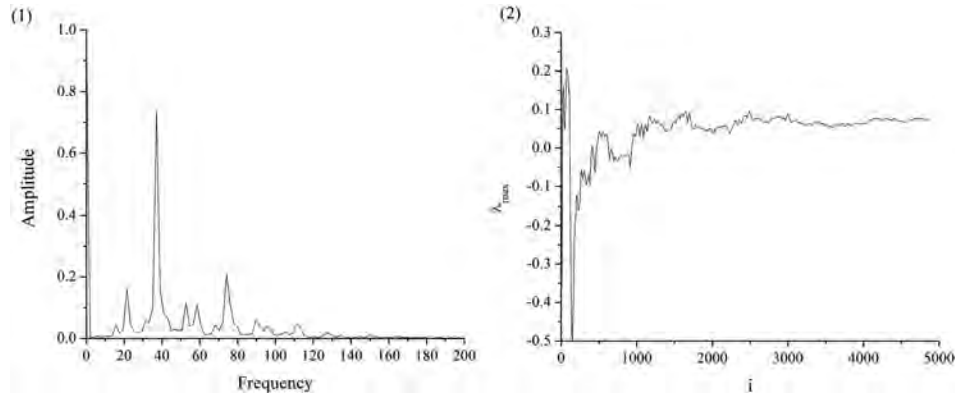


**Fig. 9** Maximal Lyapunov exponent converges well to  $\lambda_{\max} = 0.072$ , confirming the onset of deterministic chaos. The parameter values are identical to those in Fig. 7(2).

$$\begin{aligned} \varepsilon(t) &= \varepsilon + \delta_\varepsilon \sin(\omega_\varepsilon t) \\ \zeta(t) &= \zeta + \delta_\zeta \sin(\omega_\zeta t) \end{aligned} \quad (4)$$

such that  $\delta_\varepsilon$ ,  $\delta_\zeta$ ,  $\omega_\varepsilon$ , and  $\omega_\zeta$  represent the constant oscillation amplitudes and the angular frequencies, respectively. The former satisfy the constraint  $\delta_\varepsilon \leq \varepsilon$ ,  $\delta_\zeta \leq \zeta$ , which ensures the model's consistency as it confines each perturbation term to an appropriate range of values. The introduced modification addresses the issue of the system's response to an external perturbation, this aimed at showing that even the small-amplitude influences are sufficient to profoundly change the original behavior, leading to the onset of chaos. Within this framework, the external perturbations are incorporated implicitly by assuming that they induce small oscillations near the equilibrium values of some of the system parameters but admitting the periodic motion. Such persistent time-dependent perturbations may be attributed to the earthquakes that arise from slow rupture along the faults or to some nonnatural source of vibrations, on one side [33], or Earth tides and reservoir effects, on the other side [34]. However, note that the persistence of perturbations should be assessed in relative terms, meaning that even the impact of transient influences whose oscillation period is much shorter than the time they act on the system may still qualify for the provided description. In this context, one recalls the dynamical triggering models, which concern the possibility of earthquakes caused by the passage of seismic waves from the mainshock on some distant fault [35,36]. In particular, it has been proposed that the stress pulse emitted by the mainshock may increase another fault's slip speed or enhance triggering by reducing the associated state variable.

#### 4 Numerical Analysis

The system (3) has only one stationary solution  $(\theta, u, v) = (0, 0, 1)$ , which corresponds to steady sliding. We shall proceed in the standard way to determine and analyze the dynamics of Eq. (3) around a stationary solution  $(0, 0, 1)$ .

Let us first analyze the dynamics of the system (3) under the perturbation of one or two parameters, while the remaining ones are held fixed at values admitting the equilibrium point. To provide a point of reference, we first present the results on the stability of the equilibrium point for the autonomous system (2) if one of the parameters  $\varepsilon$  and  $\zeta$  is varied, viz. Fig. 2.

In order to gain insight on how the interplay between the parameters affects the behavior of the original system (2), we further plot the attractors in the  $(\varepsilon, \zeta)$  parameter plane, which is obtained analytically (Fig. 3). The corresponding diagrams for the other pairs of parameters are qualitatively similar. Corresponding time series and phase portraits for points 1 and 2 (in Fig. 3) are shown in Fig. 4. One learns that the variation of each of the parameters

$\varepsilon$  or  $\zeta$  leads the system through the supercritical Hopf bifurcation, such that the equilibrium point goes unstable and a new stable limit cycle is created.

Periodic motion of the block is confirmed by calculating the Fourier power spectrum (Fig. 5).

As stated earlier, the main goal of the analysis is to examine whether some sinusoidal perturbations acting in the system may change its underlying dynamics, giving rise to the chaotic solutions. The perturbations are introduced in an implicit fashion, assuming that they induce oscillations of the system parameters near their equilibrium values before and after the bifurcation occurs in the original system (2) (Fig. 3). Our strategy consists of varying the parameters in the vicinity of their respective equilibrium values, verifying if the periodic perturbation of a certain amplitude and frequency can elicit the chaotic behavior in the system, whereas the perturbation amplitudes have to comply with the elementary constraint  $\delta_\varepsilon \leq \varepsilon$  and  $\delta_\zeta \leq \zeta$ , the corresponding frequencies can assume a broader range of values.

The systematic exploration along these lines reveals the following results. First we address the issue of what occurs if only a single parameter,  $\varepsilon$  or  $\zeta$ , undergoes periodic oscillations, while the other parameter is fixed. Note that the chosen parameter values would lead to the limit cycle in the unperturbed system (2). We start by changing the angular frequency of periodic oscillations of parameter  $\varepsilon$ , for the fixed upper limit value of amplitude

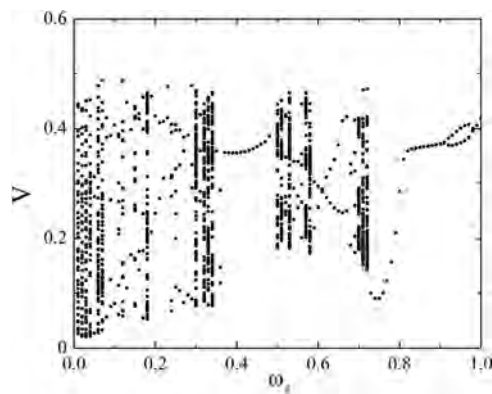


**Fig. 10** Bifurcations of the system (3) under the variation of the parameter  $\zeta$ . Orbital diagram is constructed for the section with plane  $\theta = 1$ , and calculation step  $\omega_\zeta = 0.01$ , showing the asymptotic dynamics after  $4 \times 10^6$  time units. At each instance, the parameters held constant are awarded values near the equilibrium point, but admitting the limit cycle,  $\varepsilon = 0.4$ ,  $\zeta = 0.5$  ( $\delta_\zeta = 0.4$ ), and  $\gamma = 0.8$ . Corresponding time series and phase portraits for quasi-periodic motion are shown in Fig. 11.

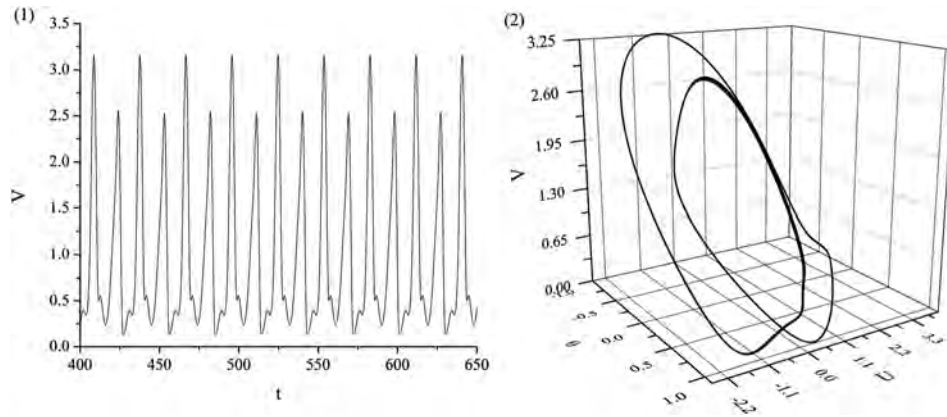


**Fig. 11** Temporal evolution of variable  $V(t)$  and the appropriate phase portrait (2) for  $\omega_\xi = 0.65$  (quasi-periodic motion). At each instance, the parameters held constant are awarded the values near the equilibrium point, but admitting the limit cycle,  $\varepsilon = 0.4$  ( $\delta_\varepsilon = 0.4$ ),  $\xi = 0.5$ , and  $\gamma = 0.8$ .

( $\delta_\varepsilon = 0.4$ ). It turns out that as the parameter  $\omega_\varepsilon$  takes smaller values at each step in the range  $[0,1]$ , a transition from periodic motion to deterministic chaos is observed, with periodic and quasi-periodic windows interspersed between chaotic clouds of dots (Fig. 6). Note that in all of the examined cases trajectory intersects Poincaré surface in only one direction. The typical time series and phase portraits for the corresponding time series are displayed in Fig. 7.

The transition to chaos is verified by calculating the Fourier power spectra for the time series presented in Fig. 7, with the results displayed in Fig. 8. The first maximal peak for fundamental frequency and several smaller peaks for harmonics (as integer multiples of the fundamental frequency) in Fig. 8(1) imply the periodic evolution of the system. The broadband noise in Fig. 8(2) suggests the emergence of a strange attractor. Maximal Lyapunov exponent, which is determined using the method of Wolf et al. [37] converges well to a positive value ( $\lambda_{\max} \approx 0.072$ ), indicating the onset of deterministic chaos (Fig. 9).

The analysis of the system's dynamics when the perturbation of the parameter  $\xi$  ( $\omega_\xi$ ) is assumed (also for the fixed upper value of amplitude,  $\delta_\xi = 0.4$ ) indicates a more complex picture, with successive transition from periodic and quasi-periodic motion to deterministic chaos, interspersed with periodic and quasi-periodic windows (Fig. 10). The corresponding time series and phase portrait for quasi-periodic motion are shown in Fig. 11.

The quasi-periodic motion is further verified by several incommensurate frequencies in Fourier power spectra (Fig. 12) for the time series presented in Fig. 11.

Although the onset of chaos is observed due to a single parameter perturbation, the drawback of such an approach is that the associated perturbation amplitude has to be comparable to the parameter's equilibrium value ( $\delta_\varepsilon = \delta_\xi = 0.4$ ). This is why we conducted additional analysis of complex dynamics of the model (3) by choosing a value of angular frequency admitting the periodic motion of the block in an unperturbed state, while the dynamics is observed by changing the perturbation amplitudes for each of the observed parameter separately (Fig. 13).

As it is clear from Fig. 13, in case of perturbing only a single parameter ( $\varepsilon$  or  $\xi$ ), there is a direct transition to deterministic chaos for both amplitude values  $\delta_\varepsilon$  and  $\delta_\xi$  in the range  $[0,0.4]$ . This type of scenario to chaos could imply the existence of some global bifurcation. One should note that for  $\delta_\xi > 0.4$ , system (3) becomes extremely stiff in the plausible parameter domains, meaning that an exceedingly small iteration step ( $<10^{-5}$ ) is required to carry out the numerical integration.

In the next step of our analysis, we examined another case of a single amplitude perturbation, only this time with higher frequency values ( $\omega_\varepsilon = \omega_\xi = 0.9$ ). As it can be seen in Fig. 14, for

the higher frequency values, a transition from periodic motion to deterministic chaos is observed, which is a type of dynamics already captured in Fig. 6. By comparing orbital diagrams in Figs. 13 and 14, it is clear that the onset of chaos could be controlled only by tuning the angular frequencies of assumed periodic perturbation of the selected parameters ( $\varepsilon$  or  $\xi$ ).

We further proceed by analyzing what occurs if both  $\varepsilon$  and  $\xi$  undergo small oscillations. As a first step in the analysis, we choose values of angular frequencies admitting the periodic motion of the block in an unperturbed state and observe the dynamics of the model (3) by simultaneously changing the amplitude values for both parameters  $\varepsilon$  and  $\xi$  (Fig. 15).

In this case, a transition from periodic motion to deterministic chaos is observed (Fig. 16), with the onset of chaos for higher perturbation amplitudes in comparison to Figs. 13 and 14. The conclusions on the character of the observed behavior rely on the two commensurate frequencies and well-developed continuous noise in the power spectrum for the time series  $V(t)$ , provided in Figs. 17(1) and 17(2), respectively.

Deterministic chaos is further corroborated by calculating the positive value of the maximal Lyapunov exponent, as indicated in Fig. 18, using two different methods [37,38].

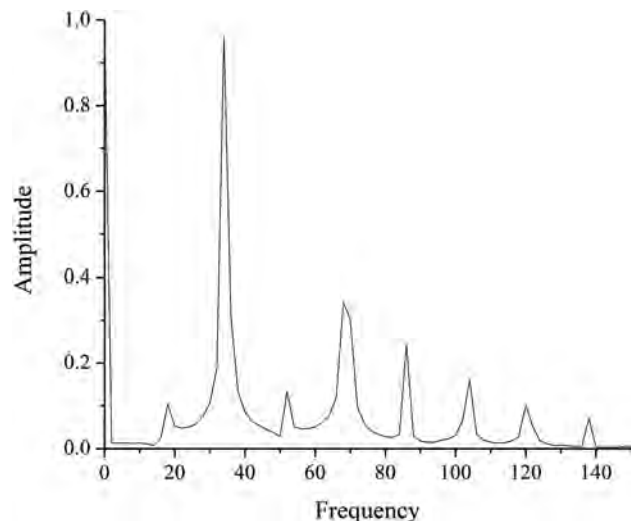


**Fig. 12** Several incommensurate frequencies in Fourier power spectrum indicate quasi-periodic motion. Parameter values are the same as in Fig. 11.

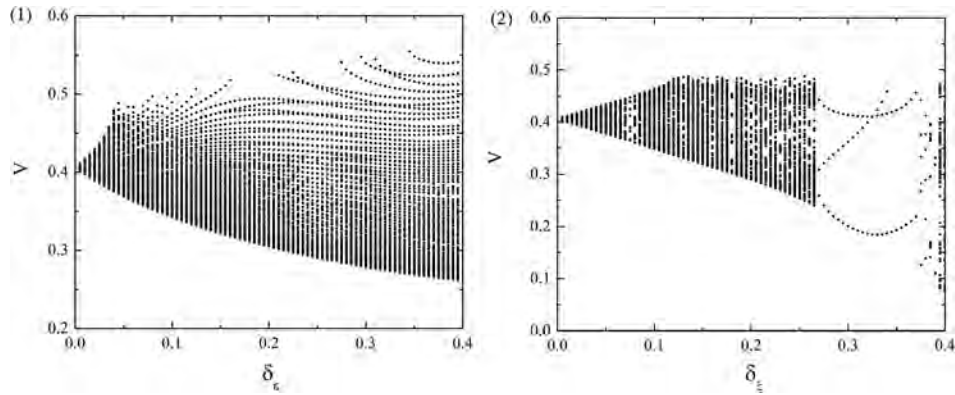


**Fig. 13** Bifurcations of the system (4), for different perturbation amplitudes  $\delta_\varepsilon$  and  $\delta_\zeta$ : (1)  $\omega_\varepsilon = 0.2$ ; (2)  $\omega_\zeta = 0.3$ . In both cases, orbital diagram is constructed for the section with plane  $\theta = 1$ , and calculation step  $\omega_\varepsilon = \omega_\zeta = 0.01$ , showing the dynamics after  $8 \times 10^6$  and  $4 \times 10^6$  time units, respectively. At each instance, the parameters held constant are awarded values near the equilibrium point, but admitting the limit cycle,  $\varepsilon = 0.4$ ,  $\zeta = 0.5$ , and  $\gamma = 0.8$ .

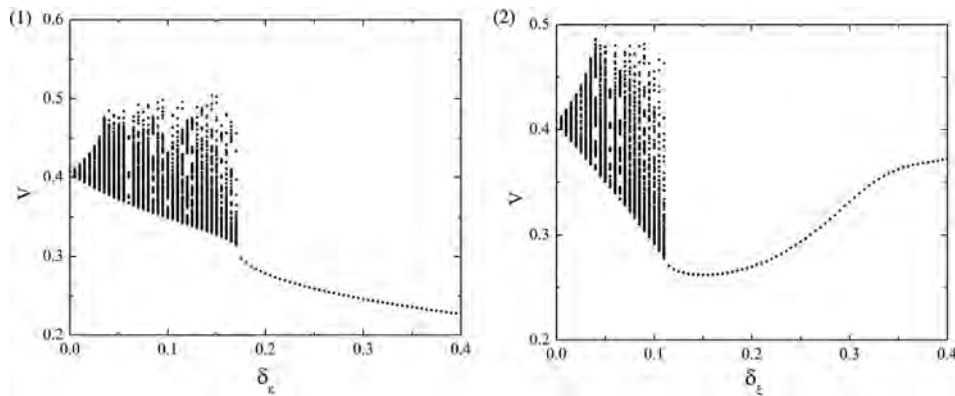


**Fig. 14** Bifurcations of the system (3), for different perturbation amplitudes  $\delta_\varepsilon$  and  $\delta_\zeta$ : (1)  $\omega_\varepsilon = 0.9$ ; (2)  $\omega_\zeta = 0.9$ . In both cases, orbital diagram is constructed for the section with plane  $\theta = 1$ , and calculation step  $\omega_\varepsilon = \omega_\zeta = 0.01$  showing the dynamics after  $8 \times 10^6$  time units. At each instance, the parameters held constant are awarded values near the equilibrium point but admitting the limit cycle,  $\varepsilon = 0.4$ ,  $\zeta = 0.5$ , and  $\gamma = 0.8$ .

If we proceed with further analysis, this time by assuming high constant perturbation frequencies ( $\omega_\varepsilon = \omega_\zeta = 0.9$ ) and by simultaneously changing the amplitude values for both parameters  $\varepsilon$  and  $\zeta$ , in the range  $[0, 0.4]$ , the system (3) exhibits only the periodic motion.

## 5 Concluding Remarks

In this paper, we analyze the effect of periodic parameter perturbation on the onset of complex dynamics in Burridge–Knopoff single-block model. In the first phase of the research, we examine the impact of a single parameter perturbation ( $\varepsilon$  or  $\zeta$ ) on the system's dynamics. The results indicate that the complex dynamics are observed only under a single parameter perturbation for limit amplitude values, with transition from periodic and quasi-periodic motion to deterministic chaos, interspersed with periodic and quasi-periodic windows between chaotic clouds of dots. An interesting finding is that the onset of chaos is observed for the frequencies of a single parameter perturbation near the frequency of periodic motion of the block in an unperturbed state ( $\omega_\varepsilon = 0.2$ ,  $\omega_\zeta = 0.3$ ). In an earthquake analogy, it means that the instability of motion along the fault could be generated by small-amplitude oscillations with a frequency value admitting the aseismic motion along the fault. Further analysis of the system's dynamics with oscillation frequencies assumed constant

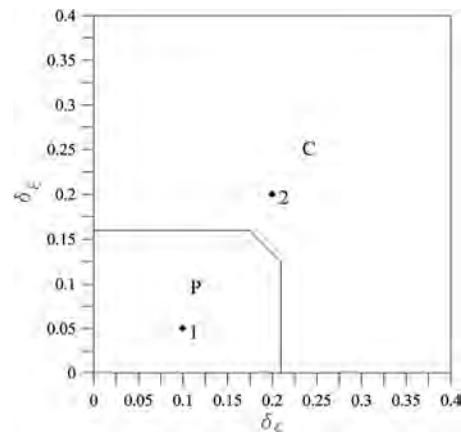


**Fig. 15** Attractors of the system (3) in parameter plane  $\delta_\varepsilon - \delta_\zeta$ , for the frequencies near the frequency of the block in unperturbed state, admitting chaos due to a single parameter perturbation ( $\omega_\varepsilon = 0.2$ ,  $\omega_\zeta = 0.3$ ). Diagram is constructed for the grid  $0.01 \times 0.01$ . At each instance, the parameters held constant are awarded the values near the equilibrium point but admitting the limit cycle,  $\varepsilon = 0.4$ ,  $\zeta = 0.5$ , and  $\gamma = 0.8$ . P and C are abbreviations for periodic motion and deterministic chaos, respectively. Corresponding time series and phase portraits for points 1 and 2 are shown in Fig. 16.

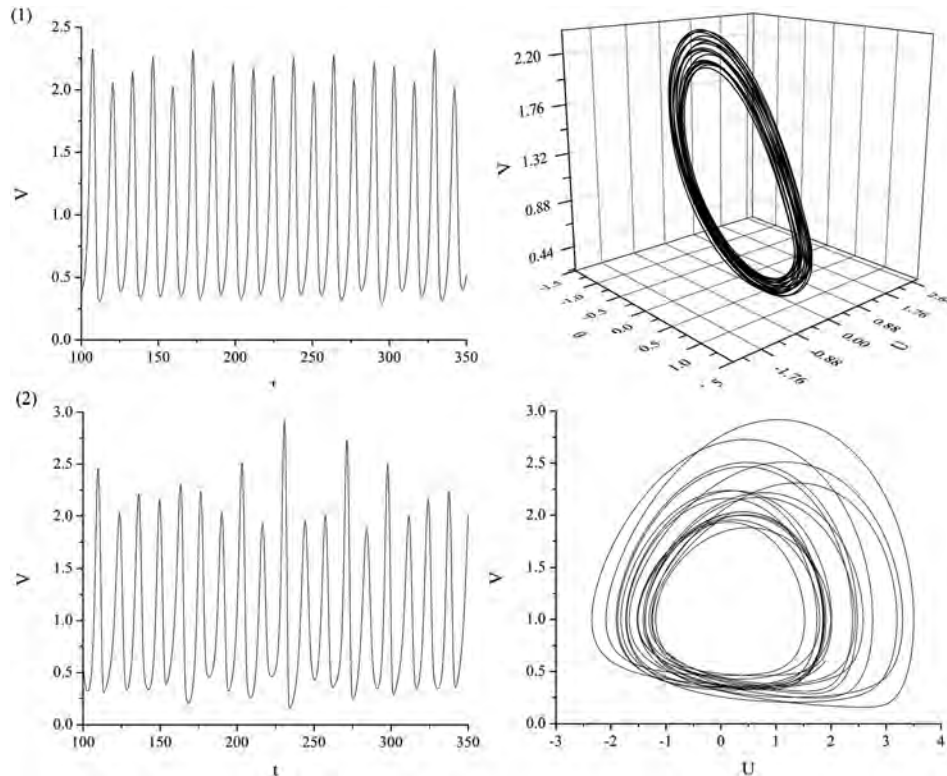


**Fig. 16** Temporal evolution of variable  $V$  and the appropriate phase portraits for points 1 and 2 in Fig. 15: (1)  $\delta_\varepsilon = 0.1$ ,  $\delta_\zeta = 0.05$  (periodic motion); (2)  $\delta_\varepsilon = 0.2$ ,  $\delta_\zeta = 0.2$  (deterministic chaos). At each instance, the parameters held constant are awarded values near the equilibrium point but admitting the limit cycle,  $\varepsilon = 0.4$ ,  $\zeta = 0.5$ , and  $\gamma = 0.8$ . Values of the angular frequency are chosen to be near the angular frequency of the block in an unperturbed state, admitting the onset of deterministic chaos for a single parameter perturbation:  $\omega_\varepsilon = 0.2$ ,  $\omega_\zeta = 0.3$ .

( $\omega_\varepsilon = 0.2$ ,  $\omega_\zeta = 0.3$ ) and only by changing the perturbation amplitudes  $\delta_\varepsilon$  and  $\delta_\zeta$  in the range  $[0, 0.4]$  shows a direct transition to deterministic chaos, which could indicate the existence of global bifurcations. On the other hand, for higher oscillation frequencies ( $\omega_\varepsilon = \omega_\zeta = 0.9$ ), a transition from periodic motion to deterministic chaos is observed. In this case, it is obvious that the onset of chaos could be controlled only by tuning the angular frequencies of assumed single parameter perturbation.

In the second phase of the research, we assume the coaction of both parameters  $\varepsilon$  and  $\zeta$ . By changing only the perturbation ampli-

tudes of both parameters in the range  $[0, 0.4]$  with constant values of frequencies admitting the periodic motion of the block in an unperturbed state ( $\omega_\varepsilon = 0.2$ ,  $\omega_\zeta = 0.3$ ), the results indicate the transition from periodic motion to deterministic chaos, with the onset of chaos only for higher values of perturbation amplitudes in comparison to the case when only a single parameter is perturbed. On the other side, the system (3) exhibits only the periodic motion for the coaction of both perturbed parameters if higher frequency values are presumed ( $\omega_\varepsilon = \omega_\zeta = 0.9$ ).

It has to be emphasized that sinusoidal oscillations represent an idealistic case of parameter perturbation, which rarely occurs

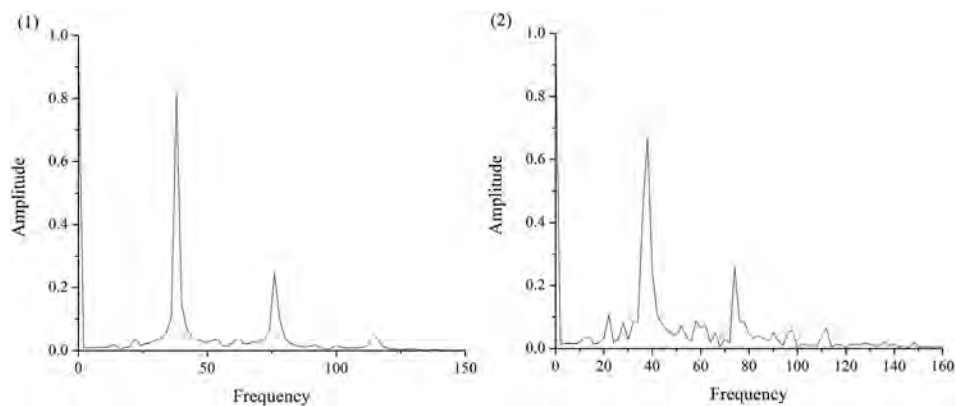


**Fig. 17** (1) Two commensurate peaks in power spectrum (first peak for the fundamental frequency, and the second peak for the harmonic) imply the periodic motion (2). The broadband noise in the Fourier power spectrum indicates the chaotic behavior of the system. The parameter values are the same as in Figs. 16(1) and 16(2), respectively.

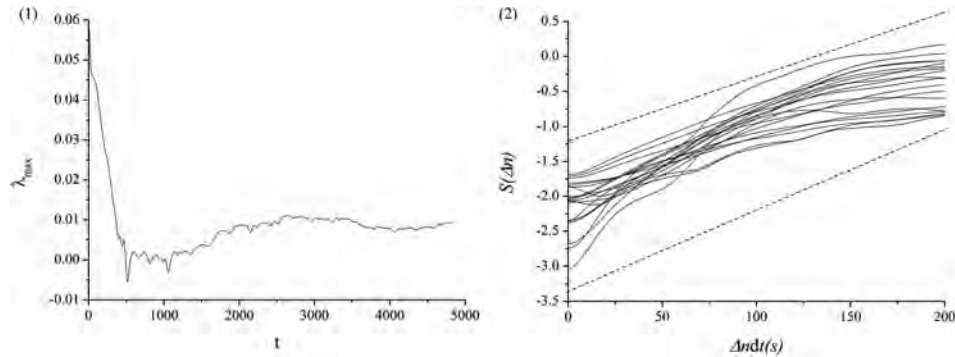


**Fig. 18** Calculation of maximal Lyapunov exponent for a time series in Fig. 17(2): (1)  $\lambda_{\max} = 0.009$  (method of Wolf et al. [37]); (2)  $\lambda_{\max} \approx 0.009$  (method of Rosenstein et al. [38]). Effective expansion rate  $S(\Delta n)$  represents the average of the logarithm of  $D_i(\Delta n)$ , defined as the average distance of all nearby trajectories to the reference trajectory as a function of the relative time  $\Delta n$ . The slope of dashed lines indicating the predominant slope of  $S(\Delta n)$  in dependence on  $\Delta n t$  presents a robust estimate for the maximal Lyapunov exponent. The results are determined for 1000 reference points and neighboring distance  $\varepsilon = 0.1-0.5$ .

under the real conditions in Earth's crust. However, as already stated in the introductory part, we believe they are of interest because of their simple shape and because a real wave pattern results in a superposition of such periodic waves. Also, some earthquakes that arise from slow rupture along the faults could generate seismic waves of such simple shape [33], or they could occur as a product of some artificial source (e.g., heavy mining machines and equipment).

Nevertheless, though the analyzed model and the assumed perturbations are rather simple, the performed analysis showed that the onset of deterministic chaos could be observed for small values of the control parameter  $\varepsilon$ , which is in contrast to the research conducted by Erickson et al. [20], who observed the occurrence of deterministic chaos in Burridge–Knopoff single-block model for  $\varepsilon = 11$ . On the other side, the results of our analysis correspond well with the research also conducted by Erickson et al. [39], where the transition to chaos is observed for  $\varepsilon = 0.5$  as the number of blocks increases from 20 to 21. This further implies that the onset of chaos does not have to be size dependent, as it was already indicated in our previous research on the dynamics of spring-block model with time delay [27].

In the present paper, the focus has been on introducing a minimal model of fault dynamics that can exhibit chaotic behavior. The possible gain from such an approach lies in highlighting the more subtle mechanisms otherwise neglected in the models that involve the compound fault structure. What we actually suggest is that the results obtained here should be viewed as complementary to those established for the more complex models. Nonetheless, the strategy we adopted can likely be replicated in case of the larger number of blocks or be incorporated into the model of a transform fault, implying that the current results may further be reevaluated under some more realistic setups.

## Acknowledgment

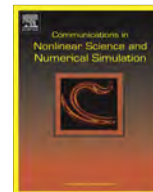
This research has been supported by the Ministry of Education, Science and Technological Development of the Republic of Serbia, Contract Nos. 176016, 171015, and 171017.

## References

- [1] Ohnaka, M., 1993, "Critical Size of the Nucleation Zone of Earthquake Rupture Inferred From Immediate Foreshock Activity," *J. Phys. Earth*, **41**, pp. 45–56.
- [2] Ellsworth, W. L., and Beroza, G. C., 1995, "Seismic Evidence for an Earthquake Nucleation Phase," *Science*, **268**, pp. 851–855.

- [3] Dodge, D. A., Beroza, G. C., and Ellsworth, W. L., 1996, "Detailed Observations of California Foreshock Sequences: Implications for the Earthquake Initiation Process," *J. Geophys. Res.*, **101**, pp. 22,371–22,392.
- [4] Abercrombie, R., and Mori, J., 1994, "Local Observations of the Onset of a Large Earthquake: 28 June 1992 Landers, California," *B. Seismol. Soc. Am.*, **84**, pp. 725–734.
- [5] Mori, J., and Kanamori, H., 1996, "Initial Rupture of Earthquakes in the 1995 Ridgecrest, California Sequence," *Geophys. Res. Lett.*, **23**, pp. 2340–2437.
- [6] Geller, R. J., 1976, "Body Force Equivalents for Stress-Drop Seismic Sources," *B. Seismol. Soc. Am.*, **66**, pp. 1801–1804.
- [7] Ben-Menahem, A., and Singh, S. J., 2000, *Seismic Waves and Sources*, Springer-Verlag, New York.
- [8] Aki, K., and Richards, P. G., 2002, *Quantitative Seismology, Theory and Methods*, Freeman, San Francisco.
- [9] Gibowicz, S. J., and Kijko, A., 1994, *An Introduction to Mining Seismology*, Academic Press, Salt Lake City, UT.
- [10] Brace, W., and Byerlee, J., 1966, "Stick-Slip as a Mechanism for Earthquakes," *Science*, **153**(3739), pp. 990–992.
- [11] Burridge, R., and Knopoff, L., 1967, "Model and Theoretical Seismicity," *B. Seismol. Soc. Am.*, **57**, pp. 341–371.
- [12] Carlson, J. M., and Langer, J. S., 1989, "Mechanical Model of an Earthquake Fault," *Phys. Rev. A*, **40**, pp. 6470–6484.
- [13] Elmer, F.-J., 1997, "Self-Organized Criticality With Complex Scaling Exponents in the Train Model," *Phys. Rev. E*, **56**, pp. R6225–R6228.
- [14] Galvanetto, U., 2002, "Some Remarks on the Two-Block Symmetric Burridge–Knopoff Model," *Phys. Lett. A*, **293**, pp. 251–259.
- [15] Popp, K., and Stelter, P., 1990, "Stick-Slip Vibrations and Chaos," *Phil. Trans. R. Soc. Lond. A*, **332**, pp. 89–105.
- [16] Galvanetto, U., 2001, "Some Discontinuous Bifurcations in a Two-Block Stick-Slip System," *J. Sound Vib.*, **248**, pp. 653–669.
- [17] Ranjith, K., and Rice, J. R., 1999, "Stability of Quasi-Static Slip in a Single Degree of Freedom Elastic System With Rate and State Dependent Friction," *J. Mech. Phys. Solids*, **47**, pp. 1207–1218.
- [18] Scholz, C. H., 2002, *The Mechanics of Earthquakes and Faulting*, Cambridge University Press, Cambridge.
- [19] Montagne, R., and Vasconcelos, G. L., 2004, "Complex Dynamics in a One-Block Model for Earthquakes," *Physica A*, **342**, pp. 178–185.
- [20] Erickson, B., Birnir, B., and Lavallee, D., 2008, "A Model for Aperiodicity in Earthquakes," *Nonlinear Proc. Geoph.*, **15**, pp. 1–12.
- [21] Pomeau, Y., and Le Berre, M., 2011, "Critical Speed-Up vs Critical Slow-Down: A New Kind of Relaxation Oscillation With Application to Stick-Slip Phenomena," arXiv: 1107.3331v1.
- [22] Ruina, A. L., 1983, "Slip Instability and State Variable Friction Laws," *J. Geophys. Res.*, **88**, pp. 10359–10370.
- [23] Tullis, T. E., and Weeks, J. D., 1986, "Constitutive Behavior and Stability of Frictional Sliding in Granite," *Pure Appl. Geophys.*, **124**, pp. 383–414.
- [24] Dieterich, J. H., 1979, "Modeling of Rock Friction, 1. Experimental Results and Constitutive Equations," *J. Geophys. Res.*, **84**, pp. 2161–2168.
- [25] Madariaga, R., and Olsen, K. B., 2002, "Earthquake Dynamics," *International Handbook of Earthquake and Engineering Seismology, Part A*, W. H. K. Lee, H. Kanamori, P. C. Jennings, and C. Kisslinger, eds., Academic Press, London, pp. 176–194.
- [26] Kawamura, H., Hatano, T., Kato, N., Biswas, S., and Chakrabarti, B. K., 2012, "Statistical Physics of Fracture, Friction and Earthquake," *Rev. Mod. Phys.*, **84**, pp. 839–884.
- [27] Kostić, S., Franović, I., Todorović, K., and Vasović, N., 2013, "Friction Memory Effect in Complex Dynamics of Earthquake Model," *Nonlinear Dynam.*, **73**(3), pp. 1933–1943.

- [28] Gombert, J., Blanpied, M., and Beeler, N., 1997, "Transient Triggering of Near and Distant Earthquakes," *B. Seismol. Soc. Am.*, **87**, pp. 294–309.
- [29] Perfettini, H., Schmittbuhl, J., and Cochard, A., 2003, "Shear and Normal Load Perturbations on a Two-Dimensional Continuous Fault: 2. Dynamic Triggering," *J. Geophys. Res.* **108**(2409), pp. 1–16.
- [30] Burić, N., and Vasović, N., 1999, "A Simple Model of the Chaotic Immune Response," *Chaos Soliton. Fract.* **10**, pp. 1185–1192.
- [31] Dieterich, J. H., and Kilgore, B. D., 1994, "Direct Observation of Frictional Contacts: New Insights for State Dependent properties," *Pure Appl. Geophys.*, **143**, pp. 283–302.
- [32] Rice, J. R., Lapusta, N., and Ranjith, K., 2001, "Rate and State Dependent Friction and the Stability of Sliding Between Elastically Deformable Solids," *J. Mech. Phys. Solids*, **49**, pp. 1865–1898.
- [33] Gombert, J., Bodin, P., Savage, W., and Jackson, M. E., 1995, "Landslide Faults and Tectonic Faults, Analogs?—The Slumgullion Earthflow, Colorado," *Geology*, **23**, pp. 41–44.
- [34] Perfettini, H., Schmittbuhl, J., Rice, J. R., and Cocco, M. J., 2001, "Frictional Response Induced by Time-Dependent Fluctuations of the Normal Loading," *Geophys. Res.*, **106**, pp. 13455–13472.
- [35] Gombert, J., Beeler, N. M., Blanpied, M. L., and Bodin, P., 1998, "Earthquake Triggering by Transient and Static Deformations," *J. Geophys. Res.*, **103**, pp. 24411–24426.
- [36] Parsons, T., 2005, "A Hypothesis for Delayed Dynamic Earthquake Triggering," *Geophys. Res. Lett.*, **32**(4), pp. 1–4.
- [37] Wolf, A., Swift, J., Swinney, H., and Vastano, J., 1985, "Determining Lyapunov Exponents From a Time Series," *Physica D*, **16**, pp. 285–317.
- [38] Rosenstein, M. T., Collins, J. J., and De Luca, C. J., 1993, "A Practical Method for Calculating Largest Lyapunov Exponents From Small Data Sets," *Physica D*, **65**, pp. 117–134.
- [39] Erickson, B. A., Birnir, B., and Lavallée, D., 2011, "Periodicity, Chaos and Localization in a Burridge–Knopoff Model of an Earthquake With Rate-and-State Friction," *Geophys. J. Int.*, **187**, pp. 178–198.



## Dynamics of landslide model with time delay and periodic parameter perturbations



Srdan Kostić<sup>a,\*</sup>, Nebojša Vasović<sup>b</sup>, Igor Franović<sup>c</sup>, Dragutin Jevremović<sup>d</sup>, David Mitrinović<sup>e</sup>, Kristina Todorović<sup>f</sup>

<sup>a</sup> Department of Geology, University of Belgrade, Faculty of Mining and Geology, Đušina 7, 11000 Belgrade, Serbia

<sup>b</sup> Department of Applied Mathematics, University of Belgrade, Faculty of Mining and Geology, Đušina 7, 11000 Belgrade, Serbia

<sup>c</sup> Department of Theoretical Mechanics, Statistical Physics, and Electrodynamics, University of Belgrade, Faculty of Physics, Studentski Trg 12, 11000 Belgrade, Serbia

<sup>d</sup> Department of Geotechnics, University of Belgrade, Faculty of Mining and Geology, Đušina 7, 11000 Belgrade, Serbia

<sup>e</sup> Institute for the Development of Water Resources "Jaroslav Černi", Jaroslava Černog 80, 11226 Belgrade, Serbia

<sup>f</sup> Department of Physics and Mathematics, University of Belgrade, Faculty of Pharmacy, Vojvode Stepe 450, 11000 Belgrade, Serbia

### ARTICLE INFO

#### Article history:

Received 11 October 2013

Received in revised form 24 January 2014

Accepted 10 February 2014

Available online 20 February 2014

#### Keywords:

Landslides

Time delay

Stress perturbation

Rate- and state-dependent friction law

### ABSTRACT

In present paper, we analyze the dynamics of a single-block model on an inclined slope with Dieterich–Ruina friction law under the variation of two new introduced parameters: time delay  $T_d$  and initial shear stress  $\mu$ . It is assumed that this phenomenological model qualitatively simulates the motion along the infinite creeping slope. The introduction of time delay is proposed to mimic the memory effect of the sliding surface and it is generally considered as a function of history of sliding. On the other hand, periodic perturbation of initial shear stress emulates external triggering effect of long-distant earthquakes or some non-natural vibration source. The effects of variation of a single observed parameter,  $T_d$  or  $\mu$ , as well as their co-action, are estimated for three different sliding regimes:  $\beta < 1$ ,  $\beta = 1$  and  $\beta > 1$ , where  $\beta$  stands for the ratio of long-term to short-term stress changes. The results of standard local bifurcation analysis indicate the onset of complex dynamics for very low values of time delay. On the other side, numerical approach confirms an additional complexity that was not observed by local analysis, due to the possible effect of global bifurcations. The most complex dynamics is detected for  $\beta < 1$ , with a complete Ruelle–Takens–Newhouse route to chaos under the variation of  $T_d$ , or the co-action of both parameters  $T_d$  and  $\mu$ . These results correspond well with the previous experimental observations on clay and siltstone with low clay fraction. In the same regime, the perturbation of only a single parameter,  $\mu$ , renders the oscillatory motion of the block. Within the velocity-independent regime,  $\beta = 1$ , the inclusion and variation of  $T_d$  generates a transition to equilibrium state, whereas the small oscillations of  $\mu$  induce oscillatory motion with decreasing amplitude. The co-action of both parameters, in the same regime, causes the decrease of block's velocity. As for  $\beta > 1$ , highly-frequent, limit-amplitude oscillations of initial stress give rise to oscillatory motion. Also for  $\beta > 1$ , in case of perturbing only the initial shear stress, with smaller amplitude, velocity of the block changes exponentially fast. If the time delay is introduced, besides the stress perturbation, within the same regime, the co-action of  $T_d$  ( $T_d < 0.1$ ) and small oscillations of  $\mu$  induce the onset of deterministic chaos.

© 2014 Elsevier B.V. All rights reserved.

\* Corresponding author. Tel.: +381 113219107.

E-mail addresses: [srdjan.kostic@rgf.bg.ac.rs](mailto:srdjan.kostic@rgf.bg.ac.rs) (S. Kostić), [nvasovic@rgf.bg.ac.rs](mailto:nvasovic@rgf.bg.ac.rs) (N. Vasović), [igor.franovic@gmail.com](mailto:igor.franovic@gmail.com) (I. Franović), [jevremovic@rgf.bg.ac.rs](mailto:jevremovic@rgf.bg.ac.rs) (D. Jevremović), [davidmitrinovic@yahoo.com](mailto:davidmitrinovic@yahoo.com) (D. Mitrinović), [kisi@pharmacy.bg.ac.rs](mailto:kisi@pharmacy.bg.ac.rs) (K. Todorović).

## 1. Introduction

Landslides constitute a major geologic hazard of strong concern in most parts of the world, posing a serious threat to highway, railway and residential areas. They commonly occur in slopes of different geological and structural setting, and can be triggered by various external factors, such as floods, earthquakes or volcanic eruptions [1]. In order to occur, forces acting on a slope must overcome the friction strength along a possible sliding surface. The traditional way to assess whether a slope is safe or not relies mainly on the use of factor of safety by assuming a limit equilibrium of the soil [2,3]. This analysis commonly uses a simple static Coulomb failure criterion, where shear strength depends on the cohesion  $c$  and the angle of internal friction  $\varphi$  [4]. Here, the constant solid friction coefficient is interpreted as an effective average friction coefficient. This failure criterion simply requires reaching a critical stress threshold  $\tau$  when instability occurs [5]. However, this failure model alone does not explain the time-dependent nature of the failure threshold and it holds only for  $V = 0$ . This temporal dependence of friction along a rough sliding surface was firstly observed in rock mass, and it has a significant impact on the earthquake nucleation [6]. Apparently, real observations, as well as laboratory experiments, indicate temporal logarithmic increase of friction coefficient during the interseismic interval or quasistationary contact between the block and rough surface in the Burridge–Knopoff model [7]. This type of friction is well described by Dieterich–Ruina rate- and state-dependent friction law, which has been studied extensively for rock joints [8–12]. Besides these experiments for dry rock joints, Skempton [13] observed similar behavior of clays in the ring shear tests, for much slower sliding rate ( $V < 0.01$  mm/min), comparing to the results obtained for Burridge–Knopoff model [8,14,15]. Following the results of Skempton [13], it is reasonable to assume that Dieterich–Ruina rate- and state dependent friction law, with logarithmic increase of friction coefficient during the quasistationary contact, also holds for the landslides. Indeed, Chau [16] suggested that Dieterich–Ruina friction law with one state variable can be used to model landslides that occur in natural infinite slope along a plane of weak surface, such as a persistent rock joint, a rock joint filled with wet gouge or soil or a soil interface. Some years later, further research conducted by Chau [17] showed that two state variables are often needed for a more complete description of the shear stress evolution with deformation, motivated by the experiments on quartzite [9], dolomite [18] and granite [12].

Triggering and propagation of shallow landslides is commonly modeled by using a discrete element method [19] or a molecular dynamics approach [20]. In this paper, following the suggestion of Chau [16] and Helmstetter et al. [1], we assume that the sliding process could be described by a single sliding block moving along the rough surface. In particular, we model a landslide as a block resting on an inclined slope forming an angle  $\varphi$  with respect to the horizontal [21–23]. This phenomenological model describes only the landslides with translational slope failures, which can be idealized by infinite slope assumptions like the Vaiont landslide or La Clapiere landslide [1]. Furthermore, we assume that a pre-existing weak plane exists within the slope, and that a landslide occurs as a consequence of the unstable slip of a creeping slope when it is subject to small external perturbation [22,24,25].

As for the nature of friction between the block and the rough surface, we suppose that it could be described by Dieterich–Ruina friction law, but with only one state variable. The effect of the other state variable, as well as the delayed increase in frictional strength, is modeled by introducing the time delay parameter  $T_d$  in friction term. This kind of analysis was already applied for the earthquake nucleation model in our previous research [26]. Another reason for inclusion of time delay in friction term is that the delayed increase of static friction coefficient is observed in laboratory experiments, as well as in the quiescent period of seismic stress drop during the recurrence interval [6]. By assuming the analogy between the landslide faults and tectonic faults [27–29], it is plausible that this feature is also inherent for the friction coefficient along the sliding surface. It has to be emphasized that our approach here differs from the research on spring-block Burridge–Knopoff model of earthquake nucleation, primarily because gravitational pull is considered instead of spring–slider system.

Besides the introduction of time delay, the second part of the analysis included the external triggering effect of earthquake, by assuming periodic sinusoidal perturbations of the initial shear stress  $s_0$ . The sinusoidal earthquake signal could correspond to long duration shear seismic wave [28,30], or it could be generated by non-natural sources such as vehicle traffic [28]. As far as the authors are aware, this analysis is new and the seismic impact on landslide dynamics has not been investigated in this way so far. However, similar analysis was conducted for some biological systems [31], where periodic

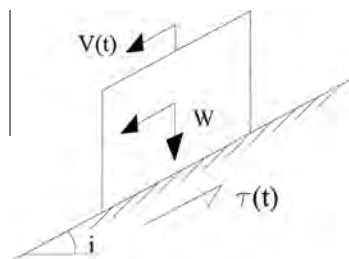


Fig. 1. The single-block model of landslide on an inclined slope with velocity  $V(t)$  under gravitational pull.



parameter perturbation are attributed to various slow internal and external changes of the surrounding environment, basic variables and processes.

The paper consists of the following sections. In the first section, original model is described together with the corresponding Dieterich–Ruina rate-and state-dependent friction law. Here we also present results of the previous research and motivate our further analysis. In the second section, time delay parameter  $T_d$  is introduced and the dynamics of the system is analyzed numerically and by the means of standard local bifurcation analysis. In the third section we assume periodic perturbation of initial shear stress  $\mu$ , and observe the changes in the landslide dynamics. In the fourth section, we analyze the co-action of both parameters  $T_d$  and  $\mu$ . In the final section, we give discussion on the obtained results, together with the proposal for the future research.

## 2. Description of the original model and its derivatives

The aim of this paper is to provide a general framework which applies the one state variable friction law to landslide problems. To make the problem mathematically tractable, we only consider landslides which can be idealized by infinite slope assumptions (Fig. 1), as suggested in the work of Chau [16,17].

According to Chau [16], a motion of the single block on an inclined slope could be described by the system of three coupled nonlinear first-order differential equations:

$$\begin{aligned} \frac{dV}{dt} &= g \sin \alpha - \frac{\tau}{\rho h} \\ \frac{d\tau}{dt} &= \frac{d\theta}{dt} + \frac{A}{V} \frac{dV}{dt} \\ \frac{du}{dt} &= V \end{aligned} \quad (1)$$

where  $g$  is gravitational constant ( $9.81 \text{ m/s}^2$ ),  $\alpha$  is the slope angle,  $\rho$  is the mass density,  $h$  is the thickness of the overlying soil,  $\tau$  is the shear strength along the sliding surface,  $V$  and  $u$  are the velocity and displacement of the block, respectively, while  $A$  represents material constant, dependent on rock type, pressure, temperature and sliding velocity [32].

We model the shear strength along the sliding surface using a rate- and state-dependent friction law, which was originally developed to characterize laboratory observations of fault friction dependence on slip, time and sliding velocity [9]. In present paper, the choice of such friction model for sliding process was motivated by the results of laboratory analysis in the work of Skempton [13], which showed that this friction model is also valid for fluid-saturated clay and siltstone containing low clay fraction:

$$\begin{aligned} \tau &= \tau_0 + \theta + A \ln \left( \frac{V}{V_0} \right) \\ \frac{d\theta}{dt} &= -\frac{V}{L} \left[ \theta + B \ln \left( \frac{V}{V_0} \right) \right] \end{aligned} \quad (2)$$

For  $V = 0$ , it is assumed that Coulomb's friction law applies:  $\tau_0 = \mu\sigma$ , where  $\mu$  and  $\sigma$  are the frictional coefficient and the normal stress at the slip surface. In model (2)  $\tau_0$  represents the threshold shear stress at some reference sliding velocity  $V_0$ ,  $B$  is an empirical constant, depending on the properties of soil,  $L$  is a characteristic slip distance comparable to a typical asperity length (characteristic decay length scale), while  $\theta$  denotes the time-dependent state variable, which is a function of the history of sliding [33]. State variable  $\theta$  represents an evolving time scale, as a delayed reaction of friction to instantaneous changes in velocity [34]. In the static case,  $\theta = t$ , and Dieterich [8] suggested that  $\theta$  can be interpreted as the average age of contacts, i.e. the average elapsed time since the contacts were first formed. In present case, this variable is introduced to characterize the current mechanical state of the slip surface, and, in general,  $\theta$  remains constant for the steady state, but evolves for unsteady slip [16].

Following the idea of Chau [16], the model of infinite slope evolution could be expressed in the subsequent dimensionless form:

$$\begin{aligned} \frac{ds}{dT} &= -\lambda e^v [s - s_0 - (1 - \beta)v] + \frac{e^{-v}}{\kappa} (\gamma - s) \\ \frac{dv}{dT} &= \frac{e^{-v}}{\kappa} (\gamma - s) \\ \frac{d\delta}{dT} &= e^v \end{aligned} \quad (3)$$

where  $s = \tau/A$  (dimensionless stress),  $v = \ln(V/V_0)$  (dimensionless velocity),  $\delta = u/h$  (dimensionless displacement),  $T = V_0 t/h$  (dimensionless time),  $s_0 = \tau_0/A$ ,  $\kappa = \rho V_0^2/A$ ,  $\gamma = \rho g h \sin \alpha/A$ ,  $\beta = B/A$  and  $\lambda = h/L$ .

Equilibrium point for the system (3) is obtained by assuming that  $ds/dT = dv/dT = 0$ , while  $d\delta/dT = \text{const}$ . Hence, the parameter values at the equilibrium point must satisfy the following conditions:

$$\begin{aligned} s &= \gamma \\ v &= \frac{\gamma - s_0}{1 - \beta} \\ \delta &= e^v T \end{aligned} \quad (4)$$

In present analysis, the initial conditions  $(s, v, \delta)$  are set near the equilibrium point.

The dynamics of this original model [16] for various range of parameter values shows two different stability regimes depending on parameter  $\beta$ , as the control parameter whose values determine the onset of bifurcations. For  $\beta < 1$ , which corresponds to velocity strengthening behavior, the motion of the block along the slope is so slow, that it could be approximated by the steady state of the block. All the solutions approach the improper node as  $t \rightarrow \infty$ . Similarly, for  $\beta = 1$ , the block moves along the slope with constant velocity, whose magnitude rises with the change of parameter  $s_0$  in the range  $[0, 1]$ . According to Chau [16] all trajectories of the system (3) in this regime converge to neutrally stable equilibrium point. On the other hand, for  $\beta > 1$ , which represents velocity weakening friction law, the motion becomes unstable in a way that velocity of the block increases very fast and for a certain time interval, it suddenly diverges to infinity. In present paper, in contrast to Chau [16], we neglect the negative values of the block velocity, which appears for  $s_0 > 1$ . This indicates the motion of the block in opposite direction, which is not possible for natural sliding process, except for periodic perturbations due to earthquake triggering. Also, in contrast to Chau [16] we consider only the positive values of parameter  $\beta$ , since long-term or short-term stress changes cannot take negative values. Parameters  $\lambda$ ,  $\kappa$ ,  $\beta$  and  $\gamma$  have positive values.

### 3. Extended model with time delay

In the first phase of the research, we incorporate time delay in model (3) in the following way:

$$\begin{aligned} \frac{ds}{dT} &= -\lambda e^v [s(T - T_d) - s_0 - (1 - \beta)v] + \frac{e^{-v}}{\kappa} (\gamma - s) \\ \frac{dv}{dT} &= \frac{e^{-v}}{\kappa} (\gamma - s) \\ \frac{d\delta}{dT} &= e^v \end{aligned} \quad (5)$$

where meaning of all terms is the same as in (3). In this way, we also model the influence of the second state variable, introduced previously in the work of Chau [17]. Apparently, the results of previous research showed that for the two-state variable friction law bifurcation occurs when the imaginary axis is crossed, as a dividing line of stable region and unstable region (Hopf bifurcation) [17].

The introduced time delay in dimensionless shear stress term emphasizes the delayed response of the friction (along the slip surface) to the sudden increase of sliding velocity. Such an abrupt velocity change is commonly caused by the effect of rainfalls, which is usually considered as the main triggering factor of slope instability. This assumption corresponds well with the results of laboratory test on fluid-saturated clay with low sliding rates, performed by Skempton [13], which clearly show the jump in shear stress before it decreases to the steady state value. Moreover, similar assumption has already been made in the case of a spring-block model of earthquake nucleation with much higher sliding rates [26], and it lead to new dynamical features. However, direct comparison of the present analysis with the previous researches on earthquake nucleation process cannot be made, since the present non-linear system is formulated by considering gravitational pull instead of spring-slider system, despite the fact that the same Dieterich–Ruina friction law is used.

#### 3.1. Local stability and bifurcations of the stationary solution

The system (5) has only one stationary solution, namely  $(s, v) = (1, 0)$ , according to (4), for the following parameter values:  $s_0 = \gamma = 1.0$ ,  $\lambda = 1.5$ , and  $\kappa = 2.0$ . We shall proceed in a standard way to determine and analyze the characteristic equation of (5) around a stationary solution  $(1, 0)$ .

Linearization of the system (5) and substitution  $s = Ae^{\Delta T}$ ,  $v = Be^{\Delta T}$  and  $s(T - T_d) = Ae^{\Delta(T - T_d)}$  results in a system of algebraic equations for the constants  $A$  and  $B$ . This system has a nontrivial solution if the Jacobian matrix satisfies the following condition:

$$\begin{vmatrix} -\frac{1}{\kappa} - \lambda e^{-\Delta T_d} - \Delta & \lambda(1 - \beta) \\ -\frac{1}{\kappa} & -\Delta \end{vmatrix} = 0 \quad (6)$$

In other words, the characteristic equation of the system (5) must fulfill the following constraint:

$$\Delta^2 + \Delta \left( \frac{1}{\kappa} + \lambda e^{-\Delta T_d} \right) + \frac{\lambda}{\kappa} (1 - \beta) = 0 \quad (7)$$

By substituting  $\Delta = i\omega$  in (7), we obtain:

$$\frac{\omega^2 - \frac{i}{\kappa}(1 - \beta) - i\omega\frac{1}{\kappa}}{i\omega\lambda} = (\cos \omega T_d - i \sin \omega T_d) \quad (8)$$

The resulting two equations for the real and imaginary part of (8) after squaring and adding give an equation for the parameter  $\beta$  in terms of the other parameter  $\omega$ , and vice versa, and after division, an equation for  $T_d$  in terms of the parameters  $\beta$  and  $\omega$ . In this way, one obtains parametric representations of the relations between  $T_d$  and the parameters, which correspond to the bifurcation values  $\Delta = i\omega$ . The general form of such relations is illustrated by the following formula for  $\beta$  as a function of  $\omega$ :

$$\beta_{1,2} = \frac{1}{2} \left[ -\frac{8}{3}\omega^2 + 2 \pm \frac{8\sqrt{2}}{3}\omega \right] \quad (9)$$

On the other hand, for  $\omega$  as a function of  $\beta$ :

$$\omega_{1,2}^2 = \frac{(14 - 6\beta) \pm 4\sqrt{2(5 - 3\beta)}}{8} \quad (10)$$

and for  $T_d$  as a function of  $\beta$  and  $\omega$ :

$$T_d = \frac{1}{\omega} \left[ \arctg \left( \frac{2\sqrt[3]{4}(1 - \beta) - \omega^2}{\omega} \right) + k\pi \right] \quad (11)$$

where  $k$  is any nonnegative integer such that  $T_{dk} \geq 0$ .

Though the very form of the solution adopted for the characteristic equation is indicative of Hopf bifurcations, the rigorous proof of this claim is rather lengthy to convey [35–37]. Here it suffices to say that the above parametric equations for  $\beta$ ,  $\omega$  and  $T_d$  coincide with the Hopf bifurcation curves illustrated in Fig. 2 for the fixed parameter values  $s_0 = \gamma = 1.0$ ,  $\lambda = 1.5$ , and  $\kappa = 2.0$ .

Reading from Fig. 2, one learns that only by increasing the time-lag  $T_d$ , e.g. by setting  $T_d = 0.5$ ,  $T_d = 2$ ,  $T_d = 7$  and  $T_d = 10$ , and by slightly changing the other parameter values, the block dynamics changes from the fixed point, over the limit cycle oscillation (first Hopf bifurcation) and torus (second Hopf bifurcation) to chaos. In particular, the system exhibits quasiperiodic (Ruelle–Takens–Newhouse) route to chaos [38,39]. Corresponding time series and phase portraits for points  $a$ ,  $b$ ,  $c$  and  $d$  in Fig. 2, are shown in Fig. 3. Broadband noise in Fourier power spectrum (Fig. 4) confirms the onset of deterministic chaos.

### 3.2. Numerical approach

In spite of the favorable results of the previous analysis indicating the onset of complex dynamics under the variation of the introduced time delay, we stress that the local stability analysis naturally does not capture the existence of global bifurcations. This is why we extended the analysis by numerically integrating model (5) near the equilibrium point (4). Regarding the fashion in which the delay-differential equations are numerically solved, the initial function is selected such that its values within the interval  $[-T_d, 0]$  are set by the first equation in (5) with  $\lambda = 0$ . In all the examined cases we adopt Runge–Kutta fourth order numerical integration method, due to simplicity and low computational cost, with the remark that qualitatively the same results could be obtained using an implicit integration scheme (e.g. backward differentiation formula), primarily intended for solving complex systems, as the one analyzed in this case. At each instance, the parameters

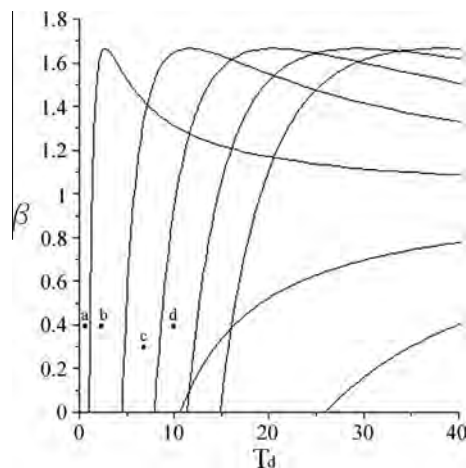


**Fig. 2.** Hopf bifurcation curves  $T_d(\beta)$ , for the fixed values of parameters  $s_0 = \gamma = 1.0$ ,  $\lambda = 1.5$ , and  $\kappa = 2.0$ . The appropriate time series and the phase diagrams corresponding to points  $a$ ,  $b$ ,  $c$  and  $d$  are shown in Fig. 3.

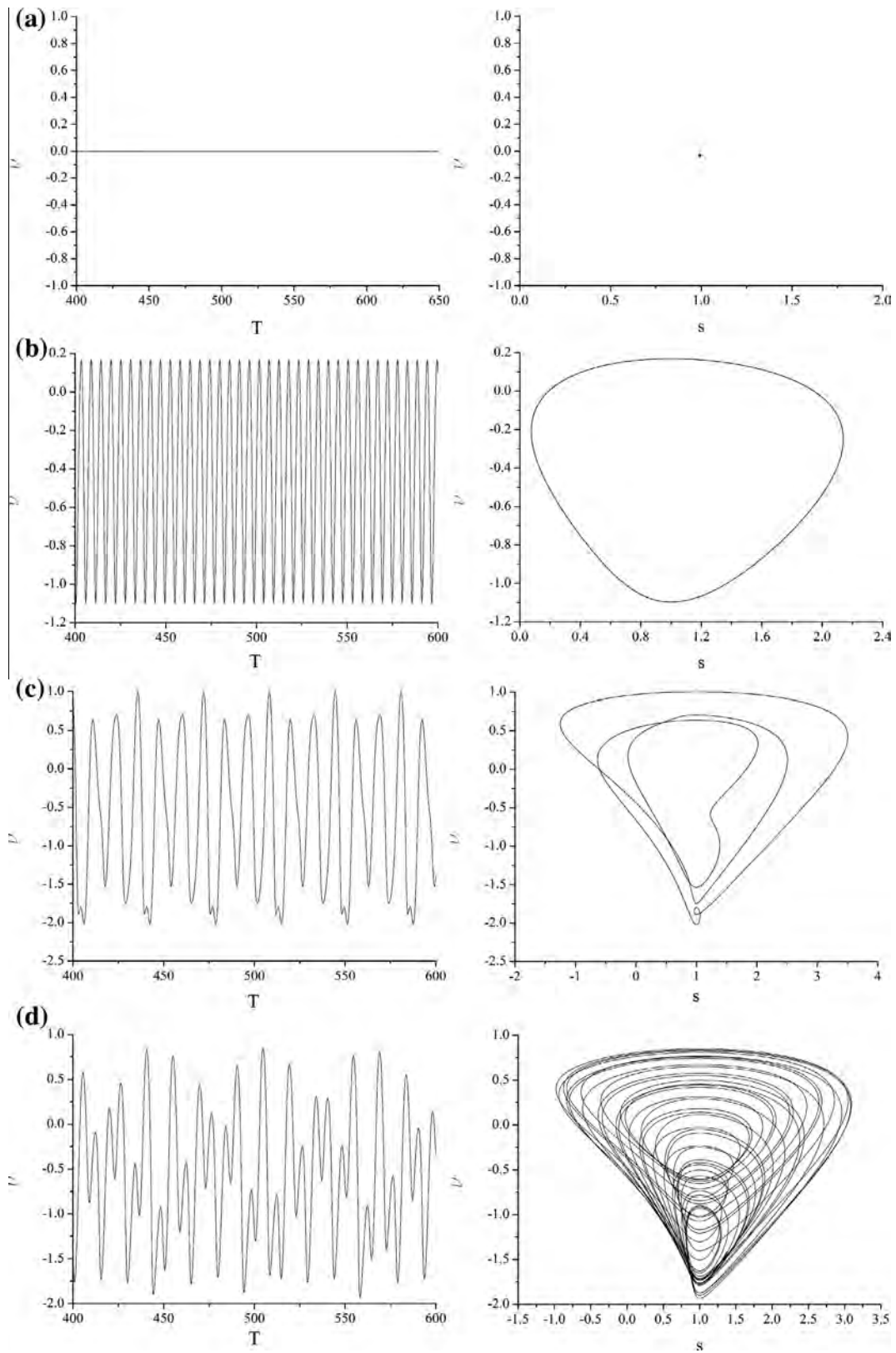


**Fig. 3.** Temporal evolution of variable  $V$  and the corresponding phase portraits for: (a)  $T_d = 0.5, \beta = 0.4$ , (equilibrium state); (b)  $T_d = 2, \beta = 0.4$  (periodic motion); (c)  $T_d = 7, \beta = 0.3$  (quasiperiodic motion); (d)  $T_d = 10, \beta = 0.4$  (deterministic chaos). In all the examined cases, other parameter values are as in Fig. 2.

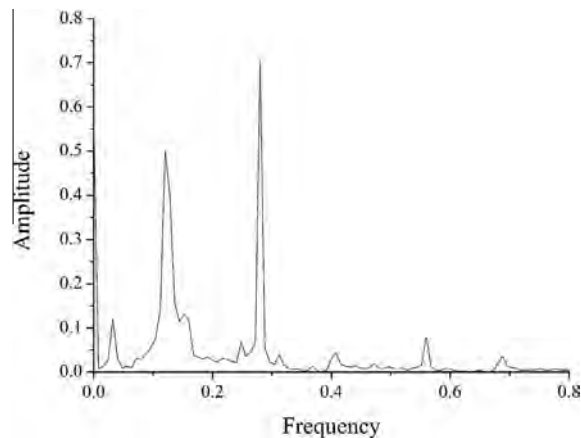


**Fig. 4.** Broadband noise in Fourier power spectrum indicates the chaotic behavior of the system. The parameter values are identical to those in Fig. 3(d).

held constant are awarded values near the equilibrium point. The dynamics of the block for  $\beta < 1$  and for  $T_d$  in range [0.1–10] is shown in Fig. 5.

If we compare Figs. 2 and 5, it is clear that numerical approach indicates much complex behavior, with small areas of quasiperiodic and chaotic motion, which imply the existence of global bifurcations, which will not be analyzed in present paper.

The scenario of deterministic chaos was further confirmed by calculation of the Fourier power spectrum for oscillations, torus and chaotic orbits (Figs. 6 and 7a). The single peak in power spectrum in Fig. 6(a) indicates the oscillatory behavior of the system under study, while the quasiperiodic behavior (torus) is verified by the second peak in Fig. 6(b). The broadband noise in Fourier power spectrum (Fig. 7a) and positive value of maximal Lyapunov exponent, calculated by method of Wolf et al. [40] indicate that the attractor is strange (Fig. 7b).

In Fig. 8, the maximal Lyapunov exponent is calculated using the method of Rosenstein et al. [41]. One could note that the obtained values of  $\lambda_{\max}$  by using the Wolf's (Fig. 7b) and Rosenstein's method (Fig. 8) are of the same order of magnitude.

For  $\beta = 1$ , system under study shows no complex dynamics under the increase of the included time delay. Apparently, for a first few values of time delay, the velocity of the block decreases in comparison to the original model, exhibiting finally a transition to equilibrium state. Further increase of time delay induce negative constant velocity of the block, meaning that block moves upwards, which is not physically possible, and this case is neglected in our analysis (Fig. 9). In other words, in

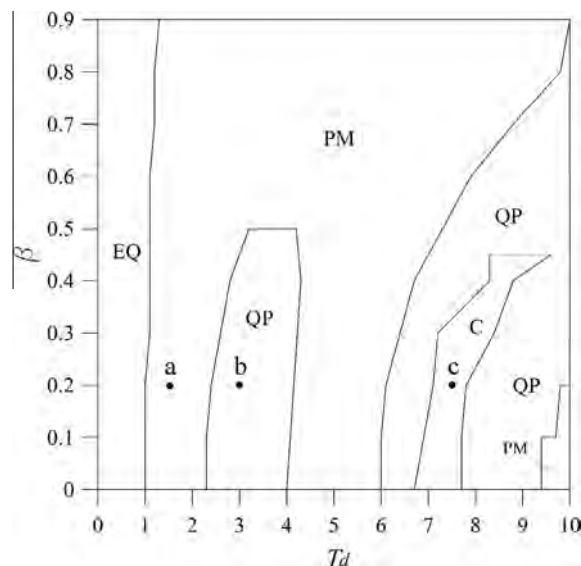


**Fig. 5.** Parameter domains ( $T_d, \beta$ ), admitting equilibrium state (EQ), periodic (PM) and quasiperiodic motion (QP) and deterministic chaos (C). Diagram is constructed numerically, for the step size equal 0.1 for both  $T_d$  and  $\beta$ . Other parameter values are:  $s_0 = 1.0$ ,  $\lambda = 1.5$ ,  $\kappa = 2.0$  and  $\gamma = 1.0$ . Corresponding power spectra for points  $a$ ,  $b$  and  $c$  are shown in Fig. 6, while the largest Lyapunov exponent is calculated for point  $c$  in Fig. 7.

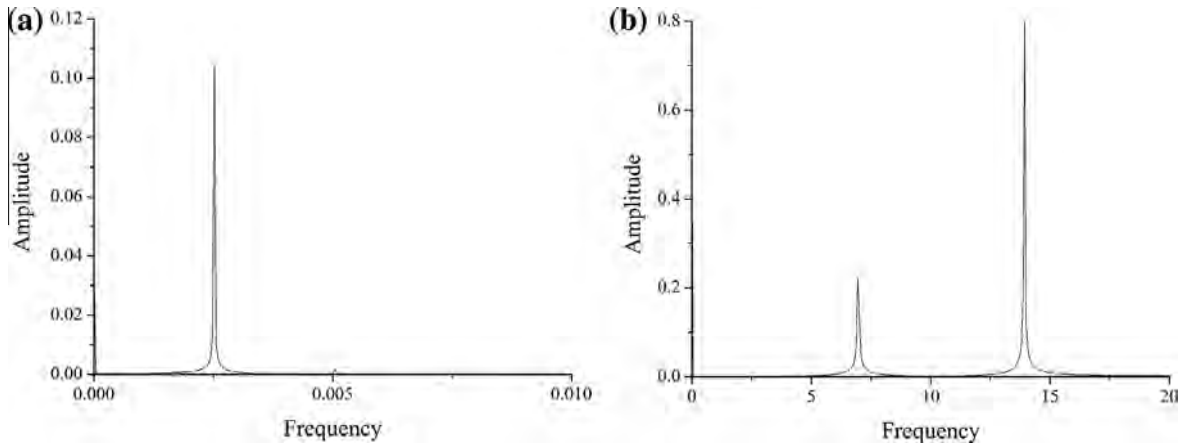


**Fig. 6.** (a) Single peak in power spectrum indicates the oscillatory behavior of the model for  $T_d = 1.5$ ,  $\beta = 0.2$  (point *a* in Fig. 5) (b) two peaks in power spectrum imply the appearance of torus for  $T_d = 3$ ,  $\beta = 0.2$  (point *b* in Fig. 5). In all the examined cases, other parameter values are as in Fig. 5.

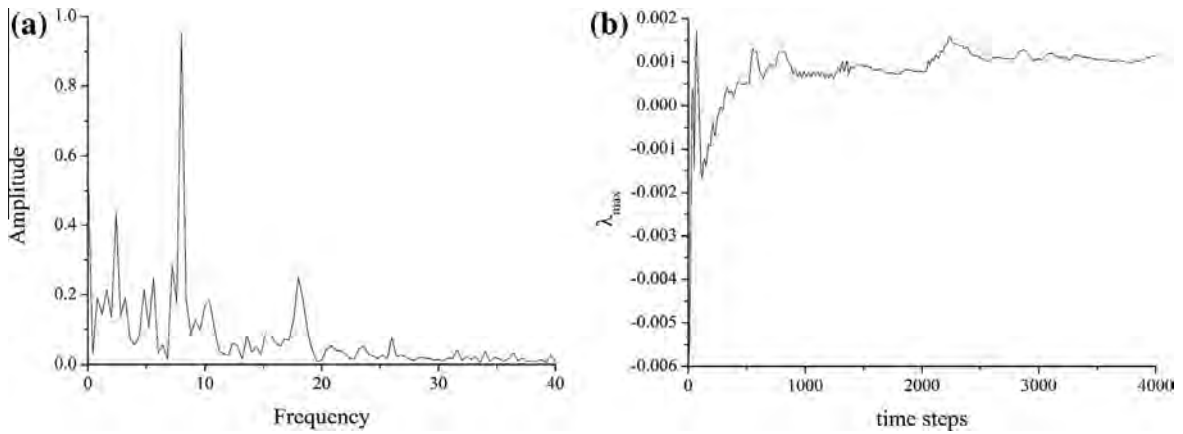


**Fig. 7.** (a) The broadband noise in Fourier power spectrum indicates the chaotic behavior of the system for  $T_d = 7.5$ ,  $\beta = 0.2$  (point *c* in Fig. 5); (b) maximal Lyapunov exponent converges well to  $\lambda_{\max} = 0.0011$ , indicating the presence of deterministic chaos. Other parameter values are as in Fig. 5.

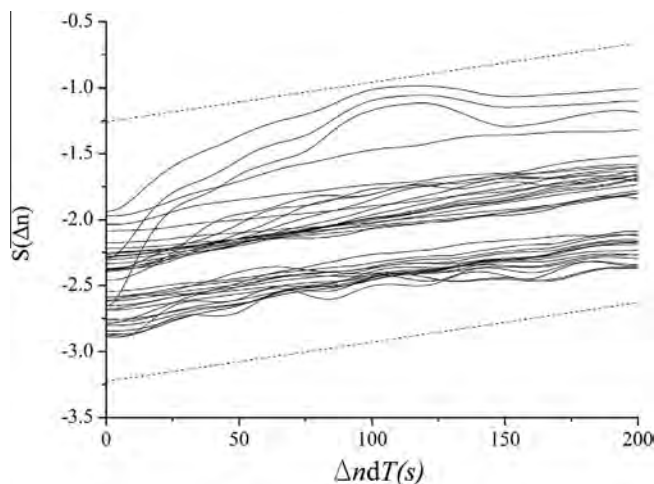


**Fig. 8.** Calculation of maximal Lyapunov exponent for the time series in Fig. 4 (4). The method of Rosenstein et al. [41], implies  $\lambda_{\max} \approx 0.003$ . Effective expansion rate  $S(\Delta n)$  represents the average of the logarithm of  $D_i(\Delta n)$ , defined as the average distance of all nearby trajectories to the reference trajectory as a function of the relative time  $\Delta n$ . The slope of dashed lines indicating the predominant slope of  $S(\Delta n)$  in dependence on  $\Delta ndT$  presents a robust estimate for the maximal Lyapunov exponent. The results are determined for 1000 reference points and neighboring distance  $\varepsilon = 0.15\text{--}0.30$ . The obtained value of maximal Lyapunov exponent is of the same order of magnitude, as in Fig. 7(b).

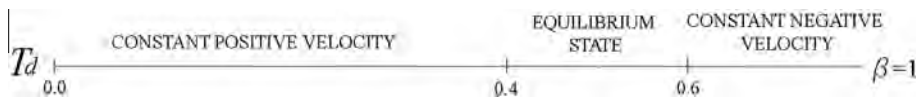


**Fig. 9.** Bifurcations of the system (5) under variation of parameter  $T_d$ , for  $\beta = 1.0$ . At each instance, the parameters held constant are awarded values near the equilibrium point:  $s_0 = 1.0$ ,  $\lambda = 1.5$ ,  $\kappa = 2.0$ , and  $\gamma = 1.0$ .

the case of  $\beta = 1$ , introduction of time delay suppresses the motion, leading eventually to equilibrium state of the block. This type of dynamics differs from the previous case, for  $\beta < 1$ , where the inclusion of  $T_d$  generated more complex behavior.

For  $\beta > 1$ , introduced time delay renders the system (5) extremely stiff in the plausible parameter domains, meaning that an exceedingly small iteration step ( $<10^{-5}$ ) is required to carry out the numerical integration. However, the results of the analysis for  $\beta = 1.1$  and  $T_d = 0.1$ , indicate the chaotic behavior of the model under study (Fig. 10), which is confirmed by continuous broadband noise in the power spectrum (Fig. 11a) and by positive value of the largest Lyapunov exponent (Figs. 11b and 12).

However, it should be emphasized that, even though the maximal Lyapunov exponent converged well to positive values in Figs. 7(b) and 11(b), the standard procedure of Wolf et al. [40] has to be complemented by performing additional averaging over a set of different initial conditions (Fig. 13), since delay-differential equation (5) represents infinite-dimensional system. It is clear that in all the examined cases, maximal Lyapunov exponent converges to positive value of the same order of magnitude as in Figs. 11(b) and 12.

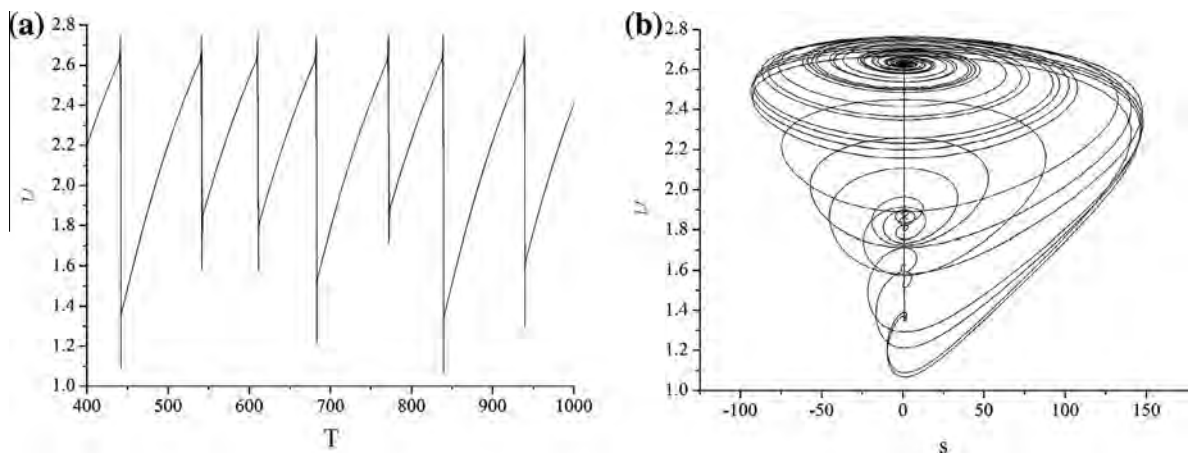


**Fig. 10.** (a) Time series  $u(T)$  and (b) phase portrait for  $\beta = 1.1$  and  $T_d = 0.1$ . Other parameter values are:  $s_0 = 1.0$ ,  $\lambda = 1.5$ ,  $k = 2.0$ , and  $\gamma = 1.0$ .

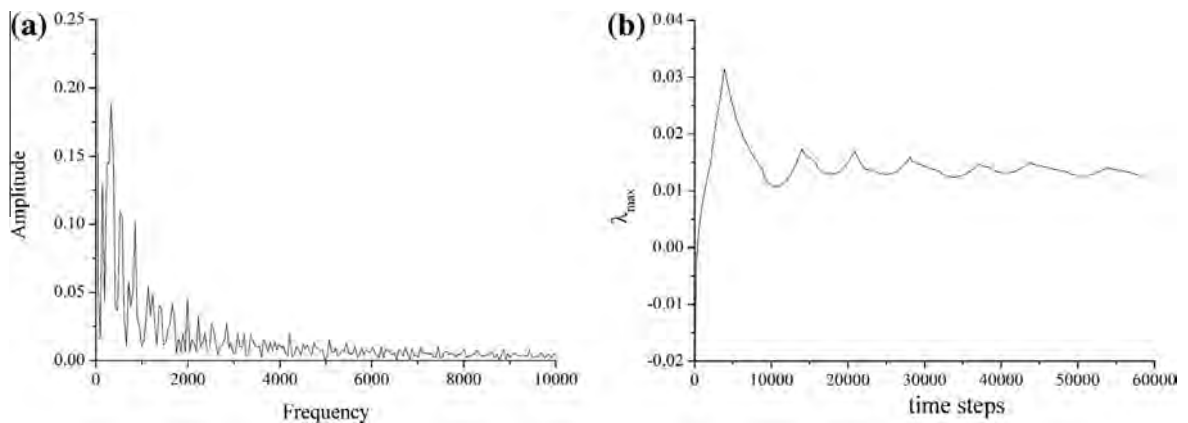


**Fig. 11.** (a) Continuous broadband noise in Fourier power spectrum confirms chaotic motion of block. (b) Maximal Lyapunov exponent converges well to positive value,  $\lambda_{\max} = 0.013$ .

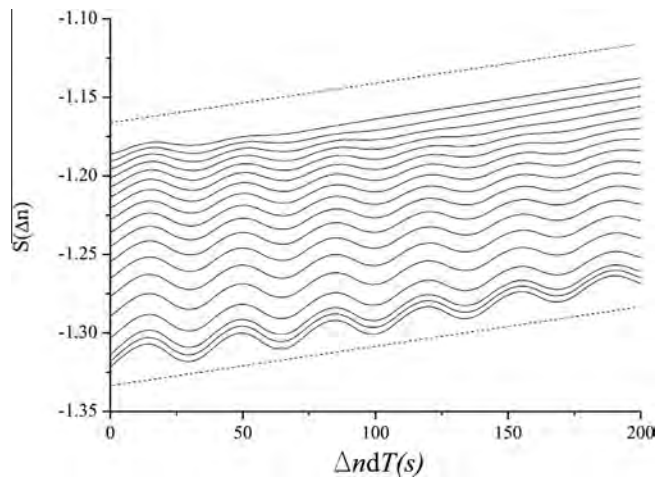


**Fig. 12.** Calculation of maximal Lyapunov exponent for the time series in Fig. 10(a). The method of Rosenstein et al. [41], implies  $\lambda_{\max} \approx 0.014$ . The results are determined for 100 reference points and neighboring distance  $\varepsilon = 0.5-1$ . The obtained value of maximal Lyapunov exponent is of the same order of magnitude, as in Fig. 11(b).

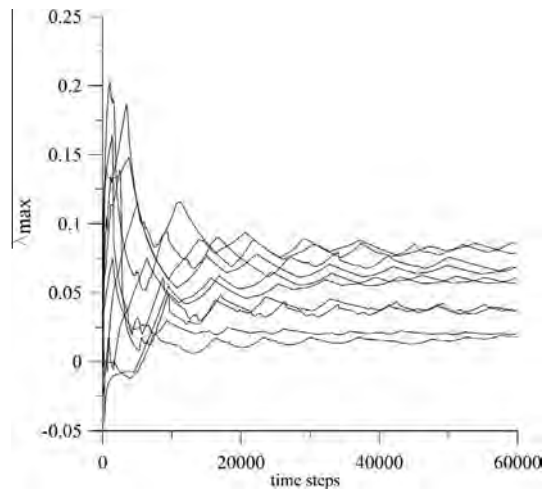


**Fig. 13.** Calculation of maximal Lyapunov exponent by performing additional averaging over a set of different initial conditions, whereby  $s_0$ ,  $v_0$  and  $\delta_0$  belong to the respective ranges  $s_0 \in [0, 1]$ ,  $v_0 \in [0, 0.5]$ ,  $\delta_0 \in [0, 1]$ . The results have been obtained by the method of Wolf et al. [41]. Maximal Lyapunov exponents converge well to positive values of the order  $10^{-2}$ , the same as in Fig. 11(b). Note that time  $t$  is expressed in the units of iteration steps.

#### 4. Extended model with stress perturbation

In the second phase of the analysis, we modified the original model (3) by assuming periodic perturbations of the initial shear stress  $s_0$  due to external earthquake triggering effect:

$$\mu(T) = s_0 + \delta_s \sin(\omega_s T) \quad (12)$$

such that  $\delta_s$ , and  $\omega_s$  represent the constant oscillation amplitude and the angular frequency, respectively. The former satisfy the constraint  $\delta_s \leq s_0$ , which ensures the model's consistency as it confines each perturbation term to an appropriate range of values. In that way, system (3) becomes nonautonomous.

For  $\beta < 1$ , by perturbing only the shear stress  $\mu$ , while the other parameters are held constant for the initially creeping slope (equilibrium state), block exhibits oscillatory behavior. This kind of motion is observed for any frequency value ( $\omega_s$ ) in the range [0.1–2.0]. It is in contrast to the original model, where only the constant positive velocity of the block is observed.

For  $\beta = 1$ , also by assuming limit amplitude oscillations of shear stress  $\mu$ , the velocity of the block takes constant negative values, meaning that block moves upward, in opposite direction, which is physically impossible. Hence, this case is neglected in our analysis.



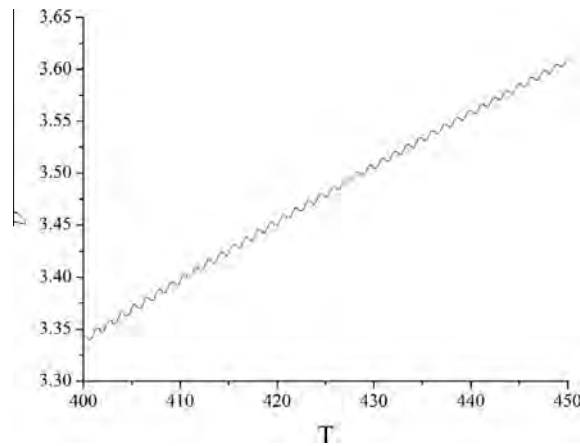


**Fig. 14.** Time series  $u(T)$  for  $\beta = 1.1$ , and for oscillation amplitude  $\delta_s = 1.0$  and frequency  $\omega_s = 5.0$ . At each instance, other parameters held constant are awarded values near the equilibrium point:  $s_0 = 1.0$ ,  $\lambda = 1.5$ ,  $\kappa = 2.0$ , and  $\gamma = 1.0$ .

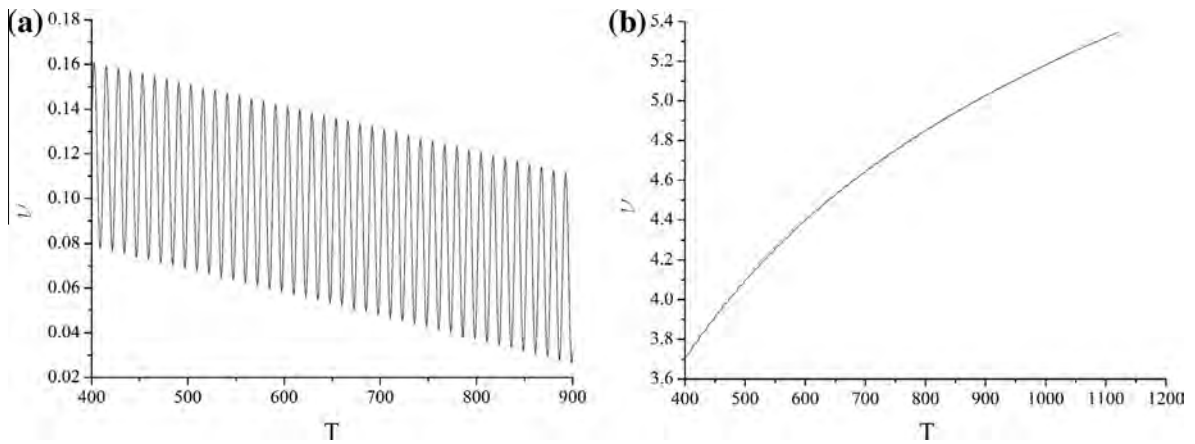


**Fig. 15.** (a) Time series  $u(T)$  for  $\beta = 1$ , under the variation of parameter  $\mu$ , with  $\delta_s = 0.06$  and  $\omega_s = 0.5$ ; (b) time series  $u(T)$  for  $\beta = 1.1$ , and for oscillation amplitude  $\delta_s = 0.2$  and frequency  $\omega_s = 0.5$ . At each instance, other parameters held constant are awarded values near the equilibrium point:  $s_0 = 1.0$ ,  $\lambda = 1.5$ ,  $\kappa = 2.0$ , and  $\gamma = 1.0$ .

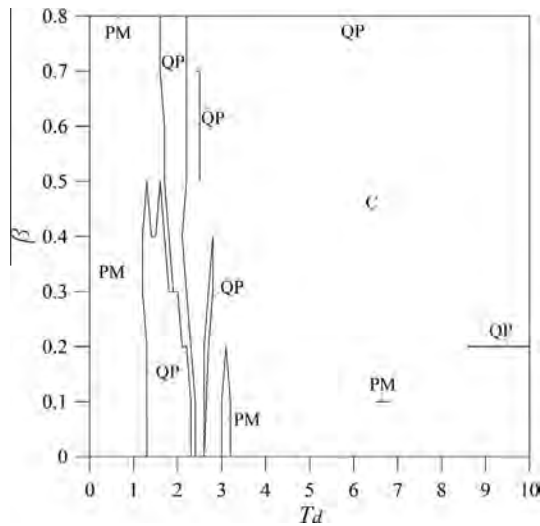


**Fig. 16.** Parameter domains  $(T_d, \beta)$  admitting periodic motion (PM), quasiperiodic motion (QP) and deterministic chaos (C), under the variation of  $\mu$ , with  $\delta_s = 1.0$  and  $\omega_s = 0.5$ . Other parameter values are:  $s_0 = 1.0$ ,  $\lambda = 1.5$ ,  $\kappa = 2.0$  and  $\gamma = 1.0$ . Diagram is constructed for step size equal 0.1 for both  $T_d$  and  $\beta$ . For  $\beta = 0.9$ , velocity of the block becomes negative, meaning that block moves upwards which is neglected in our analysis.

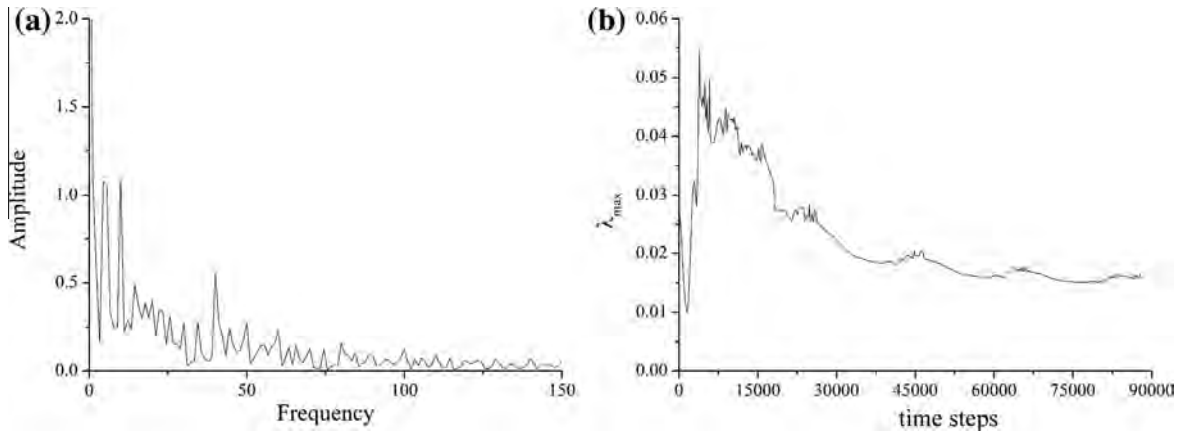


**Fig. 17.** (a) The broadband noise in the Fourier power spectrum indicates the chaotic behavior of the system for  $T_d = 5$ ,  $\beta = 0.3$ ; (b) maximal Lyapunov exponent converges well to  $\lambda_{\max} = 0.016$ , indicating the presence of deterministic chaos. Other parameter values are identical to those in Fig. 16.

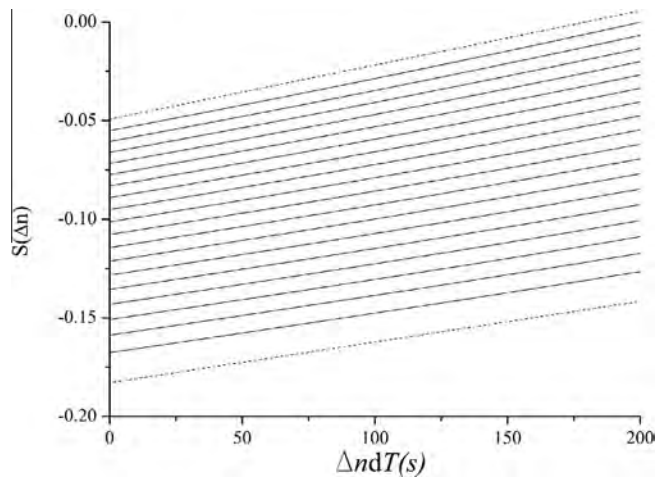


**Fig. 18.** Calculation of maximal Lyapunov exponent for the system (5) under the variation of  $\mu$ , with  $\delta_s = 1.0$  and  $\omega_s = 0.5$ . Other parameter values are:  $T_d = 5$ ,  $\beta = 0.3$ ,  $s_0 = 1.0$ ,  $\lambda = 1.5$ ,  $\kappa = 2.0$  and  $\gamma = 1.0$ . The method of Rosenstein et al. [41], implies  $\lambda_{\max} \approx 0.012\text{--}0.016$ . The results are determined for 100 reference points and neighboring distance  $\varepsilon = 1\text{--}3$ . The obtained value of maximal Lyapunov exponent is of the same order of magnitude, as in Fig. 17(b).

On the other hand, for  $\beta > 1$ , also by perturbing only the shear stress  $\mu$ , velocity of the block takes negative values until  $\omega_s = 4.9$ , after which it becomes positive again and further increasing (Fig. 14). It has to be emphasized that in this case, similar to the previous one with time delay, system (12) is very stiff in numerical sense.

However, one could note that the observed dynamics is generated for the limit amplitude values ( $\delta_s = s_0 = 1.0$ ), which are rarely observed in real conditions. In other words, it is highly unlikely to expect that the shear stress along the slip surface would change from maximum to zero value, since both field and laboratory tests indicate that even in the steady state, shear stress retains a certain minimum positive value. Hence, it is of special interest to investigate whether small parameter perturbations could lead to complex dynamics. Following this idea, additional analysis is conducted for all three dynamical regimes ( $\beta < 1$ ,  $\beta = 1$ ,  $\beta > 1$ ), by decreasing oscillation amplitudes, while other parameter values are being held constant. For  $\beta < 1$ , variation of amplitude value does not render any new dynamics (it remains oscillatory). However, for  $\beta = 1$ , velocity of the block changes periodically for  $\delta_s \leq 0.11$  (Fig. 15a). As for  $\beta > 1$ , velocity of the block rises exponentially for amplitude values  $\delta_s \leq 0.22$  (Fig. 15b).

**5. Co-effect of time delay and stress perturbation**

In the final phase of the analysis, the periodic perturbation of parameter  $s_0$  is assumed in system (5) with included time delay  $T_d$ , for  $\delta_s = 1.0$  (limit amplitude value) and  $\omega_s = 0.5$ . In this case, attractors of the system (5) are shown in Fig. 16 for  $\beta < 1$  and for  $T_d$  in range [0.1–10].

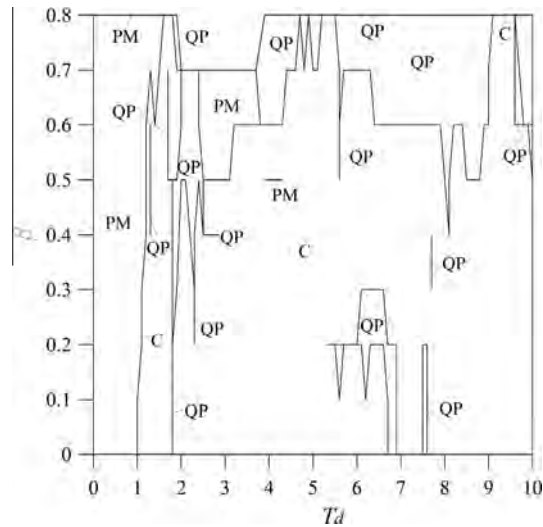


**Fig. 19.** Parameter domains  $(T_d, \beta)$  admitting periodic motion (PM), quasiperiodic motion (QP) and deterministic chaos (C), under the variation of  $\mu$ , with  $\delta_s = 0.5$  and  $\omega_s = 0.5$ . Other parameter values are:  $s_0 = 1.0$ ,  $\lambda = 1.5$ ,  $\kappa = 2.0$  and  $\gamma = 1.0$ . Diagram is constructed for step size equal 0.1 for both  $T_d$  and  $\beta$ . For  $\beta = 0.9$ , velocity of the block becomes negative, meaning that block moves upwards which is neglected in our analysis.

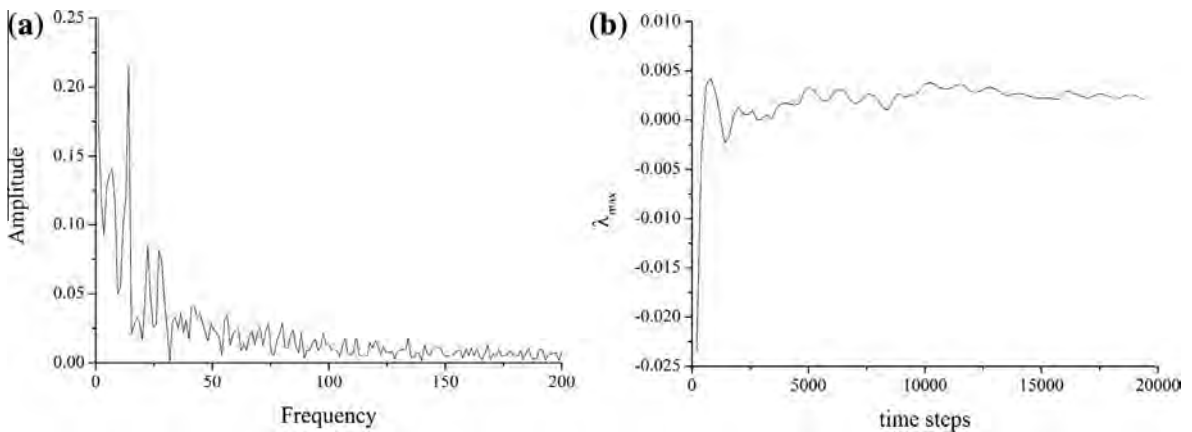


**Fig. 20.** (a) Continuous broadband noise in Fourier power spectrum confirms chaotic motion of block for  $\beta = 1.1$ ,  $T_d = 0.1$ ,  $\delta_s = 0.15$  and  $\omega_s = 0.5$ ; (b) maximal Lyapunov exponent converges well to positive value,  $\lambda_{\max} = 0.002$ . Other parameter values are:  $s_0 = 1.0$ ,  $\lambda = 1.5$ ,  $\kappa = 2.0$  and  $\gamma = 1.0$ .

The onset of deterministic chaos is corroborated by broadband noise in power spectrum (Fig. 17a) and positive value of the largest Lyapunov exponent (Figs. 17b and 18).

It should be noted that the complex dynamics (Fig. 16) is observed for the limit amplitude value of initial stress oscillation ( $\delta_s = 1.0$ ). The results of additional analysis, for  $\beta < 1$  and for smaller amplitude values indicated even more complex behavior. Diagram in Fig. 19 is constructed for oscillation amplitude  $\delta_s = 0.5$ .

For  $\beta = 1$  and for  $\beta > 1$ , and for the limit perturbation amplitudes ( $\delta_s = 1.0$ ), block's velocity is changing periodically in negative domain, which is neglected in our analysis. However, if we assume smaller shear perturbation amplitudes, complex dynamical behavior emerges. For  $\beta = 1$ , if we take that  $\delta_s = 0.06$  (as in Fig. 15), while the other parameter values are as in Fig. 19, the introduction of time delay  $T_d$  slows down the block, and for  $T_d = 0.4$ , the block's velocity becomes negative. Similar behavior is observed for other amplitude values in the range  $[0, 1]$ . As for  $\beta > 1$ , systematic exploration reveals the following dynamics. For  $T_d = 0.1$ , system (5) exhibits chaotic dynamics, if the perturbation amplitude is  $\delta_s \leq 0.18$ , while for  $\delta_s > 0.18$ , as already stated, block's velocity is changing periodically in negative domain. Deterministic chaos is further corroborated by broadband noise in Fourier power spectrum and by positive value of maximal Lyapunov exponent (Figs. 20 and 21).

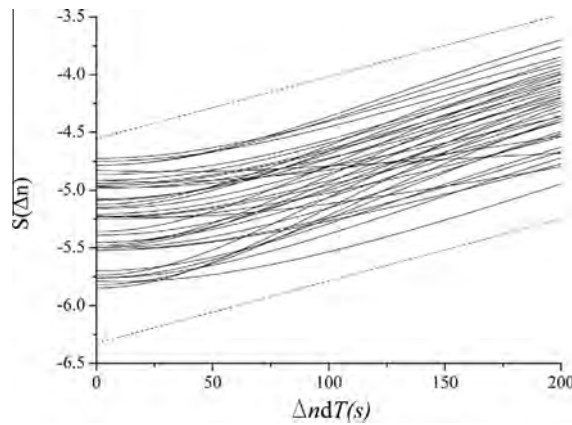


**Fig. 21.** Calculation of maximal Lyapunov exponent for the system (5) under the variation of  $\mu$ , with  $\delta_s = 0.15$  and  $\omega_s = 0.5$ . Other parameter values are:  $\beta = 1.1$ ,  $T_d = 0.1$ ,  $s_0 = 1.0$ ,  $\lambda = 1.5$ ,  $\kappa = 2.0$  and  $\gamma = 1.0$ . The method of Rosenstein et al. [41], implies  $\lambda_{\max} \approx 0.005$ . The results are determined for 1000 reference points and neighboring distance  $\varepsilon = 0.005$ – $0.015$ . The obtained value of maximal Lyapunov exponent is of the same order of magnitude, as in Fig. 20(b).

## 6. Discussion and conclusion

In present paper, we examined the dynamics of the block along the inclined slope, under the variation of two parameters: time delay  $T_d$  and initial shear stress  $s_0$ . We assume that this model phenomenologically describes sliding along the infinite slope. Parameter  $T_d$  mimics the memory effect of the sliding surface, and it is usually interpreted as a function of history of sliding. Also, it could be related to the initial retarded period of the frictional healing during quasistationary contact, which is a feature commonly observed in dynamics of earthquake faults [6,26]. In the same time, this parameter serves as a replacement for the second state variable  $\theta$ , bringing closer in that way the effects of one-state and two-state Dieterich–Ruina friction law. On the other hand, external dynamic effect of long lasting shear waves or traffic vibrations is modeled by periodic perturbations of initial shear stress  $\mu$ . It has to be emphasized that sinusoidal oscillations represent idealistic case of perturbations, which rarely occur in natural conditions. However, as already stated in the introductory part, we believe they are of interest because of their simple shape, and because a real wave pattern results in a superposition of such periodic waves. Also, some long-lasting earthquakes could generate seismic waves of such simple shape [28], or they could occur as a product of some artificial source, e.g. mining vibrations. They also represent the basis for more complex periodic perturbations represented by a sine wave scaled by a Gaussian pulse [42].

In the first phase of the research, each parameter is varied separately, in order to estimate their independent effect on dynamics of motion. The variation of these parameters generate various types of dynamics depending on parameter  $\beta$ , which is confirmed by previous research [16,17] as a control parameter that primarily defines the stability of the system. For  $\beta < 1$ , the change of parameter  $T_d$  renders rich dynamical behavior, with transition from equilibrium state through periodic and quasiperiodic motion to deterministic chaos (Fig. 2). This type of dynamics significantly differs from the original case without  $T_d$ , when the block is in the creeping phase, with the equilibrium point as an improper node [16]. It has to be emphasized that the dynamics of the model (5) with the introduced time delay was examined in two ways: using the standard local bifurcation analysis and numerical approach. Even though the results in both cases are qualitatively similar and indicate the existence of complex dynamics, numerical approach showed additional small areas of complex behavior that were not captured by local bifurcation analysis. This type of behavior could be explained by the effect of global bifurcations, which were not analyzed in present paper. However, by introducing the oscillatory character of the shear stress  $\mu$  without the influence of time delay, while the other parameters are held constant for the initially creeping slope, the analysis shows that block exhibits only oscillatory behavior. For  $\beta = 1$ , the introduction of time delay has an opposite effect – it suppresses the motion, by slowing down the block and generating transition to equilibrium state (Fig. 9). This is contrast to the original model, where only the constant positive velocity of the block is observed, with equilibrium point as a neutrally stable one. On the other hand, perturbation of stress parameter  $\mu$  for  $\beta = 1$  generates negative velocity of the block, which is the case that is not observed in nature. This type of dynamics occurs for limit amplitude values ( $\delta_s = s_0 = 1.0$ ). By decreasing the amplitude values, it is observed that for  $\delta_s \leq 0.11$ , velocity of the block changes periodically, simultaneously decreasing with time (Fig. 15a). For  $\beta > 1$  and with introduced  $T_d$ , system (5) becomes very stiff in numerical sense, so the analysis was done only for  $\beta = 1.1$ , when the chaotic behavior is observed (Figs. 10 and 11). On the other hand, perturbation of  $\mu$  for  $\beta > 1$  (and for limit amplitude value) renders the physically acceptable behavior only for high frequencies ( $\omega_s > 4.9$ ), when the oscillatory motion of the block with increasing amplitude occurs (Fig. 14). By decreasing the amplitude value, for  $\delta_s \leq 0.22$  velocity of the block rises exponentially (Fig. 14b).

In the second phase of the research, combined effect of both parameters is analyzed for the limit amplitude values ( $\delta_s = s_0 = 1.0$ ). For  $\beta < 1$ , complex dynamic behavior is also observed, with transition from periodic and quasiperiodic motion to deterministic chaos (Fig. 16). As it is obvious, dynamics of the model is more complex in this case, meaning that the onset

of chaos is observed for much lower values ( $T_d = 2.3$ ,  $\beta = 0.5$ ) in comparison to the previous one, when only parameter  $T_d$  is varied ( $T_d = 6.7$ ,  $\beta = 0.1$ ). Moreover, if we assume initial shear oscillations of smaller amplitudes ( $\delta_s = s_0 = 0.5$ ) more complex behavior occurs (Fig. 19). In real conditions, it means that external triggering effect of earthquake or some other source of vibrations of any amplitude could easily generate instability and occurrence of sliding along the slope. For  $\beta = 1$  and for  $\beta > 1$ , the velocity of the block is negative, which does not correspond to real conditions on an inclined slope. However, if we assume smaller perturbation amplitude values, complex dynamical behavior emerges. For  $\beta = 1$  and for the amplitude values in the range  $[0, 1]$  the introduction of time delay  $T_d$  slows down the block, and for  $T_d = 0.4$ , block takes negative velocity. As for  $\beta > 1$ , the introduction of time delay  $T_d$  (while in the same time initial stress is periodically perturbed), systematic exploration reveals the following dynamics. For  $T_d = 0.1$ , system (5) exhibits chaotic dynamics, if the perturbation amplitude is  $\delta_s \leq 0.18$  (Fig. 20). For  $T_d > 0.1$  and for  $\delta_s < 0.18$ , system (5) becomes extremely stiff in numerical sense, meaning that very small iteration steps are required in order to conduct numerical integration.

The performed analysis showed that the most complex dynamics of motion along the slope is observed for  $\beta < 1$ , which corresponds well to the experimental results of Skempton [13]. Apparently, this velocity-strengthening behavior is observed in ring shear laboratory tests for friction stress variations with slip rate changes, for Kalabagh Dam clay and siltstone with low clay fraction. The results of these experiments indicated that the decrease of frictional stress with the ongoing slip ( $B$ ) was lower in comparison to the increase of shear stress along the slip surface ( $A$ ) when the sudden increase in velocity occurs ( $B < A$ ).

In comparison to the original model (3), our analysis shows that the instability of motion along the slope could occur even for  $\beta < 1$  with introduced time delay, while Chau [16] observed the appearance of instable motion only for  $\beta > 1$ , which is, as already stated, the case that is not detected in laboratory conditions [13]. In present analysis, complex dynamics in velocity-weakening regime occurs only for small values of time delay ( $T_d = 0.1$ ) and relatively small perturbation amplitudes ( $\delta_s \leq 0.18$ ).

We have to emphasize that the idea of a chaotic landslide dynamics has already been suggested in [43], where it is shown that chaos appears in the evolutionary process of a slope. Moreover, Qin et al. [44] reported that slope body evolves from a chaotic through periodic and deterministic motion.

Interesting result is certainly the dual effect of time delay  $T_d$  on the motion of the block (meaning that it renders the complex dynamics, and, in the same time, stabilizes the motion of the block) depending on the value of the control parameter  $\beta$ . As it was shown, for  $\beta < 1$ , introduction and variation of  $T_d$  generates complex dynamics, with the complete Ruelle–Takens–Newhouse route to chaos. On the other side, for  $\beta = 1$ , time delay has opposite effect, rendering the transition to equilibrium state.

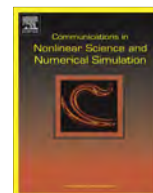
## Acknowledgments

This research has been supported by the Ministry of Education, Science and Technological development of the Republic of Serbia, Contracts No. 176016, 171015 and 171017.

## References

- [1] Helmstetter A, Sornette D, Grasso J-R, Andersen JV, Gluzman S, Pisarenko V. Slider-block friction model for landslides: application to Vaiont and La Clapiere landslides. *J Geophys Res Sol Ea* 2004;109:B02409.
- [2] Skempton AW. Long-term stability of clay slopes. *Geotechnique* 1964;14:77–102.
- [3] Wang J. Comparisons of limit analysis solutions and random search solutions on slope critical slip surface. *Commun Nonlinear Sci* 1998;3:66–71.
- [4] Labuz J, Zang A. Mohr–Coulomb failure criterion. *Rock Mech Rock Eng* 2012;45:975–9.
- [5] Gomberg J, Beeler N, Blanpied M. On rate-state and Coulomb failure models. *J Geophys Res* 2000;105:7857–71.
- [6] Marone C. The effect of loading rate on static friction and the rate of fault healing during the earthquake cycle. *Nature* 1998;391:69–72.
- [7] Scholz C. Earthquakes and friction laws. *Nature* 1998;391:37–42.
- [8] Dieterich JH. Modeling of rock friction – 1. Experimental results and constitutive equations. *J Geophys Res* 1979;84:2161–8.
- [9] Ruina A. Slip instability and state variable friction laws. *J Geophys Res* 1983;88:359–70.
- [10] Rice JR, Ruina A. Stability of steady frictional slipping. *Trans Am Soc Mech Eng* 1983;50:343–9.
- [11] Gu J-C, Rice JR, Ruina AL, Tse ST. Slip motion and instability of a single degree of freedom elastic system with rate and state dependent friction. *J Mech Phys Solids* 1984;32:167–96.
- [12] Tullis TE, Weeks JD. Constitutive behavior and stability of frictional sliding of granite. *Pure Appl Geophys* 1986;124:383–414.
- [13] Skempton AW. Residual strength of clays in landslides, folded strata and the laboratory. *Geotechnique* 1985;35:3–18.
- [14] Carlson JM, Langer JS. Mechanical model of an earthquake fault. *Phys Rev A* 1989;40:6470–84.
- [15] Erickson B, Birmir B, Lavallee D. A model for aperiodicity in earthquakes. *Nonlinear Process Geophys* 2008;15:1–12.
- [16] Chau KT. Landslides modeled as bifurcations of creeping slopes with nonlinear friction law. *Int J Solids Struct* 1995;32:3451–64.
- [17] Chau KT. Onset of natural terrain landslides modeled by linear stability analysis of creeping slopes with a two-state variable friction law. *Int J Numer Anal Methods* 1999;23:1835–55.
- [18] Weeks JD, Tullis TE. Frictional sliding of dolomite: a variation in constitutive behavior. *J Geophys Res* 1985;90:7821–6.
- [19] Crosta G, Imposimato S, Roddeman D. Numerical modelling of large landslides stability and runoff. *Nat Hazards Earth Syst Sci* 2003;523–38.
- [20] Martelloni G, Bagnoli F, Massaro E. A computational toy model for shallow landslides: molecular dynamics approach. *Commun Nonlinear Sci* 2013;18:2479–92.
- [21] Eisbacher GH. Cliff collapse and rock avalanches in the Mackenzie Mountains, Northwestern Canada. *Can Geotech J* 1979;16:309–34.
- [22] Davis RO, Smith NR, Salt G. Pore fluid frictional heating and stability of creeping landslides. *Int J Numer Anal Methods* 1990;14:427–43.
- [23] Durville JL. Study of mechanisms and modeling of large slope movements. *Bull Eng Geol Environ* 1992;45:25–42.
- [24] Savage WZ, Chleborad AF. A model for creeping flow in landslides. *Bull Eng Geol Environ* 1982;19:333–8.
- [25] Davis RO, Desai CS, Smith NR. Stability of motion of translational landslides. *J Geotech Eng ASCE* 1993;119:420–32.
- [26] Kostić S, Franović I, Todorović K, Vasović N. Friction memory effect in complex dynamics of earthquake model. *Nonlinear Dyn* 2013;73:1933–43.

- [27] Fleming RW, Johnson AM. Structures associated with strike-slip faults that bound landslide elements. *Eng Geol* 1989;27:39–114.
- [28] Gomberg J, Bodin P, Savage W, Jackson ME. Landslide faults and tectonic faults, analogs? – The slumgullion earthflow, Colorado. *Geology* 1995;23:41–4.
- [29] Peng Z, Gomberg J. An integrated perspective of the continuum between earthquakes and slow-slip phenomena. *Nat Geosci* 2010;3:599–607.
- [30] Schreyer HL. Inverse solutions for one-dimensional seismic waves in elastic, inhomogeneous media. *J Appl Mech* 1997;44:469–74.
- [31] Burić N, Vasović N. A simple model of the chaotic immune response. *Chaos Solitons Fractals* 1999;10:1185–92.
- [32] C. Scholz, *The mechanics of earthquakes and faulting*, Cambridge University Press, United Kingdom; 2002. p. 471.
- [33] Clancy I, Corcoran D. State-variable friction for the Burridge–Knopoff model. *Phys Rev E* 2009;80:016113.
- [34] Y. Pomeau, M. Le Berre, Critical speed-up vs critical slow-down: a new kind of relaxation oscillation with application to stick-slip phenomena, arXiv: 1107.3331v1 (2011) pp. 1–8.
- [35] Belair J, Campbell SA. Stability and bifurcations of equilibria in a multiple delayed differential equation. *SIAM J Appl Math* 1994;54:1402–24.
- [36] Wiggins S. *Introduction to applied nonlinear dynamical systems and chaos*. New York: Springer; 2003.
- [37] Kuznetsov YA. *Elements of the applied bifurcation theory*. New York: Springer-Verlag; 2004.
- [38] Ruelle D, Takens F. On the nature of turbulence. *Commun Math Phys* 1971;20:167–72.
- [39] Newhouse S, Ruelle D, Takens F. Occurrence of strange axiom-A attractors near quasiperiodic flow on  $T^m$ ,  $m > 3$ . *Commun Math Phys* 1978;64:35–44.
- [40] Wolf A, Swift J, Swinney H, Vastano J. Determining Lyapunov exponents from a time series. *Physica D* 1985;16:285–317.
- [41] Rosenstein MT, Collins JJ, De Luca CJ. A practical method for calculating largest Lyapunov exponents from small data sets. *Physica D* 1993;65:117–34.
- [42] Gomberg J, Blanpied M, Beeler N. Transient triggering of near and distant earthquakes. *Bull. Seismolog Soc Am* 1997;87:294–309.
- [43] Qin S, Jiao JJ, Wang S, Long H. A nonlinear catastrophe model of instability of planar-slip slope and chaotic dynamical mechanisms of its evolutionary process. *Int J Solids Struct* 2001;38:8093–109.
- [44] Qin S, Jiao JJ, Wang S. A nonlinear dynamical model of landslide evolution. *Geomorphology* 2002;43:77–85.



# Stability, coherent spiking and synchronization in noisy excitable systems with coupling and internal delays

Igor Franović<sup>a</sup>, Kristina Todorović<sup>b</sup>, Nebojša Vasović<sup>c</sup>, Nikola Burić<sup>d,\*</sup>

<sup>a</sup> Faculty of Physics, University of Belgrade, PO Box 44, 11001 Belgrade, Serbia

<sup>b</sup> Department of Physics and Mathematics, Faculty of Pharmacy, University of Belgrade, Vojvode Stepe 450, Belgrade, Serbia

<sup>c</sup> Department of Applied Mathematics, Faculty of Mining and Geology, University of Belgrade, PO Box 162, Belgrade, Serbia

<sup>d</sup> Scientific Computing Lab., Institute of Physics, University of Beograd, PO Box 68, 11080 Beograd-Zemun, Serbia

## ARTICLE INFO

### Article history:

Received 7 November 2013

Received in revised form 11 February 2014

Accepted 17 February 2014

Available online 26 February 2014

### Keywords:

Time-delay

Noise

Coherent spiking

## ABSTRACT

We study the onset and the adjustment of different oscillatory modes in a system of excitable units subjected to two forms of noise and delays cast as external or internal according to whether they are associated with inter- or intra-unit activity. Conditions for stability of a single unit are derived in case of the linearized perturbed system, whereas the interplay of noise and internal delay in shaping the oscillatory motion is analyzed by the method of statistical linearization. It is demonstrated that the internal delay, as well as its coaction with external noise, drive the unit away from the bifurcation controlled by the excitability parameter. For the pair of interacting units, it is shown that the external/internal character of noise primarily influences frequency synchronization and the competition between the noise-induced and delay-driven oscillatory modes, while coherence of firing and phase synchronization substantially depend on internal delay. Some of the important effects include: (i) loss of frequency synchronization under external noise; (ii) existence of characteristic regimes of entrainment, where under variation of coupling delay, the optimized unit (noise intensity fixed at resonant value) may be controlled by the adjustable unit (variable noise) and vice versa, or both units may become adjusted to coupling delay; (iii) phase synchronization achieved both for noise-induced and delay-driven modes.

© 2014 Elsevier B.V. All rights reserved.

## 1. Introduction

Generation of different oscillatory modes and their mutual adjustment constitute the basic paradigm behind the local and cooperative dynamics in a wide variety of biological and inorganic systems. Modeling complex multi-scale systems often consists in singling out the components showing typical and well controllable behavior into a few selected degrees of freedom, whereas their interactions incorporate explicit time-delays and different forms of noise. The stochastic component is intended to approximate variations within the embedding environment, as well as the fluctuations due to processes taking place at smaller spatial and temporal scales. The delays typically emerge due to complexity of interactions. In particular, the origin of delay between a sending and a receiving element may be linked to (i) intrinsic times of signal generation in the sending element, (ii) the finite propagation velocity of signals, and (iii) the latency in signal processing of the receiving element [1]. By their characteristic spatial and time-scales, the delays and sources of noise can naturally be associated with the

\* Corresponding author. Tel.: +381 11 3160260; fax: +381 11 3162190.

E-mail address: [buric@ipb.ac.rs](mailto:buric@ipb.ac.rs) (N. Burić).

degrees of freedom pertaining to a single unit (“internal” noise and delays) or those related to the interactions between the units (“external/interaction” noise and delays).

The existence of multiple noises and delays, together with the vast separation of characteristic time scales of the underlying processes, are inevitable features accompanying the modeling of many different biological systems. While the mere presence of these ingredients may be thought of as universal, the prevalence of one type of noise/delay over the other in regard to impact on the system dynamics is an individual feature of any particular system. For instance, the external (synaptic) noise is the dominant factor in the evolution of neuronal systems [2], whereas the internal (biochemical) noise, arising due to small numbers of reactants’ molecules [3], is likely the most prominent form of noise for the dynamics of gene expression regulatory networks [4,5]. Nonetheless, in neuronal systems the conduction delays of type (ii) are manifested more strongly than the delays of type (iii), while in gene networks the coupling delays of types (i) and (iii) occur naturally due to multistage synthesis of the reactants and the complex kinetics of intercellular signaling [5,6]. Regarding the photosynthesis and the related photo-respiration cycle, it has been indicated that the primary stochastic component comes from biochemical noise due to small numbers of reacting molecules [7], whereas the delay may be associated with the multistage assembly of reactants, the processes one would expect to naturally involve memory effects. Notably, there is ample evidence that in many biological systems noise and delay, alone or combined, play a significant role. Apart from the well known impact of these ingredients on neuronal systems [8–12], it has also been found that noise substantially affects the gene expression [13–15]. Also, the delayed negative feedback loops induce oscillations in gene transcription networks [16,6], whereas the interplay of randomness and delay has been demonstrated to accelerate signaling in genetic pathways [17,18,6]. As for photosynthesis, it has been suggested that the optimal amount of noise may enhance efficiency of energy transfer at certain stages of the process [19].

In this paper, the aim is to study in detail the interplay of internal and interaction delays and noise on formation and adjustment of oscillatory modes. This issue is especially intricate if the system is not made up of autonomous oscillators, but rather of excitable units [20]. Excitability rests on the point that equilibrium is poised close to a bifurcation toward periodic activity, whereby a unit may produce oscillations under permanent perturbation. If additional ingredients, such as delays, lead to coexistence of equilibrium and certain oscillatory states, then it becomes interesting to examine how excitability feature is modified due to multistability. Note that the body of work referring to models involving coaction of noise and delays is significantly less compared to those where either of them acts alone. Reluctance to consider nonlinear stochastic models with delays is mainly caused by the fact that the underlying systems of nonlinear stochastic delay-differential equations (SDDEs) are rarely tractable analytically [21,22].

The research here is focused on interaction of stochastic excitable units, whose dynamics is influenced by the coupling and intrinsic delays. We consider a pair of Fitzhugh–Nagumo (FHN) elements, which may be viewed as a basic motif of some complex network. While two distinct forms of perturbation are included as additive noise within the fast and slow subsystems, the model also features two types of delays, one incorporated into the coupling terms and the other related to the recovery mechanism of individual units. Our main goal is to study the particular roles and the co-effects of internal and interaction noise and delays on stability of equilibrium and the onset of different oscillatory modes, further examining regularity of spiking and certain forms of coordinated behavior cast within the framework of stochastic synchronization. Note that the combined effects of two types of noise on a single unit have been considered in [23,24], whereas synchronization of interacting stochastic units in the absence of coupling delays has been analyzed in [25,26]. On the other hand, the results on bifurcations and stability of exact synchronization in the unperturbed system admitting interaction delays have been reported in [27]. Compared to these studies, the novel points here concern (i) the presence of internal delays in each unit, (ii) application of several analytical techniques on the underlying model, including calculation of the stability conditions for the linearized system under perturbation and the method of statistical linearization, as well as (iii) putting emphasis on the competition between the noise-induced and delay-driven oscillatory modes, especially in terms of how it is reflected on the frequency and phase synchronization between the units.

The paper is organized as follows. Section 2 concerns the details of the model, specifying the background and the role of the introduced stochastic terms and delays. Section 3 provides the analysis on stability of a single unit. Apart from considering the local and global bifurcations controlled by intrinsic delay in the deterministic system, we derive the appropriate Fokker–Planck equation and determine stability conditions for the first two moments of the linearized system under perturbation. Method of statistical linearization is applied to study how coaction of noise and delay affects the unit’s oscillatory motion. In Section 4, a pair of interacting units is approached by performing bifurcation analysis for the noiseless case, which demonstrates the prevalence of bistable regimes, either between equilibrium and the oscillatory states or between the different oscillation modes. Section 5 contains numerical results, intended to gain insight into the competition between the delay- and noise-driven modes. The issues of spiking coherence and stochastic synchronization are systematically examined under variation of delays, while letting the noise amplitudes take values below, about and above the resonant ones. Concluding remarks are provided in Section 6.

## 2. Details of the applied model

We consider a couple of identical excitable elements subjected to two types of noise and delay. In its most general form, the model dynamics is given by



$$\begin{aligned} \epsilon dx_i &= [x_i - x_i^3/3 - y_i(t - \tau_{in})]dt + \sqrt{\epsilon} \sqrt{2D_1^i} dW_1^i + c[x_j(t - \tau_{ex}) - x_i(t)]dt, \\ dy_i &= (x_i + b)dt + \sqrt{2D_2^i} dW_2^i, \end{aligned} \quad (1)$$

where  $i, j \in \{1, 2\}$ ,  $i \neq j$  denote unit indices. Parameter  $\epsilon = 10^{-2}$  is set to a small value to ensure a sharp time scale separation between the activator variables  $x_i$  and the respective recovery variables  $y_i$ . In the context of neuroscience, FHN model is regarded as phenomenological, but an analogy may still be drawn between the behavior of the fast variables and the evolution of membrane potential [20]. One may further compare the action of slow variables to a group of complementing relaxation processes, where the most salient is driven by the potassium gating channels. The terms  $dW_1^i$  and  $dW_2^i$  stand for the stochastic increments of the independent Wiener processes. Their expectations and correlations satisfy  $\langle dW_k^i(t) \rangle = 0$  and  $\langle dW_k^i(t) dW_l^j(t') \rangle = \delta_{kl} \delta_{ij} dt$ , having introduced  $k, l \in \{1, 2\}$  to distinguish whether noise acts within the fast or slow subsystem of each unit. Extending the above arguments, the role of stochastic terms in  $x_i$  dynamics may be compared to synaptic noise, made up of random inputs continuously impinging on any given cell from its peer neurons. Note that the synaptic noise constitutes by far the most important noise source in cortical neurons, arising due to the combination of sustained irregular activity and the typically high connectivity of units [2]. As for the stochastic terms in  $y_i$  dynamics, one may conditionally interpret them as thermal noise triggering the random conformation changes of ion-gating channels in the neuron's semi-permeable membrane [23,28]. Since the random fluctuations introduced into fast-variable subsystems may be attributed to the effects of surrounding, whereas the stochastic component in the  $y_i$  dynamics may be associated with the intra-unit sources, in the rest of the paper we refer to them as *external* and *internal noise* [2], respectively.

The form of interaction between the excitable units depends on the particular physical system the model refers to. The most elementary interaction is given by the linear coupling, which in neuronal modeling conforms to electrical synapse. The difference between the characteristic time-scale of  $x_i(t)$  and the one at which the interactions take place justifies the assumption that the coupling terms should include an explicit time-delay  $\tau_{ex}$ . The latter corresponds to the time it takes an excitation to travel between the two connected units at finite propagation speed. Parameter  $c$  characterizes the coupling strength. Following a more detailed analysis of (1), one may argue that there are three qualitatively different domains of  $c$  values. For sufficiently small  $c$ , the units act as if they were independent. Nonetheless, in the noiseless and delay-free case, for comparably large  $c$  the total system behaves as a single multidimensional oscillator. Adding noise and delay then induces only quantitative changes in the properties of the multidimensional oscillations. Therefore,  $c$  is fixed to an intermediate value  $c = 0.1$ , so that variation of delay and noise may introduce qualitative changes in the system dynamics.

Our model also features the intrinsic time delay  $\tau_{in}$ , which is an order of magnitude smaller than the characteristic time-scale set by  $y_i(t)$ . Its role is to modify the relaxation process by influencing the refractory stage after a spike has been elicited. In terms of neuronal modeling, if the analogy between the dynamics of  $y_i(t)$  and the ion-gating channels is accepted, one should also appreciate the point that the channels themselves are composed of subunits which have to act in concert to reach the open state. The time necessary to do so, accounted for by  $\tau_{in}$ , effectively becomes prevalent in the “slope” describing recovery of  $x_i(t)$  to the rest state. In a broader sense,  $\tau_{in}$  specifies an intermediate time-scale, nested between the ones defined by  $x_i(t)$  and  $y_i(t)$ . Such a setup is not unlike the already considered scenario where the FHN units are exposed to colored noise [29], whose correlation time lies between  $\mathcal{O}(\epsilon)$  and  $\mathcal{O}(1)$ . Note that though the internal delay and internal noise may be conditionally associated with the dynamics of ion-channel gating, the mechanisms contributing them are independent. To clarify this, one may invoke a comparison between a certain system influenced by inherent randomness, e.g. internal noise, and a system where the stochastic component coexists with the memory effects. While the former would be described by a set of stochastic differential equations, the dynamics of the latter would be represented by a system of stochastic delay-differential equations, where the terms accounting for the noise and delay are not related.

To briefly explain excitability, let us temporarily confine the discussion to an isolated unit with  $\tau_{in} = 0$ . Excitability rests on the proximity of equilibrium to a bifurcation toward the oscillatory state. FHN model belongs to type II excitability class, which implies that the unit undergoes direct supercritical Hopf bifurcation at the critical threshold [20]. In our case, the bifurcation parameter is  $b$ , whose critical value is given by  $|b| = 1$ : for  $|b| > 1$  the unit lies at equilibrium, whereas for  $|b| < 1$  there exists a limit cycle. Since (1) is invariant under the transformation  $(x_i, y_i, b) \rightarrow (-x_i, -y_i, -b)$ , it suffices to consider only the case  $b > 0$ . For a slightly supra-critical  $b$ , say  $b = 1.05$ , the value fixed throughout the paper, a unit is in the excitable regime: under weak perturbation, it rapidly relaxes back to equilibrium, but an adequate perturbation may elicit a spike, associated with the representative point making a large excursion in phase space before equilibrium is regained.

In model (1), the oscillation modes can be induced by any of the time delays or by any of the noise terms. It is well known that  $\tau_{ex}$  introduces oscillatory motion via the local Hopf or by the global fold-cycle bifurcation, whereby a similar point will be shown for  $\tau_{in}$ . The modes derived from these two scenarios are rather different. Nonetheless, under permanent perturbation, excitable units generate oscillations, which can become coherent at an optimal noise intensity. Two profoundly distinct resonance mechanisms have been established for the additive noise influencing either the activator or the recovery variable. In case of coherence resonance (CR), occurring under internal noise, the stochastic limit cycle is just the precursor of the deterministic one [30,31]. Its phase portrait is akin to the those found in relaxation oscillators, with the two pieces of slow motion  $\mathcal{O}(1)$  connected by the two fast transients  $\mathcal{O}(\epsilon)$ , see Fig. 1(a). The resonance mechanism is based on a trade-off between the durations of the activation and the relaxation times. Nevertheless, in case of self-induced stochastic resonance (SISR), taking place under external noise, the phase portrait of the stochastic cycle is substantially different from the one found in the supercritical deterministic system [31,24], especially with respect to escape from the refractory and the spiking

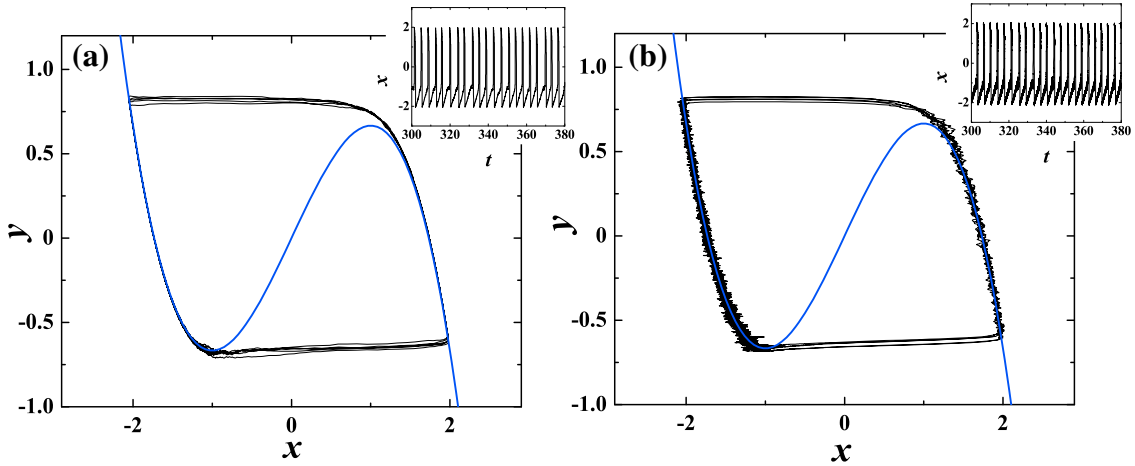


**Fig. 1.** (a) and (b) show phase portraits typical for oscillations induced by internal and external noise, respectively. The noise intensities  $D_2 = 0.0021$  and  $D_1 = 0.0009$  are close to resonant values. In the CR case, the orbit follows the refractory and the spiking branch given by the activator nullcline  $x - x^3/3 = y$ , whereas the points of escape from the branches approximately coincide with the knees  $(x_l, y_l) = (-1, -2/3)$  and  $(x_r, y_r) = (1, 2/3)$  of the nullcline. Under the SISr scenario, the stochastic limit cycle is not the precursor of the deterministic one. In the insets are displayed the corresponding  $x(t)$  series.

branches, cf. Fig. 1(b). The resonance mechanism is much more intricate, and is based on keeping the phase point frustrated at the refractory branch so it can never reach the branch’s knee. In qualitative sense, note that the action of internal noise has a clear interpretation, as it modifies the position of the recovery variable’s nullcline, given by  $x_i = -b$ . This can make the equilibrium unstable, temporarily pushing the system over the critical threshold. Role of external noise cannot be interpreted in a similar fashion.

Given the arguments above and the stated objective to understand the interplay of noise,  $\tau_{ex}$  and  $\tau_{in}$  on systems of excitable units, we treat the cases with external and internal noise separately. This is done so because otherwise the co-effects of noise terms and the co-effects of noise and delays become rather difficult to distinguish.

### 3. Analysis of the single unit’s dynamics

#### 3.1. Derivation of the Fokker–Planck equation

Having made an overview of the dynamics exhibited by a single unit under the influence of noise, let us turn to the analysis of the co-effects of noise and the internal delay. Our intention is to first illustrate the obstacles one is faced with when attempting to tackle this problem via the Fokker–Planck formalism. To this end, we derive the appropriate Fokker–Planck equation assuming the general case of a unit subjected to both external and internal noise ( $c = 0, D_1 > 0, D_2 > 0$ ). Since system (1) features only additive noise, the result is independent on whether Itô or Stratonovich interpretation has been adopted [32]. To begin with, note that the probability distribution of  $x$  and  $y$  is defined by  $p(x, y, t) = \langle \delta[x(t) - x] \delta[y(t) - y] \rangle$ , where  $\langle \cdot \rangle$  denotes averaging over the realizations of the stochastic processes, and the unit index has been dropped for simplicity. Taking the time derivative of the above expression and using the properties of the Dirac delta function, one arrives at

$$\begin{aligned} \frac{\partial}{\partial t} p(x, y, t) = & -\frac{\partial}{\partial x} \langle \delta[x(t) - x] f(x(t), y_{\tau_{in}}) \rangle \langle \delta[y(t) - y] \rangle - \frac{\partial}{\partial y} \langle \delta[y(t) - y] \rangle \langle \delta[x(t) - x] g(x(t)) \rangle \\ & - \sqrt{\frac{2D_1}{\epsilon}} \frac{\partial}{\partial x} \langle \delta[x(t) - x] \xi_1(t) \rangle \langle \delta[y(t) - y] \rangle - \sqrt{2D_2} \frac{\partial}{\partial y} \langle \delta[y(t) - y] \xi_2(t) \rangle \langle \delta[x(t) - x] \rangle, \end{aligned} \tag{2}$$

where the notation  $y_{\tau_{in}} \equiv y(t - \tau_{in})$ ,  $\xi_1(t) = dW_1/dt$ ,  $\xi_2(t) = dW_2/dt$ , as well as  $f(x(t), y_{\tau_{in}}) = [x(t) - x^3(t)/3 - y(t - \tau_{in})]/\epsilon$ ,  $g(x(t)) = x(t) + b$  has been introduced for shorthand. The averages containing stochastic terms can be handled by the Furutsu–Novikov formula [21], which here results in

$$\langle \delta[x(t) - x] \xi_1(t) \rangle = \int_0^t \langle \xi_1(t) \xi_1(t') \rangle \left\langle \frac{\delta\{\delta[x(t) - x]\}}{\delta \xi_1(t')} \right\rangle dt' = \left\langle \frac{\delta\{\delta[x(t) - x]\}}{\delta \xi_1(t)} \right\rangle \tag{3}$$

and the analogous relation for  $\langle \delta[y(t) - y] \xi_2(t) \rangle$ , having applied  $\langle \xi_1(t) \xi_1(t') \rangle = \delta(t - t')$  and  $\langle \xi_2(t) \xi_2(t') \rangle = \delta(t - t')$ . Employing again the properties of the delta function, the functional derivative in (3) may be written as

$$\left\langle \frac{\delta\{\delta[x(t) - x]\}}{\delta\xi_1(t)} \right\rangle = \left\langle -\frac{\partial}{\partial x} \delta[x(t) - x] \frac{\delta x(t)}{\delta\xi_1(t)} \right\rangle, \tag{4}$$

with the similar relation obtained for  $\left\langle \frac{\delta\{\delta[y(t) - y]\}}{\delta\xi_2(t)} \right\rangle$ . From (1) it follows that  $\frac{\delta x(t)}{\delta\xi_1(t)} = \sqrt{\frac{2D_1}{\epsilon}}$  and  $\frac{\delta y(t)}{\delta\xi_2(t)} = \sqrt{2D_2}$ . Knowing that the average  $\langle \delta[x(t) - x] \rangle$  may be calculated as  $\langle \delta[x(t) - x] \rangle = \int_{-\infty}^{\infty} \int_{-\infty}^{\infty} \delta[x(t) - x] p(x, y, t) dx dy$ , one finds

$$\langle \delta[x(t) - x] \xi_1(t) \rangle = -\sqrt{\frac{2D_1}{\epsilon}} \frac{\partial}{\partial x} p(x, y, t), \tag{5}$$

and by the same token,

$$\langle \delta[y(t) - y] \xi_2(t) \rangle = -\sqrt{2D_2} \frac{\partial}{\partial y} p(x, y, t). \tag{6}$$

The results so far refer to the final two terms on the right side of (2). Regarding the first term, by using the law of total expectation, it follows that

$$\langle \delta[x(t) - x] \delta[y(t) - y] f(x(t), y_{\tau_{in}}) \rangle = \iiint \delta[x(t) - x] \times \delta[y(t) - y] [(x(t) - x^3(t)/3 - y_{\tau_{in}})/\epsilon] p(x, y, y_{\tau_{in}}) dx dy dy_{\tau_{in}}. \tag{7}$$

Under general conditions, one cannot assume the statistical independence between  $x(t)$  and  $y(t)$  on one hand and  $y(t - \tau_{in})$  on the other. Therefore, the probability  $p(x, y, y_{\tau_{in}})$  may only be written in the form  $p(x, y, y_{\tau_{in}}) = p(y_{\tau_{in}} | x, y) p(x, y)$ , where  $p(y_{\tau_{in}} | x, y)$  presents the conditional probability of finding  $y_{\tau_{in}}$  at the moment  $t - \tau_{in}$ , provided that  $(x(t), y(t)) = (x, y)$ . Inserting the expression for  $p(x, y, y_{\tau_{in}})$  into (7), we find

$$\langle \delta[x(t) - x] \delta[y(t) - y] f(x(t), y_{\tau_{in}}) \rangle = p(x, y, t) \times \frac{1}{\epsilon} \left[ x(t) - x^3(t)/3 - \int y_{\tau_{in}} p(y_{\tau_{in}} | x, y) dy_{\tau_{in}} \right], \tag{8}$$

where the last term on the right constitutes the so-called conditional drift [22,21,33]

$$\langle y_{\tau_{in}} | x(t), y(t) \rangle = \int y_{\tau_{in}} p(y_{\tau_{in}} | x, y) dy_{\tau_{in}} \tag{9}$$

emerging due to non-Markovian character of the SDDE system (1). Collecting the above results and substituting them into (2), we obtain the Fokker–Planck equation for a FHN unit subjected to external and internal noise, as well as internal delay

$$\begin{aligned} \frac{\partial}{\partial t} p(x, y, t) = & -\frac{1}{\epsilon} \frac{\partial}{\partial x} [x(t) - x^3(t)/3 - \langle y_{\tau_{in}} | x(t), y(t) \rangle] \times p(x, y, t) - \frac{\partial}{\partial y} [x(t) + b] p(x, y, t) + \frac{2D_1}{\epsilon} \frac{\partial^2}{\partial x^2} p(x, y, t) + 2D_2 \\ & \times \frac{\partial^2}{\partial y^2} p(x, y, t). \end{aligned} \tag{10}$$

The standard way to proceed would be to determine the stationary solution of (10), whereby the conditions for system's stability should be inferred by calculating the parameter values under which the stationary distribution can no longer be normalized [21]. The main obstacle for completing this task lies in the inability to resolve the conditional drift term (9) analytically, which forces us to explore other means of estimating the co-effects of noise and internal delay on stability of the stationary solution.

### 3.2. Deterministic system and stability of the linearized system under stochastic perturbation

To get a sense on the impact of  $\tau_{in}$  on the dynamics of a single unit, we analyze its behavior in the deterministic case, obtained from (1) by setting  $c = 0, D_1 = 0, D_2 = 0$ . The index of the selected unit has again been dropped for simplicity. Stability of the stationary solution is determined by the roots of the characteristic equation. The first step in deriving the latter is to linearize the system describing the isolated unit around the fixed point  $(x_0, y_0) = (-b, -b + b^3/3)$ . Assuming that the deviations are of the form  $\delta x(t) = Ae^{\lambda t}, \delta y(t) = Be^{\lambda t}$  and  $\delta y(t - \tau_{in}) = Be^{\lambda(t - \tau_{in})}$ , one arrives at a system of algebraic equations over the coefficients  $A$  and  $B$ . The condition for this system to possess a nontrivial solution is provided by the characteristic equation

$$\epsilon \lambda^2 - \lambda(1 - b^2) + e^{-\lambda \tau_{in}} = 0, \tag{11}$$

whose transcendental form reflects the presence of time delay in the unit's dynamics [34–36]. For the parameter values  $(\epsilon, b) = (0.01, 1.05)$  kept throughout the paper, we have numerically found that the two complex-conjugate roots of (11) cross the imaginary axes at  $\tau_{in}^H = 0.118$ , which indicates the onset of a limit cycle via Hopf bifurcation. Note that the roots

of (11) obtained for small  $\tau_{in}, \lambda_{\pm} = \frac{1 + \tau_{in} - b^2 \pm \sqrt{(1 + \tau_{in} - b^2)^2 - 4\epsilon}}{2\epsilon}$ , imply that the addition of intrinsic delay drives the system away from the critical threshold of the Hopf bifurcation controlled by the parameter  $b$ , meaning that a unit becomes less excitable.

Nevertheless, it turns out that the complete knowledge on the system's behavior with  $\tau_{in}$  cannot be gained by performing just the local bifurcation analysis. Apart for the Hopf bifurcation,  $\tau_{in}$  gives rise to another oscillatory mode by inducing a

global (direct) fold-cycle bifurcation in which an unstable and a large stable limit cycle are born. This global event occurs around  $\tau_{in}^{FC} = 0.106$ , a value smaller than  $\tau_{in}^H$ . Since the fold-cycle bifurcation does not affect the local stability of the fixed point, a deterministic unit exhibits bistability, i.e. coexistence between the equilibrium and the limit cycle within the interval  $\tau_{in}^{FC} < \tau_{in} < \tau_{in}^H$ . However, we also report on an interesting interplay between the local and the global bifurcation for  $\tau_{in} > \tau_{in}^H$ . It turns out that the incipient cycle, emerging around the position of the former equilibrium for  $\tau_{in} = \tau_{in}^H$  grows only until colliding with the unstable cycle born in the global bifurcation. These two cycles get annihilated in an inverse fold-cycle bifurcation, such that the large cycle, created in the direct fold-cycle bifurcation at  $\tau_{in} = \tau_{in}^{FC}$ , remains as the only attractor. Phase portrait of the large cycle is substantially distinct from those of cycles emerging due to noise, cf. Fig. 2(a) and what is shown in Fig. 1(a) and (b). The apparent differences in the relaxation stage are consistent with the role of  $\tau_{in}$ , as explained in Section 2.

Intuitively, adding external or internal noise to physical picture governed by  $\tau_{in}$  could result in several effects. For  $\tau_{in} < \tau_{in}^{FC}$ , a coherent noise-driven mode will emerge at an optimal noise-intensity, whereas rare spiking or fast incoherent spiking will occur at small or large noise intensities, respectively. Within the interval  $\tau_{in}^{FC} < \tau_{in} < \tau_{in}^H$ , the system is likely to become monostable even for very small noise, because stability of equilibrium would be rather sensitive to its presence. The similar point on the loss of bistability also applies to  $\tau_{in}$  values slightly above  $\tau_{in}^H$ , where the deterministic system displays coexistence between a small and a large limit cycle. For any  $\tau_{in} > \tau_{in}^{FC}$ , under increasing noise one is likely to first encounter competition between the delay- and the noise-driven mode, whereas at some point, the stochastic component would overwhelm the deterministic one. We point out that the period of the mode elicited by  $\tau_{in}$  is typically larger than the average ISI characterizing the noise-led oscillations, cf.  $T = 4.44$  for the cycle in Fig. 2(a) vs  $\langle T \rangle = 3.8$  for that in Fig. 1(a). This will prove useful in interpreting the outcome of the competition between the noise- and delay-driven modes later on.

Before considering the effects of perturbation on stability, we make a brief qualitative remark on the interplay of internal noise and  $\tau_{in}$ . For small  $\tau_{in}$ , one can expand the term  $y(t - \tau_{in})$  to first order  $y(t - \tau_{in}) \approx y(t) - \tau_{in} \frac{dy}{dt}$ , which may be used to transform the equations for a single unit into

$$\begin{aligned} \epsilon dx &= (x - x^3/3 - y(t))dt + \tau_{in}(x(t) + b)dt + \tau_{in}\sqrt{2D_2}dW_2, \\ dy &= (x + b)dt + \sqrt{2D_2}dW_2, \end{aligned} \tag{12}$$

This reveals an interesting point that the co-effect of internal delay and internal noise may actually be treated by drawing an analogy to a delay-free system subjected to noise in both the slow and the fast variable, whereby the latter is an order of magnitude smaller than the former. Note that the system described by (12) can be fully analyzed within the Fokker-Planck formalism.

As a final point on the stability of a single unit, we discuss the stability of the system linearized around the stationary solution  $(x_0, y_0) = (-b, -b + b^3/3)$  under stochastic perturbation [21,38,37]. Given that the perturbation is provided by the Gaussian distributed white noise with zero mean and a delta function autocorrelation, it is sufficient to consider the stability of the first  $(\langle \delta x(t) \rangle, \langle \delta y(t) \rangle)$  and second moments  $(\langle \delta x^2(t) \rangle, \langle \delta y^2(t) \rangle, \langle \delta x(t) \delta y(t) \rangle)$  of the solution [38,37], where  $\delta x(t) = x(t) - x_0$  and  $\delta y(t) = y(t) - y_0$ . To derive the equations describing the dynamics of the first moments, one starts off from the linearized system

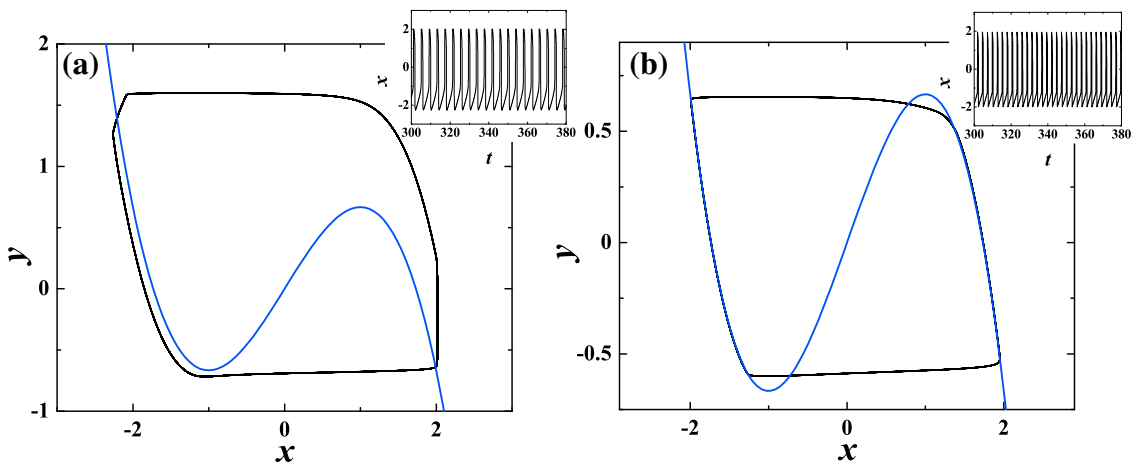


Fig. 2. (a) and (b) show phase portraits corresponding to limit cycles born in global fold-cycle bifurcations induced by  $\tau_{in}$  and  $\tau_{ex}$ , respectively. Note that the former does not follow the cubic nullcline during the declining stage of spike, whereas the latter's orbit involves escaping the slow branches before reaching the knees of the nullcline. In the insets are shown the corresponding  $x(t)$  series. (a) is obtained for a single noiseless unit at  $\tau_{in} = 0.4$ , while (b) refers to a setup with interacting noiseless units for  $(c, \tau_{ex}) = (0.1, 1.2)$ .

$$\begin{aligned} d\delta x(t) &= \frac{1}{\epsilon} [(1-b^2)\delta x(t) - \delta y(t - \tau_{in})]dt + \sqrt{\frac{2D_1}{\epsilon}} dW_1(t), \\ d\delta y(t) &= \delta x(t)dt + \sqrt{2D_2} dW_2(t). \end{aligned} \quad (13)$$

Carrying out integration from 0 to  $t$ , taking the expectation and finally differentiating with respect to  $t$ , from (13) we arrive at

$$\begin{aligned} d\langle \delta x(t) \rangle &= \frac{1}{\epsilon} [(1-b^2)\langle \delta x(t) \rangle - \langle \delta y(t - \tau_{in}) \rangle]dt, \\ d\langle \delta y(t) \rangle &= \langle \delta x(t) \rangle dt, \end{aligned} \quad (14)$$

which is completely analogous to the set of equations determining the stability of the unperturbed unit. Thus, stability of the first moments is readily solved by applying the results reached for the deterministic system.

As far as the equations governing the dynamics of the second moments are concerned, we begin the derivation by taking the Itô derivative [32,46] of  $\delta x^2(t)$  and  $\delta y^2(t)$ . If the steps from above are repeated, using the linearized system (12) and the properties of the stochastic integrals in the Itô interpretation [32], one arrives at

$$\begin{aligned} \frac{d}{dt} \langle \delta x^2(t) \rangle &= \frac{2}{\epsilon} \left[ (1-b^2)\langle \delta x^2(t) \rangle - \langle \delta x(t)\delta y_{\tau_{in}} \rangle + D_1 \right], \\ \frac{d}{dt} \langle \delta y^2(t) \rangle &= 2\langle \delta x(t)\delta y(t) \rangle + 2D_2, \\ \frac{d}{dt} \langle \delta x(t)\delta y(t) \rangle &= \frac{1}{\epsilon} \left[ (1-b^2)\langle \delta x(t)\delta y(t) \rangle - \langle \delta y(t)\delta y_{\tau_{in}} \rangle \right] + \langle \delta x^2(t) \rangle. \end{aligned} \quad (15)$$

Stability of the second-order moments can be analyzed by introducing the two-time correlation functions  $C_{xx}(t, t') \equiv \langle \delta x(t)\delta x(t') \rangle$ ,  $C_{yy}(t, t') \equiv \langle \delta y(t)\delta y(t') \rangle$  and  $C_{xy}(t, t') \equiv \langle \delta x(t)\delta y(t') \rangle$ . From (15) one finds that their stationary values are determined by the noise amplitudes, as well as the parameters  $\epsilon$  and  $b$ :  $C_{xx}^0 = -\frac{D_1+D_2}{1-b^2}$ ,  $C_{yy}^0 = -D_2(1-b^2) - \epsilon\frac{D_1+D_2}{1-b^2}$  and  $C_{xy}^0 = -D_2$ . The system (15) can be linearized about these stationary values, considering the perturbations of the form  $K_{xx} = C_{xx}(t, t') - C_{xx}^0 = Ae^{\lambda t}e^{\lambda t'}$ ,  $K_{yy} = C_{yy}(t, t') - C_{yy}^0 = Be^{\lambda t}e^{\lambda t'}$  and  $K_{xy} = C_{xy}(t, t') - C_{xy}^0 = Ce^{\lambda t}e^{\lambda t'}$ . For fixed  $b = 1.05$  and  $\epsilon = 0.01$ , the ensuing characteristic equation  $2\epsilon^2\lambda^3 - 3\epsilon\lambda^2(1-b^2) + \lambda(1-b^2)^2 - (1-b^2)e^{-\lambda\tau_{in}} = 0$  indicates that the stability of the stationary solution depends solely on  $\tau_{in}$ . It may be shown numerically that the critical value of  $\tau_{in}$  for the second moments is virtually indistinguishable from the critical threshold  $\tau_{in}^H$  obtained for the first moments.

### 3.3. Method of statistical linearization

As a means of characterizing the co-effects of noise and  $\tau_{in}$  on the behavior of a single unit, we invoke an approach that belongs to a corpus of statistical linearization techniques [40,39]. Such methods have originally been developed to gain insight into the interplay of noise and nonlinearity in stochastically perturbed systems. The general idea is to substitute the nonlinear terms with their stationary values calculated in the self-consistent fashion, whereby the impact of noise on the system's dynamics is ultimately reduced to a dependence on the noise amplitude. Note that the latter property is reminiscent to what is typically obtained by the mean-field approaches [41–45].

The immediate goal is to translate the original dynamics of a single unit into an analogous two-dimensional Ornstein-Uhlenbeck process, described by a system of linear SDEs of the form [46]

$$d\mathbf{x}_s(t) = -\hat{A}\mathbf{x}_s(t)dt + \hat{B}d\mathbf{W}(t), \quad (16)$$

where bold letters indicate vectors,  $\hat{A}$  and  $\hat{B}$  are the appropriate two-dimensional matrices, and the index  $s$  refers to the stationary process with a zero mean. Principal gain from the transformation is related to the point that the result for the stationary variance matrix  $\hat{\sigma}$  of an Ornstein-Uhlenbeck process in two dimensions is well known and can be applied to calculate the second moments of the fast and slow variables. In order to proceed, one is required to introduce two approximations: (i)  $\tau_{in}$  is small so that the expansion of the term containing delay  $y(t - \tau_{in}) \approx y(t) - \tau_{in}\frac{dy}{dt}$  to the first order is sufficient, and (ii) the nonlinear term  $x^3(t)$  is replaced by  $x^3(t) \approx \langle x^2 \rangle_t x(t)$ , where the  $t$  index on angled brackets denotes a stationary, i.e. time-averaged quantity.

As an example, we consider the scenario with external noise, which is also preferred given the approximation (i). Moving to a new set of coordinates shifted for the position of the equilibrium  $(x_0, y_0)$  and having implemented (i) and (ii), one finds that

$$\hat{A} = \begin{pmatrix} -\mu/\epsilon & 1/\epsilon \\ -1 & 0 \end{pmatrix}, \quad \hat{B} = \begin{pmatrix} \sqrt{2D_1/\epsilon} & 0 \\ 0 & 0 \end{pmatrix}, \quad \mathbf{x}_s = \begin{pmatrix} x \\ y \end{pmatrix}, \quad (17)$$

with  $\mu = 1 - b^2 + \tau_{in} - \frac{1}{3}\langle x^2 \rangle_t$ .  $\langle x^2 \rangle_t$  may be calculated in a self-consistent fashion by using the expression for the stationary variance matrix of a two-dimensional Ornstein-Uhlenbeck process [46]

$$\hat{\sigma} = \frac{(\text{Det}\hat{A})\hat{B}\hat{B}^T + [\hat{A} - \text{Tr}\hat{A}\hat{I}]\hat{B}\hat{B}^T[\hat{A} - \text{Tr}\hat{A}\hat{I}]^T}{2\text{Tr}\hat{A}\text{Det}\hat{A}}, \tag{18}$$

where the superscript  $T$  refers to a transposed matrix and  $\hat{I}$  denotes the identity matrix. In particular, one can demonstrate that from (18) follows

$$\hat{\sigma}_{11} = \langle x^2 \rangle_t = -D_1/\mu = -D_1 / \left[ 1 - b^2 + \tau_{in} - \frac{1}{3} \langle x^2 \rangle_t \right], \tag{19}$$

which presents a second order equation over  $\langle x^2 \rangle_t$ . Given that the solution has to be positive, we finally obtain

$$\langle x^2 \rangle_t = \frac{1}{2} \left[ 3(1 - b^2 + \tau_{in}) + \sqrt{12D_1 + 3(1 - b^2 + \tau_{in})^2} \right]. \tag{20}$$

Inserting this result into the above expression for  $\mu$ , it is easy to show that  $\mu < 1 - b^2 + \tau_{in}$  holds for any  $D_1$  and reasonably small  $\tau_{in}$  under  $b = 1.05$ , the value kept throughout the paper. This is important because the stability of the equilibrium for the linearized system given by (17) is determined by the characteristic roots  $\lambda_{\pm} = \frac{\mu \pm \sqrt{\mu^2 - 4\epsilon}}{2\epsilon}$ , where  $\mu$  plays a key role. What the above point actually means is that the net effect of external noise, contributing via the  $\langle x^2 \rangle_t$  term, is to drive the system away from the critical threshold of the Hopf bifurcation controlled by  $b$ . In other words, presence of  $D_1$  makes the unit “less” excitable, which is the same type of influence already attributed to  $\tau_{in}$ .

Nevertheless, our main result obtained by the method of statistical linearization concerns the interplay of external noise and  $\tau_{in}$ . To assess how these ingredients affect the unit’s oscillatory behavior, one may consider the dependence of correlation time  $t_{corr}$  as a function of  $D_1$  and  $\tau_{in}$ . The latter provides a useful measure for regularity of oscillations, and may indicate how the competition between the noise- and the delay-driven mode is resolved for the given parameter set. Note that the correlation time [29,39] is defined by

$$t_{corr} = \int_0^\infty |G_{xx}(s)| ds, \tag{21}$$

where  $G_{xx}(s)$  stands for the normalized autocorrelation function  $G_{xx}(s) = \frac{1}{\sigma_x^2} \langle x(t-s)x(t) \rangle_t$ , knowing that  $\langle x \rangle_t = 0$ . In general, the expression for the time correlation matrix of a multivariate stationary Ornstein–Uhlenbeck process reads [46]

$$\hat{G}(s) = \langle \mathbf{x}(t-s), \mathbf{x}^T(t) \rangle_t = \hat{\sigma} \exp[-\hat{A}^T s], \tag{22}$$

which may be applied to calculate  $t_{corr}$  from (21).

Skipping the more involved details of the calculation, here we just report on the results, given in Fig. 3 in terms of the family of curves  $t_{corr}(D_1)$  for a set of relevant  $\tau_{in}$  values  $\tau_{in} \in \{0, 0.1, 0.2, 0.4\}$ . One first learns that the applied method provides accurate qualitative predictions regarding the effects of  $\tau_{in}$ : for  $\tau_{in} = \{0, 0.1\}$  there is no delay-driven mode, so the corresponding curves lie below the ones for  $\tau_{in} = \{0.2, 0.4\}$  within the entire range of  $D_1$  values. Also, for larger  $D_1$ , all the curves approach each other, indicating that the delay-led behavior is completely overwhelmed by noise. The values of  $t_{corr}$  for  $\tau_{in} = \{0.2, 0.4\}$  are very large only for small  $D_1 \sim 10^{-4}$  and decay rapidly with increasing noise. The point that  $t_{corr}$  is three orders of magnitude smaller at intermediate noise  $D_1 \sim 10^{-3}$  than at  $D_1 \sim 10^{-4}$  but is still above the curves for  $\tau_{in} = \{0, 0.1\}$  implies that some form of coherent motion exists, but is not prevalingly deterministic, i.e. it is not driven by the delay. This is consistent with the numerical findings on the average ISIs, e.g. at  $\tau_{in} = 0.4$ , the average ISI for  $D_1 = 0.002$ ,  $\langle T \rangle = 2.52$ , is substantially distinct from  $\langle T \rangle = 4.29$  obtained for  $D_1 = 0.0001$ .

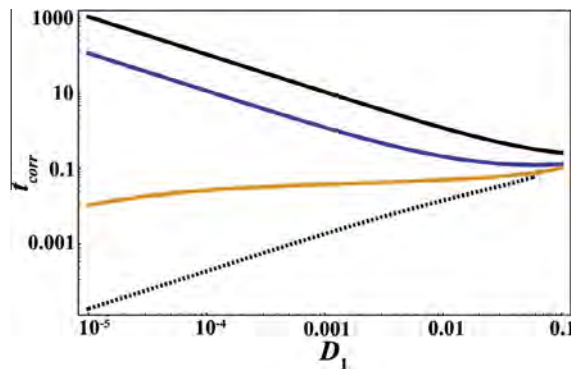


**Fig. 3.** Variation of correlation time  $t_{corr}$  with external noise  $D_1$  for a single unit, as obtained by the method of statistical linearization. The curves from bottom to top correspond to  $\tau_{in} = 0, 0.1, 0.2$  and  $0.4$ , respectively.

#### 4. Stability analysis for the system of interacting units

Having considered the issues related to stability of an single unit in presence of noise and  $\tau_{in}$ , here we address the analogous problem for the system of two interacting FHN excitable elements, which involves coupling delay  $\tau_{ex}$  as an additional ingredient. For the most part, the analysis is focussed on the deterministic version of (1) with  $c > 0, D_1 = D_2 = 0$ . This approach is taken for two reasons: (i) due to interplay of  $\tau_{in}$  and  $\tau_{ex}$ , the deterministic system alone displays intricate behavior, including bistable regimes between the different oscillatory modes in multiple parameter domains, and (ii), conditions for stability of the unperturbed system coincide with those for the first moments of the linearized system influenced by noise. Naturally, the bifurcation analysis to follow will provide a useful tool for interpretation of the numerically obtained results on the competition between the noise- and the delay-driven modes, serving as the reference point to clearly isolate the stochastic effects.

The characteristic equation describing local stability of equilibrium  $(x_i, y_i) = (-b, -b + b^3/3), i \in \{1, 2\}$  for the deterministic version of system (1) reads

$$\lambda^2 [\epsilon\lambda - (1 - b^2 - c)]^2 + 2\lambda [\epsilon\lambda - (1 - b^2 - c)] e^{-\lambda\tau_{in}} - \lambda^2 c^2 e^{-2\lambda\tau_{ex}} - e^{-2\lambda\tau_{in}} = 0. \quad (23)$$

Given the complexity of the above expression, local stability analysis has been carried out numerically by the *DDE – biftool* [47,48], an adaptable package of *MATLAB* routines suitable for handling the sets of DDE with constant delays. The issue of particular interest is how the behavior of coupled units is influenced by variation of  $\tau_{in}$  and  $\tau_{ex}$  while  $c$  is kept fixed. It turns out that the system undergoes a sequence of supercritical and subcritical Hopf bifurcations, whereby the former (latter) result in creation of a stable (unstable) limit cycle. Recall that both types of Hopf bifurcation can further be cast as direct or inverse [49], which indicates whether an unstable two-dimensional manifold for the fixed point appears or vanishes when crossing the bifurcation curve, causing the fixed point to unfold on the unstable or the stable side, respectively. In the following, we use the notation where the  $+/-$  sign reflects the direct/inverse character of bifurcation, whereas the numerical indices refer to the order in which the successive branches of bifurcation curves are encountered as  $\tau_{ex}$  is increased.

Bifurcation diagram in the  $\tau_{ex} - \tau_{in}$  parameter plane for the moderate coupling strength  $c = 0.1$  is shown in Fig. 4. We stress that the complete knowledge on the system's behavior cannot be gained by performing the local bifurcation analysis alone, since  $\tau_{ex}$  and  $\tau_{in}$  each give rise to a global fold-cycle bifurcation as well. Due to global character of such events, the fashion in which the observed dynamics is shaped may be interpreted as if the effects of coupling were just superimposed on the behavior governed by the intrinsic properties of units, which results in multistable regimes for most of the relevant parameter domains. Focussing first on the case  $\tau_{ex} = 0$ , we note that the scenario for the onset of oscillations exactly matches the one that holds for an isolated unit. In brief, under increasing  $\tau_{in}$ , the system first undergoes fold-cycle bifurcation at  $\tau_{in}^{FC} = 0.106$ , see the point denoted by an open circle in Fig. 4, and then displays a subtle interplay between the local Hopf and the global bifurcation around  $\tau_{in}^0 = 0.118$ . The latter rests on the fact that the incipient cycle emerging from the Hopf bifurcation lies enclosed by the saddle-cycle left over from the global bifurcation, which for some weakly supercritical  $\tau_{in}$  leads to their collision and disappearance following an inverse fold-cycle bifurcation. Consequently, after a small interval of bistability, the system's unique attractor for  $\tau_{ex} = 0$  and  $\tau_{in} \gg \tau_{in}^0$  is the large cycle, whose existence is unaffected by the local bifurcations.

On the other hand, for  $\tau_{in} = 0$ , one finds that a fold-cycle bifurcation controlled by  $\tau_{ex}$  occurs around  $\tau_{ex}^{FC} = 1.16$ , cf. the black circle in Fig. 4. Therefore, in terms of stability, the system lies in the stationary state for  $\tau_{ex} < \tau_{ex}^{FC}, \tau_{in} < \tau_{in}^{FC}$ , whereas the domain  $\tau_{ex} \geq \tau_{ex}^{FC}, \tau_{in} < \tau_{in}^{FC}$  is characterized by a coexistence between the fixed point and a limit cycle, whose basins of attraction are separated by the saddle-cycle created in the global bifurcation. Note that the large cycles emerging from the global bifurcations evoked by  $\tau_{ex}$  or  $\tau_{in}$  have very distinct phase portraits, cf. Fig. 2. The orbit of the former mostly follows

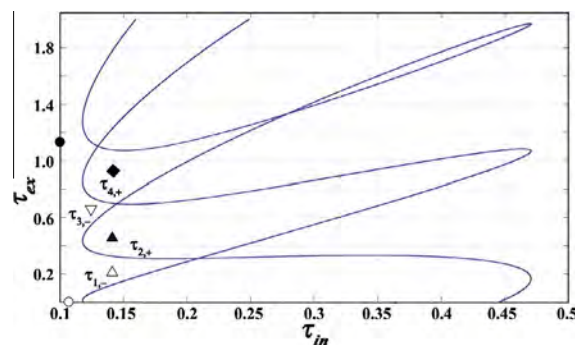


**Fig. 4.** Bifurcation diagram  $\tau_{ex} - \tau_{in}$  for the two interacting units in the noiseless case. Stability of equilibrium is influenced by a sequence of direct and inverse supercritical and subcritical Hopf bifurcations. Critical values for the global fold-cycle bifurcations are indicated by an open and solid circle. Coupling strength is set to  $c = 0.1$ .

the cubic nullcline, whereas the latter one's traverses a large section away from the nullcline. Furthermore, the period associated with oscillations at  $\tau_{ex}^{FC}, T_* = 2.42$ , is significantly smaller than  $T_\circ = 3.96$ .

Let us now turn to the sequence of local bifurcations occurring under increasing  $\tau_{ex}$  for  $\tau_{in} \gtrsim \tau_{in}^0$ . In the domain indicated by an open up-triangle in Fig. 4, stability of equilibrium is regained as a result of an inverse subcritical Hopf bifurcation which the system undergoes at  $\tau_{1,-}$ . This means that the region  $\tau_{1,-} < \tau_{ex} < \tau_{2,+}$  admits a bistable regime where the large cycle and the stationary state coexist. Note that the unstable cycle born in the Hopf bifurcation acts like a threshold switching between the two stable solutions. Stepping into the area marked by a solid up-triangle in Fig. 5, the equilibrium becomes unstable due to a direct supercritical Hopf bifurcation at  $\tau_{2,+}$ . However, one finds that another bistable regime is established, which involves coexistence between two limit cycles, a large one created in the fold-cycle bifurcation and the other emerging from the Hopf bifurcation. Crossing the curve  $\tau_{3,-}$  from below, cf. the domain marked by an open down-triangle in Fig. 5, the fixed point loses an unstable plane due to an inverse subcritical Hopf bifurcation, thus becoming stable again. In the region bounded by  $\tau_{3,-}$  and  $\tau_{4,+}$ , bistability between two oscillatory states is replaced by a regime where the stationary state coexists with an oscillatory solution. Above  $\tau_{4,+}$ , the most important point is that the equilibrium is no longer stable for any  $\tau_{ex}$ . Apart from the direct supercritical Hopf bifurcation which the system undergoes at  $\tau_{4,+}$ , this is further linked with the fact that the increase of  $\tau_{ex}$  gives rise to a global fold-cycle bifurcation, as explained earlier. Just below  $\tau_{ex}^{FC}$ , it is difficult to discern between the modes arising from the local bifurcation and the global bifurcation induced by  $\tau_{in}$ , with the associated periods becoming barely distinguishable. Above  $\tau_{ex}^{FC}$ , one could in principle expect a multistable regime characterized by three oscillations modes, one elicited by the local, and the remaining two by the global events. Nevertheless, it turns out that the structure of phase space may support only two coexisting oscillatory states. Apparently, the limit cycle born via Hopf bifurcation vanishes by a scenario involving an inverse fold-cycle bifurcation, where it collides with one of the saddle cycles.

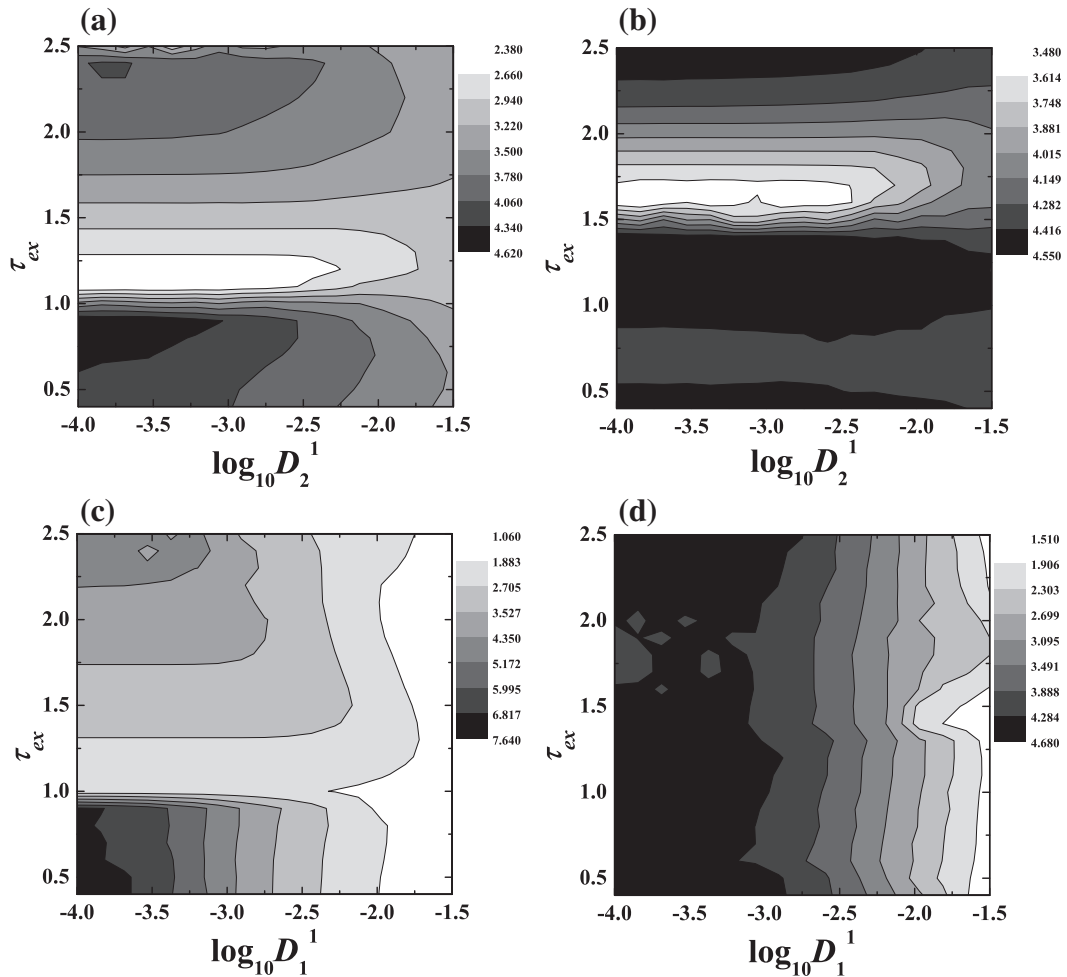


**Fig. 5.** Indication on competition between the noise-induced and delay-driven modes. Average ISIs ( $T_1$ ) for the adjustable unit are plotted as a function of its noise intensity and  $\tau_{ex}$ . The top row refers to setup with internal, and the bottom row with external noise. The left and right columns show the fields obtained for  $\tau_{in} = 0$  and  $\tau_{in} = 0.4$ , respectively.



As a result, a bistable regime is established, such that the two large cycles from the global bifurcations coexist, with the corresponding attraction basins separated by the remaining saddle cycle. For  $\tau_{in} \gtrsim \tau_{in}^0$ , the given oscillation modes have clearly distinct periods.

Detailed analysis on the deterministic system has mostly been motivated by its specific feature that the dynamics is substantially influenced by the global, rather than local bifurcations. A question that naturally arises is how is this point reflected in the stability of the system influenced by noise. As explained in case of an isolated unit, conditions for the stability of the deterministic system exactly match those associated with the first moments of the perturbed system. The dynamics of second moments is given by a complex set of equations, which are best treated numerically. However, judging by the above findings, even the complete knowledge on the stability of the linearized system would be insufficient to fully understand the behavior displayed by the interacting units under stochastic perturbation. On the other hand, note that the results obtained for the deterministic system also hold for the perturbed system in the limit of small noise, though some of the bistable regimes, especially those involving the equilibrium, are likely to be highly sensitive to stochastic effects. Apart from disturbing the stability of equilibrium, stronger noise may affect the attraction basins of coexisting attractors thereby modifying the asymptotic dynamics, or can give rise to certain transient phenomena, such as mixing between the different oscillatory modes. Analysis on these issues, as well as coherence and synchronization properties of interacting units under a wide range of noise amplitudes has been performed by numerical means.

## 5. Numerical results on the interplay of noise and the delays

In this section, the goal is to demonstrate how is the competition between the delay- and noise-driven modes reflected in the coherence of individual firing series and the units' synchronization. Since oscillatory motion is either induced or perturbed by noise, a quantity appropriate to characterize the degree of coherence over a long series  $x_i(t)$  is the ratio of the time-averaged ISI and the standard deviation of the ISI distribution [50]

$$S_i = \frac{\langle T_{i,k} \rangle_t}{\sqrt{\langle T_{i,k}^2 \rangle_t - \langle T_{i,k} \rangle_t^2}}. \quad (24)$$

In (24),  $i$  specifies the particular unit,  $T_{i,k} = t_{i,k+1} - t_{i,k}$  refers to the  $k$ th interspike interval, and the spike time  $t_{i,k}$  is defined as the moment of crossing the threshold  $x_i(t) = 1$  under condition  $x_i'(t_k) > 0$ . Note that  $S_i$ , often referred to as regularity, may be interpreted as a signal-to-noise ratio [25], in a sense that it compares the recorded noisy signal to a periodic one, whose  $P(T_{i,k})$  distribution would conform to a delta-function. In neuroscience, quantity  $S_i$  is deemed relevant because it can be linked to the timing precision of information processing [51].

Given the noisy nature of oscillations, coordinated activity between the units is considered within the framework of stochastic synchronization. This concept comprises frequency synchronization, where the time-scales characterizing oscillatory motion of the involved systems are adjusted, or phase synchronization, which refers to scenario where an approximately constant phase difference between the units is maintained. On the former, note that the appropriate time-scale for each unit is associated with the average ISI, whose reciprocal value can be viewed as the firing frequency. Therefore, as a measure of frequency synchronization one may use the ratio of time-averaged ISIs,  $r = \langle T_{1,k} \rangle_t / \langle T_{2,k} \rangle_t$  [29]. The case of special interest concerns frequency entrainment between the units where  $r \approx 1$ . We stress that the latter condition does not imply per se that the oscillatory motions of the two units take place on the same attractor. In particular,  $r$  merely refers to adjustment of time-scales between oscillatory motions regardless of their specific features, such as the oscillation amplitudes or phases.

To examine coordination of units' spiking at an arbitrary moment of time, we define the phase [52,53]

$$\phi_i(t) = 2\pi \frac{t - t_{i,k-1}}{t_{i,k} - t_{i,k-1}} + 2\pi(k - 1), \quad (25)$$

where the notation is analogous to that in (24). For systems comprised of coupled autonomous oscillators, phase synchronization, or rather phase locking, would imply that the phase difference  $\Delta\phi(t) = \phi_1(t) - \phi_2(t)$  remains constant during the evolution. In presence of noise,  $\Delta\phi(t)$  cannot maintain a stationary value, but its fluctuations may appear nearly stationary for most of the time if perturbation is weak. Nevertheless, even then the abrupt jumps are bound to occur due to phase slips [29,53], where  $\Delta\phi(t)$  changes by  $\pm 2\pi$ . Consequently, better phase synchronization between the units effectively implies that the intervals with nearly constant relative phase last longer. The degree of phase synchronization is quantified by the synchronization index  $\gamma$  [53,29]

$$\gamma = \sqrt{\langle \cos \Delta\phi(t) \rangle_t^2 + \langle \sin \Delta\phi(t) \rangle_t^2}, \quad (26)$$

which can vary within  $\gamma \in [0, 1]$  interval, such that values approaching 1 describe approximate phase synchronization. Note that  $\gamma$  by construction refers only to adjustment of phases between the oscillating units, independent on the potentially different oscillation amplitudes [53]. This is convenient, because we encounter instances where the two units lie on distinct limit cycles, but the associated characteristic time-scales are closely matched.

The strategy adopted to systematically examine the co-effects of noise,  $\tau_{ex}$  and  $\tau_{in}$  on behavior of two interacting excitable units is as follows. We distinguish between two basic setups, characterized by whether perturbation derives from external or

internal sources. In both instances, action of noise is analyzed by having an “adjustable” unit (index  $i = 1$ ) with variable noise amplitude  $D_1^1$  or  $D_1^2$ , and a unit that is “optimized” ( $i = 2$ ) in a sense that  $D_2^1$  or  $D_2^2$  are kept at the appropriate resonant value, be it the CR or the SISR case. Coupling delay spans the interval  $\tau_{ex} \in [0.4, 2.5]$ , selected such that the lowest value is an order of magnitude less than the typical ISI, whereas the highest value is comparable to it. Coupling strength is fixed to an intermediate value  $c = 0.1$ , which is sufficient to facilitate coordinated activity between the units, rather than let their dynamics remain independent. Qualitative impact of intrinsic delay is outlined by comparing the system’s behavior for domains where  $\tau_{in}$  lies below or above  $\tau_{in}^{FC}$ , having them represented by  $\tau_{in} = 0$  and  $\tau_{in} = 0.4$ , respectively.

In the discussion below, the aim is to numerically demonstrate four points, conditionally divided into primarily stochastic and primarily deterministic effects. Regarding the first group, one finds that the distinction between external/internal character of noise crucially influences (i) the ability of entrainment to a single frequency and (ii) the fashion in which the competition between the delay- and noise-driven modes is resolved. As for the second group,  $\tau_{in}$  is established to substantially influence (i) regularity of firing and (ii) the properties of phase synchronization between the units. Note that the dependencies of  $S_i$  and  $\gamma$  on  $D_1^1$  or  $D_1^2$  and the delays are obtained by performing time-averages over long  $x_i(t)$  series, as well as the stochastic averages over an ensemble of  $\sim 10^2$  realizations, making certain that the transients have been eliminated and that further increasing of the ensemble size does not significantly affect the results stated. Numerical integration has been carried out by the Euler integration scheme with time step 0.001. We have adopted the standard and physically plausible initial functions, based on the assumption that the units evolve independently within the time interval  $t \in [-\tau_{min}, 0]$ , where  $\tau_{min} = \min\{\tau_{in}, \tau_{ex}\}$ . In effect, for the specified interval, the system (1) has been integrated by setting aside the interaction terms, with the initial conditions lying in close vicinity of equilibrium.

### 5.1. Frequency synchronization and the competition between the delay-driven and noise-induced modes

Regarding frequency entrainment, a qualitatively different picture emerges for the setups involving external or internal noise. In the latter case, one finds that the units exhibit frequency synchronization within all the considered parameter domains. This has been verified by determining that  $r \approx 1$  holds for all the plausible values of  $\tau_{in}$  under variation of  $\tau_{ex}$  and  $D_1^2$ . On the other hand, under external noise, for  $\tau_{in} = 0$  or any relevant  $\tau_{in} > 0$ , frequency synchronization is gradually lost with  $D_1^1$ , whereby the decline of  $r$  becomes marginally steeper at higher  $\tau_{in}$ . In other words, frequency entrainment is more sensitive to external than the internal perturbation. Note that by increasing external noise at adjustable unit, its average firing frequency is enhanced, but it fails to control the optimized unit, so the two eventually act as if they were independent. Naturally, existence of a prevailing mode in the system’s behavior can only be considered if there is frequency entrainment.

The point on the prevailing oscillatory modes is best illustrated by examining variation of the average ISIs in the  $\tau_{ex} - D_2^1$  ( $\tau_{ex} - D_1^1$ ) plane for internal (external) noise. In Fig. 5, and Fig. 5(b) are shown the fields  $\langle T_1 \rangle(\tau_{ex}, D_2^1)$  referring to the cases  $\tau_{in} = 0$  and  $\tau_{in} = 0.4$ , respectively. Given the frequency synchronization, nearly identical results would be obtained by plotting  $\langle T_2 \rangle(\tau_{ex}, D_2^2)$  instead. For  $\tau_{in} = 0$ , one learns that three qualitatively distinct regimes are clearly discernible under increasing  $\tau_{ex}$ , which may be explained by invoking the arguments from Section 4. In the domain below the fold-cycle bifurcation ( $\tau_{ex} \lesssim \tau_{ex}^{FC}$ ), the adjustable unit is able to entrain the optimized one, which is corroborated by the fact that the average ISI strongly depends on  $D_2^2$ . Once the global bifurcation has occurred ( $\tau_{ex}^{FC} \approx 1.16$ ), there is an interval of  $\tau_{ex}$  values where the units’ oscillatory motion is dominated by the coupling delay. This point is verified by the rather weak dependence of  $\langle T_1 \rangle$  on  $D_2^1$ . Note that the characteristic time-scale of oscillations in this region is described by an approximate relation  $\langle T_1 \rangle \approx 2\tau_{ex}$ .

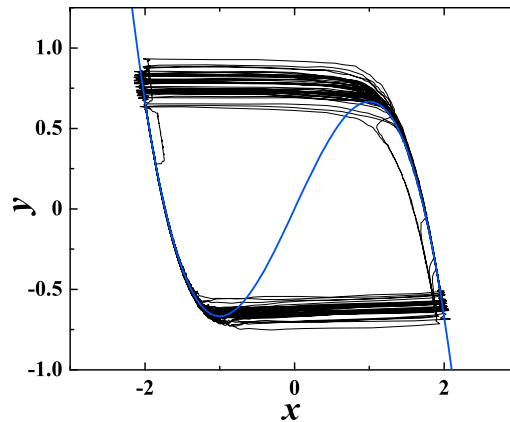


**Fig. 6.** Noise may induce stochastic switching between different oscillatory modes. The phase portrait corresponds to the adjustable unit under internal noise, with the parameters set to  $D_2^1 = 0.001$ ,  $D_2^2 = 0.00255$ ,  $\tau_{ex} = 1.7$ ,  $\tau_{in} = 0$ . In the particular instance, noise causes mixing between the mode driven by  $\tau_{ex}$  and the noise-induced mode derived from the optimized unit. The cubic nullcline is drawn to indicate the distinction between the two types of orbits more clearly.

Entrainment with coupling delay is gradually lost as  $\tau_{ex}$  further departs from  $\tau_{ex}^{FC}$ . Before the third regime actually sets in, one encounters an interval of coupling delays ( $\tau_{ex} \approx 1.7$ ), where the distributions of ISIs  $P(T_{i,k})$  are not unimodal even for very small  $D_2^1$ . In particular, a typical  $P(T_{i,k})$  for long  $x_i(t)$  series in this  $\tau_{ex}$  range indicates strong mixing between the  $\tau_{ex}$ -driven mode and the noise-induced mode of the optimized unit, whereby the latter component eventually prevails. Stochastic switching between the limit cycles characterizing the two modes is illustrated in Fig. 6. Note that despite the mixing, in statistical sense the units display the same average behavior, such that the ratio  $r \approx 1$  is maintained. The delays  $\tau_{ex} \geq 1.9$  admit the regime where, at variance with the case  $\tau_{ex} \lesssim \tau_{ex}^{FC}$ , the optimized unit is able to entrain the adjustable one. Naturally, such form of motion is likely to be susceptible to noise if  $D_2^1 > D_2^2$ , which is confirmed by the shape of the field  $\langle T_1 \rangle(\tau_{ex}, D_2^1)$ , cf. Fig. 5(a).

The picture described so far is substantially modified by the non-trivial  $\tau_{in} > \tau_{in}^{FC}$ , see Fig. 5(b). For this setup, there are two qualitatively different regimes, but the one where the characteristic time-scales of both units are controlled by  $\tau_{in}$  prevails for most of the  $(\tau_{ex}, D_2^1)$  parameter values. It is interesting that the coupling term is able to suppress such a behavior only for  $\tau_{ex} \in (1.6, 1.9)$ . Within this interval, the characteristic time-scale for the  $\tau_{ex}$ -driven mode approximately matches the one for the noise-driven mode at the optimized unit. Above  $\tau_{ex} \approx 1.9$ , the mode owing to  $\tau_{in}$  wins over again, such that the units display longer average ISIs, cf. Fig. 5(b).

Now let us turn to the scenario involving external noise. Given the loss of frequency synchronization for larger  $D_1^1$ , the average dynamics of units 1 and 2 is governed independently. In Fig. 5(b) and (d) we have plotted the fields  $\langle T_1 \rangle(\tau_{ex}, D_1^1)$  corresponding to  $\tau_{in} = 0$  and  $\tau_{in} = 0.4$ , respectively. The behavior of unit 1 is illustrated rather than that of unit 2, because it is more strongly affected by the change from internal to external noise. Note that below  $\tau_{ex}^{FC}$ , the prevailing dynamics of the optimized unit conforms to the paradigm involving three characteristic regimes, similar to what is shown in Fig. 5(a). As for the adjustable unit, once  $D_1^1$  becomes sufficiently strong ( $D_1^1 \gg D_2^1$ ), it completely overwhelms all the other influences, implying that the unit 1 can no longer be entrained either by  $\tau_{ex}$  or the optimized unit. This is reflected by the virtual independence of  $\langle T_1 \rangle$  on  $\tau_{ex}$  for larger  $D_1^1$ , cf. Fig. 5(c). For  $\tau_{in}$  above  $\tau_{in}^{FC}$ , it turns out that the effects of coupling are felt even less than for the

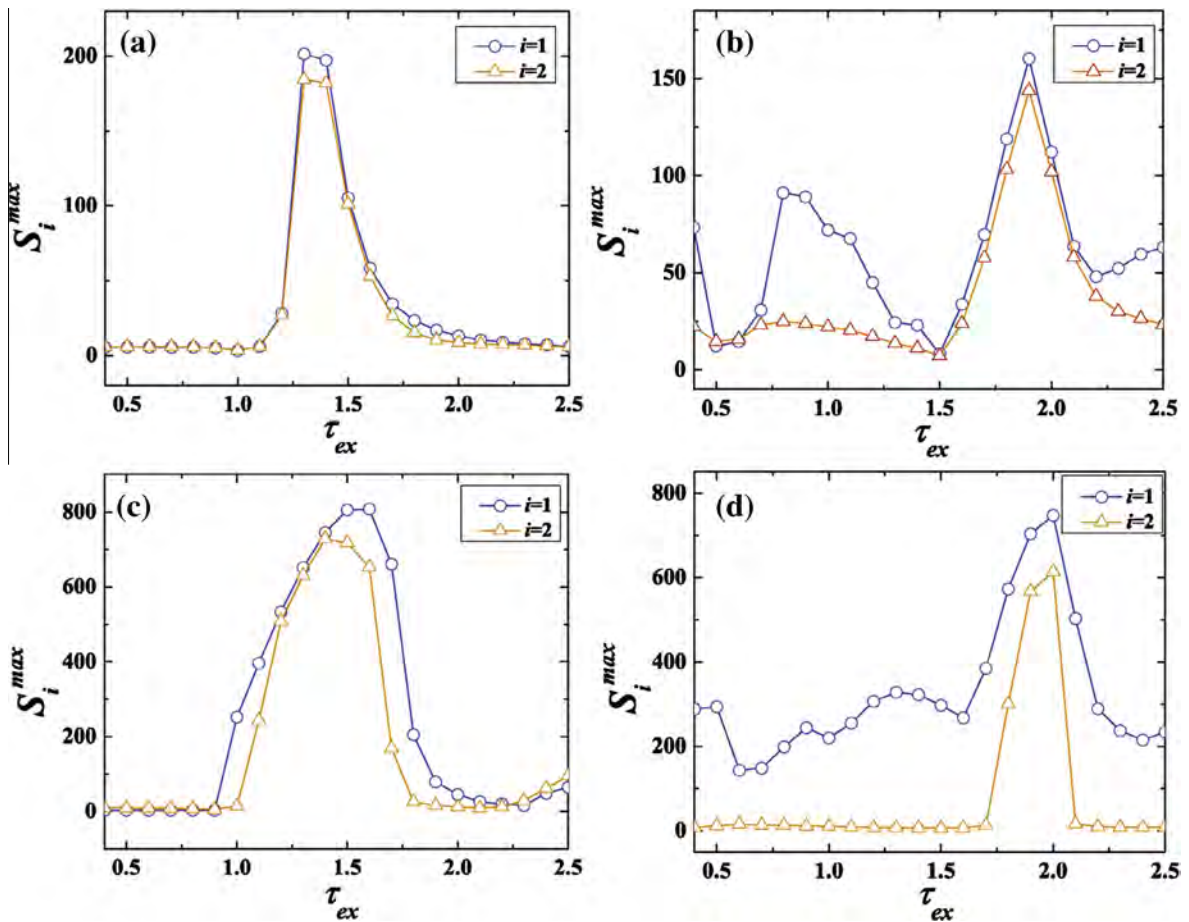


Fig. 7. Families of curves  $S_i^{max}(\tau_{ex})$ , whereby open circles (triangles) refer to unit  $i = 1$  ( $i = 2$ ). The presentation scheme is such that the top and bottom rows concern the scenarios with internal and external noise, respectively, whereas the left column illustrates the case  $\tau_{in} = 0$ , and the right one the case  $\tau_{in} = 0.4$ . The profile of curves suggests that firing coherence is substantially influenced by  $\tau_{in}$ .

analogous scenario with internal noise. This may be attributed to the point that the coupling term itself attains a noisy component, at variance with the previous setup. While the dynamics of unit 2 is completely controlled by  $\tau_{in}$ , the data in Fig. 5(d) demonstrate that unit 1 exhibits a  $\tau_{in}$ -driven mode only for smaller  $D_1^1$ , approximately given by the condition  $D_1^1 < D_2^1$ . In line with the results derived in subSection 3.3, for larger  $D_1^1$  the characteristic time-scale of oscillations at unit 1 is set by noise. This is corroborated by the fact that  $\langle T_1 \rangle$  strongly changes with  $D_1^1$ , but remains unaffected by the increase of  $\tau_{ex}$ , see Fig. 5(d).

## 5.2. Regularity of firing and phase synchronization

In order to isolate the key ingredients influencing regularity, one first performs a kind of coarse-graining over the effects of noise. The latter consists in determining  $S_i^{max}(\tau_{ex}, \tau_{in})$ , which present the largest values of signal-to-noise ratio over the considered range of noise amplitudes ( $D_1^1$  or  $D_2^1$ ) acting on unit 1 under the fixed pair of delays ( $\tau_{ex}, \tau_{in}$ ). In Fig. 7 are illustrated the dependencies  $S_i^{max}(\tau_{ex})$  for external (top row) and internal noise (bottom row), whereas the left and right columns refer to cases  $\tau_{in} = 0$  and  $\tau_{in} = 0.4$ , respectively. At first sight, it becomes apparent that the prevailing behavior is determined by the intrinsic delay, while variation with the type of noise is only a secondary effect. For  $\tau_{in}$  below  $\tau_{in}^{FC}$ , the peak in  $S_i^{max}(\tau_{ex})$  reflects the onset of the fold-cycle bifurcation controlled by  $\tau_{ex}$ . Nevertheless, the peak's profile and the position of its maximum relative to  $\tau_{ex}^{FC}$  is influenced by the form of noise. In particular, it seems likely that the peak's maximum coincides with the  $\tau_{ex}$  value where the noise-induced oscillations at unit 2 provide the weakest perturbation to the  $\tau_{ex}$ -driven mode.

For intrinsic delays above  $\tau_{in}^{FC}$ , both  $S_1^{max}(\tau_{ex})$  and  $S_2^{max}(\tau_{ex})$  exhibit a sharp peak around  $\tau_{ex} \approx 2$ . Nonetheless, motion of the adjustable unit is further characterized by the secondary peak or peaks, contingent on the external/internal character of noise. Note that Fig. 7 refers only to coupling delays that satisfy  $\tau_{ex} > \tau_{in}$ , so the regularity peak corresponding to oscillations induced by the  $\tau_{in}$ -controlled global bifurcation is not visible. The primary peak itself in Fig. 7(c) and (d) can be linked to scenario where the characteristic time-scales of the  $\tau_{ex}$ -induced mode and the noise-driven mode at the optimized unit are most closely matched, such that the stochastic effects are minimized. On the other hand, increase of  $S_1^{max}$  at smaller  $\tau_{ex}$  values actually reflects the adjustable unit's motion for very small  $D_1^1$  or  $D_2^1$ , which warrant that the  $\tau_{in}$ -driven mode is perturbed the least.

The latter point suggests one should examine in greater detail how much the maximal regularities represent the general tendencies in system's behavior, taking into account both the character of noise and its magnitude. It turns out that the above description is more accurate if the perturbation is due to internal, than the external sources. In the latter instance, the provided picture is valid only for small  $D_1^1$ , where the frequency synchronization is still maintained. In this context, one should also make it explicit how the coaction of non-trivial  $\tau_{in} > \tau_{in}^{FC}$  and noise affects  $S_i$  at specific  $\tau_{ex}$  values. For  $\tau_{ex}$  below  $\tau_{ex}^{FC}$ , it is readily seen that the deterministic component emerging due to  $\tau_{in} > \tau_{in}^{FC}$  improves the firing coherence of both units compared to what is found at  $\tau_{in} < \tau_{in}^{FC}$ . Such a behavior is illustrated in Fig. 8(a) showing families of curves  $S_i(D_2^1)$  for  $\tau_{in} = 0$  and  $\tau_{in} = 0.4$  at fixed  $\tau_{ex} = 0.8$ . On the other hand, for  $\tau_{ex} > \tau_{ex}^{FC}$  the stochastic effects come into play more strongly. In the domain  $\tau_{ex} \in (1.2, 1.9)$ , the intrinsic delay above  $\tau_{in}^{FC}$  may promote or suppress regularity for small noise, depending on whether it derives from external or internal sources. Under larger perturbation, regularity tends to decrease due to stochastic switching between the two deterministic modes, one driven by  $\tau_{ex}$ , and the other by  $\tau_{in}$ . An example where setting intrinsic delay above  $\tau_{in}^{FC}$  is accompanied by the nontrivial dependence of  $S_i$  on noise is illustrated in Fig. 8(b), which shows how  $S_i$  vary with  $D_2^1$  for  $\tau_{in} = 0$  and  $\tau_{in} = 0.4$  at fixed  $\tau_{ex} = 1.7$ .

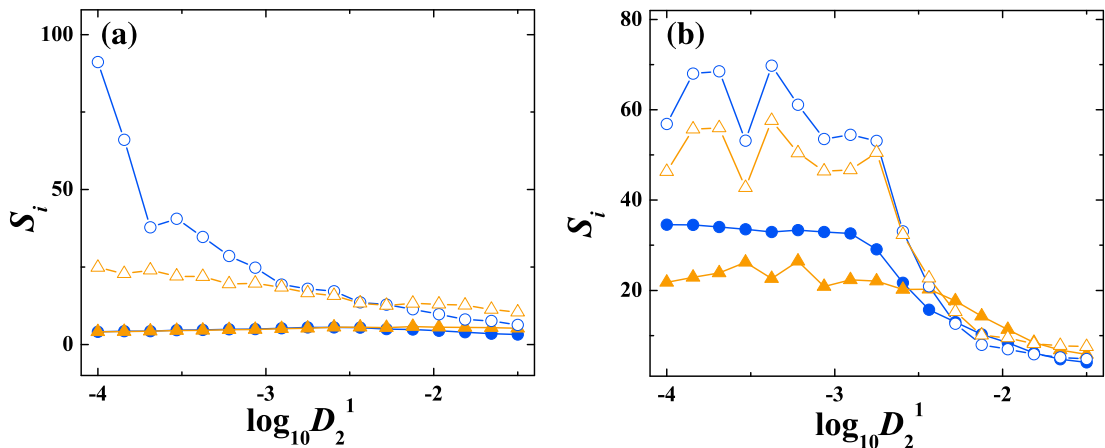


**Fig. 8.** Whether and how much setting  $\tau_{in}$  above  $\tau_{in}^{FC}$  contributes to spiking coherence depends nontrivially on  $\tau_{ex}$  and noise at unit 1. (a) and (b) show  $S_i(D_2^1)$  families of curves for  $\tau_{in} = 0$  (solid symbols) and  $\tau_{in} = 0.4$  (open symbols), obtained under fixed  $\tau_{ex} = 0.8$  and  $\tau_{ex} = 1.7$ , respectively. The circles (triangles) are reserved for unit 1 (2). The data in both instances refer to setup including internal noise with  $D_2^2 = 0.00255$ .

As announced at the beginning of this section, we address the issue of phase synchronization by considering variation of the synchronization index  $\gamma$ . Adhering to the scheme of analysis so far, in Fig. 9 are illustrated the dependencies  $\gamma(\tau_{ex}, D_2^1)$  (top row) and  $\gamma(\tau_{ex}, D_1^1)$  (bottom row) obtained for internal and external sources of noise, whereas the left and right columns refer to cases  $\tau_{in} = 0$  and  $\tau_{in} = 0.4$ , respectively. In the insets are shown the auxiliary plots  $\gamma^{max}(\tau_{ex})$ , intended to help in identifying the domains supporting phase synchronization. Note that  $\gamma^{max}$  follow from the same coarse-graining procedure as  $S_1^{max}$  introduced earlier on.

For  $\tau_{in}$  below  $\tau_{in}^{FC}$ , one finds three  $\tau_{ex}$  domains admitting approximate phase synchronization independent on the source of noise. It is interesting that each domain coincides with one of the characteristic regimes identified when discussing Fig. 5(a). In particular, at small and large  $\tau_{ex}$ , there is phase synchronization between the oscillations prevailing influenced by noise, see Fig. 10(a), whereas at intermediate  $\tau_{ex}$  a nearly stationary relative phase is maintained for the  $\tau_{ex}$ -driven mode at both units, cf. Fig. 10(b). The actual phase shift for  $\tau_{ex} < \tau_{ex}^{FC}$  is small, while for intermediate and larger  $\tau_{ex}$  the units are almost perfectly synchronized in anti-phase. The source of noise is only reflected in the point that the corresponding  $\gamma$  values at  $\tau_{ex} \approx 1$  and  $\tau_{ex} \approx 2$  are slightly higher in Fig. 9(c) than in Fig. 9(a), which is a consequence of the known fact that the oscillations under optimal noise in the SISR case are more regular than those in the CR case.

For  $\tau_{in}$  above  $\tau_{in}^{FC}$ , there are more apparent secondary effects reflecting the external/internal character of noise. Under internal noise, an almost constant relative phase is achieved at  $\tau_{ex} \approx 2$ , where the prevailing behavior corresponds to a mode driven by  $\tau_{in}$ . In particular, coupling delays from the interval  $\tau_{ex} \in (1.9, 2.1)$  seem to affect the units' behavior in a stabilizing fashion, suppressing the noise-induced fluctuations around the typical orbit, which facilitates the establishment of a nearly stationary relative phase. One may show that the units in this domain are synchronized in anti-phase. On the other hand, the co-effects of coupling delay and external noise lead to a different picture within the interval  $\tau_{ex} \in (1.6, 2.3)$ . At variance with Fig. 9(b), their interplay is found to promote phase synchronization, cf. Fig. 9(d). The important contribution from the stochastic effects is corroborated by the point that the  $\gamma^{max}$  values in the inset of Fig. 9(d) correspond to non-negligible noise amplitudes at unit 1. Note that such  $D_1^1$  values are not large enough to disturb the adjustment between the units' characteristic time-scales. As for the actual phase differences, around  $\tau_{ex} \approx 2$  the units are approximately synchronized in anti-phase, whereas the in-phase synchronization sets in closer to the boundaries of the  $\tau_{ex} \in (1.6, 2.3)$  interval.

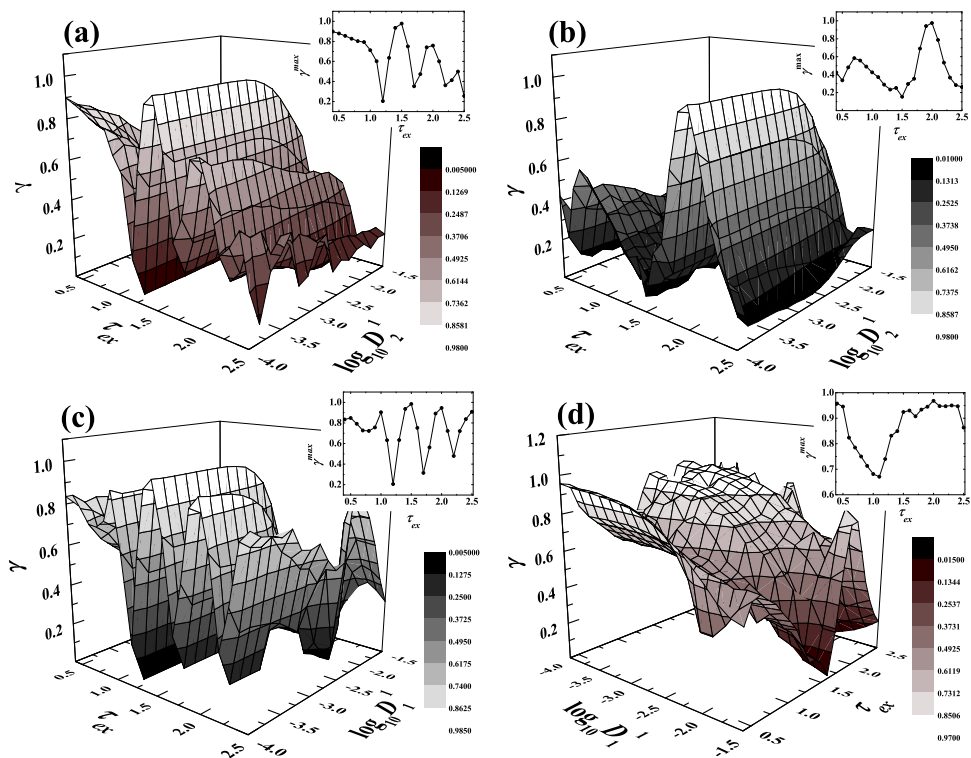


**Fig. 9.** The main frames display synchronization index  $\gamma$  as a function of  $\tau_{ex}$  and noise intensity at the adjustable unit. The top (bottom) row refers to setup with internal (external) noise, whereas the left and right columns are obtained for  $\tau_{in} = 0$  and  $\tau_{in} = 0.4$ , respectively. In the insets are shown the corresponding dependencies of the coarse-grained index  $\gamma^{max}$  on  $\tau_{ex}$ .

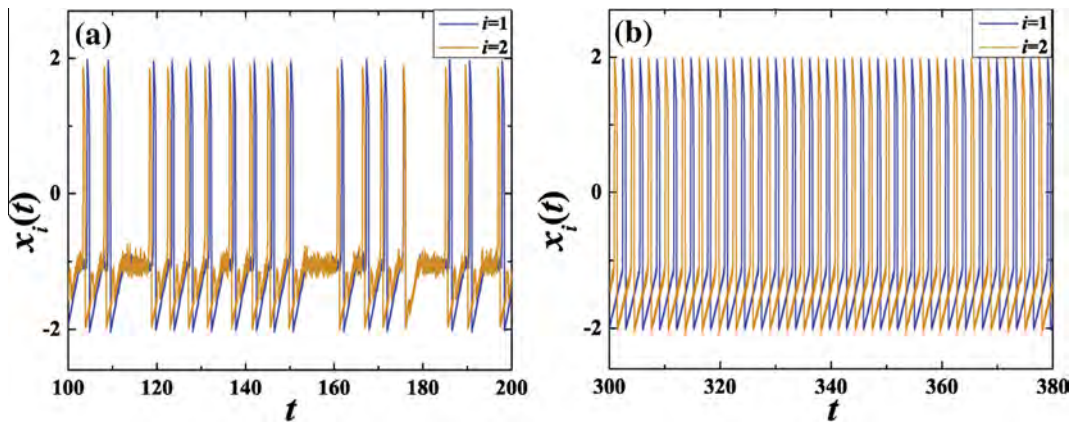


**Fig. 10.** (a) and (b) refer to scenarios where phase synchronization is achieved between the noise-induced oscillations and oscillations controlled by the coupling delay, respectively.  $x_i(t)$  series in both cases are obtained for external noise with  $\tau_{ex} = 0.9$  in (a) and  $\tau_{ex} = 1.5$  in (b). Remaining parameters are  $D_1^i = 0.0002$ ,  $D_2^i = 0.00087$ ,  $\tau_{in} = 0$ .

## 6. Conclusion

In this paper, we have examined how the behavior of a typical class II excitability model is altered by incorporating an intermediate characteristic time-scale, nested between the ones defined by the activator and the recovery variable. Introduced in the FHN model, such a time-scale is associated with intrinsic delay  $\tau_{in}$ , whose role is to modify the relaxation process, affecting both the declining stage of spike and the slope describing how the rest state is regained. Drawing analogy to neuroscience, the former may partly be motivated as means to approximate the gross effects of certain microscopic processes in the ion-gating channels of neuron membrane. For the paradigmatic cases, including a single unit under additive noise from external or internal sources, as well as a pair of delay-coupled noisy units, the main goal has been to understand how the competition between the noise-induced and the delay-driven (noise perturbed) oscillation modes is resolved, further considering its impact on regularity of units' firing and their synchronizability.

Given the additional ingredient in the single unit model, its stability and the onset of oscillations have been addressed in detail. Apart from carrying out the bifurcation analysis of the unperturbed system and determining the conditions for the stability of the linearized system under perturbation, we have also extended the method of statistical linearization to gain further insight into the interplay of noise and  $\tau_{in}$  in light of competition between the different oscillatory modes. Regarding the role of  $\tau_{in}$ , the key result on the deterministic system is that the equilibrium loses stability via the direct supercritical Hopf bifurcation at  $\tau_{in}^H$ , but the unit's oscillatory motion is primarily shaped by the global fold-cycle bifurcation occurring for  $\tau_{in}^{FC} < \tau_{in}^H$ . In effect, a sophisticated interplay between the local and global events renders the large cycle emerging from the latter as the unique attractor already for  $\tau_{in}$  slightly above  $\tau_{in}^H$ . An interesting qualitative point on  $\tau_{in}$  in relation to excitability is that it shifts the system away from the Hopf bifurcation controlled by  $b$ , making the unit less excitable.

Stability of the perturbed unit cannot be treated within the Fokker–Planck formalism due to inability to resolve the conditional drift term. Nevertheless, in case of the linearized system it is demonstrated that the critical  $\tau_{in}$  values for the first two moments of the solutions are only marginally different, though the respective characteristic equations are distinct. Focussing on the setup admitting external noise, the method of statistical linearization has proven useful for two reasons. First, one infers that the time-averaged effect of external noise  $D_1$  consists in suppressing the unit's excitability, quite similar to the impact of  $\tau_{in}$ . The other result concerns families of curves obtained for the correlation time as a function of  $D_1$  at different  $\tau_{in}$ . These dependencies provide indirect evidence on the prevailing factor in the unit's oscillatory motion, such as the point that the  $\tau_{in}$ -driven mode is strongly susceptible to external perturbation, giving way to the noise-induced mode already at intermediate  $D_1$ .

In the noiseless case, we have shown that the system of coupled units displays bistability in most  $(\tau_{ex}, \tau_{in})$  domains, which is a corollary of an intricate interplay between the local and global bifurcations. While the equilibrium undergoes a sequence of direct and inverse supercritical and subcritical Hopf bifurcations with increasing  $\tau_{ex}$  at any  $\tau_{in} > \tau_{in}^H$ , the  $\tau_{in}$ -controlled fold-cycle bifurcation inherited from the single unit is complemented by the fold-cycle bifurcation due to  $\tau_{ex}$ . For any  $\tau_{in} > \tau_{in}^H$ , there exists a coupling delay  $\tau_{ex}$  slightly smaller than the fold-cycle threshold  $\tau_{ex}^{FC}$ , above which the fixed point is no longer stable. As for the oscillatory state, the large cycles elicited in global bifurcations typically survive, whereas the cycles emerging from Hopf bifurcations get annihilated in scenarios involving inverse fold-cycle bifurcation. Adding stochastic terms affects asymptotic dynamics (novel oscillatory modes, certain bistable regimes lost), but also leads to some transient phenomena (stochastic switching between oscillatory modes).

Interaction of noisy units is examined for two basic setups involving perturbation from external or internal sources. In both instances, the impact of  $\tau_{in}$  is assessed by comparing two representative cases, characterized by  $\tau_{in}$  lying below or above

$\tau_{in}^{FC}$ . While regularity of firing is quantified by the signal-to-noise ratio  $S$ , coordination of activities has been treated within the framework of stochastic synchronization. The latter refers to frequency synchronization, described by the ratio of average ISIs  $r$ , and the adjustment at an arbitrary moment of time, measured by the synchronization index  $\gamma$ .

We have numerically demonstrated that the external/internal character of noise crucially influences (i) the ability of entrainment to a single frequency and (ii) the fashion in which the competition between the delay- and noise-driven modes is resolved. Regarding (i), note that frequency synchronization turns out to be resilient against intrinsic noise, whereas it is violated by external noise if the adjustable unit is sufficiently perturbed. On the prevailing oscillatory mode, both forms of noise yield a similar paradigm for  $\tau_{in} < \tau_{in}^{FC}$ , whereas the differences become apparent for non-trivial  $\tau_{in} > \tau_{in}^{FC}$ . Below  $\tau_{in}^{FC}$ , under increasing  $\tau_{ex}$  the characteristic scale of oscillations is first controlled by the adjustable unit, then by the coupling delay and finally by the optimized unit. Above  $\tau_{in}^{FC}$ , the scenarios with different noise terms are manifestly distinct because the  $\tau_{in}$ -driven mode is more susceptible to external perturbation.

Deterministic effects due to intrinsic delay have been shown to strongly influence (i) regularity of firing and (ii) the properties of phase synchronization between the units. With respect to (i), for  $\tau_{in} < \tau_{in}^{FC}$ , maximal regularity reflects the onset of the fold-cycle bifurcation controlled by  $\tau_{ex}$ , whereas above  $\tau_{in}^{FC}$ , regularity peaks if the characteristic time-scale of the noise-induced oscillations at the optimized unit matches that of the  $\tau_{ex}$ -driven mode. On (ii), note that for  $\tau_{in} < \tau_{in}^{FC}$  three characteristic regimes admitting phase synchronization may be found. At small and large  $\tau_{ex}$ , phase synchronization arises between the modes prevalently influenced by noise, whereas at intermediate  $\tau_{ex}$  a nearly stationary relative phase is achieved for the  $\tau_{ex}$ -driven modes. Above  $\tau_{in}^{FC}$ , stochastic effects are more expressed under external noise, as its coaction with  $\tau_{ex}$  can give rise to phase synchronization.

In this paper we have examined how introducing an intermediate characteristic time-scale affects the regularity and phase synchronization of class II excitable units subjected to external and internal sources of noise, as well as coupling delays. The fashion in which the competition between the noise-induced and delay-driven (noise-perturbed) oscillation modes is resolved can also have merit from the aspect of controlling the noise-induced oscillations through coupling delay. It would be interesting to study the similar set of issues in case of type I excitable units, represented by the Morris–Lecar model.

## Acknowledgement

This work was supported in part by the Ministry of Education and Science of the Republic of Serbia, under Project Nos. 171017 and 171015.

## References

- [1] Ares S, Morelli LG, Jörg DJ, Oates AC, Jülicher F. *Phys Rev Lett* 2011;106:058102.
- [2] Destexhe A, Rudolph-Lilith M. *Neuronal noise*. New York: Springer; 2012.
- [3] Sagués F, Sancho JM, García-Ojalvo J. *Rev Mod Phys* 2007;79:829.
- [4] Pedraza JM, Paulsson J. *Science* 2008;319:339.
- [5] Galla T. *Phys Rev E* 2009;80:021909.
- [6] Gupta C, Lopez JM, Ott W, Josić K, Bennett MR. *Phys Rev Lett* 2013;111:058104.
- [7] Roussel MR, Igamberdiev AU. *Biosystems* 2011;103:230.
- [8] Dhamala M, Jirsa VK, Ding M. *Phys Rev Lett* 2004;92:074104.
- [9] Popovych OV, Hauptmann C, Tass PA. *Phys Rev Lett* 2005;94:164102.
- [10] McDonnell MD, Ward LM. *Nat Rev Neurosci* 2011;12:415.
- [11] Ramana Reddy DV, Sen A, Johnson GL. *Phys Rev Lett* 1998;80:5109.
- [12] Pikovsky A, Zaikin A, de la Casa MA. *Phys Rev Lett* 2002;88:050601.
- [13] Elowitz MB, Levine AJ, Siggia ED, Swain PS. *Science* 2002;297:1183.
- [14] Raser JM, O’Shea EK. *Science* 2004;304:1811.
- [15] Blake WJ, Kaern M, Cantor CR, Collins JJ. *Nature (London)* 2003;422:633.
- [16] Gaudreault M, Drolet F, Vials J. *Phys Rev E* 2012;85:056214.
- [17] Bratsun D, Volfson D, Tsimring LS, Hasty J. *Proc Natl Acad Sci USA* 2005;102:14593.
- [18] Jia T, Kulkarni RV. *Phys Rev Lett* 2011;106:058102.
- [19] Lim J, Ryu J, Lee C, Yoo S, Jeong H, Lee J. *New J Phys* 2011;13:103002.
- [20] Izhikevich EM. *Dynamical systems in neuroscience: the geometry of excitability and bursting*. Cambridge, Massachusetts: MIT Press; 2007.
- [21] Gaudreault M, Lépine F, Vials J. *Phys Rev E* 2009;80:061920.
- [22] Gaudreault M, Berbert JM, Vials J. *Phys Rev E* 2011;83:011903.
- [23] Khovanov IA, Polovinkin AV, Luchinsky DG, McClintock PVE. *Phys Rev E* 2013;87:032116.
- [24] Muratov CB, Vanden-Eijnden E. *CHAOS* 2008;18:015111.
- [25] Zhang J, Yuan Z, Wang J, Zhou T. *Phys Rev E* 2008;77:021101.
- [26] Hauschildt B, Janson NB, Balanov A, Schöll E. *Phys Rev E* 2006;74:051906.
- [27] Burić N, Todorović D. *Phys Rev E* 2003;67:066222.
- [28] Schmid G, Goychuk I, Hänggi P. *Fluct Noise Lett* 2004;4:L33.
- [29] Brandstetter S, Dahlem MA, Schöll E. *Philos Trans R Soc A* 2010;368:391.
- [30] Pikovsky AS, Kurths J. *Phys Rev Lett* 1997;78:775.
- [31] Lee DeVille RE, Vanden-Eijnden E, Muratov CB. *Phys Rev E* 2005;72:031105.
- [32] Risken H. *The Fokker–Planck equation: methods of solutions and applications*. 2nd ed. Berlin, Heidelberg: Springer-Verlag; 1989.
- [33] Guillozic S, L’Heureux I, Longtin A. *Phys Rev E* 1999;59:3970.
- [34] Atay FM, editor. *Complex time-delay systems: theory and applications*. Berlin, Heidelberg: Springer; 2010.
- [35] Campbell SA. Time delays in neural systems. In: McIntosh R, Jirsa VK, editors. *Handbook of brain connectivity*. Berlin, Heidelberg: Springer-Verlag; 2007. p. 65–90.

- [36] Campbell SA. Calculating centre manifolds for delay differential equations using Maple. In: Balachandran B, Kalmar-Nagy T, Gilsinn D, editors. Delay differential equations: recent advances and new directions. New York: Springer-Verlag; 2009. p. 221–45.
- [37] Mackey MC, Nechaeva IG. Phys Rev E 1995;52:3366.
- [38] Lei J, Mackey MC. SIAM J Appl Math 2007;67:387.
- [39] Pomplun J, Amann A, Schöll E. EuroPhys Lett 2005;71:366.
- [40] Kottalam J, Lindenberg K, West BJ. J Stat Phys 1986;42:979.
- [41] Lindner B, Garcia-Ojalvo J, Neiman A, Schimansky-Geier L. Phys Rep 2004;392:321.
- [42] Zaks MA, Neiman AB, Feistel S, Schimansky-Geier L. Phys Rev E 2003;68:066206.
- [43] Franović I, Todorović K, Vasović N, Burić N. Phys Rev E 2013;87:012922.
- [44] Franović I, Todorović K, Vasović N, Burić N. Phys Rev Lett 2012;108:094101.
- [45] Hasegawa H. Phys Rev E 2004;70:021911.
- [46] Gardiner CW. Handbook of stochastic methods for physics, chemistry and the natural sciences. 3rd ed. Berlin, Heidelberg: Springer-Verlag; 2004.
- [47] Engelborghs K, Luzyanina T, Samaey G. Technical report TW-330, Department of Computer Science, K.U. Leuven Leuven, Belgium; 2001.
- [48] Engelborghs K, Luzyanina T, Roose D. ACM Trans Math Softw 2002;28:1.
- [49] Wiggins S. Introduction to applied nonlinear dynamical systems and chaos. 2nd ed. New York, Cambridge: Springer; 2000.
- [50] Hu B, Zhou C. Phys Rev E 2000;61:R1001.
- [51] Pei X, Wilkens L, Moss F. Phys Rev Lett 1996;77:4679.
- [52] Neiman A, Silchenko A, Anishchenko V, Schimansky-Geier L. Phys Rev E 1998;58:7118.
- [53] Rosenblum M, Pikovsky A, Kurths J, Schäfer C, Tass PA. Phase synchronization: from theory to data analysis. In: Moss F, Gielen S, editors. Neuroinformatics and neural modelling. Amsterdam, The Netherlands: North-Holland; 2001. p. 279–322.



## Persistence and failure of mean-field approximations adapted to a class of systems of delay-coupled excitable units

Igor Franović,<sup>1</sup> Kristina Todorović,<sup>2</sup> Nebojša Vasović,<sup>3</sup> and Nikola Burić<sup>4,\*</sup>

<sup>1</sup>*Faculty of Physics, University of Belgrade, P. O. Box 44, 11001 Belgrade, Serbia*

<sup>2</sup>*Department of Physics and Mathematics, Faculty of Pharmacy, University of Belgrade, Vojvode Stepe 450, Belgrade, Serbia*

<sup>3</sup>*Department of Applied Mathematics, Faculty of Mining and Geology, University of Belgrade, P. O. Box 162, Belgrade, Serbia*

<sup>4</sup>*Scientific Computing Laboratory, Institute of Physics, University of Beograd, P. O. Box 68, 11080 Beograd-Zemun, Serbia*

(Received 2 July 2013; revised manuscript received 25 December 2013; published 28 February 2014)

We consider the approximations behind the typical mean-field model derived for a class of systems made up of type II excitable units influenced by noise and coupling delays. The formulation of the two approximations, referred to as the Gaussian and the quasi-independence approximation, as well as the fashion in which their validity is verified, are adapted to reflect the essential properties of the underlying system. It is demonstrated that the failure of the mean-field model associated with the breakdown of the quasi-independence approximation can be predicted by the noise-induced bistability in the dynamics of the mean-field system. As for the Gaussian approximation, its violation is related to the increase of noise intensity, but the actual condition for failure can be cast in qualitative, rather than quantitative terms. We also discuss how the fulfillment of the mean-field approximations affects the statistics of the first return times for the local and global variables, further exploring the link between the fulfillment of the quasi-independence approximation and certain forms of synchronization between the individual units.

DOI: [10.1103/PhysRevE.89.022926](https://doi.org/10.1103/PhysRevE.89.022926)

PACS number(s): 05.45.Xt, 02.30.Ks

### I. INTRODUCTION

When modeling macroscopic systems comprised of coupled oscillating units, one is often required to incorporate noise and interaction delays, whose separate or combined effects may substantially alter the “bare” dynamics, unattended by these two ingredients. The systems where coaction of noise and delays should be taken into account appear to be common, rather than rare [1,2], with the most prominent examples derived from the biophysiological context [3] or involving laser dynamics [4]. The interplay of noise and delays becomes especially intricate if the units making up the system are not self-oscillating, but excitable [5]. For such a setup, the local and collective dynamics rest on the competition between the delay-driven and the noise-induced oscillation modes [6,7].

In mathematical terms, the described models are usually stated in terms of systems of nonlinear stochastic delay-differential equations (SDDE), whose general form is given by

$$d\mathbf{x}_i(t) = f(\mathbf{x}_i(t)) + \sum_{i,j} g_{ij}(\mathbf{x}_i(t), \mathbf{x}_j(t - \tau_j)) + \sigma_i dW_i, \quad (1)$$

where  $i, j = 1, \dots, N$ ,  $\mathbf{x}_i$  are vectors of dynamical variables for the  $i$ th unit,  $f$  is a nonlinear function,  $\tau_i$  are the coupling delays, and  $dW_i$  are stochastic increments of the independent Wiener processes. For systems like (1), the standard Fokker-Planck formalism can rarely provide useful results that may serve for qualitative analysis of stochastic stability and stochastic bifurcations [8–11], with its use severely constrained by the non-Markovian character and nonlinearity of the equations [12]. In particular, for univariate systems one may only consider the limits of small delay or delay larger than the system’s correlation time [12–15], whereas for the

setup involving multiple units, even the delay-free case under the assumption of molecular chaos cannot be analytically resolved [16], though efficient numerical methods are available [17].

The failure of Fokker-Planck formalism implies the necessity for considering approximate methods, one of them being the mean-field (MF) approach. The gains from the latter can in general be cast as twofold. On one hand, an accurate MF model substantially reduces the computational time for numerical integration [18], which for the exact system grows as  $\sim N^2$  with its size [19]. The other gain lies in the ability to translate the problem of stochastic bifurcations displayed by the exact system into bifurcations of the compact deterministic MF system [20–22]. The stochastic bifurcations have so far been characterized phenomenologically, relying on the point that a certain time-averaged quantity, such as the asymptotic probability distributions of the relevant variables or the associated power spectra undergo some qualitative change [17,20,23,24]. For instance, it has been shown that the stochastic Hopf bifurcation from a stochastically stable fixed point to a stochastically stable limit cycle is accompanied by the loss of Gaussian property for the asymptotic distributions of the appropriate variables [20]. In parallel, the degree by which the distribution departs from the normal one with supercriticality depends on the particular system at hand. However, the onset of stochastic bifurcation and the loss of Gaussian property for asymptotic distributions alone do not imply the failure of the MF approximate model. In fact, such a correspondence would apply only if the MF approximation were based on the notion that the described stochastic process is a Gaussian one. Nevertheless, such a requirement is too strong, in a sense that the validity of the MF model is then satisfied trivially. Moreover, examples have already been found where the MF system can accurately predict the properties of the oscillatory state, including the oscillation frequency [25,26].

\*buric@ipb.ac.rs

The arguments above justify more elaborate research on the approximations behind the MF model and the conditions for their validity. On one hand, one may ask whether the MF approximations (MFAs) are universal as might be expected at first sight, or should in fact be modified to account for the properties of the system at hand. The second question we address is whether the dynamics of the MF model itself may point to parameter domains where the MF approximation fails. At variance with the earlier work, this set of issues is completely unrelated to the asymptotic distributions of the underlying variables.

As an example of a system conforming to (1), we consider an assembly of delay-coupled noisy class II excitable units [5], represented by the generic Fitzhugh-Nagumo model. For such a system, we demonstrate that the MFAs should be precisely adapted to its properties, explicitly incorporating the key ingredients of type II excitability, such as relaxation character of oscillations, in the definition of the MFAs and the methods by which their validity is verified. The main benefit from the refined definitions is that they provide rationale on why the predictions provided by the MF model successfully extend to parameter domains admitting oscillatory states, where the trivial Gaussian approximation would necessarily be violated. The other important point shown in the paper is that the dynamics of the MF model may indicate in the self-consistent fashion the domains where one of the MFAs we introduced fails. In particular, such a breakdown of the MF approximate model is found to be linked with the noise-induced bistability in the MF dynamics. Note that the term noise-induced bistability refers to either coexistence of the fixed point and a limit cycle or two limit cycles, which emerge due to action of the noise intensity parameter. The appearance of these regimes is associated with the global fold-cycle (tangent) bifurcation controlled by the noise intensity.

The paper is organized as follows. In Sec. II, we precisely define the two main approximations behind the MF model, dubbed Gaussian approximation and the quasi-independence approximation, whose formulations are adapted to reflect the qualitative properties of type II excitable units. Section III is concerned with identifying the typical dynamical scenarios where the MFAs are seen to hold or fail, whereby the tests applied to verify the validity of the MFAs are accommodated to class II excitable systems. In Sec. IV we discuss one of the key points, consisting in the ability to deduce the parameter domains where the quasi-independence approximation fails solely by the dynamics of the MF model. Section V deals with several miscellaneous topics, including how the fulfillment of the MFAs is manifested in the statistics of the first return times for the local and collective variables, as well as the link between synchronization and the fulfillment of the quasi-independence approximation. Section VI contains a summary of the main points of the paper.

## II. EXACT SYSTEM, MFAs, AND MF MODEL

### A. Background on the exact system

The validity of the MFAs is analyzed in the case of a collection of  $N$  Fitzhugh-Nagumo excitable units, whose

dynamics is set by

$$\begin{aligned} \epsilon dx_i &= (x_i - x_i^3/3 - y_i)dt + \frac{c}{N} \sum_{j=1}^N [x_j(t - \tau) - x_i]dt, \\ dy_i &= (x_i + b)dt + \sqrt{2D}dW_i, \quad i = 1, \dots, N. \end{aligned} \quad (2)$$

Each unit interacts with every other via diffusive delayed couplings, whereby the coupling strength  $c$  and the time lag  $\tau$  are taken uniform. Parameters  $\epsilon = 0.01$  and  $b = 1.05$  are such that the isolated units display excitable behavior, having a stable fixed point (FP) as the only attractor. The terms  $\sqrt{2D}dW_i$  represent stochastic increments of the independent Wiener processes, viz.,  $dW_i$  satisfy  $E(dW_i) = 0$ ,  $E(dW_i dW_j) = \delta_{i,j}dt$ , where  $E(\cdot)$  denotes the expectation over different realizations of the stochastic process.

Having proposed that the nontrivial conditions for the fulfillment of the MFAs derive from the qualitative properties of the underlying dynamics, we first summarize the typical regimes exhibited by  $[x_i(t), y_i(t)]$ , beginning with the deterministic case  $D = 0$ . For small  $c$  and  $\tau$ , the only attractor of each unit is FP and the dynamics is excitable. For larger  $c$  and/or larger  $\tau$ , the FP undergoes a Hopf bifurcation and the asymptotic dynamics resides on a stable limit cycle (LC). The LC conforms to relaxation oscillations, with two clearly distinguished slow branches, the refractory and the spiking one, and two fast transients in between [cf. Fig. 1(b) where small noise perturbations are added]. Small  $D$  induces small fluctuations around the attractor of the deterministic dynamics. If the latter motion lies on LC, the impact of  $D$  is reflected mostly in the fluctuations of phase of the oscillatory dynamics between the different stochastic realizations. Apart from the increase of fluctuation amplitudes, enhancing  $D$  may give rise to the transition from the stochastically stable FP to the noise-induced spiking. The latter can appear as nearly periodic or irregular depending on  $c$ ,  $\tau$ , and  $D$ . It is known that in systems of excitable units subjected to  $D$  and  $\tau$ , the length of interspike intervals (ISIs) is influenced by the competition between two characteristic time scales [6,7]. One is set by the self-oscillation “period”  $T_0(D)$  obtained for  $\tau = 0$ , whereas the other is adjusted with  $\tau$ . Loosely speaking, for  $\tau < T_0(D)$  and intermediate  $c$ , the noise-led dynamics characterized by  $T_0(D)$  prevails over the delay-driven one unless  $\tau$  is commensurate or comparable to  $T_0(D)$ . This paradigm may carry over to the collective motion due to synchronization of individual units.

### B. Formulation of MFAs

The first MFA derives from the strong law of large numbers, by which the sample average  $S_N = N^{-1} \sum_{i=1}^N s_i$  of  $N$  independent and identically distributed random variables  $s_i$  converges almost surely to the expectation value  $E(s_i)$  for  $N \rightarrow \infty$ . How  $S_N$  approaches  $E(s_i)$  for large, but finite  $N$  and finite variances of  $s_i$  distributions  $\sigma^2$ , is specified by the central limit theorem, which implies that  $S_N$  follow the normal distribution  $\mathcal{N}(E(s_i), \sigma^2/N)$ . In our setup, the subsets  $\{x_i(t)|i = 1, \dots, N\}$  and  $\{y_i(t)|i = 1, \dots, N\}$  at any given  $t$  are obviously not made up of independent variables, but one may still consider the influence of interaction terms negligible if  $N$  is sufficiently large. The latter is referred to

as the quasi-independent approximation (QIA), whose precise formulation is as follows.

*Approximation 1 (QIA).* Random variables  $\{x_i(t)|i = 1, \dots, N\}$  and  $\{y_i(t)|i = 1, \dots, N\}$  for each  $t$  and sufficiently large  $N$  satisfy the approximate equalities

$$\begin{aligned} X(t) &\equiv \frac{1}{N} \sum_i^N x_i(t) \approx E[x_i(t)], \\ Y(t) &\equiv \frac{1}{N} \sum_i^N y_i(t) \approx E[y_i(t)]. \end{aligned} \quad (3)$$

On the left of (3) are the *spatial averages*, used to define the global variables  $X(t)$  and  $Y(t)$ . Note that the method implemented in Sec. III to test the validity of the QIA will reflect the relaxation character of oscillations typical for class II excitable systems.

The need for the second approximation becomes apparent after carrying out the spatial average and applying the QIA on (2). The fashion in which the terms  $E[x_i^3(t)]$  are to be treated is resolved by the *Gaussian approximation* (GA), given as follows.

*Approximation 2 (GA).* For most time instances  $t_0$ , the small random increments  $dx_i(t), dy_i(t)$  for  $t \in (t_0, t_0 + \delta t)$  can be computed with sufficiently good accuracy by assuming that the random variables  $x_i(t), y_i(t)$  for each  $i = 1, \dots, N$  and for  $t \in (t_0, t_0 + \delta t)$  are normally distributed around  $(E[x_i(t)], E[y_i(t)]) \approx [X(t), Y(t)]$ .

GA is intentionally stated in a weak sense, containing the phrases ‘‘sufficiently good accuracy’’ and ‘‘for most time instances.’’ The former implies that the approximate solution should have the same qualitative features as the exact one. Nevertheless, the phrase ‘‘for most time instances’’ is crucial, because it specifically targets the class II excitable systems, being introduced to account for the relaxation character of oscillations, as explicitly demonstrated in Sec. III. Further note that the GA does not require  $\{x_i(t)|i = 1, \dots, N\}$  and  $\{y_i(t)|i = 1, \dots, N\}$  to be Gaussian processes over asymptotically large time intervals, but rather to be Gaussian over small intervals  $(t, t + \delta t)$ , with the latter supposed to hold for most values of  $t$ . For such  $t$  one can express all the higher-order moments that appear in the expressions for  $dX(t)$  and  $dY(t)$  in terms of only the means, viz.,  $X(t)$  and  $Y(t)$ , and the second-order moments, including variances  $s_x(t) = E[n_{x_i}^2(t)], s_y(t) = E[n_{y_i}^2(t)]$  and the covariance  $u(t) = E[n_{x_i}(t)n_{y_i}(t)]$ , where  $n_{x_i}(t) = X(t) - x_i(t)$ ,  $n_{y_i}(t) = Y(t) - y_i(t)$ . Here, the QIA is reflected in the fashion in which the spatial and the stochastic averages are related. Use of the GA in deriving the MF model rests on the notion that the fraction of time where GA fails will not introduce significant differences between the MF and the exact solutions.

The MF counterpart of (2), incorporating the QIA and GA, has been derived in [25]. It constitutes the following system of five deterministic DDE:

$$\begin{aligned} \epsilon \dot{m}_x &= m_x(t) - m_x(t)^3 - s_x(t)m_x(t) - m_y(t) \\ &\quad + c[m_x(t - \tau) - m_x(t)], \\ \dot{m}_y &= m_x(t) + b, \\ \frac{\epsilon}{2} \dot{s}_x &= s_x(t)[1 - m_x(t)^2 - s_x(t) - c] - u(t), \end{aligned}$$

$$\frac{1}{2} \dot{s}_y = u(t) + D,$$

$$\dot{u} = [u(t)/\epsilon][1 - m_x(t)^2 - s_x(t) - c] - s_y(t)/\epsilon + s_x(t), \quad (4)$$

assuming that the MF solutions satisfy  $m_x(t) \approx X(t)$ ,  $m_y(t) \approx Y(t)$ . Note that some more sophisticated MF approaches [19,27] adopt the Gaussian decoupling approximation, yet do not require a QIA, as their final form accounts for spatial averages of fluctuations of both local and global variables.

### III. TESTING THE VALIDITY OF MFAs AND THE GENERIC REGIMES WHERE THEY HOLD OR FAIL

The goal is to first explain the two generic scenarios where both the MFAs hold, outlining the parameter domains where the pertaining local and global dynamics typically occur. We also illustrate the case where both the MFAs fail, independently demonstrating that the GA and the QIA are violated. As indicated in the Introduction, the methods applied to verify the validity of the MFAs for the oscillatory state are adapted to the essential properties of the class II excitable systems. Note that in this section, which contains the numerical results on the exact system, one is primarily concerned with the fulfillment of the GA. This is done deliberately, given that the breakdown of the QIA can be deduced from the dynamics of the MF model, as demonstrated in Sec. IV.

Intuitively, one would expect that both the MFAs are satisfied if  $c$  and  $D$  are small. Though this is indeed so, the general conclusion on the simultaneous validity of both the MFAs is less straightforward, and should refer to the qualitative properties of the system’s dynamics, rather than alluding to certain parameter domains. As a preview of this result, it may be stated that the GA and the QIA hold if the local and the global dynamics are characterized by a single attractor of the same type, either a FP or a LC, provided that  $D$  is not too large. Conversely, if the local and the collective variables yield qualitatively different dynamics or exhibit multistability, the validity of either or both the MFAs is lost. Nevertheless, note that the separate conditions for failure of each of the MFAs can be put in a more succinct form, which will be clarified below.

The discussion above implies that there are two paradigmatic scenarios where both the GA and the QIA hold. By one, the local and the collective dynamics display stochastically stable FP, whereas in the other, the local and the collective dynamics exhibit the stochastically stable LC. These two cases are addressed in Figs. 1(a) and 1(b), respectively, whereby the intention is to first verify the validity of GA. Before proceeding in this direction, note that the value  $c = 0.1$ , fixed in both instances, is chosen from an intermediate range to stress that the MFAs’ validity extends into such a domain. Nonetheless, the data in Fig. 1(a) are obtained for small  $D_1 = 0.0002$  and small  $\tau_1 = 0.2$ , while the setup in Fig. 1(b) involves  $D_2 = D_1$  but the much larger  $\tau_2 = 2.7$ .

As an illustration of the qualitative similarity between the individual realizations and the expectations, the main frames of Figs. 1(a) and 1(b) show three different stochastic realizations  $(x_{5,r}, y_{5,r})$ , encoded in black solid, dashed, and dotted lines,

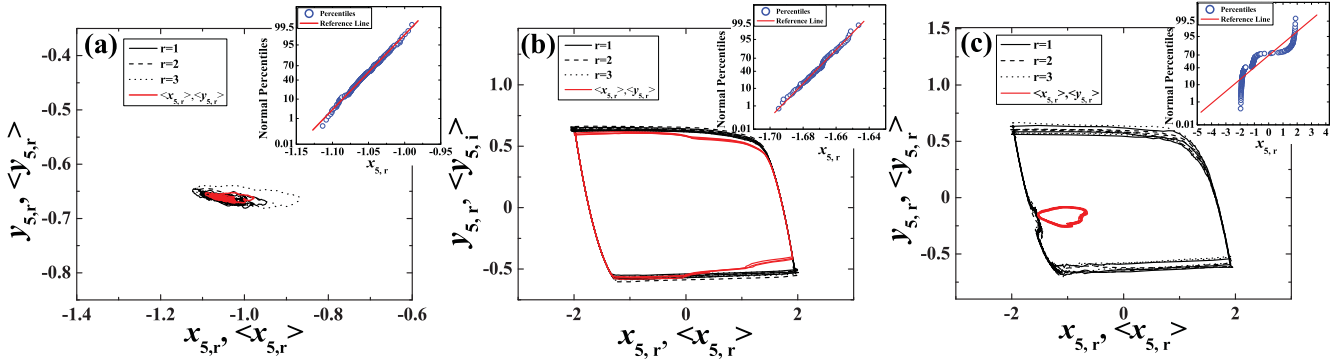


FIG. 1. (Color online) Impact of noise on the validity of GA. (a) and (b) refer to typical scenarios where the GA holds, while (c) concerns one of the cases where it fails. For an arbitrary unit, here denoted with index 5, the main frames of (a), (b), and (c) show orbits corresponding to three different stochastic realizations  $(x_{5,r}, y_{5,r})$  (black solid, dashed, and dotted lines), as well as the respective expectations  $[E(x_{5,r}), E(y_{5,r})]$  for an ensemble of ten realizations, having indicated the latter by the solid red (gray) lines. In the insets of (a), (b), and (c) are displayed the appropriate graphic normality tests, such that the red (gray) lines conform to theoretical data sets obeying the Gaussian distribution, whereas the circles reflect the data for  $x_{5,r}$  actually collected over different realizations. The parameter sets are  $(c, D, \tau) = (0.1, 0.0002, 0.2)$  in (a),  $(c, D, \tau) = (0.1, 0.0002, 2.7)$  in (b), and  $(c, D, \tau) = (0.1, 0.003, 1.5)$  in (c).

as well as the expectation values  $[E(x_{5,r}), E(y_{5,r})]$  over an ensemble of ten realizations, having plotted them by the solid red (gray) lines. The data are representative of the dynamics of an arbitrary neuron, whereby the particular example refers to the unit  $i = 5$ . The index  $r$  accounts for the realizations. In the case of Fig. 1(a), for any  $t$ , the expectation closely matches either of the realizations trivially. Nevertheless, for the scenario with the LC attractor, the analogous statement holds if  $t$  is such that  $(E[x_{i,r}(t)], E[y_{i,r}(t)]) \approx [X(t), Y(t)]$  lies on the slow branches of the given orbit. At variance with this, if  $(E[x_{i,r}(t)], E[y_{i,r}(t)])$  falls onto one of the transients, the expectation departs substantially from the realizations [cf. Fig. 1(b)]. The two latter points are consistent with the relaxation character of oscillations, and as such are accounted for by the definition of GA. Invoking the definition, it follows that the GA's validity is upheld if the number of instances where the expectations closely match the individual realizations strongly prevails over the number of instances where such a correspondence is lost. In other words, the GA holds if the expectations preserve the relaxation character of oscillations exhibited by the realizations. Though this requirement is qualitative in nature, one may still attempt to attribute it a certain quantitative measure. For instance, for the  $(c, D_2, \tau_2)$  parameter set from Fig. 1(b), it may be shown that the ratio of points lying on the transients vs those on the slow branches is small ( $n_t/n_s \approx 0.1$ ) over the sufficiently long time period along the trajectory of  $(E[x_{i,r}(t)], E[y_{i,r}(t)])$ .

Figure 1(c) refers to the case where GA no longer holds. The illustrated local dynamics is obtained for comparably large  $D_3 = 0.003$ ,  $c = 0.1$ , and intermediate  $\tau_3 = 1.5$ , such that the individual stochastic realizations fluctuate around the single LC. However, the noise-induced fluctuations are large enough to throw the different realizations out of step, resulting in the strong misalignment between the pertaining oscillation phases. Therefore, at variance with Fig. 1(b), the expectation substantially departs from each of the realizations at *any*  $t$ . For  $(c, D_3, \tau_3)$ , one can no longer interpret  $(E[x_{i,r}(t)], E[y_{i,r}(t)])$  in terms of clearly discernible slow and fast motions, so that the ratio  $n_t/n_s$  cannot be determined.

Apart from characterizing it by the  $n_t/n_s$  ratio, the GA validity has been tested directly for an arbitrary neuron at the given  $(c, D, \tau)$ . Having run many different realizations of the processes  $x_i(t), y_i(t)$  for the same initial function, we have examined the properties of the distribution of different realizations  $x_{i,r}(t_0 + \delta t), y_{i,r}(t_0 + \delta t)$  for small  $\delta t$ , taken to be of the order, in tens or hundreds of iteration steps. For the LC dynamics,  $[x_{i,r}(t_0), y_{i,r}(t_0)]$  has been set on the refractory branch. The insets of (a), (b), and (c) display graphic normality tests, where the red lines indicate the theoretical percent of data points that would lie below the given value if obeying the Gaussian distribution, while the blue circles refer to the cumulative distribution of  $(x_{5,r}, y_{5,r})$  for an ensemble of over 200 realizations. Apparently, the distributions corresponding to  $(c, D, \tau)$  in Figs. 1(a) and 1(b) are Gaussian, whereas the one for Fig. 1(c) is not. Results of the graphic tests are corroborated by the standard numerical Shapiro-Wilk method.

Having seen that the criteria for the validity of GA is primarily qualitative, it is still of interest to find some indication of how the fulfillment of GA deteriorates with variation of the system parameters. Naturally, the most relevant question is to assess the rate at which the validity reduces with increasing  $D$  for fixed  $c$  and  $\tau$ . The quantity appropriate to characterize this is determined as follows. For very small  $D = 0.0002$ , we select an arbitrary neuron and fix a point on the refractory branch of its LC orbit. Then, a large number of different stochastic realizations  $N_r$  for the given parameter set  $(D, c, \tau) = (0.0002, 0.1, 2.7)$  is run. The goal is to find the maximal number of iteration steps  $T_{\max}$ , for which the representative point in all the realizations still lies on the refractory branch. Enhancing  $D$  while  $T_{\max}$  is kept fixed, one naturally encounters realizations where the latter condition is no longer satisfied. In Fig. 2 we demonstrate how the fraction of realizations  $N_{\text{out}}/N_r$  in which the representative point has escaped the refractory branch in less than or exactly  $T_{\max}$  steps increases with  $D$ . Along with allowing one to quantify the gradual loss of the GA's validity, this dependence may also be interpreted as an indication of how  $D$  gives rise to the number of moments  $t$  where  $(E[x_{i,r}(t)], E[y_{i,r}(t)])$  belong

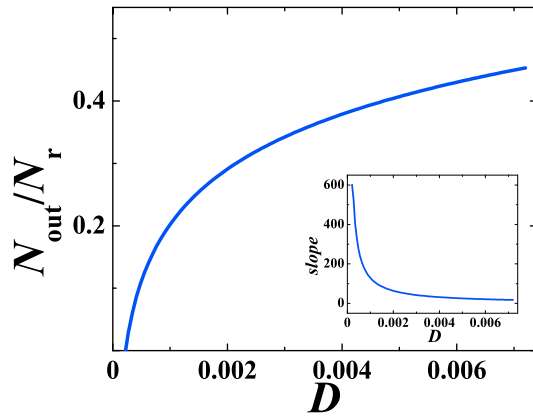


FIG. 2. (Color online) Estimating rate by which the validity of GA deteriorates with increasing  $D$ . The plot shows a fraction of stochastic realizations  $N_{out}/N_r$  in dependence of  $D$  for  $(c, \tau) = (0.1, 2.7)$ .  $N_{out}$  accounts for the instances where the representative point escapes the refractory branch of slow motion within the given number of iteration steps  $T_{max}$ . The results converge to the displayed curve as  $N_r$  is increased. The inset refers to the variation of the slope of the curve from the main frame with noise.

to fast transients, rather than the two slow branches. In this context, it is interesting to explain why the curve's slope shows a significant change in behavior around  $D_0 \approx 0.0014$  (cf. the inset in Fig. 2). Below  $D_0$ , the fluctuations of phase between the different stochastic realizations systematically grow, but the physical picture by which the LC for the expectations  $(E[x_{i,r}(t)], E[y_{i,r}(t)])$  is described in terms of two pieces of slow motion connected by the two rapid jumps still applies. Nevertheless, about  $D \simeq D_0$ , such a picture has to be abandoned, because the LC generated by the expectations no longer matches the phase portrait of individual realizations. In particular, the  $(E[x_{i,r}(t)], E[y_{i,r}(t)])$  cycle lies inside that for the single realizations, as it fails to reach the latter's spiking branch. Once the framework involving qualitative equivalence between the dynamics of realizations and the expectations has been broken,  $N_{out}/N_r$  for  $D > D_0$  loses its original meaning, but its steady increase reflects the tendency for growing irregularity in the unit's behavior.

We now turn to the analysis on the fulfillment of the QIA. The intention here is just to briefly mention the two methods that may be used to verify the validity of the QIA by examining the exact system, whereas the main point, lying in the ability to predict the failure of the QIA solely by the dynamical

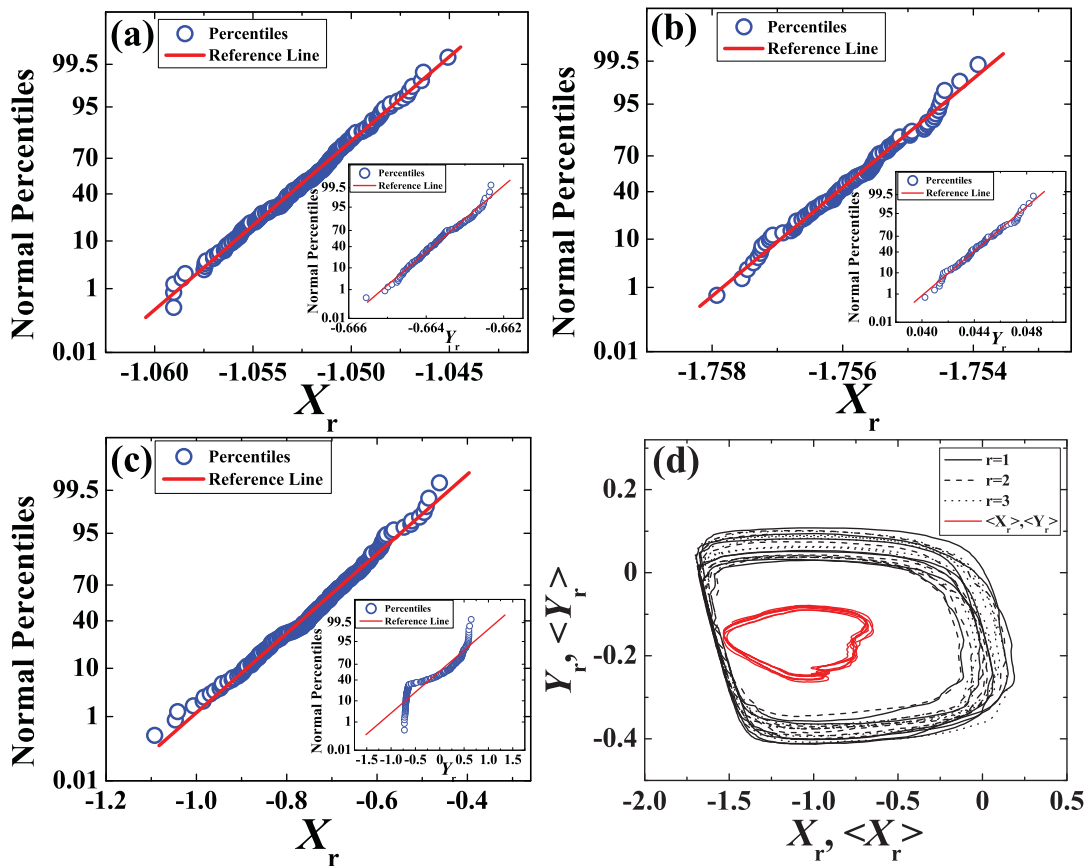


FIG. 3. (Color online) Examining the validity of the QIA. Consistent with the theorem of large numbers, confirming the validity of GA for the global variables corroborates that the QIA holds for the local variables. The main frames (insets) of (a), (b), and (c) refer to the graphic normality tests for the collective variables  $X(t)$  [ $Y(t)$ ], whereby the respective parameter sets correspond to those in Figs. 1(a)–1(c). In (a) and (b) is demonstrated that  $X_r(t)$  and  $Y_r(t)$  for different stochastic realizations are Gaussian distributed, whereas (c) indicates a substantial departure from the normal distribution in the case of  $Y_r(t)$ . (d) illustrates the loss of qualitative analogy between the oscillations characterizing the individual realizations and the expectation for  $(c, D, \tau)$  from (c).

features of the MF model is left for the next section. Considering the exact system, one may either take (i) an indirect approach, derived from a corollary of the QIA formulation, or (ii) the direct approach, based on the notion that approximate synchronization between the units may render them virtually independent. Since the more comprehensive discussion on the relation between different types of synchronization and the QIA is provided in Sec. VB, we focus on the indirect approach (i). One first invokes the central limit theorem, by which for large, but finite  $N$  holds that if the local variables are normally distributed for most  $t$ , so too are the collective variables. Hence, the validity of GA for  $X(t)$  and  $Y(t)$  should imply that the local variables are independent. The normality tests on  $X(t)$  and  $Y(t)$  are carried out analogously to those for  $x_i(t)$  and  $y_i(t)$ . The main frames (insets) of Figs. 3(a)–3(c) refer to graphic normality tests on the variable  $X(t)$  [ $Y(t)$ ] for the parameter sets exactly matching those in Figs. 1(a)–1(c). Figures 3(a) and 3(b) indicate the validity of GA for  $X(t)$  and  $Y(t)$  distributions, thereby suggesting that the QIA also applies. The positive result in Fig. 3(b), which is associated with the oscillatory state, again draws on the main feature of the class II excitable systems. An interesting point regarding Fig. 3(c) is that the distribution of  $X_r(t_0 + \delta t)$  over stochastic realizations conforms to, and the one for  $Y_r(t_0 + \delta t)$  sharply deviates from the Gaussian form. Such a violation of the QIA is mostly found for intermediate  $D$  and  $\tau$ . Figure 3(d) further illustrates the loss of qualitative analogy between the oscillations for the individual realizations and the expectation, with the latter failing to preserve the relaxation character.

#### IV. PREDICTING THE FAILURE OF QIA BY THE DYNAMICS OF THE MF MODEL

The aim in this section is to demonstrate how the failure of the QIA is indicated by the dynamics of the MF model. To this end, we first present the results of the bifurcation analysis for the approximate system. Note that the analysis has not been carried out on the full system (4), but rather on its counterpart obtained by retaining the equations for the first moments under the “adiabatic” approximation that the evolution of second moments is slow and can be cast as stationary. The main reason for this lies in the fact that the reduced system, unlike the original one, is analytically tractable.

The approximate model is found to display a sequence of supercritical and subcritical Hopf bifurcations, whereby the former (latter) result in the creation of a stable (unstable) limit cycle. Recall that both types of Hopf bifurcation can further be cast as direct or inverse [28], which refers to whether the fixed point unfolds on the unstable or the stable side, respectively. The final expression for the critical time delay in dependence of  $c$  and  $D$  reads [25,26]

$$\begin{aligned} \tau_{\pm}^j &= [\arccos(-\kappa\epsilon/c) + 2j\pi]/\omega_{\pm}, \\ &\text{if } \frac{-\omega_{\pm}^2 + 1/\epsilon}{c\omega_{\pm}/\epsilon} \geq 0, \quad \text{or} \\ \tau_{\pm}^j &= [-\arccos(-\kappa\epsilon/c) + 2(j+1)\pi]/\omega_{\pm}, \\ &\text{if } \frac{-\omega_{\pm}^2 + 1/\epsilon}{c\omega_{\pm}/\epsilon} < 0, \end{aligned} \quad (5)$$

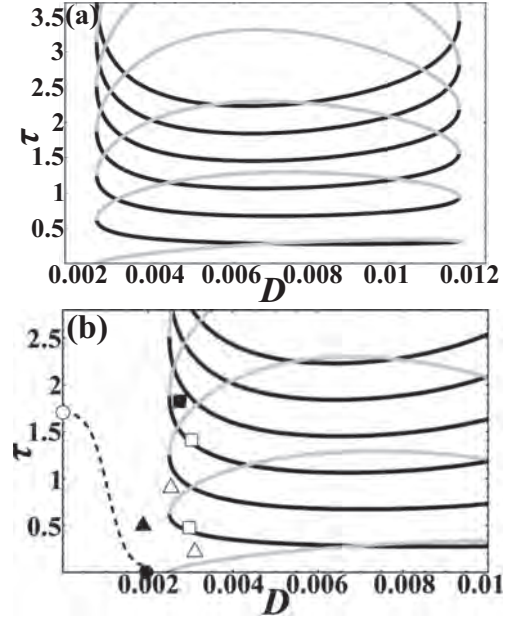


FIG. 4. (a) First few branches  $j = 0, 1, \dots, 6$  of the Hopf bifurcation curves  $\tau_{\pm}^j(D)$  for the MF model. (b) A close-up view of (a), but including the additional indication on the parameter values where the global fold-cycle bifurcations occur. Stability of equilibrium is influenced by a sequence of direct (supercritical) and inverse (subcritical) Hopf bifurcations, shown by the black and gray lines, respectively. In (b), the critical values  $D_{fc}$  and  $\tau_{fc}$  for the  $D$ - and  $\tau$ -controlled fold-cycle bifurcations are indicated by the solid and the open circle lying at  $(D, \tau) = (D_{fc}, 0)$  and  $(D, \tau) = (0, \tau_{fc})$ . The dashed line approximately highlights the parameter values above which the dynamics of the MF model always involves a large cycle born via the global bifurcation. The bistable regimes emerging due to global bifurcations involve the coexistence of FP and LC (instances indicated by the triangles) or two LCs (instances indicated by the squares). For  $D > D_H$ , the existence of bistable regimes and their form depend on the complex interplay between the local and the global bifurcations. Coupling strength is fixed at  $c = 0.1$ .

where the (+) (−) sign reflects the direct (inverse) character of bifurcation,  $j = 0, 1, 2, \dots$  and  $\omega_{\pm} = \omega_{\pm}(c, D)$ ,  $\kappa = \kappa(c, D)$ . It can be shown by a rather lengthy calculation that the direct (inverse) bifurcations are always supercritical (subcritical) [25]. The first few branches  $j = 0, 1, \dots, 6$  of the Hopf bifurcation curves  $\tau_{\pm}^j(D)$  for the intermediate coupling strength  $c = 0.1$  are presented in Fig. 4. In particular, Fig. 4(a) is focused on the Hopf curves alone, whereas Fig. 4(b) presents a zoomin of Fig. 4(a), but also contains additional information, as explained below. Note that the presentation scheme in both figures is such that the curves coinciding with the direct (supercritical) Hopf bifurcations are indicated by the black lines, while those corresponding to inverse (subcritical) Hopf bifurcations are plotted by the gray lines.

Apart from the local bifurcations which affect the stability of equilibrium, the MF dynamics are influenced in a highly nontrivial fashion by the two global fold-cycle (tangent) bifurcations, one controlled by  $D$  and the other by  $\tau$ . Note that the direct fold-cycle bifurcation gives rise to a stable large cycle and a saddle cycle. The point  $(D, \tau) = (D_{fc}, 0)$  where the noise alone is sufficient to induce the global bifurcation is

indicated by the solid circle in Fig. 4. In an analogous fashion, the point  $(D, \tau) = (0, \tau_{fc})$  where solely the delay gives rise to the global bifurcation is denoted by the open circle. The dashed line connecting the open and the solid circle approximately highlights the parameter values above which the dynamics of the MF model always involves a large cycle born via the global bifurcation. One should caution that in the parameter domains allowing for the local bifurcations, the existence of a large cycle *per se* does not warrant multistability in the MF dynamics. Later on, it is shown that multistability in such domains depends on a complex interplay between the attractors and saddles resulting from the local and global bifurcations.

Due to global bifurcations, the MF model exhibits two types of bistable regimes, one involving the coexistence between the FP and the LC, and the other characterized by the coexistence of two LCs. In the former case, the LC corresponds to a large cycle born in the fold-cycle bifurcation. The latter scenario may be realized either by the coaction of the local (direct supercritical) Hopf bifurcation and the global fold-cycle bifurcation, which mainly occurs for  $\tau < \tau_{fc}$ , or the two cycles may both derive from the fold-cycle bifurcations ( $\tau > \tau_{fc}$ ). In most cases, bistability emerges due to the action of noise, i.e., is facilitated by the  $D$ -controlled global bifurcation. Such regimes are referred to as the noise-induced bistability to distinguish them from the scenario involving the coexistence between the FP and the large cycle born in the  $\tau$ -controlled global bifurcation, which occurs for  $\tau > \tau_{fc}$ ,  $D < D_{fc}$ .

Our main point is that the noise-induced bistability in the dynamics of the MF model provides the necessary condition for the failure of the QIA, and therefore the failure of MF approximation as a whole. In other words, the qualitative features of the dynamics displayed by the MF model can be used to predict in a self-consistent fashion the  $(\tau, D)$  parameter domains where the QIA is bound to fail. Before explaining this point in more detail, we make a remark on why the noise-induced bistability is distinguished from the one owing solely to the  $\tau$ -controlled global bifurcation. Though the MF model makes no qualitative distinction between  $D$  and  $\tau$ , which are both considered as equally valid bifurcation parameters, the exact system is naturally sensitive to the deterministic or stochastic character of the effects they generate. In this context, for  $\tau > \tau_{fc}$  and sufficiently small noise, the oscillations displayed by the exact system retain their primarily deterministic character and as such satisfy the MF approximation trivially. Nonetheless, using the method described in Sec. III, we have verified that the stochastic perturbation becomes large enough to compromise the validity of the QIA for  $D$  fairly close to  $D_{fc}$ , the noise intensity marking the onset of the  $D$ -controlled global bifurcation in the MF model.

Next we show how the noise-induced bistability of the MF model is reflected in the dynamics of the exact system. First note that the illustrative examples of parameter values admitting bistability between the FP and the LC are indicated in Fig. 4 by the triangles, whereas the squares are reserved for the typical cases facilitating coexistence between the two LCs. In particular, we have singled out three instances related to bistability between the FP and the LC. The point denoted by the solid triangle ( $\blacktriangle$ ) refers to the case bearing no influence from the local Hopf bifurcations, given that

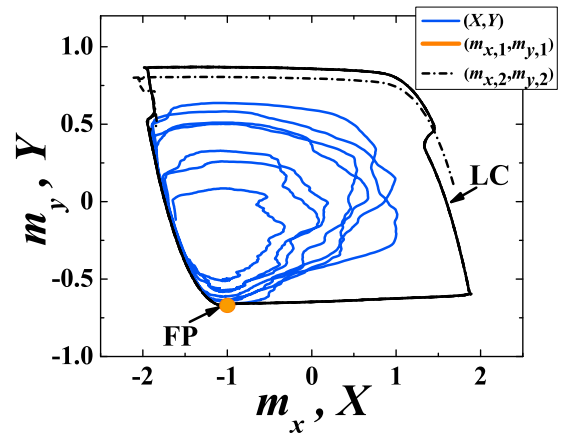


FIG. 5. (Color online) Bistability exhibited by the approximate model allows one to gain insight into the parameter domains where the QIA breaks down. In the example provided, the MF dynamics  $[m_x(t), m_y(t)]$  shows coexistence of the FP, denoted by the orange (light gray) dot, and the LC (black dashed line) born via the global fold-cycle bifurcation. Influenced by noise, the typical orbit  $[X(t), Y(t)]$  of the exact system, displayed by the blue (dark gray) solid line, is found to fluctuate between the two attractors of the MF model. Failure of GA for the global variables may be considered indirect evidence of the failure of the QIA on the level of local variables. The data are obtained for the parameter set  $(c, D, \tau) = (0.1, 0.0029, 0.3)$ .

$D < D_H$ , where  $D_H \approx 0.0025$  marks the onset of the Hopf bifurcations. Nevertheless, in the two examples indicated by the open triangles ( $\Delta$ ), such form of bistability occurs because the equilibrium is stabilized via the inverse subcritical Hopf bifurcation, whereby the unstable cycle born in the Hopf bifurcation acts like a threshold switching between the two stable solutions. Implementing the method introduced in Sec. III, it has been verified that the QIA is violated in all three described instances. For the case  $(c, D, \tau) = (0.1, 0.0029, 0.3)$ , we have illustrated the phase portraits corresponding to the two attractors of the MF model and the appropriate orbits for the collective variables of the exact system (see Fig. 5). The rationale for the failure of the QIA rests on the point that the mixed mode of the exact system may be interpreted as stochastic switching between the two attractors of the deterministic MF model. Naturally, the ensuing orbits are not normally distributed around the respective averages.

The analogous explanation also applies for the scenario where the MF model displays coexistence between the two LCs. In Fig. 4, we have indicated three parameter domains supporting such form of bistability. In the cases denoted by the open squares ( $\square$ ), the large cycle from the global bifurcation coexists with the incipient cycle, emerging from the direct supercritical Hopf bifurcation. Nonetheless, the solid square ( $\blacksquare$ ) points to an instance where the two large cycles coexist, one of them created in the  $D$ -controlled, and the other in the  $\tau$ -controlled global bifurcation. It has been verified that the QIA breaks down in all of the stated instances.

One should note that crossing the Hopf bifurcation curves alone does not immediately imply the failure of the QIA. Nevertheless, due to interplay with the  $D$ -controlled global bifurcation, crossing the curves may become associated with the violation of the QIA in two cases, one where the

supercritical regime involves bistability of the FP and the LC (inverse subcritical Hopf bifurcation), and the other, which includes coexistence between two LCs (direct supercritical Hopf bifurcation). The occurrence of such cases is mostly confined to  $\tau \lesssim \tau_{fc}$ , because above  $\tau_{fc}$  the MF dynamics is primarily influenced by the two global bifurcations.

## V. MISCELLANEOUS TOPICS

### A. Fulfillment of MFAs and the statistics of the first return times

This section provides a discussion on some of the corollaries related to the fulfillment of the MFAs. Before elaborating on the relation between the synchronization properties and the fulfillment of the QIA, we make two auxiliary notes qualifying more closely the terms “frequency” and “phase” used later on. The immediate aim is to show that the effective frequency and phase description of system dynamics may be appropriate if the MFAs hold. Regarding frequency, we present the results on the distribution of ISIs for  $X(t)$ . Note that there are two types of collective modes, one where the ISIs are dominated by  $T_0(D)$ , which occurs for small and intermediate  $D$  under very small  $\tau$ , and the other corresponding to the delay-led dynamics, which is typically seen for small and intermediate  $D$  under large  $\tau$ . Either way, we have verified that ISIs are normally distributed for an arbitrary stochastic realization under long simulation times. In Fig. 6(a), the normality test is provided for the more interesting case, showing persistence of Gaussian distribution for the noise-led dynamics under fairly large  $D = 0.0015$  at  $\tau = 0$ . Since the analogous conclusion is readily reached for the delay-driven collective mode, one may state that the description of collective motion in terms of the average period (frequency) appears justified if the MFAs apply.

A question that naturally arises is whether the fulfillment of the MFAs implies that the distributions of the return points  $P(X_r)$  and  $P(Y_r)$  sampled at intervals equal to the average ISI of the macroscopic dynamics are also Gaussian.  $P(X_r)$  and  $P(Y_r)$  are calculated in two steps: One first lets the simulation run for a sufficiently long time to determine the average ISI for  $X(t)$ , and then carries on by collecting data on the return points for another very long time period. The first point  $(X_0, Y_0)$  is chosen to lie on the refractory branch of the LC. In Fig. 6(b) is displayed the graphic normality

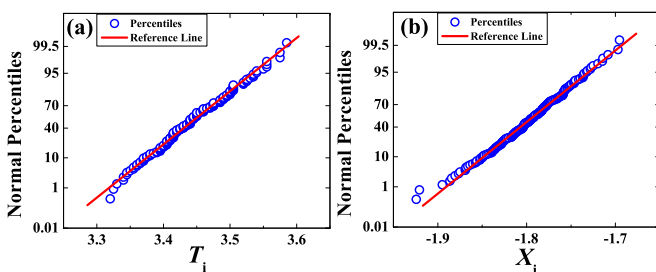


FIG. 6. (Color online) Characterizing the distribution of the return times and the return points for the macroscopic dynamics of the exact system. In (a) and (b) are displayed the graphic normality tests respectively indicating that the ISIs and the return points for  $X(t)$  are Gaussian distributed. The data refer to the case of noise-led dynamics at  $(c, D, \tau) = (0.1, 0.0015, 0)$ , but one may arrive at qualitatively similar results for the delay-driven dynamics.

test for  $P(X_r)$  along an arbitrary stochastic trajectory under the same parameter set as in Fig. 6(a). The demonstrated normality of distribution indicates that, in a statistical sense, the return points remain fairly close to the “average” LC. From a broader perspective, one may think of this result in the context of building an effective phase description for the collective motion [29–31].

Another point of interest is to verify whether the analogous conclusions hold for the local, rather than the global variables. Under the same parameter set as in Figs. 6(a) and 6(b), one can demonstrate for an arbitrary unit that the ISIs over a very long time series indeed conform to Gaussian distribution if the data from less than 10% of realizations are discarded. However, the return points  $P(x_r)$ , sampled at  $t_n = n * T_s$ , where  $T_s$  denotes the average ISI for the given unit, turn out not to be normally distributed. This is so because the Gaussian distribution for the local ISIs is comparably broader than that for the global variables. Still, starting off from any point on the refractory or the spiking branch of slow motion, the successive return points, recorded at  $T_s$  long intervals, always fall on the “right” branch, determined by the location of the initial point. Therefore, the above results suggest an interesting point that if the MFAs are satisfied, the use of terms frequency and phase is more appropriate to describe the dynamics of the global, than the local variables.

### B. Fulfillment of QIA and synchronization

Having gained insight into the competition between the noise-led and the delay-driven dynamics, as well as the statistical features providing the context for the effective use of terms frequency and phase, we proceed with the analysis of the relation between the synchronization of the individual units and the fulfillment of the QIA. To begin with, one notes that for being stochastic and excitable in nature, the units cannot exhibit complete synchronization. However, the discussion above suggests that it is reasonable to speak of approximate frequency (FS) and phase synchronization (PS) in conditional terms, viz., if the MFAs are satisfied. The presence or absence of these forms of synchronization may give rise to three types of collective states: (i) coherent states where single units display both the approximate FS and PS, (ii) states that exhibit FS, but lack PS, and (iii) collective states where approximate FS is not established. One may infer the relation between synchronization and QIA by examining the linear interaction terms of the form  $c * [x_i(t - \tau) - x_j(t)]$ . If there is approximate lag synchronization, the latter become very small, which leaves the neurons virtually independent. Therefore, by identifying conditions under which the approximate lag synchronization is achieved, one effectively looks for the parameter domains where QIA applies.

We have established that there exist only two scenarios for the approximate lag synchronization, both of which amount to cases of approximate FS and PS. The interaction terms may substantially reduce either (i) for noise-led dynamics at  $\tau \simeq 0$ , or (ii) for delay-driven dynamics at very large  $\tau \sim T_0(D)$ . A way to characterize the approximate FS for the given parameter set is to calculate the ratio  $r = \Delta T / \langle \bar{T}_i \rangle$ , where  $\Delta T = \max |\bar{T}_i - \bar{T}_j|$  is the maximal difference between the time-averaged ISIs  $\bar{T}_i$  of individual units, whereas  $\langle \bar{T}_i \rangle$  denotes



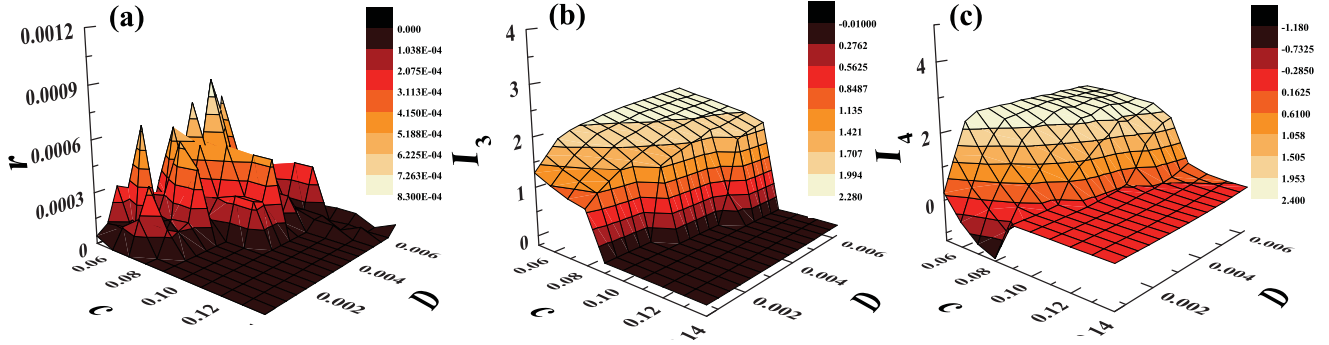


FIG. 7. (Color online) Focus on identifying the parameter domains that admit frequency and phase synchronization between the single units, which effectively provides an indication of where the QIA holds. (a) shows  $r(c, D)$  for the delay-driven dynamics at  $\tau = 2.7$ . In (b) and (c) are illustrated the corresponding  $\bar{I}_3(c, D)$  and  $\bar{I}_4(c, D)$  distributions for  $\tau = 2.7$ , respectively. Comparing (a), (b), and (c), note the overlap between the regions displaying near-zero values for the  $r$  ratio,  $\bar{I}_3$  and  $\bar{I}_4$ . The analogous result can be obtained for the noise-driven dynamics at  $\tau = 0$ .

the population average  $\langle \bar{T}_i \rangle = N^{-1} \sum_{i=1}^N \bar{T}_i$ . The smaller  $r$  becomes, the better FS between the units is achieved. The results for  $r(c, D)$  plotted in Fig. 7(a) refer to the (ii) case at  $\tau = 2.7$ . We have verified that setting  $\tau = 0$ , which corresponds to case (i), yields qualitatively similar results. As the main point, note a very large domain where  $r$  is small, which indicates the approximate FS. Expectedly, for small  $c$  and large  $D$ ,  $r$  is seen to rise sharply, implying that FS is lost.

The drawback of the method above is that one cannot distinguish whether approximate FS is or is not accompanied by PS. To do so, we consider the time-averaged third- and fourth-order moments of the local potentials  $P[x_i(t)]$  for the given parameter set, taking the average over a very long stochastic realization. Note that if the ergodic hypothesis applied, such an average would equal that over an ensemble of realizations. Nevertheless, whether this holds or not is of marginal significance because the results below are not intended to be rigorous, but should rather provide an illustration on the link between PS and the fulfillment of QIA. Therefore, the discussion on the asymptotic distributions here is independent and should by no means be confounded with the results from Sec. III, which only concern averaging over an ensemble of stochastic realizations.

As for the moments, the third-order average moment is defined by  $\bar{I}_3 = (1/T) \sum_{t=1}^T I_3(t)$ , where  $I_3(t) = \sum_{x_i} [x_i - X(t)]^3 P[x_i(t)]$ . The analogous relation holds for  $\bar{I}_4$ .  $P[x_i(t)]$  is obtained by dividing the range of possible  $x_i$  values into 110 bins  $[x, x + \delta x]$ , whereby one records the fraction of units whose potential falls within the given bin. If there is an approximate FS and PS, one expects  $x_i$  for most  $t$  to be Gaussian distributed around the mean  $X(t)$ . Then, both  $\bar{I}_3$  and  $\bar{I}_4$  should lie close to zero. If there is approximate FS, but PS is lacking,  $\bar{I}_3 \approx 0$  should hold, whereas  $\bar{I}_4$  should substantially depart from zero. Finally, if there is no approximate FS, both  $\bar{I}_3$  and  $\bar{I}_4$  are supposed to lie away from zero. Results on  $\bar{I}_3$  and  $\bar{I}_4$  at  $\tau = 2.7$  for a wide range of  $(c, D)$  values [cf. Figs. 7(b) and 7(c)] suggest that domains with approximate FS closely match those with PS. Note the overlap between the areas with the smallest  $r$ ,  $\bar{I}_3 \approx 0$  and  $\bar{I}_4 \approx 0$  in Figs. 7(a)–7(c), where the QIA should hold.

## VI. CONCLUSION

The reduction of computational demand and the possibility of describing the stochastic stability and the stochastic bifurcations can be cast as general reasons for introducing the MF approximate model for an arbitrary set of SDDEs. Given the apparent relevance of the MF method, an issue of considerable importance is to be able to determine the domains where such an approach may provide accurate qualitative predictions. The approximations behind the MF model are often considered in a simplistic fashion, as if they were completely independent of the class of systems which the model under study belongs to. Such a view results by invoking the (stereo)typical requirements for small noise intensity and weak couplings as the main conditions for the validity of the MF model.

In the present paper, the issue of the MF approximations and their validity is highlighted by taking the example of a system of delay-coupled noisy type II excitable units, represented by the generic Fitzhugh-Nagumo model. What we actually show is that, though they contain certain commonly stated elements, the MFAs relevant for the given system also include ingredients that should be precisely adapted to its essential dynamical properties. In particular, the inherent features of class II excitable systems, such as relaxation character of oscillations, have been explicitly incorporated into the definitions of the two MFAs we introduced. This point is particularly apparent in the definition of the GA, and is further reflected in the fashion in which the validity of both the GA and the QIA has been verified.

It is found that the requirements for the joint validity of the GA and QIA may be expressed in terms of a single qualitative statement, by which the two apply if the local and global dynamics exhibit a unique attractor of the same type, either a FP or a LC, provided that  $D$  is not overly large. Of the two generic scenarios, the one involving the stochastically stable FP is fairly trivial, whereas the one associated with the LC is more intricate and makes apparent the need for introducing the refined MFAs considered in the paper.

Focusing on each of the approximations independently, it is shown that the validity of the GA cannot be explicitly tied to certain parameter domains, but rather comes down to a

qualitative requirement for not too large a noise intensity. This is the main corollary of the actual statement on the validity of the GA, by which the GA is satisfied if the qualitative similarity between the individual realizations and the appropriate expectations is maintained for the given parameter set. For the oscillatory state, the notion of qualitative similarity effectively refers to the point that the expectations preserve the relaxation character of oscillations. In this context, we have attempted to provide some quantitative measure of the validity of GA by determining the variation of the  $N_{\text{out}}/N_r$  ratio with  $D$  (see Sec. III).

Nonetheless, our main conclusion regarding the validity of the MF approximation is associated with the fulfillment of the QIA. What we have demonstrated is that the failure of the QIA can explicitly be related to the noise-induced bistability of the MF model. Such bistable regimes, involving either the coexistence between the FP and the LC or the two LCs, are influenced by the global fold-cycle (tangent) bifurcation controlled via the noise intensity parameter. In this fashion, the  $(\tau, D)$  parameter domains where the MF approximation is bound to fail are identified with the domains admitting noise-induced bistability for the MF model's dynamics. In other words, the noise-induced bistability of the MF model provides the necessary condition for the failure of the QIA, and thus the MF approximation. Note that such parameter domains do not exhaust all the cases where the MF approximation fails, because the breakdown may also be caused by the violation of GA.

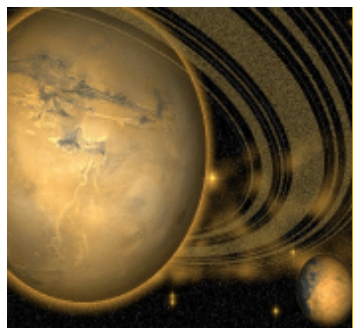
As for the relationship between the Hopf bifurcation curves determined for the MF model and the failure of MF

approximation, we stress that crossing the curves itself does not imply the failure. It has already been pointed out that the latter would mean that the MF model could never account for the collective oscillatory states, which is not true. Though the asymptotic distribution for the collective variables in the exact system indeed loses the Gaussian property if the curve corresponds to the stochastic Hopf bifurcation, this fact alone has no bearing on the MF approximations we introduced. However, in the interplay with the  $D$ -controlled global bifurcation, crossing the Hopf bifurcation curves may involve the onset of two different bistable regimes in the MF model, and as such, may contribute to the violation of the QIA, and thereby the MF approximation as a whole. It is reasonable to expect that the scope of the conclusion on the relationship between the noise-induced bistability of the MF model and the failure of MF approximation may likely be extended to a broader range of systems, since it draws only on the qualitative properties of the system dynamics. For future research, it would be interesting to examine the refined MFAs and their validity by carrying out an analysis similar to ours in the case of the MF models derived for systems exhibiting complex multiscale oscillations, such as bursting, when subjected to noise and coupling delays.

#### ACKNOWLEDGMENT

This work was supported in part by the Ministry of Education and Science of the Republic of Serbia, under projects No. 171017 and No. 171015.

- 
- [1] L. S. Tsimring and A. Pikovsky, *Phys. Rev. Lett.* **87**, 250602 (2001).
  - [2] A. Pototsky and N. B. Janson, *Phys. Rev. E* **77**, 031113 (2008).
  - [3] Y. Chen, M. Ding, and J. A. Scott Kelso, *Phys. Rev. Lett.* **79**, 4501 (1997).
  - [4] C. Masoller, *Phys. Rev. Lett.* **86**, 2782 (2001).
  - [5] E. M. Izhikevich, *Dynamical Systems in Neuroscience: The Geometry of Excitability and Bursting* (MIT Press, Cambridge, MA, 2007).
  - [6] I. Franović, K. Todorović, N. Vasović, and N. Burić, *Chaos* **22**, 033147 (2012).
  - [7] I. Franović, K. Todorović, N. Vasović, and N. Burić, *Phys. Rev. Lett.* **108**, 094101 (2012).
  - [8] *Complex Time-Delay Systems: Theory and Applications*, edited by F. M. Atay (Springer, Berlin, 2010).
  - [9] C. W. Gardiner, *Handbook of Stochastic Methods for Physics, Chemistry and the Natural Sciences*, 3rd ed. (Springer-Verlag, Berlin, 2004).
  - [10] X. Mao, *Exponential Stability of Stochastic Differential Equations* (Marcel Dekker, New York, 1994).
  - [11] *Stochastic Methods in Neuroscience*, edited by C. Laing and G. J. Lord (Oxford University Press, New York, 2010).
  - [12] S. Guillouzic, I. L'Heureux, and A. Longtin, *Phys. Rev. E* **59**, 3970 (1999).
  - [13] M. Gaudreault, F. Lépine, and J. Vinals, *Phys. Rev. E* **80**, 061920 (2009).
  - [14] M. Gaudreault, J. M. Berbert, and J. Vinals, *Phys. Rev. E* **83**, 011903 (2011).
  - [15] D. Bratsun, D. Volfson, L. S. Tsimring, and J. Hasty, *Proc. Natl. Acad. Sci. USA* **102**, 14593 (2005).
  - [16] M. A. Zaks, X. Sailer, L. Schimansky-Geier, and A. B. Neiman, *Chaos* **15**, 026117 (2005).
  - [17] J. A. Acebrón, A. R. Bulsara, and W.-J. Rappel, *Phys. Rev. E* **69**, 026202 (2004).
  - [18] *Numerical Solution of Stochastic Differential Equations*, edited by P. E. Kloeden and E. Platen (Springer, Berlin, 1999).
  - [19] H. Hasegawa, *Physica D* **237**, 137 (2008).
  - [20] S. Tanabe and K. Pakdaman, *Phys. Rev. E* **63**, 031911 (2001).
  - [21] B. Lindner, J. Garcia-Ojalvo, A. Neiman, and L. Schimansky-Geier, *Phys. Rep.* **392**, 321 (2004).
  - [22] M. A. Zaks, A. B. Neiman, S. Feistel, and L. Schimansky-Geier, *Phys. Rev. E* **68**, 066206 (2003).
  - [23] L. Arnold, *Random Dynamical Systems* (Springer-Verlag, Berlin, 1999).
  - [24] H. Hasegawa, *Phys. Rev. E* **70**, 021911 (2004).
  - [25] N. Burić, D. Ranković, K. Todorović, and N. Vasović, *Physica A* **389**, 3956 (2010).
  - [26] I. Franović, K. Todorović, N. Vasović, and N. Burić, *Phys. Rev. E* **87**, 012922 (2013).
  - [27] H. Hasegawa, *Phys. Rev. E* **70**, 021912 (2004).
  - [28] S. Wiggins, *Introduction to Applied Nonlinear Dynamical Systems and Chaos*, 2nd ed. (Springer, New York, 2000).
  - [29] J. T. C. Schwabedal and A. Pikovsky, *Phys. Rev. E* **81**, 046218 (2010).
  - [30] Z. Levnajić and A. Pikovsky, *Phys. Rev. E* **82**, 056202 (2010).
  - [31] J. T. C. Schwabedal and A. Pikovsky, *Phys. Rev. Lett.* **110**, 204102 (2013).



[ACCOUNT](#) [VIEW CART](#)  
  
[Home](#) [Books](#) [Series](#) [Journals](#) [Reference](#) [eBooks](#) [Information](#) [Sales](#) [Imprints](#) [for Authors](#)

[Top » Catalog » Books » Natural Disasters »](#)

[My Account](#) | [Cart Contents](#) | [Checkout](#)

**Quick Find**

Use keywords to find the product you are looking for.  
**Advanced Search**

**What's New?** →

Iraq: The Continuing Challenges in the Post-Saddam Hussein Era  
 \$73.80

**Shopping Cart** →

0 items

**Information**

[Shipping & Returns](#)  
[Privacy Notice](#)  
[Conditions of Use](#)  
[Contact Us](#)

**Bestsellers**

01. Future Systems for Earthquake Early Warning
02. The Phoenix of Natural Disasters: Community Resilience
03. Recent Progress on Earthquake Geology
04. Droughts: Causes, Effects and Predictions
05. Landslides: Causes, Types and Effects
06. Mass Trauma: Impact and Recovery Issues
07. Meltdown: Climate Change, Natural Disasters and other Catastrophes - Fears and Concerns for the Future
08. Crisis Management
09. Disaster Relief: Organizations, Speed and Efficiency of Response and Roles
10. Earthquake Engineering: New Research

**Notifications** →

Notify me of updates to **Earthquakes: Monitoring**

## Earthquakes: Monitoring Technology, Disaster Management and Impact Assessment

Retail Price: **\$160.00**  
**10% Online Discount**  
 You Pay: **\$144.00**

Editors: Wayne Coleman

**Book Description:**

In recent years, a number of disasters caused by earthquakes have demonstrated the vulnerability of both the developing and the developed world. This book provides new research on earthquakes. Chapter One focuses on the behavior of a simple spring-block model from the viewpoint of nonlinear dynamics and seismology. Chapter Two employs a new technique based on Extreme Learning Machine (ELM) for determination of liquefaction susceptibility of soil based on Standard Penetration Test (SPT) and Cone Penetration Test (CPT) from the Chi-Chi earthquake. Chapter Three presents a review of earthquake phenomenon in Nigeria, the occurrence and available data. Chapter Four describes the behavior and failure mechanisms of unreinforced masonry buildings and different rehabilitation and strengthening techniques. Chapter Five presents the results related to the preferred sources of information related to Risk, Hazard and Natural disaster. Chapter Six presents results regarding urban and semi-rural schoolchildren's seismic risk perception, awareness and preparedness of a highly seismic region, in the state of Oaxaca, Mexico. Chapter Seven reviews the anomalous decrease in groundwater radon before the Taiwan large earthquakes. (Imprint: Nova)



[Click to enlarge](#)

We've partnered with Copyright Clearance Center to make it easy for you to request permissions to reuse Nova content.

For more information, [click here](#) or click the "Get Permission" button below to link directly to this book on Copyright Clearance Center's website.



**Table of Contents:**

**Special Focus Titles**

01. Heart Failure: What a Non-Heart Failure Specialist Needs to Know
02. Bottle-Feeding: Perceptions, Practices, and Health Outcomes
03. Between Success and Failure: Assessment of Aspirations and Risk (CD Included)
04. Understanding Left and Right: An Illustrated Guide to the Political Divide
05. Phytoremediation: Methods, Management and Assessment
06. "Waste-to-Profit" (W-t-P): Value added Products to Generate Wealth for a Sustainable Economy. Volume 1
07. The Impact and Implications of Crisis: A Comprehensive Approach Combining Elements of Health and Society
08. When "We" Are Stressed: A Dyadic Approach to Coping with Stressful Events
09. The Man Brand: Why Public Campaigns Hide Half of Intimate Partner Violence
10. The Life of Abraham Lincoln: Drawn from Original Sources and Containing Many Speeches, Letters and Telegrams Hitherto Unpublished. Volume One
11. Life of Charles Dickens
12. The Inventions and Discoveries of the World's Most Famous Scientists



Technology, Disaster  
Management and  
Impact Assessment

Tell A Friend



Tell someone you know about  
this product.

## Preface

Chapter 1. Nonlinear Dynamics Behind The Seismogenic Fault Motion - A Review On Dynamics Of Single-Array Spring-Block Models => pp. 1-60

(Srđan Kostić, Nebojša Vasović, Kristina Todorović, and Igor Franović, Institute for Development of Water Resources "Jaroslav Černi", Jaroslava Černog, Belgrade, Serbia, and others)

Chapter 2. Modeling of Seismic Liquefaction Data Using Extreme Learning Machine => pp. 61-70

(Pijush Samui, Sanjiban Sekhar Roy, Pradeep Kurup, and Yıldırım Dalkılıç, Associate Professor, Department of Civil Engineering, NIT Patna, Bihar, India, and others)

Chapter 3. Mitigating Ground Shaking Construction Activities in Coastal Cities of Nigeria: An Earthquake Preventive Measure => pp. 71-100

(P. O. Awoyera, B. U. Ngene, G. A. Adeyemi and P. A. Aderonmu, Department of Civil Engineering, Covenant University, Ota, Nigeria, and others)

Chapter 4. Protection of Cultural Heritage Buildings Against Earthquakes from a Sensitized Structural Engineering Perspective => pp. 101-128

(Adolfo Preciado, Osmar Rodriguez, Alejandro Ramirez-Gaytan, Nayar Gutierrez, David Vargas, and Gil Ochoa, Departamento del Hábitat y Desarrollo Urbano, Instituto Tecnológico y de Estudios Superiores de Occidente (ITESO), Tlaquepaque, Jalisco, México, and others)

Chapter 5. Seismic Risk Knowledge Sources and Perception: The Case of Preparatory School Students in Mexico City => pp. 129-150

(Jaime Santos-Reyes, Tatiana Gouzeva and Galdino Santos-Reyes, Grupo de Investigación SARACS, ESIME, ZAC., Instituto Politecnico Nacional, México)

Chapter 6. Seismic Risk Perception and Preparedness of Primary Schoolchildren: The Case of Huajuapán, Oaxaca, Mexico => pp. 151-168

(Jaime Santos-Reyes, Galdino Santos-Reyes and Tatiana Gouzeva, Grupo de Investigación SARACS, ESIME, ZAC., Instituto Politecnico Nacional, México)

Chapter 7. Anomalous Decrease in Groundwater Radon before the Taiwan Large Earthquakes => pp. 169-182

(T. Kuo, Department of Mineral and Petroleum Engineering, National Cheng Kung University, Tainan, Taiwan)

## Index

### Series:

Natural Disaster Research, Prediction and Mitigation

**Binding:** Hardcover

**Pub. Date:** 2017 - 1st Quarter

**Pages:** 6x9 - (NBC-R)

**ISBN:** 978-1-53610-342-7

**Status:** AV



Status Code	Description
AN	Announcing
FM	Formatting
PP	Page Proofs
FP	Final Production
EP	Editorial Production
PR	At Prepress
AP	At Press
AV	Available

 [Add to Cart](#)

Monday 16 April, 2018

Nova Science Publishers  
© Copyright 2004 - 2018

NATURAL DISASTER RESEARCH, PREDICTION AND MITIGATION

## **EARTHQUAKES**

**MONITORING TECHNOLOGY,  
DISASTER MANAGEMENT  
AND IMPACT ASSESSMENT**

# **NATURAL DISASTER RESEARCH, PREDICTION AND MITIGATION**

Additional books in this series can be found on Nova's website  
under the Series tab.

Additional e-books in this series can be found on Nova's website  
under the eBooks tab.

**NATURAL DISASTER RESEARCH, PREDICTION AND MITIGATION**

# **EARTHQUAKES MONITORING TECHNOLOGY, DISASTER MANAGEMENT AND IMPACT ASSESSMENT**

**WAYNE COLEMAN  
EDITOR**

Copyright © 2017 by Nova Science Publishers, Inc.

All rights reserved. No part of this book may be reproduced, stored in a retrieval system or transmitted in any form or by any means: electronic, electrostatic, magnetic, tape, mechanical photocopying, recording or otherwise without the written permission of the Publisher.

We have partnered with Copyright Clearance Center to make it easy for you to obtain permissions to reuse content from this publication. Simply navigate to this publication's page on Nova's website and locate the "Get Permission" button below the title description. This button is linked directly to the title's permission page on copyright.com. Alternatively, you can visit copyright.com and search by title, ISBN, or ISSN.

For further questions about using the service on copyright.com, please contact:

Copyright Clearance Center  
Phone: +1-(978) 750-8400 Fax: +1-(978) 750-4470 E-mail: info@copyright.com.

### NOTICE TO THE READER

The Publisher has taken reasonable care in the preparation of this book, but makes no expressed or implied warranty of any kind and assumes no responsibility for any errors or omissions. No liability is assumed for incidental or consequential damages in connection with or arising out of information contained in this book. The Publisher shall not be liable for any special, consequential, or exemplary damages resulting, in whole or in part, from the readers' use of, or reliance upon, this material. Any parts of this book based on government reports are so indicated and copyright is claimed for those parts to the extent applicable to compilations of such works.

Independent verification should be sought for any data, advice or recommendations contained in this book. In addition, no responsibility is assumed by the publisher for any injury and/or damage to persons or property arising from any methods, products, instructions, ideas or otherwise contained in this publication.

This publication is designed to provide accurate and authoritative information with regard to the subject matter covered herein. It is sold with the clear understanding that the Publisher is not engaged in rendering legal or any other professional services. If legal or any other expert assistance is required, the services of a competent person should be sought. FROM A DECLARATION OF PARTICIPANTS JOINTLY ADOPTED BY A COMMITTEE OF THE AMERICAN BAR ASSOCIATION AND A COMMITTEE OF PUBLISHERS.

Additional color graphics may be available in the e-book version of this book.

### Library of Congress Cataloging-in-Publication Data

Names: Coleman, Wayne C., editor.  
Title: Earthquakes : monitoring technology, disaster management, and impact assessment / Wayne Coleman, editor.  
Description: Hauppauge, New York : Nova Science Publishers, Inc., [2016] | Series: Natural disaster research, prediction, and mitigation | Includes index.  
Identifiers: LCCN 2016045423 (print) | LCCN 2016047160 (ebook) | ISBN 9781536103427 (hardcover) | ISBN 9781536103564  
Subjects: LCSH: Earthquakes. | Earthquake hazard analysis. | Earthquake resistant design.  
Classification: LCC QE534.3 .E3745 2016 (print) | LCC QE534.3 (ebook) | DDC 551.22--dc23  
LC record available at <https://lccn.loc.gov/2016045423>

Published by Nova Science Publishers, Inc. † New York

## CONTENTS

<b>Preface</b>	vii
<b>Chapter 1</b>	1
Nonlinear Dynamics Behind the Seismogenic Fault Motion: A Review on Dynamics of Single-Array Spring-Block Models <i>Srdan D. Kostić, Nebojša Vasović, Kristina Todorović and Igor Franović</i>	
<b>Chapter 2</b>	61
Modeling of Seismic Liquefaction Data Using Extreme Learning Machine <i>Pijush Samui, Sanjiban Sekhar Roy, Pradeep Kurup and Yildirim Dalkılıç</i>	
<b>Chapter 3</b>	71
Mitigating Ground Shaking Construction Activities in Coastal Cities of Nigeria: An Earthquake Preventive Measure <i>P. O. Awoyera, B. U. Ngene, G. A. Adeyemi and P. A. Aderomnu</i>	
<b>Chapter 4</b>	101
Protection of Cultural Heritage Buildings against Earthquakes from a Sensitized Structural Engineering Perspective <i>Adolfo Preciado, Osmar Rodriguez, Alejandro Ramirez-Gavilan, Nayar Gutierrez, David Vargas and Gil Ochoa</i>	



<b>Chapter 5</b>	Seismic Risk Knowledge Sources and Perception: The Case of Preparatory School Students in Mexico City <i>Jaime Santos-Reyes, Tatiana Gouzeva and Galdino Santos-Reyes</i>	<b>129</b>
<b>Chapter 6</b>	Seismic Risk Perception and Preparedness of Primary Schoolchildren: The Case of Huajuapán, Oaxaca, Mexico <i>Jaime Santos-Reyes, Galdino Santos-Reyes and Tatiana Gouzeva</i>	<b>151</b>
<b>Chapter 7</b>	Anomalous Decrease in Groundwater Radon Before the Taiwan Large Earthquakes <i>T. Kuo</i>	<b>169</b>
<b>Index</b>		<b>183</b>

## PREFACE

In recent years, a number of disasters caused by earthquakes have demonstrated the vulnerability of both the developing and the developed world. This book provides new research on earthquakes. Chapter One focuses on the behavior of a simple spring-block model from the viewpoint of nonlinear dynamics and seismology. Chapter Two employs a new technique based on Extreme Learning Machine (ELM) for determination of liquefaction susceptibility of soil based on Standard Penetration Test (SPT) and Cone Penetration Test (CPT) from the Chi-Chi earthquake. Chapter Three presents a review of earthquake phenomenon in Nigeria, the occurrence and available data. Chapter Four describes the behavior and failure mechanisms of unreinforced masonry buildings and different rehabilitation and strengthening techniques. Chapter Five presents the results related to the preferred sources of information related to Risk, Hazard and Natural disaster. Chapter Six presents results regarding urban and semi-rural schoolchildren's seismic risk perception, awareness and preparedness of a highly seismic region, in the state of Oaxaca, Mexico. Chapter Seven reviews the anomalous decrease in groundwater radon before the Taiwan large earthquakes.

Chapter 1 – Present chapter is focused on the behavior of a simple spring-block model from the viewpoint of nonlinear dynamics and seismology. In particular, authors briefly describe the previously applied methods of nonlinear dynamics for the analysis of the motion of several different models: mono-block model, two-block model and models with an array of blocks with global coupling and varying neighboring interactions, by assuming the rate dependent and rate-and state-dependent friction law. Dynamics of such models is examined under the impact of frictional memory effect, delayed and varying interaction among the blocks, transient and continuous perturbations and

random seismic noise. Results of the previous studies show that irregular motion of the examined models, as an analog of the seismogenic fault motion, could be identified as an example of deterministic chaos, or it could occur due to effect of the introduced seismic noise or the existence of global attractor. In such regime, it is confirmed that recorded displacements of spring-block models obey Gutenberg-Richter power law distribution. In case when only the first Hopf bifurcation is detected, proposed models could be used as reliable characteristic earthquake models. Phase response curves of fault dynamics indicated the following: (1) for a mono-block fault model, single pulse perturbation delays the oscillation cycle phase, while two successive pulses induce two different mechanisms of phase advancement; (2) for a homogeneous two-block fault model, when each block is affected by a single pulse perturbation, both blocks exhibit the advance of oscillation phase, (3) for a heterogeneous two-block fault model, a single pulse perturbation has a destabilizing effect of perturbation via interaction between the blocks is non-negligible and its influence of non-perturbed block is destabilizing. Results of previous studies presented in this chapter confirm the reliability of the use of simple spring-block models as phenomenological models of seismogenic fault motion.

Chapter 2 – Seismic liquefaction is a major concern for any earthquake prone area. This article employs a new technique based on Extreme Learning Machine (ELM) for determination of liquefaction susceptibility of soil based on Standard Penetration Test (SPT) and Cone Penetration Test (CPT) from the Chi-Chi earthquake. ELM is the modified version of Single-hidden Layer Feed forward Neural Network. Different input combinations have been tried to get best performance. A comparative study has been carried out between the SPT and CPT based models. CPT based models give better performance than the SPT based model. The developed ELM model shows that Cone Resistance ( $q_c$ ) and Peck Ground Acceleration (PGA) are sufficient parameters for determination of liquefaction susceptibility of soil.

Chapter 3 – This chapter presents a review of earthquake phenomenon in Nigeria, the occurrence and available data. The review also includes recommendation to government agencies and designers of Engineering Structures on the need to accommodate mitigating efforts to avoid possible future disasters occasioned by earthquake occurrence. Nigeria may not be presently in high impact zone of earthquake phenomenon, but what the future portends cannot be easily predicted. Hence there is necessity for long term planning to avoid being caught unaware of the possible effect of sudden high impact earthquake in its shores. Thus, the need for the application of cutting

edge Information Technology and adoption of mitigation techniques in the reduction of earthquake effects cannot be overemphasized. Environmental impact assessment prior to construction should indicate the seismic performance of concrete frames, perhaps under simulated earthquake excitations. Also significant is the effect of rapid urbanization and consequent construction of heavy engineering structures that require deep foundation in coastal cities of Nigeria. The effect of such construction activities can trigger earth movement in the area. Thus, the destructive impacts of earthquake, both on lives and properties could be ameliorated by taking mitigation measures of risks connected to earthquake. Mainly, through adherence to effective town planning and land use plans, enforcement of standard building codes and good construction practices. Moreover, adequate early warning systems, awareness creation and community preparedness would serve as protective mechanism. Finally, hazard and risk mapping and analyses should be carried out on a national and regional basis, so as to enhance emergency preparedness, rescue operation planning and resources allocation.

Chapter 4 – The most common construction techniques for heritage buildings were mainly based on basic geometric rules about stability and earthquake damage observations. This situation led to the construction of massive structures with structural elements of great thickness, but still with poor seismic performance because damage was continuously presented. These restrictions have made historical buildings extremely vulnerable against earthquakes, presenting partial and total collapses. Thus, becomes evident the need of suitable technical solutions to protect them. This chapter describes the behavior and failure mechanisms of unreinforced masonry buildings and different rehabilitation and strengthening techniques. Both techniques are aimed at keeping good deformation compatibility between materials without affecting the architectonic value of the monument. Advantages and disadvantages of different rehabilitation and strengthening proposals are discussed from a sensitized structural engineering perspective taking into account that this type of buildings are very different from modern structures. These techniques aim at protecting cultural heritage against earthquakes by inducing a modified failure mechanisms that involves more energy dissipation than the original structural system.

Chapter 5 – The chapter presents the results related to the preferred sources of information related to Risk, Hazard and Natural disaster. Also, some results of seismic risk perception and the preferred sources of education on seismic risk are presented. The sample size of the cross-sectional study was  $N = 1489$  that included six Preparatory school located in Mexico City. The

main findings of the study have been the following: a) overall, the results show that the students are well aware of the words 'Hazard' (99.6%, Mean = 2.00, SD = 0.063), 'Risk' (99.5%, Mean = 2.00, SD = 0.069), and 'Natural disaster' (99.2%, Mean = 2.00, SD = 0.118); b) the main source of information associated with the term 'Risk' (Mean = 3.27, SD = 0.891) was the "School;" The term 'Natural disaster', on the other hand, has been found to be "TV" (Mean = 1.87, SD = 0.334); c) regarding the participants' knowledge on the three seismic zones of the Capital City, the overwhelming majority of them did not know this fact (89.1%, Mean = 1.10, SD = 0.294); d) students perceived that an earthquake could occur "At any time" (86.9%, Mean = 4.72, SD = 0.816); e) students prefer to learn more on seismic risk by the following sources and in this particular order: "Civil protection" (44%), "School" (22%), and "Internet" (20%); f) In general, the participants of the study showed a lack of knowledge on seismic risk (see c) above), even though, they are well aware that an earthquake could happen at any time (see d) above). It is hoped that the preliminary results presented here may serve as the basis for a more in-depth analysis, for example, of mass media, social networks related to earthquakes, in the context of the Mexican culture. The paper gives an account of an ongoing research project.

Chapter 6 – The chapter presents results regarding urban and semi-rural schoolchildren's seismic risk perception, awareness and preparedness of a highly seismic region, in the state of Oaxaca, Mexico. The sample of the study was N = 819 (Urban sample size = 522; Semi-rural sample size = 297). The main findings of the cross-sectional study have been the following: a) overall, urban schoolchildren demonstrated a generalized awareness of the seismic area where they live; however, this was not the case for semi-rural schoolchildren; educational campaigns may be needed to further enhance seismic awareness of both urban and semi-rural areas of the region; b) the two hazards associated with earthquakes and crime have been perceived to represent the two major threats to them at school and at home, and for both urban and semi-rural schoolchildren; c) schoolchildren emotions are not consistent when asked whether they would be able to control themselves during an earthquake; d) seismic risk communication takes place at school and at home; this may be regarded as encouraging in order to further educate children on seismic risk; however, more is needed to better educate them on important aspects regarding what to do before, during and after an earthquake and this may well prove to be an effective way to share their knowledge with their parents (most of them are not well educated) and contribute to build a resilient community to earthquakes; e) the preliminary findings of the study

are consistent with has been found in similar studies; i.e., "children were able to identify higher frequency events at a higher frequency and lower frequency events at a relatively lower frequency."

Chapter 7 – In southwestern Taiwan, radon anomalous declines prior to the 2010 Mw 6.3 Jiasian and 2016 Mw 6.4 Meinong earthquakes were recorded at the Paihe spring. The above-mentioned earthquakes are the two strongest since 1964 that have occurred near the area southeast of Chiayi. The Paihe spring (P1) is located 46 km and 45 km, respectively, from the epicenters of the 2010 Mw 6.3 Jiasian and 2016 Mw 6.4 Meinong earthquakes. Specifically, the concentration of groundwater radon decreased from background levels of  $144 \pm 7$  and  $137 \pm 8$  pCi/L to minima of  $104 \pm 8$  and  $97 \pm 9$  pCi/L prior to the 2010 Mw 6.3 Jiasian and 2016 Mw 6.4 Meinong earthquakes, respectively. The Paihe spring is from an unconfined limestone aquifer surrounded by ductile shale and sandy shale. The v-shaped pattern of radon behavior in the Paihe spring is quite similar to those radon decreases that were measured in the confined andesite aquifer at Antung in eastern Taiwan.

Recurrent anomalous declines in the concentration of groundwater radon were observed at well D1 in the Antung hot spring in eastern Taiwan prior to the five major earthquakes –2003 Mw 6.8 Chengkung, 2006 Mw 6.1 and Mw 5.9 Taitung, 2008 Mw 5.4 Antung, and 2011 Mw 5.0 Chimei. Well D1 is located 24 km, 52 km, 47 km, 13 km, and 32 km, respectively, from the epicenters of the 2003 Mw 6.8, 2006 Mw 6.1 and Mw 5.9, 2008 Mw 5.4, and 2011 Mw 5.0 earthquakes. The 2003 Mw 6.8 Chengkung was the strongest earthquake near the Chengkung area in eastern Taiwan since 1951. Specifically, radon decreased from a background level of  $787 \pm 42$  pCi/L to a minimum of  $326 \pm 9$  pCi/L prior to the 2003 Mw 6.8 Chengkung earthquake. In a brittle aquifer under un-drained conditions (Antung and Paihe), the dilation of brittle rock mass occurred at a rate faster than the recharge of pore water and gas saturation developed in newly created cracks preceding the earthquake. Radon partitioning into the gas phase may explain the anomalous decrease of groundwater radon prior to the 2003 Chengkung earthquake.

Both observations at Paihe and Antung suggest that in-situ radon volatilization offers an attractive mechanism for a premonitory decrease in groundwater radon. "A low-porosity brittle aquifer with un-drained conditions" is a suitable geological site to consistently detect precursory declines in groundwater radon prior to local large earthquakes. A long-term monitoring of precursory declines in groundwater radon at a suitable geological site can be a useful means for forecasting local disastrous

earthquakes. At a suitable geological site, it is of a great practical value to develop the correlations among the scale of radon decline, precursory time, and earthquake magnitude for a given seismogenic fault.

In: Earthquakes

Editor: Wayne Coleman

ISBN: 978-1-53610-342-7

© 2017 Nova Science Publishers, Inc.

### Chapter 1

## NONLINEAR DYNAMICS BEHIND THE SEISMOGENIC FAULT MOTION: A REVIEW ON DYNAMICS OF SINGLE-ARRAY SPRING-BLOCK MODELS

*Srdan D. Kostić<sup>1,\*</sup>, PhD, Nebojša Vasović<sup>2,†</sup>, PhD,  
Kristina Todorović<sup>3,‡</sup>, PhD, and Igor Franović<sup>4,§</sup>, PhD*

<sup>1</sup>Institute for Development of Water Resources "Jaroslav Černi,"  
Belgrade, Serbia

<sup>2</sup>University of Belgrade Faculty of Mining and Geology, Belgrade, Serbia

<sup>3</sup>University of Belgrade Faculty of Pharmacy, Belgrade, Serbia

<sup>4</sup>University of Belgrade Institute of Physics, Belgrade, Serbia

### ABSTRACT

Present chapter is focused on the behavior of a simple spring-block model from the viewpoint of nonlinear dynamics and seismology. In particular, authors briefly describe the previously applied methods of nonlinear dynamics for the analysis of the motion of several different models: mono-block model, two-block model and models with an array

\* [srdjan.kostic@jcemi.co.rs](mailto:srdjan.kostic@jcemi.co.rs).

† [nebojsa.vasovic@rgf.bg.ac.rs](mailto:nebojsa.vasovic@rgf.bg.ac.rs).

‡ [kisi@pharmacy.bg.ac.rs](mailto:kisi@pharmacy.bg.ac.rs).

§ [franovic@ipb.ac.rs](mailto:franovic@ipb.ac.rs).

of blocks with global coupling and varying neighboring interactions, by assuming the rate dependent and rate-and state-dependent friction law. Dynamics of such models is examined under the impact of frictional memory effect, delayed and varying interaction among the blocks, transient and continuous perturbations and random seismic noise. Results of the previous studies show that irregular motion of the examined models, as an analog of the seismogenic fault motion, could be identified as an example of deterministic chaos, or it could occur due to effect of the introduced seismic noise or the existence of global attractor. In such regime, it is confirmed that recorded displacements of spring-block models obey Gutenberg-Richter power law distribution. In case when only the first Hopf bifurcation is detected, proposed models could be used as reliable characteristic earthquake models. Phase response curves of fault dynamics indicated the following: (1) for a mono-block fault model, single pulse perturbation delays the oscillation cycle phase, while two successive pulses induce two different mechanisms of phase advancement; (2) for a homogeneous two-block fault model, when each block is affected by a single pulse perturbation, both blocks exhibit the advance of oscillation phase, (3) for a heterogeneous two-block fault model, a single pulse perturbation has a destabilizing effect of perturbation via interaction between the blocks is non-negligible and its influence of non-perturbed block is destabilizing. Results of previous studies presented in this chapter confirm the reliability of the use of simple spring-block models as phenomenological models of seismogenic fault motion.

**Keywords:** spring-block models, bifurcation analysis, random noise, mean-field approximation, deterministic chaos, power law, time delay, transient perturbation, phase response curve

## 1. INTRODUCTION

In present chapter, nonlinear dynamics in the background of the seismogenic fault motion is explained through the analysis of motion of spring-block models in the following form:

- mono-block model;
- two-block model;
- one-dimensional array of blocks,

with the assumed rate-dependent and rate-and state-dependent friction law. Since the analyzed models are one-dimensional, present analysis is restricted only to the temporal irregularities. Dynamics of these models is analyzed under the influence of:

- friction memory effect (time delay in friction term);
- delayed interaction among the blocks;
- transient and continuous perturbations;
- random seismic noise;
- varying neighboring interactions.

In the first part of the chapter, dynamics of the mono-block model with the assumed Dieterich-Ruina rate-and state-dependent friction is examined under the impact of friction memory effect, continuous and transient perturbations. Friction memory effect is modeled by assuming by that friction is a function of velocity with a time delay, which was previously shown to be in the range 3-9 ms in laboratory conditions [1], depending on the viscosity and contact load. Standard local bifurcation analysis, demonstrates that the mono-block model with the introduced time delay in the friction term exhibits Ruelle-Takens-Newhouse route to chaos. Results of the performed analysis reveal that small perturbations of the control parameters lead to deterministic chaos, which could be treated as the onset of instability. On the other hand, if regular periodic change of the control parameters is assumed, revealing the effect of the continuous external signal, such as the work of the mining machines, or the traffic impact, results of the performed analysis indicate that deterministic chaos may emerge when some of the parameters are assumed to undergo small oscillations near the equilibrium values, but admitting the periodic motion. In particular, the Ruelle-Takens-Newhouse route to chaos is observed for the cases of limit amplitude perturbations. On the other side, when the angular frequency is assumed constant for the value near the periodic motion of the block in an unperturbed case, variation of oscillation amplitudes probably gives rise to global bifurcations, with immediate occurrence of chaotic behavior. When two perturbed parameters are assumed, further analysis shows that a transition from periodic motion to chaotic behavior occurs for oscillation frequencies of periodic motion in an unperturbed case. Regarding the influence of transient perturbations, the effect of transient external force induced by a passing seismic wave on fault motion is introduced as a change of block acceleration in the form of a sine wave scaled by an exponential pulse. Results obtained indicate the transition to quasiperiodic - or chaos-like

motion, which could be attributed to the precursory creep regime and seismic motion, respectively, when fault motion is exposed to external force in the inter-seismic creep regime.

One should note that the introduction of time delay in order to mimic the memory effect, as well as the effect of noise on dynamics of natural systems, although new for theoretical computational geophysics, has already been successfully applied in the area of computational neuroscience [2-14]. Indeed, a very active relationship has been develop between the theory of nonlinear dynamics and neuroscience in the last 20 years, which resemble of positive recurrent feedback. On one hand, application of methods of nonlinear dynamics has substantially contributed to the physical modelling of neural systems. On the other hand, features detected in neural systems has motivated the development of new concepts in theory of nonlinear dynamics, including excitability, different forms of synchronization and chaotic itinerancy.

In the second part of the chapter, an array of blocks is examined under the impact of the seismic noise, varying neighboring interactions and delayed interactions among the blocks. In particular, an array of 100 blocks is examined with two different types of interaction: (1) all-to-all interaction, (2) varying number of block coupling with  $2K$  neighboring units ( $1 \leq 2K \leq N$ ,  $N = 100$ ). In case of global coupling, results obtained indicate there are local bifurcations from equilibrium state to periodic oscillations, with an occurrence of irregular aperiodic behavior when initial conditions are set away from the equilibrium point. Such a behavior indicates a possible existence of a bi-stable dynamical regime, due to effect of the introduced seismic noise or the existence of global attractor. In this bi-stable regime, distribution of event magnitudes follows Gutenberg-Richter power law with satisfying statistical accuracy, including the  $b$ -value within the real observed range. In case when each block is coupled to a varying number of  $2K$  neighboring units, results of the performed analysis indicate the occurrence of direct supercritical Hopf bifurcation, implying a transition from equilibrium state to periodic oscillations under the variation of coupling delay. For loosely coupled blocks and low values of friction, observed system does not exhibit any bifurcation, regardless of the assumed noise amplitude in the expected range of values. Distribution of event magnitudes, as a sum of squared displacements, is found to correspond well to periodic (characteristic) earthquake model.

In the third part of the chapter, the qualitative analysis is focused on determining the first- and second-order phase response curves for models of a simple monoblock fault and paradigmatic two-block complex faults, which display relaxation oscillations in the stick-slip regime [15-18]. Given their

strong nonlinear character and the stiffness property, the considered models of earthquake faults are expected to display a number of intricate behaviors, such that their response to perturbation may qualitatively depend on different system parameters, as well as the fault complexity. The main corpus of issues we address includes (i) the sensitivity of a simple monoblock fault to external perturbation, (ii) the influence of system parameters on the profile of phase response curves, (iii) the effect of two consecutive pulse perturbations, as well as (iv) the responses of complex faults, either homogeneous or heterogeneous, to external perturbation. Apart from considering the first-order phase response curves, our interest also lies with the second-order phase response curves because their nontrivial behavior may indicate a potential long-term effect of external perturbation on the duration of an earthquake cycle.

It should be emphasized that results of previous studies which are briefly reviewed in this chapter primarily refer to the description of dynamics of strike-slip fault motion, since the effect of gravity is not taken into account. Nevertheless, the presented methods and approach could be also applied for the analysis of induced seismicity, primarily under the effect of deep underground excavation. In this case, influence of continuous and transient signals on fault motion could be ascribed to different triggering factors, including the effect of blasting and/or drilling or the impact of the vibrations induced by the work of the mining machines.

Present chapter is composed of three different sections. Authors provide brief review of the results of previous studies in Section 2. Dynamics of a mono-block model is given in Section 3, including the description of original model and its derivatives. The main focus of this section will be on frictional memory effect and on the impact of continuous and transient perturbations [19-20]. Dynamics of a chain of 100 blocks is analyzed in Section 4, where the main focus is on the effect of seismic noise, varying neighbor interactions and delayed transition of motion among the blocks [21-22]. Section 5 is devoted to analysis of the external perturbation on earthquake fault dynamics using phase response curves. In Subsection 5.1 we consider the case of a monoblock fault, first analyzing the impact of a single and two successive pulse perturbations, and then demonstrating how the profile of phase response curves depends on the fault parameters. Subsection 5.2 concerns the behavior of the homogeneous and the heterogeneous two-block complex faults. For the homogeneous fault, it is determined how the system responds if each of the blocks is perturbed, but the perturbations arrive with a certain phase lag. For the heterogeneous fault, it is examined how the system response changes

depending on whether the block with the shorter or the longer oscillation period is perturbed.

## 2. BACKGROUND – LITERATURE REVIEW

It is commonly considered that earthquakes occur as a result of the sudden release of energy within some confined region of undergoing deformation. At the contact of two tectonic plates (interplate earthquakes), or two different lithological units (intraplate earthquakes), energy is stored in the rocks in a form of elastic strain. Faulting occurs when the accumulated strain exceeds the strength of the rock, after which the opposite sides of the fault rebound to equilibrium state (Figure 1). During this process, a part of the stored energy is usually released in a form of heat, other part is used for rock deformation, while the rest of energy propagates as seismic waves. This explanation of earthquake nucleation is known as the elastic rebound theory, formulated by Reid [23] as a result of his studies of the geodetic measurements along the San Andreas fault during the San Francisco earthquake in 1906.

However, even though Reid's hypothesis is quite generally accepted, the main problem arises when the earthquakes occur along the existing faults (reactivated faults). Recent evidence indicates the existence of an aseismic creep along the fault, i.e., the motion along the fault exists without the occurrence of an earthquake. This kind of motion is not predicted by Reid's rebound theory, so there has to be another mechanism that may account for such a motion. One plausible explanation is that any variation of frictional resistance during sliding could induce a dynamic instability, which often occurs repetitively – the instability is followed by a period of no motion during which the stress is recharged, followed by another instability. This common frictional behavior is called the regular stick slip [24].

A stick-slip with friction at the contact of blocks of rocks is considered by many researchers as one of the most simplified and probable analogs of the earthquake source. It is well-known that the major portion of earthquakes occurs in accordance with the scenario corresponding to the model of unstable stick-slip [25].

The suggestion of regular stick-slip motion as a possible mechanism of motion along the fault originally came from Brace and Byerlee [26], who studied the behavior of the granite samples in triaxial shear apparatus. The primary significance of the Brace and Byerlee paper is in the emphasis on stability and the effect of friction, not strength, in explaining the mechanism of earthquakes.

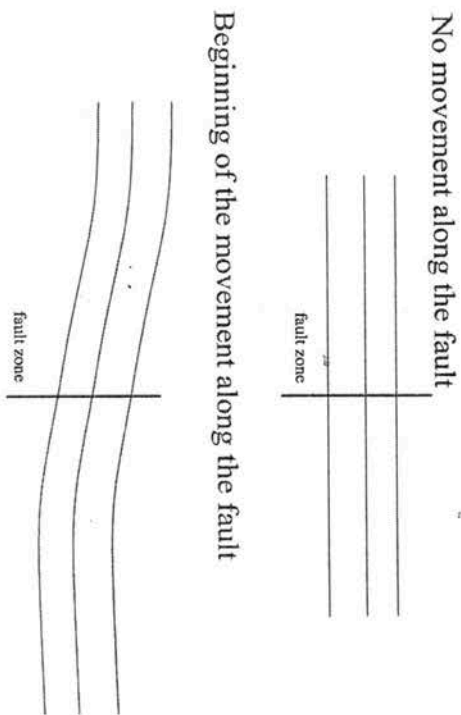


Figure 1. Earthquake nucleation according to Reid's elastic rebound theory.

On the basis of the suggestion by Brace and Byerlee [26], Burridge and Knopoff [27] set an array of blocks interconnected with elastic springs, which are driven along the rough surface by the driving plate. Connection of blocks with the driving plate is also provided by the series of elastic springs. Thereby, they assumed that the main nonlinearity in the analyzed system comes from the specific friction law between the moving block and the rough surface of the lower plate. In this paper, Burridge and Knopoff assumed velocity-dependent friction law of the following form:

$$F = -E\dot{x} + F(x) \quad (1)$$

where the first term represents the force due to radiation and the second term combines the viscous and friction effects.

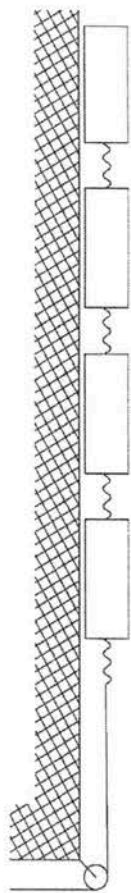


Figure 2. Sketch of the original Burridge-Knopoff model.

Following this suggestion of Brace and Byerlee [26] that stick-slip occurring in laboratory sliding experiments may be analogous to the mechanism of crustal earthquakes, Burridge and Knopoff [27] simulated this stick-slip motion in laboratory conditions, using an array of several blocks. Eight masses and eight springs were placed upon a long, horizontal, plane surface (Figure 2). Approximately uniform friction existed everywhere between the masses and the surface.

Burridge and Knopoff [27] measured the potential energy in the system released during any shock, by assuming Hookean elasticity for all the springs.

The results for the case when all springs are equal show that the parameter values of Gutenberg-Richter law are  $a = 2.76$ ,  $b = 0.42$ , with good approximation ( $R^2 = 0.996$ ), which are the usual values of parameters for the most observed earthquakes.

In order to compare these values with the real observed data, Kostić et al. [28] conducted a statistical analysis of 483 earthquakes in Serbia with the magnitude range 1.8-5.4, for the period 10/11/2004 - 03/10/2011, according to the data of European-Mediterranean Seismological Centre [28]. The results obtained indicate that the earthquake distribution for the territory of Serbia also follows Gutenberg-Richter law ( $R^2 = 0.86$ ) with parameters  $a = 2.64$ , and  $b = 0.46$  (Figure 3).

In the same paper, Burridge and Knopoff [27] observed the occurrence of aftershocks, relating it to the widely known Omori-Utsu law [29-30]. For this purpose, they observed an array of ten blocks, interconnected by harmonic springs, and also attached through springs to a driving upper plate, which cause the whole system to move in a stick-slip fashion along the rough surface of the lower plate. The histogram for the sequence of 69 aftershocks is shown in Figure 4. Analysis performed by Kostić et al. [28] indicated that the values of parameters of Omori-Utsu law are  $c = 0.068$ , and  $d = 0.012$ , with the correlation coefficient  $R^2 = 0.916$ .

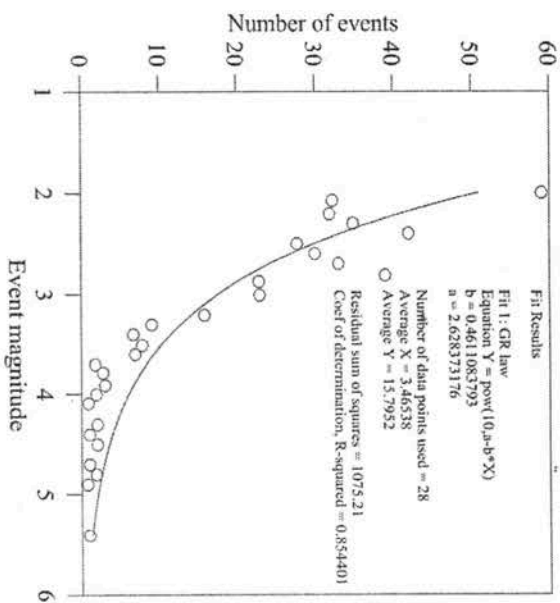


Figure 3. Gutenberg-Richter law for earthquakes in Serbia recorded in the period 2004-2011.

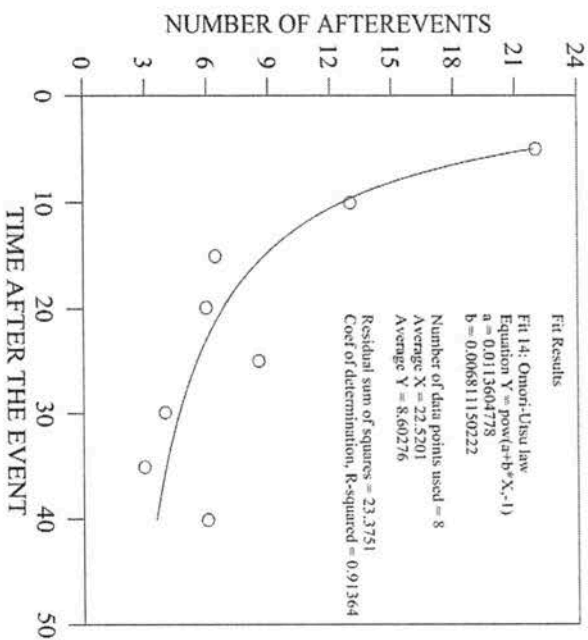


Figure 4. Histogram for number of aftershocks in a time interval of  $5 \times 10^5$  units.



Kostić et al. [28] also conducted a statistical analysis of aftershock sequence from 03/11 to 25/11/2011 was done, for the shock following the Kraljevo M5.4 earthquake recorded on November 3rd in 2010 in Serbia. As it can be seen in Figure 5, aftershock sequence of 91 events obey Omori-Utsu law, with the following parameters:

$$N = 1 / (-0,06 + 0,015t) \quad (2)$$

with the correlation coefficient  $R^2 = 0,98$ .

The main contribution of the work of Burridge and Knopoff is two-fold:

- they proposed an experimental setup that mimics the stick-slip behavior, and that phenomenologically resembles the motion along the seismicogenic fault;
- they showed that the distribution of bursts of motion follows the two significant macroseismological laws: Gutenberg-Richter and Omori-Utsu law.

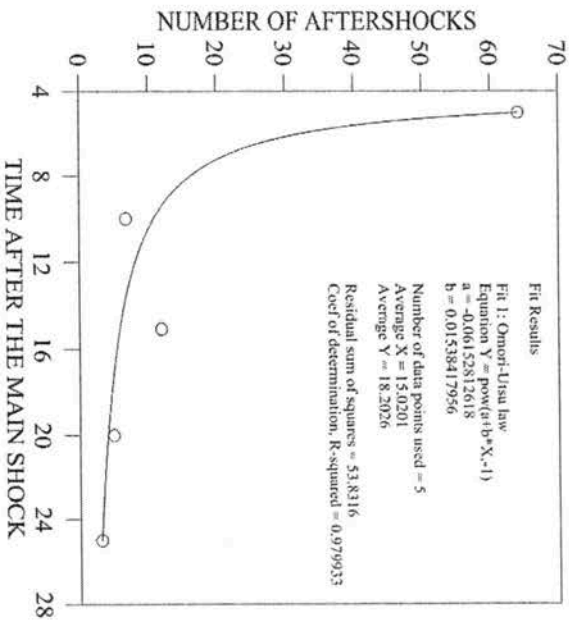


Figure 5. Omori law for aftershock sequence of 2010 Kraljevo M5.8 earthquake in Serbia.

Since the work of Burridge and Knopoff [27], spring-block models have been widely recognized as convenient phenomenological models of fault motion. In particular, a setup consisting of interconnected blocks moving along a rough surface was shown to exhibit stick-slip dynamics, which resembles to real observed movement along the seismicogenic faults. Such models have been widely used to mimic the fault motion, in order to capture the main dynamical mechanism behind the fault dynamics. For a very nice review on the existing spring-block model and their main features from the viewpoint of statistical physics, one should refer to the work of Kawamura et al. [31].

After the work of Burridge and Knopoff [27], the subsequent significant study on this topic was performed by Carlson and Langer [32], who analyzed dynamics of a Burridge-Knopoff spring-block model with up to 400 blocks in a row, and by assuming the velocity-dependent friction law:

$$F \begin{pmatrix} \dot{x} \\ v_1 \end{pmatrix} = F_0 \phi \begin{pmatrix} \dot{x} \\ v_1 \end{pmatrix} \quad (3)$$

where  $\phi$  vanishes at large values of its argument and is normalized so that  $\phi(0) = -\phi'(0) = 1$ , and  $v_1$  is some speed that characterizes the velocity dependence of  $F$ . Results of their analysis indicate occurrence of three distinct events: microscopic events (including only one or a few blocks), localized events (when triggering pulse excites only the blocks within the starting slipping zone) and delocalized events (when triggering pulse excites the blocks outside the starting slipping zone). With the transition from microscopic to delocalized events, the average velocity increases (approaching unity for delocalized events), and also the event irregularities are being amplified. From the seismological viewpoint, Carlson and Langer provided the relationship between the number of displaced blocks and the frequency of events, as an analogous version of the Gutenberg-Richter power law. In particular, they provided several characteristic magnitude vs. frequency diagrams for different values of control parameters and observed the following. Large number of microscopic events falls at the small end of the magnitude distribution, while localized events, as moderately large events, appear at the center of these diagrams. Distribution of these localized events corresponds well with the Gutenberg-Richter law. In fact, for the value of critical parameter  $\alpha = 2.5$ , parameter  $b = 1$ , which is in agreement with the Gutenberg-Richter law. At the large end of the magnitude distribution, delocalized great events appear, which

are too frequent to be consistent with the Gutenberg-Richter power law. Results of their research also indicated that dimensionless parameter  $\alpha$  (as a rate at which disturbances are amplified as a result of velocity-weakening friction) and fault length have a significant impact on the role of delocalized great events. In particular, great events have a predominant influence in moving the system forward on average at the loading speed and are more nearly periodic on shorter faults and for larger values of  $\alpha$ .

Another important paper dealing with the spring-block models from the viewpoint of nonlinear dynamics comes from Vieira [33]. In her paper, Vieira analyzed two-block and three-block model, by assuming also the velocity depending friction law, without the possibility of the backward motion. Results of her research indicated that for a certain parameter values, two-block model exhibits periodic, quasiperiodic and chaotic behavior, with the route to chaos from period one to period two and then directly into chaos. Also, Vieira showed the chaotic synchronization could occur in a three-block model, which could have a significant impact on earthquake prediction, since synchronization decreases the dimensionality of the attractor.

Among the recent research, one should single out the work by Erickson et al. [34-35], who studied the dynamics of a mono-block and a three-block model [34] and model with an array of blocks [35] by assuming the Dieterich-Ruina rate- and state-dependent friction law [36, 37]:

$$\mu(V, \theta) = \mu_0 + A \ln \left( \frac{V}{V_0} + B \ln \left( \frac{V_0 \theta}{D_c} \right) \right) \quad (4)$$

where  $\mu_0$  is a friction constant for steady-state slip at velocity  $V_0$ ,  $V$  is the velocity of the block,  $D_c$  ( $L$ ) is the critical length, that one block needs to move in order to replace the asperity contact,  $\theta$  is a state variable, and  $A$  and  $B$  are empirical constants. State variable  $\theta$  secures the fading memory of previous states [38]. It represents the delayed reaction of the friction to instantaneous change of the velocity. Material constants  $A$  and  $B$  strongly depends on the temperature and stress state, and, consequently, they change their values with the depth of the Earth's crust. In particular, parameter ( $A$ - $B$ ) actually denotes the conditions for the earthquake to occur along the crustal faults. Depending on the sign of this parameter, conditions from the ground surface up to 50km depth change from stable through conditionally stable to unstable, where unstable conditions correspond to the possibility of earthquake occurrence. Indeed, the majority of the recorded earthquake foci is located within the

unstable zone, where ( $A$ - $B$ ) parameter is with the negative sign [39]. When parameter ( $A$ - $B$ ) is with the negative sign, then one talks about the velocity-weakening law, while positive ( $A$ - $B$ ) indicates velocity-strengthening law. In order for instability to occur, observed model should exhibit velocity-weakening law. It is interesting to notice that similar law is also observed for the "weak" rock masses (clays), which further implies that such law could be also significant for the landslide activation and its dynamics.

In order to model the details of friction arising from perturbations in average contact lifetime (state) or slip velocity, equation (4) must be coupled with a description of state evolution:

$$\dot{\theta} = 1 - \left( \frac{V\theta}{D_c} \right) \quad (5)$$

Equation (4) has been referred to as the slowness law and the Dieterich-Ruina law (Figure 6). In this equation, state, and thus friction, evolve even for truly stationary contact with  $V = 0$ , which has been referred to as aging [40-44].

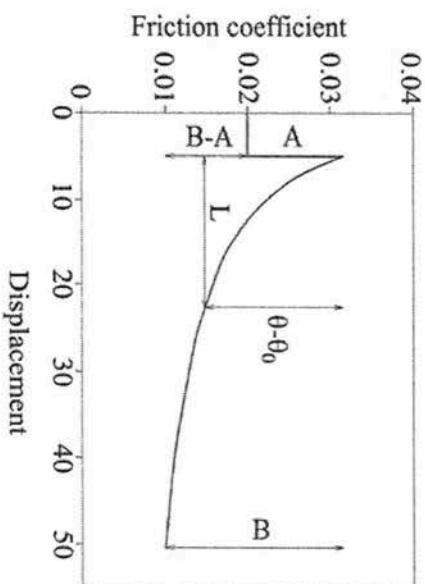


Figure 6. Dieterich-Ruina rate- and state-dependent friction law.

It should be emphasized that Dieterich-Ruina friction law is applicable not only for describing the contact of rock masses, but also for metals, paper and other materials. Nevertheless, despite its universality and wide applicability, some of the previous studies indicate that Dieterich-Ruina law could not be

assumed for high sliding velocities, which could be explained by the occurrence of different mechanical and chemical reactions which arise due to frictional melting, which lubricates the contact surfaces. Such reactions include body heating, frictional melting and production of silicate gelatin or granular mass along the contact.

Except from Dietrich-Ruina friction law, there are other formulation of rock friction laws, that are also frequently assumed in the analysis of the spring-block model dynamics (For a very nice and thorough review on the laboratory-derived friction laws, please refer to Marone, [45]). For instance, Ruina [37] proposed a different evolution law in which velocity and displacement were of primary importance:

$$\begin{aligned} \mu(V, \theta) &= \mu_0 + A \ln \left( \frac{V}{V_0} + B \ln \left( \frac{V_0 \theta}{D_c} \right) \right) \\ \dot{\theta} &= - \left( \frac{V \theta}{D_c} \right) \ln \left( \frac{V \theta}{D_c} \right) \end{aligned} \quad (6)$$

A third law by Perrin, Rice, and Zheng [42] exhibits both aging and symmetry with respect to velocity changes:

$$\begin{aligned} \mu(V, \theta) &= \mu_0 + A \ln \left( \frac{V}{V_0} + B \ln \left( \frac{V_0 \theta}{2D_c} \right) \right) \\ \dot{\theta} &= 1 - \left( \frac{V \theta}{2D_c} \right)^2 \end{aligned} \quad (7)$$

Although the distinction between the two views of friction evolution is fundamental in terms of micromechanical interpretation of the underlying processes, the laws reproduce laboratory data in a similar fashion.

It has to be emphasized that the friction relations have been extended to include variations in normal stress [46-47], which we do not consider here.

For a mono-block model, Erickson et al. [34] revealed an occurrence of deterministic chaos for a certain parameter values, which is rather interesting result, concerning the dimensionality of the analyzed dynamical system. For a three-block model, chaotic solution occur for smaller values of control parameters when compared to the case of only a single block. Similar conclusion was drawn for the one-dimensional spring-block model in the continuum limit, including the presence of soliton and breather solutions [35].

As it can be seen from this brief review, phenomenological models are widely used in the study of fault motion. Except from these aforementioned models, there are also cellular automata models, two fractal overlap models or fiber bundle models (which represent a classical model of material failure rarely used in seismic analysis) and a dislocation model, which is still the most useful kinematic description of an earthquake.

The most commonly used cellular automata model as a representation of fault dynamics is suggested by Olami, Feder, and Christensen (1992). In general, cellular automata represent mathematical idealizations of physical system in which space and time are discrete, and it commonly consists of a regular uniform lattice, usually infinite in extent, with a discrete variable at each "cell". A cellular automaton evolves in discrete time steps, with the values of the variable at a single cell being affected by the values of variable at cells in its neighborhood on the previous time step. The variables at each site are updated simultaneously, based on the values of the variables in their neighborhood at the preceding time step, and according to a definite set of local rules. It is interesting to notice that cellular automata were originally introduced by von Neumann and Ulam (as a possible idealization of biological systems (1963), with the particular purpose of modeling biological self-reproduction.

Regarding the fractal models, a simple model was proposed by Chakrabarti and Stinchcombe (1999), in a form of a pair of dynamically overlapping Cantor sets, which allow one to study in detail the statistics of the overlap of one fractal object on another. The two fractal overlap (magnitude) changes in time as one fractal moves over the other. The overlap (magnitude) time series, which are changing as one fractal moves over the other, could be studied as a model time series of earthquake avalanche dynamics. In particular, the strain energy grown between the two surfaces due to a stick period is taken to be proportional to the overlap between them. Considering that slips occur at intervals proportional to the length corresponding to that area, previous studies indicated that a power-law, similar to Gutenberg-Richter law, for the frequency distribution of the energy release could be obtained.

As for the analysis of the effect of different perturbation on earthquake fault dynamics using phase response curves, such an approach has first been adopted in our recent paper [48], though the formalism related to phase description of nonlinear oscillators has already been invoked in the context of earthquake fault dynamics [24, 49-52]. So far, the phase response curves have often been used in theoretical neuroscience [53-56] and the general theory of coupled phase oscillators [57-60] as a tool to study the response of systems to

external stimuli, as well as the ability of coupled systems to synchronize their activity.

Present chapter is majorly composed on the basis of the results of the following previous studies:

- Kostić, S., Franović, I., Todorović, K., Vasović, N. *Nonlinear Dyn*, 2013, 73, 1933-1943 [19]
- Vasović N., Kostić S., Franović I., Todorović K. *Commun Nonlin Sci*, 38, 117-129 [21]
- Kostić, S., Franović, I., Perc, M., Vasović, N., Todorović, K. *Sci. Rep.: Nature Publishing Group*, 2014, 4, 5401 [20]
- Kostić, S., Vasović, N., Franović, I., Todorović, K. *Nonlinear Proc Geophys*, 2013, 20, 857-865 [61]
- Kostić, S., Vasović, N., Franović, I., Todorović, K., Klinshov, V., Nekorkin, V. *Submitted to Nonlinear Dynamics (under review)*, 2016 [22]
- Franović, I., Kostić S., Perc, M., Klinshov, V., Nekorkin, V., Kurths, J. *Chaos*, 2016, 26, 063105-1-12 [48]
- Kostić, S., Vasović, N., Franović, I., Todorović, K.. *J Comput Nonlin Dyn* 2013, 9, 031019 [62].

In present chapter, analysis of dynamics of spring-block models is conducted under the assumption that a single movement of a block or average displacement of a chain of blocks mimic the earthquake, which enables a qualitative analogy between the long-term dynamics of a block or a group of blocks and different regimes of fault motion. Thereby, transition between these regimes implies the occurrence of bifurcation due to subtle variation of control parameters, or under the impact of newly introduced factors. Considering the fact that sequence of earthquakes along a single fault is irregular in space, time and in size, a dynamics of a corresponding spring-block model should also be irregular. In case of a one-dimensional chain of blocks (i.e., interconnected blocks are moving in a single direction), one could observe the irregular dynamics only in time and size, which could correspond to the onset of deterministic chaos [35], or it could arise as a consequence of the effect of seismic noise [21].

### 3. NONLINEAR DYNAMICS – THEORETICAL BACKGROUND

In present chapter, nonlinear dynamics refers to the branch of physics that provides the description of complex natural phenomena using nonlinear differential equations. Moreover, we assume that such systems (dynamical systems) could be sensitive to initial conditions, which could further indicate a possible existence of a deterministic chaos. Although there is no formal and widely accepted definition of deterministic chaos, in present chapter we assume that deterministic chaos denotes the long-term aperiodic behavior of a dynamical system, which is highly sensitive to initial conditions (i.e. a small change of initial conditions commonly induce a large change in behavior of the observed dynamical system after a certain amount of time), and which, finite amount of time, converges towards the strange attractor. Famous mathematician, Ian Stewart, also defined it as the ability of simple models, without inbuilt random features to generate highly irregular behavior. In order for deterministic chaos to occur, observed dynamical system needs to go through a series of dynamical changes, i.e. bifurcations. There are three common ways how one could induce an onset of deterministic chaos: period-doubling, quasiperiodic and intermittent route to chaos. Period-doubling bifurcations occur at logistic mapping, where stable fixed point becomes unstable after a series of flip bifurcations (where fixed point loses its stability, with the occurrence of a limit cycle). Quasiperiodicity occurs for Van der Pol oscillator, where spiral node becomes unstable and a limit cycle occurs through a Hopf bifurcation. Torus appears after the second Hopf bifurcation. Further parameter change leads to decomposition of torus and the observed dynamical system settles on a constrained strange attractor, implying the occurrence of deterministic chaos. Such quasiperiodic route to chaos is also known as the Ruelle-Takens-Newhouse route to chaos. The third, intermittent route to chaos is characterized by a saddle-node bifurcation in high-dimensional systems, where saddle node and a stable node coalesce and disappear, finally giving rise to trajectory with chaotic periods which are interspersed with regular oscillations.

It should be emphasized that besides differential equations, which describes the system's behavior in continuous time, there are also difference equations (iterative mapping), which describe the behavior of dynamical systems in discrete time intervals. Expect from this division of dynamical systems, there are also autonomous and nonautonomous equations, which describe explicit and implicit temporal dependence of the observed dynamical

system, respectively. In current chapter, analyzed dynamical systems are described using autonomous ordinary first-order differential equations.

Dynamics of the systems observed in present chapter is usually determined by several control parameters, whose fine tuning induce specific transitions between different dynamical regimes, i.e. occurrence of bifurcations. Bifurcations represent qualitative, topological changes of the behavior of the observed dynamical system due to variation of values of control parameters. Number of parameters, whose tuning leads to the onset of bifurcation, commonly denotes the co-dimension of bifurcation. The most common bifurcations of co-dimension 1 are saddle-node bifurcation, transcritical and pitchfork bifurcation, Hopf bifurcation and period-doubling bifurcation. Homoclinic and heteroclinic bifurcations are the most frequent representatives of bifurcations of co-dimension 2. From the strict mathematical viewpoint, bifurcation occurs when eigenvalues of the characteristic equation of the observed system change their sign. In case characteristic equation has conjugate-complex solutions, real part of the solution needs to change the sign in order to induce a bifurcation. In present chapter, only the occurrence of a Hopf bifurcation is analyzed. This type of bifurcation actually represents a local bifurcation when a fixed point loses its stability and a pair of conjugate-complex eigenvalues of the linearized system in the neighborhood of the fixed point crosses the imaginary axis of the complex plane. Supercritical Hopf bifurcation occurs when the fixed point loses its stability with the parameter change, giving rise to the onset of a stable limit cycle. On the other hand, subcritical Hopf bifurcation arises when the increase of the value of control parameter further induce the coalescence of the stable fixed point and a stable limit cycle, eventually giving rise to the large stable limit cycle.

One should note that in present chapter only the results of the local bifurcation analysis are discussed. Global bifurcation, when larger dynamical sets, like periodic orbits, coalesce with the fixed point, or between each other, are analyzed only numerically.

There are two ways how models presented in current chapter are analyzed. One approach assumes linearization of the observed ordinary differential equations around the equilibrium state. Another approach, which is applied for stochastic differential equations, assumes the introduction of mean-field method.

Linearization of the observed dynamical systems (i.e. ordinary differential equations) is performed since according to Hartman-Grobman theorem, behavior of a dynamical system near the hyperbolic fixed point is qualitatively the same as the behavior of linearized system near the fixed point, under the

condition that all eigenvalues of linearized system have the real part  $Re(\lambda) \neq 0$ . In that way, analysis of the behavior of dynamical system in a small neighborhood of the equilibrium state (fixed point) is more convenient after the performed linearization. After the performed linearization, one proceeds with determination of the characteristic equation of the observed system, which is further solved for eigenvalues  $\lambda_i$ . After the eigenvalues are determined, one continues with solving the relations between the examined control parameters of the observed system. Once these relations are determined, bifurcation curves are constructed, which denote the transition between different dynamical regimes. The next step assumes calculation of derivatives along the obtained bifurcation curves. In particular, in specific chosen points on the curve, one calculates the first derivative of the eigenvalue for the chosen control parameter. The obtained positive derivative indicates the existence of a direct Hopf bifurcation, while negative derivative denotes the inverse Hopf bifurcation. Unfortunately, local bifurcation analysis does not enable the determination of the exact type of Hopf bifurcation (whether it is a supercritical or subcritical), concerning the fact that global bifurcation could not be captured solely by the means of local analysis.

It is necessary to emphasize that, before conducting a linearization of the observed system, one should introduce convenient dimensionless parameters, especially in the case when a large number of potentially important parameters exist, so that their grouping into small number would make the analysis easier.

Regarding the application of the mean-field approach, we started from the initial assumption that modeling complex systems which comprise multiple characteristic spatial and time-scales inevitably incorporates a coarse-graining procedure, which consists in singling out the components that show a well controllable behavior into a few selected degrees of freedom, whereas the variations within the embedding environment, as well as the fluctuations associated to processes that take place at smaller spatial and temporal scales are approximated by introducing the different types of noise. Apart from noise, modeling of macroscopic systems often requires one to explicitly take into account the effects of interaction delays, which may derive from finite velocities of signal propagation and/or a latency of response of system's units to input variations. The separate or combined effects of noise and coupling delays may substantially alter the "bare" dynamics, unattended by these two ingredients. Among other effects of their interplay, one may find complex multistable behavior and competition between the delay-driven and the noise-induced oscillation modes.

The described models are mathematically stated in terms of systems of nonlinear stochastic delay-differential equations (SDDE). The analysis of stability and bifurcations of such systems presents a highly nontrivial problem. From qualitative perspective, the stochastic component may give rise to stochastic bifurcations, the kind of phenomenon fundamentally distinct from what is found in deterministic systems. The stochastic bifurcations have so far been characterized phenomenologically, in a sense that a certain time-averaged quantity, such as the asymptotic probability distributions of the relevant variables or the associated power spectra, may undergo some qualitative change under variation of noise intensity. For instance, it has been shown that the stochastic Hopf bifurcation from a stochastically stable fixed point to a stochastically stable limit cycle is accompanied by the loss of Gaussian property for the asymptotic distributions of the appropriate variables. In parallel, the degree by which the distribution departs from the normal one with super criticality depends on the particular system at hand. At variance with bifurcations in deterministic systems, where one may clearly identify a critical value of the control parameter, the change of system's behavior in noise-induced transitions is gradual.

The largest obstacle for analytically treating SDDE systems lies in the fact that the standard Fokker-Planck formalism cannot provide useful results concerning the qualitative analysis of stochastic stability and stochastic bifurcations of systems of SDDEs. The use of such an approach is severely constrained by the non-Markovian character and the nonlinearity of the underlying equations. In particular, the non-Markovian character is reflected in the occurrence of the so-called "conditional drift term". Even for univariate systems, the latter may only be resolved by an approximation, considering either the limit of a small delay or the limit of large delay, which substantially exceeds the system's correlation time. Nevertheless, for the setup involving multiple units, even the delay-free case under the assumption of molecular chaos cannot be handled analytically, though efficient numerical methods are available.

The failure of Fokker-Planck formalism implies the necessity for considering approximate methods, which should satisfy two criteria. On one hand, a viable approximate method should allow us to analyze the stability and stochastic bifurcations of the large systems of nonlinear SDDEs, whereas on the other hand, the approximation should be self-contained, in a sense that the parameter domains where it applies or fails are mathematically tractable.

One of the most frequently used approximate methods is the mean-field approach, which consists in deriving a low-dimensional reduced set of

effective deterministic equations which may qualitatively account for the stability and bifurcations of the original set of  $N$  coupled SDDEs. The ensuing mean-field model is given by a set of delay-differential equations, where the influence of noise is manifested only by the noise intensity. The gains from introducing a mean-field model can in general be cast as twofold. On one hand, if it captures the behavior of the exact system with sufficient accuracy, the mean-field model substantially reduces the computational time for numerical integration, which in case of the exact system grows as  $\approx N^2$  with its size. The other advantage lies in the ability to translate the highly nontrivial problem of stochastic bifurcations displayed by the exact system into a study of the compact deterministic mean-field system, which is amenable to standard bifurcation analysis, whereby the noise intensity acts as an additional bifurcation parameter.

In order to build a mean-field model for a general system of stochastic differential equations, one may adopt two different approaches. One approach is to consider the time dependence of a hierarchy of probability densities formally derived from the appropriate Fokker-Planck equation, whereas the other approach consists in focusing on the evolution of cumulants, whereby the full density of states is factorized into a series of marginal densities. In presence of coupling delay, the latter alternative is clearly a preferred one, and it further allows for a number of convenient approximations to be introduced in a controlled fashion. Note that one is bound to make certain simplifying approximations due to nonlinearity of the original system. In particular, the nonlinearity causes the cumulants of a given order to become linked to the ones of the higher order, which apparently renders the underlying series unclosed. The way to resolve this consists in truncating the series by introducing a closure hypothesis. A typical closure hypothesis integrates the cumulant approach with the Gaussian approximation, according to which all the cumulants above second order are assumed to vanish. By this approach, starting from the exact system of  $kN$  SDDEs, where  $k$  denotes the number of local degrees of freedom, one ends up with a set of  $k(k+3)/2$  deterministic delay-differential equations describing the collective dynamics in terms of the means, as well as the appropriate variances and the covariances.

The described mean-field method has so far mainly been applied in the field of neuroscience, where the use of effective low-dimensional approximate models has a long history. In particular, the mean-field method has proven successful in qualitative analysis of stability of collective dynamics in assemblies of delay-coupled noisy excitable elements. Nonetheless, it has also been demonstrated to successfully capture the scenarios for the onset and the

delay-induced suppression of the collective mode, showing that the bifurcations displayed by the approximate model can qualitatively account for the stochastic bifurcations displayed by the exact system. It has also been indicated that the mean-field model can provide accurate quantitative predictions, reflected in a close agreement between its oscillation period and the average oscillation period of the exact system. Apart from systems with all-to-all (global) connectivity, the method has also been extended to cases with more complex connection topology, including random networks and paradigmatic modular networks. Note that the intricacies regarding the approximations behind the described mean-field approach, called the Gaussian approximation and the quasi-independence approximation, have been analyzed in detail, not only in terms of precise formulations, but also with respect to parameter domains that warrant their validity. In this context, it has been reported that the dynamics of the mean-field model can indicate in a self-consistent fashion the parameter domains where the mean-field approximations break down.

In light of the application of nonlinear dynamics in seismology, two different approaches are currently in the focus. One approach concerns the analysis of dynamics of spring-block models, which are assumed to mimic the movement along strike-slip faults in the Earth's crust. These models could be constrained to dynamics of a single block, or several blocks are mutually connected in a single array or within a two-dimensional plane. Previous studies have shown that distribution of displacements of a single unit or group of units follow characteristic seismological laws: Gutenberg-Richter and Omori-Utsu law. Analysis of such models also enables determination of key factors that control the onset of instability, which is considered to be analogous to the start of seismic fault motion. Another approach concerns the analysis of recordings of real earthquakes, or the analysis of the temporal and spatial distribution of main events, using method of nonlinear time series analysis. Such application could provide useful data for prediction of the size and location of the next great event (earthquake) or aftershock, and could be also advantageous for engineering design.

It should be emphasized that presented approach could be also used for modeling of movement along a reactivated fault, mainly due to the change of stress-strain conditions under the impact of deep underground excavation. Previous recordings and studies imply that earthquakes generated due to reactivated movement along the existing faults are by far the most frequent seismic feature in large mining fields. Moreover, such seismic events could occur with the magnitude up to M6, and with the intensity of VI-VIII degrees

according to Modified Mercalli scale. There are many examples of such seismic events, including those at Lubin copper field and Silesia coal field in Poland (M4.5 and M4.3, respectively), at coal mines in France (up to M2.5), at coal mines in Germany (up to M4), at coal mines in USA (up to M3.5) and at lead, silver and zinc mines in USA (up to M3). The necessary triggering factor for the reactivation of fault movement could occur as a continuous signal, originating from the work of large mining machines, or as a transient signal, due to effect of blasting and drilling at the excavation front. Such external perturbations could cause a change of the stress-strain conditions near the existing inactive fault, which could further induce a movement along the normal, reverse and strike-slip fault. Besides the activated movement, such changes of stress-strain conditions could also cause specific features, including rockbursts, pillar bursts, outbursts and bumps.

One should note that approach presented in current chapter is restricted to dimensionless phenomenological models. In particular, one cannot use the actually measured values for the analysis, but examined models could serve only for qualitative assessment of dynamics of the earthquake nucleation process. Reason for this lies in the fact that analyzed spring-block models, for a certain parameter values, exhibit stick-slip motion, which resembles the seismogenic fault dynamics. Also, such models are very convenient for qualitative analysis of the effect of different factors, including background seismic noise, transient impact of a passing seismic wave from near or distant earthquake or the influence of different types of interaction between different parts of the fault.

Other techniques of nonlinear dynamics, like nonlinear time series analysis, could be used to examine the recorded accelerograms of the past earthquakes. Such time series actually represent the motion of the ground surface due to passage of seismic waves, and the results of such analysis could be directly beneficial for urban planning and civil engineering. This techniques include, but are not restricted to: false nearest neighbor method, mutual information method, deterministic test, stationarity test, surrogate data testing or calculation of maximal Lyapunov exponent. This techniques could also be used for the analysis of time series of different origin, including volcanic seismicity, blasting, etc. In general, application of these methods should lead to full characterization of recorded signal, which could further enable its prediction, at least for the near future.

### 3. DYNAMICS OF A MONO-BLOCK MODEL

Kostić et al. [19] analyzed model proposed by Madariaga [34], which describes the motion of a single block along the rough surface coupled with Dieterich - Ruina rate and state dependent friction law:

$$\begin{aligned} \dot{\theta} &= -\left(\frac{\nu}{L}\right)\left(\theta + B \log\left(\frac{\nu}{\nu_0}\right)\right) \\ \dot{u} &= \nu - \nu_0 \\ \dot{\nu} &= \left(-\frac{L}{M}\right)\left(ku + \theta + A \log\left(\frac{\nu}{\nu_0}\right)\right) \end{aligned} \quad (8)$$

with the following parameter used:

- $k$  - spring stiffness,
- $M$  - mass of the block,
- $L$  (Dc) - critical sliding distance necessary to replace the population of asperity contacts,
- $A, B$  - empirical constants (dependent on the material properties).

For convenience, system (8) could be formulated in non-dimensional fashion by defining the new variables  $\theta', \nu', u'$  and  $t'$ :  $\theta = A\theta', \nu = \nu_0\nu', u = Lu', t = (L/\nu_0)t'$ . After returning to the use of  $\theta, \nu, u$  and  $t$ , system (8) becomes:

$$\begin{aligned} \dot{\theta} &= -\nu(\theta + (1 + \varepsilon)\log(\nu)) \\ \dot{u} &= \nu - 1 \\ \dot{\nu} &= -\gamma^2 \left[ u + (1/\xi)(\theta + \log(\nu)) \right] \end{aligned} \quad (9)$$

where  $\varepsilon = (B-A)/A$  measures the sensitivity of the velocity relaxation,  $\xi = (kL)/A$  is the nondimensional spring constant, and  $\gamma = (kM)^{1/2}(L/\nu_0)$  is the nondimensional frequency [34].

#### 3.1. Frictional Memory Effect

Frictional memory effect is analyzed by introducing the time delay  $\tau$  in system (9) [19]:

$$\begin{aligned} \dot{\theta} &= -\nu[(\theta + (1 + \varepsilon)\log(\nu(t - \tau)))] \\ \dot{u} &= \nu - 1 \\ \dot{\nu} &= -\gamma^2 \left[ u + (1/\xi)(\theta + \log(\nu)) \right] \end{aligned} \quad (10)$$

The system of first-order ordinary differential equations (10) has a unique stable stationary solution  $(\theta, U, V) = (0, 0, 1)$ , which corresponds to the steady sliding of the block. Hence, by this model, the fault is in a state of constant motion, which could correspond to some plate boundary segments, like an Eastern California shear zone, where the average repeat time of fault seismic motion is of the order of thousands of years [20].

The main motivation for including the time delay in friction term lies in the nature of the rock friction itself – change in velocity of the block does not instantaneously induce a corresponding change. On the contrary, there is a certain time delay between the change of velocity and change of friction, which could be modeled as it is suggested in Eq. (10). Another motivation for the introduction of time delay comes from the similarity of the dynamics of spring-block model with the relaxation oscillator. In particular, stick-slip motion represents an inherent property of the relaxation oscillators, whose main mark is the existence of two time scales: the slow one, during the energy accumulation (the so-called stick phase) and the fast one, during the energy release (to so-called slip phase).

Standard bifurcation analysis leads to the following expression for  $\varepsilon$  as a function of  $\omega$ :

$$\varepsilon = -1 + \sqrt{\left[ \omega^3 - \omega\gamma^2 \left( \frac{1 + \varepsilon}{\xi} \right) \right]^2 + \left[ \omega^2 \left( \frac{\gamma^2}{\xi} + 1 \right) - \gamma^2 \right]^2} \quad (11)$$

and for  $\tau$  as a function of  $\omega$ :



$$\tau = \tau_c = \frac{1}{\omega} \left[ \arctg \left( \frac{-\omega^2 \left( \frac{\gamma^2}{\xi} + 1 \right) + \gamma^2}{-\omega^3 + \omega \gamma^2 \left( \frac{1 + \xi}{\xi} \right)} \right) + k\pi \right] \quad (12)$$

where  $k$  is any nonnegative integer such that  $\tau_k \geq 0$ .

The above parametric equations for  $\varepsilon$ ,  $\xi$  and  $\tau$  coincide with the Hopf bifurcation curves illustrated in Figure 7, where the bifurcation curves  $\tau(\varepsilon)$  are shown at the fixed parameter values  $\xi = 0.5$  and  $\gamma = 0.8$ . Two different scenarios could occur when increasing the value of time delay. On one hand, the increase of time delay could induce the so-called amplitude or oscillatory death, indicating a transition between the different regimes of periodic oscillations, or the return to equilibrium state, respectively. On the other hand, increase of frictional delay could destabilize the system, with the final occurrence of deterministic chaos. Apparently, the system exhibits quasiperiodic route to chaos [63-64], such that after two supercritical Hopf bifurcations, the dynamics falls onto the strange attractor. Apparently, only by increasing the time-lag  $\tau$ , e.g., by setting  $\tau = 0$ ,  $\tau = 10$ ,  $\tau = 12$ , to  $\tau = 20$ , and by slightly changing the other parameter values, the block dynamics changes from the fixed point, over the limit cycle oscillation (first Hopf bifurcation) and torus (second Hopf bifurcation) to chaos (Figure 8).

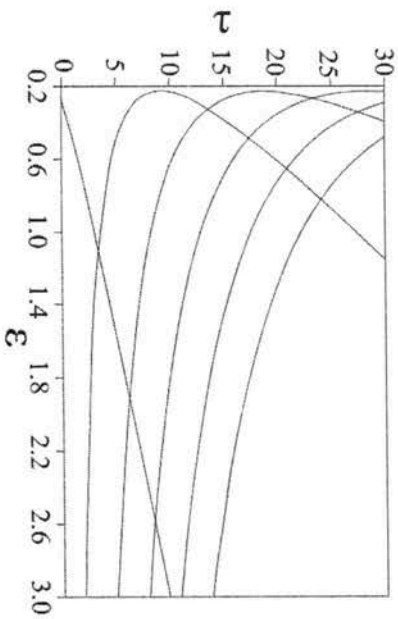


Figure 7. Hopf bifurcation curves  $\tau(\varepsilon)$ , for the fixed values of parameters  $\xi = 0.48$ , and  $\gamma = 0.8$ . The appropriate time series and the phase diagrams corresponding to particular points are shown in Figure 8.

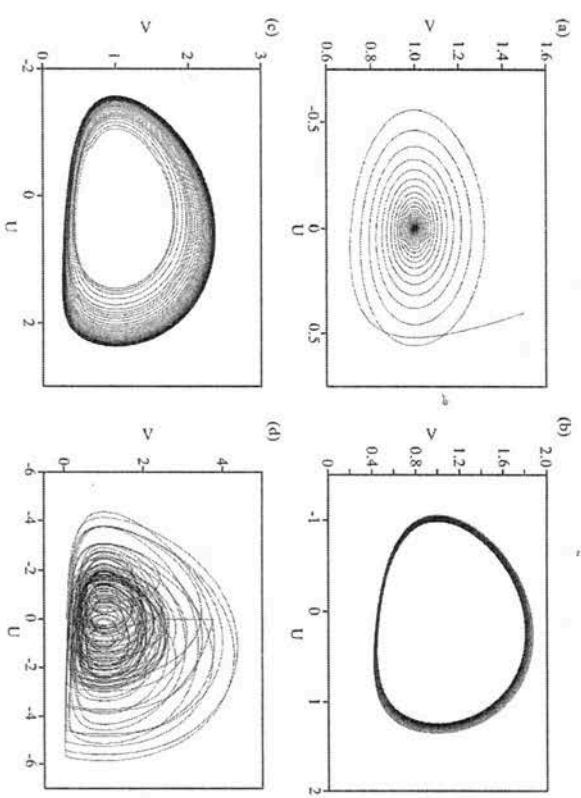


Figure 8. Phase portraits of variable  $v$  for a.  $\tau = 0$ ,  $\varepsilon = 0.23$ ,  $\xi = 0.48$  and  $\gamma = 0.8$  (fixed point); b.  $\tau = 10$ ,  $\varepsilon = 0.3$ ,  $\xi = 0.48$  and  $\gamma = 0.8$  (limit cycle); c.  $\tau = 12$ ,  $\varepsilon = 0.5$ ,  $\xi = 0.48$  and  $\gamma = 0.8$  (torus); d.  $\tau = 20$ ,  $\varepsilon = 0.5$ ,  $\xi = 0.48$  and  $\gamma = 0.8$  (deterministic chaos). Parameter values are determined by the position of Hopf bifurcation curves in Figure 7.

### 3.2. Impact of Transient Perturbations

Kostić et al. [20] also examined the effect of a passing seismic wave on the dynamics of a spring-block model by introducing the following transient perturbation of the block acceleration:

$$\begin{aligned} \dot{\theta} &= -V(\theta + (1 + \varepsilon)\log(V)) \\ \dot{U} &= V - 1 \\ \dot{V} &= -\gamma^2 [U + (1/\xi)(\theta + \log(V))] + A \sin\left(\frac{2\pi t}{T}\right) e^{\{[(t-t_0)/t_0]^r\}} \end{aligned} \quad (13)$$

with the following parameters:

- $A$  - maximum amplitude of the induced change,

- $T$  - wave period,
- $t_0$  - moment for which the perturbation amplitude reaches its maximum value,
- $t_w$  - half width of the induced perturbation,
- $n$  - integer that controls the rise-time.

In terms of real earthquakes, more rapidly varying (short-period) transient changes of block acceleration could correspond to the effect of closer, smaller earthquakes, while more slowly varying (long-period) transient changes might describe larger, more remote earthquakes [20]. Parameters are set with respect to the periodic oscillations of the unperturbed system (13) just above the bifurcation curve ( $A_0 = 0.6$ ,  $T_0 \approx 12$ ). In this context, we have considered the short-period ( $T < 12$ ) and long-period ( $T > 12$ ) acceleration changes of different duration  $t_w$  [3, 100]. Kostić et al. [20] conducted the numerical analysis of the system (12) using Runge-Kutta fourth order system by assuming parameter values before and after the bifurcation curve. In the former case, the only relevant result occur when introducing the long-term transient changes which cause weakly irregular oscillations, that could be treated as an example of transient chaotic behavior, indicating the mechanism of instantaneous earthquake triggering. In the latter case, long-term high-frequency transient acceleration change induces the onset of quasiperiodic-like motion with modulated amplitude, indicating a possible transition to a precursory creep regime. On the other hand, longer low-frequency transient perturbations induce irregular oscillations which could correspond to transient seismic motion along the fault.

The main starting assumption of the work by Kostić et al. [20] is that different stages of block motion separated by the Hopf bifurcation curve correspond to the different creeping regimes along the fault. In particular, the uniform motion of the block is treated as a model of fault slip in the post-seismic creep regime, just after the last seismic event has occurred. The periodic oscillatory motion is considered to correspond to inter-seismic creep regime, which could be characteristic of more "mature" faults during the period of slow accumulation of elastic. One should note that model (13) only describes the different stages of the creeping aseismic displacement along the fault, whereas the onset of transient quasiperiodic-like (precursory creep regime) and irregular chaos-like motion (co-seismic dynamics) occurs only under the effect of external perturbation. The two latter types of motion are assumed to correspond to the precursory creep regime and the seismic motion, respectively. In this context, Kostić et al. [20] analyzed only the possibility of

generating the complex behavior, while common approach differs assumes that the dynamic instability arises when the sliding velocity exceeds some pre-defined threshold value [65-69].

Under the assumption that a passing seismic wave propagates along the fault, dynamics of system (12) reveals the following picture. In case when the generated change is of longer duration ( $t_w = 100$ ), high-frequency acceleration changes in the inter-seismic creep-regime lead to quasiperiodic-like dynamics (precursory creep regime), while long-period changes of acceleration in both post-seismic and inter-seismic creep regimes invoke irregular oscillations or chaos-like behavior (seismic motion). It is clear that the longer low-frequency transients could excite a seismic motion even if the fault is in an uniform creep regime. Such type of triggering has been observed in real conditions [70-71].

Significantly longer acceleration changes (e.g.,  $t_w = 800$ ) induce a temporary transition from oscillatory to uniform motion, after which the system converges to a stable limit cycle. San Andreas fault system, for example, did not experience significant triggering by the Landers earthquake, since its thicker and more deformed fault gouge requires greater stress change to induce a rupture [72].

The performed analysis has confirmed the occurrence of immediate or instantaneous dynamic triggering effect of a passing seismic wave, which has already been observed in situ following Landers [73], Denali [74] and Izmit earthquake [70]. Kostić et al. [20] determined that the long-period transients, which are assumed to correspond to the effect of distant earthquakes, have the strongest impact on the fault motion, leading to irregular chaos-like behaviors. On the other hand, the high-frequency transients, presumably originating from the nearby earthquakes, induce a transition to quasiperiodic-like motion (precursory creep regime).

It should be emphasized that the analysis performed by Kostić et al. [20] revealed that the low-amplitude variations have no significant impact on the dynamics of system (14). Nevertheless, previous studies indicated that even very small dynamic changes (down to  $3 \times 10^{-9}$ ) could trigger faults that are sufficiently near failure [75-76]. This discrepancy could be explained by the fact that model analyzed by Kostić et al. [20] represents only the fault creeping that is relatively stable with respect to the short-lived perturbations and that the dynamics of this model does not exhibit transient or asymptotic instability without the external perturbation of sufficiently high amplitude.

The results of Kostić et al. [20] are consistent with the work of Gombert et al. [77-78], who indicated that the transient dynamic stresses could not explain the delay triggering. Also, Belardinelli et al. [79] found that a dynamic

stress pulse is able to promote a nearly instantaneous failure, but cannot induce delayed triggering.

### 3.3. Impact of Continuous Perturbations

In the work of Kostić et al. [62], effect of continuous perturbations is analyzed by assuming the time dependent character of  $\varepsilon$  and  $\xi$  in the following way:

$$\begin{aligned}\dot{\theta} &= -V[\theta + (1 + \varepsilon + \delta_\varepsilon \sin(\omega_\varepsilon t))\log V] \\ \dot{U} &= V - 1 \\ \dot{V} &= -\gamma^2 [U + (1/\xi + \delta_\xi \sin(\omega_\xi t))(\theta + \log V)]\end{aligned}\quad (14)$$

where  $\delta_\varepsilon$ ,  $\delta_\xi$ ,  $\omega_\varepsilon$  and  $\omega_\xi$  represent the constant oscillation amplitudes and the angular frequencies, respectively ( $\delta_\varepsilon \leq \varepsilon$ ,  $\delta_\xi \leq \xi$ ). It is assumed that external perturbations induce small oscillations near the equilibrium values of some of the system parameters, but admitting the periodic motion, which could arise from slow rupture along the faults or to some non-natural source of vibrations, on one side [80], or Earth tides and reservoir effects, on the other side [81].

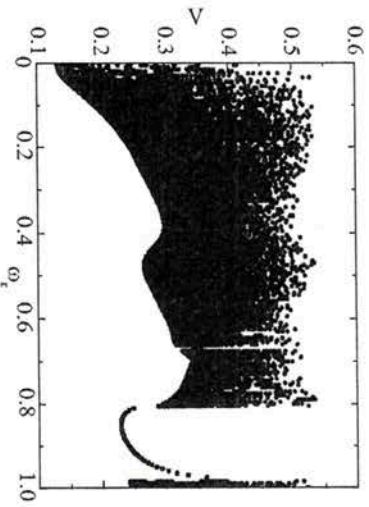


Figure 9. Projection of the attractors in the Poincaré section onto the V-coordinate vs the bifurcation parameter  $\omega_\varepsilon$ . The sections are provided for the plane  $\theta = 1$  and  $\omega_\xi$  and with the sampling step of 0.01, obtained after  $8 \times 10^6$  iteration steps for the fixed parameters admitting the limit cycle:  $\varepsilon = 0.4$  ( $\delta_\varepsilon = 0.3$ ),  $\xi = 0.5$  and  $\gamma = 0.7$ .

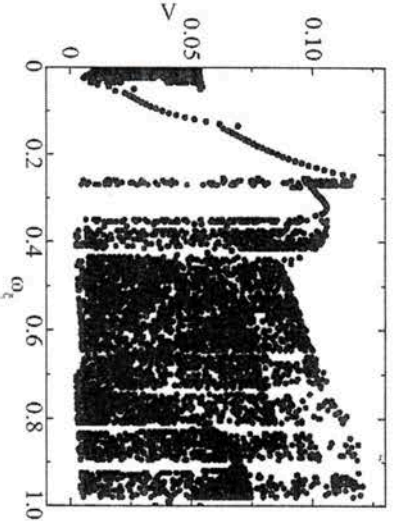


Figure 10. V-coordinates of the respective Poincaré sections under the variation of  $\omega_\varepsilon$ . The sections are provided for the plane  $\theta = 1$ , having sampled  $\omega_\xi$  with the 0.01 step size, obtained after  $4 \times 10^6$  time steps, for the fixed parameter values admitting the limit cycle:  $\varepsilon = 0.4$ ,  $\xi = 0.1$  ( $\delta_\xi = 0.3$ ) and  $\gamma = 0.7$ .

If only a single parameter,  $\varepsilon$  or  $\xi$ , undergoes periodic oscillations, while the other parameter is fixed, it turns out that as the parameter  $\omega_\varepsilon$  takes smaller values at each step in the range  $[0, 1]$ , a transition from periodic motion to deterministic chaos is observed, with periodic and quasiperiodic windows interspersed between chaotic clouds of dots (Figure 9).

The analysis of the system's dynamics when the perturbation of the parameter  $\xi$  ( $\omega_\xi$ ) is assumed (also for the fixed upper value of amplitude,  $\delta_\xi = 0.4$ ) indicates more complex picture, with successive transition from periodic and quasiperiodic motion to deterministic chaos, interspersed with periodic and quasiperiodic windows (Figure 10).

Although the onset of chaos is observed due to a single parameter perturbation, the drawback of such an approach is that the associated perturbation amplitude has to be comparable to the parameter's equilibrium value ( $\delta_\varepsilon = \delta_\xi = 0.4$ ). This is why we conducted additional analysis of complex dynamics of the examined model by choosing a value of angular frequency admitting the periodic motion of the block in an unperturbed state, while the dynamics is observed by changing the perturbation amplitudes for each of the observed parameter separately (Figure 11).

As it is clear from Figure 11 (upper figures), in case of perturbing only a single parameter ( $\varepsilon$  or  $\xi$ ), there is a direct transition to deterministic chaos for both amplitude values,  $\delta_\varepsilon$  and  $\delta_\xi$ , in the range  $[0, 0.4]$ . This type of scenario to chaos could imply the existence of some global bifurcation.

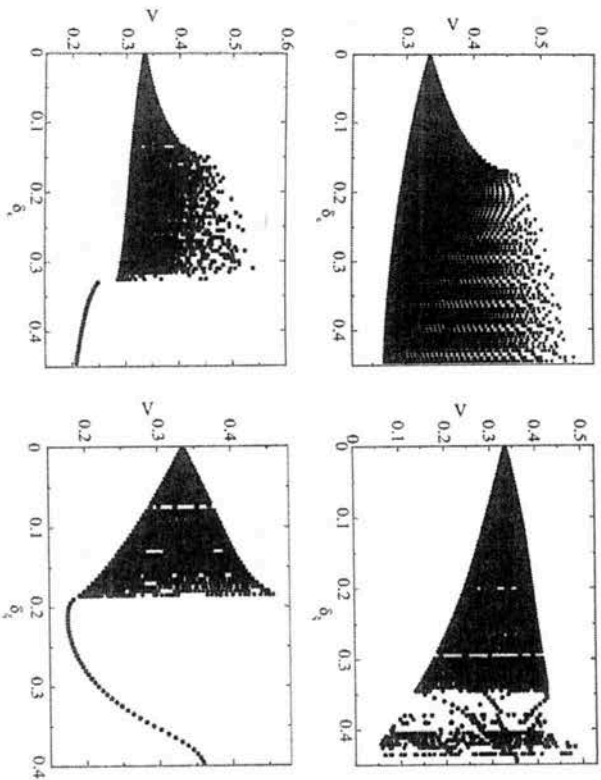


Figure 11. Orbital diagrams for the system (14) under the variation of the perturbation amplitude  $\delta_\varepsilon$  and  $\delta_\xi$ , with the associated frequencies fixed at  $\omega_\varepsilon = \omega_\xi = 0.3$  (upper figures) and  $\omega_\varepsilon = \omega_\xi = 0.8$  (lower figures), constructed for the plane  $\theta = 1$ , adopting the 0.01 sampling step after  $8 \times 10^6$  iteration steps. The remaining parameters admit the limit cycle:  $\varepsilon = 0.4$ ,  $\xi = 0.5$  and  $\gamma = 0.7$ .

In the work of Kostić et al. [62] they also analyzed a case of a single amplitude perturbation, only this time with higher frequency values ( $\omega_\varepsilon = \omega_\xi = 0.9$ ). As it can be seen in Figure 11 (lower figures), for the higher frequency values, a transition from periodic motion to deterministic chaos is observed. By comparing orbital diagrams in Figure 11 (lower figures), it is clear that the onset of chaos could be controlled only by tuning the angular frequencies of assumed periodic perturbation of the selected parameters ( $\varepsilon$  or  $\xi$ ).

One should note that although the assumed perturbations are rather simple, the performed analysis showed that the onset of deterministic chaos could be observed for smaller values of the control parameter  $\varepsilon$ , in comparison to the results of Erickson et al. [34], who observed irregular aperiodic oscillations for  $\varepsilon = 11$ . On the other side, results of Kostić et al. [62] are comparable with the research also conducted by Erickson et al. [35], where the transition to chaos is observed for  $\varepsilon = 0.5$ .

## 4. DYNAMICS OF A CHAIN OF BLOCKS

### 4.1. Global Coupling

Vasović et al. [21] examined the chain of all-to-all coupled blocks (each of  $i = 1, 2, \dots, N$  units is coupled with each other unit):

$$\begin{aligned} \dot{U}_{2i}(t) &= U_{2i}(t) \\ dU_{2i}(t) &= \left\{ -U_{1i}(t) + \Phi(U_{2i} + v) - \Phi(v) + \frac{K}{N} \sum_{j=1}^N [U_{1j}(t - \tau) - U_{1i}(t)] \right\} dt + \sqrt{2D} dW_i, \end{aligned} \quad (15)$$

where:

- $U_{1i}, U_{2i}$  - displacement and velocity of the  $i$ -th block, respectively,
- $K$  - spring constant,
- $\Phi$  - friction force,  $\Phi(V) = -(\mu_0 + a \ln(V))$  ( $\mu_0$  - steady-state friction,  $a$  - material property),
- $\tau$  - time delay,
- $v$  - nondimensional pulling background velocity,
- $\sqrt{2D} dW_i$  - stochastic increments of independent Wiener process,  $E(dW_i) = 0, E(dW_i dW_j) = \delta_{ij} dt$ , ( $E()$  - expectation over many realizations of the stochastic process,  $D$  - intensity of additive local noise).

One should note that rate-dependent nature of friction law has been indicate by previous studies [82-83].

Starting from model (15), Vasović et al. [21] developed the following averaged mean-field model:

$$\begin{aligned}
 \dot{m}_{U_2}(t) &= m_{U_2}(t), \\
 \dot{m}_{U_1}(t) &= -m_{U_1}(t) + ahv - ah(m_{U_2} + v) + \frac{a}{2} \frac{1}{(m_{U_2} + v)^2} s_{U_2} + \frac{a}{4} \frac{1}{(m_{U_2} + v)^4} 3s_{U_2}^2 + \\
 &+ K[m_{U_1}(t - \tau) - m_{U_1}(t)] \\
 \frac{1}{2} \dot{s}_{U_1}(t) &= s_{U_1} \\
 \frac{1}{2} \dot{s}_{U_2}(t) &= s_{U_2} \left[ \frac{a}{(m_{U_2} + v)} - \frac{a}{(m_{U_2} + v)^3} s_{U_2} \right] - (K + 1)s_{U_2} + D, \\
 \dot{s}_{U_1 U_2} &= -s_{U_1 U_2} \left[ \frac{a}{(m_{U_2} + v)} + \frac{a}{(m_{U_2} + v)^3} s_{U_2} \right] - (K + 1)s_{U_1} + s_{U_2}(t)
 \end{aligned}
 \tag{16}$$

where:  $m_{U_1}(t) = \langle U_1(t) \rangle$ ,  $m_{U_2}(t) = \langle U_2(t) \rangle$ ,  $s_{U_1}(t) = \langle \dot{m}_{U_1}^2(t) \rangle$ ,  $s_{U_2}(t) = \langle \dot{m}_{U_2}^2(t) \rangle$ ,  $s_{U_1 U_2}(t) = \langle \dot{m}_{U_1} \cdot \dot{m}_{U_2} \rangle$ , and  $n_{U_j}(t) = m_{U_j}(t) - U_j(t)$ ,  $j = 1, 2$ . In their work, Vasović et al. [21] showed mean-field approximated model (16) describes the dynamics of the starting model (15) accurately enough, so the obtained bifurcation curves in general correspond to bifurcations of the original system. Local bifurcation analysis of system (15) indicates a transition from equilibrium state to periodic oscillations for certain parameter values (Figure 12). From the seismological viewpoint, fixed point corresponds to absence of movement or steady sliding along the fault, while limit cycle denotes the aseismic creep along the fault [84-85].

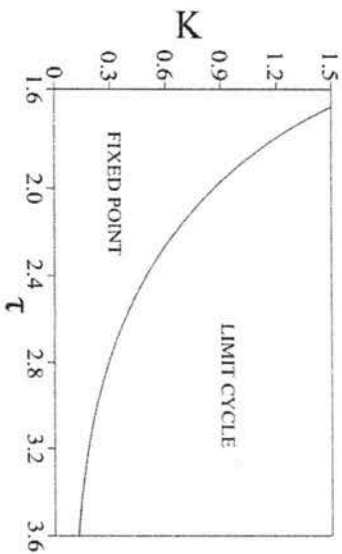


Figure 12. Parameter domain (K,  $\tau$ ) admitting fixed point or limit cycle of the mean-field approximated model (16). For a given parameter domain, other parameters are held constant:  $v = 1.2$ ,  $D = 0.002$ ,  $a = 0.1$ .

According to Vasović et al. [21], derived model (16) is in equilibrium state when the initial conditions are set near the fixed point. However, when initial conditions are assumed to take values away from the equilibrium point, mean-field model (16) could be both in equilibrium state or exhibit periodic regular oscillations, as a consequence of a global bifurcation or due to impact of the introduced random seismic noise when the starting stochastic system is near the bifurcation curve.

From the viewpoint of seismology, performed bifurcation analysis indicates that earthquakes could be expected to occur only in a bi-stable dynamical regime in the vicinity of a bifurcation curve provided that initial conditions along the fault are far from the equilibrium state (the case of active fault). In particular, irregular oscillations with amplitude higher than assumed noise level arise only for this regime, as an effect of either the introduced noise or the global attractor. Regular periodic oscillations of the starting system (16) above the bifurcation curve rarely occur in real conditions, since periodic occurrence of earthquakes is captured in the real conditions only for the strongest earthquakes at certain locations in the Earth's crust [86]. However, occurrence of all earthquakes within certain area is aperiodic. This means that periodic oscillations also represent an example of aseismic creep, which is frequently observed in real conditions [84-85].

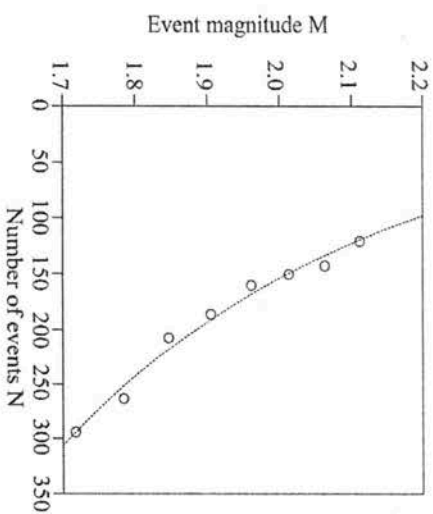


Figure 13. Examples of power-law behavior of system (15) away from the equilibrium point in a bi-stable regime near the bifurcation curve. It is clear that for different parameter values magnitude-frequency distribution follows the Gutenberg-Richter law ( $b = 0.99$ ) with satisfying statistical accuracy ( $a = 0.1$ ;  $D = 0.001$ ;  $\tau = 2$ ;  $K = 0.865$ ;  $v = 1.2$ ).

According to Vasović et al. [21], performed statistical analysis indicated that distribution of observed event magnitudes follows the Gutenberg-Richter power law with high values of  $R^2$  and low residual sum of squares and with the b-value  $\approx 0.99$  (Figure 13). Similar power law behavior is observed in neural networks [87]. In this case, event magnitude is defined as a natural logarithm of displacement sums for all blocks.

### 4.2. Varying Neighboring Interactions

Kostić et al. [22] analyzed a system comprised of  $N$  blocks, whereby each block  $i$  interacts with  $2K$  nearest neighbors:

$$\begin{aligned} & \bullet \quad u_i = v_i \\ & \bullet \quad \dot{v}_i = -u_i + \Phi(v_i + v_0) - \Phi(v_0) + \frac{C}{N} \sum_{j \in J} \left( u_{i+j} (t - \tau) - u_i \right) + \sqrt{2D} \xi_i(t), \end{aligned} \tag{17}$$

where  $J$  denotes the set of indices  $J = \{-K, \dots, K\} \setminus \{0\}$ ,  $C$  is the coupling strength,  $\tau$  is uniform interaction delay, often previously assumed in the case of neural chains [88-90],  $v_0$  is the pulling velocity of the upper moving plate,  $\xi_i(t)$  - independent Gaussian white noise ( $\langle \xi_i \rangle = 0, \langle \xi_i \xi_j \rangle = \delta_{ij}$ ), deriving from various sources [91-92] and  $\Phi$  is the frictional force  $\Phi(v) = \mu_0 - a \ln(v)$ , where  $\mu_0$  and  $a$  are the same as in Equation (15).

Impact of coupling strength on the dynamics of the observed system arises from the effect of the crushed material along the fault zone, which commonly represents a cohesionless unconsolidated material composed of finely crushed particles. Influence of this material primarily depends on its composition, zone width and fault depth.

One should note that blocks at the end of the array are connected to neighboring blocks only on one side.

Starting from model (16), Kostić et al. [22] derive the following mean-field approximated model with qualitatively the same dynamics as in Eq. (17):

$$\begin{aligned} \dot{m}_u(t) &= m_v(t) \\ \dot{m}_v(t) &= -m_u(t) + a \ln(v_0) - a \ln(m_u + v_0) + \frac{1}{2} \frac{D}{(m_u + v_0)} + \frac{2KC}{N} (m_u(t - \tau) - m_u(t)) \end{aligned} \tag{18}$$

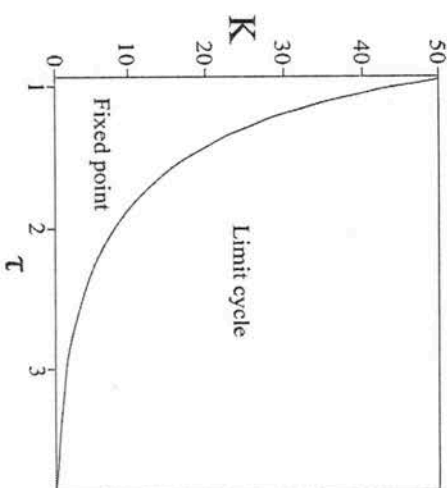


Figure 14.  $K(\tau)$  bifurcation curve describing the destabilization of fixed point in the mean-field model (18). The remaining system parameters are fixed at  $C = 5$ ,  $D = 0.0001$ ,  $a = 0.1$ ,  $v_0 = 1.2$ .

Analysis performed by Kostić et al. [22] showed that a supercritical Hopf bifurcation occurs indicating a transition from fixed point to a limit cycle, solely by increasing the time delay in interaction (Figure 14). For relatively high values of  $\tau$ , bifurcation can arise even in case of very small range of interactions ( $K = 3$ ). On the other hand, bifurcation could occur only by increasing the number of interacting blocks for a constant  $\tau$ . From the seismological viewpoint, this means that seismic fault movement could be induced solely by increasing the active length under the condition that there is a delayed interaction among different fault segments [22].

According to Kostić et al. [22], effect of seismic noise on dynamics of system (17) is negligible for the common ratio of coseismic slip rate vs. seismic noise is in the range  $10^{-2}$ - $10^{-7}$ .

One should note that bifurcation in the starting stochastic system (17) occurs solely by increasing the coupling strength  $C$  provided the delayed interaction between the units.

Furthermore, the results of analysis performed by Kostić et al. [22] obtained indicate the occurrence of an inverse supercritical Hopf bifurcation,

induced by the decrease the friction, which is expected in real conditions, since friction usually decreases with the increase of fault motion velocity. This means that a reduction of friction along the fault zone under the impact of pore water or similar, could induce the onset of bifurcation, under the assumed delayed interactions among different fault segments.

According to Kostić et al. [22], a group of coupled blocks with the largest displacements in the considered array (17) could be considered as a model for a hypocenter of a seismic event. In this case, they assume that event magnitude is defined as a natural logarithm of a sum of squares of displacements:

$$M = \ln \left( \sum_{i=1}^N (u_i)^2 \right) \quad (19)$$

where  $N$  is the total number of blocks in the observed system. Here, Kostić et al. [22] take the sum of squared displacement for each block as a measure of accumulated potential energy released during a single event. One should note that this is in no way in contrast to the assumptions made regarding the Figure 13. In essence, distribution of events remains the same. Nevertheless, authors consider the equation (18) to be a more reasonable assumption, concerning the definition of the potential energy itself. The distribution of the events with the largest magnitudes of displacements, is nearly periodic, so the suggested model (17) could be treated as a periodic or characteristic earthquake model [93].

## 5. PHASE RESPONSE CURVES FOR EARTHQUAKE FAULT DYNAMICS

The fault dynamics is often represented by the class of spring-slider block models incorporating different forms of constitutive friction laws. Such models can qualitatively account for the relevant regimes of fault dynamics, including the aseismic creep motion or the stick-slip motion, whereby the latter is signature for earthquakes. The studies based on these models have so far mainly aspired to gain insight into the scaling laws and the occurrence of characteristic events, as well as to elucidate the relation between small and large earthquakes. A substantially different approach is adopted in the work of Franović et al. [48]. Rather than examining the statistical features of the underlying time series or assessing the earthquake hazard, they to analyze a

representative class of fault models from the perspective of nonlinear dynamics theory.

The physical background for taking such an approach can be described as follows. Apart from the scale-invariant statistical features reflected in several well-known empirical scaling laws, certain earthquakes may exhibit characteristic features, manifested in "characteristic earthquakes" with the well-defined time or energy scales [24, 93-94]. The presence of a typical timescale implies that the fault fails in a pseudo-periodic series, making its dynamics reminiscent of that of a relaxation oscillator. The underlying oscillations are likely to be sensitive to external perturbations, which may derive from various forms of additional forcing whose duration and magnitude are small compared to the tectonic load. In general, if the perturbation is sufficiently small, it does not influence the amplitude of oscillations, but may considerably affect their phase. Then, an important conceptual issue, especially from the seismological point of view, becomes to determine whether and how the phase of stick-slip oscillations, and thereby the characteristic event itself, is delayed or advanced by such perturbations.

The motion of blocks comprising the complex fault is given by a simple generalization of the form:

$$\begin{aligned} \frac{d\theta_i}{dt} &= -\nu_i (\theta_i + (1 + \epsilon_i) h \nu_i) \\ \frac{du_i}{dt} &= \nu_i - 1 \\ \frac{d\nu_i}{dt} &= \gamma_i^2 (c(u_i - u_j) + u_i + (1/\epsilon_i)(\theta_i + h \nu_i)) \end{aligned} \quad (20)$$

where  $i, j \in \{1, 2\}$ ,  $i \neq j$  while  $c$  denotes the coupling strength.

As already indicated, the pseudo-periodic recurrence times have primarily been associated with large characteristic earthquakes [52, 95-99]. By one scenario, the latter involve breaking of the most part of or the entire seismogenic zone [24, 93, 100-101], whereas by the other scenario they emerge due to breaking of similar sections of complex faults [24, 102]. Well-known examples are earthquakes in the Nankaido region (Japan), the northern, southern and Parkfield sections of the San Andreas Fault [103], and several regions in China [104-105]. Apart from these large characteristic earthquakes, the description of fault dynamics in terms of relaxation oscillator models may also be justified for certain small repeating earthquakes [106]. One should note that many of the relevant models of fault dynamics may yield periodic

sequences of events or series with a strong periodic component. For instance, such behavior has been found for the one- and two-dimensional versions of the Burridge-Knopoff model [107-109], as well as in case of the Oiami-Feder-Christensen model [110]. It has also been suggested that models of coupled relaxation oscillators displaying the stick-slip dynamics may account for a phase-locking mechanism behind earthquake clusters. The latter conform to rupture patterns where the main events occur in groups comprising nearby or distributed faults with similar characteristic periods [49-50, 111].

## 5.1. Phase Response Curves for the Monoblock Fault

### 5.1.1. Theoretical Background

Phase response curve is an inherent feature of an arbitrary oscillator, which reflects its sensitivity to a brief pulse-like stimulus. Phase response curve is given by the dependence of the phase shift, induced by a perturbation, as a function of the oscillation phase at which the perturbation has occurred. The effect of phase resetting due to pulse perturbation may formally be treated as follows. Let us first consider a one-dimensional oscillator, described only by a continuously increasing phase variable  $\varphi$  which evolves as  $\dot{\varphi} = \omega$ . Then the system's phase just after a pulse stimulus of strength  $\kappa$  introduced at the moment  $t_p$  can be written as [18, 55].

$$\varphi_+(t_p) = \varphi(t_p) + \kappa Z(\varphi, \kappa) \quad (21)$$

where  $Z(\varphi, \kappa)$  stands for the phase response curve. In a more general case, periodic oscillations are characterized by a limit-cycle attractor  $X_0(t)$  in an  $N$ -dimensional phase space. Nevertheless, the notion of isochrones [112-113] still allows one to consider a phase space representation of the form  $(a, \varphi)$  where  $a$  is an  $(N-1)$ -dimensional "amplitude," and  $\varphi$  is the regular phase variable obeying  $\dot{\varphi} = \omega$  [55]. Without loss of generality, one may assume that the "amplitude" vanishes on the limit cycle ( $a = 0$ ). In this setup, if a kick is introduced at the moment  $t_p$ , the reset of the state  $(a, \varphi)$  just after  $t_p$  may be expressed as [55]:

$$\begin{aligned} \mathbf{a}_+(t_p) &= \mathbf{a}(t_p) + \kappa A(\mathbf{a}(t_p), \varphi(t_p), \kappa) = \kappa A(0, \varphi(t_p), \kappa) \\ \varphi_+(t_p) &= \varphi(t_p) + \kappa \Phi(\mathbf{a}(t_p), \varphi(t_p), \kappa) = \varphi(t_p) + \kappa Z(\varphi(t_p), \kappa) \end{aligned} \quad (22)$$

The above equations take into account that the initial state lies on the limit cycle ( $a = 0$ ), such that  $\Phi(0, \varphi, \kappa) = Z(\varphi, \kappa)$  holds. In terms of application, phase response curves were first introduced in the study of oscillations in biological systems, including cardiac cells, fireflies populations and especially neural networks [114-120]. Within these fields, as well the general theory of coupled phase oscillators, the method has facilitated an analysis of the units' interaction properties, including stability, synchronization or clustering. The concept of phase response curves allows one to reduce complex models of oscillators to simple phase models which still reflect important features of the original oscillators, such as the point that the effect of perturbation depends on the dynamical state of the oscillator. By this physical picture, each oscillator possesses a characteristic phase response curve that can be computed numerically or measured experimentally [121-123].

In a general multidimensional system, the kick may be applied to any of the system variables. In the work of Franović et al. [48], a perturbation is added to the second equation of the system (20), which is the most plausible choice, because it may be interpreted as a small variation at the loading point. The corresponding equation then takes the form  $dw/dt = v-1 + f(t)$ , where  $f(t)$  is the perturbation term. In real faults, such perturbations may derive from various natural and artificial sources, including rock break, pressure fluctuations or crack vibration due to movement of magma and volcanic gases [124], sudden stress drops [125-126] drilling and blasting in underground mining activities [127-128], as well as micro earthquakes due to hydraulic fracturing or deep injection of waste fluids [129].

In order to determine the phase response curves, one does not have to carry out an explicit phase reduction of the underlying systems, but may rather focus on the occurrence of characteristic events. The latter are associated to large spikes of velocity of the block and are representative of earthquakes within the given models. With this in mind, one may effectively determine the phase response curves in complete analogy to the method typically applied for systems of spiking neurons. In particular, the impact of a perturbation is such that it locally changes the oscillation period of a system from the default value  $T_0$  (period in the absence of perturbation) to a different value  $T$ . This may be used to numerically determine the phase shift  $\Delta\varphi$  by measuring the relative change of the period [18, 55, 130]:



$$\Delta\varphi(\varphi) = \frac{T_0 - T_1}{T_0} \quad (23)$$

The phase shift  $\Delta\varphi$  plotted as a function of the phase  $\varphi$  when a perturbation has kicked in constitutes precisely the phase response curve. If  $T_1 < T_0$ , the stimulus advances the cycle and vice versa. The change of period of the oscillation cycle where a perturbation has occurred defines the first-order phase response curve. Perturbations may also affect the duration of the next oscillation cycle  $T_2$ , which corresponds to the second-order phase response curve, where the phase shift is given by:

$$\Delta\varphi^{(2)}(\varphi) = \frac{T_0 - T_2}{T_0} \quad (24)$$

In the seismological context, a nontrivial profile of the second-order phase response curve would qualitatively reflect the long-term effects exerted on fault dynamics by the pulse perturbation, bearing in mind that the interseismic periods typically comprise very long time scales.

By implementing the described method, Franović et al. [48] determine the first- and second-order phase response curves for different models of fault dynamics. Apart from a single pulse perturbation, they also consider scenarios where two subsequent pulses are introduced within a given oscillation cycle. The form of the perturbation involves the standard  $\alpha$  function

$$f(t) = C * [(-1/t_r) * \exp(-(t-t_p)/t_r) + (1/t_r) * \exp(-(t-t_p)/t_r)] \Theta(t-t_p) \quad (25)$$

whereby the Heaviside  $\Theta$  function is used for shifting along the time-axis. Naturally, the rise and decline characteristic times  $t_r$  and  $t_f$  are selected so that the perturbation maintains a narrow profile compared to the oscillation period ( $t_r = 0.15$ ,  $t_f = 0.4$ ), whereas  $C$  is kept sufficiently small so that the perturbation does not affect the amplitude of the underlying oscillations ( $C = 5$ ). Note that in all the considered instances, zero phase is assigned to the maximum amplitude of the  $u$  variable, which makes a natural choice in the seismological interpretation, because it corresponds to the occurrence of the characteristic event (earthquake).

### 5.1.2. Phase Response Curves for a Single Pulse Perturbation

The profiles of the first- and second-order phase response curves are provided in Figure 15(a), whereby the phase values are expressed in units of  $\pi$ . An important point regarding Figure 15(a) is that the first-order curve shows a phase advancement in a narrow phase interval lying at a small distance from the earthquake event, which is attributed to the phase  $\varphi = 0$ . Nevertheless, the external stimulus introduced at all the other points of the oscillation cycle has a retardation effect, viz. it acts to postpone the next characteristic event. The change of sensitivity to a perturbation is expectedly found close to the end of the seismic cycle. In that phase domain, the delay effect is weaker, but the perturbation still cannot advance the cycle. Franović et al. [48] have verified that the characteristic profile of the phase response curve is not modified under variation of the perturbation amplitude within the relevant range of values [48].

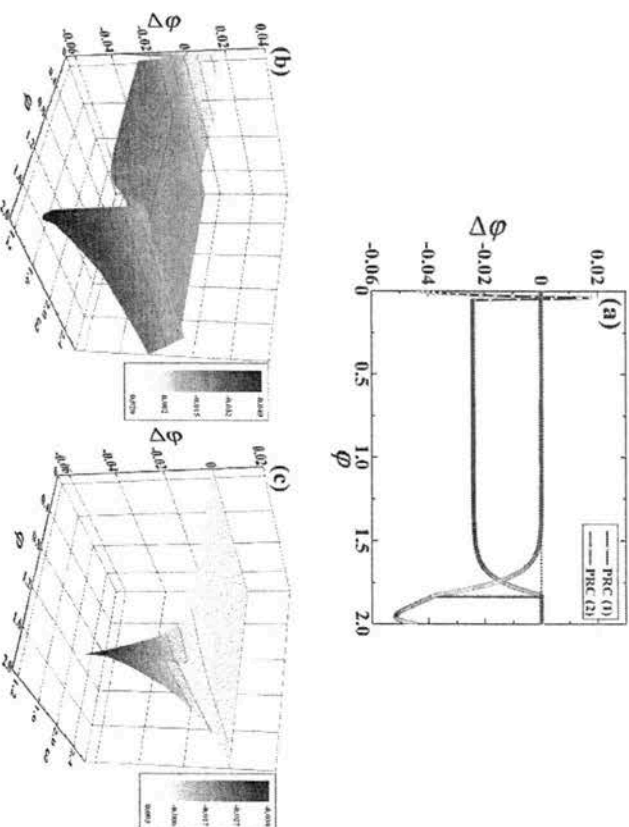


Figure 15. (a) Phase response curves of the first (blue circles) and second order (red circles) for a monoblock fault in the stick-slip regime. The fault parameters are ( $\epsilon, \xi, \gamma$ ) = (1.5, 0.5, 1000). (b) and (c) respectively show the families of first- and second-order PRCs  $\Delta\varphi(\varphi, \epsilon)$  for a monoblock fault under variation of  $\epsilon$ . The remaining parameters are the same as in (a).

As to be expected, the second order curve in Figure 15 (a) corroborates that the perturbation typically has a negligible impact on the duration of the next seismic cycle. Nevertheless, an interesting point concerns a long-term retardation effect exhibited for  $\varphi \approx 1.8\pi$ . Note that this delaying effect occurs precisely in the phase domain where the first-order phase response curves show a reduced retardation.

An important issue is to examine how robust are the obtained phase response curve profiles against variation of fault parameters. Note that the parameters  $\xi$  and  $\gamma$  are less specific to particular faults, so that the impact of their variation may be of lesser significance compared to the one of changing  $\varepsilon$ , which is highly specific to particular faults [48]. An important finding is that the curve profiles from Figure 15 turn out to be generic, viz. they remain qualitatively unaffected by changing  $\xi$  or  $\gamma$  for fixed  $\varepsilon$ . The effects of varying  $\varepsilon$  under fixed  $\xi$  and  $\gamma$  are illustrated in Figure 15 (b) and Figure 15 (c). These figures refer to phase shifts corresponding to first- and second-order phase response curves respectively, whereby  $\varepsilon$  attains values from the seismologically relevant range  $\varepsilon \in (1, 3)$ , while  $\xi$  and  $\gamma$  are fixed at values from Figure 15 (a).

Regarding the first-order curve, the effect of advancing the seismic cycle by a perturbation introduced within a preferred time interval just after the earthquake persists for the most part of the relevant  $\varepsilon$  range, but declines with increasing  $\varepsilon$ . In fact, one also finds a critical  $\varepsilon$  value above which there is no phase advance, cf. Figure 15 (b). The other interesting effect, which consists in a reduced phase delay if the perturbation occurs close to the end of the seismic cycle, appears unaffected by variation of  $\varepsilon$ . Also, the delay effect characteristic for the most of phase domain becomes less pronounced with increasing  $\varepsilon$ . Therefore, the profile of the first-order curve in general becomes more flat as  $\varepsilon$  is enhanced. Similar may be stated in case of the second-order phase response curve. In particular, Figure 15 (c) clearly shows that the delay effect associated to perturbation occurring by the end of the oscillation cycle is gradually lost with  $\varepsilon$ .

### 5.1.3. Two-Pulse Phase Response Curves for a One-Block Fault

Franović et al. [48] further consider the sensitivity of a one-block fault in the regime of stick-slip oscillations to two successive pulse perturbations. The first pulse acts at the phase  $\varphi_1$  of the oscillation cycle, whereas the other pulse is introduced at the phase  $\varphi_2$ . In both instances, the form of applied perturbation is assumed to be the same. Under real conditions, the occurrence

of multiple perturbations during a single oscillation cycle may be attributed to a number of different phenomena, both natural and artificial.

The first-order phase response curve is shown in Figure 16 (a). Note that the term "phase response curve" is kept for simplicity, though the plot actually shows the dependence of a phase reset  $\Delta\varphi$  in terms of  $\varphi_1$  and  $\varphi_2 - \varphi_1$ . The same terminology is maintained when describing the analogous three-dimensional plots below. From Figure 16 (a) one learns of two different mechanisms that may give rise to advancement of the phase of the seismic cycle [48]. First, if the initial pulse is applied in a narrow interval sufficiently close to the last seismic event ( $\varphi = 0$ ), the fault's phase is substantially advanced, irrespective of the precise point when the second perturbation occurs. Nonetheless, the advancing effect of two pulses is amplified compared to that of a single pulse, cf. Figure 16. The second mechanism is associated to the domain of  $\varphi_1$  values away from the characteristic event. There, the earlier arrival of the first perturbation typically requires a late arrival of the second perturbation in order to induce a substantial phase advancement. However, for sufficiently large  $\varphi_1$ , the phase of seismic cycle is advanced only within a narrow interval of preferred  $\varphi_2$  values, where the second pulse arrives in a relatively close succession to the first one. Outside of the described ( $\varphi_1$ ,  $\varphi_2$ ) domains, the impact of two successive pulse perturbations consists in delaying the next characteristic event, viz. the perturbations have a stabilizing effect on the fault dynamics.

Regarding the second-order phase response curve shown in Figure 16 (b), one notes a sizeable long-term effect if the first pulse arrives early (small  $\varphi_1$ ), and the second pulse is applied sufficiently late within the given cycle (large  $\varphi_2 - \varphi_1$ ). It is interesting that the long-term effect may either result in fault destabilization (advanced phase of oscillation) or fault stabilization (delayed phase of oscillation), which depends sensitively on the phase of the second pulse. Note that we interpret phase advancement (retardation) of the seismic cycle as destabilization (stabilization) of the fault because its next characteristic event is precipitated (postponed) by the perturbation. The presence of both types of behavior is quite distinct from what is found for a single pulse perturbation in Figure 16 (b), where the only pronounced effect consists in delaying the next oscillation cycle.

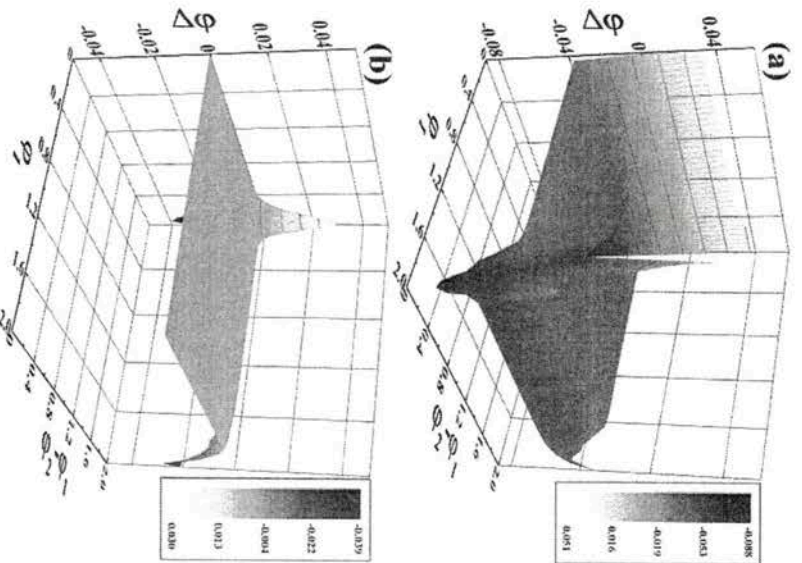


Figure 16. (a) and (b) respectively show the phase response curves of first and second order when a mono-block fault is subjected to two successive pulse perturbations. The first perturbation is introduced at the phase  $\varphi_1$ , and the second one is applied with the phase difference  $\varphi_2 - \varphi_1$ . The fault parameters are set to  $\varepsilon = 1.5$ ,  $\xi = 0.5$ ,  $\gamma = 1000$ .

## 5.2. Phase Response of Complex Faults

This subsection concerns the behavior of complex faults, whose structure generally involves multiple segments with potentially different elastic and frictional properties.

In particular, Franović et al. [48] analyze the sensitivity to perturbation of a homogeneous fault ( $\varepsilon_1 = \varepsilon_2$ ,  $\xi_1 = \xi_2$ ,  $\gamma_1 = \gamma_2$ ) built of identical blocks, as well as the heterogeneous complex fault [48]. Heterogeneity is confined to the scenario of two blocks with disparate  $\varepsilon$ ,  $\varepsilon_1 \neq \varepsilon_2$ , which results in distinct periods

of the respective stick-slip oscillations. Both for the homogeneous and the heterogeneous two-segment faults,  $c$  is taken sufficiently weak so that the interaction does not perturb the respective oscillation cycles of the blocks.

### 5.2.1. Phase Response Curves for the Fault Comprised of Two Identical Blocks

For the homogeneous complex fault, Franović et al. [48] analyze the scenario where perturbation on block 1 acts at phase  $\varphi_1$  of its oscillation cycle, whereas block 2 receives a kick with the phase difference  $\varphi_2 - \varphi_1 > 0$ . The form of perturbation to both blocks is assumed to be identical.

The first- and second-order phase response curves are illustrated in Figure 17. The respective phase shifts are denoted by  $\Delta\varphi_{ij}$ , where the first index denotes a particular block, and the second index refers to the first/second order of the phase response. It is interesting to compare the first-order phase response curves in Figure 17 (a) and Figure 17 (c), because this indicates how the interaction affects the response of individual blocks. In particular, the phase of both blocks is significantly advanced if the first block is stimulated immediately after the characteristic event. In this case, a perturbation of the first block induces a strong destabilization of the second block, regardless of the moment when the second block is perturbed. Just beyond the described region of  $\varphi_1$  values, one encounters a narrow domain where the external stimuli delay the cycles of both blocks. Nevertheless, the most interesting point concerns the differences between  $\Delta\varphi_{11}$  and  $\Delta\varphi_{21}$  dependencies. Namely, Franović et al. [48] have found that  $\Delta\varphi_{21}$  shows a much larger  $(\varphi_1, \varphi_2)$  domain where the phase of the cycle is strongly advanced compared to  $\Delta\varphi_{11}$ . This point corroborates that the dynamics of block 2 is substantially affected by the perturbation of block 1 conveyed via the interaction term. In fact, within the indicated  $(\varphi_1, \varphi_2)$  domain, the destabilization effect on block 2 is amplified by the co-action of two pulses, reflected in an indirect influence of a perturbation applied to the first block, and a direct impact of the subsequent pulse. Note that the destabilization effect on block 2 is more pronounced if the perturbation on block 1 arrives by the end of its oscillation cycle.

As far as the second order phase response curves are concerned, Figure 17 (b) and Figure 17 (d) both show quite large  $(\varphi_1, \varphi_2)$  domains of substantial phase advancement and phase retardation. Such nontrivial long-term effects are caused by the interaction between the blocks. Nevertheless, note that for the same  $(\varphi_1, \varphi_2)$  values, the long-term effects on two blocks are asymmetric, in a sense that the stabilization (phase delay) of one block is accompanied by the destabilization (phase advancement) of the other block.

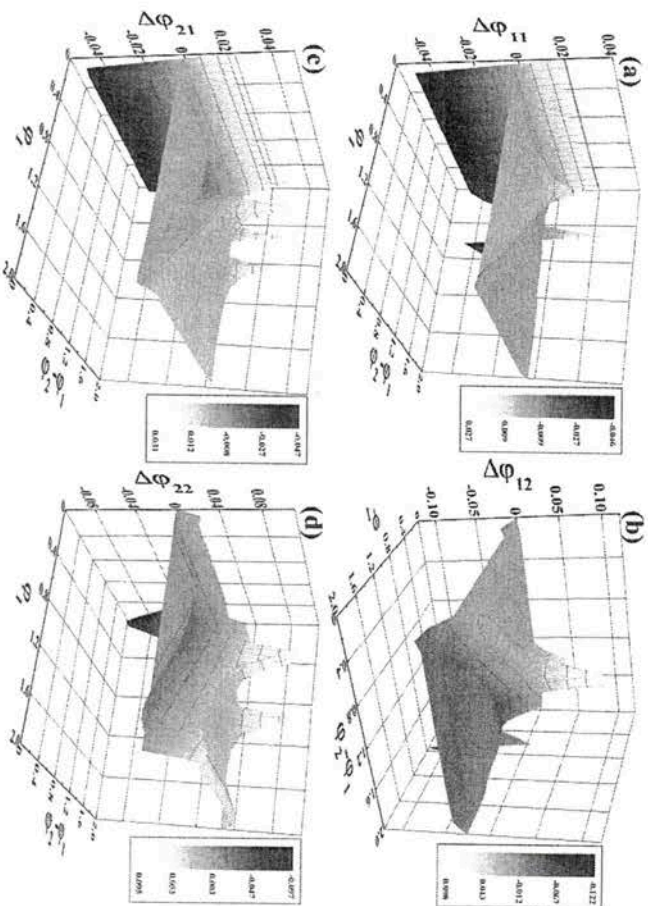


Figure 17. The top (bottom) row shows the phase responses of the first (left column) and second order (right column) for block 1 (2) in dependence of  $\phi_1$  and  $\phi_2$ . The blocks are assumed to be identical, and are characterized by parameters  $\varepsilon = 1.5$ ,  $\xi = 0.5$ ,  $\gamma = 1000$ . The interaction strength  $c = 0.1$  lies well below the critical bifurcation value and warrants that the periodic oscillations on the coupled blocks are not substantially different from those in the uncoupled case (For interpretation of the references to colour in this figure legend, the reader is referred to the web version of this chapter).

### 5.2.2. Phase Response Curves for the Two-Block Inhomogeneous Fault

Eranović et al. [48] further determine the phase response curves for an inhomogeneous fault comprised of two blocks with distinct  $\varepsilon$  values. The latter are such that the respective oscillation periods of blocks are substantially different, with  $T_1 \approx 52$  and  $T_2 \approx 77$ . Two generic scenarios are considered: in the first instance, perturbation is applied only to the block with the shorter oscillation period (here block 1), whereas in the second instance one perturbs the block with the longer oscillation period (here block 2). The numerical experiments are carried out so that at the moment when the stimulus arrives to one block, the other block always attains the same phase.

The results for the first scenario (perturbation applied to block 1 at phase  $\phi_1$ ) are illustrated in Figure 18, whereby Figure 18 (a) and Figure 18 (b) refer to first- and second-order responses of blocks 1 and 2, respectively. Note that Figure 18 (c) shows the average responses  $\Delta\phi_i = (\Delta\phi_{1,i} + \Delta\phi_{2,i})/2$  for the total system (complex fault), where  $i \in \{1, 2\}$  stands for the first- or second-order response.

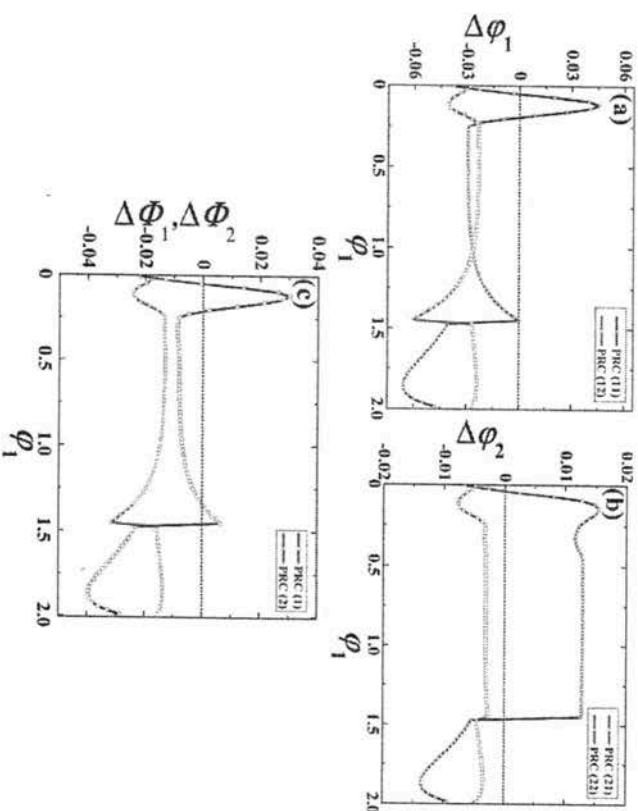


Figure 18. Scenario where pulse perturbation is introduced to the block with shorter oscillation period. In (a) are shown the first- (blue circles) and second-order phase response curves (red squares) for block 1, which is subjected to pulse perturbation. (b) illustrates the first- and second-order phase response curves for block 2 which is influenced by perturbation only via interaction with block 1. (c) provides an indication on the average phase response  $\Delta\phi_i$ ,  $i \in \{1, 2\}$  for the total system, viz. the complex fault, whereby index  $i$  refers to the first- or second-order dependence. The block parameters kept fixed are  $\xi = 0.5$ ,  $\gamma = 1000$ , whereas  $\varepsilon$  values on particular blocks are  $\varepsilon_1 = 1.45$  and  $\varepsilon_2 = 2$  (For interpretation of the references to colour in this figure legend, the reader is referred to the web version of this chapter).

As expected, for block 1, the first- and second-order phase response curves are qualitatively similar to that of an uncoupled block, cf. Figure 18 (a). As far as block 2 is concerned, note that Figure 18 (b) shows the dependence

$\Delta\varphi_2(\varphi_1)$  obtained for a fixed value of the phase of the second block. In other words, a perturbation is applied at different phases of the cycle of block 1, whereas block 2 at the moment of pulse arrival to block 1 always acquires certain fixed phase  $\varphi_2$ . The first-order response of block 2 implies that the interaction may play an important role in destabilization of the fault. In particular, it strikes that a perturbation acting on the block with a shorter oscillation period (block 1) is found to substantially advance the phase of the block with the longer oscillation period (block 2) for a broad interval of  $\varphi_1$  values [48]. Note that Figure 18 (c) implies that the average response of the two-block fault is mostly shaped by the behavior of block 1 which actually receives the stimulus.

In analogy to the previous setup, perturbation is applied at different phases of the cycle of block 2, whereas block 1 at the moment of pulse arrival to block 2 always has a fixed phase  $\varphi_1$ . The first-order responses of the blocks are shown in Figure 19 (a), whereas Figure 19 (b) refers to the second-order responses. The average first- and second-order responses of the complex two-block fault are provided in Figure 19 (c).

At variance with the scenario from Figure 18, the first-order phase response curve for the kicked block now shows two phase intervals which admit an advancement of the seismic cycle, whereby one is closely after the characteristic event ( $\varphi_2 \approx 0.1\pi$ ), while the other is located by the end of the seismic cycle ( $\varphi_2 \approx 1.5$ ). Nevertheless, an important qualitative finding on the first-order response of block 1 is that for almost all  $\varphi_2$ , the perturbation on block 2 advances the oscillation cycle on block 1. The analogous effect of advancing the phase of the respective block which is not subjected to pulse perturbation has already been observed in Figure 18 (b), but not in such a broad domain of perturbation phases. This point clearly evinces that (i) the effect of perturbation conveyed via interaction between the blocks is non-negligible, and (ii) that its impact on the block that has not directly received the pulse perturbation is typically destabilizing. As far as the total system is concerned, the first-order response is mostly influenced by the behavior of the block explicitly affected by the perturbation, whereas the leading delay effect in the second-order response derives from the other block, cf. Figure 18 (c).

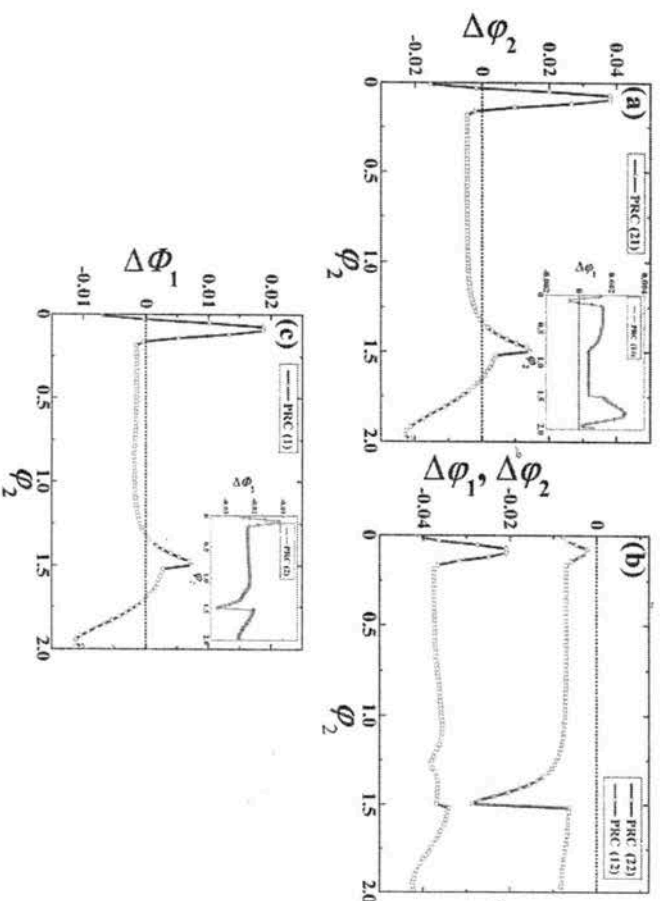


Figure 19. Scenario where pulse perturbation acts on the block with longer oscillation period. The main frame and inset in (a) shows the first-order phase response curve for block 2 and block 1, respectively. In (b) are shown the second-order phase response curves, whereby the blue circles (red squares) are reserved for block 2 (block 1). The main frame and the inset in (c) illustrate the average first- and second-order phase response for the complex fault, respectively. The block parameters are the same as in Figure 18 (For interpretation of the references to colour in this figure legend, the reader is referred to the web version of this chapter).

## CONCLUSION

In this chapter, authors provide a brief review of the main results regarding the dynamics of one-dimensional spring-block models under the impact of the following controlling factors:

- Delayed interaction among the blocks within array
- Delayed friction response to the change in velocity
- Incoherent random noise
- Various friction strength

- Continuous and transient perturbations.

This chapter represents the retrospective of the authors' work, since it is mainly based on the previous studies by Kostić et al [19, 20, 22, 61, 62], Franović et al. [48] and Vasović et al. [21]. Different setups of spring-block models, including a mono-block model, two-block model and an array of blocks, are derived from the original Burridge-Knopoff model, which is comprised of a series of interconnected blocks that are moving in a stick-slip fashion along the rough plane, in which way they mimic the seismogenic fault motion. Dynamics of such models is analyzed using standard method of nonlinear dynamics: bifurcation analysis, mean-field method, construction of phase response curves and numerical analysis. Such an approach that is based on the application of techniques from theoretical physics to geophysical research is new for the seismological community, and it provides a new perspective on the qualitative analysis of the earthquake nucleation process.

Previous studies aim to explain the very nature of the complex earthquake fault motion, starting from the simple dynamical systems, which assume that the main nonlinearity comes from the specific friction between the moving blocks and the rough plane, including rate-dependent and rate – and state – dependent friction law. However, if no additional assumption is made, analyzes show that such models are incapable of reproducing any relevant dynamical features. On the other hand, if supplementary presumption are made, including the delayed response of friction on the velocity change, delayed interaction among the block, the effect of random seismic noise or the influence of continuous or transient perturbation, one could easily detect rich dynamical behavior of these simple starting models. New features that arise include the following:

- direct or inverse Hopf bifurcations, with transition from equilibrium state (fixed point), through periodic (limit cycle) and quasiperiodic (torus) oscillations to long-term aperiodic irregular behavior (deterministic chaos), giving rise to the occurrence of complex fault motion;
- amplitude or oscillation death, preventing the occurrence of complex fault motion;
- advancement or retardation of the seismic cycle, in dependence on the nature of the assumed perturbation.

Assumption of delayed friction response to the velocity change results in two possible scenarios. Depending on the values of the control parameters, time delay could act both as a stabilizing and destabilizing factor. In the latter case, increase of time delay in friction could induce the more complex dynamics of fault motion, eventually leading to the onset of deterministic chaos. In the former case, increase of time delay could also lead to amplitude or oscillation death, acting, in that way, as a stabilizing factor.

If one assumes transient perturbation of a velocity in a form of sine wave scaled by an exponential pulse, which could correspond to the effect of a passing seismic wave from near or distant earthquake, transitions to different seismic regimes could be observed as a function of the assumed duration, frequency and the perturbation moment. In particular, if high-frequency acceleration changes are presumed in the inter-seismic creep-regime, this could lead to quasiperiodic-like dynamics, while long-period changes of acceleration in both post-seismic and inter-seismic creep regimes induce chaos-like behavior, which can be treated as an onset of the seismic motion.

If change of control parameters is assumed in a form of continuous periodical regular wave, which could correspond to the regular periodic influence of mining machines, then a direct transition from periodic motion to deterministic chaos could be observed in dependence on the assumed perturbation frequency. Moreover, the obtained results indicate the predominant impact of the assumed perturbation amplitude, which acts a controlling factor for the occurrence of a long-term irregular aperiodic behavior.

Except from introducing new parameters to the existing models, which triggered the occurrence of new dynamical regimes, previous studies on this topic also included the application of mean-field approach, which turned out to be a very useful technique when analyzing stochastic dynamical systems with large number of units. In particular, this method enables derivation of a simple deterministic model governed by a small number of equations, which exhibits qualitatively the same dynamical features as the starting stochastic model with a large number of equations. In this way, one could discuss about the conditions for specific transitions of the complex system by analyzing the reduced deterministic system.

Also, authors present the analysis of the perturbation by applying the theory of phase response curves, which provided more extended picture of the changes in dynamics of a mono-block and two-block models under the influence of external perturbation. The resulting first-order and second-order phase response curves imply the occurrence of seismic cycle advancement or

delay in dependence on the model setup (mono-block, homogeneous or heterogeneous two-block model) and on the arriving time of the presumed single-pulse or two-pulse stimulus.

In relation to seismology, it is interesting to note that the observed dynamics of the analyzed spring-block models, in certain cases, exhibit power-law behavior. In particular, if the sum of displacements of all the blocks in an array is treated as analogous to the earthquake magnitude, one could easily show that distribution of different events, regarding their number and size, is accurately described by Gutenberg-Richter law, with near  $b \approx 1$  value.

The presented analysis of the dynamics of the spring-block models enables the following:

- determination of the key parameters that control the system dynamics,
- qualitative assessment of the effect of various parameters on the changes of dynamical regimes,
- easier inquiry of the complex stochastic model by deriving the reduced, simpler deterministic model with qualitatively the same dynamical features as the stochastic model.

The main limitation of the presented approach lies in definition of the starting model, which is a dimensionless representation of the real fault motion. This means in the analysis one deals with parameter values which strictly do not correspond to the real observed data. Concerning this, one is able to infer about the qualitative influence of the parameter on the dynamics of the observed system, i.e., whether the increase or decrease of parameter values affect the system's dynamics, and how subtle those changes need to be.

Further research of the dynamics of spring-block models could include the analysis of two-dimensional models, which, besides temporal, also include the spatial variations and irregularities. Such models are definitely closer to the real observed fault motion, and, therefore, could more closely capture the specifics of movement along the fault plane. On the other hand, future analysis could also be oriented towards the application of different techniques of nonlinear time series analysis in order to capture the main dynamical mechanism behind the strong ground motion. Such study could result in useful data for engineering design, by providing the more accurate mathematical description of earthquake ground motion, or by determining the critical parameter values for which strong irregular ground motion occurs. Another approach that could be also implemented concerns the analysis of the effect of

normal and shear stress on the earthquake nucleation process, including both the normal (reverse) and strike-slip faults.

#### ACKNOWLEDGMENTS

The work on this chapter was partly supported by the Ministry of Education, Science and Technological Development of the Republic of Serbia (Contracts No. 176016 and 171017).

#### REFERENCES

- [1] Hess, D. P., Soom, A. *J Tribol*, 1990, 112, 147 - 152.
- [2] Burić, N., Mudrinić, M., Vasović, N. *Chaos Soliton Fract*, 2001, 12, 483-489.
- [3] Burić, N., Grozdanović, I., Todorović, K., Vasović, N. *J Stat Phys*, 2011, 145, 175-186.
- [4] Burić, N., Ranković, d., Todorović, K., Vasović, N. *Physica A*, 2010, 389, 3956-3964.
- [5] Burić, N., Grozdanović, I., Vasović, N. *Chaos Soliton Fract*, 2004, 22, 731-740.
- [6] Burić, N., Grozdanović, I., Vasović, N. *Chaos Soliton Fract*, 2005, 23, 1221-1233.
- [7] Burić, N., Vasović, N. *Chaos Soliton Fract*, 2007, 31, 336-342.
- [8] Vasović, N., Burić, N., Todorović, K., Grozdanović, I. *Chinese Phys B*, 2012, 21, 010203.
- [9] Burić, N., Todorović, K., Vasović, N. *Physical Review E*, 2010, 82, 037201.
- [10] Burić, N., Todorović, K., Vasović, N. *Chaos Soliton Fract*, 2009, 40, 2405-2413.
- [11] Burić, N., Todorović, K., Vasović, N. *Phys Rev E*, 2007, 75, 026209.
- [12] Burić, N., Todorović, K., Vasović, N. *Chaos Soliton Fract*, 2009, 40, 1127-1135.
- [13] Burić, N., Todorović, K., Vasović, N. *Phys Rev E*, 2008, 78, 036211.
- [14] Burić, N., Todorović, K., Vasović, N. *Phys Rev E*, 2007, 75, 067204.
- [15] Kuramoto, Y. *Chemical Oscillations, Waves, and Turbulence*: Dover, Mineola: New York, USA, 2003; 176 p.

- [16] Winfree, A. T. *The Geometry of Biological Time*; Springer: Berlin, 1980; 779 p.
- [17] Tass, P. A. *Phase Resetting in Medicine and Biology: Stochastic Modeling and Data Analysis*; Springer: Berlin Heidelberg, 2007; 329 p.
- [18] Schultzeiss, N. W., Prinz, A. A., Butera, R. J. (Eds.). *Phase Response Curves in Neuroscience: Theory, Experiment, and Analysis*; Springer: New York, 2012; 518 p.
- [19] Kostić, S., Franović, I., Todorović, K., Vasović, N. *Nonlinear Dynam.* 2013, 73, 1933-1943.
- [20] Kostić, S., Franović, I., Perc, M., Vasović, N., Todorović, K. *Sci Rep: Nature Publishing Group*, 2014, 4, 5401.
- [21] Vasović N., Kostić S., Franović I., Todorović K. *Commun Nonlinear Sci*, 2016, 38, 117-129.
- [22] Kostić, S., Vasović, N., Franović, I., Todorović, K., Klinsnov, V., Nekorkin, V. Submitted to *Nonlinear Dynam.* 2016 (under review).
- [23] Reid, H. F. Report of the State Investigation Commission, Vol. 2, Carnegie Institution of Washington, Washington, D. C. 1910, pp. 16-28.
- [24] Scholz, C. H. The mechanics of earthquakes and faulting, Cambridge University Press: Cambridge, 2002; 504 p.
- [25] Bykov, V. G. *Acta Geophys*, 2008, 56, 270-285.
- [26] Brace, W., Byerlee, J. *Science*, 1966, 153, 990-992.
- [27] Burridge, K., Knopoff, L. *Bull. Seismol. Soc. Am.* 1967, 57, 341-371.
- [28] Kostić, S., Vasović, N. *Tehnika*, 2011, 67, 61-66.
- [29] Omori, F. *J Coll Sci, Imperial University of Tokyo*. 1894, 7, 111-200.
- [30] Utsu, T. *Geophysical Magazine*, 1961, 30, 521-605.
- [31] Kawamura, H., Hatano, T., Kato, N., Biswas, S., Chakrabarti, B. K. *Rev Mod Phys*, 2012 84, 839-884.
- [32] Carlson, J. M., Langer, J. S. *Phys Rev A*, 1989, 40, 6470-6484.
- [33] De Sousa Vieira, M. *Phys Rev Lett*, 1999, 82, 201-204.
- [34] Erickson, B., Birnir, B., Lavallee, D. *Nonlinear Proc Geophi*, 2008, 15, 1-12.
- [35] Erickson, B. A., Birnir, B., Lavallée, D. *Geophys J Int*, 2011, 187, 178-198.
- [36] Dieterich, J. H. *J Geophys Res*, 1979, 84, 2161-2168.
- [37] Ruina, A. L. *J Geophys Res*, 1983, 88, 10359-10370.
- [38] Clancy, I., Corcoran, D. *Phys Rev E*, 2009, 80, 016113.
- [39] Scholz, C. H. *Nature*, 1998, 391, 37-42
- [40] Tullis, T. E., Beeler, N. M., Weeks, J. D. *Eos, Trans Am Geophys Union*, 1993, 74, 296.

- [41] Beeler, N. M., Tullis, T. E., Weeks, J. D. *Geophys Res Lett*, 1994, 21, 1987-1990.
- [42] Perrin, G., Rice, J. R., Zheng, G. *J Mech Phys Solids*, 1995, 43, 1461-1495.
- [43] Scholz, C. H., Molnar, P., Johnson, T. *J Geophys Res*, 1972, 77, 6392-6406.
- [44] Baumberger T., Heslot F., Perrin B. *Nature*, 1994, 367, 544-546.
- [45] Marone, C. *Ann Re. Earth Planet Sci*, 1998, 26, 643-696.
- [46] Linker, M. F., Dieterich, J. H. *J Geophys Res*, 1992, 97, 4923-4940.
- [47] Wang, W., Scholz, C. H. *Pure Appl Geophys*, 1994, 143, 303-316.
- [48] Franović, I., Kostić S., Perc, M., Klinsnov, V., Nekorkin, V., Kurths, J. *Chaos*, 2016, 26, 063105-1-12.
- [49] Scholz, C. H. *Bull Seismol Soc Am*, 2010, 100, 901-909.
- [50] Sugijura, N., Hori, T., Kawamura, Y. *Nonlin Proc Geophys*, 2014, 21, 251-267.
- [51] Lurmsanashvili, O., Paatashvili, T., Gheonjian, L., in *Synchronization and Triggering: from Fracture to Earthquake Processes*; Editors, de Rubels, V., Czechowski, Z., Teisseyre, R., Springer-Verlag: Berlin-Heidelberg, 2010, pp. 305-322.
- [52] Vasudevan, K., Cavers, M., Ware, A. *Nonlin Proc Geophys*, 2015, 22, 499-512.
- [53] Perez Velazquez, J. L., Galan, R. F., Garcia Dominguez, L., Leshchenko, Y., Lo, S., Belkas, J., Guevara Erra, R., *Phys Rev E*, 2007, 061912.
- [54] Tateno, T., Robinson, H. P. C. *Biophys J*, 2007, 92, 683-695.
- [55] Krishnan, G. P., Bazhenov, M., Pikovsky, A. *Phys Rev E*, 2013, 88, 042902.
- [56] Achuthan, S., Canavier, C. C. *J Neurosci*, 2009, 29, 5218-5233.
- [57] Kawamura, Y., Nakao, H., Arai, K., Kori, H., Kuramoto, Y. *Phys Rev Lett*, 2008, 101, 024101.
- [58] Kori, H., Kawamura, Y., Nakao, H., Arai, K., Kuramoto, Y. *Phys Rev E*, 2009, 80, 036207.
- [59] Ko, T. W., Ermentrout, G. B. *Phys Rev E*, 2009, 79, 016211.
- [60] Levnajić, Z., Pikovsky, A. *Phys Rev E*, 2010, 82, 056202.
- [61] Kostić, S., Vasović, N., Franović, I., Todorović, K. *Nonlin Proc Geophys*, 2013, 20, 857-865.
- [62] Kostić, S., Vasović, N., Franović, I., Todorović, K. *J Comput Nonlin Dyn*, 2013, 9, 031019.



- [63] Prasad, A., Dhamala, M., Adhikari, B. M., Ramaswamy, R., *Phys Rev E*, 2010, 81, 027201.
- [64] Newhouse, S., Ruelle, D., Takens, F. *Commun Math Phys*, 1978, 64, 35–44.
- [65] Bizzari, A. *Earth-Sci Rev*, 2012, 115, 304–318.
- [66] Day, S. M., Dalgner, L. A., Lapusta, N., Liu, Y. *J Geophys Res*, 2005, 110, B12307.
- [67] Bizzari, A., Belardinelli, M. E. *Geophys J Int*, 2008, 173, 906–921.
- [68] Rubin, A. M., Ampuero, J. P. *J Geophys Res*, 2005, 110, B11312.
- [69] Bizzari, A., Spudich, P. *J Geophys Res*, 2008, 113, B05304.
- [70] Brodsky, E. E., Karakostas, V., Kanamori, H. *Geophys Res Lett*, 2000, 27, 2741–2744.
- [71] Brodsky, E. E., Prejean, S. G. *J Geophys Res*, 2005, 110, B04302.
- [72] Freed, A. M. *Annu Rev Earth Planet Sci*, 2005, 33, 335–367.
- [73] Hill, D. P. et al. *Science*, 1993, 260, 1617–1623.
- [74] Prejean et al. *Bull Seismol Soc Am*, 2004, 94, 348–359.
- [75] Van Der Elst, N. J., Brodsky, E. E. *J Geophys Res*, 2010, 115, B07311.
- [76] Van Der Elst, N. J. The effect of seismic waves on earthquake nucleation and fault strength. University of California, Santa Cruz, PhD dissertation, 2012; 210 p.
- [77] Gombert, J., Blanpied, M. L., Beeler, N. M. *Bull Seismol Soc Am*, 1997, 87, 294–309.
- [78] Gombert, J., Beeler, N. M., Blanpied, M. L., Bodin, P. *J Geophys Res*, 1998, 103, B10, 24411–24426.
- [79] Belardinelli, M. E., Bizzari, A., Cocco, M. *J Geophys Res*, 2003, 108, 2135.
- [80] Gombert, J., Bodin, P., Savage, W., Jackson, M. E., *Geology*, 1995, 23, 41–44.
- [81] Perfettini, H., Schmitzbuhl, J., Rice, J. R., Cocco, M. *J Geophys Res*, 2001, 106, 13455–13472.
- [82] Sone, H., Shinamoto, T. *Nat Geosci*, 2009, 2, 705–708.
- [83] Lapusta N.: The roller coaster of fault friction. *Nat Geosci*, 2009, 2, 676–677.
- [84] Lienkaemper, J. J. et al. *Bull Seismol Soc Am*, 2012, 102, 31–41.
- [85] Galehouse, J. S., Lienkaemper, J. *Bull Seismol Soc Am*, 2004, 93, 2415–2433.
- [86] Parsons, T., Console, R., Falcone, G., Murru, M., Yamashina, K. *Geophys J Int*, 2012, 190, 1673–1688.
- [87] Franović, I., Miljković, V. *Eur Phys J B*, 2010, 763, 613–624.

- [88] Franović, I., Miljković, V. *Chaos Soliton Frac*, 2011, 44, 122–130.
- [89] Franović, I., Miljković, V. *Commun Nonlin Sci*, 2011, 16, 623–633.
- [90] Franović, I., Miljković, V. *EPL* 92, 2010, 68007.
- [91] Telford, W. M., Geldart, L. P., Sheriff, R. E. *Applied Geophysics*; Cambridge University Press: Cambridge, 1990; 792 p.
- [92] Ryabov, V. B., Correig, A. M., Urquiza, M., Zaitin, A. A. *Chaos Soliton Fract*, 2003, 16, 195–210.
- [93] Kanamori, H. (Ed.) *Earthquake Seismology: Treatise on Geophysics*; Elsevier: Amsterdam, 2009; Volume 4, 653 p.
- [94] Bhattacharyya, P., Chakrabarti, B. (Eds.), *Modeling Critical and Catastrophic Phenomena in Geoscience*; Springer: Berlin Heidelberg, 2006; 527 p.
- [95] Wesnousky, S. G. *Bull Seismol Soc Am*, 1994, 84 1940–1959.
- [96] Sieh, K. *Proc Natl Acad Sci USA*, 1996, 93, 3764–3771.
- [97] Tapponnier, P., Ryerson, F. J., Van der Woerd, J., Meriaux, A. S., Lasserre, C. *C R Acad Sci*, 2001, 333, 483–494.
- [98] Nishenko, S. P., Buland, R. *Bull Seismol Soc Am*, 1987, 77, 1382–1399.
- [99] Parsons, T. *Geophys Res Lett*, 2008, 35 L21301.
- [100] Sykes, L. R., Menke, W. B. *Seismol Soc Am*, 2006, 96, 1569–1596.
- [101] Ishibashi, K. *Ann Geophys*, 2004, 47, 339–368.
- [102] Benedetti, L. et al. *J Geophys Res Solid Earth*, 2013, 118, 4948–4974.
- [103] Schärer, K. M., Biasi, G. P., Weldon, R. J., Fumal, T. E. *Geology*, 2010, 38, 555–558.
- [104] Klinger, Y., Etchebes, M., Tapponnier, P., Narteau, C. *Nat Geosci*, 2011, 4, 389–392.
- [105] Haibing, L., Van der Woerd, J., Tapponnier, P., Klinger, Y., Xuexiang, Q., Jingsuia, Y., Yintang, Z. *Earth Planet Sci Lett*, 2005, 237, 285–299.
- [106] Matsuzawa, T., Igarashi, T., Hasegawa, A. *Geophys Res Lett*, 2002, 29, 1543.
- [107] Carlson, J. M. *Phys Rev A*, 1991, 44, 6226.
- [108] Mori, T., Kawamura, H. *Phys Rev Lett*, 2005, 94, 058501.
- [109] Mori, T., Kawamura, H. *J Geophys Res*, 2006, 111, B07302.
- [110] Kotani, T., Yoshino, H., Kawamura, H. *Phys Rev E*, 2008, 010102(R).
- [111] Sammis, C. G., Smith, S. W. *Tectonophysics*, 2013, 589, 167–171.
- [112] Guckenheimer, J. *J Math Biol*, 1975, 1, 259–273.
- [113] Schwabedal, J. T. C., Pikovsky, A. *Phys Rev Lett*, 2013, 110, 204102.
- [114] Mirollo, R. E., Strogatz, S. H. *SIAM J Appl Math*, 1990, 50, 1645–1662.
- [115] Ermentrout, G. B., Koppel, N. *J Math Biol*, 1991, 29, 195–217.
- [116] Kuramoto, Y. *Physica D*, 1991, 50, 15–30.

- [117] Bottani, S. *Phys Rev Lett*, 1995, 74, 4189.
- [118] Glass, L. *Nature*, 2001, 410, 277-284.
- [119] Glass, L., Nagai, Y., Hall, K., Talajić, M., Nattel, S. *Phys Rev E*, 2002, 65, 021908.
- [120] Canavier, C. C., Achuthan, S. *Math Biosci*, 2010, 226, 77-96.
- [121] Ermentrout, G. B. *Neural Comput*, 1996, 8, 979-1001.
- [122] Ermentrout, G. B., Beverin Bryce, I. I., Troyer, T., Netoff, T. *J Comput Neurosci*, 2011, 31, 185-197.
- [123] Galan, R. F., Ermentrout, G. B., Urban, N. N. *Phys Rev Lett*, 2005, 94, 158101.
- [124] Chouet, B. A. *Nature*, 1996, 380, 309-316.
- [125] Belardinelli, M. E., Bizzarri, A., Cocco, M. *J Geo Res*, 2003, 108, 2135.
- [126] Perfetini, H., Schmitzbuhl, J., Cochard, A. *J Geophys Res*, 2003, 108(b9), 2409.
- [127] Lu, W., Yang, J., Yan, P., Chen, M., Zhou, C., Luo, Y., Jin, L. *Int J Rock Mech Min Sci*, 2012, 53, 129-141.
- [128] Mulargia, F., Bizzarri, A. *Sci Rep*, 2014, 4, 6100.
- [129] Ellsworth, W. L. *Science*, 2013, 341, 1225942.
- [130] Ermentrout, G. B., Terman, D. H. *Mathematical Foundations of Neuroscience*. Springer: New York, 2010; 422 p.

In: Earthquakes

Editor: Wayne Coleman

ISBN: 978-1-53610-342-7

© 2017 Nova Science Publishers, Inc.

## Chapter 2

# MODELLING OF SEISMIC LIQUEFACTION DATA USING EXTREME LEARNING MACHINE

Pijush Samui<sup>1,\*</sup>, Sanjiban Sekhar Roy<sup>†</sup>,  
Pradeep Kurup<sup>3,‡</sup> and Yildirim Dalkılıç<sup>4,§</sup>

<sup>1</sup>Department of Civil Engineering,

NIT Patna, Bihar, India

<sup>2</sup>SCOPE, VIT University, Vellore, India

<sup>3</sup>Department of Civil and Environmental Engineering,

University of Massachusetts Lowell, Lowell, MA, US

<sup>4</sup>Faculty of Engineering,

Civil Engineering Department, Erzinçan University, Turkey

## ABSTRACT

Seismic liquefaction is a major concern for any earthquake prone area. This article employs a new technique based on Extreme Learning Machine (ELM) for determination of liquefaction susceptibility of soil based on Standard Penetration Test (SPT) and Cone Penetration Test (CPT) from the Chi-Chi earthquake. ELM is the modified version of

\* Email: pijush.phd@gmail.com.

† Email: sanjibanroy09@gmail.com.

‡ Email: Pradeep\_Kurup@uml.edu.

§ Email: yildirim.dalkilic@gmail.com.

